Alexander I. Bobenko *Editor*

Advances in Discrete Differential Geometry

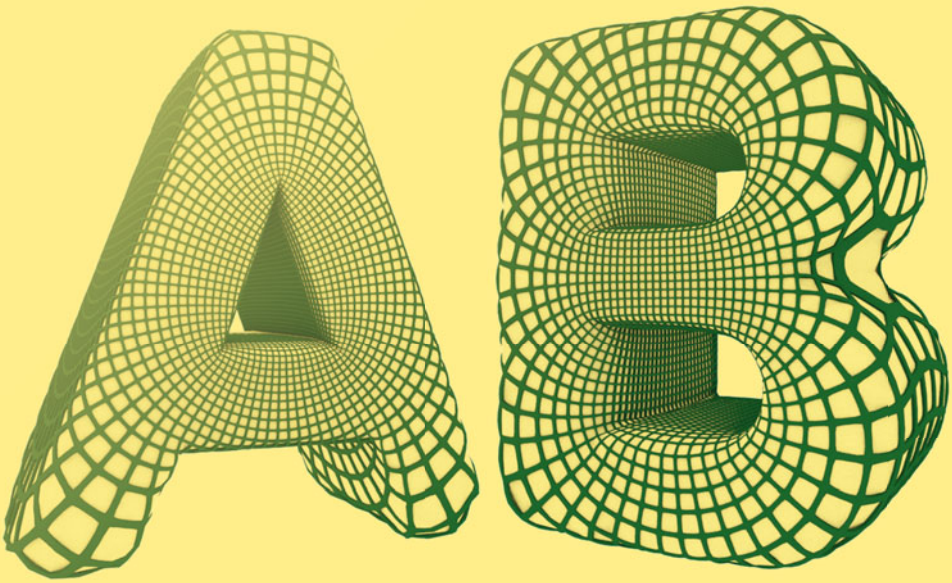

Springer Open

Advances in Discrete Differential Geometry

Alexander I. Bobenko
Editor

Advances in Discrete Differential Geometry

Springer Open

Editor
Alexander I. Bobenko
Institut für Mathematik
Technische Universität Berlin
Berlin
Germany

ISBN 978-3-662-50446-8 ISBN 978-3-662-50447-5 (eBook)
DOI 10.1007/978-3-662-50447-5

Library of Congress Control Number: 2016939574

Printed on acid-free paper

This Springer imprint is published by Springer Nature
The registered company is Springer-Verlag GmbH Berlin Heidelberg

Preface

In this book we take a closer look at discrete models in differential geometry and dynamical systems. The curves used are polygonal, surfaces are made from triangles and quadrilaterals, and time runs discretely. Nevertheless, one can hardly see the difference to the corresponding smooth curves, surfaces, and classical dynamical systems with continuous time. This is the paradigm of structure-preserving discretizations. The common idea is to find and investigate discrete models that exhibit properties and structures characteristic of the corresponding smooth geometric objects and dynamical processes. These important and characteristic qualitative features should already be captured at the discrete level. The current interest and advances in this field are to a large extent stimulated by its relevance for computer graphics, mathematical physics, architectural geometry, etc.

The book focuses on differential geometry and dynamical systems, on smooth and discrete theories, and on pure mathematics and its practical applications. It demonstrates this interplay using a range of examples, which include discrete conformal mappings, discrete complex analysis, discrete curvatures and special surfaces, discrete integrable systems, special texture mappings in computer graphics, and freeform architecture. It was written by specialists from the DFG Collaborative Research Center "Discretization in Geometry and Dynamics". The work involved in this book and other selected research projects pursued by the Center was recently documented in the film "The Discrete Charm of Geometry" by Ekaterina Eremenko.

Lastly, the book features a wealth of illustrations, revealing that this new branch of mathematics is both (literally) beautiful and useful. In particular the cover illustration shows the discretely conformally parametrized surfaces of the inflated letters A and B from the recent educational animated film "conform!" by Alexander Bobenko and Charles Gunn.

At this place, we want to thank the Deutsche Forschungsgesellschaft for its ongoing support.

Berlin, Germany
November 2015

Alexander I. Bobenko

Contents

Contributors

Alexander I. Bobenko Inst. für Mathematik, Technische Universität Berlin, Berlin, Germany

Raphael Boll Inst. für Mathematik, Technische Universität Berlin, Berlin, Germany

Folkmar Bornemann Zentrum Mathematik – M3, Technische Universität München, Garching bei München, Germany

Ulrike Bücking Inst. für Mathematik, Technische Universität Berlin, Berlin, Germany

Felix Günther Inst. für Mathematik, Technische Universität Berlin, Berlin, Germany

Tim Hoffmann Zentrum Mathematik – M10, Technische Universität München, Garching bei München, Germany

Alexander Its Department of Mathematical Sciences, Indiana University–Purdue University, Indianapolis, IN, USA

Caigui Jiang King Abdullah Univ. of Science and Technology, Thuwal, Saudi Arabia

Michael Joswig Inst. für Mathematik, Technische Universität Berlin, Berlin, Germany

Felix Knöppel Inst. für Mathematik, Technische Universität Berlin, Berlin, Germany

Hana Kouřimská Inst. für Mathematik, Technische Universität Berlin, Berlin, Germany

Wai Yeung Lam Technische Universität Berlin, Inst. Für Mathematik, Berlin, Germany

Daniel Matthes Zentrum Mathematik – M8, Technische Universität München, Garching bei München, Germany

Milan Mehner Inst. für Mathematik, Technische Universität Berlin, Berlin, Germany

Sheehan Olver School of Mathematics and Statistics, The University of Sydney, Sydney, Australia

Arnau Padrol Institut de Mathématiques de Jussieu - Paris Rive Gauche, UPMC Univ Paris 06, Paris Cedex 05, France

Matteo Petrera Inst. für Mathematik, Technische Universität Berlin, Berlin, Germany

Ulrich Pinkall Inst. für Mathematik, Technische Universität Berlin, Berlin, Germany

Helmut Pottmann Vienna University of Technology, Wien, Austria

Stefan Sechelmann Inst. für Mathematik, Technische Universität Berlin, Berlin, Germany

Lara Skuppin Inst. für Mathematik, Technische Universität Berlin, Berlin, Germany

Boris Springborn Inst. für Mathematik, Technische Universität Berlin, Berlin, Germany

Xiang Sun King Abdullah Univ. of Science and Technology, Thuwal, Saudi Arabia

Yuri B. Suris Inst. für Mathematik, Technische Universität Berlin, Berlin, Germany

Jan Techter Inst. für Mathematik, Technische Universität Berlin, Berlin, Germany

Mats Vermeeren Inst. für Mathematik, Technische Universität Berlin, Berlin, Germany

Johannes Wallner Graz University of Technology, Graz, Austria

Georg Wechslberger Zentrum Mathematik – M3, Technische Universität München, Garching bei München, Germany

Günter M. Ziegler Inst. für Mathematik, Freie Universität Berlin, Berlin, Germany

Discrete Conformal Maps: Boundary Value Problems, Circle Domains, Fuchsian and Schottky Uniformization

Alexander I. Bobenko, Stefan Sechelmann and Boris Springborn

Abstract We discuss several extensions and applications of the theory of discretely conformally equivalent triangle meshes (two meshes are considered conformally equivalent if corresponding edge lengths are related by scale factors attached to the vertices). We extend the fundamental definitions and variational principles from triangulations to polyhedral surfaces with cyclic faces. The case of quadrilateral meshes is equivalent to the cross ratio system, which provides a link to the theory of integrable systems. The extension to cyclic polygons also brings discrete conformal maps to circle domains within the scope of the theory. We provide results of numerical experiments suggesting that discrete conformal maps converge to smooth conformal maps, with convergence rates depending on the mesh quality. We consider the Fuchsian uniformization of Riemann surfaces represented in different forms: as immersed surfaces in $\mathbb{R}^3$, as hyperelliptic curves, and as $\mathbb{CP}^1$ modulo a classical Schottky group, i.e., we convert Schottky to Fuchsian uniformization. Extended examples also demonstrate a geometric characterization of hyperelliptic surfaces due to Schmutz Schaller.

1 Introduction

Not one, but several sensible definitions of discrete holomorphic functions and discrete conformal maps are known today. The oldest approach, which goes back to the early finite element literature, is to discretize the Cauchy–Riemann equa-

A.I. Bobenko · S. Sechelmann · B. Springborn (✉)
Inst. für Mathematik, Technische Universität Berlin, Straße des 17. Juni 136,
10623 Berlin, Germany
e-mail: boris.springborn@tu-berlin.de

A.I. Bobenko
e-mail: bobenko@math.tu-berlin.de

S. Sechelmann
e-mail: sechel@math.tu-berlin.de

A.I. Bobenko (ed.), *Advances in Discrete Differential Geometry*,
DOI 10.1007/978-3-662-50447-5_1

tions [10–14, 27]. This leads to linear theories of discrete complex analysis, which have recently returned to the focus of attention in connection with conformal models of statistical physics [8, 9, 22, 23, 29, 40–42], see also [4].

The history of nonlinear theories of discrete conformal maps goes back to Thurston, who introduced patterns of circles as elementary geometric way to visualize hyperbolic polyhedra [45, Chapter 13]. His conjecture that circle packings could be used to approximate Riemann mappings was proved by Rodin and Sullivan [35]. This initiated a period of intensive research on circle packings and circle patterns, which lead to a full-fledged theory of discrete analytic functions and discrete conformal maps [44].

A related but different nonlinear theory of discrete conformal maps is based on a straightforward definition of discrete conformal equivalence for triangulated surfaces: Two triangulations are discretely conformally equivalent if the edge lengths are related by scale factors assigned to the vertices. This also leads to a surprisingly rich theory [5, 17, 18, 28]. In this article, we investigate different aspects of this theory (Fig. 1).

We extend the notion of discrete conformal equivalence from triangulated surfaces to polyhedral surfaces with faces that are inscribed in circles. The basic definitions and their immediate consequences are discussed in Sect. 2.

In Sect. 3, we generalize a variational principle for discretely conformally equivalent triangulations [5] to the polyhedral setting. This variational principle is the main tool for all our numerical calculations. It is also the basis for our uniqueness proof for discrete conformal mapping problems (Theorem 3.9).

Section 4 is concerned with the special case of quadrilateral meshes. We discuss the emergence of orthogonal circle patterns, a peculiar necessary condition for the existence of solutions for boundary angle problems, and we extend the method of constructing discrete Riemann maps from triangulations to quadrangulations.

In Sect. 5, we briefly discuss discrete conformal maps from multiply connected domains to circle domains, and special cases in which we can map to slit domains.

Section 6 deals with conformal mappings onto the sphere. We generalize the method for triangulations to quadrangulations, and we explain how the spherical version of the variational principle can in some cases be used for numerical calculations although the corresponding functional is not convex.

Section 7 is concerned with the uniformization of tori, i.e., the representation of Riemann surfaces as a quotient space of the complex plane modulo a period lattice. We consider Riemann surfaces represented as immersed surfaces in $\mathbb{R}^3$, and as elliptic curves. We conduct numerical experiments to test the conjectured convergence of discrete conformal maps. We consider the difference between the true modulus of an elliptic curve (which can be calculated using hypergeometric functions) and the modulus determined by discrete uniformization, and we estimate the asymptotic dependence of this error on the number of vertices.

In Sect. 8, we consider the Fuchsian uniformization of Riemann surfaces represented in different forms. We consider immersed surfaces in $\mathbb{R}^3$ (and S^3), hyperelliptic curves, and Riemann surfaces represented as a quotient of $\hat{\mathbb{C}}$ modulo a classical Schottky group. That is, we convert from Schottky uniformization to Fuchsian uniformization. The section ends with two extended examples demonstrating, among

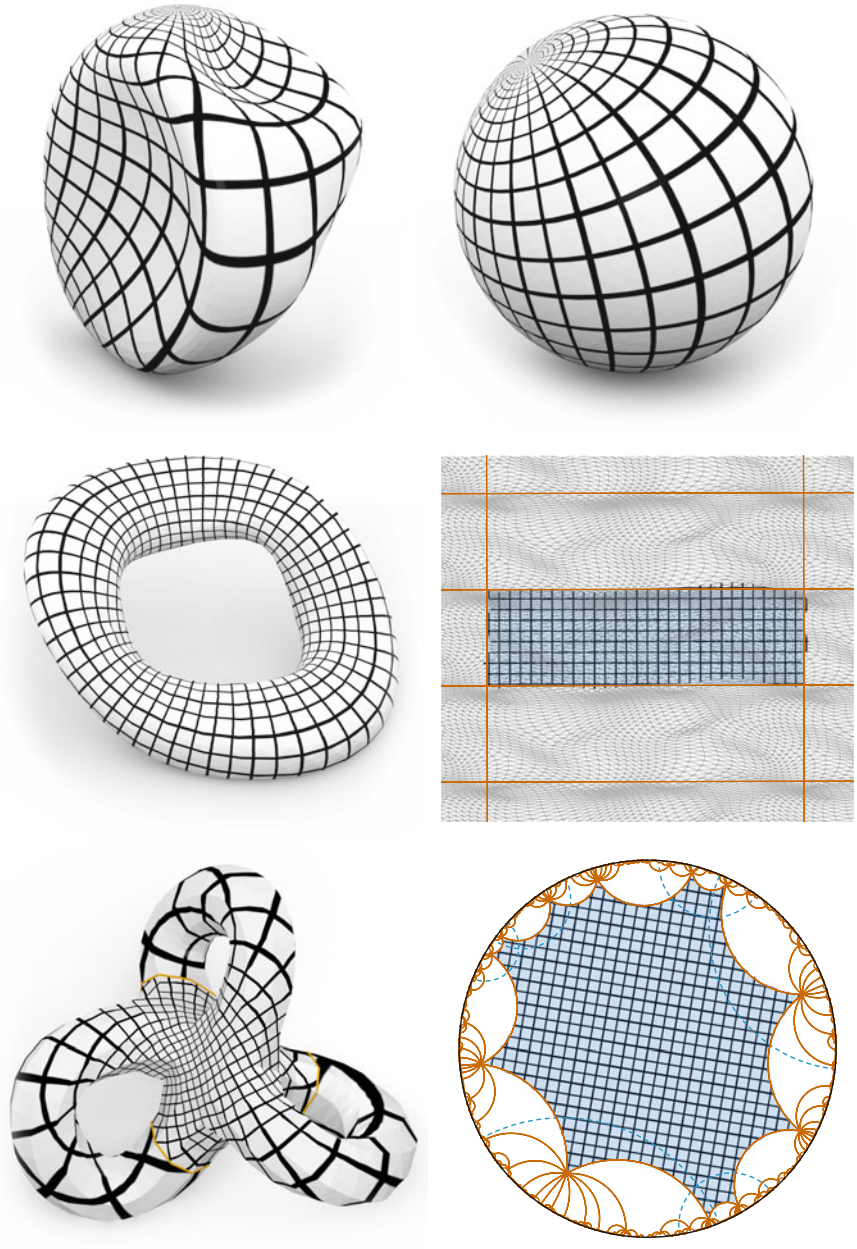

Fig. 1 Uniformization of compact Riemann surfaces. The uniformization of spheres is treated in Sect. 6. Tori are covered in Sect. 7, and Sect. 8 is concerned with surfaces of higher genus

other things, a remarkable geometric characterization of hyperelliptic surfaces due to Schmutz Schaller.

2 Discrete Conformal Equivalence of Cyclic Polyhedral Surfaces

2.1 Cyclic Polyhedral Surfaces

A *euclidean polyhedral surface* is a surface obtained from gluing euclidean polygons along their edges. (A *surface* is a connected two-dimensional manifold, possibly with boundary.) In other words, a euclidean polyhedral surface is a surface equipped with, first, an intrinsic metric that is flat except at isolated points where it has cone-like singularities, and, second, the structure of a CW complex with geodesic edges. The set of vertices contains all cone-like singularities. If the surface has a boundary, the boundary is polygonal and the set of vertices contains all corners of the boundary.

Hyperbolic polyhedral surfaces and *spherical polyhedral surfaces* are defined analogously. They are glued from polygons in the hyperbolic and elliptic planes, respectively. Their metric is locally hyperbolic or spherical, except at cone-like singularities.

We will only be concerned with polyhedral surfaces whose faces are all cyclic, i.e., inscribed in circles. We call them *cyclic polyhedral surfaces*. More precisely, we require the polygons to be cyclic before they are glued together. It is not required that the circumcircles persist after gluing; they may be disturbed by cone-like singularities. A polygon in the hyperbolic plane is considered cyclic if it is inscribed in a curve of constant curvature. This may be a circle (the locus of points at constant distance from its center), a horocycle, or a curve at constant distance from a geodesic.

A *triangulated surface*, or *triangulation* for short, is a polyhedral surface all of whose faces are triangles. All triangulations are cyclic.

2.2 Notation

We will denote the sets of vertices, edges, and faces of a CW complex Σ by V_Σ, E_Σ, and F_Σ, and we will often omit the subscript when there is no danger of confusion. For notational convenience, we require all CW complexes to be *strongly regular*. This means that we require that faces are not glued to themselves along edges or at vertices, that two faces are not glued together along more than one edge or one vertex, and that edges have distinct end-points and two edges have at most one endpoint in common. This allows us to label edges and faces by their vertices. We will write $ij \in E$ for the edge with vertices $i, j \in V$ and $ijkl \in F$ for the face with vertices $i, j, k, l \in V$. We will always list the vertices of a face in the correct cyclic order, so that for example the face $ijkl$ has edges ij, jk, kl, and li. The only reason for restricting our discussion to strongly regular CW complexes is to be able to use this simple notation. Everything we discuss applies also to general CW complexes.

2.3 Discrete Metrics

The *discrete metric* of a euclidean (or hyperbolic or spherical) cyclic polyhedral surface Σ is the function $\ell : E_\Sigma \to \mathbb{R}_{>0}$ that assigns to each edge $ij \in E_\Sigma$ its length ℓ_{ij}. It satisfies the polygon inequalities (one side is shorter than the sum of the others):

$$\left.\begin{aligned} -\ell_{i_1 i_2} + \ell_{i_2 i_3} + \ldots + \ell_{i_{n-1} i_n} &> 0 \\ \ell_{i_1 i_2} - \ell_{i_2 i_3} + \ldots + \ell_{i_{n-1} i_n} &> 0 \\ &\vdots \\ \ell_{i_1 i_2} + \ell_{i_2 i_3} + \ldots - \ell_{i_{n-1} i_n} &> 0 \end{aligned}\right\} \quad \text{for all } i_1 i_2 \ldots i_n \in F_\Sigma \tag{1}$$

In the case of spherical polyhedral surfaces, we also require that

$$\ell_{i_1 i_2} + \ell_{i_2 i_3} + \ldots + \ell_{i_{n-1} i_n} < 2\pi. \tag{2}$$

The polygon inequalities (1) are necessary and sufficient for the existence of a unique cyclic euclidean polygon and a unique cyclic hyperbolic polygon with the given edge lengths. Together with inequality (2) they are necessary and sufficient for the existence of a unique cyclic spherical polygon. For a new proof of these elementary geometric facts, see [24]. Thus, a discrete metric determines the geometry of a cyclic polyhedral surface:

Proposition and Definition 2.1 *If Σ is a surface with the structure of a CW complex and a function $\ell : E_\Sigma \to \mathbb{R}_{>0}$ satisfies the polygon inequalities (1), then there is a unique euclidean cyclic polyhedral surface and also a unique hyperbolic cyclic polyhedral surface with CW complex Σ and discrete metric ℓ. If ℓ also satisfies the inequalities (2), then there is a unique spherical cyclic polyhedral surface with CW complex Σ and discrete metric ℓ.*

We will denote the euclidean, hyperbolic, and spherical polyhedral surface with CW complex Σ and discrete metric ℓ by $(\Sigma, \ell)_{euc}$, $(\Sigma, \ell)_{hyp}$, and $(\Sigma, \ell)_{sph}$, respectively.

2.4 Discrete Conformal Equivalence

We extend the definition of discrete conformal equivalence from triangulations [5, 28] to cyclic polyhedral surfaces in a straightforward way (Definition 2.2). While some aspects of the theory carry over to the more general setting (e.g., Möbius invariance, Proposition 2.5), others do not, like the characterization of discretely conformally equivalent triangulations in terms of length cross-ratios (Sect. 2.5). We will discuss similar characterizations for polyhedral surfaces with 2-colorable vertices and the particular case of quadrilateral faces in Sects. 2.7 and 2.8.

We define discrete conformal equivalence only for polyhedral surfaces that are combinatorially equivalent (see Remark 2.4). Thus, we may assume that the surfaces share the same CW complex Σ equipped with different metrics ℓ, $\tilde{\ell}$.

Definition 2.2 *Discrete conformal equivalence* is an equivalence relation on the set of cyclic polyhedral surfaces defined as follows:

- Two *euclidean* cyclic polyhedral surfaces $(\Sigma, \ell)_{euc}$ and $(\Sigma, \tilde{\ell})_{euc}$ are *discretely conformally equivalent* if there exists a function $u : V_\Sigma \to \mathbb{R}$ such that

$$\tilde{\ell}_{ij} = e^{\frac{1}{2}(u_i+u_j)}\ell_{ij}. \tag{3}$$

- Two *hyperbolic* cyclic polyhedral surfaces $(\Sigma, \ell)_{hyp}$ and $(\Sigma, \tilde{\ell})_{hyp}$ are *discretely conformally equivalent* if there exists a function $u : V_\Sigma \to \mathbb{R}$ such that

$$\sinh\left(\frac{\tilde{\ell}_{ij}}{2}\right) = e^{\frac{1}{2}(u_i+u_j)} \sinh\left(\frac{\ell_{ij}}{2}\right). \tag{4}$$

- Two *spherical* cyclic polyhedral surfaces $(\Sigma, \ell)_{sph}$ and $(\Sigma, \tilde{\ell})_{sph}$ are *discretely conformally equivalent* if there exists a function $u : V_\Sigma \to \mathbb{R}$ such that

$$\sin\left(\frac{\tilde{\ell}_{ij}}{2}\right) = e^{\frac{1}{2}(u_i+u_j)} \sin\left(\frac{\ell_{ij}}{2}\right). \tag{5}$$

We will also consider mixed versions:

- A euclidean cyclic polyhedral surface $(\Sigma, \ell)_{euc}$ and a hyperbolic cyclic polyhedral surface $(\Sigma, \tilde{\ell})_{hyp}$ are discretely conformally equivalent if

$$\sinh\left(\frac{\tilde{\ell}_{ij}}{2}\right) = e^{\frac{1}{2}(u_i+u_j)}\ell_{ij}. \tag{6}$$

- A euclidean cyclic polyhedral surface $(\Sigma, \ell)_{euc}$ and a spherical cyclic polyhedral surface $(\Sigma, \tilde{\ell})_{sph}$ are discretely conformally equivalent if

$$\sin\left(\frac{\tilde{\ell}_{ij}}{2}\right) = e^{\frac{1}{2}(u_i+u_j)}\ell_{ij}. \tag{7}$$

- A hyperbolic cyclic polyhedral surface $(\Sigma, \ell)_{hyp}$ and a spherical cyclic polyhedral surface $(\Sigma, \tilde{\ell})_{sph}$ are discretely conformally equivalent if

$$\sin\left(\frac{\tilde{\ell}_{ij}}{2}\right) = e^{\frac{1}{2}(u_i+u_j)} \sinh\left(\frac{\ell_{ij}}{2}\right). \tag{8}$$

Remark 2.3 Note that relation (5) for spherical edge lengths is equivalent to relation (3) for the euclidean lengths of the chords in the ambient $\mathbb{R}^3$ of the sphere (see

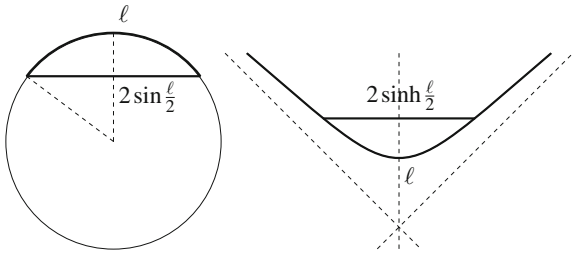

Fig. 2 Spherical and hyperbolic chords

Fig. 2, left). Likewise, relation (4) for hyperbolic edge lengths is equivalent to (3) for the euclidean lengths of the chords in the ambient $\mathbb{R}^{2,1}$ of the hyperboloid model of the hyperbolic plane (see Fig. 2, right).

Remark 2.4 For triangulations, the definition of discrete conformal equivalence has been extended to meshes that are not combinatorially equivalent [5, Definition 5.1.4] [17, 18]. It is not clear whether or how the following definitions for cyclic polyhedral surfaces can be extended to combinatorially inequivalent CW complexes.

The discrete conformal class of a cyclic polyhedral surface embedded in n-dimensional euclidean space is invariant under Möbius transformations of the ambient space:

Proposition 2.5 (Möbius invariance) *Suppose P and $\tilde{P}$ are two combinatorially equivalent euclidean cyclic polyhedral surfaces embedded in $\mathbb{R}^n$ (with straight edges and faces), and suppose there is a Möbius transformation of $\mathbb{R}^n \cup \{\infty\}$ that maps the vertices of P to the corresponding vertices of $\tilde{P}$. Then P and $\tilde{P}$ are discretely conformally equivalent.*

Note that only vertices are related by the Möbius transformation, not edges and faces, which remain straight. The simple proof for the case of triangulations [5] carries over without change.

2.5 Triangulations: Characterization by Length Cross-Ratios

For euclidean triangulations, there is an alternative characterization of conformal equivalence in terms of length cross-ratios [5]. We review the basic facts in this section.

For two adjacent triangles $ijk \in F$ and $jil \in F$ (see Fig. 3), the *length cross-ratio* of the common interior edge $ij \in E$ is defined as

$$\operatorname{lcr}_{ij} = \frac{\ell_{il}\ell_{jk}}{\ell_{lj}\ell_{ki}}. \tag{9}$$

(If the two triangles are embedded in the complex plane, this is just the modulus of the complex cross-ratio of the four vertices.) This definition of length cross-ratios

Fig. 3 Length cross-ratio

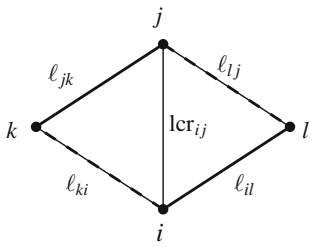

implicitly assumes that an orientation has been chosen on the surface. For non-orientable surfaces, the length cross-ratio is well-defined on the oriented double cover.

The product of length cross-ratios around an interior vertex $i \in V$ is 1, because all lengths cancel:

$$\prod_{ij \ni i} \mathrm{lcr}_{ij} = 1. \tag{10}$$

Proposition 2.6 *Two euclidean triangulations $(\Sigma, \ell)_{euc}$ and $(\Sigma, \tilde{\ell})_{euc}$ are discretely conformally equivalent if and only if for each interior edge $ij \in E^{int}_{\Sigma}$, the induced length cross-ratios agree.*

Remark 2.7 Analogous statements hold for spherical and hyperbolic triangulations. Equation (9) has to be modified by replacing ℓ with $\sin \frac{\ell}{2}$ or $\sinh \frac{\ell}{2}$, respectively (compare Remark 2.3).

2.6 Triangulations: Reconstructing Lengths from Length Cross-Ratios

To deal with Riemann surfaces that are given in terms of Schottky data (Sect. 8.2) we will need to reconstruct a function $\ell : E_\Sigma \to \mathbb{R}_{>0}$ satisfying (9) from given length cross-ratios. (It is not required that the function ℓ satisfies the triangle inequalities.) To this end, we define auxiliary quantities c^i_{jk} attached to the angles of the triangulation. The value at vertex i of the triangle $ijk \in F$ is defined as

$$c^i_{jk} = \frac{\ell_{jk}}{\ell_{ij}\ell_{ki}}. \tag{11}$$

Then (9) is equivalent to

$$\mathrm{lcr}_{ij} = \frac{c^i_{jk}}{c^i_{lj}}. \tag{12}$$

Now, given a function $\mathrm{lcr} : E^{int} \to \mathbb{R}_{>0}$ defined on the set of interior edges E^{int} and satisfying the product condition (10) around interior vertices, one can find parame-

ters c^i_{jk} satisfying (11) by choosing one value at each vertex and then successively multiplying length cross-ratios. The corresponding function ℓ is then determined by

$$\ell_{ij} = \frac{1}{\sqrt{c^i_{jk}c^j_{ki}}} = \frac{1}{\sqrt{c^i_{lj}c^j_{il}}}. \tag{13}$$

2.7 Bipartite Graphs: Characterization by Length Multi-Ratios

A different characterization of discrete conformal equivalence in terms of length multi-ratios holds if the 1-skeleton of the polyhedral surface is bipartite, i.e., if the vertices can be colored with two colors so that no two neighboring vertices share the same color.

Proposition 2.8 *(i) If two combinatorially equivalent euclidean cyclic polyhedral surfaces* $(\Sigma, \ell)_{euc}$ *and* $(\Sigma, \tilde{\ell})_{euc}$ *with discrete metrics* ℓ *and* $\tilde{\ell}$ *are discretely conformally equivalent, then the* length multi-ratios *for even cycles*

$$i_1i_2, i_2i_3, \ldots, i_{2n}i_1$$

are equal:

$$\frac{\ell_{i_1i_2}\ell_{i_3i_4}\cdots\ell_{i_{2n-1}i_{2n}}}{\ell_{i_2i_3}\ell_{i_4i_5}\cdots\ell_{i_{2n}i_1}} = \frac{\tilde{\ell}_{i_1i_2}\tilde{\ell}_{i_3i_4}\cdots\tilde{\ell}_{i_{2n-1}i_{2n}}}{\tilde{\ell}_{i_2i_3}\tilde{\ell}_{i_4i_5}\cdots\tilde{\ell}_{i_{2n}i_1}}. \tag{14}$$

(ii) If the 1*-skeleton of* Σ *is bipartite, i.e., if all cycles are even, then this condition is also sufficient: If the length multi-ratios are equal for all cycles, then the polyhedral surfaces are discretely conformally equivalent.*

Proof (i) This is obvious, because all scale factors e^u cancel. (ii) It is easy to see that Eq. (3) can be solved for the scale factors $e^{u/2}$ if the length multi-ratios are equal. Note that the scale factors are not uniquely determined: they can be multiplied by λ and $1/\lambda$ on the two vertex color classes, respectively. To find a particular solution, one can fix the value of $e^{u/2}$ at one vertex, and find the other values by alternatingly dividing and multiplying by $\tilde{\ell}/\ell$ along paths. The equality of length multi-ratios implies that the obtained values do not depend on the path. □

Remark 2.9 If a polyhedral surface is simply connected, then its 1-skeleton is bipartite if and only if all faces are even polygons. If a polyhedral surface is not simply connected, then having even faces is only a necessary condition for being bipartite.

A polyhedral surface with bipartite 1-skeleton has even faces. If a polyhedral surface has even faces and is simply connected, then its 1-skeleton is bipartite, and the face boundaries generate all cycles. Thus, Proposition 2.8 implies the following corollary.

Corollary 2.10 *Two simply connected combinatorially equivalent euclidean cyclic polyhedral surfaces with even faces and with discrete metrics ℓ and $\tilde{\ell}$ are discretely conformally equivalent if and only if the multi-ratio condition* (14) *holds for every face boundary cycle.*

Remark 2.11 Analogous statements hold for spherical and hyperbolic cyclic polyhedral surfaces. In the multi-ratio condition, one has to replace non-euclidean lengths ℓ with $\sin\frac{\ell}{2}$ or $\sinh\frac{\ell}{2}$, respectively (compare Remark 2.3).

2.8 Quadrangulations: The Cross-Ratio System on Quad-Graphs

The case of cyclic quadrilateral faces is somewhat special (and we will return to it in Sect. 4), because equal length cross-ratio implies equal complex cross-ratio:

Proposition 2.12 *If two euclidean polyhedral surfaces with cyclic quadrilateral faces are discretely conformally equivalent, then corresponding faces $ijkl \in F$ have the same complex cross-ratio (when embedded in the complex plane):*

$$\frac{(z_i - z_j)(z_k - z_l)}{(z_j - z_k)(z_l - z_i)} = \frac{(\tilde{z}_i - \tilde{z}_j)(\tilde{z}_k - \tilde{z}_l)}{(\tilde{z}_j - \tilde{z}_k)(\tilde{z}_l - \tilde{z}_i)}$$

Proof This follows immediately from Proposition 2.8: The length multi-ratio of a quadrilateral is the modulus of the complex cross-ratio. If the (embedded) quadrilaterals are cyclic, then their complex cross-ratios are real and negative, so their arguments are also equal. □

For planar polyhedral surfaces, i.e., for quadrangulations in the complex plane, Proposition 2.12 connects discrete conformality with the cross-ratio system on quad-graphs. A *quad-graph* in the most general sense is simply an abstract CW cell decomposition of a surface with quadrilateral faces. Often, more conditions are added to the definition as needed. Here, we will require that the surface is oriented and that the vertices are bicolored black and white. For simplicity, we will also assume that the CW complex is strongly regular (see Sect. 2.2). The *cross-ratio system* on a quad-graph Σ imposes equations (15) on variables z_i that are attached to the vertices $i \in V_\Sigma$. There is one equation per face $ijkl \in F_\Sigma$:

$$\frac{(z_i - z_j)(z_k - z_l)}{(z_j - z_k)(z_l - z_i)} = Q_{ijkl}, \tag{15}$$

where we assume that i is a black vertex and the boundary vertices $ijkl$ are listed in the positive cyclic order. (Here we need the orientation). On the right hand side of the equation, $Q : F_\Sigma \to \mathbb{C} \setminus \{0, 1\}$ is a given function. In particular, it is required that the values z_i, z_j, z_k, z_l on a face are distinct.

By Proposition 2.12, two discretely conformally equivalent planar quadrangulations correspond to two solutions of the cross-ratio system on the same quad-graph with the same cross-ratios Q. The following proposition says that in the simply connected case, one can find complex factors w on the vertices whose absolute values $|w| = e^{u/2}$ govern the length change of edges according to (3), and whose arguments govern the rotation of edges. Note that (3) is obtained from (16) by taking absolute values.

Proposition 2.13 *Let Σ be a simply connected quad-graph. Two functions $z, \tilde{z} : V_\Sigma \to \mathbb{C}$ are solutions of the cross-ratio system on Σ with the same cross-ratios Q if and only if there is a function $w : V_\Sigma \to \mathbb{C}$ such that for all edges $ij \in E_\Sigma$*

$$\tilde{z}_j - \tilde{z}_i = w_i w_j (z_j - z_i). \tag{16}$$

Proof As in the proof of Proposition 2.8, it is easy to see that the system of equations (16) is solvable for w if and only if the complex multi-ratios for even cycles are equal. Because Σ is simply connected, this is the case if and only if the complex cross-ratios of corresponding faces are equal. □

Remark 2.14 The cross-ratio system on quad-graphs (15) is an integrable system (in the sense of 3D consistency [6, 7]) if the cross-ratios Q "factor", i.e., if there exists a function on the set of edges, $a : E_\Sigma \to \mathbb{C}$, that satisfies the following conditions for each quadrilateral $ijkl \in F$:

(i) It takes the same value on opposite edges,

$$a_{ij} = a_{kl}, \quad a_{jk} = a_{li}. \tag{17}$$

(ii)

$$Q_{ijkl} = \frac{a_{ij}}{a_{jk}}. \tag{18}$$

In Adler et al. classification of integrable equations on quad-graphs [2], the integrable cross-ratio system is called $(\mathrm{Q1})_{\delta=0}$. It is also known as the discrete Schwarzian Korteweg–de Vries (dSKdV) equation, especially when it is considered on the regular square lattice [33] with constant cross-ratios.

If the cross-ratios Q have unit modulus, the cross-ratio system on quad-graphs is connected with circle patterns with prescribed intersection angles [6, 7].

Remark 2.15 The system of equations (16) is also connected with an integrable system on quad-graphs. Let $b_{ij} = z_j - z_i$, so b is a function on the oriented edges with $b_{ij} = -b_{ji}$. Let us also assume that the quad-graph Σ is simply connected. Then the system (16) defines a function $z : V \to \mathbb{C}$ (uniquely up to an additive constant) if and only if the complex scale factors $w : V_\Sigma \to \mathbb{C}$ satisfy, for each face $ijkl \in F$ the closure condition

$$b_{ij} w_i w_j + b_{jk} w_j w_k + b_{kl} w_k w_l + b_{li} w_l w_i = 0. \tag{19}$$

This system for w is integrable if, for each face $ijkl \in F$,

$$b_{ij} + b_{kl} = 0 \quad \text{and} \quad b_{jk} + b_{li} = 0.$$

In this case, (19) is known as discrete modified Korteweg–de Vries (dmKdV) equation [33], or as Hirota equation [6, 7].

3 Variational Principles for Discrete Conformal Maps

3.1 Discrete Conformal Mapping Problems

We will consider the following discrete conformal mapping problems. (The notation $(\Sigma, \ell)_g$ was introduced in Definition 2.1.)

Problem 3.1 (*prescribed angle sums*) **Given**

- A euclidean, spherical, or hyperbolic cyclic polyhedral surface $(\Sigma, \ell)_g$, where $g \in \{euc, hyp, sph\}$,
- a desired total angle $\Theta_i > 0$ for each vertex $i \in V_\Sigma$,
- a choice of geometry $\tilde{g} \in \{euc, hyp, sph\}$,

find a discretely conformally equivalent cyclic polyhedral surface $(\Sigma, \tilde{\ell})_{\tilde{g}}$ of geometry $\tilde{g}$ that has the desired total angles Θ around vertices.

For interior vertices, Θ prescribes a desired cone angle. For boundary vertices, Θ prescribes a desired interior angle of the polygonal boundary. If $\Theta_i = 2\pi$ for all interior vertices i, then Problem 3.1 asks for a flat metric in the discrete conformal class, with prescribed boundary angles if the surface has a boundary.

More generally, we will consider the following problem, where the logarithmic scale factors u (see Definition 2.2) are fixed at some vertices and desired angle sums Θ are prescribed at the other vertices. The problems to find discrete Riemann maps (Sect. 4.2) and maps onto the sphere (Sect. 6.1) can be reduced to this mapping problem with some fixed scale factors.

Problem 3.2 (*prescribed scale factors and angle sums*) **Given**

- A euclidean, spherical, or hyperbolic cyclic polyhedral surface $(\Sigma, \ell)_g$, where $g \in \{euc, hyp, sph\}$,
- a partition $V_\Sigma = V_0 \dot{\cup} V_1$

- a prescribed angle $\Theta_i > 0$ for each vertex $i \in V_1$,
- a prescribed logarithmic scale factor $u_i \in \mathbb{R}$ for each vertex $i \in V_0$,
- a choice of geometry $\tilde{g} \in \{euc, hyp, sph\}$,

find a discretely conformally equivalent cyclic polyhedral surface $(\Sigma, \tilde{\ell})_{\tilde{g}}$ of geometry $\tilde{g}$ that has the desired total angles Θ around vertices in V_1 and the fixed scale factors u at vertices in V_0.

Note that for $V_0 = \emptyset$, $V_1 = V$, Problem 3.2 reduces to Problem 3.1.

3.2 Analytic Formulation of the Mapping Problems

We rephrase the mapping Problem 3.2 analytically as Problem 3.4. The sides of a cyclic polygon determine its angles, but practical explicit equations for the angles as functions of the sides exist only for triangles, e.g., (21). For this reason it makes sense to triangulate the polyhedral surface. For the angles in a triangulation, we use the notation shown in Fig. 4. In triangle ijk, we denote the angle at vertex i by α^i_{jk}. We denote by β^i_{ij} the angle between the circumcircle and the edge jk. The angles α and β are related by

$$\alpha^i_{jk} + \beta^j_{ki} + \beta^k_{ij} = \pi,$$

so betas determine alphas and vice versa:

$$2\beta^i_{jk} = \pi + \alpha^i_{jk} - \alpha^j_{ki} - \alpha^k_{ij}, \ \ldots \tag{20}$$

For euclidean triangles,

$$\alpha^i_{jk} + \alpha^j_{ki} + \alpha^k_{ij} = \pi, \qquad \beta^i_{jk} = \alpha^i_{jk}.$$

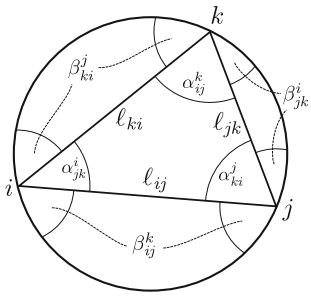

Fig. 4 Notation of lengths and angles in a triangle $ijk \in F$

The half-angle equation can be used to express the angles as functions of lengths:

$$\tan\left(\frac{\alpha_{jk}^{i}}{2}\right)=\begin{cases}\left(\dfrac{(-\ell_{ij}+\ell_{jk}+\ell_{ki})(\ell_{ij}+\ell_{jk}-\ell_{ki})}{(\ell_{ij}-\ell_{jk}+\ell_{ki})(\ell_{ij}+\ell_{jk}+\ell_{ki})}\right)^{\frac{1}{2}} & (euc)\\ \left(\dfrac{\sinh\left((\ell_{ij}-\ell_{jk}+\ell_{ki})/2\right)\sinh\left((\ell_{ij}+\ell_{jk}-\ell_{ki})/2\right)}{\sinh\left((-\ell_{ij}+\ell_{jk}+\ell_{ki})/2\right)\sinh\left((\ell_{ij}+\ell_{jk}+\ell_{ki})/2\right)}\right)^{\frac{1}{2}} & (hyp)\\ \left(\dfrac{\sin\left((\ell_{ij}-\ell_{jk}+\ell_{ki})/2\right)\sin\left((\ell_{ij}+\ell_{jk}-\ell_{ki})/2\right)}{\sin\left((-\ell_{ij}+\ell_{jk}+\ell_{ki})/2\right)\sin\left((\ell_{ij}+\ell_{jk}+\ell_{ki})/2\right)}\right)^{\frac{1}{2}} & (sph)\end{cases} \tag{21}$$

Lemma 3.3 (analytic formulation of Problem 3.2) *Let*

- *the polyhedral surface* $(\Sigma,\ell)_g$,
- *the partition* $V_0\dot\cup V_1$,
- Θ_i *for* $i\in V_1$,
- u_i *for* $i\in V_0$,
- *the geometry* $\tilde g\in\{euc,hyp,sph\}$

be given as in Problem 3.2. Let Δ *be an abstract triangulation obtained by adding non-crossing diagonals to non-triangular faces of* Σ. *(So* $V_\Sigma=V_\Delta$, $E_\Sigma\subseteq E_\Delta$, *and the set of added diagonals is* $E_\Delta\setminus E_\Sigma$.*) For* $ij\in E_\Sigma$, *define* λ_{ij} *by*

$$\lambda_{ij}=\begin{cases}2\log\ell_{ij} & \text{if}\quad g=euc\\ 2\log\sinh\frac{\ell_{ij}}{2} & \text{if}\quad g=hyp\\ 2\log\sin\frac{\ell_{ij}}{2} & \text{if}\quad g=sph\end{cases} \tag{22}$$

Then solving Problem 3.2 is equivalent to solving Problem 3.4 with $E_0=E_\Sigma$ *and* $E_1=E_\Delta\setminus E_\Sigma$.

Problem 3.4 Given

- an abstract triangulation Δ,
- a partition $V_\Delta=V_0\dot\cup V_1$,
- $u_i\in\mathbb{R}$ for $i\in V_0$
- $\Theta_i\in\mathbb{R}_{>0}$ for $i\in V_1$,
- a partition $E_\Delta=E_0\dot\cup E_1$,
- λ_{ij} for $ij\in E_0$,
- $\tilde g\in\{euc,hyp,sph\}$,

find $u_i\in\mathbb{R}$ for $i\in V_1$ and λ_{ij} for $ij\in E_1$ such that

$$\tilde\ell:E_\Delta\to\mathbb{R}_{>0}$$

defined by

$$\tilde{\lambda}_{ij} = u_i + u_j + \lambda_{ij}, \tag{23}$$

and

$$\tilde{\ell}_{ij} = \begin{cases} e^{\frac{1}{2}\tilde{\lambda}_{ij}} & \text{if } \tilde{g} = euc \\ 2\,\mathrm{arsinh}\, e^{\frac{1}{2}\tilde{\lambda}_{ij}} & \text{if } \tilde{g} = hyp \\ 2\arcsin e^{\frac{1}{2}\tilde{\lambda}_{ij}} & \text{if } \tilde{g} = sph \end{cases} \tag{24}$$

satisfies for all $ijk \in F_\Delta$ the triangle inequalities

$$\tilde{\ell}_{ij} < \tilde{\ell}_{jk} + \tilde{\ell}_{ki}, \qquad \tilde{\ell}_{jk} < \tilde{\ell}_{ki} + \tilde{\ell}_{ij}, \qquad \tilde{\ell}_{ki} < \tilde{\ell}_{ij} + \tilde{\ell}_{jk}, \tag{25}$$

and for $\tilde{g} = sph$ also

$$\tilde{\ell}_{ij} + \tilde{\ell}_{jk} + \tilde{\ell}_{ki} < 2\pi, \tag{26}$$

and such that

$$\sum_{jk:ijk\in F_\Delta} \tilde{\alpha}^i_{jk} = \Theta_i \quad \text{for all} \quad i \in V_1, \tag{27}$$

$$\tilde{\beta}^k_{ij} + \tilde{\beta}^l_{ji} = \pi \quad \text{for all} \quad ij \in E_1, \tag{28}$$

where $\tilde{\alpha}$ and $\tilde{\beta}$ are defined by (21) and (20) (with α, β, ℓ replaced by $\tilde{\alpha}, \tilde{\beta}, \tilde{\ell}$). Note that for $\tilde{g} = sph$ it is also required that $\tilde{\lambda} < 0$ for $\tilde{\ell}$ to be well-defined.

Proof (of Lemma 3.3) Note that (27) says that the angle sums at vertices in V_1 have the prescribed values, and (28) says that neighboring triangles of $(\Delta, \tilde{\ell})_{\tilde{g}}$ belonging to the same face of Σ share the same circumcircle. So deleting the edges in $E_\Delta \setminus E_\Sigma$, one obtains a cyclic polyhedral surface $(\Sigma, \tilde{\ell}|_{E_\Sigma})_{\tilde{g}}$. □

3.3 Variational Principles

Definition 3.5 For an abstract triangulation Δ and a function $\Theta \in \mathbb{R}^{V_\Delta}_{>0}$, define the three functions

$$E^{euc}_{\Delta,\Theta}, E^{hyp}_{\Delta,\Theta}, E^{sph}_{\Delta,\Theta} : \mathbb{R}^{E_\Delta} \times \mathbb{R}^{V_\Delta} \longrightarrow \mathbb{R},$$
$$(\lambda, u) \longmapsto E^{\tilde{g}}_{\Delta,\Theta}(\lambda, u)$$

by

$$E^{\tilde{g}}_{\Delta,\Theta}(\lambda, u) = \sum_{ijk\in F_\Delta} \left(f^{\tilde{g}}(\tilde{\lambda}_{ij}, \tilde{\lambda}_{jk}, \tilde{\lambda}_{ki}) - \frac{\pi}{2}(\tilde{\lambda}_{jk} + \tilde{\lambda}_{ki} + \tilde{\lambda}_{ij}) \right) + \sum_{i\in V_\Delta} \Theta_i u_i, \tag{29}$$

where $\tilde{g} \in \{euc, hyp, sph\}$, $\tilde{\lambda}$ is defined as function of λ and u by (23), and the functions f^{euc}, f^{hyp}, f^{sph} are defined in Sect. 3.4.

We will often omit the subscripts and write simply E^{euc}, E^{hyp}, E^{sph} when this is unlikely to cause confusion.

Definition 3.6 We define the *feasible regions* of the functions $E^{\tilde{g}}_{\Delta,\Theta}$ as the following open subsets of their domains:

- The feasible region of E^{euc} and E^{hyp} is the set of all $(\lambda, u) \in \mathbb{R}^{E_\Delta} \times \mathbb{R}^{V_\Delta}$ such that $\tilde{\ell} \in \mathbb{R}^E_{>0}$ defined by (23) and (24) satisfies the triangle inequalities (25)
- The feasible region of E^{sph} is the set of all $(\lambda, u) \in \mathbb{R}^{E_\Delta} \times \mathbb{R}^{V_\Delta}$ such that $\tilde{\lambda}$ defined by (23) is negative, and $\tilde{\ell}$, which is then well-defined by (24), satisfies the triangle inequalities (25) and the inequalities (26).

Theorem 3.7 (Variational principles) *Every solution $(\Sigma, \tilde{\ell})_{\tilde{g}}$ of Problem 3.2 corresponds via (23) and (24) to a critical point $(\lambda, u) \in \mathbb{R}^{E_\Delta} \times \mathbb{R}^{V_\Delta}$ of the function $E^{\tilde{g}}_{\Delta,\Theta}$ under the constraints that λ_{ij} and u_i are fixed for $ij \in E_0$ and $i \in V_0$, respectively. (The triangulation Δ, and $E_0 = E_\Sigma$ and $E_1 = E_\Delta \setminus E_\Sigma$ are as in Lemma 3.3, and the given function Θ is extended from V_1 to V by arbitrary values on V_0.)*

Conversely, if $(\lambda, u) \in \mathbb{R}^{E_\Delta} \times \mathbb{R}^{V_\Delta}$ is a critical point of the function $E^{\tilde{g}}_{\Delta,\Theta}$ under the same constraints, and if (λ, u) is contained in the feasible region of $E^{\tilde{g}}_{\Delta,\Theta}$, then $(\Sigma, \tilde{\ell})_{\tilde{g}}$ defined by (23) and (24) is a solution of Problem 3.2.

Proof This follows from the analytic formulation of Problem 3.2 (see Sect. 3.2) and Proposition 3.8. □

Proposition 3.8 (First derivative of $E^{\tilde{g}}$) *The partial derivatives of $E^{\tilde{g}}$ are*

$$\frac{\partial E^{\tilde{g}}}{\partial u_i}(\lambda, u) = \Theta_i - \sum_{ijk \ni i} \tilde{\alpha}^i_{jk} \tag{30}$$

$$\frac{\partial E^{\tilde{g}}}{\partial \lambda_{ij}}(\lambda, u) = \tilde{\beta}^k_{ij} + \tilde{\beta}^l_{ij} - \pi. \tag{31}$$

Here $\tilde{\alpha}$, $\tilde{\beta}$ are defined by (21) and (20) (with α, β, ℓ replaced by $\tilde{\alpha}$, $\tilde{\beta}$, $\tilde{\ell}$) if (λ, u) is contained in the feasible region of $E^{\tilde{g}}$. For (λ, u) not contained in the feasible region, the definition of $\tilde{\alpha}$, $\tilde{\beta}$ is extended like in Definition 3.12.

Proof Equations (30) and (31) follow from the definition of $E^{\tilde{g}}$ and Proposition 3.14 on the partial derivatives of f^g. □

Theorem 3.9 (Uniqueness for mapping problems) *If Problem 3.2 with target geometry $\tilde{g} \in \{euc, hyp\}$ has a solution, then the solution is unique—except if*

$\tilde{g} = euc$ and $V_0 = \emptyset$ (the case of Problem 3.1). In this case, the solution is unique up to scale.

The critical point $(\lambda, u) \in \mathbb{R}^{E_\Delta} \times \mathbb{R}^{V_\Delta}$ that corresponds, via (23) and (24), to a solution $(\Sigma, \tilde{\ell})_{\tilde{g}}$ of Problem 3.2 with $\tilde{g} \in \{euc, hyp\}$ is a minimizer of $E^{\tilde{g}}_{\Delta,\Theta}$ under the constraints described in Theorem 3.7. The minimizer is unique except in the following cases. If $\tilde{g} = euc$ and $V_0 = \emptyset$, then $E^{\tilde{g}}_{\Delta,\Theta}$ is constant along all lines in the "scaling direction" $(0, 1_{V_\Delta}) \in \mathbb{R}^{E_\Delta} \times \mathbb{R}^{V_\Delta}$. If the 1-skeleton of Σ is bipartite and $V_0 = \emptyset$, then $E^{\tilde{g}}_{\Delta,\Theta}$ is constant in the direction that is ± 1 on the two color classes of V_Δ, respectively, and takes appropriate values on $E_\Delta \setminus E_\Sigma$ so that $\tilde{\lambda}_{ij}$ defined by (23) remains constant for all $ij \in E_\Delta$. (In both exceptional cases, one can obtain a unique minimizer by adding the constraint of fixing u_i for some $i \in V_\Delta$.)

Proof The theorem follows from Theorem 3.7 and the following observations.

(1) If the point $(\lambda, u) \in \mathbb{R}^{E_\Delta} \times \mathbb{R}^{V_\Delta}$ corresponds to a solution of Problem 3.2, it is contained in the feasible region of $E^{\tilde{g}}_{\Delta,\Theta}$.
(2) By (29) and Proposition 3.16, the functions E^{euc} and E^{hyp} are convex.
(3) For (λ, u) in the feasible region, the second derivative $D^2E^{hyp}(\lambda, u)$ is a positive definite quadratic form of $d\tilde{\lambda}$, i.e., $D^2E^{hyp}(\lambda, u)(\dot{\lambda}, \dot{u}) \geq 0$ for all $(\dot{\lambda}, \dot{u}) \in \mathbb{R}^{E_\Delta} \times \mathbb{R}^{V_\Delta}$ and $D^2E^{hyp}(\lambda, u)(\dot{\lambda}, \dot{u}) = 0$ if and only if

$$\dot{\lambda}_{ij} + \dot{u}_i + \dot{u}_j = 0 \quad \text{for all } ij \in E_\Delta.$$

(4) Similarly, for (λ, u) in the feasible region, the second derivative $D^2E^{euc}(\lambda, u)$ is a positive semidefinite quadratic form with $D^2E^{euc}(\lambda, u)(\dot{\lambda}, \dot{u}) = 0$ if and only if

$$\dot{\lambda}_{ij} + \dot{u}_i + \dot{u}_j = c \quad \text{for all } ij \in E_\Delta, \text{ for some } c \in \mathbb{R}. \qquad \square$$

In the following proposition, we collect explicit formulas for the second derivatives of the functions $E^{\tilde{g}}$. They are useful for the numerical minimization of E^{euc} and E^{hyp}, and even for finding critical points of E^{sph}, as explained in Sect. 6.2.

Proposition 3.10 (Second derivative of $E^{\tilde{g}}$) *The second derivatives of E^{euc}, E^{hyp}, and E^{sph} are the quadratic forms*

$$D^2E^{\tilde{g}}(\lambda, u) = \frac{1}{2} \sum_{ijk \in F_\Delta} \left(q^k_{ij}(\lambda, u) + q^i_{jk}(\lambda, u) + q^j_{ki}(\lambda, u) \right),$$

where $q^k_{ij}(\lambda, u) = 0$ if $\tilde{\ell}_{ij}, \tilde{\ell}_{jk}, \tilde{\ell}_{ki}$ defined by (23), (24) violate the triangle inequalities (25), or, in the case of $\tilde{g} = sph$, inequality (26). Otherwise, the quadratic forms $q^k_{ij}(\lambda, u)$ are defined by

$$q_{ij}^k = \begin{cases} \cot \tilde{\alpha}_{ij}^k \, (d\lambda_{ki} - d\lambda_{jk} + du_i - du_j)^2 & (euc) \\ \cot \tilde{\beta}_{ij}^k \left((d\lambda_{ik} - d\lambda_{kj} + du_i - du_j)^2 + \tanh^2 \left(\frac{\tilde{\ell}_{ij}}{2} \right) (d\lambda_{ij} + du_i + du_j)^2 \right) & (hyp) \\ \cot \tilde{\beta}_{ij}^k \left((d\lambda_{ik} - d\lambda_{kj} + du_i - du_j)^2 - \tan^2 \left(\frac{\tilde{\ell}_{ij}}{2} \right) (d\lambda_{ij} + du_i + du_j)^2 \right) & (sph) \end{cases}$$

where $\tilde{\alpha}$, $\tilde{\beta}$ are defined by (21) and (20) (with α, β, ℓ replaced by $\tilde{\alpha}$, $\tilde{\beta}$, $\tilde{\ell}$).

Proposition 3.10 follows from (29) and Proposition 3.15 about the second derivatives of f^g.

3.4 The Triangle Functions

This section is concerned with three real valued functions f^{euc}, f^{hyp}, f^{sph} of three variables that are the main building blocks for the action functions E^{euc}, E^{hyp}, E^{sph} of the variational principles. Since we consider single triangles in this section, not triangulations, we can use simpler notation. For $\{i, j, k\} = \{1, 2, 3\}$, let

$$\lambda_i = \lambda_{jk}, \quad \ell_i = \ell_{jk}, \quad \alpha_i = \alpha_{jk}^i, \quad \beta_i = \beta_{jk}^i.$$

The terminology introduced in the following definition makes Definition 3.12 easier to state.

Definition 3.11 Let the *feasible region* of f^{euc} and f^{hyp} be the open subset of all $\lambda \in \mathbb{R}^3$ such that $\ell \in \mathbb{R}^3_{>0}$ determined by (22) satisfies the triangle inequalities, i.e.,

$$\ell_k < \ell_i + \ell_j \tag{32}$$

for $\{i, j, k\} = \{1, 2, 3\}$.

Let the *feasible region* of f^{sph} be the open subset of all $\lambda \in \mathbb{R}^3$ such that $\lambda < 0$, and such that $\ell \in \mathbb{R}^3_{>0}$, which is then well-defined by (22), satisfies the triangle inequalities (32) and

$$\ell_1 + \ell_2 + \ell_3 < 2\pi. \tag{33}$$

Definition 3.12 We define the three functions

$$f^{euc}, f^{hyp}, f^{sph} : \mathbb{R}^3 \to \mathbb{R}$$

by

$$\begin{aligned} f^g(\lambda_1, \lambda_2, \lambda_3) = {} & \beta_1\lambda_1 + \beta_2\lambda_2 + \beta_3\lambda_3 + \Pi(\alpha_1) + \Pi(\alpha_2) + \Pi(\alpha_3) \\ & + \Pi(\beta_1) + \Pi(\beta_2) + \Pi(\beta_3) + \Pi\left(\tfrac{1}{2}(\pi - \alpha_1 - \alpha_2 - \alpha_3)\right), \end{aligned} \tag{34}$$

where $g \in \{euc, hyp, sph\}$, $\Pi(x)$ denotes Milnor's Lobachevsky function [30]

$$\text{Л}(x) = -\int_0^x \log\left|2\sin(t)\right| dt, \tag{35}$$

and,

- if λ is in the feasible region of f^g, then the angles α, β are defined as the angles (shown in Fig. 4) in a euclidean, hyperbolic, or spherical triangle (depending on g) with sides ℓ_1, ℓ_2, ℓ_3 determined by (22). That is, α and β are defined by (21) and (20).
- Otherwise, if $g = sph$, and if either at least two λs are non-negative or $\lambda < 0$ and inequality (33) is violated, let

$$\alpha_k = \alpha_i = \alpha_j = \pi, \quad \beta_k = \beta_i = \beta_j = 0.$$

- Otherwise, if the triangle inequality (32) is violated, or if $g = sph$ and $\lambda_k \geq 0$, let

$$\alpha_k = \beta_k = \pi, \quad \alpha_i = \alpha_j = \beta_i = \beta_j = 0.$$

Figure 5 shows a graph of Milnor's Lobachevsky function. It is continuous, π-periodic, odd, has zeros at the integer multiples of $\pi/2$, and is real analytic except at integer multiples of π, where the derivative tends to $+\infty$.

Remark 3.13 In the euclidean case, (34) simplifies to

$$f^{\text{euc}}(\lambda) = \alpha_i\lambda_i + \alpha_j\lambda_j + \alpha_k\lambda_k + 2\text{Л}(\alpha_i) + 2\text{Л}(\alpha_j) + 2\text{Л}(\alpha_k). \tag{36}$$

This follows immediately from $\alpha_1 + \alpha_2 + \alpha_3 = \pi$, $\alpha = \beta$, and $\text{Л}(0) = 0$.

Proposition 3.14 (first derivative) *The functions f^g, $g \in \{euc, hyp, sph\}$, are continuously differentiable and*

$$\frac{\partial f^g}{\partial \lambda_i} = \beta_i. \tag{37}$$

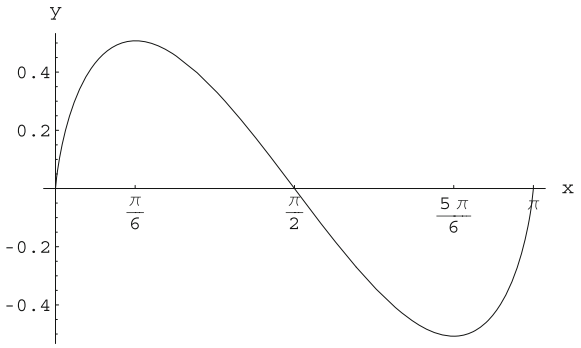

Fig. 5 Graph of Milnor's Lobachevsky function, $y = \text{Л}(x)$

Proof Note that the angles α, β are continuous functions of λ on $\mathbb{R}^3$. Hence f^g defined by (34) is also continuous. We will show that f^g is continuously differentiable with derivative (37) on an open dense subset of the domain, namely, the union of (a) the feasible region and (b) the interior of its complement. Since f^g is continuous and df^g extends continuously to $\mathbb{R}^3$, the claim follows.

(a) First, suppose λ is contained in the feasible region of f^g. By symmetry, it suffices to consider the derivative with respect to λ_1. From (34) and (35) one obtains

$$\frac{\partial f^g}{\partial \lambda_1} = \beta_1 + \sum_{i=1}^{3} \Big(\big(\lambda_i - \log(2\sin\beta_i)\big) \frac{\partial \beta_i}{\partial \lambda_1} + \big(-\log(2\sin\alpha_i) + \tfrac{1}{2}\log\big|2\sin(\tfrac{\pi-\alpha_1-\alpha_2-\alpha_3}{2})\big|\big) \frac{\partial \alpha_i}{\partial \lambda_1} \Big) \tag{38}$$

For hyperbolic and spherical triangles, one derives from the respective cosine rules

$$\sinh^2 \frac{\ell_i}{2} = \frac{\sin\beta_i \sin\frac{\pi-\alpha_1-\alpha_2-\alpha_3}{2}}{\sin\alpha_2 \sin\alpha_3} \qquad \text{(hyperbolic)},$$

$$\sin^2 \frac{\ell_i}{2} = \frac{\sin\beta_i \sin\frac{\alpha_1+\alpha_2+\alpha_3-\pi}{2}}{\sin\alpha_2 \sin\alpha_3} \qquad \text{(spherical)}.$$

In both cases, expand the fraction on the right hand side by four and take logarithms to find

$$\lambda_i = \log(2\sin\beta_i) + \log\big|2\sin\tfrac{\pi-\alpha_1-\alpha_2-\alpha_3}{2}\big| - \log(2\sin\alpha_j) - \log(2\sin\alpha_k).$$

Substitute this expression for λ_i in (38) and use $d\beta_i = \frac{1}{2}(d\alpha_i - d\alpha_j - d\alpha_k)$ to see that all terms on the right hand side of (38) cancel, except β_1.

For euclidean triangles, (38) simplifies to

$$\frac{\partial f^g}{\partial \lambda_1} = \beta_1 + \sum_{i=1}^{3} \big(\lambda_i - 2\log(2\sin\alpha_i)\big) \frac{\partial \alpha_i}{\partial \lambda_1},$$

where

$$\lambda_i - 2\log(2\sin\alpha_i) = 2\log\frac{\ell_i}{2\sin\alpha_i} = 2\log R$$

does not depend on i. (R denotes the circumradius.) Equation (37) follows because the angle sum is constant.

(b) Now suppose λ is contained in the interior of the complement of the feasible region of f^g. Since $\beta_1, \beta_2, \beta_3$ are constant on each connected component of the complement of the feasible region, and since

$$f^g(\lambda_1, \lambda_2, \lambda_3) = \beta_1\lambda_1 + \beta_2\lambda_2 + \beta_3\lambda_3,$$

outside the feasible region, Eq. (37) holds also in this case. This completes the proof. □

Proposition 3.15 (second derivative) *For $g \in \{euc, hyp, sph\}$ the function f^g is twice continuously differentiable on its feasible set and the second derivative is*

$$D^2 f^{euc} = \frac{1}{2}\sum_{i=1}^{3} \cot\alpha_i \, (d\lambda_j - d\lambda_k)^2, \tag{39}$$

$$D^2 f^{hyp} = \frac{1}{2}\sum_{i=1}^{3} \cot\beta_i \left((d\lambda_j - d\lambda_k)^2 + \tanh^2\left(\tfrac{\ell_i}{2}\right) d\lambda_i^2\right), \tag{40}$$

$$D^2 f^{sph} = \frac{1}{2}\sum_{i=1}^{3} \cot\beta_i \left((d\lambda_j - d\lambda_k)^2 - \tan^2\left(\tfrac{\ell_i}{2}\right) d\lambda_i^2\right). \tag{41}$$

On each component of the complement of its feasible set, the function f_g is linear so the second derivative vanishes.

A proof of (39) is contained in [5] (Proposition 4.2.3), see Remark 3.17 below. Equations (40) and (41) can be derived by lengthy calculations.

Proposition 3.16 *(i) The function f^{euc} is convex. On its feasible set, the second derivative $D^2 f^{euc}$ is positive semidefinite with one-dimensional kernel spanned by the "scaling direction"* (1, 1, 1).

(ii) The function f^{hyp} is convex. On its feasible set, the second derivative $D^2 f^{hyp}$ is positive definite, so the functions is locally strictly convex.

Part (i) is proved in [5] (Propositions 4.2.4, 4.2.5, note the following remark) directly from (39). We do not know a similarly straightforward proof of part (ii). The proof in [5] (Sect. 6.2) is based on a connection with 3-dimensional hyperbolic geometry: f^{hyp} is the Legendre dual of the volume of an ideal hyperbolic prism considered as a function of the dihedral angles. This volume function is strictly concave, as shown by Leibon [26]. His argument uses the decomposition of an ideal prism into three ideal tetrahedra.

Remark 3.17 The functions f and $\hat{V}_h$ defined in [5] (equations (4-3), (6-4)) are related to the functions f^{euc} and f^{hyp} by

$$f^{euc}(\lambda_1, \lambda_2, \lambda_3) = 2f(\tfrac{\lambda_1}{2}, \tfrac{\lambda_2}{2}, \tfrac{\lambda_3}{2}), \tag{42}$$

$$f^{hyp}(\lambda_1, \lambda_2, \lambda_3) = 2\hat{V}_h(\lambda_1, \lambda_2, \lambda_3, 0, 0, 0). \tag{43}$$

4 Conformal Maps of Cyclic Quadrangulations

Having introduced the mapping problems and variational principles, we return to conformal maps of cyclic quadrangulations. Some basic facts were already discussed in Sect. 2.8. Here, in Sect. 4.1, we consider a simple experiment that demonstrates the somewhat unexpected appearance of orthogonal circle patterns, and also a necessary condition for the boundary angles. In Sect. 4.2, we discuss a discrete version of the Riemann mapping problem for quadrangulations.

4.1 Emerging Circle Patterns and a Necessary Condition

Consider the two discrete conformal maps shown in the two rows of Fig. 6. The domains (shown left) are a square and a rectangle, subdivided into 6×6 and 6×5 squares, respectively. We solve the mapping Problem 3.1 by minimizing E^{euc} as explained in Sect. 3.3, prescribing boundary angles to obtain maps to parallelograms: $\Theta = 50°$ and $130°$ for the corner vertices, $\Theta = 180°$ for the other boundary vertices, and $\Theta = 360°$ for interior vertices. The resulting quadrangulations are shown in the middle.

On first sight, the 6×6 example shown in the top row behaves rather like one would expect from a conformal map. The horizontal and vertical "coordinate lines" of the domain are mapped to polygonal curves that look more or less like they could be discretizations of reasonable smooth curves. In the 6×5 example shown in the bottom row, the images of the vertical lines zigzag noticeably.

A closer look at the 6×6 example reveals a remarkable phenomenon. Let us bicolor the vertices black and white so that neighboring vertices have different

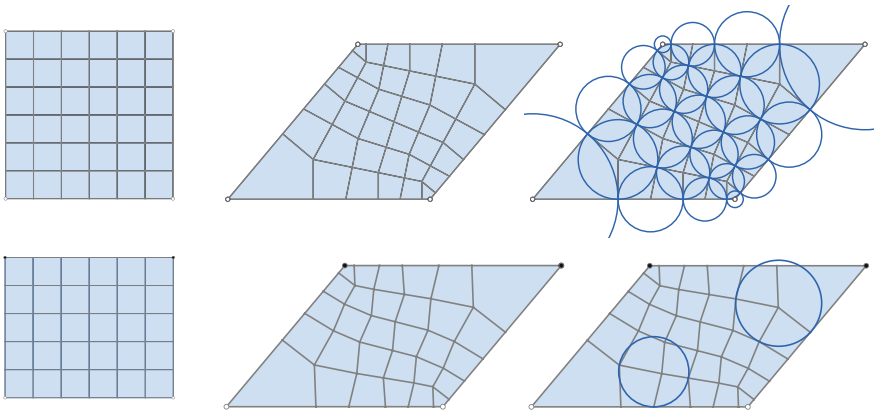

Fig. 6 Mapping a rectangle to a parallelogram. Note the orthogonal circle pattern in the *top row* and the wiggly vertical lines in the *bottom row*

colors, with the corners colored white. Then, in the image quadrangulation, the edges incident with a black vertex meet at right angles, and the edges incident with a white vertex have the same length. One can therefore draw a circle around each white vertex through the neighboring black vertices as shown in Fig. 6 (top right). At the black vertices, these circles touch and intersect orthogonally. Such circle patterns were studied by Schramm [38] as discrete analogs of conformal maps.

Given such a circle pattern with orthogonally intersecting circles, the quadrangulation formed by drawing edges between circle centers and intersection points consists of quadrilaterals that are right-angled kites. Such kites have complex cross-ratio -1. Hence, the quadrangulation coming from an orthogonal circle pattern is discretely conformally equivalent (in our sense) to a combinatorially equivalent quadrangulation consisting of squares.

The conformal map shown in the top row of Fig. 6 "finds" the orthogonal circle pattern because that circle pattern exists and the conformal map is unique (by Theorem 3.9). For the 6×5 example shown in the bottom row, a corresponding orthogonal circle pattern does not exist. No matter which coloring is chosen, there are two black vertices at which the total angle changes (from 90° to 50° and 130°, respectively). The neighbors of a vertex do not lie on a circle. Figure 6 (bottom right) shows two circles drawn through three out of four neighbors.

If we map an $m \times n$ square grid to a parallelogram like in Fig. 6, an orthogonal circle pattern will appear if m an n are even. No such pattern will appear if one of the numbers is even and the other is odd. What happens if both m and n are odd? In this case, the conformal map does not exist. The corners with increasing angle and the corners with decreasing angle would have different colors. This violates the necessary condition expressed in the following theorem.

Theorem 4.1 (Necessary condition for the existence of a conformal map) *Let Σ be an abstract quadrangulation of the closed disk, and let*

$$z, \tilde{z} : V_\Sigma \to \mathbb{C}$$

determine two discretely conformally equivalent immersions of Σ into the complex plane. Denote their angle sums at boundary vertices $v \in V_\Sigma$ by Θ_v and $\tilde{\Theta}_v$, respectively. Since the 1-skeleton of Σ is bipartite, we may assume the vertices are colored black and white. Let V_b^∂ and V_w^∂ denote the sets of black and white boundary vertices of Σ. Then

$$\sum_{v \in V_b^\partial} (\tilde{\Theta}_v - \Theta_v) \equiv 0 \pmod{2\pi}, \tag{44}$$

$$\sum_{v \in V_w^\partial} (\tilde{\Theta}_v - \Theta_v) \equiv 0 \pmod{2\pi}. \tag{45}$$

(Since $\sum_{V_b^\partial \cup V_w^\partial} (\tilde{\Theta}_v - \Theta_v) = 0$, equations (45) and (44) are equivalent.)

Proof Since z and $\tilde{z}$ are two solutions of the cross-ratio system on Σ with the same cross-ratios (see Sect. 2.8), there exists by Proposition 2.13 a function $w : V_\Sigma \to \mathbb{C}$ such that (16) holds for all edges $ij \in E_\Sigma$. Now suppose $v_0, \ldots, v_{2n-1} \in V_\Sigma$ are the boundary vertices in cyclic order (with indices taken modulo $2n$). Then

$$e^{i(\tilde{\Theta}_{v_k} - \Theta_{v_k})} = \frac{(\tilde{z}_{v_{k+1}} - \tilde{z}_{v_k})(z_{v_{k-1}} - z_{v_k})}{(\tilde{z}_{v_{k-1}} - \tilde{z}_{v_k})(z_{v_{k+1}} - z_{v_k})} = \frac{w_{v_{k+1}}}{w_{v_{k-1}}},$$

so

$$\prod_{k=0}^{n-1} e^{i(\tilde{\Theta}_{v_{2k}} - \Theta_{v_{2k}})} = \prod_{k=0}^{n-1} e^{i(\tilde{\Theta}_{v_{2k+1}} - \Theta_{v_{2k+1}})} = 1.$$

Equations (44) and (45) follow. □

4.2 Riemann Maps with Cyclic Quadrilaterals

Consider the following discrete version of the Riemann mapping problem: Map a cyclic polyhedral surface that is topologically a closed disk discretely conformally to a planar polygonal region with boundary vertices on a circle. An example is shown in Fig. 7, top row. This type of problem can often be reduced to Problem 3.2. Then, by the variational principle, if a solution exists, it can be found by minimizing a convex function. For triangulations, the reduction of the discrete Riemann mapping problem to Problem 3.2 is explained in [5] (Sect. 3.3). Here, we consider the case of quadrangulations. (The arguments can be extended to even polygons with more than four sides. We restrict our attention to quadrilaterals because the combinatorial restrictions discussed in the following paragraph become even more involved for surfaces with hexagons, octagons, etc.)

The basic idea is the same as for triangulations: First, map the polyhedral surface to the half plane with one boundary vertex at infinity. Then apply a Möbius transformation. This leads to a combinatorial restriction: No face may have more than one edge on the boundary. (The face would degenerate when the boundary is mapped to a straight line.) For triangulations, this means that no triangle may be connected to the surface by only one edge. If this condition is violated, cutting off such "ears" often leads to an admissible triangulation. For quadrangulations, this fix does not work in typical situations. Instead, if a quadrilateral contains two consecutive edges on the boundary, cut off a triangle. The resulting polyhedral surface will consist mostly of quadrilaterals with some triangles on the boundary, as in the example shown in Figs. 7, 8.

Suppose $(\Sigma, \ell)_{euc}$ is a euclidean cyclic polyhedral surface that is homeomorphic to the closed disk and consists mostly of quadrilaterals. (For the following construction we really only need a boundary vertex that is incident with quadrilateral faces.) To map it to a polygonal region inscribed in a circle, proceed as follows (see Fig. 7):

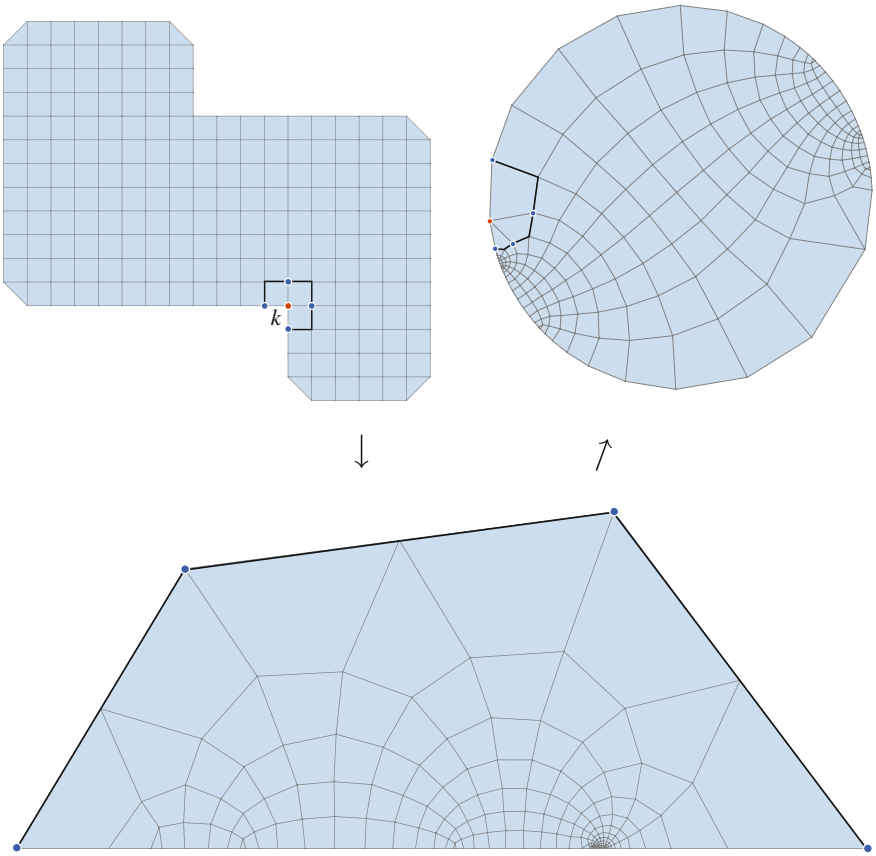

Fig. 7 Riemann mapping with cyclic quadrilaterals

(1) Choose a vertex k on the boundary of Σ such that all incident faces are quadrilaterals.
(2) Apply a discrete conformal change of metric (3) such that all edges incident with k have the same length. One may choose $u = 0$ for all vertices except the neighbors of k. It does not matter if polygon inequalities are violated after this step.
(3) Let $(\Sigma', \ell')_{euc}$ be the cyclic polyhedral complex obtained by removing vertex k and all incident quadrilaterals.
(4) Solve Problem 3.2 for $(\Sigma', \ell')_{euc}$ with prescribed total angles $\Theta_i = 2\pi$ for interior vertices of Σ', $\Theta_i = \pi$ for boundary vertices of Σ' that were not neighbors of k in Σ, and fixed logarithmic scale factors $u_i = 0$ for those that were neighbors of k. The result is a planar polyhedral surface as shown in Fig. 7, bottom. The boundary consists of one straight line segment containing all boundary edges of Σ' that were also boundary edges of Σ, and two or more straight

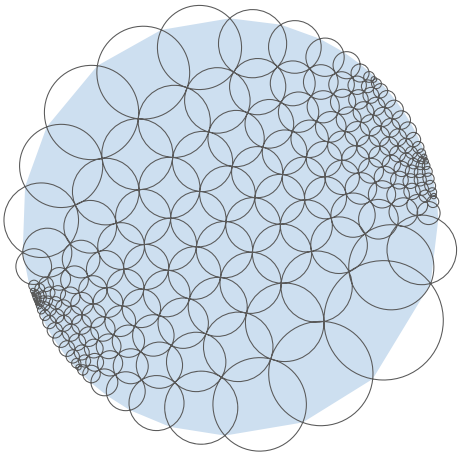

Fig. 8 Here we show the face circumcircles of the solution to the Riemann mapping problem of Fig. 7. It looks conspicuously like an orthogonal circle pattern. But the face circumcircles intersect only approximately but not exactly at right angles

line segments, each consisting of two edges that were incident with a removed quadrilateral.

(5) Apply a Möbius transformation (e.g., $z \mapsto 1/z$) to the vertices that maps the boundary vertices of Σ to a circle and the other vertices to the inside of this circle. Reinsert k at the image point of ∞ under this Möbius transformation. Each face $ijmk \in \Sigma$ incident with k is cyclic because the three vertices i, j, and m are contained in a line before transformation.

(6) Optionally apply a 2-dimensional version of the Möbius normalization described in Sect. 6.3.

Proposition 4.2 *The result of this procedure is a planar cyclic polyhedral surface that is discretely conformally equivalent to* $(\Sigma, \ell)_{euc}$ *and has its boundary polygon inscribed in a circle.*

Proof That the boundary polygon is inscribed in a circle is obvious from the construction. Using the Möbius invariance of discrete conformal equivalence (Proposition 2.5), it is not difficult to see that the surfaces without quadrilaterals incident with k are discretely conformally equivalent. To show that the whole surfaces are equivalent, it suffices to show that corresponding quadrilaterals incident with k have the same complex cross-ratio.

After step (2), the length cross-ratio of a quadrilateral incident with k is equal to the simple length ratio of the two edges that are not incident with k.

After step (4), the length cross-ratio of these edges is unchanged due to the fixed logarithmic scale factors $u = 0$ on the neighbors of k. Also, these edges are now collinear because of the prescribed angle $\Theta = \pi$ between them.

After applying the Möbius transformation in step (5), the image of the point at infinity and the other three vertices of our quadrilateral incident with k form again a cyclic quadrilateral with the same complex cross-ratio as in the beginning. □

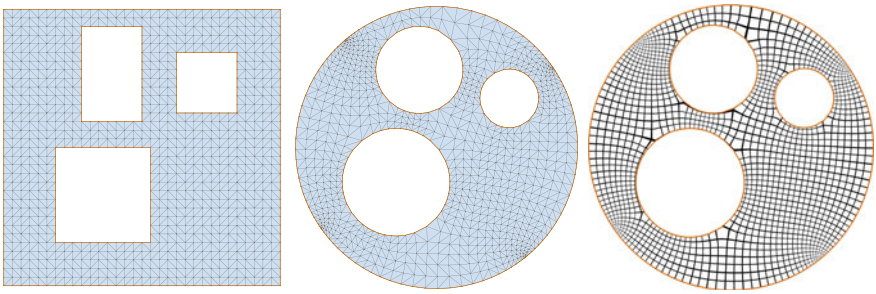

Fig. 9 Discrete conformal map of a multiply-connected domain (*left*) to a circle domain (*middle*). The images of vertical and horizontal "parameter lines" are shown on the *right*

5 Multiply Connected Domains

5.1 Circle Domains

Koebe's generalization of the Riemann mapping theorem says that multiply connected domains are conformally equivalent to domains bounded by circles, and the uniformizing map to such a circle domain is unique up to Möbius transformations. A method to construct discrete Riemann maps is described in [5] (Sect. 3.3) for triangulations and for mostly quadrilateral meshes in the previous Sect. 4.2. Having generalized the notion of discrete conformal equivalence from triangulations to cyclic polyhedral surfaces, it is straightforward to adapt this method to construct discrete maps to circle domains:

(1) Fill holes by gluing faces to all but one boundary component, so that the resulting surface is homeomorphic to a disk.
(2) Construct the discrete Riemann map.
(3) Remove the faces that were added in step (1).

Figure 9 shows an example.

5.2 Special Slit Domains

Any multiply connected domain can be mapped to the complex plain with parallel slits [32]. In principle, it is possible to construct discrete conformal maps that map holes to slits by solving Problem 3.1. On each boundary component that should be mapped to a slit, set the desired total angle $\Theta = 2\pi$ for the two vertices that should be mapped to the endpoints of the slit, and set $\Theta = \pi$ for all other vertices on that boundary component. However, this will not work in general. While the resulting surface will be flat, the developing map to the plane will in general have translational

monodromy for a cycle around the hole. The surface will only close up in the plane if the vertices that should be mapped to the endpoints of the slit are chosen exactly right. (This will in general require modifying the original mesh.)

Sometimes, the symmetry of the problem determines the right positions of the end-vertices, so that discrete conformal maps to slit surfaces can be computed. The first two rows of Fig. 10 show examples. The bottom row visualizes a discrete con-

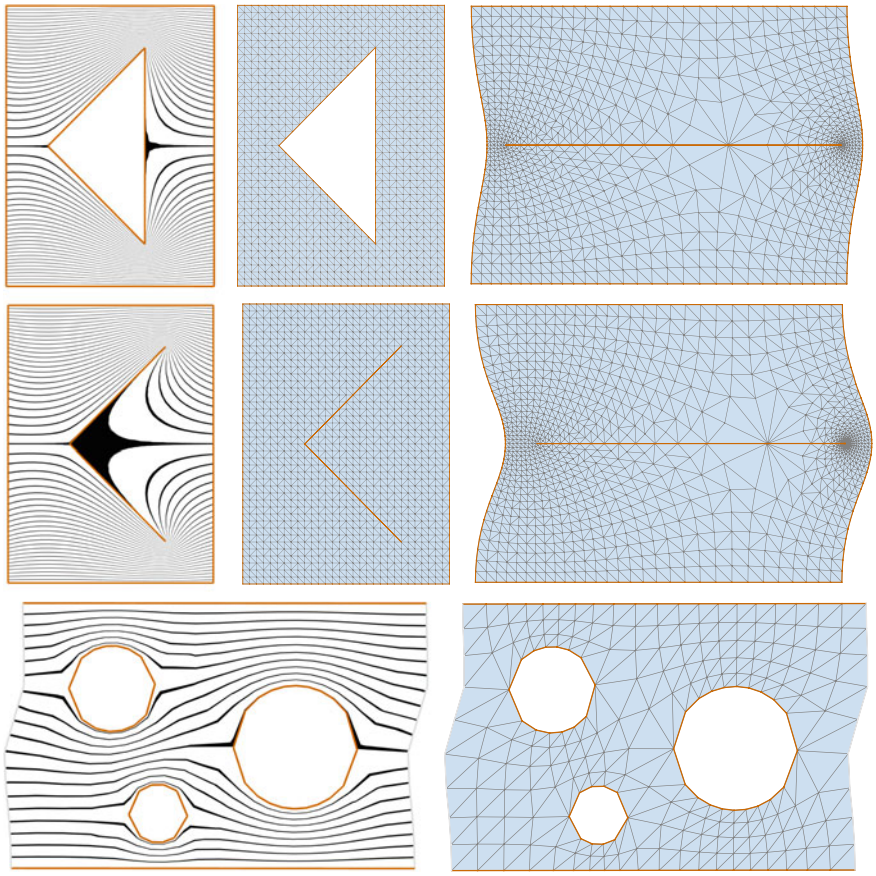

Fig. 10 Mapping surfaces with holes to slit surfaces. In all images, the *left* and *right* parts of the boundary are identified by a horizontal translation. Preimages of horizontal lines visualize the flow of an incompressible inviscid fluid around the hole in a channel with periodic boundary conditions. *Top row* A cylinder with a triangular hole is mapped to a cylinder with a slit. One vertex of the triangle and the midpoint of the opposite side are mapped to the endpoints of the slit. *Middle row* An arrow shaped slit is mapped to a straight slit. The two vertices at the arrow's tip, on either side of the slit, are mapped to the endpoints of the straight slit. *Bottom row* Three circular boundary components are mapped to horizontal slits (The slit surface is not shown.)

formal map where circular holes are mapped to slits. Here, we use the following trick: We start with the slit surface and map it to a surface with circular holes as described in Sect. 5.1.

6 Uniformization of Spheres

This section is concerned with discrete conformal maps of polyhedral surfaces of genus 0 onto the round sphere. For triangulations, this is described in [5] (Sect. 3.2). In Sect. 6.1, we adapt this method to quadrangulations. This is similar to the discrete Riemann mapping with quadrilaterals described in Sect. 4.2. Effectively, this method reduces the problem to minimizing the convex euclidean functional E^{euc}. The spherical version of the variational principle (Theorem 3.7) involves the non-convex function E^{sph}. It is not as practical for calculations, because one has to find a saddle point instead of a minimum. Nevertheless, the spherical functional can often be used to calculate maps to the sphere. This is explained in Sect. 6.2.

6.1 Uniformizing Quadrangulations of the Sphere

Suppose $(\Sigma, \ell)_{euc}$ is a cyclic polyhedral surface with quadrilateral faces that is homeomorphic to the sphere.

(1) Choose a vertex $k \in V_\Sigma$.
(2) Apply a discrete conformal change of metric (3) such that all edges incident with k have the same length. One may choose $u = 0$ for all vertices except the neighbors of k. It does not matter if polygon inequalities are violated after this step.
(3) Let $(\Sigma', \ell')_{euc}$ be the complex obtained by removing vertex k and all incident quadrilaterals.
(4) Solve Problem 3.2 for $(\Sigma', \ell')_{euc}$ with prescribed total angles $\Theta_i = 2\pi$ for interior vertices of Σ', $\Theta_i = \pi$ for boundary vertices of Σ' that were not neighbors of k in Σ, and fixed scale factors $u_i = 0$ for vertices that were neighbors of k in Σ. The result is a planar polyhedral surface with cyclic quadrilaterals. Consecutive boundary edges that belonged to a face incident with vertex k in Σ are contained in a straight line.
(5) Map the vertices to the unit sphere by stereographic projection and reinsert the vertex k at the image point of ∞.
(6) Optionally apply Möbius normalization, see Sect. 6.3.

Proposition 6.1 *The result is a cyclic polyhedral surface with vertices on the unit sphere that is discretely conformally equivalent to* $(\Sigma, \ell)_{euc}$.

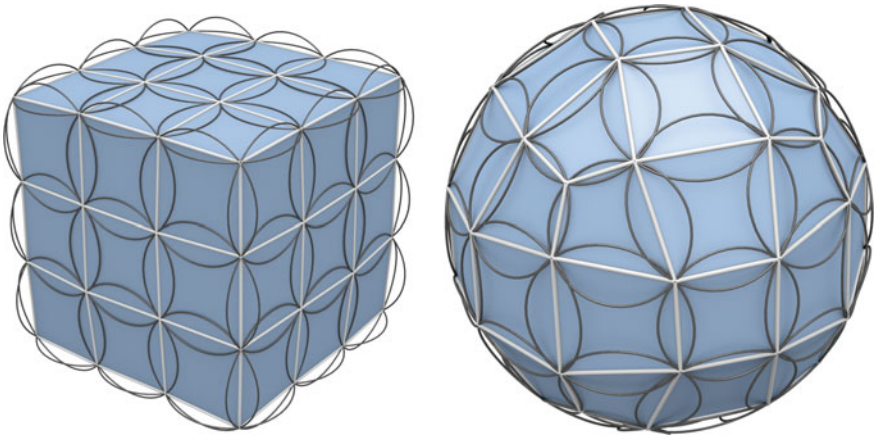

Fig. 11 Discrete conformal map from the cube to the sphere, calculated with the method described in Sect. 6.1. We apply Möbius normalization (Sect. 6.3) to the polyhedral surface with vertices on the sphere to achieve rotational symmetry

This can be seen in the same way as the corresponding statement about discrete Riemann maps with quadrilaterals (Proposition 4.2). Figure 11 shows a discrete conformal map calculated by this method.

6.2 Using the Spherical Functional

It is possible to use the spherical functional E^{sph} to calculate maps to the sphere even though it is not convex. For simplicity, we consider only triangulations, so all λ variables are fixed and we may consider E^{sph} as function of the logarithmic scale factors u only (see Sect. 3.3). A numerical method has to find a saddle point of $E^{sph}(u)$.

Note that the scaling direction $1_{V_\Delta} \in \mathbb{R}^{V_\Delta}$ is a negative direction of the Hessian at a critical point: Suppose $(\Delta, \ell)_{sph}$ is a spherical triangulation with the desired angle sum Θ_i at each vertex i. Then $0 \in \mathbb{R}^{V_\Delta}$ is a critical point of $E^{sph}_{\Delta,\Theta}(u)$. If we enlarge all edge lengths by a common factor $e^h > 1$, then all angles become larger, so every component (30) of the gradient of E^{sph} becomes negative. Following the negative gradient would result in even larger lengths.

The following minimax method works in many cases. Define the function $\tilde{E}$ by *maximizing* the functional E^{sph} in the scaling direction,

$$\tilde{E}(u) = \max_{h\in\mathbb{R}} \left\{ E^{sph}(u + h1_{V_\Delta}) \right\}. \tag{46}$$

Minimize functional $\tilde{E}$ in a hyperplane of $\mathbb{R}^{V_\Delta}$ transverse to the direction 1_{V_Δ}.

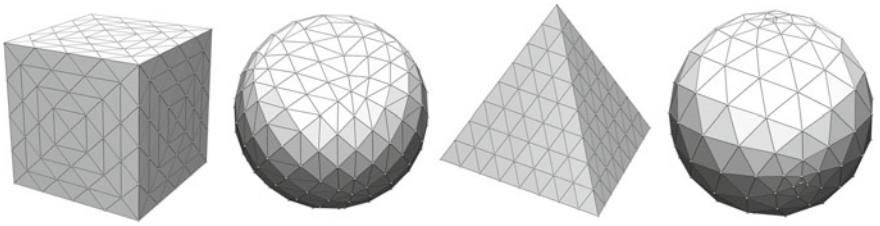

Fig. 12 Mapping conformally to the sphere using the spherical functional. The spherical surfaces are Möbius-normalized to achieve rotational symmetry

Figure 1 (top) and Fig. 12 show examples of discrete conformal maps to polyhedral surfaces inscribed in a sphere that were calculated using this method.

6.3 Möbius Normalization

The notion of discrete conformal equivalence of euclidean polyhedral surfaces $(\Sigma, \ell)_{euc}$ in $\mathbb{R}^3$ is Möbius invariant (Proposition 2.5). If all vertices $v \in V_\Sigma$ are contained in the unit sphere $S^2 \subset \mathbb{R}^3$, then there is a Möbius transformation T of S^2 such that the center of mass of the transformed vertices is the origin [43],

$$\sum_{v \in V_\Sigma} T(v) = 0.$$

The Möbius transformation T is uniquely determined up to post-composition with a rotation around the origin.

The following method can be used to calculate such a Möbius transformation: Find the unique minimizer of the function δ defined below. Then choose for T a Möbius transformation that maps S^2 to itself and the minimizer to the origin. Here, we only provide explicit formulas for the function δ and its first two derivatives. For a more detailed account, we refer the reader to [43]. The function δ is defined on the open unit ball in $\mathbb{R}^3$ by

$$\delta(x) = \sum_{v \in V} \log\left(\frac{-\langle x, v\rangle}{\sqrt{-\langle x, x\rangle}}\right), \tag{47}$$

where

$$\langle x, y\rangle = x_1 y_1 + x_2 y_2 + x_3 y_3 - 1. \tag{48}$$

The gradient and Hessian matrix of δ are

$$\operatorname{grad}\delta(x) = \sum_{v\in V}\left(\frac{v}{\langle x, v\rangle} - \frac{x}{\langle x, x\rangle}\right), \tag{49}$$

$$\operatorname{Hess}\delta(x) = \sum_{v\in V}\left(2\frac{x^T x}{\langle x, x\rangle^2} - \frac{v^T v}{\langle x, v\rangle^2} - \operatorname{diag}\left(\frac{1}{\langle x, x\rangle}\right)\right). \tag{50}$$

7 Uniformization of Tori

Every Riemann surface R of genus one is conformally equivalent to a flat torus, i.e., to a quotient space $\mathbb{C}/\Gamma$, where $\Gamma = \mathbb{Z}\omega_1 + \mathbb{Z}\omega_2$ is some two-dimensional lattice in $\mathbb{C}$. The biholomorphic map from R to $\mathbb{C}/\Gamma$, or from the universal cover of R to $\mathbb{C}$, is called a uniformizing map. For a polyhedral surface of genus one, constructing a discrete uniformizing map amounts to solving Problem 3.1 with prescribed total angle $\Theta = 2\pi$ at all vertices. This provides us with a method to calculate approximate uniformizing maps for Riemann surfaces of genus one given in various forms. We consider examples of tori immersed in $\mathbb{R}^3$ in Sect. 7.1 and elliptic curves in Sect. 7.2. (We will also consider tori in the form of Schottky uniformization in Sect. 8.2, as a toy example after treating the higher genus case.)

The belief that discrete conformal maps approximate conformal maps is not based on a proven theorem but on experimental evidence like the Wente torus example of Sect. 7.1 and the numerical experiments of Sect. 7.4.

7.1 Immersed Tori

First we consider a simple example with quadrilateral faces. Figure 13 (left) shows a coarse discretization of a torus. The faces are isosceles trapezoids, so they are inscribed in circles. On the right, the figure shows the uniformization obtained by solving Problem 3.1 with prescribed total angle $\Theta = 2\pi$ at all vertices.

To test the numerical accuracy of our discrete uniformizing maps, we consider the famous torus of constant mean curvature discovered by Wente [47]. Explicit doubly periodic conformal immersion formulas (i.e., formulas for the inverse of a uniformizing map) are known in terms of elliptic functions [1, 3, 46].

Figure 14 (left) shows a triangulated model of the Wente torus constructed by sampling an explicit immersion formula [3] on a nearly square lattice containing the period lattice Γ. On the right, the figure shows the discrete uniformization, which reproduces the regular lattice Γ to high accuracy. The modulus $\tau = \omega_2/\omega_1$ of the Wente torus has been determined numerically [19] as $\tau = 0.41300\ldots + i\ 0.91073\ldots$. The modulus of the discrete uniformization of the discretized surface shown in the figure is $\tilde{\tau} = 0.41341\ldots + i\ 0.91061\ldots$.

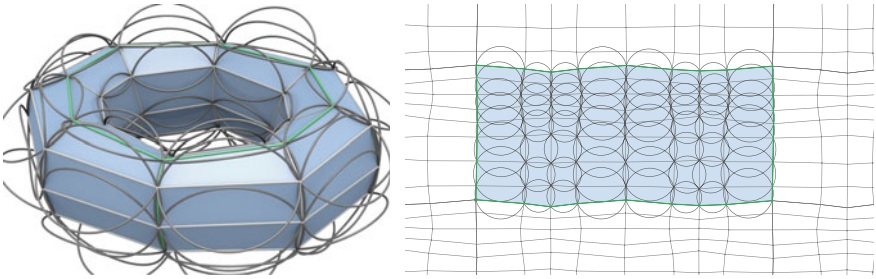

Fig. 13 Uniformization of an immersed torus with cyclic quadrilateral faces

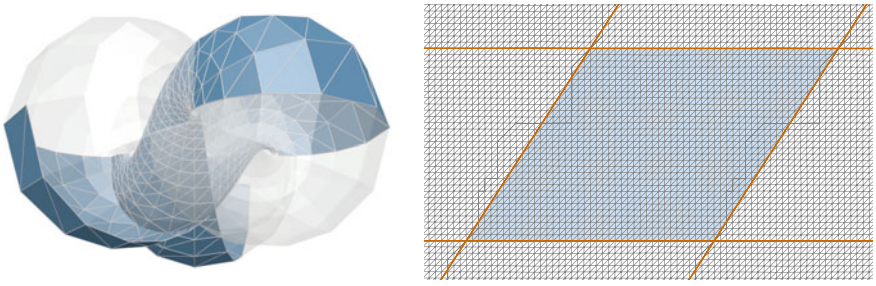

Fig. 14 Uniformization of the Wente torus

7.2 Elliptic Curves

An algebraic curve of the form

$$\mu^2 = a \prod_{j=1}^{k} (\lambda - \lambda_j), \tag{51}$$

where the $\lambda_j \in \mathbb{C}$ are distinct and $k = 3$ (an elliptic curve) or $k = 4$ (with the singularity at infinity resolved), represents a Riemann surface of genus one as branched double cover of the λ-sphere $\mathbb{C}\mathrm{P}^1$, which we identify conformally with the unit sphere $S^2 \subset \mathbb{R}^3$. The branch points are $\lambda_1, \lambda_2, \lambda_3, \infty$ if $k = 3$ and $\lambda_1, \lambda_2, \lambda_3, \lambda_4$ if $k = 4$. Every Riemann surface of genus one can be represented in this way.

We construct a discrete model for a double cover of S^2 branched at four points $\lambda_1, \ldots, \lambda_4$ in the following way. Choose n other points $p_1, \ldots, p_n \in S^2$ and let P be the boundary of the convex hull of the points $\{\lambda_1, \ldots, \lambda_4, p_1, \ldots, p_n\}$. Then P is a convex polyhedron with $n + 4$ vertices and with faces inscribed in circles. (Generically, the faces will be triangles. In Sect. 7.3 we explain the method we used to obtain "good" triangles.) Find two disjoint simple edge paths γ_1, γ_2 joining the branch points λ_j in pairs. Take a second copy $\hat{P}$ of the polyhedron P. Cut and glue P and $\hat{P}$ along the paths γ_1, γ_2 to obtain a polyhedral surface of genus 1. Uniformize it

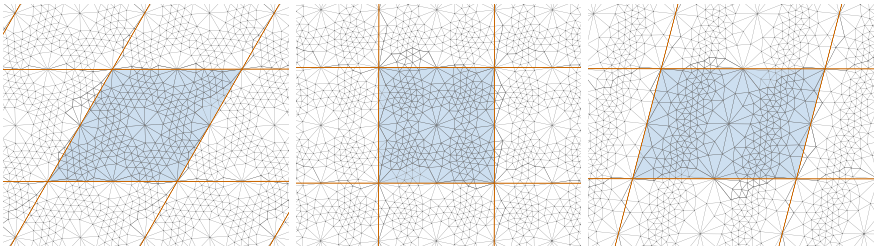

Fig. 15 Discrete uniformization of elliptic curves. *Left* If the branch points in S^2 are the vertices of a regular tetrahedron, period lattice is very close to a hexagonal lattice. *Middle* If the branch points form a square on the equator, the period lattice is very close to a square lattice. *Right* an example with branch points in unsymmetric position

by solving Problem 3.1. One obtains a discrete conformal map to a flat torus, whose inverse can be seen as a discrete elliptic function. Figure 15 shows examples. We will treat hyperelliptic curves in a similar fashion in Sect. 8.3.

Remark 7.1 Instead of constructing a doubly covered convex euclidean polyhedron with vertices on the unit sphere as described above, one could also construct a spherical triangulation of the doubly covered sphere that is invariant under the elliptic involution (exchanging sheets). These two approaches are in fact equivalent due to Remark 2.3.

Mapping a flat torus to an elliptic curve. We can also go the opposite way, mapping a flat torus to a double cover of S^2. Start with a triangulated flat torus. The triangulation should be symmetric with respect to the elliptic involution, i.e., symmetric with respect to a half turn around one vertex (which is then also a half turn around three other vertices). The quotient space of the triangulated torus modulo the elliptic involution is then a triangulated sphere. Map it to the sphere by the procedure explained in [5] (Sect. 3.2), see also Sect. 6.1 of the present article.

Figures 16 and 17 show examples where we started with a hexagonal and a square torus respectively.

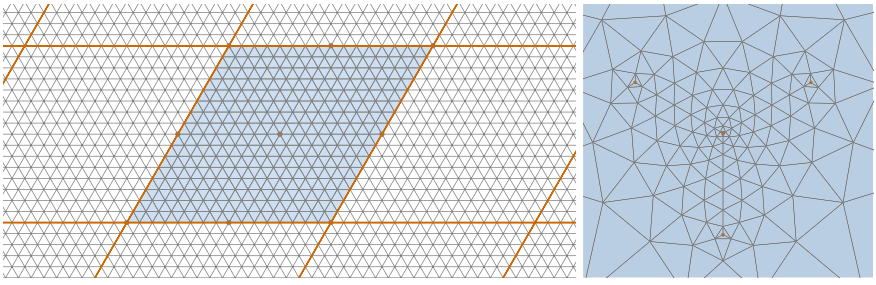

Fig. 16 Mapping the hexagonal torus $\mathbb{C}/(\mathbb{Z}+\tau\mathbb{Z})$, $\tau = \frac{1}{2} + i\frac{\sqrt{3}}{2}$ (*left*) to a double cover of the sphere (*right*). Because the regular triangulation of the torus on the *left* is symmetric with respect to the elliptic involution, its image projects to a triangulation of the sphere seen on the *right*

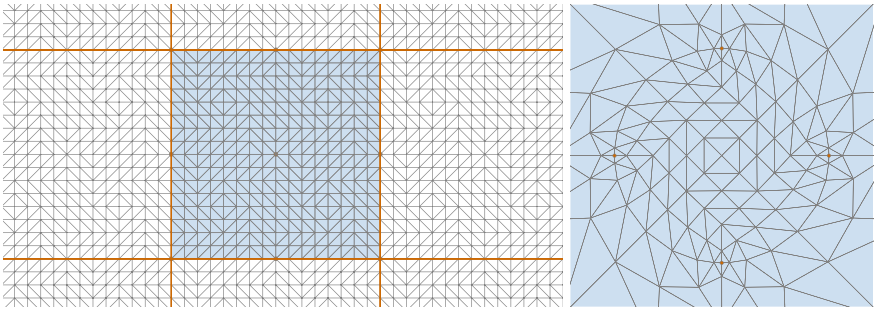

Fig. 17 Mapping the square torus $\mathbb{C}/(\mathbb{Z}+i\mathbb{Z})$ (*left*) to a double cover of the sphere (*right*). Again, the triangulation on the *left* is symmetric with respect to the elliptic involution, so the image on the *right* projects to a triangulation of the sphere

7.3 Choosing Points on the Sphere

The uniformization procedure for elliptic curves described in Sect. 7.2 requires choosing points on the sphere in addition to the four given branch points. For numerical reasons, these points should be chosen so that taking the convex hull leads to triangles that are close to equilateral. We obtained good triangulations by minimizing the following energy for n points in $\mathbb{R}^3$ while fixing the subset of branch points:

$$\mathcal{E} = n^2 \sum_{v \in V} (\langle v, v \rangle - 1)^2 + \sum_{\substack{v,w \in V \\ w \neq v}} \frac{1}{\langle w - v, w - v \rangle}, \tag{52}$$

where $\langle ., . \rangle$ denotes the standard euclidean scalar product of $\mathbb{R}^3$. We do not enforce the constraint that the points should lie in the unit sphere S^2. Instead, we simply project back to S^2 after the optimization.

As initial guess we choose points uniformly distributed in S^2. To achieve this we choose points with normally distributed coordinates and project them to S^2 [31].

7.4 Numerical Experiments

Given the branch points of an elliptic curve, the modulus τ can be calculated in terms of hypergeometric functions. In this section, we compare the theoretical value of τ with the value $\hat{\tau}$ that we obtain by the discrete uniformization method explained in Sect. 7.2.

We consider elliptic curves in Weierstrass normal form

$$\begin{aligned} \mu^2 &= 4(z - \lambda_1)(z - \lambda_2)(z - \lambda_3) \\ &= 4z^3 - g_2 z - g_3, \end{aligned} \tag{53}$$

so the branch points $\lambda_1, \lambda_2, \lambda_3, \infty$ satisfy $\lambda_1 + \lambda_2 + \lambda_3 = 0$, and

$$g_2 = -4(\lambda_1\lambda_2 + \lambda_2\lambda_3 + \lambda_3\lambda_1), \qquad g_3 = 4\lambda_1\lambda_2\lambda_3. \tag{54}$$

We calculate the modulus τ with Mathematica using the built-in function `WeierstrassHalfPeriods[{g2, g3}]`. We normalize τ and the value $\hat{\tau}$ obtained by discrete uniformization so that they lie in the standard fundamental domain of the modular group, $|\tau| > 1$ and $|\operatorname{Re}(\tau)| < \frac{1}{2}$, and we consider the error $|\tau - \hat{\tau}|$. (We stay away from the boundary of the fundamental domain.)

Subdivided icosahedron. In this experiment we start with the twelve vertices of a regular icosahedron and choose the branch points $\lambda_1, \ldots, \lambda_4$ among them. The remaining points act the role of $p_1, \ldots, p_n$. To study the dependence of $|\tau - \hat{\tau}|$ on the number of points we repeatedly subdivide all triangles into four similar triangles and project the new vertices to S^2. The number of vertices grows exponentially while the triangles remain close to equilateral. Figure 18 shows the result of this experiment. It suggests the error behaves like

$$|\tau - \hat{\tau}| = \mathcal{O}(n^{\alpha}), \quad \alpha \approx -0.88. \tag{55}$$

Dependence on mesh quality. In the second experiment we choose the additional points randomly to analyze how the quality of the triangulation affects the approximation error. We use the following quantities to measure the quality of the triangulation based on length cross-ratios for edges:

$$Q_{\mathrm{lcr}}(e) := \frac{1}{2}\left(\mathrm{lcr}(e) + \frac{1}{\mathrm{lcr}(e)}\right) - 1,$$
$$Q_{\mathrm{lmr}}(f) := \frac{1}{2}\left(\mathrm{lmr}(f) + \frac{1}{\mathrm{lmr}(f)}\right) - 1,$$

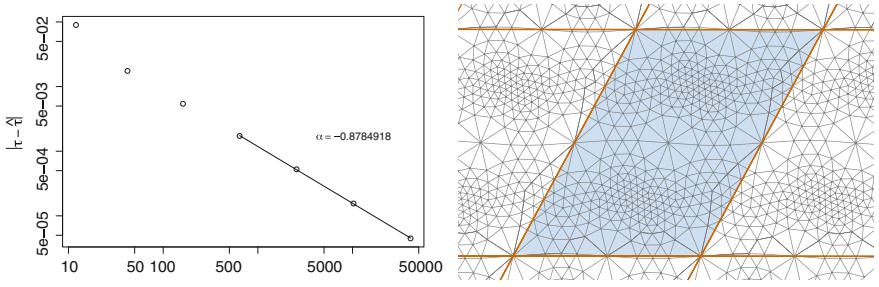

Fig. 18 *Left* Error for zero to six subdivision steps. The log-log plot shows the error $|\tau - \hat{\tau}|$ against the number of vertices of the subdivided icosahedron (i.e., in one sheet of the doubly covered sphere). To estimate the asymptotic behavior of the error, we determine the slope $\alpha \approx -0.88$ of a line through the last four points by linear regression. *Right* Result of the discrete uniformization after two subdivision steps

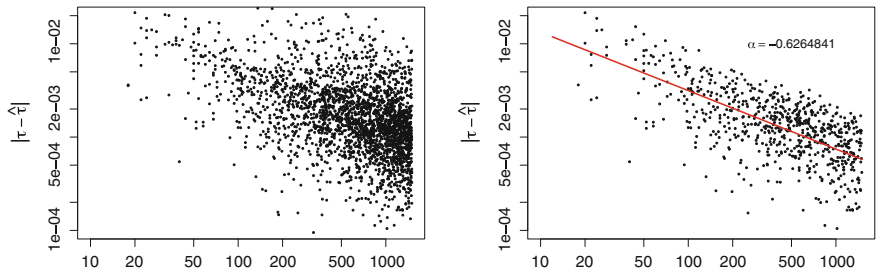

Fig. 19 *Left* log-log plot of the error $|\tau - \hat{\tau}|$ against the number of vertices for a sample of optimized random triangulations with no quality constraint. *Right* Only triangulations with $\max_e\{Q_{\mathrm{lmr}}(e)\} < 0.3$ are considered. The regression line with slope $\alpha \approx -0.63$ is shown in *red*

where lcr denotes the length cross-ratio (9) of an edge, and lmr denotes the length multi-ratio defined for faces by $\mathrm{lmr}(f) = \prod_{e \in f} \mathrm{lcr}(e)$. If $Q_{\mathrm{lcr}} = 0$ for all edges, then the mesh is discretely conformally equivalent to a mesh consisting of equilateral triangles. So less is better for these quality measures. To get enough "good" triangulations in our samples, we improve random meshes with the procedure described in Sect. 7.3.

Figure 19 (left) shows a plot of 2600 triangulations ranging from $n = 20$ to $n = 1500$ vertices. No clear convergence rate is discernible. The situation improves when only samples with a certain minimal mesh quality are considered. For the plot in Fig. 19 (right) we selected only triangulations with $\max_e\{Q_{\mathrm{lmr}}(e)\} < 0.3$. (The results are similar when using the quality measures $\max_e\{Q_{\mathrm{lcr}}(e)\} < x$ or $\mathrm{mean}_e\{Q_{\mathrm{lcr}}(e)\} < x$.)

The results from these two experiments suggest that the error depends on the number n of vertices asymptotically like n^α, where the exponent $\alpha < 0$ depends on the mesh.

7.5 *Putting a Square Pattern on a Spherical Mesh*

We can use a variant of the discrete uniformization of elliptic curves (Sect. 7.2) to put a square pattern on a surface that is homeomorphic to a sphere. Figure 20 shows an example.

Pick four vertices of the mesh as ramification points and create a two-sheeted branched cover of the mesh by gluing two copies along paths connecting the selected vertices. The resulting surface is a torus. It can be uniformized using the euclidean functional. The uniformizing group is generated by two translations. This group is a subgroup of the group generated by rotations around the branch vertices. Hence we can achieve the same result as follows. Instead of doubling the surface, prescribe total angles $\Theta = \pi$ at the ramification vertices and $\Theta = 2\pi$ at all other vertices. The result is a flat surface with four cone-like singularities of cone-angle π. The

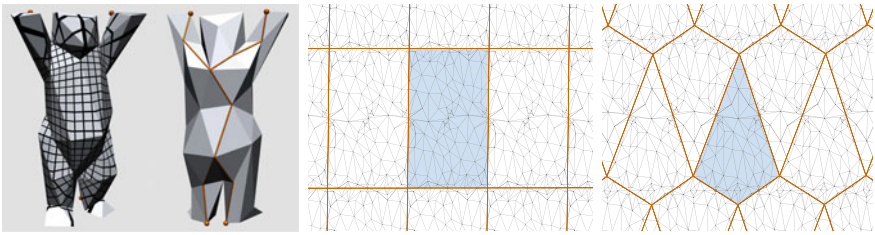

Fig. 20 The discrete "Berlin Buddy Bear", a mascot of the SFB/Transregio 109 "Discretization in Geometry and Dynamics". The square pattern is put on a bear model as described in Sect. 7.5. Four ramification vertices (marked in *red*) are chosen at the paws. The uniformization of the branched double cover is shown in the *middle*. Each fundamental domain covers the bear twice. Fundamental domains of the group generated by rotations around the branch points are shown on the *right*. Each covers the bear once

monodromy of the developing map is generated by half-turns. Avoiding the double cover is more efficient because one only has to minimize a function of (approximately) half the number of variables.

8 Uniformization of Surfaces of Higher Genus

As in the case of tori (Sect. 7), we can find uniformizing maps for cyclic polyhedral surfaces of genus $g \geq 2$ by solving the hyperbolic version ($\tilde{g} = hyp$) of Problem 3.1 with prescribed total angle $\Theta = 2\pi$ at all vertices. (We will only consider

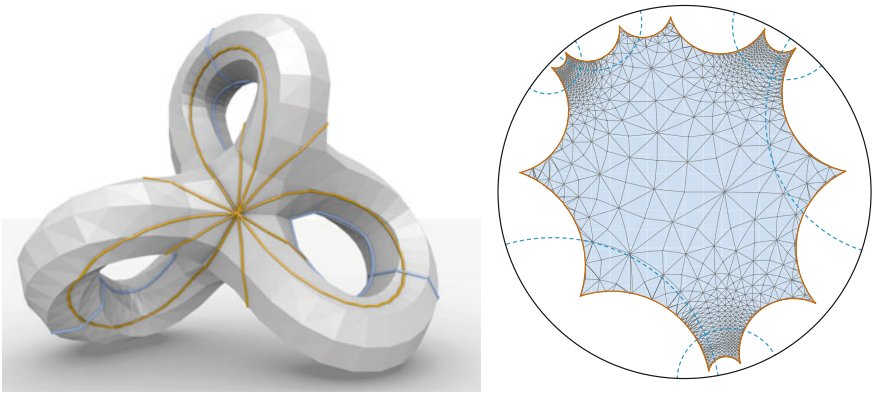

Fig. 21 Discrete uniformization of an embedded triangulated surface of genus 3. A fundamental polygon with "canonical" edge pairing is shown on the *right* together with the image mesh. The edges of the polygon (*brown*) and the axes of the edge-pairing translations (*blue*) are pulled back to the embedded surface shown on the *left*

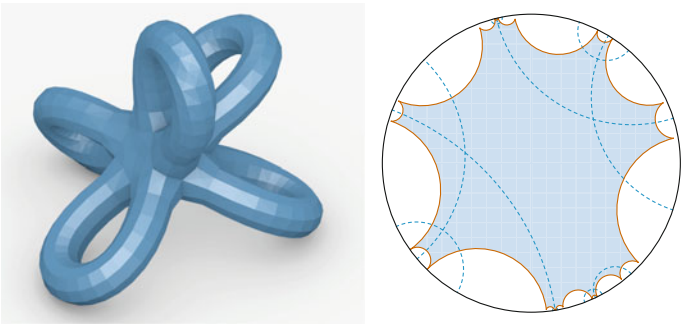

Fig. 22 *Left* An embedded triangulated surface of genus 5. *Right* Fundamental polygon with non-canonical edge-pairing. The axes of the edge pairing translations are shown in *blue*

triangulations in the following.) This allows us to calculate approximate uniformizations for Riemann surfaces of genus $g \geq 2$ given in various forms, by approximating them with polyhedral surfaces.

In Sect. 8.1, we briefly discuss how to construct fundamental polygons and group generators.

Not much needs to be said about the uniformization of immersed surfaces. Examples are shown in Figs. 1 (bottom), 21, and 22. In Sect. 5.1 we discussed mappings from multiply connected domains to circle domains. Analogously, one can construct uniformizations of polyhedral surfaces of genus $g \geq 2$ with holes over the hyperbolic plane with circular holes. An example is shown in Fig. 23. More precisely, the holes are bounded by hyperbolic polygons with vertices on a circle.

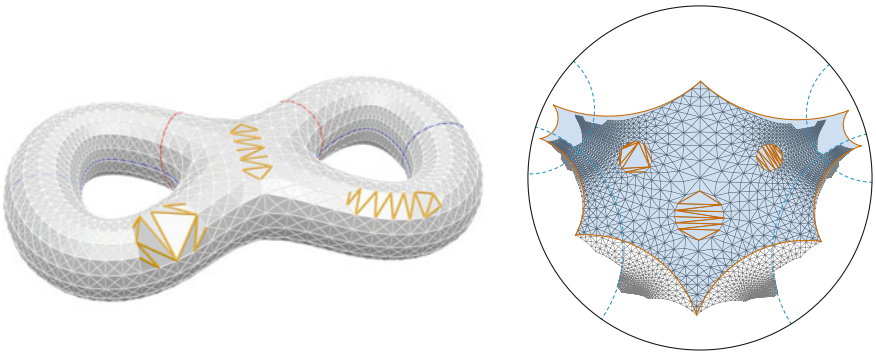

Fig. 23 Uniformization of a genus 2 surface with three boundary components over the hyperbolic plane with three circular holes. The three holes are filled with polygons, which are then triangulated during the calculation, see Sects. 5.1 and 3

We explain how to calculate the Fuchsian uniformization for Riemann surfaces given in the form of a Schottky uniformization in Sect. 8.2. We discuss the uniformization of hyperelliptic curves in Sect. 8.3 and a geometric characterization of hyperelliptic Riemann surfaces in Sect. 8.4.

8.1 Fundamental Polygons and Group Generators

Basic facts and notation. Every compact Riemann R of genus $g \geq 2$ can be represented as the quotient of the hyperbolic plane H^2 modulo the action of a discrete group G of hyperbolic translations,

$$R = H^2/G. \tag{56}$$

Presentations of the group G play an important role. We will denote generators by capital letters and their inverses by primes,

$$A' := A^{-1} \in G. \tag{57}$$

The uniformization group G can be presented with a finite set of generators

$$A, B, C, D, \ldots \in \mathrm{Isom}(H^2)$$

subject to a single relation $r = 1$,

$$G = \langle A, B, C, D, \ldots \mid r = 1 \rangle, \tag{58}$$

where r is a product in which all generators and their inverses appear exactly once. Such presentations are closely related with fundamental polygons: Every fundamental polygon in which all vertices are identified leads to such a presentation.

A fundamental domain of G is an open connected subset D of the hyperbolic plane such that the G-orbit of the closure $\bar{D}$ covers H^2, and $gD \cap D = \emptyset$ for all $g \in G \setminus \{1\}$. A fundamental polygon of G is a fundamental domain with polygonal boundary, i.e., the boundary consists of geodesic segments, the *edges* of the fundamental polygon, which are identified in pairs by the action of the group G. For each edge a, there is exactly one partner edge a' such that there exists a translation $A \in G$ mapping a to a'. These edge-gluing translations form a generating set of G. If all vertices of the fundamental polygon are identified (i.e., they belong to the same G-orbit), then the fundamental polygon has $4g$ edges. In this case there is only one relation for these generators. The relation can be determined from the edge labels, which we always list in counterclockwise order. For example, if the edges of an octagon are labeled "canonically",

$$aba'b'cdc'd', \tag{59}$$

then the relation for the corresponding edge pairing translations is

$$DC'D'CBA'B'A, \tag{60}$$

and if opposite edges are identified,

$$abcda'b'c'd', \tag{61}$$

then the relation is

$$DC'BA'D'CB'A = 1. \tag{62}$$

Computational aspects. Let (Σ, ℓ) be a closed (euclidean, spherical, or hyperbolic) triangulated surface of genus $g \geq 2$. We solve Problem 3.1 to obtain a combinatorially equivalent hyperbolic triangulated surface $(\Sigma, \tilde{\ell})_{hyp}$ with angle sum $\Theta = 2\pi$ at every vertex. We lay out the triangles in the hyperbolic plane one-by-one, following a breadth-first search of the the 1-skeleton of the dual cell complex of Σ. (Alternatively, one could use a shortest spanning tree of the 1-skeleton of the dual complex [15].) The result is a fundamental polygon with many vertices. An example is shown in Fig. 24a.

We simplify this fundamental polygon by connecting vertices that are identified with more than one partner by geodesic arcs, as shown in Fig. 24b. The resulting polygon has in general more than one vertex class.

Now we perform the standard algorithm involving cut-and-glue operations (see, e.g., [20]) to obtain a fundamental polygon with one vertex class and so-called canonical edge identification

$$aba'b'cdc'd' \ldots . \tag{63}$$

During this process we maintain edge-identification transformations, which we represent as $SO^+(2, 1)$ matrices.

Hyperbolic translations tend to accumulate numerical errors quite fast when building products. The situation could be ameliorated somewhat by using the $PSL(2, \mathbb{R})$-representation of hyperbolic isometries [16], but the fundamental problem remains. For this reason, it is desirable to perform the cut-and-glue algorithm in such a way that the number of matrix products required to maintain the gluing translations is small. We follow the following greedy approach. Repeatedly we have to choose labels x, y such that the order in the polygon is $x \cdots y \cdots x' \cdots y'$, and then perform a cut-and-glue sequence to bring the labels next to each other, $xyx'y'$. We always choose a pair x, y, for which this requires the minimal number of matrix multiplications.

The polygon with canonical edge identifications may not be convex. Following Keen [21], we can transform this domain into a strictly convex fundamental polygon by choosing a different base vertex for the same group of transformations. Let $aba'b'cdc'd' \ldots$ be a fundamental polygon and let

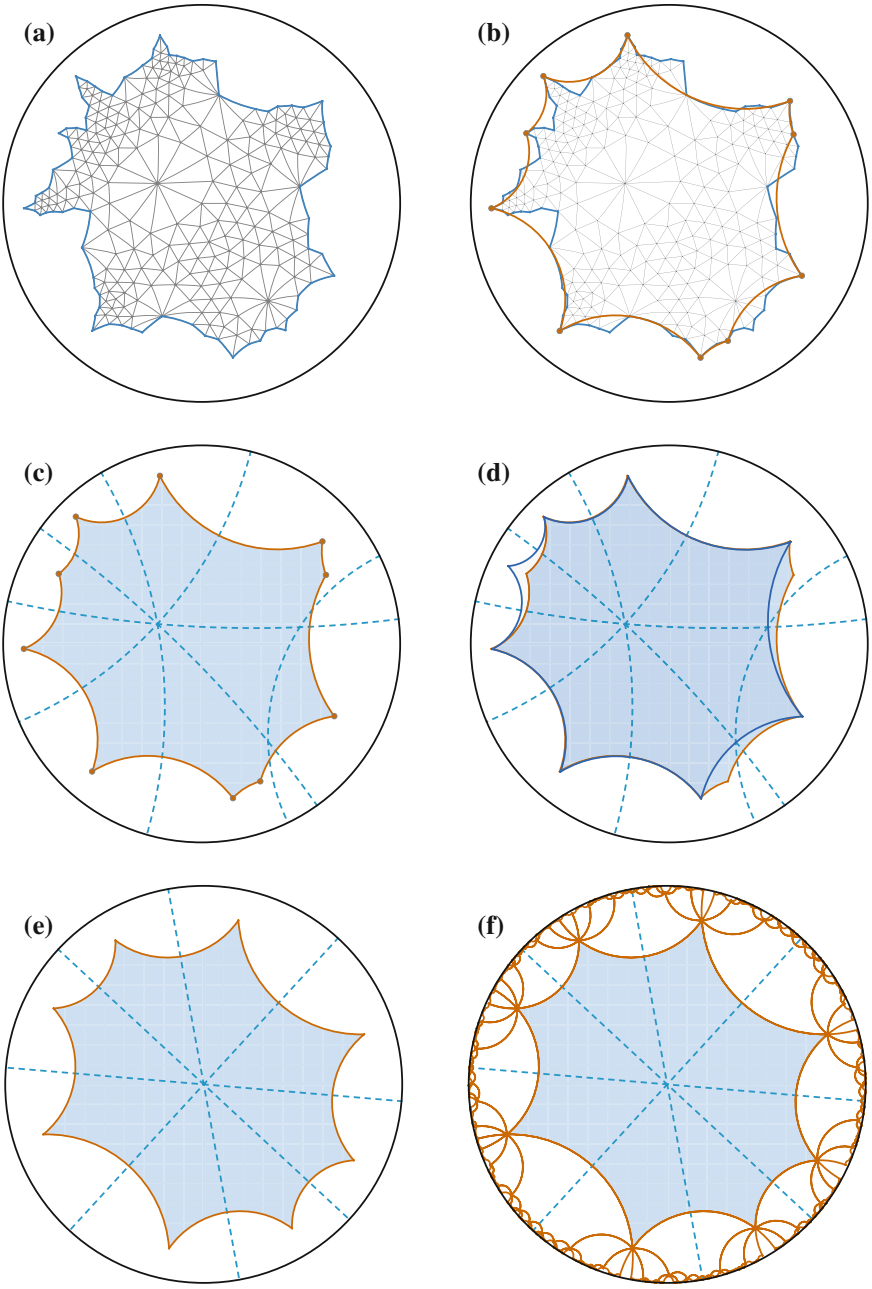

Fig. 24 Constructing a fundamental polygon with opposite edges identified. **a** Laying out hyperbolic triangles creates a fundamental polygon with many vertices. **b** Straighten the edges between vertices that are identified with more than one partner (shown in *red*). **c** Axes of the edge-pairing translations are shown in *blue*. **d**, **e** Two cut-and-paste operations lead to a fundamental polygon with one vertex class and opposite edges identified. The axes intersect in one point (see Sect. 8.4). We move this point to the origin. **f** Tiling the hyperbolic plane with fundamental polygons

$$G = \langle A, B, C, D, \ldots \in PSL(2, \mathbb{R}) \mid \ldots DC'D'CBA'B'A = 1 \rangle \qquad (64)$$

be the corresponding presentation of the uniformization group, see Fig. 25 (left). Then the axes of the generators A and B intersect in a point p_0. Choosing p_0 as the base point of a new fundamental polygon as shown in Fig. 25 (right) renders it convex and uniquely determined for the given group and presentation.

Fundamental polygons with opposite sides identified. When we consider the geometric characterization of hyperelliptic surfaces in Sect. 8.4, we want to transform fundamental polygons into fundamental polygons with opposite sides identified, i.e., polygons with edge labeling

$$abcd \cdots a'b'c'd' \cdots .$$

Any fundamental polygon can be transformed into a fundamental polygon with opposite edges identified by cut-and-glue operations: First transform the polygon to canonical form $aba'b'cdc'd' \ldots$ by the standard algorithm. Playing a sequence of steps that transforms a polygon with opposite edges identified to canonical form backwards, transforms the canonical polygon to a polygon with opposite edges identified.

This algorithm is not optimal with respect to the number of multiplications necessary to maintain the edge-gluing translations. Especially if the original polygon is already "close" to one with opposite sides identified, the detour via a canonical polygon is inefficient.

In all examples, we use a heuristic method based on the following idea: Find a longest sequence of different letters in the edge labeling (ignoring primes), and then try to move a different letter into this sequence by cutting and gluing.

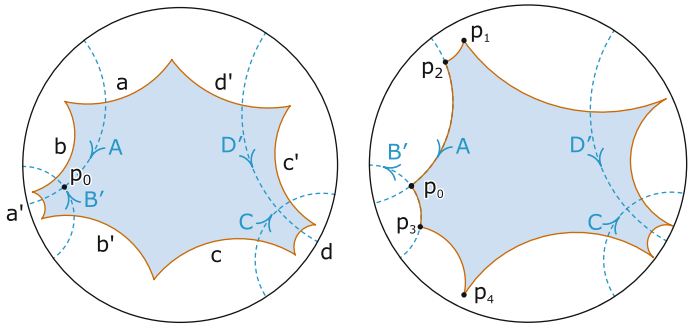

Fig. 25 The algorithm of Linda Keen to construct strictly convex fundamental polygons. Start with any canonical fundamental polygon $aba'b'cdc'd'$ with a corresponding relation $DC'D'CBA'B'A = 1$ (*left*). We choose the intersection p_0 of the axes of transformations A and B as base point for the new domain. The new vertices of the fundamental domain are calculated as $p_1 = A'Bp_0$, $p_2 = A'p_0$, $p_3 = Bp_0$, and $p_4 = BA'p_0$. The other vertices are obtained similarly from p_4 by applying C and D

8.2 From Schottky to Fuchsian Uniformization

In this section, we consider Riemann surfaces presented as quotient spaces of classical Schottky groups.

Definition 8.1 Let $C_1, C_1' \ldots, C_g, C_g'$ be circles in $\hat{\mathbb{C}}$ that bound disjoint disks. A *classical Schottky group* is a Kleinian group generated by Möbius transformations $\sigma_1, \ldots, \sigma_g$, where σ_j maps the outside of C_j onto the inside of C_j'.

Each generator σ_j has fixed points A_j, B_j inside C_j and C_j', respectively. The limiting set A of G is the union of orbits of the fixed points A_j, B_j. G acts freely and properly discontinuously on the domain of discontinuity $\Omega = \hat{\mathbb{C}} \setminus A$. The quotient space $R = \Omega/G$ is a Riemann surface of genus g. The domain outside all of the circles is a fundamental domain of G. The identified pairs of circles form handles.

We discretize the Riemann surface $R = \Omega/G$ determined by a classical Schottky group G as follows. First, construct a triangulation of Ω whose vertex set and combinatorics are invariant under the action of G. (Ignore the fact that a Möbius transformation maps straight edges to circular arcs as in Proposition 2.5 on the Möbius invariance of conformal classes.) For example, the triangulation may be the Delaunay triangulation of a G-invariant point set. The following construction avoids Delaunay triangulations of infinite (but symmetric) point configurations:

If necessary, choose a Möbius normalization for which the fundamental domain is bounded in $\mathbb{C}$. For each pair of circles C_j, C_j' we construct polygons $p_{1j}, \ldots, p_{n_j j}$ inscribed in C_j and $p'_{1j}, \ldots, p'_{n_j j}$ inscribed in C' such that $\sigma_j(p_{kj}) = p'_{kj}$. For example, we may choose a regular n-gon inscribed in C_j and map the vertices by σ_j to C_j'. Triangulate the compact region bounded by these polygons, adding vertices in the interior as wanted. (For example, use a constrained Delaunay triangulation.) The images of this triangulation under the action of G (again, considering only combinatorics and vertex positions) form a G-invariant triangulation $\hat{\Delta}$ of the universal cover of R, hence a triangulation Δ of R. More precisely, the triangulations $\hat{\Delta}$ and Δ are only defined up to isotopy fixing the vertices. The edge-lengths $\hat{\ell}$ (distances of vertices) do not project from $\hat{\Delta}$ to Δ, but the length cross-ratios $\widehat{\text{lcr}}$ calculated from these edge lengths do, because they are Möbius invariant. The projected length cross-ratios lcr determine a discrete conformal class for Δ (see Sect. 2.5).

To obtain a Fuchsian uniformization of R, construct edge lengths ℓ from the length cross-ratios lcr as described in Sect. 2.6. Then solve Problem 3.1 (or rather the corresponding analytic version, Problem 3.4) for $(\Delta, \ell)_{euc}$ with $\tilde{g} = hyp$ and desired angle sums $\Theta = 2\pi$ at all vertices.

Note that the lengths ℓ calculated from length cross-ratios lcr may not satisfy all triangle inequalities. This does not matter for the corresponding analytic Problem 3.4 (with $V = V_1$, $E = E_1$). If Problem 3.4 has a solution, it is in the discrete conformal class determined by the length cross-ratios lcr. Also, whether or not Problem 3.4 has a solution does not depend on the choice of edge lengths ℓ provided they lead to the same length cross-ratios.

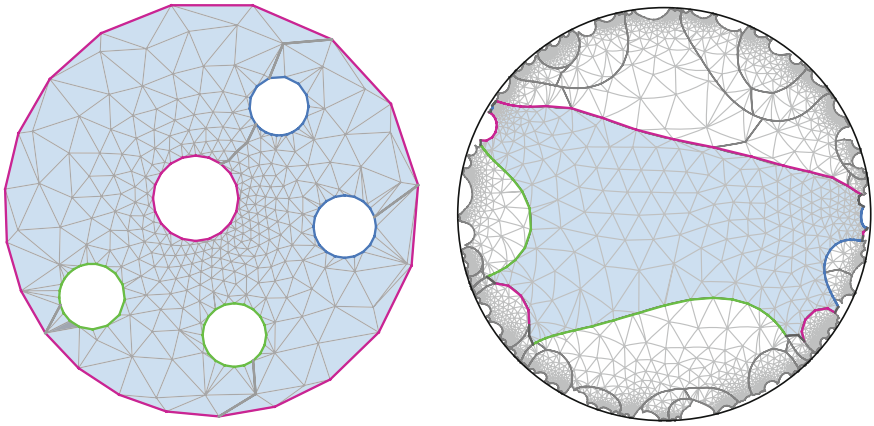

Fig. 26 Discrete Riemann surface of genus 3 given by Schottky data (*left*) and its Fuchsian uniformization (*right*). Circles with the same color are identified. The extra points of the triangulation are chosen so that the triangles are close to equilateral where possible. The *shaded region* in the *right image* corresponds to the fundamental domain of the Schottky group in the *left image*. Its boundary consists of curves corresponding to the circles and curves corresponding to lines connecting the circles (drawn in *gray*)

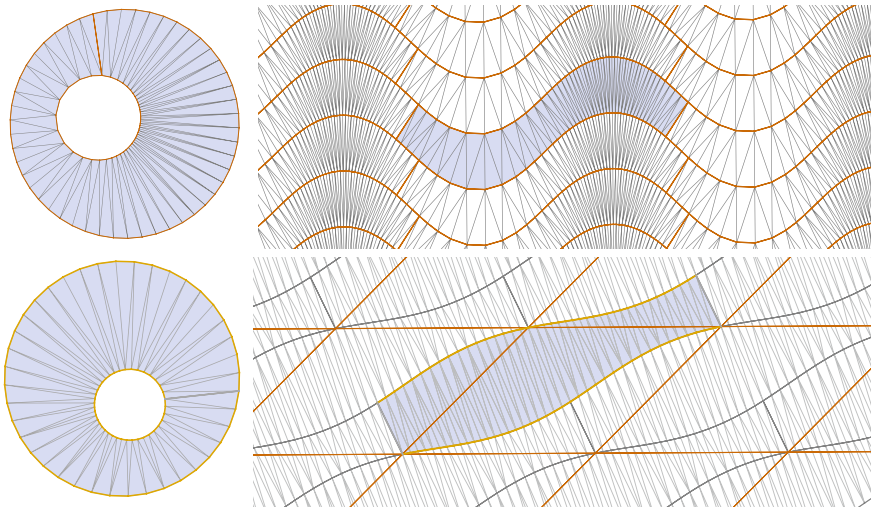

Fig. 27 *Left* Fundamental domains of Riemann surfaces of genus 1 given by Schottky data C, C', A, B, μ (see (65)). The triangulations use only points on the circles C, C'. We deliberately chose non-concentric circles, i.e., with centers $A \neq B$. *Right* Representation of the same surfaces as $\mathbb{C}/\Gamma$ for a lattice Γ. *Top* For real $\mu = 0.3$ we get a rectangular lattice. *Bottom* $\mu = 0.08 + 0.01i$ yields a parallelogram

Figure 26 shows an example of the Fuchsian uniformization of a genus three surface presented by its Schottky uniformization.

Tori given by Schottky data. For tori, the Schottky data consist of one generator

$$\frac{\sigma(z) - A}{\sigma(z) - B} = \mu \frac{z - A}{z - B} \tag{65}$$

and one pair of circles. To find a uniformization $\mathbb{C}/\Gamma$ is elementary. It suffices to consider the case where $A = B = 0$ (and C, C' are concentric circles around 0 with radii i and μ. Figure 27 shows two examples where we apply the discrete method without adding extra points inside the fundamental domain of the Schottky group.

8.3 Hyperelliptic Curves

A hyperelliptic curve is a complex algebraic curve of the form

$$\mu^2 = p(\lambda), \tag{66}$$

where p is a polynomial of degree $d \geq 5$ with d distinct roots. For $d = 2g + 2$ or $d = 2g + 1$, the hyperelliptic curve becomes a compact Riemann surface of genus g after singularities at infinity are resolved. For our purposes, a hyperelliptic curve is just a branched double cover of the λ-sphere with branch points $\lambda_1, \ldots, \lambda_{2g+1}, \infty$ if $d = 2g + 1$ and branch points $\lambda_1, \ldots, \lambda_{2g+2}$ if $d = 2g + 2$.

We construct a polyhedral approximation of a hyperelliptic curve in the same way as for elliptic curves (Sect. 7.2). We choose points $p_1, \ldots, p_n$ in addition to the $2g + 2$ branch points and take the convex hull. We cut the resulting polyhedron open along edge paths joining pairs of branch points and glue a second copy along the cuts.

Figure 28 shows uniformizations of the curves

$$\mu^2 = \lambda \prod_{k=1}^{2g} \left(\lambda - e^{\frac{ik\pi}{g}}\right) \tag{67}$$

for $g = 2, 3, 4$ that were obtained this way. The curves are branched at the $2g$th roots of unity and at 0 and ∞.

Mapping a polyhedral surface to a hyperelliptic curve. We can also map a triangulated surface of genus g to a branched double cover of the sphere, provided it is symmetric with respect to a discrete conformal involution with $2g + 2$ fixed points, which are vertices. In the simplest case, the involution is an isometry. (Compare Sect. 7.2, where we map flat tori to elliptic curves.) Taking the quotient of the trian-

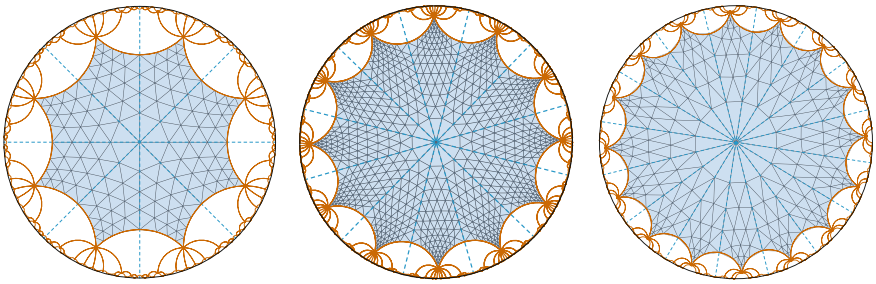

Fig. 28 Uniformizations of the hyperelliptic curves (67) with genus 2, 3, and 4. The triangulation of the surfaces is a regular 1-to-4 subdivision of the convex hull of the branch points. Due to the symmetries of these curves, the fundamental domains are regular hyperbolic $4g$-gons. Since the triangulation is as symmetric as the curves, and because the solution of the discrete uniformization problem is unique, the fundamental domains of the polyhedral surfaces are also exactly regular hyperbolic $4g$-gons. Any error in the domains is therefore due to numerics, and not due to the discretization

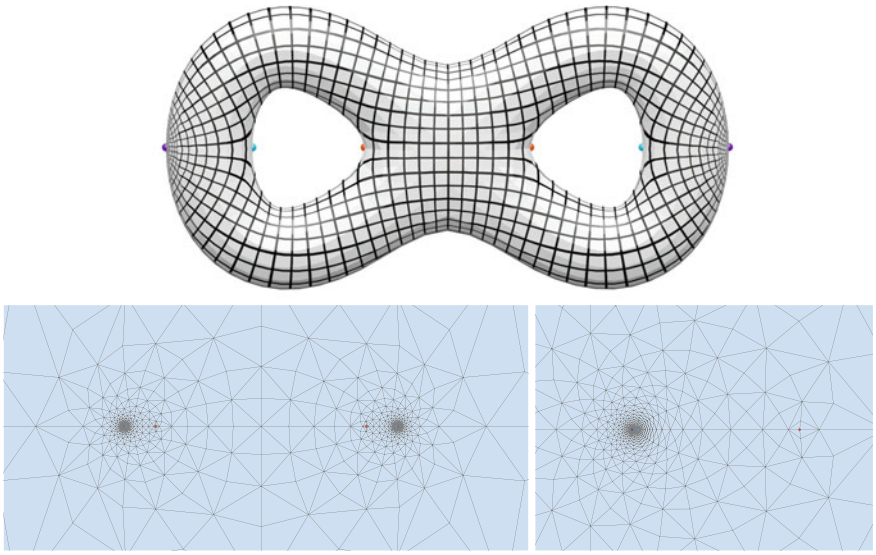

Fig. 29 A triangulated genus 2 surface is mapped to a branched cover of $\hat{\mathbb{C}}$. The 180° rotation about the horizontal symmetry axis is a discrete conformal involution with 6 fixed points marked in *red*, *blue*, and *purple*. The texture is a square grid in the plane, pulled back to the doubly covered sphere by Mercator projection, then pulled back to the surface. *Bottom* Branched cover of $\hat{\mathbb{C}}$, and a closeup of three branch points

gulation with respect to the involution, we get a triangulated sphere with a discrete conformal structure, which we map discretely conformally to the sphere. Figure 29 shows an example.

8.4 Geometric Characterization of Hyperelliptic Surfaces

A Riemann surface R of genus $g \geq 2$ is called *hyperelliptic*, if one of the following equivalent conditions is true (and hence all are):

1. R is conformally equivalent to some hyperelliptic curve.
2. R is conformally equivalent to a branched cover of the sphere with $2g + 2$ branch points.
3. There is a conformal involution $\tau : R \to R$ with exactly $2g + 2$ fixed points.

The involution τ is called the *hyperelliptic involution* of R. By the Riemann-Hurwitz formula, the quotient surface R/τ is a sphere.

All Riemann surfaces of genus two are hyperelliptic, but for every genus greater than two, there are Riemann surfaces that are not hyperelliptic. The following geometric characterization of hyperelliptic Riemann surfaces is due to Schmutz Schaller [36, 37].

Theorem 8.2 *Let R be a closed hyperbolic surface of genus g. Then the following statements are equivalent:*

(i) *R is hyperelliptic.*
(ii) *R has a set of $2g - 2$ simple closed geodesics which all intersect in one point and which intersect in no other point.*
(iii) *R has a set of $2g$ simple closed geodesics which all intersect in one point and which intersect in no other point.*
(iv) *R has a fundamental polygon that is a $4g$-gon with opposite sides identified and equal opposite angles.*

The fundamental polygon of condition (iv) is symmetric with respect to a 180° rotation around its center, which corresponds to the hyperelliptic involution on R. The $2g + 2$ fixed points on R are the vertex of the polygon, its center, and the $2g$ edge midpoints. The axes of the $2g$ edge-gluing translations all go through the center. They project to $2g$ simple closed geodesics on R which all intersect in one point and intersect in no other point.

8.5 Example: Deforming a Hyperelliptic Surface

We uniformize a hyperelliptic surface obtaining a centrally symmetric fundamental polygon with opposite edges identified as predicted by Theorem 8.2. The axes of the generators meet in one point. Then we deform the surface slightly to a non-hyperelliptic surface to see how the fundamental polygon and the axes change. The result is shown in Fig. 30.

For this example, we construct an elliptic-hyperelliptic triangulated surface with additional symmetry. A surface is called *elliptic-hyperelliptic* if it is conformally equivalent to a two-sheeted branched cover of the torus.

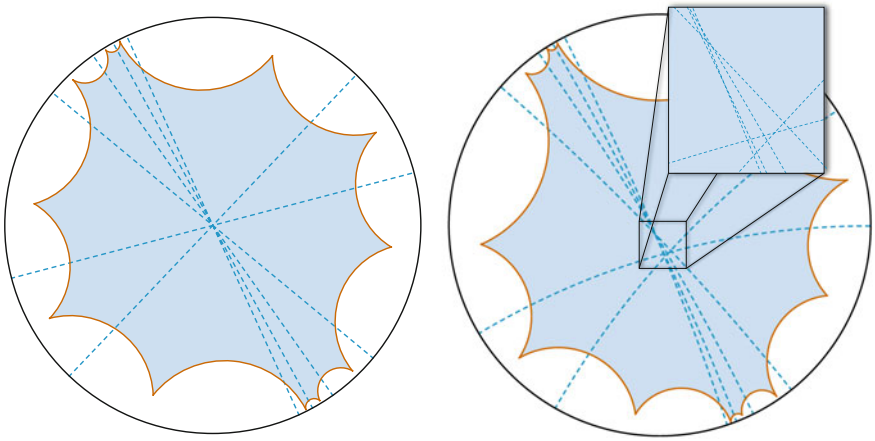

Fig. 30 Hyperelliptic versus non-hyperelliptic. *Left* Uniformization of a hyperelliptic surface with a centrally symmetric fundamental polygon. The axes of the generators meet in a common point. *Right* Uniformization of the deformed surface, which is not hyperelliptic. The axes do not meet in one point

Take two regular tetrahedra (the faces of which are subdivided several times to obtain a finer mesh), cut them across pairs of opposite edges and glue them together to obtain a two-sheeted cover of a tetrahedron branched at the four vertices. Now choose two paths in one of the sheets that connect the centers of the tetrahedron's faces in pairs. Cut the surface along these paths, take another copy of this cut surface and glue corresponding cuts together to form an elliptic-hyperelliptic surface of genus three that is a four-fold cover of a regular tetrahedron. The surface possesses six anti-holomorphic involutions corresponding to the six reflectional symmetries of the tetrahedron, and three holomorphic involutions corresponding to the rotational symmetries of the tetrahedron of order two. Each of the holomorphic involutions has eight fixed points covering the midpoints of a pair of opposite edges. Thus, this elliptic-hyperelliptic surface is also hyperelliptic.

Figure 30 (left) shows a uniformization of the hyperelliptic elliptic-hyperelliptic surface. Destroying the symmetry by moving all points of the polyhedral surface in space by a small random offset destroys the hyperellipticity of the surface, see Fig. 30 (right).

Numerical Data. We list the numerical $SO^+(2,1)$ matrices of the generators of the group

$$\langle T_1, T_2, T_3, T_4, T_5, T_6 \mid T_6 T_5^{-1} T_4 T_3^{-1} T_2 T_1^{-1} T_6^{-1} T_5 T_4^{-1} T_3 T_2^{-1} T_1 = 1 \rangle \qquad (68)$$

representing the hyperelliptic elliptic-hyperelliptic surface constructed in this section (see Fig. 31). The matrices satisfy the relation with error $\approx 10^{-7}$.

Fig. 31 Generator labels

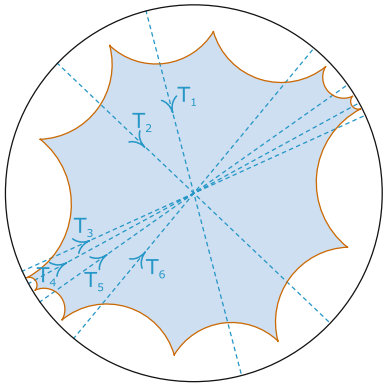

$$T_1 = \begin{bmatrix} 2.05443154523212 & -4.021591426903446 & -4.403849064057392 \\ -4.021591427085276 & 16.338309707059754 & 16.796236533536394 \\ -4.403849064222335 & 16.796236533484112 & 17.392741252301292 \end{bmatrix}$$

$$T_2 = \begin{bmatrix} 7.906334736200989 & -6.57792280760043 & -10.236171033333449 \\ -6.5779228079025245 & 7.265127613618063 & 9.749417813849163 \\ -10.236171033527825 & 9.749417813638956 & 14.171462349831586 \end{bmatrix}$$

$$T_3 = \begin{bmatrix} 933.210063638192 & 509.0929753776527 & 1063.0407708335915 \\ 509.09297492442374 & 279.0228056502974 & 580.5414569092936 \\ 1063.0407706165242 & 580.5414573067374 & 1211.2328692884857 \end{bmatrix}$$

$$T_4 = \begin{bmatrix} 47.8208492808903 & 21.282776040302117 & -52.33345184418173 \\ 21.28277609643665 & 10.67424906068982 & -23.788571865092973 \\ -52.333451867010325 & -23.788571814871467 & 57.49509834158029 \end{bmatrix}$$

$$T_5 = \begin{bmatrix} 933.2100574645401 & 509.09297238055706 & -1063.040763978619 \\ 509.092972765322 & 279.02280467565924 & -580.5414545474814 \\ -1063.0407641628826 & -580.5414542100707 & 1211.2328621402066 \end{bmatrix}$$

$$T_6 = \begin{bmatrix} 128.62265665383228 & 90.05086671584104 & -157.0093831621644 \\ 90.05086668827934 & 64.5401174556973 & -110.78621463208009 \\ -157.00938314635744 & -110.78621465448322 & 192.16277410952506 \end{bmatrix}$$

8.6 Example: Different Forms of the Same Genus-2 Surface

In this section we present Fuchsian uniformizations of the same Riemann surface represented in three different ways:

- as hyperelliptic curve $\mu^2 = \lambda^6 - 1$ (Fig. 32),
- as Lawson's genus 2 minimal surface in S^3 [25] (Fig. 33),
- and as a surface glued from six squares (Fig. 34).

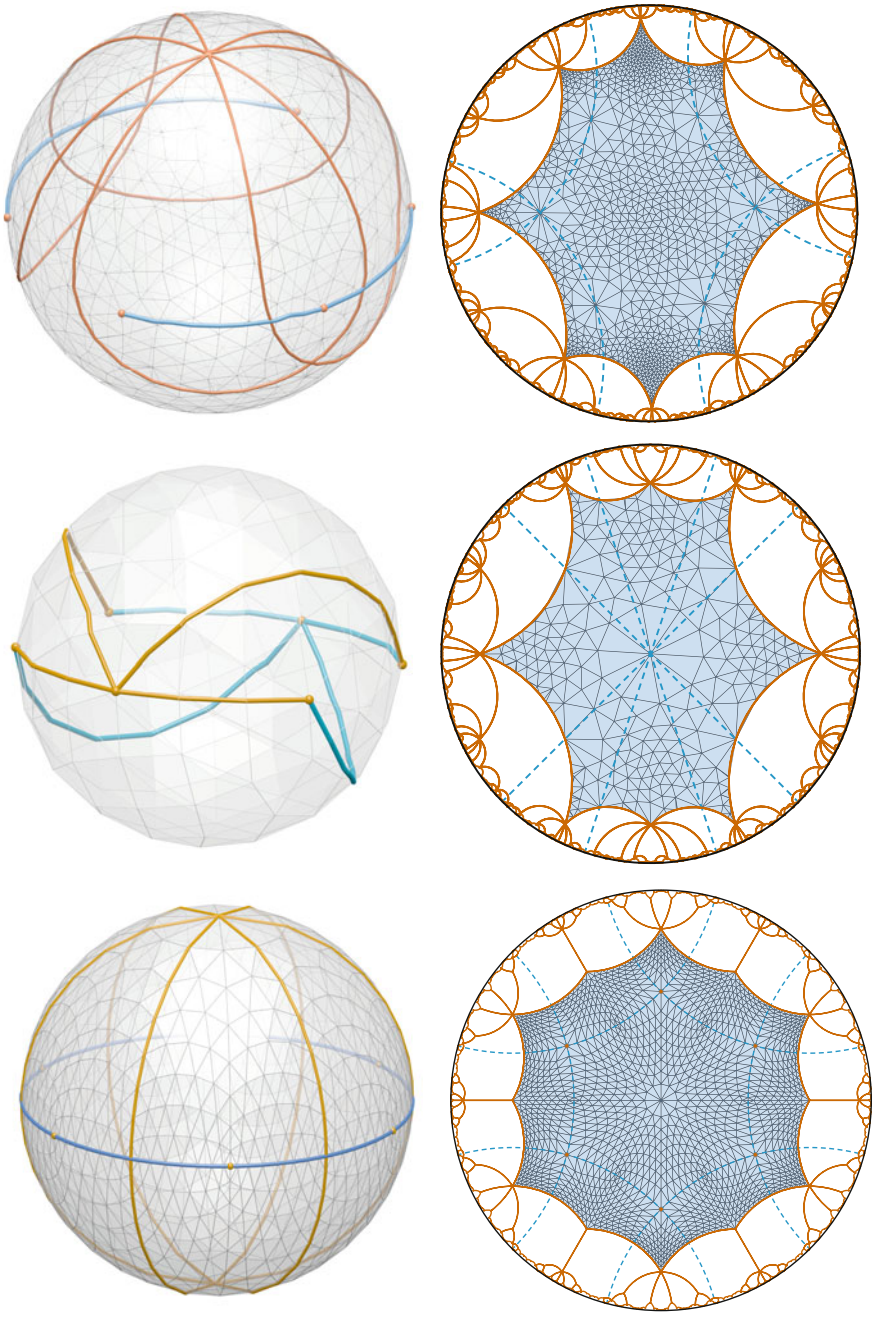

Fig. 32 Uniformization of the hyperelliptic curve $\mu^2 = \lambda^6 - 1$. *Left* Triangulated double cover of the sphere branched at the 6th roots of unity, with the boundary of the fundamental domain shown in *brown* and the axes of generators shown in *blue*. *Right* Fuchsian uniformization and fundamental polygons. Canonical polygon (*top*), polygon with opposite sides identified (*middle*), and 12-gon specially adapted to the six-squares surface (*bottom*)

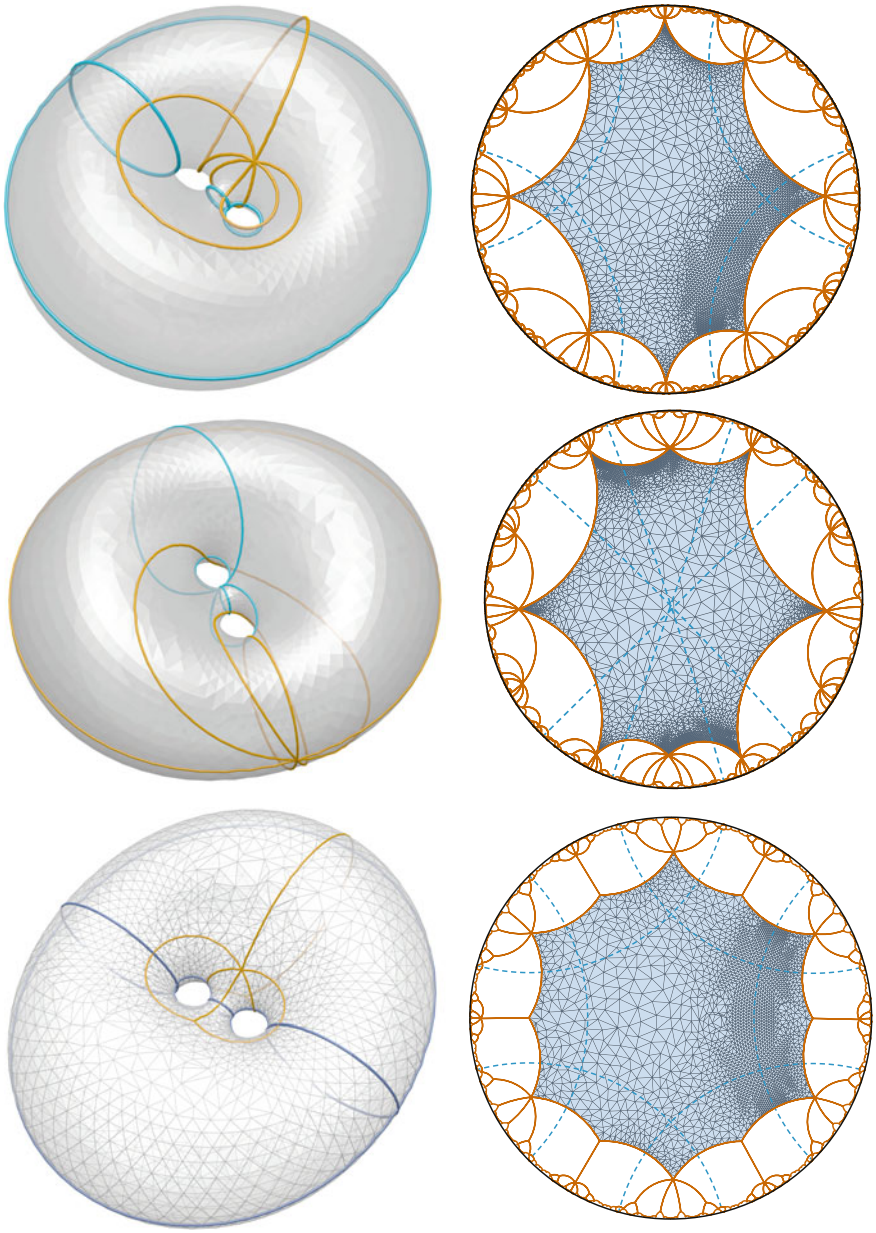

Fig. 33 Uniformization of Lawson's surface. *Left* Triangulated model [34], with the boundary of the fundamental domain shown in *brown* and the axes of the generators shown in *blue*. *Right* Fuchsian uniformizations and fundamental domains. Canonical domain (*top*), opposite sides domain (*middle*), and 12-gon (*bottom*)

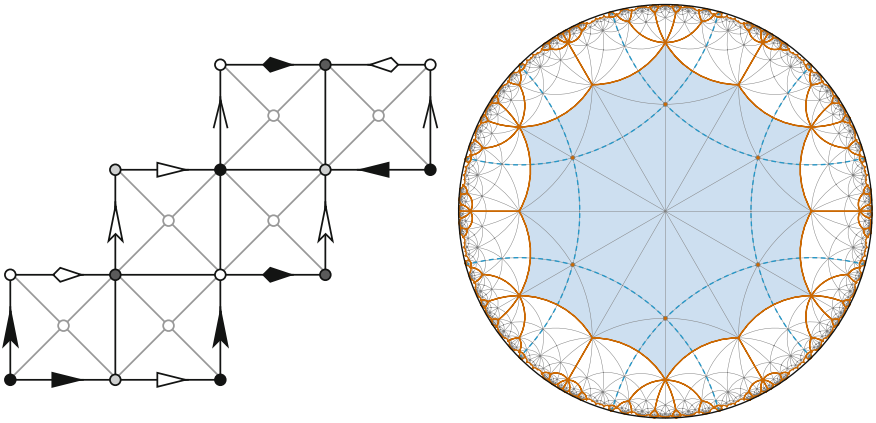

Fig. 34 *Left* A surface glued from six squares. *Right* Fuchsian uniformization and fundamental domain

For each representation we choose corresponding fundamental polygons that allow the comparison of the uniformization:

- an octagon with canonical edge pairing $aba'b'cdc'd'$,
- an octagon with opposite sides identified, $abcda'b'c'd'$,
- a 12-gon that is adapted to the six-squares surface.

All data presented in this section is available on the DGD Gallery webpage [39].

Hyperelliptic curve. We uniformize the hyperelliptic curve $\mu^2 = \lambda^6 - 1$ as described in Sect. 7.2. The results are shown in Fig. 32.

To understand the cuts on the hyperelliptic surface that lead to the 12-gon in the bottom row, imagine taking the canonical system of loops in the top row, meeting at the north pole, and deform them until they also meet at the south pole. This introduces a second vertex class in the fundamental polygon.

Lawson's surface. Figure 33 shows Fuchsian uniformizations of Lawson's minimal surface in S^3. The triangulated surface model was kindly provided by Konrad Polthier [34].

This model of the Lawson surface realizes the hyperelliptic involution as a euclidean rotational symmetry. Its symmetry axis meets the surface in six points. These fixed points of the hyperelliptic involution correspond to the branch points of the hyperelliptic curve representation. This allows us to uniformize the model with corresponding fundamental domains.

Six-squares surface. Figure 34 (left) shows a surface glued from six squares, which is conformally equivalent to Lawson's surface and the hyperelliptic curve. Edges with the same marking are glued together. We calculate a uniformization using the triangulation with vertices added in the centers of the squares as shown. An adapted fundamental domain for this square-tiled translational surface arranges all squares around a single vertex, see Fig. 34 (right). By comparison with Fig. 32 (bottom) we

see that the vertices in the center of the squares correspond to the branch points of the hyperelliptic representation of the surface. The black, gray, and white vertices correspond to the north and south pole of the hyperelliptic representation.

Acknowledgments This research was supported by DFG SFB/TRR 109 "Discretization in Geometry and Dynamics".

References

1. Abresch, U.: Constant mean curvature tori in terms of elliptic functions. J. Reine Angew. Math. **374**, 169–192 (1987)
2. Adler, V.E., Bobenko, A.I., Suris, Y.B.: Classification of integrable equations on quad-graphs. The consistency approach. Commun. Math. Phys. **233**(3), 513–543 (2003)
3. Bobenko, A.I.: All constant mean curvature tori in R^3, S^3, H^3 in terms of theta-functions. Math. Ann. **290**(2), 209–245 (1991)
4. Bobenko, A.I., Günther, F.: Discrete complex analysis on planar quad-graphs. In this volume
5. Bobenko, A.I., Pinkall, U., Springborn, B.: Discrete conformal maps and ideal hyperbolic polyhedra. Geom. Topology **19**(4), 2155–2215 (2015)
6. Bobenko, A.I., Suris, Y.B.: Integrable systems on quad-graphs. Int. Math. Res. Not. **11**, 573–611 (2002)
7. Bobenko, A.I., Suris, Y.B.: Discrete Differential Geometry-Integrable Structure, Graduate Studies in Mathematics, vol. 98. American Mathematical Society, Providence (2008)
8. Chelkak, D., Smirnov, S.: Discrete complex analysis on isoradial graphs. Adv. Math. **228**(3), 1590–1630 (2011)
9. Chelkak, D., Smirnov, S.: Universality in the 2D Ising model and conformal invariance of fermionic observables. Invent. Math. **189**(3), 515–580 (2012)
10. Courant, R., Friedrichs, K., Lewy, H.: Über partielle Differentialgleichungen der mathematischen Physik. Math. Ann. **100**, 32–74 (1928)
11. Duffin, R.J.: Discrete potential theory. Duke Math. J. **20**, 233–251 (1953)
12. Duffin, R.J.: Basic properties of discrete analytic functions. Duke Math. J. **23**, 335–363 (1956)
13. Duffin, R.J.: Distributed and lumped networks. J. Math. Mech. **8**, 793–826 (1959)
14. Duffin, R.J.: Potential theory on a rhombic lattice. J. Comb. Theory **5**, 258–272 (1968)
15. Erickson, J., Har-Peled, S.: Optimally cutting a surface into a disk. In: Symposium on Computational Geometry, pp. 244–253 (2002)
16. Floyd, W., Weber, B., Weeks, J.: The Achilles' heel of O(3, 1)? Experiment. Math. **11**(1), 91–97 (2002)
17. Gu, X., Luo, F., Sun, J., Wu, T.: A discrete uniformization theorem for ployhedral surfaces. arXiv:1309.4175 (2013)

18. Gu, X., Luo, F., Sun, J., Wu, T.: A discrete uniformization theorem for polyhedral surfaces II. arXiv:1401.4594 (2014)
19. Heil, M.: Numerical tools for the study of finite gap solutions of integrable systems. Ph.D. thesis, TU-Berlin (1995)
20. Jost, J.: Compact Riemann Surfaces, 3rd edn. Universitext. Springer-Verlag, Berlin (2006)
21. Keen, L.: Canonical polygons for finitely generated Fuchsian groups. Acta Math. **115**, 1–16 (1965)
22. Kenyon, R.: Conformal invariance of domino tiling. Ann. Probab. **28**(2), 759–795 (2000)
23. Kenyon, R.: The Laplacian and Dirac operators on critical planar graphs. Invent. Math. **150**(2), 409–439 (2002)
24. Kouřimská, H., Skuppin, L., Springborn, B.: A variational principle for cyclic polygons with prescribed edge lengths. In this volume
25. Lawson Jr., H.B.: Complete minimal surfaces in $\mathbb{S}^3$. Ann. Math. **92**(3), 335–374 (1970)
26. Leibon, G.: Characterizing the Delaunay decompositions of compact hyperbolic surfaces. Geom. Topol. **6**, 361–391 (2002)
27. Lelong-Ferrand, J.: Représentation conforme et transformations à intégrale de Dirichlet bornée. Gauthier-Villars, Paris (1955)
28. Luo, F.: Combinatorial Yamabe flow on surfaces. Commun. Contemp. Math. **6**(5), 765–780 (2004)
29. Mercat, C.: Discrete Riemann surfaces and the Ising model. Commun. Math. Phys. **218**(1), 177–216 (2001)
30. Milnor, J.: Hyperbolic geometry: the first 150 years. Bull. Amer. Math. Soc. (N.S.) **6**(1), 9–24 (1982)
31. Muller, M.E.: A note on a method for generating points uniformly on n-dimensional spheres. Commun. ACM **2**(4), 19–20 (1959)
32. Nehari, Z.: Conformal Mapping. McGraw-Hill Book Co., Inc., New York (1952)
33. Nijhoff, F., Capel, H.: The discrete Korteweg-de Vries equation. Acta Appl. Math. **39**(1–3), 133–158 (1995). KdV '95 (Amsterdam, 1995)
34. Oberknapp, B., Polthier, K.: An algorithm for discrete constant mean curvature surfaces. In: Hege, H.C., Polthier, K. (eds.) Visualization and Mathematics, pp. 141–161. Springer-Verlag, Berlin (1997)
35. Rodin, B., Sullivan, D.: The convergence of circle packings to the Riemann mapping. J. Differ. Geom. **26**(2), 349–360 (1987)
36. Schmutz Schaller, P.: Geometry of Riemann surfaces based on closed geodesics. Bull. Amer. Math. Soc. (N.S.) **35**(3), 193–214 (1998)
37. Schmutz Schaller, P.: Teichmüller space and fundamental domains of Fuchsian groups. Enseign. Math. (2) **45**(1-2), 169–187 (1999)
38. Schramm, O.: Circle patterns with the combinatorics of the square grid. Duke Math. J. **86**, 347–389 (1997)
39. Sechelmann, S., Bobenko, A.I., Springborn, B.: DGD Gallery, Lawson's surface uniformization. https://gallery.discretization.de/models/lawsons_surface_uniformization (2015)
40. Smirnov, S.: Critical percolation in the plane: conformal invariance, Cardy's formula, scaling limits. C. R. Acad. Sci. Paris Sér. I Math. **333**(3), 239–244 (2001)
41. Smirnov, S.: Conformal invariance in random cluster models. I. Holomorphic fermions in the Ising model. Ann. Math. (2) **172**(2), 1435–1467 (2010)
42. Smirnov, S.: Discrete complex analysis and probability. In: Proceedings of the International Congress of Mathematicians 2010 (ICM 2010), vol. I: Plenary Lectures and Ceremonies, vols. II-IV: Invited Lectures, pp. 595–621. Hyderabad, India (2010)
43. Springborn, B.: A unique representation of polyhedral types. Centering via Möbius transformations. Math. Z. **249**(3), 513–517 (2005)
44. Stephenson, K.: Introduction to Circle Packing. The Theory of Discrete Analytic Functions. Cambridge University Press, Cambridge (2005)
45. Thurston, W.P.: The geometry and topology of three-manifolds. Electronic version 1.1, March 2002, http://www.msri.org/publications/books/gt3m/

46. Walter, R.: Constant mean curvature tori with spherical curvature lines in non-Euclidean geometry. Manuscripta Math. **63**(3), 343–363 (1989)
47. Wente, H.C.: Counterexample to a conjecture of H. Hopf. Pacific J. Math. **121**(1), 193–243 (1986)

Discrete Complex Analysis on Planar Quad-Graphs

Alexander I. Bobenko and Felix Günther

Abstract We develop further a linear theory of discrete complex analysis on general quad-graphs, extending previous work of Duffin, Mercat, Kenyon, Chelkak and Smirnov on discrete complex analysis on rhombic quad-graphs. Our approach based on the medial graph leads to generalizations as well as to new proofs of previously known discrete analogs of classical theorems. New results include in particular discretizations of Green's first identity and Cauchy's integral formula for the derivative of a holomorphic function. Another contribution is a discussion on the product of discrete holomorphic functions that is itself discrete holomorphic in a specific sense. In this paper, we focus on planar quad-graphs, but many notions and theorems can be easily adapted to discrete Riemann surfaces. In the case of planar parallelogram-graphs with bounded interior angles and bounded ratio of side lengths explicit formulae for a discrete Green's function and discrete Cauchy's kernels are obtained. This slightly generalizes the previous results on rhombic lattices. When we further restrict to the integer lattice of a two-dimensional skew coordinate system a discrete Cauchy's integral formulae for higher order derivatives is derived.

Keywords Discrete complex analysis · Quad-graph · Green's function · Cauchy's integral formulae · Parallelogram-graph

1 Introduction

Linear theories of discrete complex analysis look back on a long and varied history. We refer here to the survey of Smirnov [24]. Already Kirchhoff's circuit laws describe a discrete harmonicity condition for the potential function whose gradient describes the current flowing through the electric network. A notable application

A.I. Bobenko · F. Günther (✉)
Inst. für Mathematik, Technische Universität Berlin, Straße des 17. Juni 136,
10623 Berlin, Germany
e-mail: fguenth@math.tu-berlin.de

A.I. Bobenko
e-mail: bobenko@math.tu-berlin.de

A.I. Bobenko (ed.), *Advances in Discrete Differential Geometry*,
DOI 10.1007/978-3-662-50447-5_2

of Kirchhoff's laws in geometry was the article [4] of Brooks, Smith, Stone, and Tutte, who used coupled discrete harmonic functions (in fact, discrete holomorphic functions) to construct tilings of rectangles into squares with different integral side lengths. Discrete harmonic functions on the square lattice were studied by a number of authors in the 1920s, including Courant, Friedrichs, and Lewy, who showed convergence of solutions of the Dirichlet boundary value problem to their corresponding continuous counterpart [8].

Discrete holomorphic functions on the square lattice were studied by Isaacs [14]. He proposed two different definitions for holomorphicity. The first one is not symmetric on the square lattice, but it becomes symmetric on the triangular lattice obtained by inserting all southwest-to-northeast diagonals. Dynnikov and Novikov studied an equivalent notion in [11]. His second definition was reintroduced by Lelong-Ferrand in [12]. She developed the theory to a level that allowed her to prove the Riemann mapping theorem using discrete methods [18]. Duffin also studied discrete complex analysis on the square grid [9] and was the first who extended the theory to rhombic lattices [10]. Mercat [19], Kenyon [16], Chelkak and Smirnov [6] resumed the investigation of discrete complex analysis on rhombic lattices or, equivalently, isoradial graphs. In these settings, it was natural to split the real and the imaginary part of a discrete holomorphic function to the two vertex sets of a bipartite decomposition.

Some two-dimensional discrete models in statistical physics exhibit conformally invariant properties in the thermodynamical limit. Such conformally invariant properties were established by Smirnov for site percolation on a triangular grid [25] and for the random cluster model [26], by Chelkak and Smirnov for the Ising model [7], and by Kenyon for the dimer model on a square grid (domino tiling) [15]. In all cases, linear theories of discrete analytic functions on regular grids were highly important. Kenyon [16] as well as Chelkak and Smirnov [6] obtained important analytic results that were instrumental in the proof that the critical Ising model is universal, i.e., that the scaling limit is independent of the shape of the lattice [7]. Already Mercat related the theory of discrete complex analysis to the Ising model and investigated criticality [19].

Important non-linear discrete theories of complex analysis involve circle packings or, more generally, circle patterns. Rodin and Sullivan proved that the Riemann mapping of a complex domain to the unit disk can be approximated by circle packings [22]. A similar result for isoradial circle patterns, even with irregular combinatorics, is due to Bücking [5]. In [2] it was shown that discrete holomorphic functions describe infinitesimal deformations of circle patterns. Moreover, in the case of parallelogram-graphs it was discussed that the corresponding theory is integrable by embedding the quad-graph into $\mathbb{Z}^n$.

Our setup in Sect. 2 is a strongly regular cellular decomposition of the complex plane into rectilinear quadrilaterals, called quad-graph. The medial graph of a quad-graph plays a crucial role in our work. It provides the connection between the notions of discrete derivatives of Kenyon [16], Mercat [20], Chelkak and Smirnov [6], extended from rhombic to general quad-graphs, and discrete differential forms and discrete exterior calculus as suggested by Mercat [19, 21]. Our treatment of discrete differential forms is close to what Mercat proposed in [21]. However, our version

of discrete exterior calculus is slightly more general. Having introduced the basic notations in the first two sections and the discrete exterior derivative in Sect. 2.3.1, we come to Proposition 2.13. There, it is described how the medial graph allows to multiply discrete holomorphic functions to a function that is discrete holomorphic in a certain sense, in particular that it fulfills (discrete) Morera's theorem.

The medial graph approach turns out to be quite useful for integration theory. Theorem 2.16 shows that the discrete exterior derivative is a derivation of the discrete wedge product. Many further results rely on this result and discrete Stokes' Theorem 2.9. In particular, this concerns discrete Green's identities (Theorem 2.23). A discretization of Green's second identity was one ingredient in the proof of Skopenkov's convergence result in [23]. Before the theorem is proved, we introduce the discrete wedge product, the discrete Hodge star, and the discrete Laplacian in Sects. 2.3 and 2.4.

Skopenkov's results on the existence and uniqueness of solutions to the discrete Dirichlet boundary value problem [23] help us to prove Theorem 2.30. This theorem states surjectivity of the discrete derivatives and the discrete Laplacian seen as linear operators. This implies in particular the existence of discrete Green's functions and discrete Cauchy's kernels. Furthermore, discrete Cauchy's integral formulae for discrete holomorphic functions are derived in Theorem 2.35 and for the discrete derivative of a discrete holomorphic function on the vertices of the quad-graph in Theorem 2.36. Note that discrete Cauchy's integral formula was used by Chelkak and Smirnov to derive certain asymptotic estimates in [7].

Section 3 is devoted to discrete complex analysis on planar parallelogram-graphs. There, explicit formulae for discrete Green's functions and discrete Cauchy's kernels with asymptotics similar to the functions in the rhombic case [5, 6, 16] are given (Theorems 3.7, 3.8, and 3.10). The general assumption is that the interior angles and the ratio of side lengths of all parallelograms are bounded. The construction of these functions is based on the discrete exponential introduced by Kenyon on quasicrystallic rhombic quad-graphs [16] and its extension to quasicrystallic parallelogram-graphs [2].

In the end, we close with the very special case of the integer lattice of a skew coordinate system in the complex plane. In this case, discrete Cauchy's integral formulae for higher order discrete derivatives of a discrete holomorphic function are derived in Theorem 3.11.

2 Discrete Complex Analysis on Planar Quad-Graphs

Although we focus on planar quad-graphs in this paper, many of our notions and theorems generalize to discrete Riemann surfaces. A corresponding linear theory of discrete Riemann surfaces is discussed in the subsequent paper [1] and can be found in more detail in the thesis [13].

2.1 Basic Definitions and Notation

The aim of this section is to introduce first planar quad-graphs and some basic notation in Sect. 2.1.1 and then to discuss the medial graph in Sect. 2.1.2.

2.1.1 Planar Quad-Graphs

Definition A *planar quad-graph Λ without boundary* is an infinite graph embedded into the complex plane $\mathbb{C}$ such that all edges are straight line segments and such that all faces are quadrilaterals which may be non-convex. In addition, we assume that Λ induces a cellular decomposition of the whole complex plane that is locally finite, i.e., a compact subset of $\mathbb{C}$ contains only finitely many quadrilaterals, and strongly regular, i.e., two different faces are either disjoint or share exactly one vertex or share exactly one edge (but not two edges).

Let $V(\Lambda)$ denote the set of vertices, $E(\Lambda)$ the set of edges, and $F(\Lambda)$ the set of faces of Λ.

It is well known that any planar quad-graph is bipartite. We fix one decomposition of the vertices of Λ into two independent sets and refer to the vertices of this decomposition as *black* and *white* vertices, respectively.

Definition Let Γ and Γ^* be the graphs defined on the black and white vertices where vv' is an edge of Γ (or Γ^*) if and only if its two black (or white) endpoints are vertices of a single face.

Remark The assumption of strong regularity guarantees that any edge of Γ or Γ^* is the (possibly outer) diagonal of exactly one quadrilateral.

In order to make the *duality* between Γ and Γ^* apparent, we consider just for this paragraph the edges of Γ or Γ^* as curves lying totally inside the face they are a diagonal of. Then, any *black* edge of Γ corresponds to the *white* edge of Γ^* that crosses it and vice versa. The black and white vertices are in one-to-one correspondence to the faces of Γ^* and Γ they are contained in.

Definition The complex number assigned to a vertex of Λ is the corresponding complex value of its embedding in $\mathbb{C}$. To oriented edges of Λ, Γ, Γ^* we assign the complex numbers determined by the difference of the complex numbers assigned to their two endpoints.

Remark For simplicity, we perform our calculations hereafter directly with the vertices and oriented edges of Λ, Γ, Γ^* rather than replacing them with their corresponding complex values.

Definition $\Diamond := \Lambda^*$ is the dual graph of Λ.

In general, we do not specify a planar embedding of the dual graph $\diamondsuit$. We will just identify vertices or faces of $\diamondsuit$ with their corresponding dual faces and vertices of Λ, respectively. However, in the particular case that all quadrilaterals are parallelograms, it makes sense to identify the vertices of $\diamondsuit$ (i.e., faces of the quad-graph Λ) with the centers of the parallelograms. Here, the center of a parallelogram is the point of intersection of its two diagonals. Further details will be given in Sects. 2.2.1 and 2.2.3.

Definition If a vertex $v \in V(\Lambda)$ is a vertex of a quadrilateral $Q \in F(\Lambda)$, we write $Q \sim v$ or $v \sim Q$ and say that v and Q are *incident* to each other.

Throughout our paper, we will denote the vertices of a single quadrilateral Q by b_-, w_-, b_+, w_+ in counterclockwise order, where $b_\pm \in V(\Gamma)$ and $w_\pm \in V(\Gamma^*)$.

Definition For a quadrilateral $Q \in F(\Lambda)$ we define

$$\rho_Q := -i\frac{w_+ - w_-}{b_+ - b_-}.$$

Moreover, let

$$\varphi_Q := \arccos\left(\mathrm{Re}\left(i\frac{\rho_Q}{|\rho_Q|}\right)\right) = \arccos\left(\mathrm{Re}\left(\frac{\overline{(b_+ - b_-)}(w_+ - w_-)}{|b_+ - b_-||w_+ - w_-|}\right)\right)$$

be the angle under which the diagonal lines of Q intersect.

Note that $0 < \varphi_Q < \pi$. Figure 1 shows a finite bipartite quad-graph together with the notations we have introduced for a single quadrilateral Q and the notations we are using later for the *star of a vertex* v, i.e., the set of all faces incident to v.

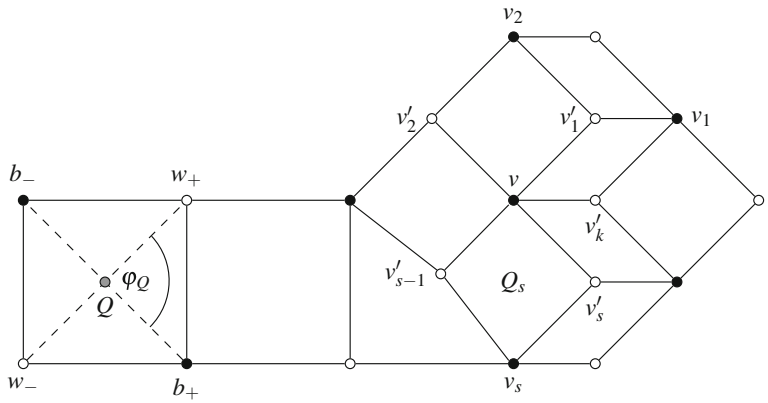

Fig. 1 Bipartite quad-graph with notations

In addition, we denote by $\Diamond_0$ a subgraph of $\Diamond$ that we always assume to be connected and by $V(\Diamond_0) \subseteq V(\Diamond)$ the corresponding subset of faces of the quad-graph Λ. Through our identification $V(\Diamond) \cong F(\Lambda)$, we can call the elements of $V(\Diamond)$ quadrilaterals and identify them with the corresponding faces of Λ.

Definition $\Diamond_0 \subseteq \Diamond$ is said to *form a simply-connected closed region* if the union of all quadrilaterals in $V(\Diamond_0)$ is a simply-connected closed region in $\mathbb{C}$.

Definition Let Λ_0 be the subgraph of Λ whose vertices and edges are exactly the corners and edges of the quadrilaterals in $V(\Diamond_0)$. The *interior faces* of Λ_0 are given by $V(\Diamond_0)$. Let Γ_0 and Γ_0^* denote the subgraphs of Γ and of Γ^* whose edges are the diagonals of quadrilaterals in $V(\Diamond_0)$ and who do not contain isolated vertices.

Remark Since $\Diamond_0 \subseteq \Diamond$ is connected, Γ_0 and Γ_0^* are connected as well. Indeed, if $Q, Q' \in V(\Diamond_0)$ are two quadrilaterals adjacent in $\Diamond_0$, then the corresponding subgraphs on Γ_0 and Γ_0^* consisting of the three black and white vertices of Q and Q' are paths of two edges each.

Definition Λ_0 is called a (planar) *quad-graph* induced by the subgraph $\Diamond_0 \subseteq \Diamond$. Its *boundary* $\partial\Lambda_0$ is the subgraph of Λ_0 that consists of all the edges of Λ_0 that belong to both a quadrilateral in $V(\Diamond_0)$ and one in $V(\Diamond)\setminus V(\Diamond_0)$.

Remark If $\Diamond_0 \subseteq \Diamond$ is finite and forms a simply-connected closed region, then the set of all interior faces of Λ_0 is homeomorphic to a disk and $\partial\Lambda_0$ is a closed broken line without self-intersections.

2.1.2 Medial Graph

Definition The *medial graph* X of Λ is defined as follows. Its vertex set is given by all the midpoints of the edges of Λ embedded in $\mathbb{C}$, and two vertices x, x' are adjacent if and only if the corresponding edges belong to the same face Q of Λ and have a vertex $v \in V(\Lambda)$ in common. We denote this edge by $[Q, v]$. Taking $[Q, v]$ as a straight line segment if v is a convex corner of the quadrilateral Q and as a curve lying inside Q that does not intersect the three other edges $[Q, v']$ ($v' \sim Q$, $v' \neq v$) inside Q if v is a concave corner, we get an embedding of X into $\mathbb{C}$. Then, the set $F(X)$ of faces of X is in bijection with $V(\Lambda) \cup V(\Diamond)$: A face F_v of X *corresponding to* $v \in V(\Lambda)$ has the midpoints of edges of Λ incident to v as vertices, and a face F_Q of X *corresponding to* $Q \in F(\Lambda) \cong V(\Diamond)$ has the midpoints of the four edges of Λ belonging to Q as vertices. The vertices of F_Q and F_v are colored gray in Fig. 2.

Remark Clearly, any pair $Q \sim v$ of a face and an incident vertex of Λ corresponds to an edge $[Q, v]$ of X. Moreover, a face F_Q lies inside Q and v is contained in F_v.

Definition As for the vertices and edges of Λ, we assign to a vertex of X the complex number corresponding to its position in $\mathbb{C}$, and to an oriented edge of X we assign the difference of the two endpoints.

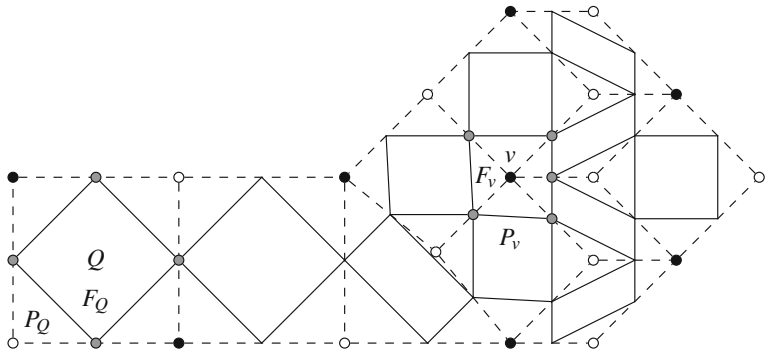

Fig. 2 Bipartite quad-graph (*dashed*) with medial graph (*solid*)

Even though not all edges of X might be straight line segments, we actually think of them as being straight since we assign the vector of its endpoints to it if the edge is oriented. In this sense, any face F_Q, $Q \in F(\Lambda)$, is a parallelogram due to Varignon's theorem. Moreover, the complex number assigned to the edge $[Q, v_0]$, $v_0 \sim Q$, if oriented from the midpoint of the edge $v_0v'_-$ to the one of the edge $v_0v'_+$ of Λ is just half of $e = v'_+ - v'_-$. We will say that $[Q, v_0]$ is *parallel* to e (disregarding the orientation), as it would be if we considered all edges of X as straight line segments.

Remark If all quadrilaterals of Λ are convex, then the embedding of X given above consists of straight line segments only. If no Varignon parallelogram of a non-convex quadrilateral contains another vertex of X apart from its corners, then the corresponding straight line realization gives an embedding equivalent to the one above. In this case, the face F_v of X corresponding to a vertex $v \in V(\Lambda)$ that is a concave corner of a quadrilateral does not contain v any longer. However, if such a Varignon parallelogram contains an additional vertex of X, then connecting adjacent vertices of X by straight line segments does not yield an embedding of X.

Definition For a connected subgraph $\diamondsuit_0 \subseteq \diamondsuit$, we denote by $X_0 \subseteq X$ the connected subgraph of X consisting of all edges $[Q, v]$ where $Q \in V(\diamondsuit_0)$ and v is a corner of Q. The *boundary* ∂X_0 is the subgraph of X_0 whose edges are exactly those $[Q, v]$ where $v \in V(\partial \Lambda_0)$ and $Q \in V(\diamondsuit_0)$ is incident to v. We consider the orientation on the boundary ∂X_0 that is induced by orienting any of its edges $[Q, v]$ counterclockwise with regard to Q. For a finite collection F of faces of X_0, ∂F denotes the union of all counterclockwise oriented boundaries of faces in F, where oriented edges in opposite directions cancel each other out.

Remark In the case that all quadrilaterals in $V(\diamondsuit_0)$ are convex, X_0 consists of all straight edges of X that lie inside the closed region formed by the quadrilaterals in $V(\diamondsuit_0)$. In any case, the medial graph X corresponds to a (strongly regular and locally finite) cellular decomposition of the plane in a canonical way. In particular, we can talk about a *topological disk D in $F(X_0)$* as a finite collection of faces of X_0 that form

a closed region homeomorphic to a disk, and we can consider its counterclockwise oriented boundary ∂D as a subgraph of X_0.

Definition For $v \in V(\Lambda)$ and $Q \in F(\Lambda)$, let P_v and P_Q be the closed paths on X connecting the midpoints of edges of Λ incident to v and Q, respectively, in counterclockwise direction. In Fig. 2, their vertices are colored gray. We say that P_v and P_Q are *discrete elementary cycles*.

2.2 Discrete Holomorphicity

To motivate the definition of discrete holomorphicity due to Mercat [21] that was also used previously in the rhombic setting by Duffin [10] and others, let us have a short look to the classical theory. There, a real differentiable complex function f defined on an open subset of the complex plane is holomorphic if and only if in any point all directional derivatives coincide. Moreover, holomorphic functions with nowhere-vanishing derivative preserve angles, and at a single point, infinitesimal lengths are uniformly scaled.

Definition Let $Q \in V(\Diamond) \cong F(\Lambda)$ and f be a complex function on the vertices b_-, w_-, b_+, w_+ of the quadrilateral Q. f is said to be *discrete holomorphic* at Q if the *discrete Cauchy-Riemann equation* is satisfied:

$$\frac{f(b_+) - f(b_-)}{b_+ - b_-} = \frac{f(w_+) - f(w_-)}{w_+ - w_-}.$$

Definition Let $f : V(\Lambda_0) \to \mathbb{C}$. f is said to be *discrete holomorphic* if f is discrete holomorphic at all $Q \in V(\Diamond_0)$.

Note that if a discrete holomorphic function f does not have the same value on both black vertices b_- and b_+, then it preserves the angle φ_Q and f uniformly scales the lengths of the diagonals of Q. However, the image of Q under f might be a degenerate or self-intersecting quadrilateral.

We immediately see that for discrete holomorphicity, only the differences at black and at white vertices matter. Hence, we should not consider constants on $V(\Lambda)$, but biconstants [20] determined by each a value on $V(\Gamma)$ and $V(\Gamma^*)$.

Definition A function $f : V(\Lambda_0) \to \mathbb{C}$ that is constant on $V(\Gamma_0)$ and constant on $V(\Gamma_0^*)$ is said to be *biconstant*.

In the following, we will define discrete analogs of ∂, $\bar{\partial}$, first of functions on $V(\Lambda)$ in Sect. 2.2.1 and later of functions on $V(\Diamond)$ in Sect. 2.2.3. Before, we introduce discrete differential forms in Sect. 2.2.2.

2.2.1 Discrete Derivatives of Functions on the Vertices of Λ

Definition Let $Q \in V(\diamondsuit) \cong F(\Lambda)$, and let f be a complex function on its vertices b_-, w_-, b_+, w_+. The *discrete derivatives* $\partial_\Lambda f$, $\bar{\partial}_\Lambda f$ are defined by

$$\partial_\Lambda f(Q) := \lambda_Q \frac{f(b_+) - f(b_-)}{b_+ - b_-} + \bar{\lambda}_Q \frac{f(w_+) - f(w_-)}{w_+ - w_-},$$
$$\bar{\partial}_\Lambda f(Q) := \bar{\lambda}_Q \frac{f(b_+) - f(b_-)}{\overline{b_+ - b_-}} + \lambda_Q \frac{f(w_+) - f(w_-)}{\overline{w_+ - w_-}},$$

where $2\lambda_Q := \exp\left(-i\left(\varphi_Q - \frac{\pi}{2}\right)\right) / \sin(\varphi_Q)$.

Remark Clearly, biconstant functions have vanishing discrete derivatives.

If the quadrilateral Q is a rhombus, then $\varphi_Q = \pi/2$ and $\lambda_Q = 1/2$. Therefore, the definition above then reduces to the previous one given by Chelkak and Smirnov [6]. The definition of discrete derivatives matches the notion of discrete holomorphicity; and the discrete derivatives approximate their smooth counterparts correctly up to order one for general quad-graphs and up to order two for parallelogram-graphs:

Proposition 2.1 *Let Q be a face of the quad-graph Λ and f be a complex function on its vertices b_-, w_-, b_+, w_+.*

(i) f is discrete holomorphic at Q if and only if $\bar{\partial}_\Lambda f(Q) = 0$.
(ii) For the function $f(v) = v$, $\bar{\partial}_\Lambda f(Q) = 0$ and $\partial_\Lambda f(Q) = 1$.
(iii) If Q is a parallelogram and $f(v) = v^2$, then $\bar{\partial}_\Lambda f(Q) = 0$, $\partial_\Lambda f(Q) = 2\hat{Q}$.
(iv) If Q is a parallelogram and $f(v) = |v|^2$, then $\bar{\partial}_\Lambda f(Q) = \overline{\partial_\Lambda f(Q)} = \hat{Q}$.

In parts (iii) and (iv), $\hat{Q}$ denotes the center of the parallelogram Q.

Proof (i) We observe that

$$\frac{2\sin(\varphi_Q)\bar{\lambda}_Q}{\overline{b_+ - b_-}} = \frac{\exp\left(i\left(\varphi_Q - \frac{\pi}{2}\right)\right)}{\overline{b_+ - b_-}} = \frac{-i\exp\left(i\varphi_Q\right)\frac{b_+ - b_-}{|b_+ - b_-|}}{|b_+ - b_-|} = \frac{-i\,(w_+ - w_-)}{|w_+ - w_-||b_+ - b_-|},$$
$$\frac{2\sin(\varphi_Q)\lambda_Q}{\overline{w_+ - w_-}} = \frac{\exp\left(i\left(\frac{\pi}{2} - \varphi_Q\right)\right)}{\overline{w_+ - w_-}} = \frac{i\exp\left(-i\varphi_Q\right)\frac{w_+ - w_-}{|w_+ - w_-|}}{|w_+ - w_-|} = \frac{i\,(b_+ - b_-)}{|w_+ - w_-||b_+ - b_-|}.$$

So if we multiply $\bar{\partial}_\Lambda f(Q)$ by $2i|w_+ - w_-||b_+ - b_-|\sin(\varphi_Q) \neq 0$, we obtain

$$(w_+ - w_-)\,(f\,(b_+) - f\,(b_-)) - (b_+ - b_-)\,(f\,(w_+) - f\,(w_-))\,,$$

which vanishes if and only if the discrete Cauchy-Riemann equation is satisfied.

(ii) Clearly, $f(v) = v$ satisfies the discrete Cauchy-Riemann equation. By the first part, $\bar{\partial}_\Lambda f(Q) = 0$. Due to $2\sin(\varphi_Q) = \exp\left(-i\left(\varphi_Q - \frac{\pi}{2}\right)\right) + \exp\left(i\left(\varphi_Q - \frac{\pi}{2}\right)\right)$, $\partial_\Lambda f(Q)$ simplifies to $\lambda_Q + \bar{\lambda}_Q = 1$.

(iii) For the function $f(v) = v^2$, the discrete Cauchy-Riemann equation is equivalent to $b_+ + b_- = w_+ + w_-$. But since Q is a parallelogram, both $(b_+ + b_-)/2$ and $(w_+ + w_-)/2$ equal its center $\hat{Q}$. Thus, f is discrete holomorphic at Q and

$$\partial_\Lambda f(Q) = \lambda_Q(b_+ + b_-) + \bar{\lambda}_Q(w_+ + w_-) = 2\hat{Q}(\lambda_Q + \bar{\lambda}_Q) = 2\hat{Q}.$$

(iv) Since f is a real function, $\bar{\partial}_\Lambda f(Q) = \overline{\partial_\Lambda f(Q)}$ follows straight from the definition. Let $z \in \mathbb{C}$ be arbitrary. If $g(v) := v\bar{z}$, then $\partial_\Lambda g(Q) = \bar{z}$ and $\partial_\Lambda \bar{g}(Q) = 0$ by the second part. So if we define the function $h(v) := |v - z|^2 = |v|^2 - v\bar{z} - \bar{v}z + |z|^2$, then $\overline{\partial_\Lambda h(Q)} = \overline{\partial_\Lambda f(Q)} - z$ using the second part and observing that constant functions have vanishing derivatives. Hence, the statement is invariant under translation, and it suffices to consider the case $\hat{Q} = 0$. Then, $b_+ = -b_-$ and $w_+ = -w_-$ since Q is a parallelogram. It follows that $f(b_-) = f(b_+)$ and $f(w_-) = f(w_+)$, so $\partial_\Lambda f(Q) = 0$.

Our first discrete analogs of classical theorems are immediate consequences of the discrete Cauchy-Riemann equation:

Proposition 2.2 *Let $f : V(\Lambda_0) \to \mathbb{C}$ be discrete holomorphic.*

(i) If f is purely imaginary or purely real, then f is biconstant.
(ii) If $\partial_\Lambda f \equiv 0$, then f is biconstant.

Proof (i) Let us assume that f is not biconstant. Then, without loss of generality, f is not constant on Γ_0. Since Γ_0 is connected, there are two adjacent vertices b_-, b_+ of Γ_0 such that $f(b_+) \neq f(b_-)$. Let $b_-, w_-, b_+, w_+ \in V(\Lambda_0)$ be the vertices of the interior face of Λ_0 with black diagonal b_-b_+. Due to the discrete Cauchy-Riemann equation,

$$\frac{f(w_+) - f(w_-)}{f(b_+) - f(b_-)} = \frac{w_+ - w_-}{b_+ - b_-}.$$

The left hand side is real and well-defined since f is purely imaginary or purely real and $f(b_+) \neq f(b_-)$. But the right hand side is not, contradicting the assumption that f is not biconstant.

(ii) Since f is discrete holomorphic,

$$\frac{f(b_+) - f(b_-)}{b_+ - b_-} = \frac{f(w_+) - f(w_-)}{w_+ - w_-}.$$

$\partial_\Lambda f \equiv 0$ then yields that both sides of the discrete Cauchy-Riemann equation equal zero, so f is constant on $V(\Gamma_0)$ and on $V(\Gamma_0^*)$ since both graphs are connected.

2.2.2 Discrete Differential Forms

In our paper, we mainly consider two type of functions, functions $f : V(\Lambda_0) \to \mathbb{C}$ and functions $h : V(\diamondsuit_0) \to \mathbb{C}$. An example for a function on $V(\diamondsuit_0)$ is $\partial_\Lambda f$.

Definition A *discrete one-form* ω is a complex function on the oriented edges of the medial graph X_0 such that $\omega(-e) = \omega(e)$ for any oriented edge e of X_0. Here, $-e$ denotes the edge e with opposite orientation.

The evaluation of ω at an oriented edge e of X_0 is denoted by $\int_e \omega$. If P is a directed path in X_0 consisting of oriented edges $e_1, e_2, \ldots, e_n$, then the *discrete integral* along P is $\int_P \omega = \sum_{k=1}^{n} \int_{e_k} \omega$. For closed paths P, we write $\oint_P \omega$ instead. If P is the oriented boundary of a topological disk D in $F(X_0)$, then we say that the discrete integral is a *discrete contour integral* with *discrete contour* P.

Since we consider the planar case, one-forms dz and $d\bar{z}$ are globally defined.

Definition The discrete one-forms dz and $d\bar{z}$ are given by $\int_e dz = e$ and $\int_e d\bar{z} = \bar{e}$ for any oriented edge e of X.

It turns out that discrete one-forms that actually come from discrete one-forms on Γ and Γ^* are of particular interest:

Definition A discrete one-form ω defined on the oriented edges of X_0 is of *type* $\diamondsuit$ if for any $Q \in V(\diamondsuit_0)$ there exist complex numbers p, q such that $\omega = pdz + qd\bar{z}$ on all edges $e = [Q, v]$, $v \in V(\Lambda_0)$ incident to Q. ω is of *type* Λ if for any $v \in V(\Lambda_0)$ there exist complex numbers p, q such that $\omega = pdz + qd\bar{z}$ on all edges $e = [Q, v]$, $Q \in V(\diamondsuit_0)$ incident to v.

Remark Discrete one-forms of type Λ do not play such an important role as discrete one-forms of type $\diamondsuit$, although they occur as discrete differentials of functions defined on $V(\diamondsuit_0)$. This will become clear in the end of Sect. 2.3.2, one of the reasons being that discrete one-forms of type Λ are not defined on discrete Riemann surfaces, but discrete one-forms of type $\diamondsuit$ are.

Definition A *discrete two-form* Ω is a complex function on the faces of X_0.

The evaluation of Ω at a face F of X_0 is denoted by $\iint_F \Omega$. If S is a set of faces $F_1, F_2, \ldots, F_n$ of X_0, then $\iint_S \Omega = \sum_{k=1}^{n} \iint_{F_k} \Omega$ is the *discrete integral* of Ω over S.

As we are mainly interested in functions $f : V(\Lambda_0) \to \mathbb{C}$ and $h : V(\diamondsuit_0) \to \mathbb{C}$, discrete two-forms of particular interest are those that vanish on faces of X_0 corresponding to vertices of either $\diamondsuit$ or Λ.

Definition A discrete two-form Ω defined on $F(X_0)$ is of *type* Λ if Ω vanishes on all faces of X_0 corresponding to $V(\diamondsuit_0)$ and of *type* $\diamondsuit$ if Ω vanishes on all faces of X corresponding to $V(\Lambda_0)$.

Remark These discrete two-forms correspond to functions on $V(\Lambda_0)$ or $V(\diamondsuit_0)$ by the discrete Hodge star that will be defined later in Sect. 2.3.3.

Since we did not give a precise embedding of the medial graph into the complex plane in the general case, we have to specify what the area of a face is. This area includes a factor of two in order to get the same coefficients in the discrete setup as in the smooth case.

Definition Let F be a face of the medial graph X. We define $\mathrm{ar}(F)$ to be twice the Euclidean area of the polygon that results from connecting adjacent vertices of F by straight line segments in the complex plane. In contrast, $\mathrm{area}(P)$ will always denote the Euclidean area of a polygon P.

Remark As we have mentioned before, our main objects either live on the quad-graph Λ or on its dual $\diamondsuit$. Thus, we have to deal with two different cellular decompositions at the same time. The medial graph has the crucial property that its faces are in one-to-one correspondence to vertices of Λ and of $\diamondsuit$, i.e., to faces of $\diamondsuit$ and of Λ. Furthermore, the Euclidean area of the Varignon parallelogram of $Q \in F(\Lambda)$ is just half of the area of Q. In some sense, a corresponding statement is true for the cells of X corresponding to vertices of Λ, i.e., faces of $\diamondsuit$. However, there is not only no canonical embedding of X, but also no natural embedding of $\diamondsuit$ in the general setting. But in the particular case of parallelogram-graphs, when we have a canonical embedding of X with rectilinear edges, we can make the statement precise: If an edge QQ' of $\diamondsuit$ is represented by the two line segments that connect the centers of the parallelograms Q and Q' with the midpoint of their common edge, then the Euclidean area of the face of X corresponding to a vertex $v \in V(\Lambda) \cong F(\diamondsuit)$ is exactly half of the area of the face of $\diamondsuit$ corresponding to v.

In summary, the medial graph allows us to deal with just one decomposition of the complex plane, but we have to count areas twice in order to get the right coefficients as in the continuous setup.

Definition The discrete two-forms Ω_Λ and $\Omega_\diamondsuit$ are defined as being zero on faces of X corresponding to vertices of $\diamondsuit$ or Λ, respectively, and defined by

$$\iint_{F_v} \Omega_\Lambda = -2i\,\mathrm{ar}(F_v) \text{ and } \iint_{F_Q} \Omega_\diamondsuit = -2i\,\mathrm{ar}(F_Q)$$

on faces F_v and F_Q corresponding to $v \in V(\Lambda)$ or $Q \in V(\diamondsuit)$. As defined above, $\mathrm{ar}(F)$ is twice the Euclidean area of the straight-line embedding of F_v or F_Q.

Remark Ω_Λ and $\Omega_\diamondsuit$ are the straightforward discretizations of $dz \wedge d\bar{z}$ having in mind that they are essentially defined on faces of $\diamondsuit$ or of Λ, respectively. It turns out that in local coordinates, we can perform our calculations with Ω_Λ and $\Omega_\diamondsuit$ in the discrete setting exactly as we do with $dz \wedge d\bar{z}$ in the smooth theory. We will see in Sect. 2.3.2 that $\Omega_\diamondsuit$ is indeed the discrete wedge product of dz and $d\bar{z}$ seen as discrete one-forms of type $\diamondsuit$. The same would be true for Ω_Λ if we considered dz and $d\bar{z}$ as being of type Λ, but the discrete wedge product is of interest just for discrete one-forms of type $\diamondsuit$ and we therefore define it just for these forms.

Definition Let $f : V(\Lambda_0) \to \mathbb{C}$, $h : V(\diamondsuit_0) \to \mathbb{C}$, ω a discrete one-form defined on the oriented edges of X_0, and Ω_1, Ω_2 discrete two-forms defined on $F(X_0)$ that are of type Λ and $\diamondsuit$, respectively. For any oriented edge $e = [Q, v]$ and any faces F_v, F_Q of X_0 corresponding to $v \in V(\Lambda_0)$ or $Q \in V(\diamondsuit_0)$, we define the products $f\omega$, $h\omega$, $f\Omega_1$, and $h\Omega_2$ by

$$\int_e f\omega := f(v)\int_e \omega \quad \text{and} \quad \iint_{F_v} f\Omega_1 := f(v)\iint_{F_v} \Omega_1, \iint_{F_Q} f\Omega_1 := 0;$$

$$\int_e h\omega := h(Q)\int_e \omega \quad \text{and} \quad \iint_{F_v} h\Omega_2 := 0, \qquad \iint_{F_Q} h\Omega_2 := h(Q)\iint_{F_Q} \Omega_2.$$

In the following table, we give a quick overview of various discrete differential forms (most of them will be discussed in Sect. 2.3) and state whether they are essentially functions on $V(\Lambda)$ (first column) or functions on $V(\diamondsuit)$ (second column) or entirely objects on the cellular decomposition X (third column). In the first row we find functions, in the second discrete one-forms, and in the third discrete two-forms. So for example, the intersection of the second row with the third column lists discrete one-forms that are entirely objects on X and cannot be reduced to functions on $V(\Lambda)$ or $V(\diamondsuit)$.

	Λ	$\diamondsuit$	X
functions	$f, g : V(\Lambda) \to \mathbb{C}$	$h_1, h_2 : V(\diamondsuit) \to \mathbb{C}$	$f \cdot g = \int (f dg + g df)$
	$\partial_\diamondsuit h, \partial_\diamondsuit h$	$\partial_\Lambda f, \partial_\Lambda f$	
1-forms	dh	df	$f dg + g df$
	$h_1 dz + h_2 d\bar{z}$	$f dz + g d\bar{z}$	$f h dz$
	η of type Λ	ω, ω' of type $\diamondsuit$	$f\omega$
2-forms	Ω_Λ	$\Omega_\diamondsuit$	
	$\star f$	$\star h$	
	$d\omega$	$d\eta$	$d(f h dz)$
	$f d\omega$	$\omega \wedge \omega'$	$d(f\omega)$

Remark Although discrete one-forms of type Λ or of type $\diamondsuit$ do not live themselves on Λ or $\diamondsuit$, they are described by two functions defined on the vertices of Λ or $\diamondsuit$, respectively.

2.2.3 Discrete Derivatives of Functions on the Faces of Λ

Before we pass on to discrete derivatives of functions on $V(\diamondsuit)$, we first prove an alternative formula for the discrete derivatives of functions on $V(\Lambda)$.

Lemma 2.3 *Let $Q \in V(\diamondsuit) \cong F(\Lambda)$ and f be a complex function on the vertices b_-, w_-, b_+, w_+ of Q. Let P_Q be the discrete elementary cycle around Q and F the face of X corresponding to Q. Then,*

$$\partial_\Lambda f(Q) = \frac{-1}{2i\,\mathrm{ar(F)}} \oint_{P_Q} f d\bar{z} \quad \text{and} \quad \bar{\partial}_\Lambda f(Q) = \frac{1}{2i\,\mathrm{ar(F)}} \oint_{P_Q} f dz.$$

Proof Since we think of F as a parallelogram (see Sect. 2.1.2), its Euclidean area is half of the area of Q. So by definition,

$$\mathrm{ar}(F) = \frac{1}{2}|b_+ - b_-||w_+ - w_-|\sin(\varphi_Q).$$

Furthermore, $f(b_+)$ and $-f(b_-)$ are multiplied by the same factor $\overline{(w_+ - w_-)}/2$ when evaluating the discrete contour integral $\oint_{P_Q} f d\bar{z}$. Therefore, the coefficient in front of $f(b_+) - f(b_-)$ in the right hand side of the first equation in the lemma is

$$i\frac{\overline{w_+ - w_-}}{4\mathrm{ar}(F)} = -\bar{i}\frac{\overline{w_+ - w_-}}{2\sin(\varphi_Q)|w_+ - w_-||b_+ - b_-|} = \frac{\exp\left(-i\left(\varphi_Q - \frac{\pi}{2}\right)\right)}{2\sin(\varphi_Q)(b_+ - b_-)} = \frac{\lambda_Q}{b_+ - b_-}$$

(compare with the proof of Proposition 2.1(i)), which is exactly the coefficient appearing in $\partial_\Lambda f(Q)$. Analogously, the coefficients in front of $f(w_+) - f(w_-)$ are equal. This shows the first equation. The second one follows from the first, noting that the coefficients in front of $f(b_+) - f(b_-)$ and $f(w_+) - f(w_-)$ on both sides of the second equation are just complex conjugates of the corresponding coefficients appearing in the first equation.

Inspired by Lemma 2.3 that is illustrated by Fig. 3a, we can now define the discrete derivatives for complex functions on $V(\Diamond)$, see Fig. 3b.

Definition Let $v \in V(\Lambda)$ and h be a complex function defined on all quadrilaterals that are incident to v. Let P_v be the discrete elementary cycle around v and F the face of X corresponding to v. Then, the *discrete derivatives* $\partial_\Diamond h$, $\bar{\partial}_\Diamond h$ at v are defined by

$$\partial_\Diamond h(v) := \frac{-1}{2i\,\mathrm{ar}(F)} \oint_{P_v} h d\bar{z} \quad \text{and} \quad \bar{\partial}_\Diamond h(v) := \frac{1}{2i\,\mathrm{ar}(F)} \oint_{P_v} h dz.$$

h is said to be *discrete holomorphic* at v if $\bar{\partial}_\Diamond h(v) = 0$.

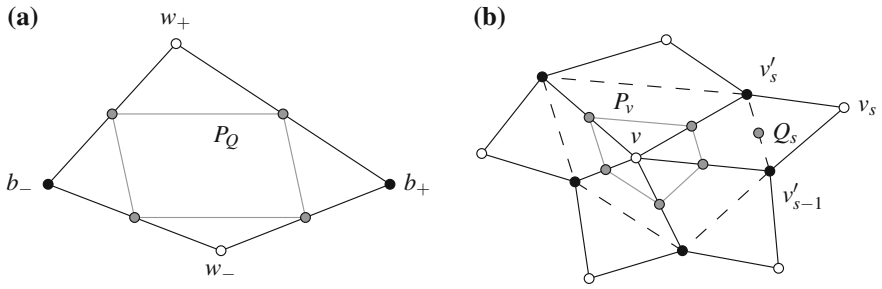

Fig. 3 Illustrations to the integration formulae for discrete derivatives. **a** Lemma 2.3 for ∂_Λ, $\bar{\partial}_\Lambda$. **b** Definitions of $\partial_\Diamond$, $\bar{\partial}_\Diamond$

Definition $h : V(\Diamond_0) \to \mathbb{C}$ is said to be *discrete holomorphic* if h is discrete holomorphic at all $v \in V(\Lambda_0)\backslash V(\partial\Lambda_0)$.

Note that in the rhombic case, our definition coincides with the one used by Chelkak and Smirnov in [6]. As an immediate consequence of the definition, we obtain a *discrete Morera's theorem*.

Proposition 2.4 *Functions $f : V(\Lambda_0) \to \mathbb{C}$ and $h : V(\Diamond_0) \to \mathbb{C}$ are discrete holomorphic if and only if $\oint_P f dz = 0$ and $\oint_P h dz = 0$ for all discrete contours P on X_0.*

Proof Clearly, $\oint_{P_v} f dz = f(v) \oint_{P_v} dz = 0$ for any discrete elementary cycle P_v around a vertex v of $V(\Lambda_0)$. Similarly, $\oint_{P_Q} h dz = 0$ for any $Q \in V(\Diamond_0)$. Using Lemma 2.3 and the definition of $\bar{\partial}_\Diamond$, f and h are discrete holomorphic if and only if $\oint_P f dz = 0$ and $\oint_P h dz = 0$ for all discrete elementary cycles P. To conclude the proof, we observe that any integration along a discrete contour can be decomposed into integrations along discrete elementary cycles since by definition, a discrete contour is the boundary of a topological disk in $F(X_0)$.

The discrete derivatives of constant functions on $V(\Diamond)$ vanish. As an analog of Proposition 2.1, we prove that the discrete derivatives $\partial_\Diamond, \bar{\partial}_\Diamond$ locally approximate their smooth counterparts correctly up to order one if the quadrilaterals in $V(\Diamond)$ are identified with the midpoints of their black or white edges. In a parallelogram-graph, these two midpoints coincide for each face, which then gives a global approximation statement. Note that even for rhombic quad-graphs, the discrete derivatives $\partial_\Diamond, \bar{\partial}_\Diamond$ generally do not coincide with the smooth derivatives in order two.

Proposition 2.5 *Let $v \in V(\Lambda)$, and let h be a complex function on all faces incident to v. As illustrated in Fig. 3b, we counterclockwise enumerate them by $Q_1, \ldots, Q_k$, where k is the degree of v in Λ, and their vertices adjacent to v by $v'_1, v'_2, \ldots, v'_k$, $v'_{k+1} = v_1$. Let $\hat{Q}_s = (v'_{s-1} + v'_s)/2$. Then, if $h(Q_s) = \hat{Q}_s$ for all s, $\bar{\partial}_\Diamond h(v) = 0$ and $\partial_\Diamond h(v) = 1$ hold true.*

Proof

$$
\begin{aligned}
4 \oint_{P_v} h dz &= \sum_{Q_s \sim v} 2h(Q_s)(v'_s - v'_{s-1}) = \sum_{Q_s \sim v} (v'_{s-1} + v'_s)(v'_s - v'_{s-1}) \\
&= \sum_{Q_s \sim v} \left((v'_s)^2 - (v'_{s-1})^2 \right) = 0, \\
4 \oint_{P_v} h d\bar{z} &= \sum_{Q_s \sim v} (v'_{s-1} + v'_s)\overline{(v'_s - v'_{s-1})} = \sum_{Q_s \sim v} \left(|v'_s|^2 - |v'_{s-1}|^2 - 2i \operatorname{Im}\left(v'_s \bar{v}'_{s-1}\right) \right) \\
&= -2i \sum_{Q_s \sim v} \operatorname{Im}\left(v'_s \bar{v}'_{s-1}\right) = -8i \operatorname{ar}(F_v).
\end{aligned}
$$

Thus, $\bar{\partial}_\diamondsuit h(v) = 0$ and $\partial_\diamondsuit h(v) = 1$. Here, we have used that by definition, $\mathrm{ar}(F_v)$ is half of the Euclidean area of the polygon $v'_1 v'_2 \dots v'_k$, so $\mathrm{ar}(F)$ equals

$$\frac{1}{2}\sum_{Q_s\sim v} \mathrm{area}(\triangle v v'_{s-1} v'_s) = \frac{1}{4}\sum_{Q_s\sim v} \mathrm{Im}\left((v'_s - v)\,\overline{(v'_{s-1} - v)}\right) = \frac{1}{4}\sum_{Q_s\sim v} \mathrm{Im}\left(v'_s \bar{v}'_{s-1}\right),$$

using that $\sum_{Q_s\sim v}\left(v\bar{v}'_{s-1} + \bar{v}v'_s\right) = \sum_{Q_s\sim v}\left(v\bar{v}'_s + \bar{v}v'_s\right)$ is real.

In [6], Chelkak and Smirnov used averaging operators to map functions on $V(\Lambda)$ to functions on $V(\diamondsuit)$ and vice versa. On parallelogram-graphs, the *averaging operator* $m(f)(Q) := \sum_{v\sim Q} f(v)/4$ actually maps discrete holomorphic functions f on $V(\Lambda)$ to discrete holomorphic functions on $V(\diamondsuit)$. Our proof will be similar as the one for rhombic quad-graphs in [6]. Note that discrete holomorphic functions on $V(\diamondsuit)$ cannot be averaged to discrete holomorphic functions on $V(\Lambda)$ in general, so the averaging operator of Chelkak of Smirnov that mapped functions on $V(\diamondsuit)$ to functions on $V(\Lambda)$ did not preserve discrete holomorphicity.

Proposition 2.6 *Let Λ be a parallelogram-graph and $f : V(\Lambda) \to \mathbb{C}$ be discrete holomorphic. Then, $m(f) : V(\diamondsuit) \to \mathbb{C}$ is discrete holomorphic.*

Proof Let us consider the star of the vertex $v \in V(\Lambda)$ and use the notation we used in Proposition 2.5 (illustrated by Fig. 3b). Since f is discrete holomorphic, the discrete Cauchy-Riemann equation is satisfied on any $Q_s \sim v$. Therefore, we can express $f(v_s)$ in terms of $f(v)$, $f(v'_s)$ and $f(v'_{s-1})$. Plugging this in the definition of the averaging operator, we obtain

$$\begin{aligned} 4m(f)(Q_s) &= 2f(v) + \frac{v_s - v + v'_s - v'_{s-1}}{v'_s - v'_{s-1}} f(v'_s) - \frac{v_s - v - v'_s + v'_{s-1}}{v'_s - v'_{s-1}} f(v'_{s-1}) \\ &= 2f(v) + 2\frac{v'_s - v}{v'_s - v'_{s-1}} f(v'_s) - 2\frac{v'_{s-1} - v}{v'_s - v'_{s-1}} f(v'_{s-1}). \end{aligned}$$

Here, we have used the properties $v_s - v'_{s-1} = v'_s - v$ and $v_s - v'_s = v'_{s-1} - v$ of the parallelogram Q_s. Hence, $m(f)$ is discrete holomorphic at v by definition due to

$$4\oint_{P_v} m(f)dz = 2f(v)\oint_{P_v} dz + \sum_{Q_s\sim v}(v'_s - v)f(v'_s) - \sum_{Q_s\sim v}(v'_{s-1} - v)f(v'_{s-1}) = 0.$$

Remark As mentioned above, our main interest lies in functions that are defined either on the vertices or the faces of the quad-graph. Now, extending $f : V(\Lambda) \to \mathbb{C}$ to a complex function on $F(X)$ by using its average $m(f)$ on $V(\diamondsuit)$ seems to be an option. However, functions on $V(\Lambda)$ and on $V(\diamondsuit)$ behave differently. In Corollary 2.11 we will see that $\partial_\Lambda f$ is discrete holomorphic if f is, but $\partial_\diamondsuit m(f)$ does not need to be discrete holomorphic in general. So to make sense of differentiating twice, we can only consider functions on $V(\Lambda)$.

Definition Let $f_1, f_2 : V(\Lambda_0) \to \mathbb{C}$ and $h_1, h_2 : V(\diamondsuit_0) \to \mathbb{C}$. Their *discrete scalar products* are defined as

$$\langle f_1, f_2 \rangle := -\frac{1}{2i} \iint_{F(X_0)} f_1 \bar{f}_2 \Omega_\Lambda \quad \text{and} \quad \langle h_1, h_2 \rangle := -\frac{1}{2i} \iint_{F(X_0)} h_1 \bar{h}_2 \Omega_\diamondsuit,$$

whenever the right hand side converges absolutely.

Proposition 2.7 *$-\partial_\diamondsuit$ and $-\bar{\partial}_\diamondsuit$ are the formal adjoints of $\bar{\partial}_\Lambda$ and ∂_Λ, respectively. That is, if $f : V(\Lambda) \to \mathbb{C}$ or $h : V(\diamondsuit) \to \mathbb{C}$ is compactly supported, then*

$$\langle \partial_\Lambda f, h \rangle + \langle f, \bar{\partial}_\diamondsuit h \rangle = 0 = \langle \bar{\partial}_\Lambda f, h \rangle + \langle f, \partial_\diamondsuit h \rangle.$$

Proof In Lemma 2.3, we showed how the discrete derivative $\partial_\Lambda f(Q)$ can be expressed as a contour integration around the face of X associated to $Q \in V(\diamondsuit)$. Using this, the definitions of Ω_Λ and $\Omega_\diamondsuit$, and $\partial_\diamondsuit \bar{h} = \overline{\bar{\partial}_\diamondsuit h}$, we get

$$\begin{aligned}
\langle \partial_\Lambda f, h \rangle + \langle f, \bar{\partial}_\diamondsuit h \rangle &= \sum_{Q \in V(\diamondsuit)} \partial_\Lambda f(Q) \bar{h}(Q) \mathrm{ar}(F_Q) + \sum_{v \in V(\Lambda)} f(v) \overline{\bar{\partial}_\diamondsuit h(v)} \mathrm{ar}(F_v) \\
&= \frac{i}{2} \sum_{Q \in V(\diamondsuit)} \bar{h}(Q) \oint_{P_Q} f d\bar{z} + \frac{i}{2} \sum_{v \in V(\Lambda)} f(v) \oint_{P_v} \bar{h} d\bar{z} \\
&= \frac{i}{2} \oint_P f \bar{h} d\bar{z} = 0,
\end{aligned}$$

where P is a large contour enclosing all the vertices of Λ and $\diamondsuit$ where f or h do not vanish. In particular, $f\bar{h}$ vanishes in a neighborhood of P. In the same way, $\langle \bar{\partial}_\Lambda f, h \rangle + \langle f, \partial_\diamondsuit h \rangle = 0$.

Remark Note that in their work on discrete complex analysis on rhombic quad-graphs, Kenyon [16] and Mercat [20] did not give explicit formulae for the discrete derivatives, but defined $-\partial_\diamondsuit$ and $-\bar{\partial}_\diamondsuit$ instead as the formal adjoints of the discrete derivatives $\bar{\partial}_\Lambda$ and ∂_Λ, respectively. In contrast, we derived the formal adjoint property from our explicit formulae for the discrete derivatives.

In Corollary 2.11, we will prove that $\partial_\Lambda f$ is discrete holomorphic if the function $f : V(\Lambda) \to \mathbb{C}$ is. Conversely, we can find discrete primitives of discrete holomorphic functions on subgraphs $\diamondsuit_0 \subseteq \diamondsuit$ that form a simply-connected closed region, extending the corresponding result for rhombic quad-graphs given by Chelkak and Smirnov [6].

Proposition 2.8 *Let $\diamondsuit_0 \subseteq \diamondsuit$ form a simply-connected closed region. Then, for any discrete holomorphic function h on $V(\diamondsuit_0)$, there is a discrete primitive $f := \int h$ on $V(\Lambda_0)$, i.e., f is discrete holomorphic and $\partial_\Lambda f = h$. f is unique up to two additive constants on Γ_0 and Γ_0^*.*

Proof Since h is discrete holomorphic, $\oint_P h dz = 0$ for any discrete contour P in X_0 by discrete Morera's Theorem 2.23. Therefore, hdz can be integrated to a well-defined function f_X on $V(X)$ that is unique up to an additive constant. The equation $f_X((v+w)/2) = (f(v)+f(w))/2$ for any edge (v, w) of Λ defines a function f on $V(\Lambda)$. Indeed, since $\diamondsuit_0$ forms a simply-connected closed region, it suffices to check the compatibility of the equations defining f just for one quadrilateral face Q. Now, the differences of f along the black and white diagonals of Q are given by integration of hdz along the edges of X that are parallel to these diagonals. Since hdz is a discrete one-form of type $\diamondsuit$, the two integrations along the edges of X parallel to one diagonal are the same if they are oriented the same, and compatibility follows. Given f_X, f is unique up to another additive constant.

In summary, f is unique up to two additive constants that can be chosen independently on Γ_0 and Γ_0^*. By construction, f satisfies

$$\frac{f(b_+) - f(b_-)}{b_+ - b_-} = h(Q) = \frac{f(w_+) - f(w_-)}{w_+ - w_-}$$

on any quadrilateral $Q \in V(\diamondsuit_0)$. So f is discrete holomorphic and $\partial_\Lambda f = h$.

2.3 Discrete Exterior Calculus

Our treatment of discrete exterior calculus is similar to the approach of Mercat in [19–21], but differs in some aspects. The main differences are due to our different notation of multiplication of functions with discrete one-forms, which allows us to define a discrete exterior derivative on a larger class of discrete one-forms in Sect. 2.3.1. It coincides with Mercat's discrete exterior derivative in the case of discrete one-forms of type $\diamondsuit$ that Mercat considers. In contrast, our definitions are based on a coordinate representation and mimic the smooth case. Eventually, they lead to essentially the same definitions of a discrete wedge product in Sect. 2.3.2 and a discrete Hodge star in Sect. 2.3.3 as in [21].

2.3.1 Discrete Exterior Derivative

Definition Let $f : V(\Lambda_0) \to \mathbb{C}$, $h : V(\diamondsuit_0) \to \mathbb{C}$. We define the *discrete exterior derivatives* df and dh as the discrete one-forms on oriented edges of X_0 given by

$$df := \partial_\Lambda f dz + \bar{\partial}_\Lambda f d\bar{z} \quad \text{and} \quad dh := \partial_\diamondsuit h dz + \bar{\partial}_\diamondsuit h d\bar{z}.$$

Definition Let ω be a discrete one-form defined on all boundary edges of a face F_v of the medial graph X corresponding to $v \in V(\Lambda)$ or on all four boundary edges of a face F_Q of X corresponding to $Q \in F(\Lambda)$. In the first case, we write $\omega = p dz + q d\bar{z}$ with functions p, q defined on all faces of Λ that are incident to v, and in the second case, we write $\omega = p dz + q d\bar{z}$ with functions p, q defined on all vertices of Λ that are incident to Q. The *discrete exterior derivative* $d\omega$ on F_v or F_Q is given by

$$d\omega|_{F_v} := \left(\partial_\diamond q - \bar{\partial}_\diamond p\right) \Omega_\Lambda \quad \text{and} \quad d\omega|_{F_Q} := \left(\partial_\Lambda q - \bar{\partial}_\Lambda p\right) \Omega_\diamond .$$

The representation of ω as $pdz + qd\bar{z}$ (p, q defined on edges of X) we have used above may be nonunique. However, $d\omega$ is well-defined by the following *discrete Stokes' theorem* that also justifies our definition of df and $d\omega$. Note that Mercat defined the discrete exterior derivative by the discrete Stokes' theorem [19].

Theorem 2.9 *Let $f : V(\Lambda_0) \to \mathbb{C}$ and ω be a discrete one-form defined on oriented edges of X_0. Then, for any directed edge e of X_0 starting in the midpoint of the edge vv'_- and ending in the midpoint of the edge vv'_+ of Λ_0 and for any finite collection of faces F of X_0 with counterclockwise oriented boundary ∂F we have:*

$$\int_e df = \frac{f(v'_+) - f(v'_-)}{2} = \frac{f(v) + f(v'_+)}{2} - \frac{f(v) + f(v'_-)}{2} \quad \text{and} \quad \iint_F d\omega = \oint_{\partial F} \omega .$$

Proof Let v_- be the other vertex of the quadrilateral Q with vertices v, v'_- and v'_+. Without loss of generality, let v be white. Since $df = \partial_\Lambda f dz + \bar{\partial}_\Lambda f d\bar{z}$, $\int_e df$ equals

$$\begin{aligned}
&\partial_\Lambda f \frac{v'_+ - v'_-}{2} + \bar{\partial}_\Lambda f \overline{\frac{v'_+ - v'_-}{2}} \\
=&\frac{1}{2}(\lambda_Q + \bar{\lambda}_Q)(f(v'_+) - f(v'_-)) + \frac{1}{2}\left(\bar{\lambda}_Q \frac{v'_+ - v'_-}{v - v_-} + \lambda_Q \overline{\frac{v'_+ - v'_-}{v - v_-}}\right)(f(v) - f(v_-)) \\
=&\frac{f(v'_+) - f(v'_-)}{2} + \mathrm{Re}\left(\bar{\lambda}_Q \frac{v'_+ - v'_-}{v - v_-}\right)(f(v) - f(v_-)) = \frac{f(v'_+) - f(v'_-)}{2}.
\end{aligned}$$

To get to the third line, we used $\lambda_Q + \bar{\lambda}_Q = 1$, and for the last step we used

$$\arg\left(\bar{\lambda}_Q \frac{v'_+ - v'_-}{v - v_-}\right) = \arg\left(\pm \exp\left(i\left(\varphi_Q - \frac{\pi}{2}\right)\right) \exp\left(-i\varphi_Q\right)\right) = \pm\pi/2.$$

The sign depends on whether v, v'_-, v_-, v'_+ denote the corners of Q in clockwise or counterclockwise order. In either case, the expression inside arg is purely imaginary.

The second identity has to be shown just for one single face of X_0. Let us write $\omega = pdz + qd\bar{z}$ on all edges of X_0 that are boundary edges of F_Q or F_v, where p, q are functions defined on the vertices of the quadrilateral $Q \in V(\diamondsuit_0)$ or on the faces incident to $v \in V(\Lambda_0)$. Then, by the representation of $\partial_\Lambda, \bar{\partial}_\Lambda$ as discrete contour integrals in Lemma 2.3 and the definition of the discrete derivatives $\partial_\diamond, \bar{\partial}_\diamond$,

$$\begin{aligned}
\iint_{F_Q} d\omega &= \iint_{F_Q} \left(\partial_\diamond q - \bar{\partial}_\diamond p\right) \Omega_\diamond = -2i\,\mathrm{ar}(F_Q)\left(\partial_\diamond q - \bar{\partial}_\diamond p\right) = \oint_{\partial F_Q} (pdz + qd\bar{z}), \\
\iint_{F_v} d\omega &= \iint_{F_v} \left(\partial_\Lambda q - \bar{\partial}_\Lambda p\right) \Omega_\Lambda = -2i\,\mathrm{ar}(F_v)\left(\partial_\Lambda q - \bar{\partial}_\Lambda p\right) = \oint_{\partial F_v} (pdz + qd\bar{z}).
\end{aligned}$$

Definition Let $\diamondsuit_0 \subseteq \diamondsuit$ form a simply-connected closed region. A discrete one-form ω defined on oriented edges of X_0 is said to be *closed* if $d\omega \equiv 0$.

Note that if ω is a discrete one-form of type $\diamondsuit$, then $\iint_F d\omega = 0$ for any face F corresponding to a face of Λ. Examples for closed discrete one-forms are discrete exterior derivatives of complex functions on $V(\Lambda)$:

Proposition 2.10 *Let $f : V(\Lambda_0) \to \mathbb{C}$. Then, $ddf = 0$ on any face F_v of X_0 corresponding to $v \in V(\Lambda_0)\backslash V(\partial\Lambda_0)$.*

Proof By discrete Stokes' Theorem 2.9, we have to show $\oint_P df = 0$ for any discrete elementary cycle P in X_0 in order to prove $ddf = 0$. Since df is of type $\diamondsuit$, the statement is trivially true if $P = P_Q$ for $Q \in V(\diamondsuit_0)$. So let $P = P_v$ for $v \in V(\Lambda_0)\backslash V(\partial\Lambda_0)$. Using discrete Stokes' Theorem 2.9 again,

$$\oint_{P_v} df = \sum_{Q_s \sim v} \frac{f(v'_s) - f(v'_{s-1})}{2} = 0.$$

An immediate corollary of the last proposition is the commutativity of discrete derivatives, generalizing the known result for rhombic quad-graphs in [6].

Corollary 2.11 *Let $f : V(\Lambda_0) \to \mathbb{C}$. Then, $\partial_\diamondsuit \bar{\partial}_\Lambda f(v) = \bar{\partial}_\diamondsuit \partial_\Lambda f(v)$ for all vertices $v \in V(\Lambda_0)\backslash V(\partial\Lambda_0)$. In particular, $\partial_\Lambda f$ is discrete holomorphic if f is discrete holomorphic.*

Proof Due to the preceding Proposition 2.10 and the definition of the discrete derivative, the equation $0 = ddf = \left(\partial_\diamondsuit \bar{\partial}_\Lambda f - \bar{\partial}_\diamondsuit \partial_\Lambda f\right) \Omega_\Lambda$ holds on all faces of X_0 corresponding to a vertex of Λ_0 that is not on the boundary $\partial\Lambda_0$. The claim follows since Ω_Λ is nonzero on these faces.

Remark Note that even in the generic rhombic case, $\partial_\Lambda \bar{\partial}_\diamondsuit h$ does not always equal $\bar{\partial}_\Lambda \partial_\diamondsuit h$ for a function $h : V(\diamondsuit) \to \mathbb{C}$ [6]. Hence, $ddh = 0$ cannot hold for such functions h in general.

Corollary 2.12 *Let $f : V(\Lambda_0) \to \mathbb{C}$. Then, f is discrete holomorphic if and only if $df = pdz$ for some $p : V(\diamondsuit_0) \to \mathbb{C}$. In the case that f is discrete holomorphic, p is discrete holomorphic as well.*

Proof Since all quadrilaterals $Q \in V(\diamondsuit_0)$ are nondegenerate, the representation of $df|_{\partial F_Q}$ as $pdz + qd\bar{z}$ is unique (see Lemma 2.14 below). Clearly, we have $df = \partial_\Lambda f dz + \bar{\partial}_\Lambda f d\bar{z}$. It follows that f is discrete holomorphic at Q if and only if $df|_{\partial F_Q} = pdz$.

Assuming that $df = pdz$ for some $p : V(\diamondsuit_0) \to \mathbb{C}$, $ddf = 0$ on any face F_v of X_0 corresponding to $v \in V(\Lambda_0)\backslash V(\partial\Lambda_0)$ by Proposition 2.10. Thus, $\bar{\partial}_\diamondsuit p(v) = 0$ for any such v and f is discrete holomorphic.

Definition Let $\diamondsuit_0 \subseteq \diamondsuit$ form a simply-connected closed region. A discrete one-form ω defined on the oriented edges of X_0 is *discrete holomorphic* if $\omega = pdz$ for some $p : V(\diamondsuit_0) \to \mathbb{C}$ and $d\omega = 0$.

Remark This notion recurs in the more general setting of discrete Riemann surfaces in [1]. By Corollary 2.12, df is discrete holomorphic if f is, and by Proposition 2.8 on the existence of a discrete primitive for discrete holomorphic functions defined on the vertices of a subset $\Diamond_0 \subseteq \Diamond$ that forms a simply-connected closed region, any discrete holomorphic one-form ω defined on the oriented edges of X_0 is the discrete exterior derivative of a discrete holomorphic function on $V(\Lambda_0)$.

Due to Chelkak and Smirnov [6], one of the unpleasant facts of all discrete theories of complex analysis is that (pointwise) multiplication of discrete holomorphic functions does not yield a discrete holomorphic function in general. We define a product of complex functions on $V(\Lambda)$ that is defined on $V(X)$ and a product of complex functions on $V(\Lambda)$ with functions on $V(\Diamond)$ that is defined on $E(X)$. In general, the product of two discrete holomorphic functions is not discrete holomorphic according to the classical quad-based definition (on planar quad-graphs different from Λ), but it will be discrete holomorphic in the sense that a discretization of its exterior derivative is closed and is of the form pdz, p defined on the edges of the medial graph of the new quad-graph, or in the sense that it fulfills a discrete Morera's theorem.

Proposition 2.13 *Let $f, g : V(\Lambda) \to \mathbb{C}$ and $h : V(\Diamond) \to \mathbb{C}$.*

(i) $fdg + gdf$ is a closed discrete one-form.
(ii) If f and h are discrete holomorphic, then $fhdz$ is a closed discrete one-form.

Proof (i) Let $\omega := fdg + gdf$. By Proposition 2.10, $ddf = 0$ and $ddg = 0$, i.e., df and dg are closed. Thus,

$$\oint_{\partial F_v} \omega = f(v) \oint_{\partial F_v} dg + g(v) \oint_{\partial F_v} df = 0$$

for any face F_v corresponding to $v \in V(\Lambda)$. Using Lemma 2.3 that relates discrete derivatives with discrete contour integration,

$$\begin{aligned} 2i\mathrm{ar}(F_Q) \oint_{\partial F_Q} \omega &= 2i\mathrm{ar}(F_Q) \oint_{\partial F_Q} \left(f\partial_\Lambda g dz + f\bar{\partial}_\Lambda g d\bar{z} + g\partial_\Lambda f dz + g\bar{\partial}_\Lambda f d\bar{z} \right) \\ &= \left(\bar{\partial}_\Lambda f \partial_\Lambda g - \partial_\Lambda f \bar{\partial}_\Lambda g + \bar{\partial}_\Lambda g \partial_\Lambda f - \partial_\Lambda g \bar{\partial}_\Lambda f \right)(Q) = 0 \end{aligned}$$

for any face F_Q corresponding to $Q \in F(\Lambda)$. It follows by discrete Stokes' Theorem 2.9 that $d\omega = 0$.

(ii) By discrete Morera's Theorem 2.23, discrete holomorphicity of f and h implies that fdz and hdz are closed. Thus, $\oint_{\partial F_v} fhdz = f(v) \oint_{\partial F_v} hdz = 0$ as well as $\oint_{\partial F_Q} fhdz = h(Q) \oint_{\partial F_Q} fdz = 0$ for any faces F_v and F_Q of X corresponding to $v \in V(\Lambda)$ and $Q \in F(\Lambda)$. Therefore, $fhdz$ is closed.

Remark In particular, for any $f, g : V(\Lambda) \to \mathbb{C}$ a product $f \cdot g : V(X) \to \mathbb{C}$ can be defined by integration of $fdg + gdf$. Note that this product $f \cdot g$ is defined up to

an additive constant. Furthermore, $f \cdot h : E(X) \to \mathbb{C}$ can be defined by "pointwise" multiplication. If f, g, h are discrete holomorphic, then $fdg + gdf = pdz$ is closed, where $p = f \cdot \partial_\Lambda g + g \cdot \partial_\Lambda f : E(X) \to \mathbb{C}$, and so to say a discrete holomorphic one-form, meaning that $f \cdot g$ is discrete holomorphic in this sense. Similarly, $fhdz$ is closed, so $f \cdot h$ is discrete holomorphic in the sense that a discrete Morera's theorem holds true. Even though $f \cdot g$ is defined on the vertices of the dual of a planar quad-graph different from Λ, as well is $f \cdot h$ on the dual of a different planar quad-graph, these products are generally not discrete holomorphic everywhere according to the quad-based definition of discrete holomorphicity on the dual of a bipartite quad-graph given by the definition in Sect. 2.2.3. To define the mentioned planar quad-graphs, we identify $Q \in V(\Diamond)$ with such a point in the interior of the face Q that all line segments connecting it to the four corners of Q lie inside the quadrilateral.

First, $f \cdot g$ is a complex function on the vertices of X. The medial graph X is the dual of the bipartite quad-graph with vertex set $V(\Lambda) \sqcup V(\Diamond)$, edges connecting points $Q \in V(\Diamond)$ with all incident vertices $v \in V(\Lambda)$, and faces in one-to-one correspondence to edges of Λ. But even if f and g are discrete holomorphic on $V(\Lambda)$, $f \cdot g$ does not need to be a discrete holomorphic function on the faces of the quad-graph we just defined. For example, consider $f(v) = 0$ if v is black and $f(v) = 1$ if v is white and a discrete holomorphic g that is not biconstant. Then, the product $f \cdot g$ is not discrete holomorphic at all $Q \in V(\Diamond)$ (seen as vertices of the quad-graph described above) where $\partial_\Lambda g(Q) \neq 0$.

Second, $f \cdot h$ is a complex function on the edges of X, so it is a function on the vertices of the medial graph of X. The medial graph of the medial graph of Λ is the dual of the quad-graph with vertex set $(V(\Lambda) \cup V(\Diamond)) \sqcup V(X)$, edges connecting points $v \in V(\Lambda)$ or $Q \in V(\Diamond)$ with the midpoints of all incident edges, and each face being in one-to-one correspondence to an edge of X. Since $fhdz$ is closed, $f \cdot h$ is discrete holomorphic on the new quad-graph at vertices of Λ or $\Diamond$ by discrete Morera's Theorem 2.23. But there is no need for $f \cdot h$ to be discrete holomorphic at vertices of X, even for constant h. For example, take the function f defined by $f(v) = 0$ if v is black and $f(v) = 1$ if v is white.

In summary, we defined products $f \cdot g$ and $f \cdot h$, where $f, g : V(\Lambda) \to \mathbb{C}$ and $h : V(\Diamond) \to \mathbb{C}$ are discrete holomorphic, that are local (on each vertex, they depend just on the values of f and g in a small neighborhood) and discrete holomorphic at least in the sense that its discrete exterior derivative is closed and of the form pdz or in the sense that it fulfills a discrete Morera's theorem.

Somehow missing is a product $h \cdot h'$, where $h, h' : V(\Diamond) \to \mathbb{C}$. In the general case, we do not know an appropriate product so far. But we want to point out that Chelkak and Smirnov showed in [7] that for so-called *spin holomorphic* functions h, h', the pointwise product satisfies $\operatorname{Re}\left(\bar{\partial}_\Diamond \left(h \cdot h'\right)\right) \equiv 0$.

2.3.2 Discrete Wedge Product

Following Whitney [27], Mercat defined in [19] a discrete wedge product for discrete one-forms living on the edges of Λ. Then, the discrete exterior derivative defined by

a discretization of Stokes' theorem is a derivation for the discrete wedge product. However, a discrete Hodge star cannot be defined on Λ. To circumvent this problem, Mercat used an averaging map to relate discrete one-forms on the edges of Λ with discrete one-forms on the edges of Γ and Γ^*, i.e., discrete one-forms of type $\diamondsuit$. Then, he could define a discrete Hodge star; however, the discrete exterior derivative was not a derivation for the now heterogeneous discrete wedge product.

In this section, a different interpretation of the discrete wedge product is proposed. Still, the notions of Mercat in [19–21] are recovered. Starting with discrete one-forms of type $\diamondsuit$ that are defined on the edges of X, a discrete wedge product on (half of) the faces of X is defined. This definition is different from Whitney's [27] and has the advantage that both a discrete wedge product and a discrete Hodge star can be defined on the same structure. In addition, the discrete exterior derivative is now a derivation for the discrete wedge product in a well-defined sense, see Theorem 2.16. It turns out that Theorem 2.16 is a powerful tool leading to discretizations of Green's identities in Sect. 2.4.1 and of a Cauchy's integral formula for the discrete derivative of a discrete holomorphic function in Sect. 2.6.

Lemma 2.14 *Let ω be a discrete one-form of type $\diamondsuit$ defined on the oriented edges of X_0. Then, there is a unique representation $\omega = pdz + q d\bar{z}$ with $p, q : V(\diamondsuit_0) \to \mathbb{C}$. On a quadrilateral $Q \in V(\diamondsuit_0)$, p and q are given by*

$$p(Q) = \lambda_Q \frac{\int_e \omega}{e} + \bar{\lambda}_Q \frac{\int_{e^*} \omega}{e^*} \quad \text{and} \quad q(Q) = \bar{\lambda}_Q \frac{\int_e \omega}{\bar{e}} + \lambda_Q \frac{\int_{e^*} \omega}{\bar{e}^*}.$$

Here, e is an oriented edge of X_0 parallel to a black edge of Γ_0, and e^* is parallel to a white edge of Γ_0^*.

Proof First, we show that a representation $\omega|_{\partial F_Q} = pdz + q d\bar{z}$ exists for any face F_Q of X_0 corresponding to a quadrilateral $Q \in V(\diamondsuit_0)$. Given ω, we have to solve the system of linear equations $\int_{e_Q} \omega = p \int_{e_Q} dz + q \int_{e_Q} d\bar{z}$ for all four boundary edges e_Q of F_Q. Since ω is of type $\diamondsuit$, we just have to consider two equations, namely one for a boundary edge e_b of F_Q parallel to a black edge of Γ_0 and one equation for a boundary edge e_w parallel to a white edge of Γ_0^*. Since all quadrilaterals are nondegenerate, the diagonals are not parallel to each other and it follows that the pair $(dz, d\bar{z})$ gives different values when integrated over e_b and e_w. Thus, this system of two linear equations in two variables is nondegenerate. It follows that p, q are uniquely defined on $V(\diamondsuit_0)$.

Furthermore, we can find for any quadrilateral $Q \in V(\diamondsuit_0) \cong F(\Lambda_0)$ a function f that is defined on the vertices $b_\pm, w_\pm$ of Q such that $2\int_e \omega = f(b_+) - f(b_-)$ and $2\int_{e^*} \omega = f(w_+) - f(w_-)$, where e is one of the two oriented edges of X_0 going from the midpoint of b_- and $w_\pm$ to the midpoint of b_+ and $w_\pm$, and e^* is one of the two edges connecting the midpoint of w_- and $b_\pm$ with the midpoint of w_+ and $b_\pm$. By discrete Stokes' Theorem 2.9, we get $\omega|_{\partial F_Q} = df = pdz + q d\bar{z}$ with $p = \partial_\Lambda f(Q)$ and $q = \bar{\partial}_\Lambda f(Q)$. Replacing the differences of f in the definition of the discrete derivative by discrete integrals of ω yields the desired result.

Definition Let $\omega = pdz + qd\bar{z}$ and $\omega' = p'dz + q'd\bar{z}$ be two discrete one-forms of type $\diamondsuit$ defined on the oriented edges of X_0. Here, $p, p', q, q' : V(\diamondsuit_0) \to \mathbb{C}$ are given by the above Lemma 2.14. Then, the *discrete wedge product* $\omega \wedge \omega'$ is defined as the discrete two-form of type $\diamondsuit$ defined on $F(X_0)$ that equals

$$\left(pq' - qp'\right) \Omega_\diamondsuit$$

on faces of X corresponding to interior faces of the quad-graph Λ_0.

Remark Note that if one considers dz and $d\bar{z}$ as discrete one-forms of type $\diamondsuit$, then $\Omega_\diamondsuit = dz \wedge d\bar{z}$.

Proposition 2.15 *Let F be a face of X_0 corresponding to $Q \in F(\Lambda_0)$, and let e, e^* be oriented edges of X parallel to the black and white diagonal of the quadrilateral Q, respectively, such that* $\operatorname{Im}(e^*/e) > 0$. *If ω, ω' are discrete one-forms of type $\diamondsuit$ defined on the oriented edges of ∂F, then*

$$\iint\limits_F \omega \wedge \omega' = 2 \int\limits_e \omega \int\limits_{e^*} \omega' - 2 \int\limits_{e^*} \omega \int\limits_e \omega'.$$

Proof Both sides of the equation are bilinear and antisymmetric in ω, ω'. Hence, it suffices to check the identity for $\omega = dz$, $\omega' = d\bar{z}$. On the left hand side, we get $\iint_F \omega \wedge \omega' = -2i\operatorname{ar}(F)$. This equals the right hand side

$$2e\bar{e}^* - 2e^*\bar{e} = 4i \operatorname{Im}(e\bar{e}^*) = -i|2e||2e^*| \sin(\varphi_Q) = -2i\operatorname{ar}(F).$$

Remark Since the complex numbers e and e^* are just half of the oriented diagonals, the above definition of the discrete wedge product is essentially the same as the one given by Mercat in [19–21].

The discrete exterior derivative is a derivation for the discrete wedge product if one considers functions on Λ and discrete one-forms of type $\diamondsuit$:

Theorem 2.16 *Let $f : V(\Lambda_0) \to \mathbb{C}$ and ω be a discrete one-form of type $\diamondsuit$ defined on the oriented edges of X_0. Then, the following identity holds on $F(X_0)$:*

$$d(f\omega) = df \wedge \omega + f d\omega.$$

Proof Let $\omega = pdz + qd\bar{z}$ with $p, q : V(\diamondsuit_0) \to \mathbb{C}$ given by Lemma 2.14. If F_v and F_Q are faces of X_0 corresponding to a vertex v and a face Q of Λ_0, then

$$\begin{aligned} d(f\omega)|_{F_v} &= \left(f(v)\left(\partial_\diamondsuit q\right)(v) - f(v)\left(\bar{\partial}_\diamondsuit p\right)(v)\right)\Omega_\Lambda = f d\omega|_{F_v}, \\ d(f\omega)|_{F_Q} &= \left(q(Q)\left(\partial_\Lambda f\right)(Q) - p(Q)\left(\bar{\partial}_\Lambda f\right)(Q)\right)\Omega_\diamondsuit = (df \wedge \omega)|_{F_Q}. \end{aligned}$$

But $(df \wedge \omega)|_{F_v} = 0$ since $\Omega_\diamondsuit|_{F_v} = 0$ and $f d\omega|_{F_Q} = 0$ since ω is of type $\diamondsuit$, so $d(f\omega) = df \wedge \omega + f d\omega$.

Remark In [19], Mercat formulated an analog of the above Theorem 2.16 in a setting where discrete one-forms are defined on edges of Λ. In the setting of discrete one-forms defined on edges of Γ and Γ^*, the claim $d(f\omega) = df \wedge \omega + f d\omega$ could not be well-defined.

Above, a discrete wedge product just of two discrete one-forms of type $\diamondsuit$ is defined. Actually, we could define a discrete wedge product of two discrete one-forms of type Λ in essentially the same way, getting a discrete two-form of type Λ. Then, the analog of Theorem 2.16 would be true for this kind of discrete wedge product and functions on $V(\diamondsuit_0)$. Also the discrete Hodge star of a discrete one-form in the next section could be defined not only for those of type $\diamondsuit$. However, there exist no analogs of Propositions 2.15 and 2.18. These propositions imply that the discrete wedge product as well as the discrete Hodge star of discrete one-forms of type $\diamondsuit$ can be defined in a chart-independent way. This enables one to consider these objects on discrete Riemann surfaces, see [1]. There are no such statements if one chooses discrete one-forms of type Λ. In fact, a discrete one-form of type Λ cannot be canonically defined on a discrete Riemann surface as opposed to discrete one-forms of type $\diamondsuit$. So since our interest lies in the latter, we do not define a discrete wedge product or a discrete Hodge star for discrete one-forms of type Λ.

2.3.3 Discrete Hodge Star

Definition Let $f : F(\Lambda_0) \to \mathbb{C}$ and $h : V(\diamondsuit_0) \to \mathbb{C}$, let $\omega = p dz + q d\bar{z}$ be a discrete one-form of type $\diamondsuit$ defined on oriented edges of X_0 with $p, q : V(\diamondsuit_0) \to \mathbb{C}$, and let $\Omega_1, \Omega_2 : F(X_0) \to \mathbb{C}$ be discrete two-forms of type Λ and $\diamondsuit$. Then, the *discrete Hodge star* is given by

$$\star f := -\frac{1}{2i} f \Omega_\Lambda; \quad \star h := -\frac{1}{2i} h \Omega_\diamondsuit; \quad \star\omega := -ip dz + iq d\bar{z};$$
$$\star\Omega_1 := -2i \frac{\Omega_1}{\Omega_\Lambda}; \quad \star\Omega_2 := -2i \frac{\Omega_2}{\Omega_\diamondsuit}.$$

If ω and ω' are both discrete one-forms of type $\diamondsuit$ defined on oriented edges of X_0, we define their *discrete scalar product*

$$\langle \omega, \omega' \rangle := \iint_{F(X_0)} \omega \wedge \star\bar{\omega}',$$

whenever the right hand side converges absolutely. Similarly, a discrete scalar product for discrete two-forms of the same type is defined.

Remark As in the classical theory, the Hodge star corresponds to a $\pi/2$-rotation: $\int_{ie} \star\omega = \int_e \omega$ where ω is a discrete one-form of type $\diamondsuit$, e an oriented edge of X and ie its (virtual) image under $\pi/2$-rotation around the origin.

Corollary 2.17 *The following statements are true:*

(i) $\star^2 = -Id$ *on discrete one-forms of type* $\diamondsuit$ *defined on oriented edges of* X_0.
(ii) $\star^2 = Id$ *on complex functions on* $V(\Lambda_0)$ *or* $V(\diamondsuit_0)$ *and discrete two-forms defined on* $F(X_0)$ *of type* Λ *or* $\diamondsuit$.
(iii) $f : V(\Lambda_0) \to \mathbb{C}$ *is discrete holomorphic if and only if* $\star df = -i df$.
(iv) $\langle f_1, f_2\rangle = \iint_{F(X_0)} f_1 \star \overline{f_2}$ *for functions* $f_1, f_2 : V(\Lambda_0) \to \mathbb{C}$ *and* $\langle h_1, h_2\rangle = \iint_{F(X_0)} h_1 \star \overline{h_2}$ *for functions* $h_1, h_2 : V(\diamondsuit_0) \to \mathbb{C}$.
(v) $\langle \cdot, \cdot \rangle$ *is a Hermitian scalar product on discrete differential forms (of type* Λ *or of type* $\diamondsuit$*).*

Proposition 2.18 *Let* $Q \in V(\diamondsuit)$*, and let* e, e^* *be oriented edges of* X *parallel to the black and white diagonal of* Q*, respectively, such that* $\operatorname{Im}(e^*/e) > 0$*. If* ω *is a discrete one-form of type* $\diamondsuit$ *defined on the oriented edges of the boundary of the face of* X *corresponding to* Q*, then*

$$\int_e \star\omega = \cot(\varphi_Q) \int_e \omega - \frac{|e|}{|e^*| \sin(\varphi_Q)} \int_{e^*} \omega,$$
$$\int_{e^*} \star\omega = \frac{|e^*|}{|e| \sin(\varphi_Q)} \int_e \omega - \cot(\varphi_Q) \int_{e^*} \omega.$$

Proof Both sides of any of the two equations are linear and behave the same under complex conjugation. Thus, it suffices to check the statement for $\omega = dz$. Hence, it remains to show that

$$-ie = \cot(\varphi_Q)\, e - \frac{|e|}{|e^*| \sin(\varphi_Q)} e^* \quad \text{and} \quad e^* = \frac{|e^*|}{|e| \sin(\varphi_Q)} e - \cot(\varphi_Q)\, e^*.$$

Now, both sides of the first equation behave the same under scaling and simultaneous rotation of e and e^*, the same statement is true for the second equation. Thus, we may assume $e = 1$ and $e^* = \cos(\varphi_Q) + i \sin(\varphi_Q)$. Multiplying both equations by $\sin(\varphi_Q)$ gives the equivalent statements

$$-i \sin(\varphi_Q) = \cos(\varphi_Q) - \left(\cos(\varphi_Q) + i \sin(\varphi_Q)\right),$$
$$-i \sin(\varphi_Q) \exp(i\varphi_Q) = 1 - \cos(\varphi_Q) \exp(i\varphi_Q).$$

Both equations are true, noting that $\cos(\varphi_Q) - i \sin(\varphi_Q) = \exp(-i\varphi_Q)$.

Remark Proposition 2.18 shows that our definition of a discrete Hodge star on discrete one-forms coincides with Mercat's definition given in [21]. But on discrete

two-forms and complex functions, our definition of the discrete Hodge star includes an additional factor of the area of the corresponding face of X.

Proposition 2.19 *$\delta := - \star d \star$ is the formal adjoint of the discrete exterior derivative d: Let $f : V(\Lambda) \to \mathbb{C}$, and let ω be a discrete one-form of type $\Diamond$ defined on the oriented edges of X and $\Omega : F(X) \to \mathbb{C}$ a discrete two-form of type Λ. Assume that all of them are compactly supported. Then,*

$$\langle df, \omega \rangle = \langle f, \delta\omega \rangle \text{ and } \langle d\omega, \Omega \rangle = \langle \omega, \delta\Omega \rangle.$$

Proof By the assumption that all forms are compactly supported, we can take a large enough finite $\Diamond_0 \subseteq \Diamond$ that forms a simply-connected closed region such that f, ω, Ω vanish outside $\Lambda_0, X_0, \Diamond_0$ and ω is zero on the boundary ∂X_0. By discrete Stokes' Theorem 2.9 and Theorem 2.16 that states that the discrete exterior derivative is a derivation for the discrete wedge product,

$$0 = \oint_{\partial X_0} f \star \bar{\omega} = \iint_{F(X_0)} d(f \star \bar{\omega}) = \iint_{F(X_0)} f d \star \bar{\omega} + \iint_{F(X_0)} df \wedge \star\bar{\omega} = \langle f, \star d \star \omega \rangle + \langle df, \omega \rangle,$$

$$0 = \oint_{\partial X_0} \star\bar{\Omega}\omega = \iint_{F(X_0)} d(\star\bar{\Omega}\omega) = \iint_{F(X_0)} \star\bar{\Omega} d\omega + \iint_{F(X_0)} (d \star \bar{\Omega}) \wedge \omega = \langle d\omega, \Omega \rangle - \langle \omega, \delta\Omega \rangle.$$

In the last equalities, we have used Corollary 2.17(ii) and (iv) (the basic properties of the discrete Hodge star) and the observation that complex conjugation commutes with the discrete Hodge star and the discrete exterior derivative. The latter observation immediately follows from the definitions that mimic the classical theory.

2.4 Discrete Laplacian

The discrete Laplacian and the discrete Dirichlet energy on general quad-graphs were introduced by Mercat in [21]. Later, Skopenkov reintroduced these definitions in [23], taking the same definition in a different notation. In our discussion of the discrete Laplacian in Sect. 2.4.1, we follow the classical approach of Mercat (up to sign) and adapt it to our notations. A feature of the medial graph approach is that it allows to formulate a discrete analog of Green's first identity from which discrete Green's second identity immediately follows.

In Sect. 2.4.2, the discrete Dirichlet energy is investigated. In particular, in Theorem 2.30 it is shown how uniqueness and existence of solutions to the discrete Dirichlet boundary value problem imply surjectivity of the discrete derivatives and the discrete Laplacian. We conclude this section with a result concerning the asymptotics of discrete harmonic functions.

2.4.1 Definition and Basic Properties

Definition The *discrete Laplacian* on functions $f : V(\Lambda) \to \mathbb{C}$, discrete one-forms of type $\diamondsuit$, or discrete two-forms of type Λ is defined as the linear operator

$$\triangle := -\delta d - d\delta = \star d \star d + d \star d \star .$$

For a connected subgraph $\diamondsuit_0 \subseteq \diamondsuit$ and $f : V(\Lambda_0) \to \mathbb{C}$, $\triangle f$ is still defined by the formula above as a complex function on $V(\Lambda_0)\backslash V(\partial\Lambda_0)$. f is said to be *discrete harmonic* at $v \in V(\Lambda_0)\backslash V(\partial\Lambda_0)$ if $\triangle f(v) = 0$. f is *discrete harmonic* if it is discrete harmonic at all such v.

The following factorization of the discrete Laplacian in terms of discrete derivatives generalizes the corresponding result given by Chelkak and Smirnov in [6] to general quad-graphs. The local representation of $\triangle f$ at $v \in V(\Lambda)$ is, up to a factor involving the area of the face F_v of X corresponding to v, the same as Mercat's [21].

Corollary 2.20 *Let* $f : V(\Lambda_0) \to \mathbb{C}$. *Then,* $\triangle f(v) = 4\partial_\diamondsuit \bar{\partial}_\Lambda f(v) = 4\bar{\partial}_\diamondsuit \partial_\Lambda f(v)$ *for all vertices* $v \in V(\Lambda_0)\backslash V(\partial\Lambda_0)$ *and*

$$\triangle f(v) = \frac{1}{2ar(F_v)} \sum_{Q_s \sim v} \frac{1}{\mathrm{Re}\,(\rho_s)} \left(|\rho_s|^2 \left(f(v_s) - f(v)\right) + \mathrm{Im}\,(\rho_s) \left(f(v'_s) - f(v'_{s-1})\right)\right).$$

Here, $\rho_s := \rho_{Q_s}$ *if* v *is black, and* $\rho_s := 1/\rho_{Q_s}$ *if* v *is white.*
In particular, $\mathrm{Re}(\triangle f) \equiv \triangle \mathrm{Re}(f)$ *and* $\mathrm{Im}(\triangle f) \equiv \triangle \mathrm{Im}(f)$.

Proof Since the definitions of the discrete Hodge star and the discrete exterior derivative mimic the classical theory and $\partial_\diamondsuit \bar{\partial}_\Lambda f(v) = \bar{\partial}_\diamondsuit \partial_\Lambda f(v)$ by Corollary 2.11,

$$\triangle f(v) = \star d \star df(v) = 2\partial_\diamondsuit \bar{\partial}_\Lambda f(v) + 2\bar{\partial}_\diamondsuit \partial_\Lambda f(v) = 4\partial_\diamondsuit \bar{\partial}_\Lambda f(v) = 4\bar{\partial}_\diamondsuit \partial_\Lambda f(v)$$

holds exactly as in the smooth setting.

For the second statement, let us assume without loss of generality that $v \in V(\Gamma_0)$. Then, we have to show that

$$\triangle f(v) = \frac{1}{2\mathrm{ar}(F_v)} \sum_{Q_s \sim v} \left(\frac{|\rho_{Q_s}|}{\sin(\varphi_{Q_s})} \left(f(v_s) - f(v)\right) - \cot(\varphi_{Q_s}) \left(f(v'_s) - f(v'_{s-1})\right)\right).$$

The structure is similar to the formula of the discrete Hodge star in Proposition 2.18. Indeed, if e_s denotes an edge of X parallel to the black diagonal vv_s and e_s^* an edge parallel to the dual diagonal, then

$$\begin{aligned}\triangle f(v) =& \frac{1}{\operatorname{ar}(F_v)} \iint_{F_v} d \star df = \frac{1}{\operatorname{ar}(F_v)} \oint_{\partial F_v} \star df \\ =& \frac{1}{\operatorname{ar}(F_v)} \sum_{Q_s \sim v} \left(\frac{|e_s^*|}{|e_s| \sin(\varphi_{Q_s})} \int_{e_s} df - \cot(\varphi_{Q_s}) \int_{e_s^*} df \right) \\ =& \frac{1}{2\operatorname{ar}(F_v)} \sum_{Q_s \sim v} \left(\frac{|\rho_{Q_s}|}{\sin(\varphi_{Q_s})} \left(f(v_s) - f(v)\right) - \cot(\varphi_{Q_s}) \left(f(v_s') - f(v_{s-1}')\right) \right),\end{aligned}$$

using discrete Stokes' Theorem 2.9 in the first and third equality, Proposition 2.18 that compares the integration of the discrete Hodge star of a discrete one-form of type $\diamondsuit$ with the integration of the discrete one-form df itself in the second equality, and $|\rho_{Q_s}| = |e_s^*|/|e_s|$ for the last step.

Remark In the case when the diagonals of the quadrilaterals are orthogonal to each other, ρ_Q is always a positive real number. In this case, the discrete Laplacian splits into two separate discrete Laplacians on Γ and Γ^*. In this case, it is known and actually an immediate consequence of the local representation in Corollary 2.20 that a discrete maximum principle holds true, i.e., a discrete harmonic function can attain its maximum only at the boundary of a closed region. This is not true for general quad-graphs, see for example Skopenkov's paper [23].

Corollary 2.21 *Let $f : V(\Lambda_0) \to \mathbb{C}$.*

(i) If f is discrete harmonic, then $\partial_\Lambda f$ is discrete holomorphic.
(ii) If f is discrete holomorphic, then f, $\operatorname{Re} f$, and $\operatorname{Im} f$ are discrete harmonic.

Proof By Corollary 2.20, $\triangle f \equiv 4\bar{\partial}_\diamondsuit \partial_\Lambda f \equiv 4\partial_\diamondsuit \bar{\partial}_\Lambda f$. In particular, $\bar{\partial}_\diamondsuit \partial_\Lambda f \equiv 0$ if $\triangle f \equiv 0$, which shows (i). Also, f is discrete harmonic if it is discrete holomorphic. Using $\operatorname{Re}(\triangle f) \equiv \triangle \operatorname{Re}(f)$ and $\operatorname{Im}(\triangle f) \equiv \triangle \operatorname{Im}(f)$, $\operatorname{Re}(f)$ and $\operatorname{Im}(f)$ are discrete harmonic if f is.

Similar to Proposition 2.1 that compares the discrete derivative ∂_Λ with the smooth derivative, the discrete Laplacian coincides with the smooth one up to order one in the general case and up to order two for parallelogram-graphs. This was already shown by Skopenkov in [23]. Since this result follows immediately from our previous ones, we give a proof here as well.

Proposition 2.22 *Let $f_\mathbb{C} : \mathbb{C} \to \mathbb{C}$ and f its restriction to $V(\Lambda)$.*

(i) If $f_\mathbb{C}(z)$ is a polynomial in $\operatorname{Re}(z)$ and $\operatorname{Im}(z)$ of degree at most one, then the smooth and the discrete Laplacian coincide on vertices: $\triangle_\mathbb{C} f_\mathbb{C}(v) = \triangle f(v) = 0$.
(ii) Let all faces of Λ be parallelograms. If $f_\mathbb{C}(z)$ is a polynomial in $\operatorname{Re}(z)$ and $\operatorname{Im}(z)$ of degree at most two, then the smooth and the discrete Laplacian coincide on vertices: $\triangle_\mathbb{C} f_\mathbb{C}(v) = \triangle f(v)$.

Proof (i) Proposition 2.1(ii) says that the function $f(v) = v$ is discrete holomorphic and Corollary 2.21(ii) that real and imaginary part of discrete holomorphic functions are discrete harmonic. Since constants are discrete harmonic, the statement follows.

(ii) In the parallelogram case, let $\hat{Q}$ denote the center of the parallelogram $Q \in F(\Lambda) \cong V(\Diamond)$. Analogously to (i), $f(v) = v^2$ is discrete harmonic by Proposition 2.1(iii) and Corollary 2.21(ii). Looking at real and imaginary part separately, $\triangle f_1^2 \equiv \triangle f_2^2$ and $\triangle(f_1 f_2) \equiv 0$ where we consider $f_1(v) = \mathrm{Re}(v)$, $f_2(v) = \mathrm{Im}(v)$. Finally,

$$\triangle |f|^2 \equiv 4\partial_\Diamond \bar{\partial}_\Lambda |f|^2 \equiv 4\partial_\Diamond h = 4$$

with $h(Q) = \hat{Q}$ for all $Q \in V(\Diamond)$, due to Propositions 2.1(iv) and 2.5 that implied $\bar{\partial}_\Lambda |f|^2 \equiv h$ and $\partial_\Diamond h \equiv 1$. Since any polynomial in $\mathrm{Re}(z)$ and $\mathrm{Im}(z)$ of monomials of degree two is a linear combination of $f_1^2 - f_2^2$, $f_1^2 + f_2^2$, and $f_1 f_2$, and since we have shown that the discrete Laplacian $\triangle$ and the smooth Laplacian $\triangle_{\mathbb{C}}$ coincide on these, we are done.

Remark The second part of the last proposition generalizes the known result for rhombi given by Chelkak and Smirnov [6]. Note that this is not true for general quadrilaterals even if one assumes that the diagonals of quadrilaterals are orthogonal to each other. For this, consider the following (finite) bipartite quad-graph of Fig. 4: the black vertex 0 is adjacent to the white vertices ± 1 and $\pm i$ in the quad-graph and adjacent to the black vertices $2 + 2i$, $-1 \pm i$, and $1 - i$ in the graph on black vertices. There are no further vertices. Then, $\triangle f(0) \neq 0$ for $f(v) = v^2$. Indeed, we would get $\triangle f(0) = 0$ if we had replaced $v = 2 + 2i$ by $v = 1 + i$ obtaining a rhombic quad-graph; but $\left(|\rho_Q|^2 / \mathrm{Re}(\rho_Q)\right)(f(v) - f(0))$ scales by a factor of 2, whereas the other nonzero summands in the formula for $\triangle f(0)$ remain invariant.

In the case of general quad-graphs, smooth functions $f_{\mathbb{C}} : \mathbb{C} \to \mathbb{C}$, and restrictions f to $V(\Lambda)$, Skopenkov compared the integral of $\triangle_{\mathbb{C}} f_{\mathbb{C}}$ over a square domain R and a sum of $\triangle f(v)$ over black vertices v in R [23]. Moreover, he showed that for $f(v) = |v|^2$,

$$\triangle f(v) = \frac{2}{\mathrm{ar}(F_v)} \sum_{Q_s \sim v} \mathrm{area}(v v'_{s-1} \hat{Q}_s v'_s)$$

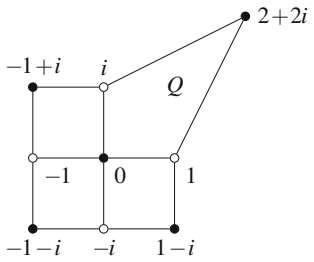

Fig. 4 $\triangle f(0) \neq 0$ for $f(v) = v^2$

when $\hat{Q}_s$ is the intersection point of the middle perpendiculars to the diagonals of the quadrilateral Q_s (which equals the intersection point of the diagonals if Q_s is a parallelogram). Note that in general, $h(Q) = \hat{Q}$ is not discrete holomorphic if $\hat{Q}$ is the intersection of these middle perpendiculars.

Definition For a finite connected subset $\diamondsuit_0 \subset \diamondsuit$, let F_0 be the set of faces of X_0 that correspond to a quadrilateral $Q \in V(\diamondsuit_0)$ that is incident to a vertex in $V(\Lambda_0)\backslash V(\partial\Lambda_0)$. Now, let $f_1 : V(\Lambda_0) \to \mathbb{C}$ and $f_2 : V(\Lambda_0)\backslash V(\partial\Lambda_0) \to \mathbb{C}$ (or vice versa) be given. Then, we denote by

$$\langle f_1, f_2\rangle := -\frac{1}{2i}\iint\limits_{F_0} f_1 \bar{f}_2 \Omega_\Lambda$$

the discrete scalar product of f_1 and f_2 seen as functions on $V(\Lambda_0)\backslash V(\partial\Lambda_0)$.

In the rhombic setup, discrete versions of Green's second identity were already stated by Mercat [19], whose integrals were not well-defined separately, and Chelkak and Smirnov [6], whose boundary integral was an explicit sum involving boundary angles. Skopenkov formulated a discrete Green's second identity with a vanishing boundary term [23].

Theorem 2.23 *Let $\diamondsuit_0 \subset \diamondsuit$ be finite, and let $f, g : V(\Lambda_0) \to \mathbb{C}$.*

(i) Discrete Green's first identity: $\langle f, \triangle g\rangle + \langle df, dg\rangle = \oint\limits_{\partial X_0} f \star d\bar{g}$.

(ii) Discrete Green's second identity: $\langle f, \triangle g\rangle - \langle \triangle f, g\rangle = \oint\limits_{\partial X_0} (f \star d\bar{g} - \bar{g} \star df)$.

Proof (i) Since the discrete exterior derivative is a derivation for the discrete wedge product by Theorem 2.16,

$$d(f \star d\bar{g}) = df \wedge \star d\bar{g} + f \star (\star d \star d\bar{g}) = df \wedge \star d\bar{g} + f \star \triangle\bar{g}.$$

Now, integration over $F(X_0)$ yields the desired result together with discrete Stokes' Theorem 2.9 and the basic properties of the discrete Hodge star given in Corollary 2.17(ii) and (iv).

(ii) Just apply twice discrete Green's first identity, once with the roles of f and g interchanged, and subtract the equations from another.

The following *discrete Weyl's lemma* is a direct consequence of discrete Green's second identity, Theorem 2.23(ii). A version for rhombic quad-graphs was given by Mercat in [19], proven by an explicit calculation.

Corollary 2.24 *$f : V(\Lambda) \to \mathbb{C}$ is discrete harmonic if and only if $\langle f, \triangle g\rangle = 0$ for every compactly supported $g : V(\Lambda) \to \mathbb{C}$.*

Skopenkov introduced the notion of discrete harmonic conjugates in [23]. We recover his definitions in our notation, observing that his discrete gradient corresponds to the discrete exterior derivative and his counterclockwise rotation by $\pi/2$ to the discrete Hodge star.

Definition Let f be a real (discrete harmonic) function on $V(\Lambda_0)$. A real discrete harmonic function $\tilde{f}$ on $V(\Lambda_0)$ is said to be a *discrete harmonic conjugate of* f if $f + i\tilde{f}$ is discrete holomorphic at all vertices of $\diamondsuit_0$.

Note that the existence of a real function $\tilde{f}$ such that $f + i\tilde{f}$ is discrete holomorphic requires already that f is discrete harmonic at all interior vertices of Λ_0 (i.e., $V(\Lambda_0)\backslash V(\partial\Lambda_0)$) due to Corollary 2.21(ii) implying that the real part of a discrete holomorphic function is discrete harmonic.

Lemma 2.25 *Let $f : V(\Lambda_0) \to \mathbb{R}$ satisfy $\triangle f(v) = 0$ for all $v \in V(\Lambda_0)\backslash V(\partial\Lambda_0)$.*

(i) The discrete harmonic conjugate $\tilde{f}$ is unique up to two additive real constants on Γ_0 and Γ_0^*.

(ii) If $\diamondsuit_0$ forms a simply-connected closed region, then a discrete harmonic conjugate $\tilde{f}$ exists.

Proof (i) If $\tilde{f}_1$ and $\tilde{f}_2$ are two real discrete harmonic conjugates, then their difference $\tilde{f}_1 - \tilde{f}_2$ is real and discrete holomorphic at all vertices of $\diamondsuit_0$. So by Proposition 2.2(ii) ($\diamondsuit_0$ is connected), it is biconstant as a real discrete holomorphic function.

(ii) Since f is harmonic, $d \star df = 0$, i.e., $\star df$ is closed and of type $\diamondsuit$. Moreover, reality of f implies $\star df = -i\partial_\Lambda f dz + i\bar{\partial}_\Lambda f d\bar{z} = 2\,\mathrm{Im}\,(\partial_\Lambda f dz)$. So in the same manner as in the proof of Proposition 2.8 (existence of a discrete primitive if $\diamondsuit_0$ forms a simply-connected closed region), $\star df$ can be integrated to a real function $\tilde{f}$ on $V(\Lambda_0)$. Since

$$d(f + i\tilde{f}) = df + i \star df = 2\,\mathrm{Re}\,(\partial_\Lambda f dz) + 2i\,\mathrm{Im}\,(\partial_\Lambda f dz) = 2\partial_\Lambda f dz$$

is of the form pdz and of type $\diamondsuit$, $f + i\tilde{f}$ is discrete holomorphic by Corollary 2.12.

Note that in the case of quadrilaterals with orthogonal diagonals, such that $\triangle$ splits into two discrete Laplacians on Γ and Γ^*, it follows that a discrete harmonic conjugate of a discrete harmonic function on $V(\Gamma)$ can be defined on $V(\Gamma^*)$ and vice versa, as was already noted by Chelkak and Smirnov in [6].

Corollary 2.26 *Let $f : V(\Lambda_0) \to \mathbb{C}$ be discrete holomorphic at all vertices of $\diamondsuit_0$. Then,* $\mathrm{Im}(f)$ *is uniquely determined by* $\mathrm{Re}(f)$ *up to two additive constants on Γ_0 and Γ_0^*.*

2.4.2 Discrete Dirichlet Energy

We follow the classical approach of discretizing the Dirichlet energy introduced by Mercat in [21]. Note that Skopenkov's definition in [23] is exactly the same. In particular, Skopenkov's results, including an approximation property of the Laplacian, convergence of the discrete Dirichlet energy to the smooth Dirichlet energy for non-degenerate uniform sequences of quad-graphs, and further theorems for quad-graphs with orthogonal diagonals apply as well in our setting. We refer to his work [23] for details on these results.

Definition For a function $f : V(\Lambda_0) \to \mathbb{C}$, we define the *discrete Dirichlet energy* of f on $\diamondsuit_0$ as $E_{\diamondsuit_0}(f) := \langle df, df \rangle \in [0, \infty]$.

If $\diamondsuit_0$ is finite, then the *discrete Dirichlet boundary value problem* asks for a real function f on $V(\Lambda_0)$ such that f is discrete harmonic at all points of $V(\Lambda_0) \backslash V(\partial \Lambda_0)$ and such that f agrees with a preassigned real function f_0 on the boundary $V(\partial \Lambda_0)$.

Proposition 2.27 *Let $\diamondsuit_0 \subseteq \diamondsuit$ be finite, and let $f : V(\Lambda_0) \to \mathbb{C}$. Then,*

$$E_{\diamondsuit_0}(f) = \sum_{Q \in V(\diamondsuit_0)} \frac{1}{2\,\mathrm{Re}\,(\rho_Q)} \left(|\rho_Q|^2\, |f(b_+) - f(b_-)|^2 + |f(w_+) - f(w_-)|^2 \right)$$
$$+ \sum_{Q \in V(\diamondsuit_0)} \frac{\mathrm{Im}\,(\rho_Q)}{\mathrm{Re}\,(\rho_Q)}\, \mathrm{Re}\left((f(b_+) - f(b_-))\, \overline{(f(w_+) - f(w_-))} \right).$$

Proof Since $E_{\diamondsuit_0}(f)$ is a sum over $Q \in V(\diamondsuit_0)$, it suffices to check the identity for just a singular quadrilateral Q. Furthermore, $E_{\diamondsuit_0}(f) = E_{\diamondsuit_0}(\mathrm{Re}(f)) + E_{\diamondsuit_0}(\mathrm{Im}(f))$ allows us to restrict to real functions f. Then, $E_Q(f)$ equals

$$\iint_{F_Q} df \wedge \star df = 4\mathrm{area}(Q) \partial_\Lambda f(Q) \bar{\partial}_\Lambda f(Q)$$
$$= 2|w_+ - w_-||b_+ - b_-| \sin(\varphi_Q) |\bar{\partial}_\Lambda f(Q)|^2.$$

Here, b_-, w_-, b_+, w_+ are the vertices of Q in counterclockwise order, starting with a black vertex, and F_Q is the face of X corresponding to Q.

In the proof of Proposition 2.1(i), we calculated

$$\bar{\partial}_\Lambda f(Q) = \frac{(w_+ - w_-)\,(f\,(b_+) - f\,(b_-)) - (b_+ - b_-)\,(f\,(w_+) - f\,(w_-))}{2i\,|w_+ - w_-||b_+ - b_-| \sin(\varphi_Q)}.$$

It follows that $E_Q(f)$ equals

$$\frac{|w_+ - w_-|}{2|b_+ - b_-| \sin(\varphi_Q)} |f(b_+) - f(b_-)|^2 + \frac{|b_+ - b_-|}{2|w_+ - w_-| \sin(\varphi_Q)} |f(w_+) - f(w_-)|^2$$
$$- \mathrm{Re}\left(\frac{(w_+ - w_-)\overline{(b_+ - b_-)}}{|w_+ - w_-||b_+ - b_-| \sin(\varphi_Q)} (f(b_+) - f(b_-))\,(f(w_+) - f(w_-)) \right).$$

Remembering $\rho_Q = -i \exp(i\varphi_Q)|w_+ - w_-|/|b_+ - b_-|$, the claim follows from

$$\frac{|w_+ - w_-|}{2|b_+ - b_-| \sin(\varphi_Q)} = \frac{|\rho_Q|^2}{2\,\mathrm{Re}\,(\rho_Q)}, \quad \frac{|b_+ - b_-|}{2|w_+ - w_-| \sin(\varphi_Q)} = \frac{1}{2\,\mathrm{Re}\,(\rho_Q)},$$
$$- \mathrm{Re}\left(\frac{(w_+ - w_-)\overline{(b_+ - b_-)}}{|w_+ - w_-||b_+ - b_-| \sin(\varphi_Q)} \right) = \frac{\mathrm{Im}(\rho_Q)}{\mathrm{Re}(\rho_Q)}.$$

The same formula of $E_{\diamondsuit_0}(f)$ was given by Mercat [21].

In the case of rhombic quad-graphs, Duffin proved in [10] that the discrete Dirichlet boundary value problem has a unique solution. The same argument applies for general quad-graphs with the discrete Dirichlet energy defined here. Using a different notation, Skopenkov proved existence and uniqueness of solutions of the discrete Dirichlet boundary value problem as well [23].

Lemma 2.28 *Let $\diamondsuit_0 \subset \diamondsuit$ be finite and $f_0 : V(\partial\Lambda_0) \to \mathbb{R}$. We consider the affine space of real functions $f : V(\Lambda_0) \to \mathbb{R}$ that agree with f_0 on the boundary.*

Then, $E_{\diamondsuit_0}$ is a strictly convex nonnegative quadratic functional in terms of the interior values $f(v)$. Furthermore,

$$-\frac{\partial E_{\diamondsuit_0}}{\partial f(v)}(f) = 2\mathrm{ar}(F_v)\triangle f(v)$$

for any $v \in V(\Lambda_0)\backslash V(\partial\Lambda_0)$. In particular, the solution of the discrete Dirichlet boundary value problem is given by the unique minimizer of $E_{\diamondsuit_0}$.

Proof By construction, $E_{\diamondsuit_0}$ is a quadratic form in the vector space of real functions $f : V(\Lambda_0)\backslash V(\partial\Lambda_0) \to \mathbb{R}$. In particular, it is convex, nonnegative, and quadratic in terms of the values $f(v)$. Thus, global minima exist. To prove strict convexity, it suffices to check that the minimum is unique.

For an interior vertex $v_0 \in V(\Lambda_0)\backslash V(\partial\Lambda_0)$, let $\phi(v) := \delta_{vv_0}$ be the Kronecker delta function on $V(\Lambda_0)$. Then,

$$\frac{\partial E_{\diamondsuit_0}}{\partial f(v_0)}(f) = \frac{d}{dt}E_{\diamondsuit_0}(f + t\phi)|_{t=0} = 2\langle df, d\phi\rangle = -2\langle \triangle f, \phi\rangle = -2\mathrm{ar}(F_{v_0})\triangle f(v_0)$$

due to Proposition 2.19 that stated that δ is the formal adjoint of d. To apply the proposition, we consider ϕ as a function on $V(\Lambda)$ and extend f to $V(\Lambda)$ by setting it zero on $V(\Lambda)\backslash V(\Lambda_0)$. This changes neither $\langle df, d\phi\rangle$ nor $2\langle \triangle f, \phi\rangle$.

It follows that exactly the minima of $E_{\diamondsuit_0}$ are discrete harmonic and therefore solve the discrete Dirichlet boundary value problem. The difference g of two minima is a discrete harmonic function vanishing on the boundary. Similar to the argument given in the previous paragraph, $E_{\diamondsuit_0}(g) = \langle dg, dg\rangle = -\langle \triangle g, g\rangle = 0$ by Proposition 2.19 since g is zero on $V(\partial\Lambda_0)$. But only biconstant functions have zero energy. Thus, the difference has to vanish everywhere, i.e., minima are unique.

In the following, we apply Lemma 2.28 to show that ∂_Λ, $\bar\partial_\Lambda$, $\partial_\diamondsuit$, $\bar\partial_\diamondsuit$, $\triangle$ are surjective operators. This implies immediately the existence of discrete Green's functions and discrete Cauchy's kernels, as we will see in Sects. 2.5 and 2.6.

Lemma 2.29 *Let $\diamondsuit_0 \subset \diamondsuit$ be finite and assume that it forms a simply-connected closed region. Then, the discrete derivatives ∂_Λ, $\bar\partial_\Lambda$, $\partial_\diamondsuit$, $\bar\partial_\diamondsuit$ and the discrete Laplacian $\triangle$ are surjective operators. That means, given any complex functions h_0 on $V(\diamondsuit_0)$ and f_0 on $V(\Lambda_0)\backslash V(\partial\Lambda_0)$, there exist functions $h_\partial, h_{\bar\partial}$ on $V(\diamondsuit_0)$ and*

f_∂, $f_{\bar\partial}$, $f_\triangle$ on $V(\Lambda_0)$ such that $\partial_\diamondsuit h_\partial = \bar\partial_\diamondsuit h_{\bar\partial} = \triangle f_\triangle = f_0$ and $\partial_\Lambda f_\partial = \bar\partial_\Lambda f_{\bar\partial} = h_0$. If f_0 is real-valued, then $f_\triangle$ can be chosen real-valued as well.

Proof Denote by B the number of vertices of $\partial\Lambda_0$. By assumption, $\partial\Lambda_0$ is a simple closed broken line with B edges.

By the previous Lemma 2.28, the space of real discrete harmonic functions on $V(\Lambda_0)$ has dimension B. Clearly, real and imaginary part of a discrete harmonic function are itself discrete harmonic. Therefore, the complex dimension of the space of complex discrete harmonic functions, i.e., of the kernel of $\triangle$, is B as well. Thus, $\triangle : \mathbb{K}^{V(\Lambda_0)} \to \mathbb{K}^{V(\Lambda_0\setminus\partial\Lambda_0)}$ is a surjective linear operator with $\mathbb{K} \in \{\mathbb{R}, \mathbb{C}\}$.

Now, $\triangle = 4\partial_\diamondsuit\bar\partial_\Lambda = 4\bar\partial_\diamondsuit\partial_\Lambda$ by Corollary 2.20, so $\partial_\diamondsuit, \bar\partial_\diamondsuit : \mathbb{C}^{V(\diamondsuit_0)} \to \mathbb{C}^{V(\Lambda_0\setminus\partial\Lambda_0)}$ are surjective as well. The kernel of $\bar\partial_\diamondsuit$ consists of all discrete holomorphic functions on $V(\diamondsuit_0)$. By Proposition 2.8 ($\diamondsuit_0$ forms a simply-connected closed region), any such function has a discrete primitive, i.e., the kernel is contained in the image of ∂_Λ. Using the surjectivity of $\triangle$, it follows that $\partial_\Lambda : \mathbb{C}^{V(\Lambda_0)} \to \mathbb{C}^{V(\diamondsuit_0)}$ is surjective. The same is true for $\bar\partial_\Lambda$.

Theorem 2.30 *The discrete derivatives ∂_Λ, $\bar\partial_\Lambda$, $\partial_\diamondsuit$, $\bar\partial_\diamondsuit$ and the discrete Laplacian $\triangle$ (defined on complex or real functions) are surjective operators on the vector space of functions on $V(\Lambda)$ or $V(\diamondsuit)$.*

Proof Let $\diamondsuit_0 \subset \diamondsuit_1 \subset \diamondsuit_2 \subset \ldots \subset \diamondsuit$ be a sequence of finite subgraphs forming simply-connected closed regions such that $\bigcup_{k=0}^\infty \diamondsuit_k = \diamondsuit$. By Λ_k we denote the subgraph of Λ whose vertices and edges are the vertices and edges of quadrilaterals in $\diamondsuit_k$.

Let us first prove that any $h : V(\diamondsuit) \to \mathbb{C}$ has a preimage under the discrete derivatives $\partial_\Lambda, \bar\partial_\Lambda$. By the previous Lemma 2.29, the affine space $A_k^{(0)}$ of all complex functions on $V(\Lambda_k)$ that are mapped to $h|_{V(\diamondsuit_k)}$ by ∂_Λ (or $\bar\partial_\Lambda$) is nonempty. Let $A_k^{(0)}\Big|_{\Lambda_j}$ denote the affine space of restrictions of these functions to $V(\Lambda_j) \subseteq V(\Lambda_k)$. Clearly,

$$A_0^{(0)} \supseteq A_1^{(0)}\Big|_{\Lambda_0} \supseteq A_2^{(0)}\Big|_{\Lambda_0} \supseteq \ldots$$

Since all affine spaces are finite-dimensional and nonempty, this chain becomes stationary at some point, giving a function f_0 on $V(\Lambda_0)$ mapped to $h|_{V(\diamondsuit_0)}$ by ∂_Λ (or $\bar\partial_\Lambda$) that can be extended to a function in $A_k^{(0)}$ for any k.

Inductively, assume that $f_j : V(\Lambda_j) \to \mathbb{C}$ is mapped to $h|_{V(\diamondsuit_j)}$ by ∂_Λ (or $\bar\partial_\Lambda$) and that f_j can be extended to a function in $A_k^{(j)}$ for all $k \geqslant j$. Let $A_k^{(j+1)}$, $k \geqslant j+1$, be the affine space of all complex functions on $V(\Lambda_k)$ that are mapped to $h|_{V(\diamondsuit_k)}$ by ∂_Λ (or $\bar\partial_\Lambda$) and whose restriction to $V(\Lambda_j)$ is equal to f_j. By assumption, all these spaces are nonempty. In the same way as above, there is a function f_{j+1} extending f_j to $V(\Lambda_{j+1})$ that is mapped to $h|_{V(\diamondsuit_{j+1})}$ by ∂_Λ (or $\bar\partial_\Lambda$) and that can be extended to a function in $A_k^{(j+1)}$ for all $k \geqslant j+1$.

For $v \in V(\Lambda_k)$, define $f(v) := f_k(v)$. f is a well-defined complex function on $V(\Lambda)$ with $\partial_\Lambda f = h$ (or $\bar\partial_\Lambda f = h$). Hence, $\partial_\Lambda, \bar\partial_\Lambda : \mathbb{C}^{V(\Lambda)} \to \mathbb{C}^{V(\diamondsuit)}$ are surjective.

Replacing $V(\Diamond_k)$ by $V(\Lambda_k)\backslash V(\partial\Lambda_k)$, we obtain with the same arguments that $\triangle$ is surjective, regardless whether $\triangle$ is defined on real or complex functions. Finally, $\partial_\Diamond, \bar{\partial}_\Diamond : \mathbb{C}^{V(\Diamond)} \to \mathbb{C}^{V(\Lambda)}$ are surjective due to $\triangle = 4\partial_\Diamond\bar{\partial}_\Lambda = 4\bar{\partial}_\Diamond\partial_\Lambda$ by Corollary 2.20.

In the case of rhombic quad-graphs with bounded interior angles, Kenyon proved the existence of a discrete Green's function and a discrete Cauchy's kernel with asymptotic behaviors similar to the classical setting [16]. But in the general case, it seems to be practically impossible to speak about any asymptotic behavior of certain discrete functions. For this reason, we will consider functions that discretize Green's functions and Cauchy's kernels apart from their asymptotics in Sects. 2.5 and 2.6. Not requiring a certain asymptotic behavior leads to non-uniqueness of these functions.

Still, one can expect results concerning the asymptotics of special discrete functions if the interior angles and the side lengths of the quadrilaterals are bounded, meaning that the quadrilaterals do not degenerate at infinity. And indeed, on such quad-graphs any discrete harmonic function whose difference functions on $V(\Gamma)$ and $V(\Gamma^*)$ have asymptotics $o(v^{-1/2})$ as $|v| \to \infty$ is biconstant. In the rhombic setting, Chelkak and Smirnov showed that a discrete Liouville's theorem holds true, i.e., any bounded discrete harmonic function on $V(\Lambda)$ vanishes [6].

Theorem 2.31 *Assume that there exist constants $\alpha_0 > 0$ and $E_1 \geqslant E_0 > 0$ such that $\alpha \geqslant \alpha_0$ and $E_1 \geqslant e \geqslant E_0$ for all interior angles α and side lengths e of quadrilaterals $Q \in F(\Lambda)$. If $f : V(\Lambda) \to \mathbb{C}$ is discrete harmonic and $f(v_+) - f(v_-) = o(v_\pm^{-1/2})$ for any two adjacent $v_\pm \in V(\Gamma)$ or $v_\pm \in V(\Gamma^*)$ as $|v_\pm| \to \infty$, then f is biconstant.*

Proof Without loss of generality, we can restrict to real functions f. Assume that f is not biconstant. Then, $df \wedge \star df$ is nonzero somewhere on a face F of X. In particular, the discrete Dirichlet energy of f is bounded away from zero if a domain contains F. Now, the idea of proof is to show that if the domain is large enough but still compact, the function being zero in the interior and equal to f on the boundary has a smaller discrete Dirichlet energy than f, contradicting Lemma 2.28 that implies that f is the unique minimizer of the discrete Dirichlet energy on that domain.

Let us first bound the intersection angles and the lengths of diagonals of the quadrilaterals. Take $Q \in F(\Lambda)$ and denote its vertices by b_-, w_-, b_+, w_+ in counterclockwise order, starting with a black vertex. Then, there are two opposite interior angles that are less than π, say $\alpha_\pm$ at vertices $b_\pm$. Since all interior angles are bounded by α_0 from below, one of $\alpha_\pm$ is less than or equal to $\pi - \alpha_0$, say $\alpha_0 \leqslant \alpha_- \leqslant \pi - \alpha_0$.

By triangle inequality, $|b_+ - b_-|, |w_+ - w_-| < 2E_1$. Twice the area of Q equals

$$|w_- - b_-||w_+ - b_-|\sin(\alpha_-) + |w_- - b_+||w_+ - b_+|\sin(\alpha_+) \geqslant E_0^2 \sin(\alpha_0),$$

so $|b_+ - b_-||w_+ - w_-|\sin(\varphi_Q) = 2\mathrm{area}(Q) \geqslant E_0^2\sin(\alpha_0)$. It follows that

$$|b_+ - b_-| \geqslant \frac{E_0^2\sin(\alpha_0)}{|w_+ - w_-|\sin(\varphi_Q)} > \frac{E_0^2\sin(\alpha_0)}{2E_1} =: E_0'.$$

Similarly, $|w_+ - w_-| > E_0'$ and $\sin(\varphi_Q) > E_0'/(2E_1)$. Thus, we can bound

$$\rho_Q = \frac{|w_+ - w_-|}{|b_+ - b_-|} \exp\left(i\left(\varphi_Q - \frac{\pi}{2}\right)\right) = \frac{|w_+ - w_-|}{|b_+ - b_-|}\left(\sin(\varphi_Q) - i\cos(\varphi_Q)\right)$$

$$\text{by } |\rho_Q| < \frac{2E_1}{E_0'} \text{ and } \operatorname{Re}\left(\rho_Q\right) > \left(\frac{E_0'}{2E_1}\right)^2.$$

For some $r > 0$, denote by $B_\diamondsuit(0, r) \subset V(\diamondsuit)$ the set of quadrilaterals that have a nonempty intersection with the open ball $B(0, r)$ around 0 and radius r. Let $R > 2E_1$, and consider the ball $B_\diamondsuit(0, R) \subset V(\diamondsuit)$. Since Λ is locally finite, $B_\diamondsuit(0, R)$ is finite. Also, if we connect two elements of $B_\diamondsuit(0, R)$ if they are adjacent in $\diamondsuit$, then we obtain a connected subgraph of $\diamondsuit$ that we will also denote by $B_\diamondsuit(0, R)$. To see that it is connected, we observe that the closed region in the complex plane formed by the quadrilaterals in $B_\diamondsuit(0, R)$ is connected, and that if $Q \in B_\diamondsuit(0, R)$, then one of its corners, say v, has to lie in $B(0, R)$ and so all quadrilaterals incident to v are in $B_\diamondsuit(0, R)$. We denote by Λ_R the subgraph of Λ that consists of all the vertices and edges of quadrilaterals in $B_\diamondsuit(0, R)$

Since edge lengths are bounded by E_1, all elements of $B_\diamondsuit(0, R)$ that are not completely contained in $B(0, R)$ are contained in $B(0, R + 2E_1)\backslash B(0, R - 2E_1)$. The area of the latter is $8\pi R E_1$. Any quadrilateral has area at least $E_0^2 \sin(\alpha_0)/2$, so at most $16\pi R E_1/(E_0^2 \sin(\alpha_0))$ quadrilaterals of $B_\diamondsuit(0, R)$ do not lie completely in $B(0, R)$. We call these quadrilaterals for short *boundary faces*.

Consider the real function f_R defined on $V(\Lambda_R)$ that is equal to f at $V(\partial\Lambda_R)$ and equal to 0 in $V(\Lambda_R)\backslash V(\partial\Lambda_R)$. When computing the discrete Dirichlet energy of f_R on $B_\diamondsuit(0, R)$, only boundary faces can give nonzero contributions. If we look at the formula of the discrete Dirichlet energy in Proposition 2.27 and use in addition that $f(v_+) - f(v_-) = o(R^{-1/2})$ for vertices of boundary faces, then we see that any contribution of a boundary face has asymptotics $o(R^{-1})$. For this, we use that $\left|\operatorname{Re}\left(\rho_Q\right)\right|$ is bounded from below by a constant and $\left|\operatorname{Im}\left(\rho_Q\right)\right| \leqslant \left|\rho_Q\right| < 2E_1/E_0'$. Using that there are only $O(R)$ faces in the boundary (the constant depending on E_0, E_1, α_0 only), the discrete Dirichlet energy $E_{B_\diamondsuit(0,R)}(f_R)$, considered as a function of R, behaves as $o(1)$. So if R is large enough, then

$$E_{B_\diamondsuit(0,R)}(f_R) < \iint_F df \wedge \star df \leqslant E_{B_\diamondsuit(0,R)}(f),$$

contradicting that f minimizes the discrete Dirichlet energy by Lemma 2.28.

2.5 Discrete Green's Functions

Definition Let $v_0 \in V(\Lambda)$. A real function $G(\cdot; v_0)$ on $V(\Lambda)$ is a *(free) discrete Green's function* for v_0 if

$$G(v_0; v_0) = 0 \text{ and } \triangle G(v; v_0) = \frac{1}{2\mathrm{ar}(F_{v_0})}\delta_{vv_0} \text{ for all } v \in V(\Lambda).$$

Remark It is important to note that discrete Green's functions as we defined them are far from being unique. The contrast to the smooth setting or the rhombic case investigated by Kenyon [16], Chelkak and Smirnov [6] is that no asymptotics are required. So it might be more appropriate to call these functions *functions of discrete Green's function type*, but for the sake of convenience, we still call them discrete Green's functions.

However, when considering planar parallelogram-graphs with bounded interior angles and bounded ratio of side lengths in Sect. 3.3, existence of a discrete Green's function with asymptotics generalizing the corresponding result for rhombic quad-graphs is proven.

As a corollary of Theorem 2.30 we get existence of discrete Green's functions.

Corollary 2.32 *A discrete Green's function exists for any* $v_0 \in V(\Lambda)$.

Proof By Theorem 2.30, $\triangle$ is surjective, so there exists a function $G : V(\Lambda) \to \mathbb{R}$ with $\triangle G(v) = \delta_{vv_0} / \left(2\mathrm{ar}(F_{v_0})\right)$. Since constant functions are discrete harmonic, we can adjust G to get $G(v_0) = 0$.

The following notion of discrete Greens' functions in a discrete domain follows the presentation of Chelkak and Smirnov in [6].

Definition Let $\Diamond_0 \subset \Diamond$ be finite and form a simply-connected closed region. For a vertex $v_0 \in V(\Lambda_0)\backslash V(\partial\Lambda_0)$, a real function $G_{\Lambda_0}(\cdot; v_0)$ on $V(\Lambda_0)$ is a *discrete Green's function in* Λ_0 *for* v_0 if

$$G_{\Lambda_0}(v; v_0) = 0 \text{ for all } v \in V(\partial\Lambda_0)$$
$$\text{and } \triangle G_{\Lambda_0}(v; v_0) = \frac{1}{2\mathrm{ar}(F_{v_0})}\delta_{vv_0} \text{ for all } v \in V(\Lambda_0)\backslash V(\partial\Lambda_0).$$

An immediate corollary of Lemma 2.29 is now the existence of these functions.

Corollary 2.33 *Let* $\Diamond_0 \subset \Diamond$ *be finite and form a simply-connected closed region. Furthermore, let* $v_0 \in V(\Lambda_0)\backslash V(\partial\Lambda_0)$. *Then, there exists a unique discrete Green's function in* Λ_0 *for* v_0.

Proof Due to our assumptions on $\Diamond_0$, existence follows from Lemma 2.29 stating surjectivity of $\triangle$ on such domains. Since the difference of two discrete Green's functions in Λ_0 for v_0 is discrete harmonic on $V(\Lambda_0)$ and equals zero on the boundary $V(\partial\Lambda_0)$, it has to be identically zero by Lemma 2.28 since the zero function is the unique solution of the corresponding discrete Dirichlet boundary value problem.

2.6 Discrete Cauchy's Integral Formulae

In this section, we first formulate discretizations of the standard Cauchy's integral formula, both for discrete holomorphic functions on $V(\Lambda)$ and $V(\diamondsuit)$. Later, we give with Theorem 2.36 a discrete formulation of Cauchy's integral formula for the derivative of a holomorphic function. We conclude this part with Sect. 2.6.1, where we relate our formulation of the discrete Cauchy's integral formula for discrete holomorphic functions on $V(\diamondsuit)$ with Chelkak's and Smirnov's notation in [6].

Definition *Discrete Cauchy's kernels with respect to* $Q_0 \in V(\diamondsuit)$ *and* $v_0 \in V(\Lambda)$ are functions $K_{Q_0} : V(\Lambda) \to \mathbb{C}$ and $K_{v_0} : V(\diamondsuit) \to \mathbb{C}$, respectively, that satisfy for all $Q \in V(\diamondsuit)$, $v \in V(\Lambda)$:

$$\bar{\partial}_\Lambda K_{Q_0}(Q) = \delta_{QQ_0} \frac{\pi}{\operatorname{ar}(F_Q)} \quad \text{and} \quad \bar{\partial}_\diamondsuit K_{v_0}(v) = \delta_{vv_0} \frac{\pi}{\operatorname{ar}(F_v)}.$$

For fixed $Q_0 \in V(\diamondsuit_0)$, $v_0 \in V(\Lambda_0) \backslash V(\partial \Lambda_0)$, functions $K_{Q_0} : V(\Lambda_0) \to \mathbb{C}$ and $K_{v_0} : V(\diamondsuit_0) \to \mathbb{C}$ satisfying the above equations for all faces $Q \in V(\diamondsuit_0)$ and vertices $v \in V(\Lambda_0) \backslash V(\partial \Lambda_0)$ are called *discrete Cauchy's kernels on* $V(\Lambda_0)$ *or* $V(\diamondsuit_0)$, respectively.

Clearly, the restrictions of discrete Cauchy's kernels to $V(\Lambda_0)$ *or* $V(\diamondsuit_0)$, respectively, are discrete Cauchy's kernels on $V(\Lambda_0)$ *or* $V(\diamondsuit_0)$, respectively.

Remark It is important to note that exactly as discrete Green's functions, discrete Cauchy's kernels as we defined them are far from being unique. Again, it might be more appropriate to call these functions *functions of discrete Cauchy's kernel type*, but we still call them discrete Cauchy's kernels.

But if interior angles and side lengths of quadrilaterals are bounded, then it follows from Theorem 2.31 that any discrete Cauchy's kernel with respect to a vertex of $\diamondsuit$ with asymptotics $o(v^{-1/2})$ as $|v| \to \infty$ is necessarily unique, but we cannot prove existence so far. In Sect. 3.4, explicit formulae for discrete Cauchy's kernels with asymptotics similar to the smooth setting are given, generalizing Kenyon's result [16] on rhombic quad-graphs to parallelogram-graphs.

The existence of discrete Cauchy's kernels follows from the surjectivity of discrete derivatives by Theorem 2.30:

Corollary 2.34 *Let* $Q_0 \in V(\diamondsuit)$ *and* $v_0 \in V(\Lambda)$ *be arbitrary. Then, discrete Cauchy's kernels with respect to* Q_0 *and* v_0 *exist.*

Theorem 2.35 *Let* f *and* h *be discrete holomorphic functions on* $V(\Lambda_0)$ *and* $V(\diamondsuit_0)$, *respectively. Furthermore, let* $v_0 \in V(\Lambda_0) \backslash V(\partial \Lambda_0)$ *and* $Q_0 \in V(\diamondsuit_0)$ *be given, and let* $K_{v_0} : V(\diamondsuit) \to \mathbb{C}$ *and* $K_{Q_0} : V(\Lambda) \to \mathbb{C}$ *be discrete Cauchy's kernels with respect to* v_0 *and* Q_0 *on* $V(\diamondsuit_0)$ *and* $V(\Lambda_0)$, *respectively.*

Then, for any discrete contours C_{v_0} *and* C_{Q_0} *on* X_0 *surrounding* v_0 *and* Q_0, *respectively, once in counterclockwise order, discrete Cauchy's integral formulae hold:*

$$f(v_0) = \frac{1}{2\pi i} \oint_{C_{v_0}} f K_{v_0} dz \quad \text{and} \quad h(Q_0) = \frac{1}{2\pi i} \oint_{C_{Q_0}} h K_{Q_0} dz.$$

Proof Let P_v and P_Q be discrete elementary cycles, v being an interior vertex and Q an interior face of Λ_0. By Lemma 2.3 that relates ∂_Λ, $\bar{\partial}_\Lambda$ with discrete contour integrals and the definition of $\bar{\partial}_\diamond$, we get:

$$\frac{1}{2\pi i} \oint_{P_v} f K_{v_0} dz = \frac{1}{\pi} \mathrm{ar}(F_v) f(v) \bar{\partial}_\diamond K_{v_0}(v) = \delta_{vv_0} f(v),$$

$$\frac{1}{2\pi i} \oint_{P_Q} f K_{v_0} dz = \frac{1}{\pi} \mathrm{ar}(F_Q) \bar{\partial}_\Lambda f(Q) K_{v_0}(Q) = 0.$$

Here, we used that the value of the product on $[Q', v'] \in E(X_0)$ is $f(v')K_{v_0}(Q')$, so in the first integration we could factor out $f(v)$, in the second one $K_{v_0}(Q)$.

By definition, the discrete contour C_{v_0} is the oriented boundary of a topological disk in $F(X_0)$, so we can decompose the integration along C_{v_0} into a couple of integrations along discrete elementary cycles P_v and P_Q as above. Summing up, only the contribution of P_{v_0} is nonvanishing, and we get the desired result. The second formula is shown in an analog fashion.

Remark In the case of rhombic quad-graphs, Mercat formulated a discrete Cauchy's integral formula for the average of a discrete holomorphic function on $V(\Lambda)$ along an edge of Λ. In [6], Chelkak and Smirnov provided a discrete Cauchy's integral formula for discrete holomorphic functions on $V(\diamondsuit)$ using an integration along cycles on Γ and Γ^*, see Sect. 2.6.1.

Theorem 2.36 *Let $f : V(\Lambda_0) \to \mathbb{C}$ be discrete holomorphic, let $Q_0 \in V(\diamondsuit_0)$, and let $K_{Q_0} : V(\Lambda_0) \to \mathbb{C}$ be a discrete Cauchy's kernel with respect to Q_0 on $V(\Lambda_0)$.*

Then, for any discrete contour C_{Q_0} in X_0 surrounding Q_0 once in counterclockwise order that does not contain any edge $[Q_0, v]$ of X_0, $v \sim Q_0$ (see Fig. 5), the discrete Cauchy's integral formula is true:

$$\partial_\Lambda f(Q_0) = -\frac{1}{2\pi i} \oint_{C_{Q_0}} f \partial_\Lambda K_{Q_0} dz.$$

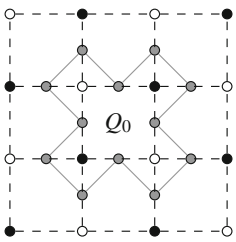

Fig. 5 Discrete contour as in Theorem 2.36

Proof Let D be the discrete domain in $F(X_0)$ bounded by C_{Q_0}. Since no edge of C_{Q_0} passes through Q_0, the discrete one-form $\bar{\partial}_\Lambda K_{Q_0} d\bar{z}$ vanishes on C_{Q_0}. Therefore, $dK_{Q_0} = \partial_\Lambda K_{Q_0} dz$ on C_{Q_0} and

$$\oint_{C_{Q_0}} f \partial_\Lambda K_{Q_0} dz = \oint_{C_{Q_0}} f dK_{Q_0} = \iint_D d(f dK_{Q_0}) = \iint_D df \wedge dK_{Q_0}$$

due to discrete Stokes' Theorem 2.9 in the second equality and Theorem 2.16 that assures that $d(f dK_{Q_0}) = df \wedge dK_{Q_0} + f dd K_{Q_0}$ and Proposition 2.10 that assures that $dd K_{Q_0} = 0$ in the third equality. Now, f is discrete holomorphic, so we obtain $df \wedge dK_{Q_0} = \partial_\Lambda f \bar{\partial}_\Lambda K_{Q_0} \Omega_\diamondsuit$. But $\bar{\partial}_\Lambda K_{Q_0}$ vanishes on all vertices of $\diamondsuit_0$ but Q_0. Finally,

$$-\frac{1}{2\pi i} \oint_{C_{Q_0}} f \partial_\Lambda K_{Q_0} dz = -\frac{1}{2\pi i} \iint_{F_{Q_0}} \partial_\Lambda f \bar{\partial}_\Lambda K_{Q_0} \Omega_\diamondsuit = \partial_\Lambda f(Q_0).$$

Remark In general, there exists no analog of the above Theorem 2.36 for the discrete derivative of a discrete holomorphic function on $V(\diamondsuit_0)$, because the discrete derivative itself does not need to be discrete holomorphic. However, in the special case of integer lattices, any discrete derivative of a discrete holomorphic function is itself discrete holomorphic. In Sect. 3.5, we will obtain discrete analogs of Cauchy's integral formulae for higher derivatives of discrete holomorphic functions.

2.6.1 A Different Notation

Let W be a cycle on the edges of Γ^*, having (ordered) white vertices $w_0, w_1, \ldots, w_m$, $w_m = w_0$. Then, any edge connecting two consecutive vertices w_k, w_{k+1} forms the diagonal of a quadrilateral face $Q(w_k, w_{k+1}) \in V(\diamondsuit)$. We denote the set of such faces together with the induced orientation of their white diagonals by $W_\diamondsuit$. For $Q \in W_\diamondsuit$, we denote its white vertices by $w_-(Q), w_+(Q)$ such that the corresponding oriented diagonal goes from $w_-(Q)$ to $w_+(Q)$. Its black vertices are denoted by $b(Q), b'(Q)$ in such a way that $w_-(Q), b(Q), w_+(Q), b'(Q)$ appear in counterclockwise order. The reason why we do not choose our previous notation of Fig. 1 is that black and white vertices now play a different role that shall be indicated by the notation.

Now, we construct a cycle B on the edges of Γ having (ordered) black vertices $b_0, b_1, \ldots, b_n$, $b_n = b_0$, in the following way. We start with $b_0 := b(Q(w_0, w_1))$. In the star of the vertex w_1, there are two simple paths on Γ connecting b_0 and $b(Q(w_1, w_2))$, and we choose the path that does not go through $Q(w_0, w_1)$. Note that it may happen that $b(Q(w_1, w_2)) = b_0$; in this case, we do not add any vertices to B. Also, $w_2 = w_0$ is possible, which causes adding the nondirect path connecting the black vertices b_0 and $b(Q(w_1, w_2)) = b'(Q(w_0, w_1))$.

Continuing this procedure till we have connected $b\,(Q\,(w_{m-1}, w_m))$ with b_0, we end up with a closed path B on Γ. Without loss of generality, any two consecutive vertices in B are different. As above, any edge connecting two consecutive vertices b_k, b_{k+1} forms the diagonal of a face $Q(b_k, b_{k+1}) \in V(\Diamond)$. We denote the set of such faces together with the induced orientation of their black diagonals by $B_\Diamond$. For $Q \in B_\Diamond$, we denote its black vertices by $b_-(Q), b_+(Q)$ such that the corresponding oriented diagonal goes from $b_-(Q)$ to $b_+(Q)$. Finally, its white vertices are denoted by $w(Q), w'(Q)$ in such a way that $b_-(Q), w'(Q), b_+(Q), w(Q)$ appear in counterclockwise order.

Definition Let W and B be cycles as above and h a function defined on $W_\Diamond \cup B_\Diamond$. We define the *discrete integrals* along W and B by

$$\oint_W h(Q)dz := \sum_{k=0}^{m-1} h\,(Q\,(w_k, w_{k+1}))\,(w_{k+1} - w_k)\,,$$

$$\oint_W h(Q)d\bar{z} := \sum_{k=0}^{m-1} h\,(Q\,(w_k, w_{k+1}))\,\overline{(w_{k+1} - w_k)};$$

$$\oint_B h(Q)dz := \sum_{k=0}^{n-1} h\,(Q\,(b_k, b_{k+1}))\,(b_{k+1} - b_k)\,,$$

$$\oint_B h(Q)d\bar{z} := \sum_{k=0}^{n-1} h\,(Q\,(b_k, b_{k+1}))\,\overline{(b_{k+1} - b_k)}.$$

In between the closed paths B and W, there is a cycle P on the medial graph X that comprises exactly all edges $[Q, v]$ with $Q \in W_\Diamond$ and $v \in B$ incident to Q and all edges $[Q, v]$ with $Q \in B_\Diamond$ and $v \in W$ incident to Q. The orientation of $[Q, v]$ is induced by the orientation of the corresponding parallel white or black diagonal. Figure 6 gives an example for this construction, where all cycles are oriented counterclockwise.

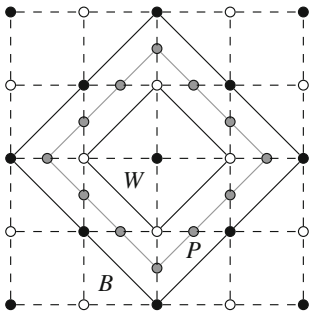

Fig. 6 Cycles W on Γ^*, B on Γ, and closed path P on X in between

Remark Note that an oriented cycle P on X induces a white cycle $W = W(P)$ and a black cycle $B = B(P)$ in such a way that W, P, and B are related as above.

Lemma 2.37 *Let P be an oriented cycle on X and let $W = W(P)$ and $B = B(P)$ be the white and black cycles it induces. Let f be a function defined on the vertices of W and B and h a function defined on $W_\diamond \cup B_\diamond$. Then,*

$$\oint_W f(b(Q))h(Q)dz + \oint_B f(w(Q))h(Q)dz = 2\oint_P fhdz.$$

Proof Any edge $e = [Q, b(Q)]\,(Q \in W_\diamond)$ or $[Q, w(Q)]\,(Q \in B_\diamond)$ of P is parallel to either an edge $w_-(Q)w_+(Q)$ of W or to an edge $b_-(Q)b_+(Q)$ of B, respectively, and vice versa. Since the complex number associated to e is just half of the corresponding parallel edge of Γ or Γ^*, $2\int_e fh = f(b(Q))\,h(Q)(w_+(Q) - w_-(Q))$ in the first and $2\int_e fh = f(w(Q))\,h(Q)(b_+(Q) - b_-(Q))$ in the second case. Therefore, the discrete integral along P decomposes into one along B and one along W.

Remark Note that the construction of B and Lemma 2.37 are also valid if W consists of a single point or of only two edges (being the same, but traversed in both directions). In both cases, P will be a discrete contour, as well when W is simple and oriented counterclockwise.

The discrete Cauchy's integral formula of Chelkak and Smirnov in [6] reads as

$$\pi i h(Q_0) = \oint_W h(Q)K_{Q_0}(b(Q))dz + \oint_B h(Q)K_{Q_0}(w(Q))dz$$

if $Q_0 \in V(\diamondsuit)$ is surrounded once by the simple closed curve W on Γ^* in counterclockwise direction, h is discrete holomorphic on $V(\diamondsuit)$, and $K_{Q_0} : V(\Lambda) \to \mathbb{C}$ is a discrete Cauchy's kernel with respect to Q_0. The above Lemma 2.37 directly relates this formulation to the one of the discrete Cauchy's integral formula in Theorem 2.35.

Finally, we conclude this section with a proposition relying on the decomposition of a discrete contour into black and white cycles. In Proposition 2.13(i), we have already seen that $fdg + gdf$ is closed for functions $f, g : V(\Lambda) \to \mathbb{C}$. Actually, a slightly stronger statement is true:

Proposition 2.38 *Let W be a closed cycle on Γ^* and B be the corresponding closed cycle on Γ as above, and let $f, g : V(\Lambda) \to \mathbb{C}$. Then,*

$$\oint_W f(b(Q))\left(\partial_\Lambda g(Q)dz + \bar{\partial}_\Lambda g(Q)d\bar{z}\right) + \oint_B g(w(Q))\left(\partial_\Lambda f(Q)dz + \bar{\partial}_\Lambda f(Q)d\bar{z}\right) = 0.$$

Proof We first rewrite the discrete integral along the cycle W. By definition, we have $dg = \partial_\Lambda g dz + \bar{\partial}_\Lambda g d\bar{z}$. By discrete Stokes' Theorem 2.9, $\int_e dg = g(w_+) - g(w_-)$ if e is an edge on X parallel to w_-w_+ and oriented the same, so

$$\oint_W f(b(Q))\left(\partial_\Lambda g(Q)dz + \bar{\partial}_\Lambda g(Q)d\bar{z}\right) = \sum_{Q\in W_\diamondsuit} f(b(Q))\left(g\left(w_+(Q)\right) - g\left(w_-(Q)\right)\right)$$
$$= -\sum_{Q\in B_\diamondsuit} g\left(w(Q)\right)\left(f\left(b_+(Q)\right) - f\left(b_-(Q)\right)\right),$$

where we changed the summation along the path W into a summation along the path B in the last step. Similar to above, we rewrite the discrete integral along B as

$$\oint_B g(w(Q))\left(\partial_\Lambda f(Q)dz + \bar{\partial}_\Lambda f(Q)d\bar{z}\right) = \sum_{Q\in B_\diamondsuit} g(w(Q))\left(f\left(b_+(Q)\right) - f\left(b_-(Q)\right)\right).$$

In summary,

$$\oint_W f(b(Q))\left(\partial_\Lambda g(Q)dz + \bar{\partial}_\Lambda g(Q)d\bar{z}\right) + \oint_B g(w(Q))\left(\partial_\Lambda f(Q)dz + \bar{\partial}_\Lambda f(Q)d\bar{z}\right) = 0.$$

3 Discrete Complex Analysis on Planar Parallelogram-Graphs

3.1 Preliminaries

Definition A *planar parallelogram-graph* Λ (without boundary) is a planar quad-graph without boundary such that all its faces are parallelograms. Its dual $\diamondsuit$ is embedded in the complex plane by placing all $Q \in V(\diamondsuit)$ at the center $\hat{Q}$ of the corresponding parallelogram Q and connecting adjacent vertices by straight line segments.

Remark Remembering the duality $V(\diamondsuit) \cong F(\Lambda)$, we will omit the hat above Q in the sequel and identify the vertex $Q \in V(\diamondsuit)$ representing a parallelogram in Λ with the corresponding point $\hat{Q}$ in the complex plane. It will be clear from the context whether Q is meant to be a face of Λ or a point in the complex plane.

In Sect. 3, discrete complex analysis on planar parallelogram-graphs Λ is discussed. As in Sect. 2, Λ is bipartite, the induced graphs on black and white vertices are denoted by Γ and Γ^*, respectively, and we assume that the cellular decomposition induced by Λ is locally finite and strongly regular (which already follows from all faces being parallelograms).

In Propositions 2.1, 2.5, and 2.22, we have already seen that discrete complex analysis on parallelogram-graphs is closer to the classical theory than on general quad-graphs. For example, $f(v) = v^2$ is a discrete holomorphic function on $V(\Lambda)$ and $\partial_\Lambda f(Q) = 2Q$; $h(Q) = Q$ is a discrete holomorphic function on $V(\diamondsuit)$ and $\partial_\diamondsuit h \equiv 1$; and the discrete Laplacian $\triangle$ approximates the smooth one correctly up to order two.

In order to concentrate on the calculation of the asymptotics of a certain discrete Green's function and discrete Cauchy's kernels, we postpone the discussion of some necessary combinatorial and geometric results on planar parallelogram-graphs to the appendix. Our setup is closely related to the quasicrystallic parallelogram-graphs discussed in [2]. There, the quad-graph was embedded into $\mathbb{Z}^n$ and explicit formulae for a discrete exponential function and a discrete logarithm were introduced. These results relied on Kenyon's formulae for a discrete exponential and a discrete Green's function in [16].

In the following, the ideas of [2] are adapted to our slightly more general setting in Sect. 3.2. The discrete exponential is the basic building block for the integral formulae of a discrete Green's function in Sect. 3.3 and discrete Cauchy's kernels in Sect. 3.4. The corresponding functions can be defined for general planar parallelogram-graphs, but we need more regularity of the graph to calculate their asymptotics. The two conditions we use are that all interior angles of the parallelograms are bounded (the same condition was used by Chelkak and Smirnov in [6]) and that the ratio of side lengths of the parallelograms is bounded as well. For rhombic quad-graphs, the second condition is trivially fulfilled; for quasicrystallic graphs, there are only a finite number of interior angles. Note that instead of using boundedness of the ratio of side lengths of the parallelograms, we can assume that the side lengths themselves are bounded. This seems to be a stronger condition at first, but actually, both conditions are equivalent, see Proposition 4.3 in the appendix.

Remark To our knowledge, it is an open problem to find an explicit formula for a discrete Green's function or a discrete Cauchy's kernel in the case of general quad-graphs as discussed in Sect. 2.

We conclude this section by a discussion of integer lattices in Sect. 3.5. On these graphs, discrete holomorphic functions can be discretely differentiated infinitely many times, and for all higher order discrete derivatives, discrete Cauchy's integral formulae with the asymptotics one expects from the asymptotics of the discrete Cauchy's integral formula for a discrete holomorphic function hold true.

Lemma 3.1 *Let $v, v' \in V(\Lambda)$, let k be an odd integer, let $e_1, \dots, e_n$ be a sequence of n oriented edges of Λ forming a directed path from v to v' on Λ, and let $f_1, \dots, f_m$ be another such sequence of m oriented edges. Then,*

$$\sum_{j=1}^{n} e_j^k = \sum_{j=1}^{m} f_j^k .$$

Here, the calculations are performed directly with edges rather than replacing them with their associated complex numbers (see Sect. 2.1.1).

Proof Consider a path p_1, p_2, p_3, p_4 of oriented edges of Λ going once around a parallelogram. Since $p_1 = -p_3$ and $p_2 = -p_4$, we have $\sum_{j=1}^{4} p_j^k = 0$. Now, any closed cycle on the planar graph Λ can be decomposed into elementary oriented cycles around faces, where edges $e, -e$ with opposite orientation cancel out, and

pairs of oppositely oriented edges (that are not necessarily successive). Using that $e^k + (-e)^k = 0$, the claim now follows from

$$\sum_{j=1}^{n} e_j^k + \sum_{j=1}^{m} (-f_j)^k = 0$$

for the cycle $e_1, \ldots, e_n, -f_1, \ldots, -f_m$ of oriented edges starting and ending in v.

In the remainder of the paper, we use the following shorthand notation.

Definition Let $v, v' \in V(\Lambda)$ and $Q, Q' \in V(\diamondsuit)$.

(i) Choose any directed path of edges $e_1, \ldots, e_n$ on Λ going from v' to v. Define

$$J(v, v') := \sum_{j=1}^{n} e_j^{-1},$$

which does not depend on the choice of path from v to v' due to Lemma 3.1.

(ii) Choose any vertex v_Q incident to Q and any directed path of edges $e_1, \ldots, e_n$ on Λ from v to v_Q. Moreover, let d_1, d_2 be the two oriented edges of Q that emanate in v_Q. We now define

$$-J(v, Q) = J(Q, v) := \sum_{j=1}^{n} e_j^{-1} + \frac{1}{2} d_1^{-1} + \frac{1}{2} d_2^{-1}.$$

Note that $J(Q, v)$ does not depend on the choice of path from v to v_Q by Lemma 3.1 nor on the choice of v_Q by a similar argument as in the proof of the above lemma.
Moreover, let $\tau(v, Q) = \tau(Q, v) := 1/(d_1 d_2)$ if v_Q, v are both in $V(\Gamma)$ or both in $V(\Gamma^*)$ and $\tau(v, Q) = \tau(Q, v) := -1/(d_1 d_2)$ otherwise. Since Q is a parallelogram, these quantities depend on v and Q only.

(iii) Choose any vertices $v_{Q'}$ incident to Q' and v_Q incident to Q and a directed path of edges $e_1, \ldots, e_n$ on Λ going from $v_{Q'}$ to v_Q. Let d_1, d_2 be the two oriented edges of Q' ending in $v_{Q'}$ and f_1, f_2 the two oriented edges of Q emanating from v_Q. Define

$$J(Q, Q') := \frac{1}{2} d_1^{-1} + \frac{1}{2} d_2^{-1} + \sum_{j=1}^{n} e_j^{-1} + \frac{1}{2} f_1^{-1} + \frac{1}{2} f_2^{-1}.$$

$J(Q, Q')$ does not depend on the choice of $v_{Q'}$ and v_Q or the path from $v_{Q'}$ to v_Q.

Furthermore, let $\tau(Q, Q') := 1/(d_1 d_2 f_1 f_2)$ if v_Q, $v_{Q'}$ are both in $V(\Gamma)$ or both in $V(\Gamma^*)$ and $\tau(Q, Q') := -1/(d_1 d_2 f_1 f_2)$ otherwise. $\tau(Q, Q')$ depends on Q and Q' only, since they are both parallelograms.

Remark In the case that all parallelograms are rhombi of side length one, we have $J(x, x') = \overline{x - x'}$.

Finally, the notion of the argument of a complex number will become important in the sequel. In our paper, it will be usually an arbitrary real number and not a number modulo 2π.

Definition For a complex number $\lambda \neq 0$, a real number ϕ such that $\lambda / \exp(i\phi)$ is a positive real number is called *argument of* λ. On the other hand, $\arg(\lambda)$ denotes the unique argument ϕ of λ that is contained in the interval $(-\pi, \pi]$.

3.2 Discrete Exponential Function

Definition Let v_0 be a vertex of Λ. Then, the *discrete exponentials* $\mathrm{e}(\lambda, \cdot; v_0)$ and $\exp(\lambda, \cdot; v_0)$ on $V(\Lambda)$ are the rational functions in the complex variable λ that are inductively defined by $\mathrm{e}(\lambda, v_0; v_0) = 1 = \exp(\lambda, v_0; v_0)$ and

$$\frac{\mathrm{e}(\lambda, v'; v_0)}{\mathrm{e}(\lambda, v; v_0)} = \frac{\lambda + (v' - v)}{\lambda - (v' - v)} \quad \text{and} \quad \frac{\exp(\lambda, v'; v_0)}{\exp(\lambda, v; v_0)} = \frac{1 + \frac{\lambda}{2}(v' - v)}{1 - \frac{\lambda}{2}(v' - v)}$$

for all vertices $v, v' \in V(\Lambda)$ adjacent to each other.

Remark Note that the quotient of e or exp at the vertices of an oriented edge e is by definition the inverse of the quotient for the edge $-e$ oriented in the opposite direction. Since all faces of Λ are parallelograms, the complex numbers associated to opposite edges oriented the same are equal and therefore are corresponding quotients of the discrete exponentials. Thus, the discrete exponentials are well-defined.

For $v \in V(\Lambda)$, $\exp(\cdot, v; v_0)$ is a rational function on $\mathbb{C}$ with poles being the complex numbers associated to the oriented edges of a shortest directed path connecting v_0 with v. It follows from Lemma 4.2 in the appendix that the arguments of all poles can be chosen to lie in an interval of length less than π. If in addition the interior angles of parallelograms are bounded from below by α_0, then the arguments of all poles can be chosen to lie even in an interval of length at most $\pi - \alpha_0$.

Remark Note that $\exp(\lambda, \cdot; v_0) = \mathrm{e}(2/\lambda, \cdot; v_0)$. Hence, e and exp are equivalent up to reparametrization. On square lattices, the discrete exponential was already considered by Ferrand [12] and Duffin [9]. The discrete exponential e on rhombic lattices was used in the papers [2, 5, 16]. To be comparable to these, we use e and not exp to perform our calculations of the asymptotic behavior. In contrast, Mercat [20], Chelkak and Smirnov [6] preferred the parametrization of exp that is closer to the smooth setting. Indeed, Mercat remarked that the discrete exponential exp in the rhombic setting is a generalization of the formula

$$\exp(\lambda x) = \left(\frac{1+\frac{\lambda x}{2n}}{1-\frac{\lambda x}{2n}}\right)^n + O\left(\frac{\lambda^3 x^3}{n^2}\right)$$

to the case when the path from the origin to x consists of $O(|x|/\delta)$ straight line segments of length δ of any directions [20].

Definition For a face $Q \in V(\Diamond)$ with incident vertices v_-, v'_-, v_+, v'_+ in counterclockwise order and $v \in V(\Lambda)$, we define the *discrete exponentials* as the following rational functions in the complex variable λ:

$$\mathrm{e}(\lambda, v; Q) := \frac{\mathrm{e}(\lambda, v; v_\pm)}{\left(\lambda - (v_\pm - v'_+)\right)\left(\lambda - (v_\pm - v'_-)\right)},$$
$$\exp(\lambda, Q; v) := \frac{\exp(\lambda, v_\pm; v)}{\left(1 - \frac{\lambda}{2}(v'_+ - v_\pm)\right)\left(1 - \frac{\lambda}{2}(v'_- - v_\pm)\right)}.$$

Remark For arbitrary $Q_0 \in V(\Diamond)$ and $v_0 \in V(\Lambda)$, the above definition yields well-defined rational functions $\mathrm{e}(\cdot, v_0; Q_0)$ and $\exp(\cdot, Q_0; v_0)$. As long as λ is not a pole, $\mathrm{e}(\lambda, \cdot; Q_0)$ is a function on $V(\Lambda)$ and $\exp(\lambda, \cdot; v_0)$ is a function on $V(\Diamond)$.

Proposition 3.2 *Let $v_0 \in V(\Lambda)$, $Q \in V(\Diamond)$. Then, for any $\lambda \in \mathbb{C}$ that is not a pole of $\exp(\cdot, v; v_0)$ for any vertex $v \sim Q$, $\exp(\lambda, \cdot; v_0)$ is discrete holomorphic at Q and*

$$\left(\partial_\Lambda \exp(\lambda, \cdot; v_0)\right)(Q) = \lambda \exp(\lambda, Q; v_0).$$

Proof Let v_-, v'_-, v_+, v'_+ be the vertices of Q in counterclockwise order. Let us denote $a := v'_+ - v_-$ and $b := v'_- - v_-$. Using Lemma 2.3 that describes $\bar\partial_\Lambda$ as a discrete contour integration, $v_+ - v_- = a + b$, $v'_+ - v'_- = a - b$, and the inductive formula for exp, we get that $\left(\bar\partial_\Lambda \exp(\lambda, \cdot; v_0)\right)(Q)$ equals

$$\begin{aligned}
&\frac{\exp(\lambda, v_-; v_0)}{2i\,\mathrm{ar}(F_Q)} \oint_{\partial F_Q} \frac{\exp(\lambda, \cdot; v_0)}{\exp(\lambda, v_-; v_0)} dz \\
=&\frac{\exp(\lambda, v_-; v_0)}{2i\,\mathrm{ar}(F_Q)} \left(\frac{a+b}{2} \cdot \left(\frac{1+\frac{\lambda}{2}b}{1-\frac{\lambda}{2}b} - \frac{1+\frac{\lambda}{2}a}{1-\frac{\lambda}{2}a}\right) + \frac{a-b}{2} \cdot \left(\frac{1+\frac{\lambda}{2}b}{1-\frac{\lambda}{2}b}\frac{1+\frac{\lambda}{2}a}{1-\frac{\lambda}{2}a} - 1\right)\right) \\
=&\frac{\exp(\lambda, v_-; v_0)}{4i\,\mathrm{ar}(F_Q)\left(1-\frac{\lambda}{2}a\right)\left(1-\frac{\lambda}{2}b\right)} \left((a+b)\,\lambda\,(b-a) + (a-b)\,\lambda\,(a+b)\right) = 0.
\end{aligned}$$

Here, F_Q is the Varignon parallelogram inside Q, and $\mathrm{ar}(F_Q) = \mathrm{area}(Q)$. Similarly, we obtain that $\left(\partial_\Lambda \exp(\lambda, \cdot; v_0)\right)(Q)$ equals

$$\begin{aligned}
&\frac{\exp(\lambda, v_-; v_0)}{4i\,\mathrm{ar}(F_Q)\left(1-\frac{\lambda}{2}a\right)\left(1-\frac{\lambda}{2}b\right)} \left(-\overline{(a+b)}\lambda\,(b-a) + \overline{(b-a)}\lambda\,(a+b)\right) \\
=&\frac{\lambda \exp(\lambda, v_-; v_0)}{2i\,|a||b|\sin(\varphi_Q)\left(1-\frac{\lambda}{2}a\right)\left(1-\frac{\lambda}{2}b\right)} 2i\,\mathrm{Im}(a\bar b) = \lambda \exp(\lambda, Q; v_0).
\end{aligned}$$

3.3 Asymptotics of the Discrete Green's Function

Following the presentation in [2], we first define a discrete logarithmic function on the lift $\tilde{\Lambda}_{v_0}$ of the quad-graph Λ onto the Riemann surface of the logarithmic function $\log(\cdot - v_0)$, which can be considered as a branched covering of the quad-graph Λ seen as a cellular decomposition of the complex plane.

Throughout the following paragraphs, fix $v_0 \in V(\Lambda)$, and let $e_1, e_2, \ldots, e_n$ be the directed edges starting in v_0, ordered according to their slopes.

Definition To each of these edges e we assign the angle $\theta_e := \arg(e) \in (-\pi, \pi]$. We assume that $\theta_{e_1} < \theta_{e_n}$. Now, define $\theta_{a+bn} := \theta_a + 2\pi b$, where $a \in \{1, \ldots, n\}$ and $b \in \mathbb{Z}$. For $m \in \mathbb{Z}$, let $e_m := e_{m \bmod n}$, considering the residue classes $\{1, 2, \ldots, n\}$.

Definition Let e be one of the e_k. The *sector* $U_e \subset \Lambda$ is the subgraph of Λ that consists of all vertices and edges of directed paths on Λ starting in v_0 whose oriented edges have arguments that can be chosen to lie in $[\arg(e), \arg(e) + \pi)$.

Definition For $m \in \mathbb{Z}$, we define the graph $\tilde{U}_m$ to be the sector U_{e_m} with the additional data that each vertex v of U_{e_m} besides v_0 is assigned the real number $\vartheta_m(v)$ given by $\vartheta_m(v) \equiv \arg(v - v_0) \bmod 2\pi$ and $\vartheta_m(v) \in [\theta_m, \theta_m + \pi)$. Then,

$$\tilde{U} := \bigcup_{m=-\infty}^{\infty} \tilde{U}_m$$

defines a graph $\tilde{\Lambda}_{v_0}$ on the Riemann surface of $\log(\cdot - v_0)$ that projects to the planar parallelogram graph Λ. Here, vertices v of U_{e_m} and v' of $U_{e_{m'}}$ are equal as vertices of $\tilde{U}_m$ and $\tilde{U}_{m'}$ if and only if $v = v'$ and either $v = v' = v_0$ or $\vartheta_m(v) = \vartheta_{m'}(v')$.

Remark Apart from the additional data of the vertices, $\tilde{U}_m$ is composed of all the vertices of edges of directed paths of edges on Λ starting in v_0 whose arguments can be chosen to lie in $[\theta_m, \theta_m + \pi)$. It follows that all $\tilde{U}_{m+bn}$, $b \in \mathbb{Z}$ and $1 \leqslant m \leqslant n$, cover the same sector U_{e_m}, and $\tilde{U}_m \cap \tilde{U}_{m'}$ contains more than just v_0 if and only if $|m - m'| < n$. In addition, Lemma 4.2 shows that the union of all U_{e_k}, $k = 1, \ldots, n$, covers the whole quad-graph Λ. It follows that $\tilde{\Lambda}_{v_0}$ is a branched covering of the cellular decomposition Λ, branched over v_0.

Definition To each vertex $\tilde{v} \in V(\tilde{\Lambda}_{v_0})$ covering a vertex $v \neq v_0$ of Λ, let us denote $\theta_{\tilde{v}} := \vartheta_m(v)$ if $\tilde{v} \in \tilde{U}_m$.

Remark $\theta_{\tilde{v}}$ increases by 2π when the vertex winds once around v_0 in counterclockwise order; and if $\tilde{v}, \tilde{v}' \neq v_0$ are adjacent vertices of $\tilde{\Lambda}_{v_0}$, then $|\theta_{\tilde{v}} - \theta_{\tilde{v}'}| < \pi$.

Note that by construction, if we connect v_0 to some $\tilde{v} \neq v_0$ by a shortest directed path of edges of $\tilde{\Lambda}_{v_0}$, then the arguments of all oriented edges can be chosen to lie all in $(\theta_{\tilde{v}} - \pi, \theta_{\tilde{v}} + \pi)$.

Definition Let $v_0 \in V(\Lambda)$ and let $\tilde{\Lambda}_{v_0}$ be the corresponding branched covering of Λ. The *discrete logarithmic function* on $V(\tilde{\Lambda}_{v_0})$ is given by $\log(v_0; v_0) := 0$ and

$$\log(\tilde{v}; v_0) := \frac{1}{2\pi i} \int_{C_{\tilde{v}}} \frac{\log(\lambda)}{2\lambda} \mathrm{e}(\lambda, v; v_0) d\lambda$$

for $\tilde{v} \neq v_0$. Here, $C_{\tilde{v}}$ is a collection of sufficiently small counterclockwise oriented loops going once around each pole of $\mathrm{e}(\cdot, v; v_0)$, $v \in V(\Lambda)$ being the projection of $\tilde{v} \in V(\tilde{\Lambda}_{v_0})$. On each loop around a pole e, we take the branch of logarithm that satisfies $\mathrm{Im}(\log(e)) \in (\theta_{\tilde{v}} - \pi, \theta_{\tilde{v}} + \pi)$.

Remark Let us suppose that v_0 is a black vertex. In the special case of a rhombic quasicrystallic quad-graph, the notion of the discrete logarithm is motivated as follows [2]: The discrete logarithm is real-valued and does not branch on black vertices; and it is purely imaginary on white points and increases by $2\pi i$ if one goes once around v_0 in counterclockwise order. Therefore, the discrete logarithm models the behavior of the real and the imaginary part of the smooth logarithm if restricted to black and white vertices, respectively. As we will see later in the proof of Proposition 3.4, the values at vertices adjacent to v_0 coincide with the smooth logarithm.

Lemma 3.3 *Let $\tilde{v}, \tilde{v}' \in V(\tilde{\Lambda}_{v_0})$ be two points that cover the same vertex $v \in V(\Lambda)$ such that $\theta_{\tilde{v}'} - \theta_{\tilde{v}} = 2\pi$. Then*

$$\log(\tilde{v}'; v_0) - \log(\tilde{v}; v_0) = 0$$

if v_0, v are both in $V(\Gamma)$ or both in $V(\Gamma^*)$, and otherwise

$$\log(\tilde{v}'; v_0) - \log(\tilde{v}; v_0) = 2\pi i.$$

Proof By definition,

$$\log(\tilde{v}'; v_0) - \log(\tilde{v}; v_0) = \int_{C_{\tilde{v}}} \frac{1}{2\lambda} \mathrm{e}(\lambda, v; v_0) d\lambda.$$

The function that is integrated is meromorphic on $\mathbb{C}$ with poles given by the one of $\mathrm{e}(\cdot, v; v_0)$ and zero. By residue formula, we can replace integration along $C_{\tilde{v}}$ by an integration along a circle centered at 0 with large radius R (such that all other poles lie inside the disk) in counterclockwise direction and an integration along a circle centered at 0 with small radius r (such that all poles lie outside the disk) in clockwise direction. Now, $\mathrm{e}(\infty, v; v_0) = 1$. If v_0, v are both in $V(\Gamma)$ or both in $V(\Gamma^*)$, then $\mathrm{e}(0, v; v_0) = 1$, otherwise $\mathrm{e}(0, v; v_0) = -1$. Hence, $\log(\tilde{v}'; v_0) - \log(\tilde{v}; v_0) = 0$ in the first and $\log(\tilde{v}'; v_0) - \log(\tilde{v}; v_0) = 2\pi i$ in the latter case.

In particular, the real part of the discrete logarithm $\log(\cdot; v_0)$ is a well-defined function on $V(\Lambda)$. Divided by 2π, one actually obtains a discrete Green's function

with respect to v_0. In the rhombic case, it coincides with Kenyon's discrete logarithm in [16] as was shown in [2].

Proposition 3.4 *Let v_0 be a vertex of $V(\Lambda)$. The function $G(\cdot; v_0) : V(\Lambda) \to \mathbb{R}$ defined by $G(v_0; v_0) = 0$ and*

$$G(v; v_0) = \frac{1}{2\pi} \operatorname{Re}\left(\frac{1}{2\pi i} \int_{C_v} \frac{\log(\lambda)}{2\lambda} e(\lambda, v; v_0) d\lambda \right)$$

for each $v \neq v_0$ is a (free) discrete Green's function with respect to v_0. Here, C_v is a collection of sufficiently small counterclockwise oriented loops going once around each pole of $e(\cdot, v; v_0)$, and on each loop around a pole e, we take the branch of log *where* $\operatorname{Im}(\log(e)) \in (\arg(v - v_0) - \pi, \arg(v - v_0) + \pi)$.

Proof When evaluating the real part of the integral, we can also take the branches of the logarithm that satisfy $\operatorname{Im}(\log(e)) \in (\arg(v - v_0) - \pi, \arg(v - v_0) + \pi) + 2k\pi$ for all poles e, where $k \in \mathbb{Z}$ is fixed. Indeed, Lemma 3.3 asserts that under this change, the discrete logarithm changes by 0 or $2k\pi i$, so the real part does not change.

Consider all faces incident to v_0 in Λ and its lift to $\tilde{\Lambda}_{v_0}$. For any vertex $v'_s \in V(\Lambda)$ adjacent to v_0, $\lambda = v'_s - v_0$ is the only pole of $e(\lambda, v'_s; v_0)$. The residue theorem shows that $\log(\tilde{v}'_s; v_0)$ and $\log(v'_s - v_0)$ coincide up to a multiple of $2\pi i$ if $\tilde{v}'_s$ covers v'_s. By a similar calculation for vertices v_s adjacent to v_0 in Γ or Γ^*, we finally get

$$G(v'_s; v_0) = \frac{1}{2\pi} \operatorname{Re}(\log(v'_s - v_0)),$$
$$G(v_s; v_0) = \frac{1}{2\pi} \operatorname{Re}\left(\left(\log\left(v'_s - v_0\right) - \log\left(v'_{s-1} - v_0\right) \right) \frac{v_s - v_0}{v'_s - v'_{s-1}} \right),$$

where v_0, v'_{s-1}, v_s, v'_s are the vertices of $Q_s \sim v_0$ in counterclockwise order.

As in Corollary 2.20, let $\rho_s := -i(v'_s - v'_{s-1})/(v_s - v_0)$. In addition, we assign angles $\theta_{v'_s} \equiv \arg\left(v'_s - v_0\right) \bmod 2\pi$ in such a way that $0 < \theta_{v'_s} - \theta_{v'_{s-1}} < \pi$. Due to $\operatorname{Re}(-i/\rho_s) = -\operatorname{Im}(\rho_s)/|\rho_s|^2$ and $\operatorname{Im}(-i/\rho_s) = -\operatorname{Re}(\rho_s)/|\rho_s|^2$,

$$\begin{aligned}
&\frac{|\rho_s|^2 (G(v_s; v_0) - G(v_0; v_0)) + \operatorname{Im}(\rho_s) \left(G(v'_s; v_0) - G(v'_{s-1}; v_0)\right)}{\operatorname{Re}(\rho_s)} \\
=&\frac{|\rho_s|^2 \operatorname{Re}(-i/\rho_s) + \operatorname{Im}(\rho_s)}{2\pi \operatorname{Re}(\rho_s)} \log\left|\frac{v'_s - v_0}{v'_{s-1} - v_0}\right| - \frac{|\rho_s|^2 \operatorname{Im}(-i/\rho_s)}{2\pi \operatorname{Re}(\rho_s)} \left(\theta_{v'_s} - \theta_{v'_{s-1}}\right) \\
=&\frac{\theta_{v'_s} - \theta_{v'_{s-1}}}{2\pi}.
\end{aligned}$$

It follows from the explicit formula for the discrete Laplacian in Corollary 2.20 that $\triangle G(v_0; v_0) = 1/(2\operatorname{ar}(F_{v_0}))$.

Now, we show that $G(\cdot; v_0)$ is discrete harmonic away from v_0. For this, we consider the star of some vertex $v \neq v_0$, i.e., all faces of Λ incident to $v \in V(\Lambda)$.

Let us assume that we can find one collection C of loops together with appropriate branches of log such that for all vertices v' of the star, $G(v'; v_0)$ can be computed by an integration along C instead of $C_{v'}$. Then, when we compute $\triangle G(v; v_0)$, we can exchange the discrete Laplacian not only with the real part, but also with the integration. Since $\mathrm{e}(\lambda, \cdot; v_0)$ is discrete holomorphic by Proposition 3.2, it is also discrete harmonic by Corollary 2.21. By this, we conclude that $\triangle G(v; v_0) = 0$.

It remains to show that there exists such a collection C of loops with corresponding branches of log. We will show that a collection of sufficiently small counterclockwise oriented loops going once around each pole of $\mathrm{e}(\cdot, v'; v_0)$, v' any vertex of the star of v, does the job, where around a pole e of $\mathrm{e}(\cdot, v'; v_0)$ that branch of logarithm is taken where $\mathrm{Im}(\log(e)) \in (\arg(v' - v_0) - \pi, \arg(v' - v_0) + \pi)$. For this, we just have to show that the branches of the logarithm are well-defined. This is the case if for two vertices v', v'' of the star and a common pole e of $\mathrm{e}(\cdot, v'; v_0)$ and $\mathrm{e}(\cdot, v''; v_0)$, there is an argument of e contained in both $(\arg(v' - v_0) - \pi, \arg(v' - v_0) + \pi)$ and $(\arg(v'' - v_0) - \pi, \arg(v'' - v_0) + \pi)$.

It easily follows from $v \neq v_0$ that if v'' is not adjacent to v', there is a vertex w adjacent to v' such that all common poles of $\mathrm{e}(\cdot, v'; v_0)$ and $\mathrm{e}(\cdot, v''; v_0)$ are also common poles of $\mathrm{e}(\cdot, v'; v_0)$ and $\mathrm{e}(\cdot, w; v_0)$. So let us assume without loss of generality that v' and v'' are adjacent. Clearly, we can also assume that both vertices are different from v_0 since $\mathrm{e}(\cdot, v_0; v_0) \equiv 1$.

Let us suppose the converse from our claim, that means suppose that there is a common pole e of $\mathrm{e}(\cdot, v'; v_0)$ and $\mathrm{e}(\cdot, v''; v_0)$ such that no argument of the edge e is contained in both the two intervals $(\arg(v' - v_0) - \pi, \arg(v' - v_0) + \pi)$ and $(\arg(v'' - v_0) - \pi, \arg(v'' - v_0) + \pi)$. This can only happen if the edge $v'v''$ intersects the ray $v_0 - te, t \geqslant 0$. But since the edge e is a pole of the discrete exponential, there is a strip with common parallel e, i.e., an infinite path in the dual graph $\Diamond$ with edges dual to edges of Λ that are parallel to e, that separates v_0 from both v' and v'' in such a way that e is pointing toward the region of v' and v'' (see the first part of the appendix for more information on a strip). In particular, the edge $v'v''$ is separated from the ray $v_0 - te$, $t \geqslant 0$, and cannot intersect it, contradiction.

Remark With almost the same arguments as in the proof of Proposition 3.4, we see that the discrete logarithm is a discrete holomorphic function on the vertices of $\tilde{\Lambda}_{v_0}$. In [2], it was shown that the discrete logarithm on rhombic quasicrystallic quad-graphs is even more than discrete holomorphic, namely isomonodromic.

Before we derive the asymptotics of the discrete Green's function given in Proposition 3.4, we state and prove some necessary estimations in two separate lemmas since we will use them later during the corresponding calculations for the discrete Cauchy's kernel in Sect. 3.4.

Lemma 3.5 *Let $E_1 \geqslant E_0 > 0$ be fixed real constants and consider a complex variable λ. Then, for any $e \in \mathbb{C} \setminus \{0\}$ satisfying $E_1 \geqslant |e| \geqslant E_0$, the following holds true, where* log *denotes the principal branch of the logarithm and constants in O-notation depend on E_0 and E_1 only:*

(i) As $\lambda \to 0$,

$$-\frac{\lambda+e}{\lambda-e} = 1 + 2\frac{\lambda}{e} + 2\frac{\lambda^2}{e^2} + O(\lambda^3),$$
$$\log\left(-\frac{\lambda+e}{\lambda-e}\right) = 2\frac{\lambda}{e} + O(\lambda^3), \quad \textit{and} \quad \log\left(-\frac{e}{\lambda-e}\right) = \frac{\lambda}{e} + O(\lambda^2).$$

(ii) As $|\lambda| \to \infty$,

$$\frac{\lambda+e}{\lambda-e} = 1 + 2\frac{e}{\lambda} + 2\frac{e^2}{\lambda^2} + O(\lambda^{-3}),$$
$$\log\left(\frac{\lambda+e}{\lambda-e}\right) = 2\frac{e}{\lambda} + O(\lambda^{-3}), \quad \textit{and} \quad \log\left(\frac{\lambda}{\lambda-e}\right) = \frac{e}{\lambda} + O(\lambda^{-2}).$$

Proof (i)

$$-\frac{\lambda+e}{\lambda-e} = \frac{1+\frac{\lambda}{e}}{1-\frac{\lambda}{e}} = \left(1+\frac{\lambda}{e}\right)\left(1+\frac{\lambda}{e}+\frac{\lambda^2}{e^2}+O(\lambda^3)\right) = 1 + 2\frac{\lambda}{e} + 2\frac{\lambda^2}{e^2} + O(\lambda^3)$$

shows the first equation and implies the second equation noting that

$$\log(1+x) = x - x^2/2 + O(x^3) \text{ as } x \to 0.$$

The series expansion for log also implies the third equation using

$$\frac{-d}{\lambda-d} = \frac{1}{1-\frac{\lambda}{d}} = 1 + \frac{\lambda}{d} + O(\lambda^2).$$

(ii) These equations are shown in a completely analogous way to (i), e/λ taking the place of λ/e.

Lemma 3.6 *Assume that there exist real constants* $\alpha_0 > 0$ *and* $E_1 \geqslant E_0 > 0$ *such that* $\alpha \geqslant \alpha_0$ *and* $E_1 \geqslant e \geqslant E_0$ *for all interior angles* α *and side lengths* e *of parallelograms of* Λ. *Let* $v_0 \in V(\Lambda)$ *and* $Q_0 \in V(\diamondsuit)$ *be fixed and consider* $v \in V(\Lambda)$ *and* $Q \in V(\diamondsuit)$ *in the following.*

(i) Let $k(v)$ *be the combinatorial distance on* Λ *between* v_0 *and* v *(or between a vertex incident to* Q_0 *and* v*).*
Then, $k(v) = \Omega(|v - v_0|)$ *(or* $k(v) = \Omega(|v - Q_0|)$*) as* $|v| \to \infty$.

(ii) $J(v, v_0) = \Omega(v - v_0)$, $J(Q, v_0) = \Omega(Q - v_0)$ *and* $J(Q, Q_0) = \Omega(Q - Q_0)$ *as* $|v|, |Q| \to \infty$.

(iii) $\tau(v, Q_0) = \Omega(1)$ *and* $\tau(Q, Q_0) = \Omega(1)$ *as* $|v|, |Q| \to \infty$.

(iv) Furthermore, assume that $|v - v_0| \geqslant 1$ *and that the arguments of all oriented edges of a shortest directed path on* Λ *from* v_0 *to* v *can be chosen to lie in* $[\theta_0, -\theta_0]$, *where* $\theta_0 := -(\pi - \alpha_0)/2$.

Then, for any $\lambda \in [-E_1\sqrt{|v-v_0|}, -E_1/\sqrt{|v-v_0|}]$:

$$|e(\lambda, v; v_0)| \leqslant \exp\left(-\frac{\cos(\theta_0)\sqrt{|v-v_0|}}{2E_1}\right).$$

Here, constants in the Ω*-notation depend on* α_0*,* E_0*, and* E_1 *only.*

Proof Let $e_1, e_2, \ldots, e_{k(v)}$ denote the oriented edges of Λ of a shortest directed path on Λ from v_0 (or a vertex incident to Q_0) to v. Due to the bound on the interior angles of parallelograms in Λ, there is a real θ_0 such that the arguments of $e_1, e_2, \ldots, e_{k(v)}$ can be chosen to lie all in $[\theta_0, \theta_0 + \pi - \alpha_0]$ by Lemma 4.2. All the claims in the first three parts stay (essentially) the same under rotation of the complex plane, so we may assume that $\theta_0 = -(\pi - \alpha_0)/2$. The same assumption is used in the fourth part.

(i) Under the assumptions above, the projections of the e_k onto the real axis lie on the positive axis and are at least $E_0\cos(\theta_0)$ long since edge lengths are bounded by E_0 from below. It follows that $k(v) \leqslant \mathrm{Re}(v-v_0)/(E_0\cos(\theta_0))$. Using in addition that $k(v) \geqslant |v-v_0|/E_1$, we get $k(v) = \Omega(|v-v_0|)$.

(ii) Using $1/|E_0| \geqslant 1/|e_j| \geqslant 1/|E_1|$ for all j, we get

$$|J(v, v_0)| = \left|\sum_{j=1}^{k(v)} e_j^{-1}\right| \leqslant \frac{k(v)}{E_0} = O(|v-v_0|),$$

$$\mathrm{Re}(J(v, v_0)) = \mathrm{Re}\left(\sum_{j=1}^{k(v)} \frac{\bar{e}_j}{|e_j|^2}\right) \geqslant \frac{1}{E_1^2}\,\mathrm{Re}\left(\sum_{j=1}^{k(v)} e_j\right) = \frac{\cos(\theta_0)|v-v_0|}{E_1^2}.$$

Hence, $J(v, v_0) = \Omega(|v-v_0|)$. This also implies that $J(Q, v_0) = \Omega(Q-v_0)$ since $|J(v, v_0) - J(Q, v_0)| \leqslant 1/|E_0|$ for any v incident to Q, which follows easily from the definition and the lower bound for edge lengths. Similarly, $J(Q, Q_0) = \Omega(Q-Q_0)$ follows from the previous statements if we take v_0 incident to Q_0.

(iii) $E_0^{-2} \geqslant |\tau(Q, Q_0)| \geqslant E_1^{-2}$ and $E_0^{-4} \geqslant |\tau(Q, Q_0)| \geqslant E_1^{-4}$ follow immediately from the definitions and the boundedness of edge lengths.

(iv) Using that $\lambda < 0$ and $\mathrm{Re}(e) > 0$, we get

$$\frac{|\lambda+e|^2}{|\lambda-e|^2} = 1 + \frac{4\lambda\,\mathrm{Re}(e)}{\lambda^2 - 2\lambda\,\mathrm{Re}(e) + |e|^2} \leqslant 1 + \frac{4\lambda\,\mathrm{Re}(e)}{(\lambda-|e|)^2} \leqslant \exp\left(\frac{4\lambda\,\mathrm{Re}(e)}{(\lambda-E_1)^2}\right).$$

Taking the product of such inequalities,

$$|\mathrm{e}(\lambda, v; v_0)| \leqslant \exp\left(\frac{2\lambda\,\mathrm{Re}(v-v_0)}{(\lambda-E_1)^2}\right) \leqslant \exp\left(\frac{2\lambda\cos(\theta_0)|v-v_0|}{(\lambda-E_1)^2}\right).$$

Now, we observe that $\lambda/(\lambda-E_1)^2$ attains its maximum on the boundary. Together with $|v-v_0| \geqslant 1$,

$$\frac{\lambda}{(\lambda - E_1)^2} \leqslant \frac{-\sqrt{|v - v_0|}}{E_1\left(1 + \sqrt{|v - v_0|}\right)^2} \leqslant \frac{-1}{4E_1\sqrt{|v - v_0|}}.$$

Plugging this into the estimation before gives the desired result.

Theorem 3.7 *Assume that there exist real constants $\alpha_0 > 0$ and $E_1 \geqslant E_0 > 0$ such that $\alpha \geqslant \alpha_0$ and $E_1 \geqslant e \geqslant E_0$ for all interior angles α and side lengths e of parallelograms of Λ. Let $v_0 \in V(\Lambda)$ be fixed. Then, the following is true:*

(i) The discrete Green's function $G(\cdot; v_0)$ given in Proposition 3.4 has the following asymptotic behavior as $|v| \to \infty$:

$$G(v; v_0) = \frac{1}{4\pi} \log \left| \frac{v - v_0}{J(v, v_0)} \right| + O\left(|v - v_0|^{-2}\right) \text{ if } v \text{ and } v_0 \text{ are of different color},$$
$$G(v; v_0) = \frac{\gamma_{Euler} + \log(2)}{2\pi} + \frac{1}{4\pi} \log |(v - v_0) J(v, v_0)| + O\left(|v - v_0|^{-2}\right) \text{ otherwise.}$$

(ii) There is exactly one discrete Green's function $G : V(\Lambda) \to \mathbb{R}$ for v_0 that behaves for $|v| \to \infty$ as

$$G(v) = \frac{1}{4\pi} \log \left| \frac{v - v_0}{J(v, v_0)} \right| + o\left(|v - v_0|^{-1/2}\right) \text{ if } v \text{ and } v_0 \text{ are of different color},$$
$$G(v) = \frac{\gamma_{Euler} + \log(2)}{2\pi} + \frac{1}{4\pi} \log |(v - v_0) J(v, v_0)| + o\left(|v - v_0|^{-1/2}\right) \text{ otherwise.}$$

Here, constants in the O-notation depend on α_0, E_0, and E_1 only, and γ_{Euler} denotes the Euler-Mascheroni constant.

Remark Note that due to Lemma 3.6(ii), $J(v, v_0) = \Omega(v - v_0)$ as $|v| \to \infty$.

By Proposition 4.3, we may replace the existence of constants $E_1 \geqslant E_0 > 0$ such that $E_1 \geqslant e \geqslant E_0$ for all side lengths e of parallelograms by the existence of q_0 such that $e/e' \geqslant q_0$ for the two side lengths e, e' of any parallelogram of Λ since the latter implies the first assumption. Then, the constants in the O-notation depend instead of E_0 and E_1 on q_0, e_0, and e_1, where e_0 and e_1 are the side lengths of an arbitrary but fixed parallelogram of Λ.

The proof of the first part follows the ideas of Kenyon [16] and Bücking [5]. Both considered just quasicrystallic rhombic quad-graphs. But the main difference to [16] is that we deform the path of integration into an equivalent one different from Kenyon's, since his approach does not generalize to parallelogram-graphs. As Chelkak and Smirnov did for rhombic quad-graphs with bounded interior angles in [6], Kenyon used that two points $v, v' \in V(\Lambda)$ can be connected by a directed path of edges such that the angle between each directed edge and $v' - v$ is less than $\pi/2$ or the angle between the sum of two consecutive edges and $v' - v$ is less than $\pi/2$. This is true for rhombic quad-graphs, but not for parallelogram-graphs. Instead, we use essentially the same deformation of the path of integration as Bücking did.

Proof (i) The poles $e_1, \dots, e_{k(v)}$ of $\mathrm{e}(\cdot, v; v_0)$ correspond to the directed edges of a path from v_0 to v of minimal length $k(v)$. By Lemma 4.2, there is a real θ_0 such that the arguments of all directed edges above can be chosen to lie in $[\theta_0, \theta_0 + \pi - \alpha_0]$. It is easy to check that the claim is invariant under rotation of the complex plane, so we can assume $\theta_0 = -(\pi - \alpha_0)/2$. By definition,

$$G(v; v_0) = \mathrm{Re}\left(\frac{1}{8\pi^2 i}\int_{C_v} \frac{\log\lambda}{\lambda}\mathrm{e}(\lambda, v; v_0)d\lambda\right),$$

where C_v is a collection of sufficiently small counterclockwise oriented loops going once around each $e_1, \dots, e_{k(v)}$ and log is the principal branch of the logarithm since it satisfies $\mathrm{Im}(\log(e_j)) \in [\theta_0, -\theta_0]$ for all j.

By residue theorem, we can deform C_v into a new path of integration C_v' that goes first along a circle centered at 0 with large radius $R(v)$ (such that all poles lie inside this disk) in counterclockwise direction starting and ending in $-R(v)$, then goes along the line segment $[-R(v), -r(v)]$ followed by the circle centered at 0 with small radius $r(v)$ (such that all poles lie outside this disk) in clockwise direction, and finally goes the line segment $[-R(v), -r(v)]$ backwards. Note that the principal branch of log jumps by $2\pi i$ at the negative real axis where the integration along the two line segments takes place.

By assumption, $E_0 \leqslant |e_j| \leqslant E_1$ for all j. Using $|v - v_0| \geqslant E_0$, it follows that

$$\frac{E_0^5}{2}|v - v_0|^{-4} \leqslant \frac{E_0}{2} < |e_j| < 2E_1 \leqslant 2\frac{E_1}{E_0^4}|v - v_0|^4.$$

In particular, we can choose

$$R(v) := 2\frac{E_1}{E_0^4}|v - v_0|^4 \text{ and } r(v) = \frac{E_0^5}{2}|v - v_0|^{-4}$$

for all $v \neq v_0$. We first look at the contributions of the circles with radii $r(v)$ and $R(v)$ to $G(v; v_0)$.

Let λ be on the small circle with radius $r(v)$. Then, $\lambda = \Omega(|v - v_0|^{-4}) \to 0$ as $|v| \to \infty$. In particular, we can apply $(-\lambda + e)/(\lambda - e) = 1 + 2\lambda/e + O(\lambda^2)$ by Lemma 3.5(i) to estimate $(-1)^{k(v)}\mathrm{e}(\lambda, v; v_0)$. More precisely, the latter is a product of $k(v) = \Omega(|v - v_0|)$ terms (see Lemma 3.6(i)) with $e = e_j$. Multiplying out and using in addition $E_0 \leqslant |e_j| \leqslant E_1$ easily gives for $|v| \to \infty$ that

$$(-1)^{k(v)}\mathrm{e}(\lambda, v; v_0) = 1 + O(|v - v_0|^{-3}).$$

Thus, we get for the integration along the small circle with radius $r(v)$:

$$\begin{aligned}
&\operatorname{Re}\left(\frac{1}{8\pi^2 i}\int_{\pi}^{-\pi}(-1)^{k(v)}\frac{\log(r(v))+i\theta}{r(v)\exp(i\theta)}\left(1+O(|v-v_0|^{-3})\right)d\left(r(v)\exp(i\theta)\right)\right)\\
&=-\operatorname{Re}\left(\frac{1}{8\pi^2}\int_{-\pi}^{\pi}(-1)^{k(v)}\left(\log(r(v))+i\theta\right)\left(1+O(|v-v_0|^{-3})\right)d\theta\right)\\
&=-\frac{(-1)^{k(v)}\log(r(v))}{4\pi}\left(1+O(|v-v_0|^{-3})\right).
\end{aligned}$$

Let us now consider λ to be on the large circle with radius $R(v)$. Then, we have $|\lambda|=\Omega(|v-v_0|^4)\to\infty$ as $|v|\to\infty$. Analogously to above, repeated use of the first equation in Lemma 3.5(ii) gives $\mathrm{e}(\lambda,v;v_0)=1+O(|v-v_0|^{-3})$ as $|v|\to\infty$. Thus, $\log(R(v))/(4\pi)\cdot\left(1+O(|v-v_0|^{-3})\right)$ is the contribution of the circle of radius $R(v)$. In total, the asymptotics for the real part of the integration along the two circles are

$$\frac{1}{4\pi}\left(\log(R(v))-(-1)^{k(v)}\log(r(v))\right)+O(|v-v_0|^{-2}).$$

The two integrations along $[-R(v),-r(v)]$ can be combined into the integral

$$\frac{1}{4\pi}\int_{-R(v)}^{-r(v)}\frac{\mathrm{e}(\lambda,v;v_0)}{\lambda}d\lambda.$$

Since we are interested in the asymptotics for $|v|\to\infty$, we can consider $|v-v_0|\geqslant 1$ large enough and split the integration into the three parts along

$$[-R(v),-E_1\sqrt{|v-v_0|}],\ [-E_1\sqrt{|v-v_0|},-\frac{E_1}{\sqrt{|v-v_0|}}],\ \text{and}\ [-\frac{E_1}{\sqrt{|v-v_0|}},-r(v)].$$

We first show that the contribution of $\lambda\in[-E_1\sqrt{|v-v_0|},-E_1/\sqrt{|v-v_0|}]$ can be neglected. Indeed, it is a consequence of the estimation in Lemma 3.6(iv) that

$$\left|\frac{1}{4\pi}\int_{-E_1\sqrt{|v-v_0|}}^{-E_1/\sqrt{|v-v_0|}}\frac{\mathrm{e}(\lambda,v;v_0)}{\lambda}d\lambda\right|\leqslant E_1\sqrt{|v-v_0|}\exp\left(-\frac{\cos(\theta_0)\sqrt{|v-v_0|}}{2E_1}\right).$$

As $|v|\to\infty$, the latter expression decays faster to zero than any power of $|v-v_0|$.

Now, consider $\lambda\in[-E_1/\sqrt{|v-v_0|},-r(v)]$. Then, $\lambda\to 0$ as $|v|\to\infty$, so using the second equation in Lemma 3.5(i) $k(v)=\Omega(|v-v_0|)$ times gives as $|v|\to\infty$:

$$\begin{aligned}
(-1)^{k(v)}\mathrm{e}(\lambda,v;v_0)&=\exp\left(2\lambda J(v,v_0)+O(k(v)\lambda^3)\right)\\
&=\exp\left(2\lambda J(v,v_0)\right)\left(1+O(|v-v_0|\lambda^3)\right).
\end{aligned}$$

Thus, the integral near the origin is equal to

$$\frac{(-1)^{k(v)}}{4\pi}\int\limits_{-E_1/\sqrt{|v-v_0|}}^{-r(v)}\left(\frac{\exp\left(2\lambda J(v,v_0)\right)}{\lambda}+\exp\left(2\lambda J(v,v_0)\right)O(|v-v_0|\lambda^2)\right)d\lambda.$$

The expansion of the integral of the second term involves two exponential factors, one for each bound: $\exp(-2J(v,v_0)r(v))$ and $\exp(-2E_1J(v,v_0)/\sqrt{|v-v_0|})$. Now, we will use that $J(v,v_0)=\Omega(|v-v_0|)$ by Lemma 3.6(ii). Since the exponent of the first factor goes to 0 in speed $|v-v_0|^{-3}$, the exponential goes exponentially fast to 1 as $|v|\to\infty$. For the second factor, we use our assumption that the arguments of all the poles can be chosen to lie in $[-(\pi-\alpha_0)/2,(\pi-\alpha_0)/2]$. It follows that $\mathrm{Re}(J(v,v_0))$ is positive and goes to infinity like $\Omega(|v-v_0|)$ as $|v|\to\infty$, such that the second exponential factor goes to zero exponentially fast. Now, it is not hard to see that the integral of $\exp\left(2\lambda J(v,v_0)\right)O(|v-v_0|\lambda^3)$ gives $O(|v-v_0|^{-2})$. For the first term, we get

$$\begin{aligned}
&\frac{(-1)^{k(v)}}{4\pi}\left(\int\limits_{-2E_1J(v,v_0)/\sqrt{|v-v_0|}}^{-1}\frac{\exp(s)}{s}ds+\int\limits_{-1}^{-2r(v)J(v,v_0)}\frac{\exp(s)-1}{s}ds\right)\\
&+\frac{(-1)^{k(v)}}{4\pi}\int\limits_{-1}^{-2r(v)J(v,v_0)}\frac{1}{s}ds\\
&=\frac{(-1)^{k(v)}}{4\pi}\left(\int\limits_{-\infty}^{-1}\frac{\exp(s)}{s}ds+\int\limits_{-1}^{0}\frac{\exp(s)-1}{s}ds\right)+\frac{(-1)^{k(v)}}{4\pi}\log(2r(v)J(v,v_0))\\
&-\frac{(-1)^{k(v)}}{4\pi}\left(\int\limits_{-\infty}^{-2E_1J(v,v_0)/\sqrt{|v-v_0|}}\frac{\exp(s)}{s}ds+\int\limits_{-2r(v)J(v,v_0)}^{0}\frac{\exp(s)-1}{s}ds\right)\\
&=\frac{(-1)^{k(v)}}{4\pi}\left(\gamma_{\text{Euler}}+\Omega(|v-v_0|^{-3})+\log(2r(v)J(v,v_0))\right).
\end{aligned}$$

To get to the last line, we used that $\mathrm{Re}(J(v,v_0))=\Omega(|v-v_0|)$ as $|v|\to\infty$ stays positive. Indeed, as $|v|\to\infty$, the first integral in the second to last line goes to zero exponentially fast (to see this, just write the integrand as $s\exp(s)/s^2$ and bound the absolute value of the integral from above by $s_0\exp(s_0)$ where s_0 denotes the term $-2E_1J(v,v_0)/\sqrt{|v-v_0|}$) and the second integral is of order $\Omega(|v-v_0|^{-3})$ as $|v|\to\infty$ as a Taylor expansion of the exponential shows.

Finally, let $\lambda\in[-R(v),-E_1\sqrt{|v-v_0|}]$. Then, $\lambda\to-\infty$ as $|v|\to\infty$, and repeated use of the second equation in Lemma 3.5(ii) gives

$$\mathrm{e}(\lambda, v; v_0) = \exp\left(\frac{2(v-v_0)}{\lambda}\right)\left(1 + O(|v-v_0|\lambda^{-3})\right)$$

as $|v| \to \infty$, so the corresponding contribution of the integral to $4\pi G(v; v_0)$ is

$$\int_{-R(v)}^{-E_1\sqrt{|v-v_0|}} \frac{\exp(\lambda, v; v_0)}{\lambda} d\lambda = \int_{-R(v)}^{-E_1\sqrt{|v-v_0|}} \frac{\exp\left(\frac{2(v-v_0)}{\lambda}\right)}{\lambda} d\lambda + O(|v-v_0|^{-2})$$

$$= \int_{-R(v)/(2(v-v_0))}^{-1} \frac{\exp\left(\frac{1}{s}\right) - 1}{s} ds + \int_{-1}^{-E_1\sqrt{|v-v_0|}/(2(v-v_0))} \frac{\exp\left(\frac{1}{s}\right)}{s} ds$$

$$+ \int_{-R(v)/(2(v-v_0))}^{-1} \frac{1}{s} ds + O(|v-v_0|^{-2})$$

$$= \gamma_{\text{Euler}} - \log\left(\frac{R(v)}{2(v-v_0)}\right) + O(|v-v_0|^{-2})$$

by a similar reasoning as above. Summing up the integrals over all four parts of the contour and taking the real part, we finally get that $4\pi G(v; v_0)$ equals

$$\left(1 + (-1)^{k(v)}\right)(\gamma_{\text{Euler}} + \log(2)) + \log|v-v_0| + (-1)^{k(v)} \log|J(v, v_0)| + O(|v-v_0|^{-2}).$$

(ii) We know from Theorem 2.31 that discrete harmonic functions of asymptotics $o(|v-v_0|^{-1/2})$ as $|v| \to \infty$ are zero. We can apply this result to the discrete harmonic function $G - G(\cdot; v_0)$, where $G(\cdot; v_0)$ from the first part has the desired asymptotics.

Remark Let us compare this result to the case of rhombi of side length one. Assume that $v_0 \in V(\Gamma)$. Then, the discrete logarithm is purely real and nonbranched on $V(\Gamma)$ and purely imaginary and branched on $V(\Gamma^*)$. It follows that $G(v; v_0) = 0$ if $v \in V(\Gamma^*)$, well fitting to the fact that $\triangle$ splits into two discrete Laplacians on Γ and Γ^*. Using $J(v, v_0) = \overline{v - v_0}$,

$$G(v; v_0) = \frac{1}{2\pi}(\gamma_{\text{Euler}} + \log(2) + \log|v-v_0|) + O(|v-v_0|^{-2})$$

as $|v| \to \infty$ for $v \in V(\Gamma)$, exactly as in the work of Bücking [5], who slightly strengthened the error term in Kenyon's work [16]. In this paper, Kenyon showed that there is no further discrete Green's function with asymptotics $o(|v-v_0|)$.

3.4 Asymptotics of Discrete Cauchy's Kernels

Let $v_0 \in V(\Lambda)$ and $Q_0 \in V(\diamondsuit)$ be given. We first give a formula for a discrete Cauchy's kernel K_{v_0} with respect to v_0 on $V(\diamondsuit)$ that has asymptotics $\Omega(|Q-v_0|^{-1})$ as $|Q| \to \infty$. Remember that the vertex $Q \in V(\diamondsuit) \cong F(\Lambda)$ is placed on the center of the corresponding parallelogram. Then, we provide a discrete Cauchy's kernel K_{Q_0} with respect to Q_0 on $V(\Lambda)$ with asymptotics $\Omega(|v-Q_0|^{-1})$ as $v \to \infty$. In both cases, there are no further discrete Cauchy's kernels with asymptotics $o(|Q-v_0|^{-1/2})$ or $o(|v-Q_0|^{-1/2})$ as $|Q|, |v| \to \infty$. In the end of this section, the asymptotics of $\partial_\Lambda K_{Q_0}$ are determined.

Theorem 3.8 *Let $G(\cdot; v_0)$ be a discrete Green's function on $V(\diamondsuit)$ for $v_0 \in V(\Lambda)$.*

(i) $K_{v_0} := 8\pi \partial_\Lambda G(\cdot; v_0)$ *is a discrete Cauchy's kernel with respect to v_0.*

(ii) Assume additionally that there exist real constants $\alpha_0 > 0$ and $E_1 \geqslant E_0 > 0$ such that $\alpha \geqslant \alpha_0$ and $E_1 \geqslant e \geqslant E_0$ for all interior angles α and side lengths e of parallelograms of Λ. Suppose that $G(\cdot; v_0)$ is the discrete Green's function given in Proposition 3.4 and K_{v_0} the discrete Cauchy's kernel given in (i). Then,

$$K_{v_0}(Q) = \frac{1}{Q-v_0} + \frac{\tau(Q, v_0)}{J(Q, v_0)} + O(|Q-v_0|^{-2})$$

as $|Q| \to \infty$. Here, constants in the O-notation depend on α_0, E_0, and E_1 only.

(iii) Under the conditions of (ii), there is exactly one discrete Cauchy's kernel with respect to v_0 with asymptotics $o(|Q-v_0|^{-1/2})$ as $|Q| \to \infty$.

Remark Note that due to Lemma 3.6(ii) and (iii),

$$\frac{\tau(Q, v_0)}{J(Q, v_0)} = \Omega\left((Q-v_0)^{-1}\right)$$

as $|Q| \to \infty$. As in Theorem 3.7, we may replace the existence of $E_1 \geqslant E_0 > 0$ such that $E_1 \geqslant e \geqslant E_0$ for all side lengths e of parallelograms by the existence of q_0 such that $e/e' \geqslant q_0$ for the two side lengths e, e' of any parallelogram of Λ since the latter implies the first assumption by Proposition 4.3. Then, the constants in the O-notation depend instead of E_0 and E_1 on q_0, e_0, and e_1, where e_0 and e_1 are the side lengths of an arbitrary but fixed parallelogram of Λ.

Proof (i) By Corollary 2.20 about the factorization of the discrete Laplacian,

$$\bar{\partial}_\diamondsuit K_{v_0}(v) = 8\pi \left(\bar{\partial}_\diamondsuit \partial_\Lambda G(\cdot; v_0)\right)(v) = 2\pi \triangle G(v; v_0) = \delta_{vv_0} \frac{\pi}{\operatorname{ar}(F_{v_0})}.$$

(ii) For the ease of notation, we assume that $v_0 \in V(\Gamma)$, but note that the other case of a white vertex v_0 can be handled in the same manner. Let b_-, w_-, b_+, w_+ denote the vertices of the parallelogram Q in counterclockwise order, starting with a black vertex. Using the asymptotics of Theorem 3.7, as $|Q| \to \infty$:

$$4\pi G(b_+;v_0) - 4\pi G(b_-;v_0) = \log\left(\frac{|J(b_+,v_0)||b_+ - v_0|}{|J(b_-,v_0)||b_- - v_0|}\right) + O(|Q-v_0|^{-2}),$$
$$4\pi G(w_+;v_0) - 4\pi G(w_-;v_0) = \log\left(\frac{|J(w_-,v_0)||w_+ - v_0|}{|J(w_+,v_0)||w_- - v_0|}\right) + O(|Q-v_0|^{-2}).$$

Let $a := w_+ - b_-$ and $b := w_- - b_-$. Using $\log|1+x| = (x+\bar{x})/2 + O(x^2)$ as $x \to 0$ and $J(Q,v_0) = \Omega(|Q-v_0|)$ as $|Q| \to \infty$ given by Lemma 3.6(ii), we get as $|Q| \to \infty$:

$$\begin{aligned}
\log|b_\pm - v_0| &= \log\left|(Q-v_0)\left(1 \pm \frac{a+b}{2(Q-v_0)}\right)\right| \\
&= \log|Q-v_0| \pm \operatorname{Re}\left(\frac{a+b}{2(Q-v_0)}\right) + O(|Q-v_0|^{-2}), \\
\log|w_\pm - v_0| &= \log|Q-v_0| \pm \operatorname{Re}\left(\frac{a-b}{2(Q-v_0)}\right) + O(|Q-v_0|^{-2}), \\
\log|J(b_\pm,v_0)| &= \log\left|J(Q,v_0)\left(1 \pm \frac{a^{-1}+b^{-1}}{2J(Q,v_0)}\right)\right| \\
&= \log|J(Q,v_0)| \pm \operatorname{Re}\left(\frac{a^{-1}+b^{-1}}{2J(Q,v_0)}\right) + O(|Q-v_0|^{-2}), \\
\log|J(w_\pm,v_0)| &= \log|J(Q,v_0)| \pm \operatorname{Re}\left(\frac{a^{-1}-b^{-1}}{2J(Q,v_0)}\right) + O(|Q-v_0|^{-2}).
\end{aligned}$$

Therefore, we get for the discrete derivative of $8\pi G(\cdot;v_0)$ at the face Q:

$$\begin{aligned}
K_{v_0}(Q) &= \lambda_Q \frac{\operatorname{Re}\left(\frac{a+b}{Q-v_0}\right) + \operatorname{Re}\left(\frac{a^{-1}+b^{-1}}{J(Q,v_0)}\right)}{a+b} + \bar{\lambda}_Q \frac{\operatorname{Re}\left(\frac{a-b}{Q-v_0}\right) - \operatorname{Re}\left(\frac{a^{-1}-b^{-1}}{J(Q,v_0)}\right)}{a-b} \\
&\quad + O(|Q-v_0|^{-2}) \\
&= \frac{1}{Q-v_0} + \frac{1}{abJ(Q,v_0)} + O(|Q-v_0|^{-2}) \\
&\quad + \frac{1}{2}\left(\lambda_Q \frac{\overline{a+b}}{a+b} + \bar{\lambda}_Q \frac{\overline{a-b}}{a-b}\right)\left(\frac{1}{\overline{Q-v_0}} + \frac{1}{\overline{abJ(Q,v_0)}}\right) \\
&= \frac{1}{Q-v_0} + \frac{\tau(Q,v_0)}{J(Q,v_0)} + O(|Q-v_0|^{-2})
\end{aligned}$$

as $|Q| \to \infty$. Here, $\lambda_Q = \exp\left(-i(\varphi_Q - \pi/2)\right)$, and we have used the identity

$$-\frac{\lambda_Q}{\bar{\lambda}_Q} = \exp\left(-2i\varphi_Q\right) = \frac{a+b}{a-b} \cdot \frac{\overline{a-b}}{\overline{a+b}} \Leftrightarrow \lambda_Q \frac{\overline{a+b}}{a+b} + \bar{\lambda}_Q \frac{\overline{a-b}}{a-b} = 0.$$

(iii) Let h be the difference of two discrete Cauchy's kernels with respect to v_0 with asymptotics $o(|Q - v_0|^{-1/2})$ as $|Q| \to \infty$. K_{v_0} in the second part is such a discrete Cauchy's kernel. Then, h is discrete holomorphic, and by Proposition 2.8, a discrete primitive f on $V(\Lambda)$ exists. By construction,

$$\frac{f(b_+) - f(b_-)}{b_+ - b_-} = \frac{f(w_+) - f(w_-)}{w_+ - w_-} = \partial_\Lambda f(Q) = h(Q) = o(|Q - v_0|^{-1/2}).$$

Since angles and edge lengths of parallelograms are bounded, the conditions of Theorem 2.31 are fulfilled, implying that f is biconstant, so h vanishes identically.

Since we do not have discrete Green's functions on $V(\diamondsuit)$, we have to derive a discrete Cauchy's kernels on $V(\Lambda)$ differently. To do so, we follow the original approach of Kenyon using the discrete exponential [16] that was reintroduced by Chelkak and Smirnov in [6].

Proposition 3.9 *Let $Q_0 \in V(\diamondsuit)$. The function defined by*

$$K_{Q_0}(v) := \frac{1}{\pi i} \int_{C_v} \log(\lambda) e(\lambda, v; Q_0) d\lambda = 2 \int_{-(v-Q_0)\infty}^{0} e(\lambda, v; Q_0) d\lambda$$

is a discrete Cauchy's kernel with respect to Q_0. Here, C_v is a collection of sufficiently small counterclockwise oriented loops going once around each pole of $e(\cdot, v; Q_0)$. On each loop around a pole e of $e(\cdot, v; Q_0)$, we take the branch of logarithm that satisfies $\mathrm{Im}(\log(e)) \in (\theta_v - \pi, \theta_v + \pi)$, where $\theta_v := \arg(v - Q_0)$. The second integration goes along the straight ray that ends in the origin in direction $(v - Q_0)$.

Proof Lemma 4.2 assures that the arguments of all poles can be indeed chosen in such a way that they lie in $(\theta_v - \pi, \theta_v + \pi)$.

By residue theorem, we can replace integration along C_v by an integration along a circle centered at 0 with large radius R (such that all poles lie inside the disk) in counterclockwise direction, an integration along a circle centered at 0 with small radius r (such that all poles lie outside the disk) in clockwise direction, and integrations along the two directions of the line segment $[-R, -r]$. Using that

$$\lim_{|\lambda| \to \infty} \lambda \mathrm{e}(\lambda, v; Q_0) \log(\lambda) = 0$$

and taking r arbitrarily small, there is a homotopy between the new integration path and the path from complex infinity to 0 and back along the ray spanned by $-(v - Q_0)$ that does not change the value of the integral. The branch of log we consider jumps by $2\pi i$ on the two sides of the ray, which shows

$$\frac{1}{\pi i} \int_{C_v} \log(\lambda) \mathrm{e}(\lambda, v; Q_0) d\lambda = 2 \int_{-(v-Q_0)\infty}^{0} \mathrm{e}(\lambda, v; Q_0) d\lambda.$$

In particular, θ_v can be replaced by any $\theta_v + 2k\pi$, $k \in \mathbb{Z}$, in the first integration.

Let us consider the parallelogram Q_0 with vertices b_-, w_-, b_+, w_+ in counterclockwise direction, starting with a black vertex, and let us denote $a := w_+ - b_-$, $b := w_- - b_-$. Without loss of generality, we rotate the complex plane in such a way that $\arg(b_+ - Q_0) = 0$. Then, $\arg(a)$ and $\arg(b)$ lie between 0 and $\pm\pi$, and using residue theorem,

$$\begin{aligned}
K_{Q_0}(b_-) &= 2\frac{(\log|a| + i\arg(a) + i\pi) - (\log|b| + i\arg(b) + i\pi)}{b-a},\\
K_{Q_0}(b_+) &= 2\frac{(\log|b| + i\arg(b)) - (\log|a| + i\arg(a))}{b-a},\\
K_{Q_0}(w_-) &= 2\frac{(\log|b| + i\arg(b) + 2i\pi) - (\log|a| + i\arg(a) + i\pi)}{a+b},\\
K_{Q_0}(w_+) &= 2\frac{(\log|a| + i\arg(a)) - (\log|b| + i\arg(b) + i\pi)}{a+b}.
\end{aligned}$$

Finally, we get by Lemma 2.3 giving an integration formula for $\bar{\partial}_\Lambda$:

$$\begin{aligned}
\bar{\partial}_\Lambda K_{Q_0}(Q_0) &= \frac{(a-b)\left(K_{Q_0}(b_+) - K_{Q_0}(b_+)\right) + (a+b)\left(K_{Q_0}(w_-) - K_{Q_0}(w_+)\right)}{4i\,\mathrm{ar}(F_{Q_0})}\\
&= \frac{\pi}{\mathrm{ar}(F_{Q_0})}.
\end{aligned}$$

By a similar argument as in the proof of Proposition 3.4, we can choose the same contours of integration for all incident vertices v of a face $Q \neq Q_0$. Then, the discrete derivative $\bar{\partial}_\Lambda$ commutes with the integration, and $\bar{\partial}_\Lambda K_{Q_0}(Q) = 0$ because $\mathrm{e}(\lambda, \cdot; Q_0)$ is discrete holomorphic by Proposition 3.2.

Theorem 3.10 *Assume that there are $\alpha_0 > 0$ and $E_1 \geqslant E_0 > 0$ such that $\alpha \geqslant \alpha_0$ and $E_1 \geqslant e \geqslant E_0$ for all interior angles α and side lengths e of parallelograms of Λ. Let $Q_0 \in V(\Diamond)$ be fixed.*

(i) The discrete Cauchy's kernel K_{Q_0} given in Proposition 3.9 has the following asymptotics as $|v| \to \infty$:

$$K_{Q_0}(v) = \frac{1}{v - Q_0} + \frac{\tau(v, Q_0)}{J(v, Q_0)} + O\left(|v - Q_0|^{-3}\right).$$

(ii) There is no further discrete Cauchy's kernel with respect to Q_0 that has asymptotics $o(|v - Q_0|^{-1/2})$ as $|v| \to \infty$.

(iii) For the discrete Cauchy's kernel K_{Q_0} given in Proposition 3.9, $\partial_\Lambda K_{Q_0}$ has the following asymptotics as $|v| \to \infty$:

$$\partial_\Lambda K_{Q_0}(Q) = -\frac{1}{(Q - Q_0)^2} - \frac{\tau(Q, Q_0)}{J(Q, Q_0)^2} + O\left(|Q - Q_0|^{-3}\right).$$

(iv) Up to two additive complex constants on Γ and Γ^*, there is no further discrete Cauchy's kernel with respect to Q_0 such that its discrete derivative has asymptotics $o(|Q-Q_0|^{-1/2})$ as $|Q|\to\infty$.

Here, constants in the O-notation depend on α_0, E_0, and E_1 only.

Remark By Lemma 3.6(ii) and (iii),

$$\frac{\tau(v,Q_0)}{J(v,Q_0)}=\Omega\left((v-Q_0)^{-1}\right)\quad\text{and}\quad\frac{\tau(Q,Q_0)}{J(Q,Q_0)^2}=\Omega\left((Q-Q_0)^{-2}\right)$$

as $|v|,|Q|\to\infty$. As in the previous Theorem 3.8, we may replace the existence of constants $E_1\geqslant E_0>0$ such that $E_1\geqslant e\geqslant E_0$ for all side lengths e of parallelograms by the existence of q_0 such that $e/e'\geqslant q_0$ for the two side lengths e,e' of any parallelogram of Λ since the latter implies the first assumption by Proposition 4.3. Then, the constants in the O-notation depend instead of E_0 and E_1 on q_0, e_0, and e_1, where e_0 and e_1 are the side lengths of an arbitrary but fixed parallelogram of Λ.

The proof of the first part follows the ideas of Kenyon [16]. Similar to the proof of Theorem 3.7, the path of integration is deformed into a path different from the one Kenyon used, $(-(v-Q_0)\infty,0]$. For the same reasons as before, his approach does not generalize to parallelogram-graphs. The second and the fourth part of the theorem are immediate consequences of Theorem 2.31; the third part is shown by a direct computation.

Proof (i) Among all the vertices incident to Q_0, let v_0 be the one that is combinatorially closest to v on Λ. Then, the poles $d_1,d_2,e_1,\dots,e_{k(v)}$ of $\mathrm{e}(\cdot,v;Q_0)$ correspond to the directed edges of a shortest path from v_0 to v of length $k(v)$ and the two directed edges of Q_0 that point toward v_0. It is easy to deduce from Lemma 4.2 that the arguments of all poles can be chosen to lie in $[\theta_0,\theta_0+\pi-\alpha_0]$. For more details, we refer to the appendix in [13]. The claim is invariant under multiplication of the complex plane, so we can assume that $\theta_0=-(\pi-\alpha_0)/2$. Then, there are no poles in the left half-plane, such that we can reduce the calculation to an integration over $\mathbb{R}$:

$$K_{Q_0}(v)=2\int_{-(v-Q_0)\infty}^{0}\mathrm{e}(\lambda,v;Q_0)d\lambda=2\int_{-\infty}^{0}\mathrm{e}(\lambda,v;Q_0)d\lambda.$$

Since we are interested in the limit $|v|\to\infty$, we take $|v-Q_0|\geqslant 1$ large enough and split the integration into the three parts along the intervals $(-\infty,-E_1\sqrt{|v-Q_0|}]$, $[-E_1\sqrt{|v-Q_0|},-E_1/\sqrt{|v-Q_0|}]$, $[-E_1/\sqrt{|v-Q_0|},0]$. Lemma 3.6(iv) shows that the contribution of the range $\lambda\in[-E_1\sqrt{|v-Q_0|},-E_1/\sqrt{|v-Q_0|}]$ decays faster to zero than any power of $v-Q_0$ as $|v|\to\infty$. By Lemma 3.6(i) and (ii) we know that $k(v)=\Omega(v-Q_0)$ and $J(v,Q_0)=\Omega(v-Q_0)$ as $|v|\to\infty$. Since the arguments of all the poles can be chosen to lie in $[-(\pi-\alpha_0)/2,(\pi-\alpha_0)/2]$, it follows even that $\mathrm{Re}(J(v,Q_0))=\Omega(|v-Q_0|)$ as $|v|\to\infty$ stays positive.

Let $\lambda \in [-E_1/\sqrt{|v-Q_0|}, 0]$. Then, $\lambda \to 0$ as $|v| \to \infty$. Repeated use of the second and the third equation in Lemma 3.5(i) yields

$$\mathrm{e}(\lambda, v; Q_0) = \tau(v, Q_0) \exp\left(2\lambda J(v, Q_0)\right) \left(1 + O(\lambda^2) + O(|v - Q_0|\lambda^3)\right)$$

as $|v| \to \infty$. Thus, the integral near the origin behaves for $|v| \to \infty$ as

$$2 \int_{-E_1/\sqrt{|v-Q_0|}}^{0} \mathrm{e}(\lambda, v; Q_0) d\lambda = \frac{\tau(v, Q_0)}{J(v, Q_0)} + O(|v - Q_0|^{-3}).$$

For this, we used that $\exp(-2E_1 J(v, Q_0)/\sqrt{|v - Q_0|})$ goes to zero exponentially fast as $|v| \to \infty$.

Now, let $\lambda \in (-\infty, -E_1\sqrt{|v - Q_0|}]$. Then, $\lambda \to -\infty$ as $|v| \to \infty$. Repeated use of the second and the third equation in Lemma 3.5(ii) shows that

$$\mathrm{e}(\lambda, v; Q_0) = \lambda^{-2} \exp\left(2(v - Q_0)/\lambda\right) \left(1 + O(\lambda^{-2}) + O(|v - Q_0|\lambda^{-3})\right)$$

as $|v| \to \infty$. Using the result of above, we get for the integral near minus infinity:

$$\begin{aligned}
&2 \int_{-\infty}^{-E_1\sqrt{|v-Q_0|}} \mathrm{e}(\lambda, v; Q_0) d\lambda \\
=&2 \int_{-\infty}^{-E_1\sqrt{|v-Q_0|}} \lambda^{-2} \exp\left(2(v - Q_0)/\lambda\right) \left(1 + O(\lambda^{-2}) + O(|v - Q_0|\lambda^{-3})\right) d\lambda \\
=&2 \int_{-1/(E_1\sqrt{|v-Q_0|})}^{0} \exp\left(2\lambda(v - Q_0)\right) \left(1 + O(\lambda^2) + O(|v - Q_0|\lambda^3)\right) d\lambda \\
=&\frac{1}{v - Q_0} + O(|v - Q_0|^{-3}).
\end{aligned}$$

Summing the contributions of the three ranges up gives the desired result and also shows the asymptotic behavior required in (ii).

(ii) The difference f of two discrete Cauchy's kernels with respect to Q_0 of asymptotics $o(|v - Q_0|^{-1/2})$ is discrete holomorphic and fulfills the conditions of Theorem 2.31. Hence, f is biconstant, so $f \equiv 0$.

(iii) Let b_-, w_-, b_+, w_+ denote the vertices of the parallelogram $Q \in V(\Diamond)$ in counterclockwise order, starting with a black vertex. Let us introduce $a := w_+ - b_-$ and $b := w_- - b_-$. Using the expansion $1/(1 + x) = 1 - x + O(x^2)$ as $x \to 0$ and the asymptotics of the first part, we get that $K_{Q_0}(b_\pm)$ and $K_{Q_0}(w_\pm)$ equal

$$\frac{1}{Q-Q_0} \mp \frac{a+b}{2(Q-Q_0)^2} + \frac{\tau(b_-, Q_0)}{J(Q, Q_0)} \mp \tau(b_-, Q_0)\frac{a^{-1}+b^{-1}}{2J(Q, Q_0)^2} + O(|Q-Q_0|^{-3}),$$
$$\frac{1}{Q-Q_0} \mp \frac{a-b}{2(Q-Q_0)^2} + \frac{\tau(w_-, Q_0)}{J(Q, Q_0)} \mp \tau(w_-, Q_0)\frac{a^{-1}-b^{-1}}{2J(Q, Q_0)^2} + O(|Q-Q_0|^{-3}),$$

respectively. By definition, $\tau(b_-, Q_0) = -\tau(w_-, Q_0)$. Therefore,

$$\begin{aligned}\partial_\Lambda K_{Q_0}(Q) =& -\lambda_Q \frac{\frac{a+b}{(Q-Q_0)^2} - \tau(b_-, Q_0)\frac{a^{-1}+b^{-1}}{J(Q,Q_0)^2}}{a+b} \\ &+ \bar{\lambda}_Q \frac{\frac{a-b}{(Q-Q_0)^2} - \tau(b_-, Q_0)\frac{a^{-1}-b^{-1}}{J(Q,Q_0)^2}}{a-b} + O(|Q-Q_0|^{-3}) \\ =& -\frac{1}{(Q-Q_0)^2} - \frac{\tau(b_-, Q_0)}{abJ(Q, Q_0)^2} + O(|Q-Q_0|^{-3}) \\ =& -\frac{1}{(Q-Q_0)^2} - \frac{\tau(Q, Q_0)}{J(Q, Q_0)^2} + O(|Q-Q_0|^{-3}).\end{aligned}$$

(iv) Let f be the difference of two discrete Cauchy's kernels with respect to Q_0 whose discrete derivatives have asymptotics $o(|Q-v_0|^{-1/2})$. Then, f is discrete holomorphic and

$$\frac{f(b_+)-f(b_-)}{b_+-b_-} = \frac{f(w_+)-f(w_-)}{w_+-w_-} = \partial_\Lambda f(Q) = o(|Q-v_0|^{-1/2}).$$

Since angles and edge lengths are bounded, the conditions of Theorem 2.31 are fulfilled. Hence, f is biconstant.

Remark Note that Kenyon [16] and Chelkak and Smirnov [6] proved in the rhombic setting the stronger result that there is a unique discrete Cauchy's kernel on $V(\Lambda)$ with respect to Q_0 with asymptotics $o(1)$ as $|v| \to \infty$.

3.5 Integer Lattice

Let us consider a planar parallelogram-graph Λ such that each vertex has degree four. With the embedding of $\diamondsuit$ described in Sect. 3.1, this happens if and only if $\diamondsuit$ is a planar quad-graph or, equivalently, if Λ has the combinatorics of the integer lattice $\mathbb{Z}^2$. The vertices of $\diamondsuit$ lie at the midpoints of edges of Γ or Γ^*. Since any vertex of Γ or Γ^* is enclosed by a quadrilateral of Γ^* or Γ, respectively, the faces of $\diamondsuit$ are parallelograms by Varignon's theorem. Thus, $\diamondsuit$ becomes a planar parallelogram-graph as well.

Of particular interest is the case that the two notions of discrete holomorphicity on $\diamondsuit$, the one coming from $\diamondsuit$ being the dual of Λ and the other coming from the quad-graph $\diamondsuit$ itself, coincide. It is not hard to show that this happens only for the integer

lattice of a skew coordinate system, onto which we restrict ourselves in the following. For more details, see [13]. If e_1, e_2 denote two spanning vectors, then $\diamondsuit$ is a parallel shift of Λ by $e_1/2 + e_2/2$. Furthermore, the discrete derivatives on $\diamondsuit$ seen as the dual of Λ coincide with the discrete derivatives on $\diamondsuit$ seen as a parallelogram-graph.

Since corresponding notions coincide and $\diamondsuit$ and Λ are congruent, we can skip all subscripts Λ and $\diamondsuit$ in the definitions of discrete derivatives. Moreover, the discrete Laplacian $\triangle$ is now defined for functions on $V(\Lambda)$ and functions on $V(\diamondsuit)$ in the same way. Due to Corollary 2.20, $4\partial\bar{\partial} = \triangle = 4\bar{\partial}\partial$ is now true on both graphs. It follows that all discrete derivatives $\partial^n f$ of a discrete holomorphic function f are discrete holomorphic themselves. Conversely, a discrete primitive exists for any discrete holomorphic function on a simply-connected domain by Proposition 2.8.

Our main interests lie in giving discrete Cauchy's integral formulae for higher order derivatives of a discrete holomorphic function and determining the asymptotics of higher order discrete derivatives of the discrete Cauchy's kernel given in Sect. 3.4. Note that due to the uniqueness statements in Theorems 3.8 and 3.10, both formulae yield the same discrete Cauchy's kernel.

Without loss of generality, we restrict our attention to functions on $V(\Lambda)$. For the ease of notation, we introduce the *discrete distance* $D(\cdot,\cdot)$ on $V(\Lambda) \cup V(\diamondsuit)$ that is induced by the $|\cdot|_\infty$-distance on the integer lattice spanned by $e_1/2, e_2/2$.

Theorem 3.11 *Let Λ be the integer lattice spanned by the pair e_1, e_2 of linearly independent complex vectors. Let $v_0 \in V(\Lambda)$, $Q_0 := v_0 + e_1/2 + e_2/2 \in V(\diamondsuit)$, let f be a discrete holomorphic function on $V(\Lambda)$, and let K_{v_0} and K_{Q_0} be discrete Cauchy's kernels with respect to v_0 and Q_0, respectively. Let n be a nonnegative integer and define $x_0 := v_0$ if n is even and $x_0 := Q_0$ if n is odd. Similarly, let $x \in V(\Lambda)$ if n is even and $x \in V(\diamondsuit)$ if n is odd.*

(i) For any counterclockwise oriented discrete contour C_{x_0} in the medial graph X enclosing all points $x' \in V(\Lambda) \cup V(\diamondsuit)$ with $D(x', x_0) \leqslant n/2$,

$$\partial^n f(x_0) = \frac{(-1)^n}{2\pi i} \oint_{C_{x_0}} f \partial^n K_{x_0} dz.$$

(ii) If K_{Q_0} is the discrete Cauchy's kernel given in Proposition 3.9, then

$$\frac{(-1)^n}{n!} \partial^n K_{Q_0}(x) = \frac{1}{(x - Q_0)^{n+1}} + \frac{\tau'(x, Q_0)}{(J(x, Q_0) e_1 e_2)^{n+1}} + O(|x - Q_0|^{-n-3})$$

as $|x| \to \infty$, where $\tau'(x, Q_0) = 1$ if x and Q_0 or $(x + e_1/2 + e_2/2)$ and Q_0 can be connected by a path on $V(\diamondsuit)$ of even length and $\tau'(x, Q_0) = -1$ otherwise. Constants in the O-notation depend on the spanning vectors e_0, e_1 only.

Remark By Lemma 3.6(ii) and (iii), we have for $|x| \to \infty$:

$$\frac{\tau'(x, Q_0)}{(J(x, Q_0)e_1e_2)^{n+1}} = \Omega\left((x - Q_0)^{-(n+1)}\right).$$

Proof (i) Let D be the discrete domain in $F(X)$ bounded by C_{x_0}. By the assumptions on C_{x_0}, the discrete one-form $\bar\partial\partial^{n-1}K_{x_0}d\bar z$ vanishes on C_{x_0}. Thus,

$$\oint_{C_{x_0}} f\partial^n K_{x_0}dz = \oint_{C_{x_0}} f d\left(\partial^{n-1}K_{x_0}\right) = \iint_D d(f d(\partial^{n-1}K_{x_0})) = \iint_D df \wedge d\left(\partial^{n-1}K_{x_0}\right)$$

by discrete Stokes' Theorem 2.9 in the second equation and Theorem 2.16 and Proposition 2.10 stating that d is a derivation for the discrete wedge product and $ddf = 0$ in the third equation. Now, f is discrete holomorphic, meaning that $\bar\partial f \equiv 0$, so $df \wedge d\left(\partial^{n-1}K_{x_0}\right) = \partial f\bar\partial\partial^{n-1}K_{x_0}\Omega_\diamondsuit$. But since the discrete derivatives commute according to Corollary 2.11, $\bar\partial\partial^{n-1}K_{x_0} = \partial^{n-1}\bar\partial K_{x_0}$ vanishes outside C_{x_0}, so by repeated use of Proposition 2.7 stating that ∂ is the formal adjoint of $-\bar\partial$,

$$\oint_{C_{x_0}} f\partial^n K_{x_0}dz = -2i\langle\partial f, \bar\partial^{n-1}\partial\bar K_{x_0}\rangle = 2i(-1)^n\langle\partial^n f, \partial\bar K_{x_0}\rangle = 2\pi i(-1)^n\partial^n f(x_0).$$

(ii) Let us define the discrete exponential $\mathrm{e}(\lambda, Q; Q_0)$ for $Q \in V(\diamondsuit)$ in the same way as a rational function in the complex variable λ as we defined $\mathrm{e}(\lambda, v; v_0)$. By inductive use of the formula for the discrete derivative of exp in Proposition 3.2 and $\exp(\lambda, \cdot; Q_0) = \mathrm{e}(2/\lambda, \cdot; Q_0)$, we get for the discrete exponential $\mathrm{e}(\lambda, \cdot; Q_0)$ that is defined on $V(\Lambda)$:

$$(\partial^n\mathrm{e}(\lambda, \cdot; Q_0))(x) = \frac{(2\lambda)^n}{((\lambda - e_1)(\lambda - e_2)(\lambda + e_1)(\lambda + e_2))^{\lceil n/2\rceil}}\mathrm{e}(\lambda, x; Q_0).$$

To compute $\partial^n K_{Q_0}(x)$, we need the values of K_{Q_0} only at vertices $v \in V(\Lambda)$ with $D(v, x) \leqslant n/2$. For these points,

$$K_{Q_0}(v) = 2\int_{-(v-Q_0)\infty}^{0} \mathrm{e}(\lambda, v; Q_0)d\lambda$$

by the formula in Proposition 3.9. If $D(x, Q_0)$ is sufficiently large, then we can choose $e \in \{e_1, e_2, -e_1, -e_2\}$ such that $D(ke, x) > n/2$ for all positive integers k. So if $D(v, x) \leqslant n/2$ and $D(x, Q_0)$ is sufficiently large, then $\mathrm{e}(\cdot, v; Q_0)$ does not have the pole e. Since $\pm e_1, \pm e_2$ are the only possible poles, it follows that there are no poles in the convex hull of all the rays $(-(v - Q_0)\infty, 0]$ for the vertices v with $D(v, x) \leqslant n/2$. By residue theorem, we can use the same path of integration for all relevant values of K_{Q_0} and get

$$\partial^n K_{Q_0}(x) = 2 \int_{-(x-Q_0)\infty}^{0} (\partial^n \mathrm{e}(\lambda, \cdot; Q_0))(x) d\lambda.$$

Now, we follow the proof of Theorem 3.10(i). Again, the claim is invariant under rotation of the complex plane, so we may assume $(x - Q_0) > 0$.

Let $E_1 := \max\{|e_1|, |e_2|\}$ and $E_0 := \min\{|e_1|, |e_2|\}$. For $|x - Q_0| \geqslant 1$ large enough, we split the integration into the three parts along $(-\infty, -E_1\sqrt{|x - Q_0|}]$, $[-E_1\sqrt{|x - Q_0|}, -E_1/\sqrt{|x - Q_0|}]$, and $[-E_1/\sqrt{|x - Q_0|}, 0]$.

By Lemma 3.6(iv), the contribution of $\lambda \in [-E_1\sqrt{|x - Q_0|}, -E_1/\sqrt{|x - Q_0|}]$ decays faster to zero than any power of $x - Q_0$ as $|x| \to \infty$. By Lemma 3.6(i) and (ii), we know that $D(x, Q_0) = \Omega(x - Q_0)$ and $J(x, Q_0) = \Omega(x - Q_0)$. Furthermore, the choice of $(x - Q_0) > 0$ implies that $\mathrm{Re}(J(x, Q_0)) = \Omega(x - Q_0)$ stays positive as $|x| \to \infty$.

Let $\lambda \in [-E_1/\sqrt{|x - Q_0|}, 0]$. Then, $\lambda \to 0$ as $|x| \to \infty$, and repeated use of the second and third equation in Lemma 3.5(i) gives that $(\partial^n \mathrm{e}(\lambda, \cdot; Q_0))(x)$ equals

$$\frac{\tau'(x, Q_0)}{(e_1 e_2)^{n+1}} (2\lambda)^n \exp(2\lambda J(x, Q_0)) \left(1 + O(\lambda^2) + O(|x - Q_0|\lambda^3)\right).$$

With a similar argument as in the proof of Theorem 3.10(i), the integral near the origin behaves for $|x| \to \infty$ as

$$\frac{(-1)^n n! \tau'(x, Q_0)}{(e_1 e_2 J(x, Q_0))^{n+1}} + O(|x - Q_0|^{-n-3}).$$

Now, let $\lambda \in (-\infty, -E_1\sqrt{|x - Q_0|}]$. For $|x| \to \infty$, $\lambda \to -\infty$, and repeated use of the second and third equation in Lemma 3.5(ii) implies that $(\partial^n \mathrm{e}(\lambda, \cdot; Q_0))(x)$ equals

$$(2\lambda)^n \lambda^{-2n-2} \exp\left(\frac{2(x - Q_0)}{\lambda}\right) \left(1 + O(\lambda^{-2}) + O(|x - Q_0|\lambda^{-3})\right).$$

Using the result of above, we get for the integral near minus infinity for $|x| \to \infty$:

$$\int_{-\infty}^{-E_1\sqrt{|x-Q_0|}} (\partial^n \mathrm{e}(\lambda, \cdot; Q_0))(x) d\lambda$$

$$= 2 \int_{-\infty}^{-E_1\sqrt{|x-Q_0|}} \left(\frac{2}{\lambda}\right)^n \lambda^{-2} \exp\left(\frac{2(x - Q_0)}{\lambda}\right) \left(1 + O(\lambda^{-2}) + O(|x - Q_0|\lambda^{-3})\right) d\lambda$$

$$= 2 \int_{-1/(E_1\sqrt{|x-Q_0|})}^{0} (2\lambda)^n \exp(2\lambda(x-Q_0)) \left(1 + O(\lambda^2) + O(|x-Q_0|\lambda^3)\right) d\lambda$$
$$= \frac{(-1)^n n!}{(x-Q_0)^{n+1}} + O(|x-Q_0|^{-n-3}).$$

Summing up the contributions of the three ranges gives

$$\frac{(-1)^n}{n!}\partial^n K_{Q_0}(x) = \frac{1}{(x-Q_0)^{n+1}} + \frac{\tau'(x,Q_0)}{(J(x,Q_0)e_1e_2)^{n+1}} + O(|x-Q_0|^{-n-3}).$$

Acknowledgments The authors thank Richard Kenyon, Christian Mercat, and Mikhail Skopenkov for fruitful discussions and helpful suggestions. In addition, we are grateful to Mikhail Skopenkov for his detailed review of previous versions and his numerous and valuable recommendations. The first author was partially supported by the DFG Collaborative Research Center TRR 109, "Discretization in Geometry and Dynamics". The research of the second author was supported by the Deutsche Telekom Stiftung. Some parts of this paper were written at the IHÉS in Bures-sur-Yvette, the INIMS in Cambridge, and the ESI in Vienna. The second author thanks the EPDI program for the opportunity to stay at these institutes. The stay at the Isaac Newton Institute for Mathematical Sciences was funded through an Engineering and Physical Sciences Research Council Visiting Fellowship, Grant EP/K032208/1.

Appendix: Planar Parallelogram-Graphs

The aim of this appendix is to discuss some combinatorial and geometric properties of parallelogram-graphs that were used in Sect. 3. The following notion of a strip is standard, see for example the book [3].

Definition A *strip* in a planar quad-graph Λ is a path on its dual $\Diamond$ such that two successive faces share an edge and the strip leaves a face in the opposite edge where it enters it. Moreover, strips are assumed to have maximal length, i.e., there are no strips containing it apart from itself.

Note that a strip is uniquely determined by the edges it passes through, meaning the edges two successive faces share.

Definition For a strip S of a parallelogram-graph Λ, there exists a complex vector a_S such that any (nonoriented) edge through which S passes is $\pm a_S$. We call a_S a *common parallel*.

a_S is unique up to sign; the choice of the sign induces an orientation on all edges. The parallel edges of the strip can be rescaled to length $|a_S| = 1$, without changing the combinatorics. Hence, rhombic planar quad-graphs and planar parallelogram-graphs are combinatorially equivalent. Rhombic planar quad-graphs are characterized by the following proposition of Kenyon and Schlenker [17]:

Proposition 4.1 *A planar quad-graph Λ admits a combinatorially equivalent embedding in $\mathbb{C}$ with all rhombic faces if and only if the following two conditions are satisfied:*

- *No strip crosses itself or is periodic.*
- *Two distinct strips cross each other at most once.*

Remark Let us prove the simpler claim that planar parallelogram-graphs fulfill these two conditions as was already noted by Kenyon in [16]. The underlying reason is that any strip S is monotone with respect to the direction ia_S: The coordinates of the endpoints of the edges parallel to a_S are strictly increasing or strictly decreasing if they are projected to ia_S. Whether the projections are decreasing or increasing depends on the direction in which the faces of S are passed through. Without loss of generality, we assume that the faces of S are passed through in such a way that the projections of the corresponding coordinates are strictly increasing. For $Q \in S$, let S^Q denote the semi-infinite part of S starting in the quadrilateral Q that passes through the faces of S in the same order.

As a consequence, no strip crosses itself or is periodic. Furthermore, S divides the complex plane into two unbounded regions, to one is a_S pointing and to the other $-a_S$. When a distinct strip S' crosses S, it enters a different region determined by S, say it goes to the one to which a_S is pointing. Due to monotonicity, the angle between $ia_{S'}$ and a_S is less than $\pi/2$. It follows that S' cannot cross S another time, since it would then go to the region $-a_S$ is pointing to, contradicting that the angle between $ia_{S'}$ and $-a_S$ is greater and not less than $\pi/2$.

In order to give explicit formulae for the discrete Green's function and the discrete Cauchy's kernels in Sects. 3.3 and 3.4, we chose a particular directed path connecting two vertices (or a face and a vertex) by edges of the parallelogram-graph Λ. This path was monotone in one direction. The existence of such a path follows from the following lemma, generalizing a result of [2] to general parallelogram-graphs. The proof bases on the same ideas.

Lemma 4.2 *Let Λ be a parallelogram-graph and let $v_0 \in V(\Lambda)$ be fixed. For a directed edge e of Λ starting in v_0, consider the subgraph $U_e \subset \Lambda$ that consists of all vertices and edges of directed paths on Λ starting in v_0 whose oriented edges have arguments that can be chosen to lie in* $[\arg(e), \arg(e) + \pi)$.

Then, the union of all U_e, e a directed edge starting in v_0, covers the whole quad-graph. If there is a constant $\alpha_0 > 0$ such that $\alpha \geqslant \alpha_0$ for all interior angles α of faces of Λ, then the same statement holds true if $[\arg(e), \arg(e) + \pi)$ *is replaced by* $[\arg(e), \arg(e) + \pi - \alpha_0]$.

Proof Let us rescale the edges such that all of them have length one. By this, we change neither the combinatorics of Λ nor the size of interior angles.

For a directed edge e starting in v_0, let U_e^- and U_e^+ denote the (directed) paths on Λ starting in v_0, obtained by choosing the directed edge with the least or largest

argument in $[\arg(e), \arg(e)+\pi)$ (or $[\arg(e), \arg(e)+\pi-\alpha_0]$) at a vertex, respectively. We first show that all vertices in between U_e^- and U_e^+ are contained in $V(U_e)$. Then, it follows that U_e is the conical sector with boundary U_e^- and U_e^+.

Suppose the contrary, i.e., suppose that there is a vertex v between U_e^- and U_e^+ to which v_0 cannot be connected by a directed path of edges whose arguments lie all in the interval $[\arg(e), \arg(e)+\pi)$ (or $[\arg(e), \arg(e)+\pi-\alpha_0]$). Let the combinatorial distance between v_0 and v be minimal among all such vertices.

In the case that interior angles of rhombi are bounded by α_0 from below, they are bounded from above by $\pi-\alpha_0$. Hence, there is a vertex v' adjacent to v such that the argument of the directed edge $v'v$ lies in $[\arg(e), \arg(e)+\pi-\alpha_0]$. Even if interior angles are not uniformly bounded, v' can be chosen in such a way that the argument of $v'v$ lies in $[\arg(e), \arg(e)+\pi)$. By construction, v' is not in $V(U_e)$, but still between U_e^- and U_e^+. Let us look at the strip S passing through $v'v$. Suppose that the common parallel a_S points from v' to v.

If S intersects U_e^- or U_e^+, then an edge parallel to a_S is contained in U_e^- or U_e^+, respectively. By construction, v_0 and v' then lie on the same side of the strip S.

If S does neither intersect U_e^- nor U_e^+, then it is completely contained in the left half space determined by the oriented line $v_0+te, t\in\mathbb{R}$, as U_e^- and U_e^+ are. Suppose S intersects the ray v_0+ta_S, $t\geqslant 0$. Again, it follows that v_0 and v' lie on the same side of S.

It remains the case that S neither intersects U_e^-, U_e^+, nor the ray v_0+ta_S, $t\geqslant 0$. Consider the quadrilateral area R in between the parallels v_0+ta_S, $v'+ta_S$ and $v_0+te, v'+te, t\in\mathbb{R}$. By assumption, the semi-infinite part of S that starts with the edge $v'v$ and then goes into R does not intersect an edge of R incident to v_0, and by monotonicity, it does not intersect $v'+ta_S$ again. Now, Λ is locally finite, such that only finitely many quadrilaterals of S are inside P. Thus, S leaves P on the edge $v'+te, t\in\mathbb{R}$, and it follows that S separates v_0 and v.

So in any case, S separates v_0 from v. Any shortest path P connecting both points has to pass through S. Let w be the first point of P that lies on the same side of S as v does. Any strip passing through an edge on the shortest path connecting w and v on S has to intersect P as well. It follows that replacing all edges of P on the same side of S as v by the path from w to v does not change its length. But then, v' is combinatorially nearer to v_0 than v, contradiction.

Finally, we can cyclically order the directed edges starting in v_0 according to their slopes. Then, the sectors U_e are interlaced, i.e., U_e contains both $U_{e_-}^+$ and $U_{e_+}^-$, where e_-, e, e_+ are consecutive according to the cyclic order. As a consequence, the union of all these U_e covers the whole Λ.

To perform our computations in Sects. 3.3 and 3.4, we needed not only that the interior angles were bounded, but also that the side lengths were bounded. We can relax the latter condition to boundedness of the ratio of side lengths.

Proposition 4.3 *Let Λ be a parallelogram-graph and assume that there are constants $\alpha_0, q_0 > 0$ such that $\alpha\geqslant\alpha_0$ and $e/e'\geqslant q_0$ for all interior angles α and two side lengths e, e' of any parallelogram of Λ. Then, $E_1\geqslant e\geqslant E_0$ for all edge lengths*

e, where $E_0 := e_0 q_0^N$ *and* $E_1 := e_1 q_0^{-N}$ *with* $N := \lceil \lfloor 2\pi/\alpha_0 \rfloor / 2 \rceil$ *and* $e_1 \geqslant e_0$ *being the side lengths of an arbitrary parallelogram of* Λ.

Proof Let $Q' \in V(\Diamond)$ be fixed with edge lengths $e_1 \geqslant e_0$ and let $Q \in V(\Diamond)$ be another parallelogram with center x. In the following, we construct a sequence of n strips such that any two consecutive strips are crossing each other, the first one contains Q', the last one contains Q, and $n \leqslant N$. Then, it follows that the side lengths of Q are bounded by E_0 and E_1.

Let S_0 be a strip containing Q'. If $Q \in S_0$, we are done. Otherwise, we choose the common parallel a_{S_0} in such a way that x lies in the region $-a_{S_0}$ is pointing to. Let $\beta_0 := \arg(a_{S_0})$. Since S_0 is monotone in the direction ia_{S_0} and interior angles are uniformly bounded, the ray $x + ta_{S_0}, t > 0$, intersects S in exactly one line segment. Let y_0 be the first intersection point and Q_0 a quadrilateral of S containing y_0.

Because Λ is locally finite, the line segment connecting x and y_0 intersects only finitely many parallelograms. Through any such parallelogram at most two strips are passing. Thus, only a finite number of strips intersect this line segment. Therefore, we can choose a strip S_1 intersecting $S_0^{Q_0}$ in a parallelogram $Q_{0,1}$ such that S_1 does not contain Q and does not intersect the line segment connecting x and y_0. Moreover, we require that $Q' \notin S_0^{Q_{0,1}}$. Now, choose the common parallel a_{S_1} of S_1 in such a way that there is an argument β_1 of a_{S_1} that satisfies $\pi + \beta_0 > \beta_1 > \beta_0$. By construction, x lies in the region $-a_{S_1}$ is pointing to. Note that $S_1^{Q_{0,1}}$ cannot cross S_0 a second time.

Suppose we have already constructed the strip S_k with common parallel a_{S_k} and argument $\beta_k, k > 0$, and x lies in the region $-a_{S_k}$ is pointing to. S_k shall not intersect the line segments connecting x and y_0 or connecting x and y_{k-1}. Moreover, assume that the semi-infinite part $S_k^{Q_{k-1,k}}$ starting in the intersection $Q_{k-1,k}$ of S_k with S_{k-1} does not cross S_0.

Let y_k be the first intersection of the ray $x + ta_{S_k}, t > 0$, with a quadrilateral Q_k of the strip S_k. By the same arguments as above, there exists a strip S_{k+1} intersecting $S_k^{Q_{k-1,k}} \cap S_k^{Q_k}$ that does not contain Q and does not intersect the line segments connecting x and y_0 or x and y_k. Choose its common parallel $a_{S_{k+1}}$ in such a way that it has an argument β_{k+1} that satisfies $\pi + \beta_k > \beta_{k+1} > \beta_k$. By construction, x lies in the region $-a_{S_{k+1}}$ is pointing to. If the semi-infinite part $S_{k+1}^{Q_{k,k+1}}$ starting in the intersection $Q_{k,k+1}$ with S_k does not cross S_0, then we continue this procedure. For a schematic picture of the proof, see Fig. 7.

After at most $l := \lceil 2\pi/\alpha_0 \rceil$ steps, we end up with a strip S_l such that $S_l^{Q_{l-1,l}}$ intersects S_0. Indeed, let us suppose the contrary, that is, let us suppose that all $S_2^{Q_{1,2}}, \ldots, S_l^{Q_{l-1,l}}$ do not cross S_0.

By assumption, $\beta_k + \pi - \alpha_0 \geqslant \beta_{k+1} \geqslant \beta_k + \alpha_0$. It follows that the first j such that β_j is greater or equal than $\beta_0 + 2\pi$ satisfies $j \leqslant \lceil 2\pi/\alpha_0 \rceil$. In addition, we have $\beta_j < \beta_0 + 3\pi - \alpha_0$.

By construction, S_j does not intersect the line segment connecting x and y_{j-1}. Moreover, $S_j^{Q_{j-1,j}}$ cannot cross S_{j-1} a second time. It follows that $S_j^{Q_{j-1,j}}$ cannot intersect the ray $x + ta_{S_{j-1}}, t > 0$.

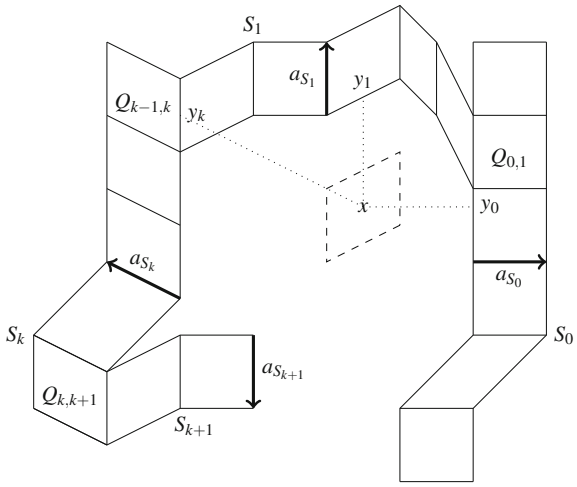

Fig. 7 Schematic picture of the proof of Proposition 4.3

Also, $S_j^{Q_{j-1,j}}$ does neither cross S_0 nor does it intersect the line segment connecting x and y_0, so it does not intersect the ray $x + ta_{S_0}, t > 0$. Thus, $S_j^{Q_{j-1,j}}$ is contained in the cone with tip x spanned by $a_{S_{j-1}}$ and a_{S_0} (with angle less than π). This contradicts the monotonicity of $S_j^{Q_{j-1,j}}$ into the direction ia_{S_j}, because the ray $x + ta_{S_j}, t > 0$, is not contained in the interior of the cone above.

In summary, we found a cycle of m strips $S_0, S_1, \ldots, S_{m-1}$ surrounding x, where $m \leqslant \lfloor 2\pi/\alpha_0 \rfloor + 1$. Actually, $m \leqslant \lfloor 2\pi/\alpha_0 \rfloor$, because the a_{S_k} are cyclically ordered. Since only finitely many strips intersect the strip S_0 in between Q' and $Q_{0,1}$, we can assume that Q' is contained in $S_0^{Q_{m-1,0}}$.

These m strips determine a bounded region x is contained in. If $Q' \neq Q_{m-1,0}$, then we look at the semi-infinite part of the strip $\tilde{S}_0$ different from S_0 that passes through Q' and goes into the interior of the bounded region above. It has to intersect one of the strips $S_1, \ldots, S_{m-1}$, say S_k. Then, $S_0, \ldots, S_k, \tilde{S}_0$ or $\tilde{S}_0, S_k, \ldots, S_{m-1}, S_0$ determine a bounded region x is contained in (Q may be an element of $\tilde{S}_0$). Clearly, they are at most $\lfloor 2\pi/\alpha_0 \rfloor$ such strips, and Q' lies on an intersection.

If $Q \notin \tilde{S}_0$, then a strip S_Q containing Q has to cross two different strips of the cycle due to local finiteness. In the same way as above, we can find a cycle of at most $m' \leqslant \lfloor 2\pi/\alpha_0 \rfloor$ strips $S'_0, S'_1, \ldots, S'_{m'-1}$ such that Q lies on one of the strips, say S'_k, and the intersection of S'_0 and $S'_{m'-1}$ is Q'. If $k \leqslant \lceil m'/2 \rceil$, then we choose the sequence of strips $S'_0, S'_1, \ldots, S'_k$; otherwise, we take $S'_{m'-1}, S'_{m'-2}, \ldots, S'_k$. Any two consecutive strips are crossing each other, Q' is on the first strip, Q on the last one, and there are at most $\lceil \lfloor 2\pi/\alpha_0 \rfloor /2 \rceil$ of them.

Remark In general, the bound $\lceil \lfloor 2\pi/\alpha_0 \rfloor /2 \rceil$ in the proof is optimal. Indeed, consider n rays emanating from 0 such that the angle between any two neighboring rays is $2\pi/n$. In each of the n segments, choose the quad-graph combinatorially equivalent to the positive octant of the integer lattice that is spanned by two consecutive rays.

For example, if $n = 4$, we obtain $\mathbb{Z}^2$. Then, any strip passes through exactly two adjacent segments, and $\lceil n/2 \rceil$ is the optimal bound.

References

1. Bobenko, A., Günther, F.: Discrete Riemann surfaces based on quadrilateral cellular decompositions (2015). Preprint arXiv:1511.00652
2. Bobenko, A., Mercat, C., Suris, Y.: Linear and nonlinear theories of discrete analytic functions. Integrable structure and isomonodromic Green's function. J. Reine Angew. Math. **583**, 117–161 (2005)
3. Bobenko, A., Suris, Y.: Discrete differential geometry: integrable structure. In: Graduate Studies in Mathematics, vol. 98. AMS, Providence (2008)
4. Brooks, R., Smith, C., Stone, A., Tutte, W.: The dissection of rectangles into squares. Duke Math. J. **7**(1), 312–340 (1940)
5. Bücking, U.: Approximation of conformal mappings by circle patterns. Geom. Dedicata **137**, 163–197 (2008)
6. Chelkak, D., Smirnov, S.: Discrete complex analysis on isoradial graphs. Adv. Math. **228**, 1590–1630 (2011)
7. Chelkak, D., Smirnov, S.: Universality in the 2D Ising model and conformal invariance of fermionic observables. Invent. Math. **189**(3), 515–580 (2012)
8. Courant, R., Friedrichs, K., Lewy, H.: Über diepartiellen Differenzengleichungen der mathematischen Physik. Math. Ann. **100**, 32–74 (1928)
9. Duffin, R.: Basic properties of discrete analytic functions. Duke Math. J. **23**(2), 335–363 (1956)
10. Duffin, R.: Potential theory on a rhombic lattice. J. Comb. Th. **5**, 258–272 (1968)
11. Dynnikov, I., Novikov, S.: Geometry of the triangle equation on two-manifolds. Moscow Math. J. **3**(2), 419–482 (2003)
12. Ferrand, J.: Fonctions préharmoniques et fonctions préholomorphes. Bull. Sci. Math. Ser. **2**(68), 152–180 (1944)
13. Günther, F.: Discrete Riemann surfaces and integrable systems. Ph.D. thesis, Technische Universität Berlin (2014). http://opus4.kobv.de/opus4-tuberlin/files/5659/guenther_felix.pdf
14. Isaacs, R.: A finite difference function theory. Univ. Nac. Tucumán. Rev. A **2**, 177–201 (1941)
15. Kenyon, R.: Conformal invariance of domino tiling. Ann. Prob. **28**(2), 759–795 (2002)
16. Kenyon, R.: The Laplacian and Dirac operators on critical planar graphs. Invent. Math. **150**, 409–439 (2002)
17. Kenyon, R., Schlenker, J.M.: Rhombic embeddings of planar quad-graphs. Trans. Amer. Math. Soc. **357**(9), 3443–3458 (2005)
18. Lelong-Ferrand, J.: Représentation conforme et transformations à intégrale de Dirichlet bornée. Gauthier-Villars, Paris (1955)

19. Mercat, C.: Discrete Riemann surfaces and the Ising model. Commun. Math. Phys. **218**(1), 177–216 (2001)
20. Mercat, C.: Discrete Riemann surfaces. In: Handbook of Teichmüller theory. Vol. I, *IRMA Lect. Math. Theor. Phys.*, vol. 11, pp. 541–575. Eur. Math. Soc., Zurich (2007)
21. Mercat, C.: Discrete complex structure on surfel surfaces. Proceedings of the 14th IAPR International Conference on Discrete Geometry for Computer Imagery. DGCI'08, pp. 153–164. Springer-Verlag, Berlin, Heidelberg (2008)
22. Rodin, B., Sullivan, D.: The convergence of circle packings to the Riemann mapping. J. Diff. Geom. **26**(2), 349–360 (1987)
23. Skopenkov, M.: The boundary value problem for discrete analytic functions. Adv. Math. **240**, 61–87 (2013)
24. Smirnov, S.: Discrete complex analysis and probability. In: Proceedings of the International Congress of Mathematicians 2010 (ICM 2010), vol. I: Plenary Lectures and Ceremonies, vols. II-IV: Invited Lectures, pp. 595–621. Hindustan Book Agency, New Delhi, India (2000)
25. Smirnov, S.: Critical percolation in the plane: conformal invariance, Cardy's formula, scaling limits. C. R. Math. Acad. Sci. Paris Sér. I **333**(3), 239–244 (2001)
26. Smirnov, S.: Conformal invariance in random cluster models. I. Holomorphic fermions in the Ising model. Ann. Math. **172**(2), 1435–1467 (2010)
27. Whitney, H.: On products in a complex. Ann. Math. **39**(2), 397–432 (1938)

Approximation of Conformal Mappings Using Conformally Equivalent Triangular Lattices

Ulrike Bücking

Abstract Two triangle meshes are conformally equivalent if their edge lengths are related by scale factors associated to the vertices. Such a pair can be considered as preimage and image of a discrete conformal map. In this article we study the approximation of a given smooth conformal map f by such discrete conformal maps f^ε defined on triangular lattices. In particular, let T be an infinite triangulation of the plane with congruent strictly acute triangles. We scale this triangular lattice by $\varepsilon > 0$ and approximate a compact subset of the domain of f with a portion of it. For ε small enough we prove that there exists a conformally equivalent triangle mesh whose scale factors are given by $\log|f'|$ on the boundary. Furthermore we show that the corresponding discrete conformal (piecewise linear) maps f^ε converge to f uniformly in C^1 with error of order ε.

1 Introduction

Holomorphic functions build the basis and heart of the rich theory of complex analysis. Holomorphic functions with nowhere vanishing derivative, also called *conformal maps*, have the property to preserve angles. Thus they may be characterized by the fact that they are infinitesimal scale-rotations.

In the discrete theory, the idea of characterizing conformal maps as local scale-rotations may be translated into different concepts. Here we consider the discretization coming from a metric viewpoint: Infinitesimally, lengths are scaled by a factor, i.e. by $|f'(z)|$ for a conformal function f on $D \subset \mathbb{C}$. More generally, on a smooth manifold two Riemannian metrics g and $\tilde{g}$ are conformally equivalent if $\tilde{g} = \mathrm{e}^{2u} g$ for some smooth function u.

U. Bücking (✉)
Inst. für Mathematik, Technische Universität Berlin, Straße des 17. Juni 136,
10623 Berlin, Germany
e-mail: buecking@math.tu-berlin.de

A.I. Bobenko (ed.), *Advances in Discrete Differential Geometry*,
DOI 10.1007/978-3-662-50447-5_3

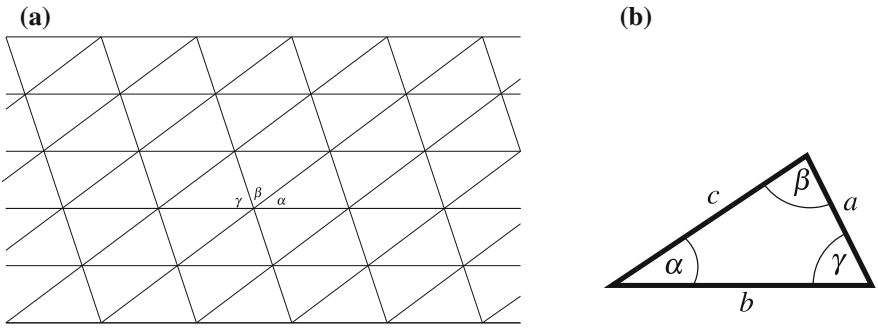

Fig. 1 Lattice triangulation of the plane with congruent triangles. **a** Example of a triangular lattice. **b** Acute angled triangle.

The smooth complex domain (or manifold) is replaced in this discrete setting by a triangulation of a connected subset of the plane $\mathbb{C}$ (or a triangulated piecewise Euclidean manifold).

1.1 Convergence for Discrete Conformal PL-Maps on Triangular Lattices

In this article we focus on the case where the triangulation is a (part of a) *triangular lattice*. In particular, let T be a lattice triangulation of the whole complex plane $\mathbb{C}$ with congruent triangles, see Fig. 1a. The sets of vertices and edges of T are denoted by V and E respectively. Edges will often be written as $e = [v_i, v_j] \in E$, where $v_i, v_j \in V$ are its incident vertices. For triangular faces we use the notation $\Delta[v_i, v_j, v_k]$ enumerating the incident vertices with respect to the orientation (counterclockwise) of $\mathbb{C}$.

On a subcomplex of T we now define a discrete conformal mapping. The main idea is to change the lengths of the edges of the triangulation according to scale factors at the vertices. The new triangles are then 'glued together' to result in a piecewise linear map, see Fig. 2 for an illustration. More precisely, we have

Definition 1.1 A *discrete conformal PL-mapping* g is a continuous and orientation preserving map of a subcomplex T_S of a triangular lattice T to $\mathbb{C}$ which is locally a homeomorphism in a neighborhood of each interior point and whose restriction to every triangle is a linear map onto the corresponding image triangle, that is the mapping is piecewise linear. Furthermore, there exists a function $u : V_S \to \mathbb{R}$ on the vertices, called *associated scale factors*, such that for all edges $e = [v, w] \in E_S$ there holds

$$|g(v) - g(w)| = |v - w| \mathrm{e}^{(u(v)+u(w))/2}, \tag{1}$$

where $|a|$ denotes the modulus of $a \in \mathbb{C}$.

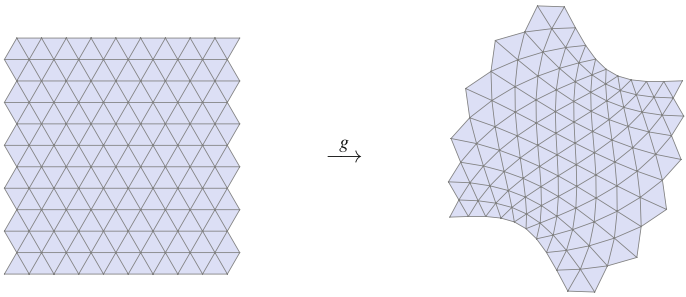

Fig. 2 Example of a discrete conformal PL-map g

Note that Eq. (1) expresses a linear relation for the logarithmic edge lengths, that is

$$2\log|g(v)-g(w)| = 2\log|v-w| + u(v) + u(w).$$

In fact, the definition of a discrete conformal PL-map relies on the notion of discrete conformal triangle meshes. These have been studied by Luo, Gu, Sun, Wu, Guo [8, 9, 14], Bobenko, Pinkall, and Springborn [1] and others.

As possible application, discrete conformal PL-maps can be used for discrete uniformization. The simplest case is a discrete Riemann mapping theorem, i.e. the problem of finding a discrete conformal mapping of a simply connected domain onto the unit disc. Similarly, we may consider a related Dirichlet problem. Given some function u_∂ on the boundary of a subcomplex T_S, find a discrete conformal PL-map whose associated scale factors agree on the boundary with u_∂. For such a Dirichlet problem (with assumptions on u_∂ and T_S) we will prove existence as part of our convergence theorem.

In this article we present a first answer to the following problem: *Given a smooth conformal map, find a sequence of discrete conformal PL-maps which approximate the given map.* We study this problem on triangular lattices T with acute angles and always assume for simplicity that the origin is a vertex. Denote by εT the lattice T scaled by $\varepsilon > 0$. Using the values of $\log|f'|$, we obtain a discrete conformal PL-map f^ε on a subcomplex of εT from a boundary value problem for the associated scale factors. More precisely, we prove the following approximation result.

Theorem 1.2 *Let $f : D \to \mathbb{C}$ be a conformal map (i.e. holomorphic with $f' \neq 0$). Let $K \subset D$ be a compact set which is the closure of its simply connected interior $int(K)$ and assume that $0 \in int(K)$. Let T be a triangular lattice with strictly acute angles. For each $\varepsilon > 0$ let T_K^ε be a subcomplex of εT whose support is contained in K and is homeomorphic to a closed disc. We further assume that 0 is an interior vertex of T_K^ε. Let $e_0 = [0, \hat{v}_0] \in E_K^\varepsilon$ be one of its incident edges.*

Then if $\varepsilon > 0$ is small enough (depending on K, f, and T) there exists a unique discrete conformal PL-map f^ε on T_K^ε which satisfies the following two conditions:

- *The associated scale factors $u^\varepsilon : V_K^\varepsilon \to \mathbb{R}$ satisfy*

$$u^\varepsilon(v) = \log|f'(v)| \quad \text{for all boundary vertices } v \text{ of } V_K^\varepsilon. \tag{2}$$

- *The discrete conformal PL-map is normalized according to $f^\varepsilon(0) = f(0)$ and* $\arg(f^\varepsilon(\hat{v}_0) - f^\varepsilon(0)) = \arg(\hat{v}_0) + \arg(f'(\frac{\hat{v}_0}{2}))$ (mod 2π).

Furthermore, the following estimates for u^ε and f^ε hold for all vertices $v \in V_K^\varepsilon$ and points x in the support of T_K^ε respectively with constants C_1, C_2, C_3 depending only on K, f, and T, but not on v or x:

(i) The scale factors u^ε approximate $\log|f'|$ uniformly with error of order ε^2:

$$\left|u^\varepsilon(v) - \log|f'(v)|\right| \leqslant C_1\varepsilon^2. \tag{3}$$

(ii) The discrete conformal PL-mappings f^ε converge to f for $\varepsilon \to 0$ uniformly with error of order ε:

$$|f^\varepsilon(x) - f(x)| \leqslant C_2\varepsilon.$$

(iii) The derivatives of f^ε (in the interior of the triangles) converge to f' uniformly for $\varepsilon \to 0$ with error of order ε:

$$\left|\partial_z f^\varepsilon(x) - f'(x)\right| \leqslant C_3\varepsilon \quad \text{and} \quad |\partial_{\bar{z}} f^\varepsilon(x)| \leqslant C_3\varepsilon$$

for all points x in the interior of a triangle Δ of T_K^ε. Here ∂_z and $\partial_{\bar{z}}$ denote the Wirtinger derivatives applied to the linear maps $f^\varepsilon|_\Delta$.

Note that the subcomplexes T_K^ε may be chosen such that they approximate the compact set K. Further notice that (3) implies that u^ε converges to $\log|f'|$ in C^1 with error of order ε, in the sense that also

$$\left|\frac{u^\varepsilon(v) - u^\varepsilon(w)}{\varepsilon} - \operatorname{Re}\left(\frac{f''((v+w)/2)}{f'((v+w)/2)}\right)\right| \leqslant \tilde{C}\varepsilon$$

on edges $[v, w]$ uniformly for some constant $\tilde{C}$.

The proof of Theorem 1.2 is given in Sect. 4. The arguments are based on estimates derived in Sect. 3.

The problem of actually computing the scale factors u for given boundary values u_∂ such that u gives rise to a discrete conformal PL-map (in case it exists) can be solved using a variational principle, see [1, 20]. Our proof relies on investigations using the corresponding convex functional, see Theorem 2.2 in Sect. 2.

Remark 1.3 The convergence result of Theorem 1.2 also remains true if linear interpolation is replaced with the piecewise projective interpolation schemes described in [1, 3], i.e., circumcircle preserving, angle bisector preserving and, generally, exponent-t-center preserving for all $t \in \mathbb{R}$. The proof is the same with only small adaptations. This is due to the fact that the image of the vertices is the same for all these interpolation schemes and these image points converge uniformly to the corresponding image points under f with error of order ε. The estimates for the derivatives similarly follow from Theorem 1.2(i).

1.2 Other Convergence Results for Discrete Conformal Maps

Smooth conformal maps can be characterized in various ways. This leads to different notions of discrete conformality. Convergence issues have already been studied for some of these discrete analogs. We only give a very short overview and cite some results of a growing literature.

In particular, linear definitions can be derived as discrete versions of the Cauchy-Riemann equations and have a long and still developing history. Connections of such discrete mappings to smooth conformal functions have been studied for example in [2, 6, 7, 13, 16, 19, 22].

The idea of characterizing conformal maps as local scale-rotations has lead to the consideration of circle packings, more precisely to investigations on circle packings with the same (given) combinatorics of the tangency graph. Thurston [21] first conjectured the convergence of circle packings to the Riemann map, which was then proven by [10, 11, 17].

The theory of circle patterns generalizes the case of circle packings. Also, there is a link to integrable structures via isoradial circle patterns. The approximation of conformal maps using circle patterns has been studied in [4, 5, 12, 15, 18].

The approach taken in this article constructs discrete conformal maps from given boundary values. Our approximation results and some ideas of the proof are therefore similar to those in [4, 5, 18] for circle patterns which also rely on boundary value problems.

2 Some Characterizations of Associated Scale Factors of Discrete Conformal PL-Maps

Consider a subcomplex T_S of a triangular lattice T and an arbitrary function $u : V_S \to \mathbb{R}$. Assign new lengths to the edges according to (1) by

$$\tilde{l}([v, w]) = |v - w| e^{(u(v)+u(w))/2} \tag{4}$$

In order to obtain new triangles with these lengths (and ultimately a discrete conformal PL-map) the triangle inequalities need to hold for the edge lengths $\tilde{l}$ on each triangle. If we assume this, we can embed the new triangles (respecting orientation) and immerse sequences of triangles with edge lengths given by $\tilde{l}$ as in (4). In order to obtain a discrete conformal PL-map, in particular a local homeomorphism, the interior angles of the triangles need to sum up to 2π at each interior vertex. The angle at a vertex of a triangle with given side lengths can be calculated. With the notation of Fig. 1b we have the half-angle formula

$$\tan\left(\frac{\alpha}{2}\right) = \sqrt{\frac{(-b+a+c)(-c+a+b)}{(b+c-a)(a+b+c)}} = \sqrt{\frac{1-(\frac{b}{a}-\frac{c}{a})^2}{(\frac{b}{a}+\frac{c}{a})^2-1}}. \tag{5}$$

The last expression emphasizes the fact that the angle does not depend on the scaling of the triangle. Careful considerations of this angle function depending on (scaled) side lengths of the triangle form the basis for our proof. In particular, we define the function

$$\theta(x,y) := 2\arctan\sqrt{\frac{1-(\mathrm{e}^{-x/2}-\mathrm{e}^{-y/2})^2}{(\mathrm{e}^{-x/2}+\mathrm{e}^{-y/2})^2-1}}, \tag{6}$$

so (5) can be written as

$$\alpha = \theta(x,y) \qquad \text{with} \quad \frac{b}{a} = \mathrm{e}^{-x/2} \quad \text{and} \quad \frac{c}{a} = \mathrm{e}^{-y/2}.$$

Summing up, we have the following characterization of scale factors associated to discrete conformal PL-maps.

Proposition 2.1 *Let T_S be a subcomplex of a triangular lattice T and $u : V_S \to \mathbb{R}$ a function satisfying the following two conditions.*

(i) For every triangle $\Delta[v_1, v_2, v_3]$ of T_S the triangle inequalities *for $\tilde{l}$ defined by (4) hold, in particular*

$$|v_i - v_j|e^{(u(v_i)+u(v_j))/2} < |v_i - v_k|e^{(u(v_i)+u(v_k))/2} + |v_j - v_k|e^{(u(v_j)+u(v_k))/2} \tag{7}$$

for all permutations (ijk) of (123).

(ii) For every interior vertex v_0 with neighbors $v_1, v_2, \ldots, v_k, v_{k+1} = v_1$ in cyclic order we have

$$\sum_{j=1}^{k} \theta(\lambda(v_0, v_j, v_{j+1}) + u(v_{j+1}) - u(v_0), \lambda(v_0, v_{j+1}, v_j) + u(v_j) - u(v_0)) = 2\pi, \tag{8}$$

where $\lambda(v_a, v_b, v_c) = 2\log(|v_b - v_c|/|v_a - v_b|)$ for a triangle $\Delta[v_a, v_b, v_c]$.

Then there is a discrete conformal PL-map (unique up to post-composition with Euclidean motions) such that its associated scale factors are the given function $u : V_S \to \mathbb{R}$.

Conversely, given a discrete conformal PL-map on a subcomplex T_S *of a triangular lattice* T*, its associated scale factors* $u : V_S \to \mathbb{R}$ *satisfy conditions (i) and (ii).*

In order to obtain discrete conformal PL-maps from a given smooth conformal map we will consider a Dirichlet problem for the associated scale factors. Therefore we will apply a theorem from [1] which characterizes the scale factors u for given boundary values using a variational principle for a functional E defined in [1, Sect. 4]. Note that we will not need the exact expression for E but only the formula for its partial derivatives. In fact, the vanishing of these derivatives is equivalent to the necessary condition (8) for the scale factors to correspond to a discrete conformal PL-map.

Theorem 2.2 *([1]) Let* T_S *be a subcomplex of a triangular lattice and let* $u_\partial : V_\partial \to \mathbb{R}$ *be a function on the boundary vertices* V_∂ *of* T_S*. Then the solution* $\tilde{u}$ *(if it exists) of Eq. (8) at all interior vertices with* $\tilde{u}|_{V_\partial} = u_\partial$ *is the unique argmin of a locally strictly convex functional* $E(u) = E_{T_S}(u)$ *which is defined for functions* $u : V \to \mathbb{R}$ *satisfying the inequalities (7).*

The partial derivative of E *with respect to* $u_i = u(v_i)$ *at an interior vertex* $v_i \in V_{int}$ *with* k *neighbors* $v_{i_1}, v_{i_2}, \ldots, v_{i_k}$ $v_{i_{k+1}} = v_{i_1}$ *in cyclic order is*

$$\frac{\partial E}{\partial u_i}(u) = 2\pi - \sum_{j=1}^{k} \theta(2\log\left(\frac{l_{i_{j+1},i_j}}{l_{i,i_{j+1}}}\right) + u_{i_j} - u_i, 2\log\left(\frac{l_{i_{j+1},i_j}}{l_{i,i_j}}\right) + u_{i_{j+1}} - u_i), \tag{9}$$

where $l_{j,k} = |v_j - v_k|$.

By Proposition 2.1 such a solution $\tilde{u}$ *are then scale factors associated to a discrete conformal PL-map.*

Remark 2.3 The functional E can be extended to a convex continuously differentiable function on $\mathbb{R}^V$, see [1] for details.

3 Taylor Expansions

We now examine the effect when we take $u = \log|f'|$ as 'scale factors', i.e. for each triangle we multiply the length $|v - w|$ of an edge $[v, w]$ by the geometric mean $\sqrt{|f'(v)f'(w)|}$ of $|f'|$ at the vertices. The proof of Theorem 1.2 is based on the idea that $u = \log|f'|$ almost satisfies the conditions for being the associated scale factors of an discrete conformal PL-map, that is conditions (i) and (ii) of Proposition 2.1, and therefore is close to the exact solution u^ε.

To be precise, suppose that εT is the equilateral triangulation of the plane. Assume without loss of generality that the edge lengths equal $\frac{\sqrt{3}}{2}\varepsilon > 0$ and edges are parallel to $e^{ij\pi/3}$ for $j = 0, 1, \ldots, 5$. Let the conformal function f, the compact set K, and the subcomplexes T_K^ε (with vertices V_K^ε and edges E_K^ε) be given as in Theorem 1.2. Let $v_0 \in V_{K,\mathrm{int}}^\varepsilon$ be an interior vertex. Here and below $V_{K,\mathrm{int}}^\varepsilon$ denotes the set of interior vertices having six neighbors in V_K^ε. Denote the neighbors of v_0 by $v_j = v_0 + \varepsilon\frac{\sqrt{3}e^{ij\frac{\pi}{3}}}{2}$ and consider the triangle $\Delta_j = \Delta[v_0, v_j, v_{j+1}]$ for some $j \in \{0, 1, \ldots, 5\}$. Taking $u = \log|f'|$, we obtain edge lengths of a new triangle $\tilde{\Delta}_j$, i.e. satisfying (7), if ε is small enough. Then the angle in $\tilde{\Delta}_j$ at the image vertex of v_0 is given by

$$\theta(\log|f'(v_0 + \varepsilon\frac{\sqrt{3}e^{ij\frac{\pi}{3}}}{2})| - \log|f'(v_0)|,\ \log|f'(v_0 + \varepsilon\frac{\sqrt{3}e^{i(j+1)\frac{\pi}{3}}}{2})| - \log|f'(v_0)|)$$

according to (6). Summing up these angles—that is inserting $\log|f'|$ into (8) instead of u at an interior vertex $v_0 \in V_{K,\mathrm{int}}^\varepsilon$—we obtain the function

$$\mathscr{S}_{v_0}(\varepsilon) = \sum_{j=0}^{5} \theta(\log|f'(v_0 + \varepsilon\frac{\sqrt{3}e^{ij\frac{\pi}{3}}}{2})| - \log|f'(v_0)|,\ \log|f'(v_0 + \varepsilon\frac{\sqrt{3}e^{i(j+1)\frac{\pi}{3}}}{2})| - \log|f'(v_0)|)$$

We are interested in the Taylor expansion of $\mathscr{S}_{v_0}$ in ε. The symmetry of the lattice T implies that $\mathscr{S}_{v_0}$ is an even function, so the expansion contains only even powers of ε^n. Using a computer algebra program we arrive at

$$\mathscr{S}_{v_0}(\varepsilon) = 2\pi + C_{v_0}\varepsilon^4 + \mathscr{O}(\varepsilon^6). \tag{10}$$

Here and below, the notation $h(\varepsilon) = \mathscr{O}(\varepsilon^n)$ means that there is a constant $\mathscr{C}$, such that $|h(\varepsilon)| \leqslant \mathscr{C}\varepsilon^n$ holds for all small enough $\varepsilon > 0$. The constant of the ε^4-term is

$$C_{v_0} = -\frac{3\sqrt{3}}{32}\mathrm{Re}\left(S(f)(v_0)\overline{\left(\frac{f''}{f'}\right)'}(v_0)\right),$$

where $S(f) = \left(\frac{f''}{f'}\right)' - \frac{1}{2}\left(\frac{f''}{f'}\right)^2$ is the Schwarzian derivative of f. We will not need the exact form of this constant, but only the fact that it is bounded on K.

Analogous results to (10) hold for all triangular lattices εT with edge lengths $a^\varepsilon = \varepsilon\sin\alpha$, $b^\varepsilon = \varepsilon\sin\beta$, $c^\varepsilon = \varepsilon\sin\gamma$, also if the angles are larger than $\pi/2$. We assume without loss of generality the edge directions being parallel to 1, $e^{i\alpha}$ and $e^{i(\alpha+\beta)}$. Arguing as above, we consider the function

$$\begin{aligned}\mathscr{S}_{v_0}(\varepsilon) = \;& \theta(2\log\frac{\sin\alpha}{\sin\gamma} + \log|\frac{f'(v_0+\varepsilon\sin\beta)}{f'(v_0)}|,\; 2\log\frac{\sin\alpha}{\sin\beta} + \log|\frac{f'(v_0+\varepsilon\sin\gamma\,\mathrm{e}^{i\alpha})}{f'(v_0)}|)\\ &+\theta(2\log\frac{\sin\beta}{\sin\alpha} + \log|\frac{f'(v_0+\varepsilon\sin\gamma\,\mathrm{e}^{i\alpha})}{f'(v_0)}|,\; 2\log\frac{\sin\beta}{\sin\gamma} + \log|\frac{f'(v_0+\varepsilon\sin\alpha\,\mathrm{e}^{i(\alpha+\beta)})}{f'(v_0)}|)\\ &+\theta(2\log\frac{\sin\gamma}{\sin\beta} + \log|\frac{f'(v_0+\varepsilon\sin\alpha\,\mathrm{e}^{i(\alpha+\beta)})}{f'(v_0)}|,\; 2\log\frac{\sin\gamma}{\sin\alpha} + \log|\frac{f'(v_0-\varepsilon\sin\beta)}{f'(v_0)}|)\\ &+\theta(2\log\frac{\sin\alpha}{\sin\gamma} + \log|\frac{f'(v_0-\varepsilon\sin\beta)}{f'(v_0)}|,\; 2\log\frac{\sin\alpha}{\sin\beta} + \log|\frac{f'(v_0-\varepsilon\sin\gamma\,\mathrm{e}^{i\alpha})}{f'(v_0)|}|)\\ &+\theta(2\log\frac{\sin\beta}{\sin\alpha} + \log|\frac{f'(v_0-\varepsilon\sin\gamma\,\mathrm{e}^{i\alpha})}{f'(v_0)}|,\; 2\log\frac{\sin\beta}{\sin\gamma} + \log|\frac{f'(v_0-\varepsilon\sin\alpha\,\mathrm{e}^{i(\alpha+\beta)})}{f'(v_0)}|)\\ &+\theta(2\log\frac{\sin\gamma}{\sin\beta} + \log|\frac{f'(v_0-\varepsilon\sin\alpha\,\mathrm{e}^{i(\alpha+\beta)})}{f'(v_0)}|,\; 2\log\frac{\sin\gamma}{\sin\alpha} + \log|\frac{f'(v_0+\varepsilon\sin\beta)}{f'(v_0)}|).\end{aligned}$$

Again, $\mathscr{S}_{v_0}$ is an even function. Using a computer algebra program we arrive at

$$\mathscr{S}_{v_0}(\varepsilon) = 2\pi + C_{v_0}\varepsilon^4 + \mathscr{O}(\varepsilon^6), \tag{11}$$

with corresponding constant

$$\begin{aligned}C_{v_0} = -\frac{\sin\alpha\sin\beta\sin\gamma}{4}\,\mathrm{Re}\Bigg(& S(f)(v_0)\overline{\left(\frac{f''}{f'}\right)'}(v_0)\\ &+c(\alpha,\beta,\gamma)\left(\frac{1}{2}\left(\frac{f''}{f'}\right)^2\left(\frac{f''}{f'}\right)' - \frac{1}{3}\left(\frac{f''}{f'}\right)'''\right)\Bigg),\end{aligned}$$

where $c(\alpha,\beta,\gamma) = \cos\beta\sin^3\beta + \cos\gamma\sin^3\gamma\,\mathrm{e}^{2i\alpha} + \cos\alpha\sin^3\alpha\,\mathrm{e}^{2i(\alpha+\beta)}$.

Our key observation is that we can control the sign of the $\mathscr{O}(\varepsilon^4)$-term in (10) if we replace $\log|f'(x)|$ by $\log|f'(x)| + a\varepsilon^2|x|^2$, where $a \in \mathbb{R}$ is some suitable constant. In particular, for positive constants $M^{\pm}$, $C^{\pm}$ consider the functions

$$w^{\pm} = \log|f'| + q^{\pm} \qquad \text{with } q^{\pm}(v) = \begin{cases}\pm\varepsilon^2(M^{\pm} - C^{\pm}|v|^2) & \text{for } v \in V_{K,\mathrm{int}}^{\varepsilon},\\ 0 & \text{for } v \in \partial V_K^{\varepsilon}.\end{cases}$$

Here and below $\partial V_K^{\varepsilon}$ denotes the set of boundary vertices of V_K^{ε}.

Then we obtain for equilateral triangulations with edge length $\frac{\sqrt{3}}{2}\varepsilon$ the following Taylor expansion for all interior vertices $v_0 \in V_{K,\mathrm{int}}^{\varepsilon}$ whose neighbors are also in $V_{K,\mathrm{int}}^{\varepsilon}$:

$$\begin{aligned}\sum_{j=0}^{5}\theta(w^{\pm}(v_0+\varepsilon\frac{\sqrt{3}}{2}\mathrm{e}^{ij\frac{\pi}{3}}) - w^{\pm}(v_0),\, w^{\pm}(v_0+\varepsilon\frac{\sqrt{3}}{2}\mathrm{e}^{i(j+1)\frac{\pi}{3}}) - w^{\pm}(v_0))\\ = 2\pi + (C_{v_0} \mp \frac{3\sqrt{3}}{2}C^{\pm})\varepsilon^4 + \mathscr{O}(\varepsilon^5).\end{aligned} \tag{12}$$

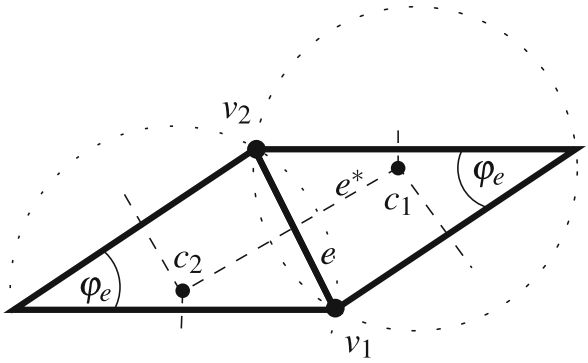

Fig. 3 Two adjacent triangles of the triangular lattice εT and orthogonal edges $e \in (\varepsilon E)$ (*solid*) and $e^* \in (\varepsilon E^*)$ (*dashed*)

Again, analogous results hold for all regular triangular lattices, where the corresponding $\mathcal{O}(\varepsilon^4)$-term then is

$$C_{v_0} \mp 4 \sin\alpha \sin\beta \sin\gamma \; C^{\pm}.$$

For interior vertices $v_0 \in V^{\varepsilon}_{K,\mathrm{int}}$ which are incident to k boundary vertices we obtain instead of the right-hand side of (12):

$$2\pi \mp k\frac{\sqrt{3}}{4}(M^{\pm} - C^{\pm}|v_0|^2)\varepsilon^2 + \mathcal{O}(\varepsilon^4).$$

For general triangular lattices we get for every edge $e = [v_0, v_j]$ which is incident to a boundary vertex $v_j \in \partial V^{\varepsilon}_K$ a term $\mp(M^{\pm} - C^{\pm}|v_0|^2)\cos\varphi_e \sin\varphi_e \varepsilon^2$ where φ_e is the angle opposite to the edge e, see Fig. 3.

The following lemma summarizes the main properties of $w^{\pm}$ which follow from the definition of $w^{\pm}$ together with the preceding estimates.

Lemma 3.1 *$w^{\pm}$ satisfies the boundary condition $w^{\pm}|_{\partial V^{\varepsilon}_K} = \log|f'|\big|_{\partial V^{\varepsilon}_K}$.*

Furthermore, $C^{\pm} > 0$ and $M^{\pm} > 0$ can be chosen such that for all ε small enough and all $v_0 \in V^{\varepsilon}_{K,int}$:

(i) $q^+(v_0) > 0$ *and* $q^-(v_0) < 0$

(ii) If $v_1, v_2, \ldots, v_6, v_7 = v_1$ denote the chain of neighboring vertices of v_0 in cyclic order and $\lambda(v_a, v_b, v_c) = 2\log(|v_b - v_c|/|v_a - v_b|)$ for any triangle $\Delta[v_a, v_b, v_c]$, we have

$$\sum_{j=1}^{6} \theta(\lambda(v_0, v_{j+1}, v_j) + w^+(v_j) - w^+(v_0), \lambda(v_0, v_j, v_{j+1}) + w^+(v_{j+1}) - w^+(v_0)) < 2\pi,$$

$$\sum_{j=1}^{6} \theta(\lambda(v_0, v_{j+1}, v_j) + w^-(v_j) - w^-(v_0), \lambda(v_0, v_j, v_{j+1}) + w^-(v_{j+1}) - w^-(v_0)) > 2\pi$$

The choices of $C^{\pm}$ and $M^{\pm}$ only depend on f (and its derivatives), K, and on the angles of the triangular lattice T.

In analogy to the continuous case we interpret Eq. (8) as a non-linear Laplace equation for u. In this spirit w^+ may be taken as superharmonic function and w^- as subharmonic function.

4 Existence of Discrete Conformal PL-Maps and Estimates

The functions $w^{\pm}$ have been introduced in order to 'catch' the solution u^{ε} in the following compact set:

$$W^{\varepsilon} = \{u : V_K^{\varepsilon} \to \mathbb{R} \mid u(v) = \log|f'(v)| \text{ for all } v \in \partial V_K^{\varepsilon}, \\ w^-(v) \leqslant u(v) \leqslant w^+(v) \text{ for all } v \in V_{K,\mathrm{int}}^{\varepsilon}\}.$$

Note that W^{ε} is a n-dimensional interval in $\mathbb{R}^n$ for $n = |V_K^{\varepsilon}|$ = number of vertices, if we identify a function $u : V_K^{\varepsilon} \to \mathbb{R}$ with the vector of its values $u(v_i)$. Also, for neighboring vertices $v_i \sim v_j$ and $u \in W^{\varepsilon}$ we have $u(v_j) - u(v_i) = \mathcal{O}(\varepsilon)$. Therefore, $u \in W^{\varepsilon}$ satisfies the triangle inequalities (7) if ε is small enough.

Our aim is to show that for ε small enough there exists a function u^{ε} satisfying conditions (i) and (ii) of Proposition 2.1 and $u^{\varepsilon}(v) = \log|f'(v)|$ for all boundary vertices $v \in \partial V_K^{\varepsilon}$. This function then defines a discrete conformal PL-map f^{ε} (uniquely if we use the normalization of Theorem 1.2).

Theorem 4.1 *Assume that all angles of the triangular lattice T are strictly smaller than $\pi/2$. There is an $\varepsilon_0 > 0$ (depending on f, K and the triangulation parameters) such that for all $0 < \varepsilon < \varepsilon_0$ the minimum of the functional E (see Theorem 2.2) with boundary conditions (2) is attained in W^{ε}.*

Corollary 4.2 *For all $0 < \varepsilon < \varepsilon_0$ there exists a discrete conformal PL-map on T_K^{ε} whose associated scale factors satisfy the boundary conditions (2).*

The proof of Theorem 4.1 follows from Lemma 4.4 below. It is based on Theorem 2.2 and on monotonicity estimates of the angle function $\theta(x, y)$ defined in (6). It is only here where we need the assumption that all angles of the triangular lattice T are strictly smaller than $\pi/2$.

Lemma 4.3 (Monotonicity lemma) *Consider the star of a vertex v_0 of a triangular lattice T and its neighboring vertices $v_1, \ldots, v_6, v_7 = v_1$ in cyclic order. Denote $\lambda_{0,k} := 2\log(|v_{k+1} - v_k|/|v_0 - v_k|)$. Assume that all triangles $\Delta(v_0, v_k, v_{k+1})$ are strictly acute angled, i.e. all angles $< \pi/2$.*

Then there exists $\eta_0 > 0$, depending on the λs, such that for all $0 \leqslant \eta_1, \ldots, \eta_6$, $\eta_7 = \eta_1 < \eta_0$ there holds

$$\sum_{k=1}^{6} \theta(\lambda_{0,k} + \eta_k, \lambda_{0,k+1} + \eta_{k+1}) \geqslant \sum_{k=1}^{6} \theta(\lambda_{0,k}, \lambda_{0,k+1}),$$

and for all $0 \geqslant \eta_1, \ldots, \eta_6, \eta_7 = \eta_1 > -\eta_0$ we have

$$\sum_{k=1}^{6} \theta(\lambda_{0,k} + \eta_k, \lambda_{0,k+1} + \eta_{k+1}) \leqslant \sum_{k=1}^{6} \theta(\lambda_{0,k}, \lambda_{0,k+1}).$$

Proof First, consider a single acute angled triangle. Observe that with the notation of Fig. 1b:

$$\frac{\partial \beta}{\partial a} = -\frac{1}{a} \cot \gamma.$$

Thus, we easily deduce that

$$\frac{\partial}{\partial \varepsilon} \theta(2 \log(\frac{a}{c}) + \varepsilon, 2 \log(\frac{a}{b}))\Big|_{\varepsilon=0} = \frac{1}{2} \cot \gamma.$$

Now the claim follows by Taylor expansion. □

Lemma 4.4 *There is an $\varepsilon_0 > 0$ such that for all $0 < \varepsilon < \varepsilon_0$ the negative gradient $-grad(E)$ on the boundary of W^ε points into the interior of W^ε.*

Proof For notational simplicity, set $u_k = u(v_k)$, $w_k^\pm = w^\pm(v_k)$ for vertices $v_k \in V_K^\varepsilon$ and $\lambda_{a,b,c} = 2 \log(|v_b - v_c|/|v_a - v_b|)$.

Consider grad(E) on a boundary face $W_i^+ = \{u \in W^\varepsilon : u_i = w_i^+\}$ of the n-dimensional interval W^ε. Let $v_1, \ldots, v_6, v_7 = v_1$ denote the neighbors of v_i in cyclic order. Note that $w_j^+ - w_j^- = \varepsilon^2(M^+ + M^- - (C^+ + C^-)|v_j|^2)$ for all vertices v_j. As K is compact we may assume that $0 < \varepsilon_0$ is such that $w_j^+ - w_j^- \leqslant \varepsilon$ for $0 < \varepsilon < \varepsilon_0$. Then using the properties of w^+ and u we obtain from Lemmas 4.3 and 3.1

$$\begin{aligned}
\frac{\partial E}{\partial u_i}(u) &= 2\pi - \sum_{j=0}^{5} \theta(\lambda_{i,j+1,j} + \underbrace{u_j - \underbrace{u_i}_{=w_i^+}}_{\leqslant w_j^+ - w_i^+}, \lambda_{i,j,j+1} + \underbrace{u_{j+1} - \underbrace{u_i}_{=w_i^+}}_{\leqslant w_{j+1}^+ - w_i^+}) \\
&\geqslant 2\pi - \sum_{j=0}^{5} \theta(\lambda_{i,j+1,j} + w_j^+ - w_i^+, \lambda_{i,j,j+1} + w_{j+1}^+ - w_i^+) \\
&> 0.
\end{aligned}$$

An analogous estimate holds for boundary faces W_i^-. □

We are now ready to deduce our convergence theorem.

Proof (of Theorem 1.2) The existence part follows from Theorem 4.1. The uniqueness is obvious as the translational and rotational freedom of the image of f^ε is fixed using values of f.

We now deduce the remaining estimates.

Part (i): Together with the definition of $w^\pm$, Theorem 4.1 implies that for $\varepsilon > 0$ small enough and all vertices $v \in V_K^\varepsilon$

$$\begin{aligned} &-\varepsilon^2(M^- - C^-|v|^2) \\ &\quad \leqslant w^-(v) - \log|f'(v)| \leqslant u^\varepsilon(v) - \log|f'(v)| \leqslant w^+(v) - \log|f'(v)| \\ &\qquad\qquad \leqslant \varepsilon^2(M^+ - C^+|v|^2). \end{aligned}$$

As K is compact, this implies estimate (3).

Part (ii): Given the scale factors u^ε associated to the discrete conformal PL-map f^ε on T_K^ε, we can in every image triangle determine the interior angles (using for example (5)). In particular, we begin by deducing from estimate (3) the change of these interior angles of the triangles.

Recall that for acute angled triangles the center of the circumcircle lies in the interior of the triangle. Joining these centers for incident triangles leads to an embedded regular graph $\varepsilon T^* = (\varepsilon V^*, \varepsilon E^*)$ which is dual to the given triangular lattice εT. In particular, the vertices εV^* are identified with the centers of the circumcircles of the triangles of εT. Furthermore, each edge $e^* \in (\varepsilon E^*)$ intersects exactly one edge $e \in (\varepsilon E)$ orthogonally, so e and e^* are dual, see Fig. 3. Consider an edge $e = [v_1, v_2] \in E_K^\varepsilon$ with dual edge $e^* = [c_1, c_2]$. Their lengths are related by $|c_2 - c_1| = |v_2 - v_1| \cot\varphi_e$, where φ_e denotes the angle opposite to e in εT. Furthermore we obtain

$$\begin{aligned} \cot\varphi_e(\log|f'(v_2)| - \log|f'(v_1)|) &= \cot\varphi_e \mathrm{Re}((\log f')'(v_1)(v_2 - v_1)) + \mathcal{O}(\varepsilon^2) \\ &= \cot\varphi_e \mathrm{Im}((\log f')'(v_1) i(v_2 - v_1)) + \mathcal{O}(\varepsilon^2) \\ &= \mathrm{Im}((\log f')'(v_1)(c_2 - c_1)) + \mathcal{O}(\varepsilon^2) \\ &= 2\mathrm{Im}((\log f')'(v_1)(c_2 - v_1)) \\ &\quad + 2\mathrm{Im}((\log f')'(v_1)(v_1 - \frac{c_2 + c_1}{2})) + \mathcal{O}(\varepsilon^2) \\ &= 2\arg f'(c_2) - 2\arg f'(\underbrace{\frac{c_2 + c_1}{2}}_{=\frac{v_2+v_1}{2}}) + \mathcal{O}(\varepsilon^2) \qquad (13) \\ &= 2\arg f'(\frac{v_2 + v_1}{2}) - 2\arg f'(c_1) + \mathcal{O}(\varepsilon^2), \qquad (14) \end{aligned}$$

where we have chosen the notation such that $(v_2 - v_1)i = (c_2 - c_1)\tan\varphi_e$.

Now we estimate the change of the angles in a triangle of T_K^ε compared with its image triangle under f^ε. Assume given a triangle $\Delta[v_0, v_1, v_2]$ and denote $e_1 = [v_0, v_1]$ and $e_2 = [v_0, v_2]$. Denote the angle at v_0 by $\theta_0 = \theta(\lambda_1, \lambda_2)$, where $l_{e_j} = |v_j - v_0|$ and $\lambda_j = 2\log(|v_1 - v_2|/l_{e_{j+1}})$ for $j = 1, 2$ and $e_3 = e_1$. Consider the Taylor expansion

$$\theta(\lambda_1 + x_1\varepsilon, \lambda_2 + x_2\varepsilon) = \theta_0 + \varepsilon(\frac{\cot\varphi_{e_1}}{2}x_1 + \frac{\cot\varphi_{e_2}}{2}x_2) + \mathcal{O}(\varepsilon^2).$$

We apply this estimate for the bounded terms

$$x_j = \frac{u^\varepsilon(v_j) - u^\varepsilon(v_0)}{\varepsilon} = \frac{\log|f'(v_j)| - \log|f'(v_0)|}{\varepsilon} + \mathcal{O}(\varepsilon)$$

for $j = 1, 2$. Denote by $\delta + \theta_0 \in (0, \pi)$ the angle at the image point of v_0 in the image triangle $f^\varepsilon(\Delta[v_0, v_1, v_2])$. Then by (13) and (14) the change of angle δ is given by

$$\delta = \arg f'(\frac{v_2 + v_0}{2}) - \arg f'(\frac{v_0 + v_1}{2}) + \mathcal{O}(\varepsilon^2) \tag{15}$$

This local change of angles is related to the angle $\psi^\varepsilon(e)$ by which each edge e of T_K^ε has to be rotated to obtain the corresponding image edge $f^\varepsilon(e)$ (or, more precisely, a parallel edge). The function ψ^ε may be defined globally on E_K^ε such that in the above notation the change of the angle at v_0 is given as $\delta = \psi^\varepsilon(e_2) - \psi^\varepsilon(e_1) \in (-\pi, \pi)$. We fix the value of ψ^ε, that is the rotational freedom of the image of T_K^ε under f^ε at the edge e_0 according to $\arg f'$, see Theorem 1.2. Then we take shortest simple paths and deduce from (15) that each edge $e = [v_j, v_{j+1}] \in E_K^\varepsilon$ is rotated counterclockwise by

$$\psi^\varepsilon(e) = \arg f'(\frac{v_j + v_{j+1}}{2}) + \mathcal{O}(\varepsilon).$$

This implies together with (3) that for all edges $e = [v_j, v_{j+1}] \in E_K^\varepsilon$ we have uniformly

$$\log f'(\frac{v_j + v_{j+1}}{2}) - \frac{u^\varepsilon(v_j) + u^\varepsilon(v_{j+1})}{2} - i\psi^\varepsilon(e) = \mathcal{O}(\varepsilon). \tag{16}$$

Therefore the difference of the smooth and discrete conformal maps at vertices $v_0 \in V_K^\varepsilon$ satisfies uniformly

$$f(v_0) - f^\varepsilon(v_0) = O(\varepsilon)$$

by suitable integration along shortest simple paths from the reference point as above. This estimate then also holds for all points in the support of T_K^ε and $\varepsilon \to 0$.

Part (iii): As last step we consider the derivatives of f^ε restricted to a triangle.

Assume given a triangle $\Delta[v_0, v_1, v_2]$ in T_K^ε. As f^ε is piecewise linear its restriction to $\Delta = \Delta[v_0, v_1, v_2]$ is the restriction of an $\mathbb{R}$-linear map L_Δ. This map can be written for $z \in \mathbb{C}$ as

$$L_\Delta(z) = f^\varepsilon(v_0) + a \cdot (z - v_0) + b \cdot \overline{(z - v_0)},$$

where the constants $a, b \in \mathbb{C}$ are determined from the conditions $L_\Delta(v_j) = f^\varepsilon(v_j)$ for $j = 0, 1, 2$. Straightforward calculation gives

$$\partial_z L_\Delta = a = \frac{(f^\varepsilon(v_2) - f^\varepsilon(v_0))\overline{(v_1 - v_0)} - (f^\varepsilon(v_1) - f^\varepsilon(v_0))\overline{(v_2 - v_0)}}{\overline{(v_1 - v_0)}(v_2 - v_0) - (v_1 - v_0)\overline{(v_2 - v_0)}}$$
$$\partial_{\bar z} L_\Delta = b = \frac{(f^\varepsilon(v_2) - f^\varepsilon(v_0))(v_1 - v_0) - (f^\varepsilon(v_1) - f^\varepsilon(v_0))(v_2 - v_0)}{\overline{(v_1 - v_0)}(v_2 - v_0) - (v_1 - v_0)\overline{(v_2 - v_0)}}.$$

Note that by definition of f^ε and ψ^ε we know that

$$f^\varepsilon(v_j) - f^\varepsilon(v_0) = (v_j - v_0)\mathrm{e}^{(u^\varepsilon(v_j)+u^\varepsilon(v_0))/2+i\psi^\varepsilon([v_j,v_0])},$$

where we use the rotation function ψ^ε on the edges as defined in the previous part (ii) of the proof. Now (16) together with the above expressions of a and b immediately implies the desired estimates

$$\partial_z f^\varepsilon|_\Delta(z) = \partial_z L_\Delta(z) = f'(z) + \mathcal{O}(\varepsilon) \quad \text{and} \quad \partial_{\bar z} f^\varepsilon|_\Delta(z) = \partial_{\bar z} L_\Delta(z) = \mathcal{O}(\varepsilon).$$

uniformly on the triangle $\Delta = \Delta[v_0, v_1, v_2]$. Also, the constants in the estimate do not depend on the choice of the triangle. This finishes the proof. □

Remark 4.5 Theorem 1.2 focuses on a particular way to approximate a given conformal map f by a sequence of discrete conformal PL-maps. Namely, we consider corresponding smooth and discrete Dirichlet boundary value problems and compare the solutions. There is of course a corresponding problem for Neumann boundary conditions, i.e. prescribing angle sums of the triangles at boundary vertices using $\arg f'$. Also, there is a corresponding variational description for conformally equivalent triangle meshes or discrete conformal PL-maps in terms of angles, see [1]. But unfortunately, the presented methods for a convergence proof seem not to generalize in a straightforward manner to this case, as the order of the corresponding Taylor expansion is lower.

Acknowledgments The author would like to thank the anonymous referees for the careful reading of the initial manuscript and various suggestions for improvement. This research was supported by the DFG Collaborative Research Center TRR 109 "Discretization in Geometry and Dynamics".

References

1. Bobenko, A.I., Pinkall, U., Springborn, B.: Discrete conformal maps and ideal hyperbolic polyhedra. Geom. Topol. **19**, 2155–2215 (2015)
2. Bobenko, A.I., Skopenkov, M.: Discrete Riemann surfaces: linear discretization and its convergence. To appear in J. Reine Angew, Math (2014)
3. Born, S., Bücking, U., Springborn, B.: Quasiconformal distortion of projective transformations, with an application to discrete conformal maps. arXiv:1505.01341 [math.CV]
4. Bücking, U.: Approximation of conformal mappings by circle patterns and discrete minimal surfaces. Ph.D. thesis, Technische Universität Berlin (2007). http://opus.kobv.de/tuberlin/volltexte/2008/1764/
5. Bücking, U.: Approximation of conformal mapping by circle patterns. Geom. Dedicata **137**, 163–197 (2008)
6. Chelkak, D., Smirnov, S.: Universality in the 2D Ising model and conformal invariance of fermionic observables. Invent. math. **189**, 515–580 (2012)
7. Courant, R., Friedrichs, K., Lewy, H.: Über die partiellen Differenzengleichungen der mathematischen Physik. Math. Ann. **100**, 32–74 (1928). English translation: IBM Journal (1967), 215–234
8. Gu, X., Guo, R., Luo, F., Sun, J., Wu, T.: A discrete uniformization theorem for polyhedral surfaces II. arXiv:1401.4594 [math.GT]
9. Gu, X., Luo, F., Sun, J., Wu, T.: A discrete uniformization theorem for polyhedral surfaces. arXiv:1309.4175 [math.GT]
10. He, Z.X., Schramm, O.: On the convergence of circle packings to the Riemann map. Invent. Math. **125**, 285–305 (1996)
11. He, Z.X., Schramm, O.: The C^∞-convergence of hexagonal disk packings to the Riemann map. Acta Math. **180**, 219–245 (1998)
12. Lan, S.Y., Dai, D.Q.: The C^∞-convergence of SG circle patterns to the Riemann mapping. J. Math. Anal. Appl. **332**, 1351–1364 (2007)
13. Lelong-Ferrand, J.: Représentation conforme et transformations à intégrale de Dirichlet bornée. Gauthier-Villars, Paris (1955)
14. Luo, F.: Combinatorial Yamabe flow on surfaces. Commun. Contemp. Math. **6**(5), 765–780 (2004)
15. Matthes, D.: Convergence in discrete Cauchy problems and applications to circle patterns. Conform. Geom. Dyn. **9**, 1–23 (2005)
16. Mercat, C.: Discrete Riemann Surfaces. In: Papadopoulos, A. (ed.) Handbook of Teichmüller theory, vol. I, pp. 541–575. Eur. Math. Soc., Zürich (Ed.) (2007)
17. Rodin, B., Sullivan, D.: The convergence of circle packings to the Riemann mapping. J. Diff. Geom. **26**, 349–360 (1987)
18. Schramm, O.: Circle patterns with the combinatorics of the square grid. Duke Math. J. **86**, 347–389 (1997)
19. Skopenkov, M.: The boundary value problem for discrete analytic functions. Adv. Math. **240**, 61–87 (2013)

20. Springborn, B., Schröder, P., Pinkall, U.: Conformal equivalence of triangle meshes. ACM Trans. Graph. **27**(3) (2008)
21. Thurston, B.: The finite Riemann mapping theorem. Invited address at the International Symposioum in Celebration of the proof of the Bieberbach Conjecture, Purdue University (1985)
22. Werness, B.M.: Discrete analytic functions on non-uniform lattices without global geometric control (2014). Preprint

Numerical Methods for the Discrete Map Z^a

Folkmar Bornemann, Alexander Its, Sheehan Olver and Georg Wechslberger

Abstract As a basic example in nonlinear theories of discrete complex analysis, we explore various numerical methods for the accurate evaluation of the discrete map Z^a introduced by Agafonov and Bobenko. The methods are based either on a discrete Painlevé equation or on the Riemann–Hilbert method. In the latter case, the underlying structure of a triangular Riemann–Hilbert problem with a non-triangular solution requires special care in the numerical approach. Complexity and numerical stability are discussed, the results are illustrated by numerical examples.

1 Introduction

Following the famous ideas of Thurston's for a *nonlinear* theory of discrete complex analysis based on circle packings, Bobenko and Pinkall [5] defined a *discrete conformal* map as a complex valued function $f : \mathbb{Z}^2 \subset \mathbb{C} \to \mathbb{C}$ satisfying

$$\frac{(f_{n,m} - f_{n+1,m})(f_{n+1,m+1} - f_{n,m+1})}{(f_{n+1,m} - f_{n+1,m+1})(f_{n,m+1} - f_{n,m})} = -1. \tag{1}$$

F. Bornemann (✉) · G. Wechslberger
Zentrum Mathematik – M3, Technische Universität München,
Boltzmannstr. 3, 85747 Garching bei München, Germany
e-mail: bornemann@tum.de

G. Wechslberger
e-mail: wechslbe@ma.tum.de

A. Its
Department of Mathematical Sciences, Indiana University–Purdue University,
402 N. Blackford, Indianapolis, IN 46202, USA
e-mail: itsa@math.iupui.edu

S. Olver
School of Mathematics and Statistics, The University of Sydney,
Sydney, NSW 2006, Australia
e-mail: sheehan.olver@sydney.edu.au

A.I. Bobenko (ed.), *Advances in Discrete Differential Geometry*,
DOI 10.1007/978-3-662-50447-5_4

That is, the cross ratio on each elementary quadrilateral (fundamental cell) of the lattice $\mathbb{Z}^2$ is -1; infinitesimally, this property characterizes conformal maps among the smooth ones. A discrete conformal map $f_{n,m}$ is called an *immersion* if the interiors of adjacent elementary quadrilaterals are disjoint.

A central problem in discrete complex analysis is to find discrete conformal analogues of classical holomorphic functions that are immersions; simply evolving just the boundary values of the classical function by (1) would not work [6]. To solve this problem, Bobenko [3] suggested to augment (1) by another equation: using methods from the theory of integrable systems it can be shown that the non-autonomous system of constraints

$$af_{n,m} = 2n\frac{(f_{n+1,m} - f_{n,m})(f_{n,m} - f_{n-1,m})}{(f_{n+1,m} - f_{n-1,m})} + 2m\frac{(f_{n,m+1} - f_{n,m})(f_{n,m} - f_{n,m-1})}{(f_{n,m+1} - f_{n,m-1})}, \tag{2}$$

obtained as an integrable discretization of the differential equation

$$af = xf_x + yf_y = zf_z$$

that would define $f(z) = z^a$ up to scaling, is compatible with (1). Agafonov and Bobenko [1] proved that, for $0 < a < 2$, the system (1) and (2) of recursions, applied to the three initial values

$$f_{0,0} = 0, \quad f_{1,0} = 1, \quad f_{0,1} = e^{ia\pi/2}, \tag{3}$$

defines a unique discrete conformal map $Z^a_{n,m} = f_{n,m}$ that is an immersion [1, Theorem 1].

Moreover, they showed [1, Sect. 3] that this discrete conformal map Z^a determines a circle pattern of Schramm type, i.e., an orthogonal circle pattern with the

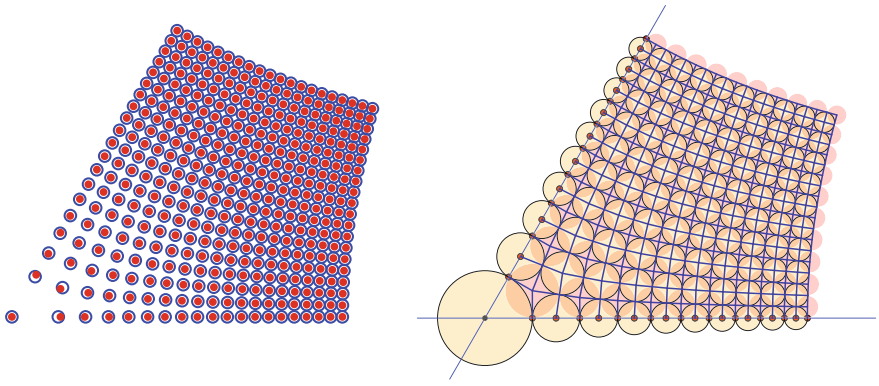

Fig. 1 *Left Red dots* are the discrete $Z^{2/3}$ for $0 \leqslant n, m \leqslant 19$; *blue circles* are the asymptotics given by (4). *Right* The Schramm circle pattern of the discrete $Z^{2/3}$ [courtesy of J. Richter-Gebert]

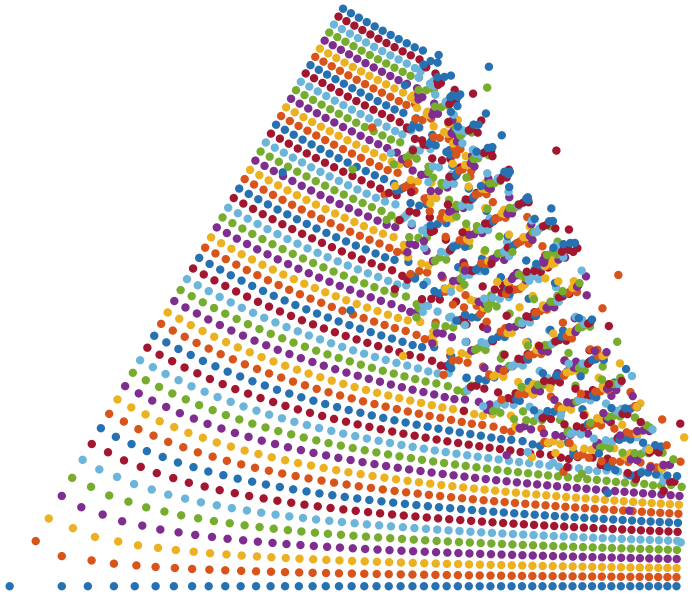

Fig. 2 Numerical discrete $Z^{2/3}_{n,m}$ $(0 \leqslant n, m \leqslant 49)$: recursing from the initial values (3) by a straightforward application of the system (1) and (2) quickly develops numerical instabilities. The color cycles with the coordinate m

combinatorics of the square grid, see Fig. 1. They conjectured, recently proved by Bobenko and Its [4] using the Riemann–Hilbert method, that asymptotically

$$Z^a_{n,m} = c_a \left(\frac{n+im}{2}\right)^a \left(1 + O\left(\frac{1}{n^2+m^2}\right)\right) \qquad (n^2+m^2 \to \infty) \tag{4a}$$

with the constant

$$c_a = \frac{\Gamma\left(1-\frac{a}{2}\right)}{\Gamma\left(1+\frac{a}{2}\right)}. \tag{4b}$$

For $0 < a \leqslant 1$, as exemplified in Fig. 1, this asymptotics is already accurate to plotting accuracy for all but the very smallest values of n and m. If $a \to 2$, however, it requires increasingly larger values of n and m to become accurate.

In this work we study the stable and accurate *numerical* calculation of Z^a; to the best of our knowledge for the first time in the literature. This is an interesting mathematical problem in itself, but the underlying methods should be applicable to a large set of similar discrete integrable systems. Now, the basic difficulty is that the evolution of the discrete dynamical system (1) and (2), starting from the initial values (3), is numerically highly unstable, see Fig. 2.[1]

[1] All numerical calculations are done in hardware arithmetic using double precision.

The support of the stencils of (1) and (2) has the form of a square and a five-point cross in the lattice $\mathbb{Z}^2$, that is,

$$\begin{matrix} f_{n,m+1} & f_{n+1,m+1} \\ f_{n,m} & f_{n+1,m} \end{matrix} \qquad \text{and} \qquad \begin{matrix} & f_{n,m+1} & \\ f_{n-1,m} & f_{n,m} & f_{n+1,m}, \\ & f_{n,m-1} & \end{matrix}$$

with the latter reducing to be dimensional along the boundary of $\mathbb{Z}^2_+$, namely

$$\begin{matrix} f_{0,m+1} \\ f_{0,m} \\ f_{0,m-1} \end{matrix}, \qquad \text{resp.} \qquad f_{n-1,0}\ f_{n,0}\ f_{n+1,0},$$

if $n = 0$ or $m = 0$. Thus, the forward evolution can be organized as follows. If $f_{n,m}$ is known for $0 \leqslant n, m \leqslant N$ the upper index N is increased to $N + 1$ according to:

(i) use (2) to compute the *boundary* values $f_{N+1,0}$ and $f_{0,N+1}$;
(ii) use (1) to compute the *row* $f_{N+1,m}$, $1 \leqslant m \leqslant N$;
(iii) use (1) to compute the *column* $f_{n,N+1}$, $1 \leqslant n \leqslant N$;
(iv) use (1) to compute the *diagonal* value $f_{N+1,N+1}$.

It is this algorithm that gives the unstable calculation shown in Fig. 2. Alternatively, one could use (2) to calculate the row values $f_{N+1,m}$, $1 \leqslant m \leqslant N-1$, and column values $f_{n,N+1}$, $1 \leqslant n \leqslant N-1$, up to the first sub- and superdiagonal (note that these calculations do *not* depend on order within the rows and columns). The missing values are then completed by using (1). However, this alternative forward evolution gives a result that is visually indistinguishable from Fig. 2.

As can be seen from Fig. 2, the numerical instability starts spreading from the diagonal elements $f_{n,n}$. In fact, there is an initial exponential growth of numerical errors to be found in the diagonal entries, see Fig. 3. Such a numerical instability of

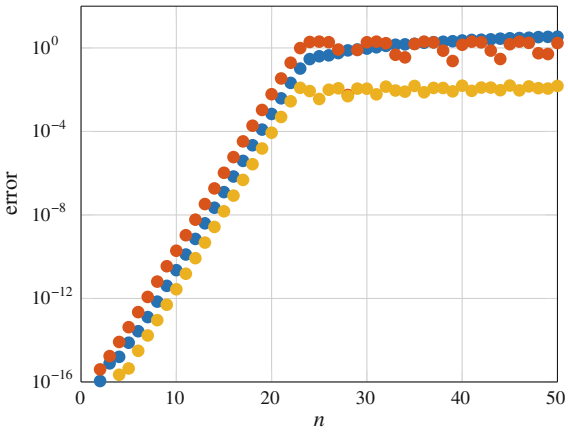

Fig. 3 Numerical error of the diagonal values $f_{n,n}$ from Fig. 2 (*blue*), of the x_n as in (5) and computed by forward evolution of the discrete Painlevé II equation (*red*), and of the corresponding invariant $|x_n| = 1$ (*yellow*); $a = 2/3$. They share the same rate of initial exponential growth

an evolution is the direct consequence of the instability of the underlying dynamical system, that is, of positive Lyapunov exponents.

As a remedy we suggest two different approaches to calculating $Z^a_{n,m}$. In Sect. 2 we stabilize the calculation of the diagonal values by solving a boundary value problem for an underlying discrete Painlevé II equation and in Sects. 3–8 we explore numerical methods based on the Riemann–Hilbert method. The latter reveals an interesting structure (Sect. 4): the Riemann–Hilbert problem has triangular data but a non-triangular solution; the operator equation can thus be written as a uniquely solvable block triangular system where the *infinite-dimensional* diagonal operators are *not* invertible. We discuss two different ways to prevent this particular structure from hurting *finite-dimensional* numerical schemes: a coefficient-based spectral method with infinite-dimensional linear algebra in Sect. 6 and a modified Nyström method based on least squares in Sect. 8.

2 Discrete Painlevé II Separatrix as a Boundary Value Problem

Since the source of the numerical instability of the direct evolution of the discrete dynamical system (1) and (2) is found in the diagonal elements $f_{n,n}$, we first express the $f_{n,n}$ directly in terms of a one-dimensional three-term recursion and then study its stable numerical evaluation. To begin with, Agafonov and Bobenko [1, Proposition 3] proved that the geometric quantities

$$x_n^2 = \frac{f_{n,n+1} - f_{n,n}}{f_{n+1,n} - f_{n,n}}, \qquad \arg x_n \in (0, \pi/2), \tag{5}$$

have invariant magnitude $|x_n| = 1$ (see the circle packing in Fig. 1) and that they satisfy the following form of the discrete Painlevé II equation

$$(n+1)(x_n^2 - 1)\left(\frac{x_{n+1} - ix_n}{i + x_n x_{n+1}}\right) - n(x_n^2 + 1)\left(\frac{x_{n-1} + ix_n}{i + x_{n-1}x_n}\right) = ax_n, \tag{6}$$

with initial value $x_0 = e^{ia\pi/4}$. Note that for $n = 0$ this nonlinear three-term recurrence degenerates and gives the missing second initial value, namely

$$x_1 = \frac{x_0(x_0^2 + a - 1)}{i((a-1)x_0^2 + 1)}. \tag{7}$$

Reversely, given the solution x_n of this equation, the diagonal elements $f_{n,n}$ can be calculated according to the simple recursion [1, p. 176]

$$u_n = \frac{r_n}{\mathrm{Re} x_n}, \quad r_{n+1} = u_n \cdot \mathrm{Im} x_n, \quad g_{n+1} = g_n + u_n, \quad f_{n+1,n+1} = g_{n+1} e^{ia\pi/4}, \tag{8}$$

with inital values $g_0 = 0$, $r_0 = 1$ (note that u_n, r_n, g_n are all positive); the sub- and superdiagonal elements $f_{n+1,n}$ and $f_{n,n+1}$ are obtained from (1) and (5) by

$$f_{n+1,n} = \frac{(x_n^2 - 1) f_{n,n} + (x_n^2 + 1) f_{n+1,n+1}}{2x_n^2}, \tag{9a}$$

$$f_{n,n+1} = \frac{(1 - x_n^2) f_{n,n} + (1 + x_n^2) f_{n+1,n+1}}{2}. \tag{9b}$$

However, given that x_n is a *separatrix* solution of the discrete Painlevé II equation [1, p. 167], we expect that a forward evolution of (6), starting with the initial values x_0 and x_1, suffers from exactly the same instability as the calculation of the diagonal values $f_{n,n}$ by evolving (1) and (2). Figure 3 shows that this is indeed the case, exhibiting the same initial exponential growth rate; it also shows that the deviation of the calculated values of $|x_n|$ from its invariant value 1 can serve as an explicitly computable error indicator.

In the continuous case of the Hastings–McLeod solution of Painlevé II, which also constitutes a separatrix, Bornemann [8, Sect. 3.2] suggested to address such problems by solving an asymptotic two-point *boundary* value problem instead of the originally given evolution problem. To this end, one has to solve the *connection problem* first, that is, one has to establish the asymptotics of x_n as $n \to \infty$. By inserting the known asymptotics (4) of $Z^a_{n,m}$ into the defining Eq. (5), we obtain

$$x_n = e^{i\pi/4}(1 + O(n^{-1})) \qquad (n \to \infty).$$

Since in actual numerical calculations we need accurate approximations already for moderately large n, we match the coefficients of an expansion in terms of n^{-1} to the discrete Painlevé II equation (6) and get, as $n \to \infty$,

$$\begin{aligned} x_n = e^{\frac{i\pi}{4}} \Bigg(1 &+ \frac{i(a-1)}{2n} + \frac{-a^2 + (2-2i)a - (1-2i)}{8n^2} - \frac{i\left(a^3 - (3-2i)a^2 - (1+4i)a + (3+2i)\right)}{16n^3} \\ &+ \frac{3a^4 - (12-12i)a^3 - (2+36i)a^2 + (28+4i)a - (17-20i)}{128n^4} \\ &+ \frac{i\left(3a^5 - (15-12i)a^4 - (30+48i)a^3 + (150+24i)a^2 - (5-48i)a - (103+36i)\right)}{256n^5} \\ &+ O(n^{-6}) \Bigg). \end{aligned}$$

We denote the r.h.s. of this asymptotic formula, without the $O(n^{-6})$ term, by $x_{n,6}$.

Next, using Newton's method, we solve the nonlinear system of $N+1$ equations in $N+1$ unknowns $x_0, \ldots, x_N$ given by the discrete Painlevé equation (6) for $1 \leqslant n \leqslant N-1$ and the two boundary conditions

$$x_1 = \frac{x_0(x_0^2 + a - 1)}{i((a-1)x_0^2 + 1)}, \qquad x_N = x_{N,6}.$$

Note that the value $x_0 = e^{ia\pi/4}$ is not explicitly used and must be obtained as output of the Newton solve, that is, it can be used as an measure of success. We choose N large enough that $|x_{N,6}| \doteq 1$ up to machine precision (about $N \approx 300$ uniformly in a). Then, using the excellent initial guesses (for the accuracy of the asymptotics cf. the left panel of Fig. 1)

$$x_0^{(0)} = e^{ia\pi/4}, \qquad x_n^{(0)} = x_{n,6} \quad (1 \leqslant n \leqslant N),$$

Newton's method will converge in about just 10 iterations to machine precision yielding a numerical solution that satisfies the invariant $|x_n| = 1$ also up to machine precision. Since the Jacobian of a nonlinear system stemming from a three-term recurrence is *tridiagonal*, each Newton step has an operation count of order $O(N)$. Hence, the overall complexity of accurately calculating the values x_n, $0 \leqslant n \leqslant N$, is of optimal order $O(N)$.

Finally, having accurate values of x_n at hand, and therefore by (8) and (9) also those of $f_{n,n}$, $f_{n+1,n}$ and $f_{n,n+1}$, one can calculate the missing values of $f_{n,m}$ row- and column-wise, starting from the second sup- and superdiagonal and evolving to the boundary, either by evolving the cross-ratio relations (1) or by evolving the discrete differential equation (2). It turns out that the first option develops numerical instabilities spreading from the boundary, see Fig. 4, whereas the second option is,

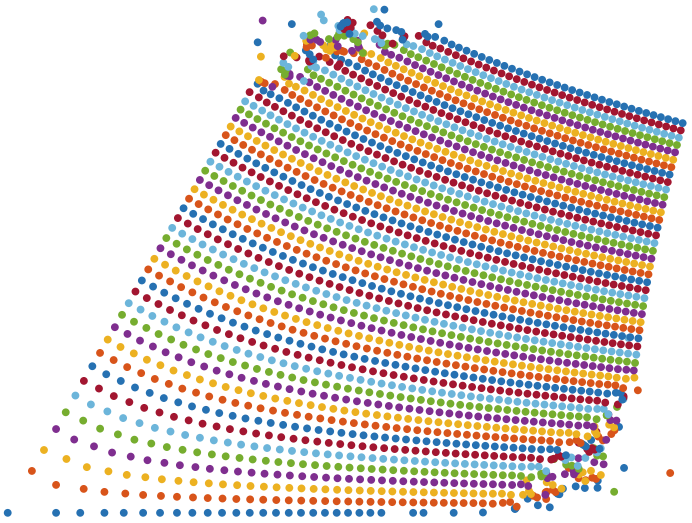

Fig. 4 Numerical discrete $Z^{2/3}_{n,m}$ $(0 \leqslant n, m \leqslant 49)$: evolving from accurate values of $f_{n,n}$, $f_{n+1,n}$, $f_{n,n+1}$ close to the diagonal back to the boundary by using the cross-ratio relations (1) develops numerical instabilities. The color cycles with the coordinate m

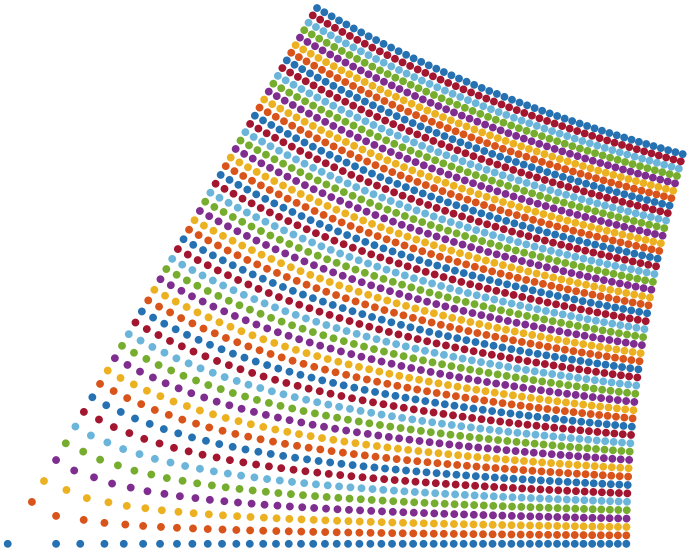

Fig. 5 Numerical discrete $Z^{2/3}_{n,m}$ ($0 \leqslant n, m \leqslant 49$): recursing from accurate values of $f_{n,n}$, $f_{n+1,n}$, $f_{n,n+1}$ close to the diagonal back to the boundary by using the discrete differential equation (2) is perfectly stable. The color cycles with the coordinate m

for a wide range of the parameter a, numerically observed to be perfectly stable, see Fig. 5. Note that this stable algorithm only differs from the alternative direct evolution discussed in the introduction in how the values close to the diagonal, that is $f_{n,n}$, $f_{n+1,n}$ and $f_{n,n+1}$, are computed.

The total complexity of this stable numerical calculation of the array $f_{n,m}$ with $0 \leqslant n, m \leqslant N$ is of optimal order $O(N^2)$.

3 The Riemann–Hilbert Method

Based on the integrability of the system (1) and (2), by identifying (1) as the compatibility condition of a Lax pair of linear difference equations [5] and by using isomonodromy, Bobenko and Its [4, p. 15] expressed the Z^a map in terms of the following Riemann–Hilbert problem (which is a slightly transformed and transposed version of the X-RHP by these authors): Let Γ_1 be the oriented contour built of two non-intersecting circles in the complex plane centered at $z = \pm 1$ (see Fig. 6 left), the holomorphic function $X : \mathbb{C} \setminus \Gamma_1 \to \mathrm{GL}(2)$ satisfies the jump condition

$$X_+(\zeta) = G_1(\zeta) X_-(\zeta) \qquad (\zeta \in \Gamma_1) \tag{10a}$$

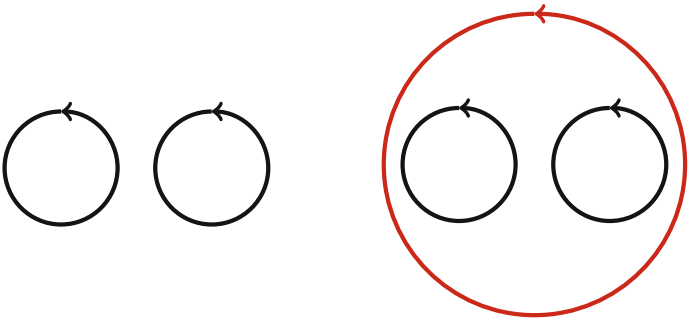

Fig. 6 Contours for the X-RHP [4, p. 15]. *Left* Two non-intersecting circles Γ_1 centered at ± 1 (*black*); *right* additional circle Γ_2 centered at 0 (*red*) for standard normalization at ∞

with the jump matrix[2]

$$G_1(\zeta) = \begin{pmatrix} 1 & 0 \\ e^{ia\pi/2}\zeta^{-a/2}(\zeta-1)^{-m}(\zeta+1)^{-n} & 1 \end{pmatrix} \tag{10b}$$

subject to the following normalization

$$X(z) = \begin{pmatrix} z^{\frac{m+n}{2}} & 0 \\ 0 & z^{-\frac{m+n}{2}} \end{pmatrix} (I + O(z^{-1})) \qquad (z \to \infty). \tag{10c}$$

Here, we restrict ourselves to values of n and m having the same parity such that $(m+n)/2$ is an integer. The discrete Z^a map is now given by the values $f_{n,m}$ extracted from an LU-decomposition at $z = 0$, namely,

$$X(0) = \begin{pmatrix} 1 & 0 \\ (-1)^{m+1} f_{n,m} & 1 \end{pmatrix} \begin{pmatrix} \bullet & \bullet \\ 0 & \bullet \end{pmatrix},$$

that is,

$$f_{n,m} = (-1)^{m+1} \frac{X_{21}(0)}{X_{11}(0)}.$$

Subsequently, using the Deift–Zhou nonlinear steepest decent method, Bobenko and Its [4] transform this X-RHP to a series of Riemann–Hilbert problems that are more suitable for asymptotic analysis. The last one of this series before introducing a

[2]To make G_1 holomorphic in the vicinity of Γ_1 we place the branch-cut of $\zeta^{-a/2}$ at the negative imaginary axis, that is, we take, using the principal branch Log of the logarithm,

$$e^{ia\pi/2}\zeta^{-a/2} = e^{ia\pi/4} e^{-\frac{a}{2}\operatorname{Log}(\zeta/i)}.$$

.

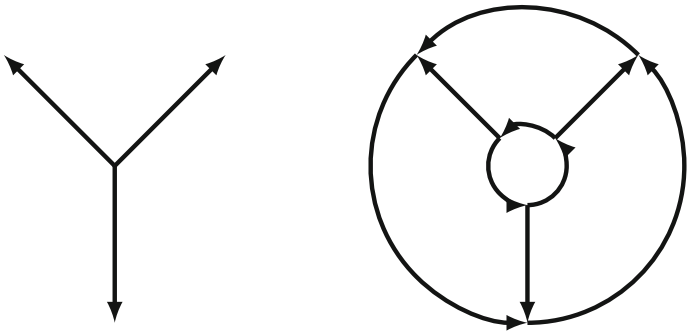

Fig. 7 *Left* Contour of the S-RHP [4, pp.24–27] centered at $z = 0$. *Right* Modified contour after normalizing the RHP at $z = 0$ and $z \to \infty$ (analogously to Fig. 6); the relative size of the inner and outer circles is chosen depending on n and m and has a major influence on the condition number of the spectral collocation method. Proper choices steer the condition number into a regime, which corresponds to a loss of about three to eight digits, see [24, Sect. 5.4]

global parametrix,[3] the S-RHP [4, pp. 24–27], is based on the contour shown in the left part of Fig. 7. This rather elaborate S-RHP is, after normalizing at $z = 0$ and $z \to \infty$ appropriately, amenable to the spectral collocation method of Olver [18]; we skip the details which can be found in the thesis of the fourth author G.W. [24, Sect. 5.4] that extends previous work on automatic contour deformation by Bornemann and Wechslberger [10, 25]. Here, the relative size of the inner and outer circles shaping the contour system shown in the right part of Fig. 7 have to be carefully adjusted to the parameters n and m to keep the condition number at a reasonable size. The complexity of computing $f_{n,m}$ for fixed n and m is then basically independent of m and n.

In the rest of this work we explore to what extent the analytic transformation from the X-RHP to the S-RHP is a necessary preparatory step also numerically, or whether one can use the originally given X-RHP as the basis for numerical calculations. To this end, we replace the normalization (10c) by the standard one, that is,

$$X(z) = I + O(z^{-1}) \qquad (z \to \infty), \tag{10d}$$

and introduce a further circle Γ_2 as shown in the right part of Fig. 6 with the jump condition

$$X_+(\zeta) = G_2(\zeta) X_-(\zeta) \quad (\zeta \in \Gamma_2), \qquad G_2(\zeta) = \begin{pmatrix} \zeta^{\frac{m+n}{2}} & 0 \\ 0 & \zeta^{-\frac{m+n}{2}} \end{pmatrix}. \tag{10e}$$

[3] Though the parametrix leads to a near-identity RHP, the actually computation of the parametrix would require solving a problem that is, numerically, of similar difficulty as the S-RHP itself.

We define $\Gamma = \Gamma_1 \cup \Gamma_2$ and put $G(\zeta) = G_j(\zeta)$ for $\zeta \in \Gamma_j$ $(j = 1, 2)$. That way, the Riemann-Hilbert problem is given in the standard form

$$X_+(\zeta) = G(\zeta)X_-(\zeta) \quad (\zeta \in \Gamma), \qquad X(z) = I + O(z^{-1}) \quad (z \to \infty). \tag{11}$$

Because of $\det G = 1$, the solution $X \in C^\omega(\mathbb{C} \setminus \Gamma, \mathrm{GL}(2))$ is unique, see [12, p. 104].

4 Lower Triangular Jump Matrices and Indices

We note that the jump matrix G defined in (10b) and (10e) is *lower triangular*. However, even though the non-singular lower triangular matrices form a multiplicative group and the normalization at $z \to \infty$ is also lower triangular, the solution X turns out to *not* be lower triangular. Arguably the most natural source of RHPs exhibiting this structure are connected to orthogonal polynomials. By renormalizing at $z \to \infty$ the standard RHP for the system of orthogonal polynomials on the unit circle with complex weight e^z, we are led to consider the following *model problem* $(m \in \mathbb{N})$[4]:

$$Y_+(\zeta) = \begin{pmatrix} \zeta^m & 0 \\ e^\zeta & \zeta^{-m} \end{pmatrix} Y_-(\zeta) \quad (|\zeta| = 1), \qquad Y(z) = I + O(z^{-1}) \quad (z \to \infty). \tag{12}$$

Though one could perform a set of transformations to this problem that are standard in the RHP approach to the asymptotics of orthogonal polynomials on the circle, basically resulting in an analogue of the S-RHP of [4], our point here is to understand the issues of a direct numerical approach to the X-RHP (11) in a simple model case. It is straightforward to check that the *unique* solution of (12) is given explicitly by

$$Y(z) = \begin{cases} \begin{pmatrix} 1 & -z^{-m}e_m(-z) \\ 0 & 1 \end{pmatrix} & (|z| > 1), \\ \begin{pmatrix} z^m & -e_m(-z) \\ e^z & z^{-m}(1 - e^z e_m(-z)) \end{pmatrix} & (|z| < 1), \end{cases}$$

[4]The standard form, see [2, p. 1124], of that orthogonal polynomial RHP would be

$$X_+(\zeta) = \begin{pmatrix} 1 & 0 \\ e^\zeta \zeta^{-m} & 1 \end{pmatrix} X_-(\zeta) \quad (|\zeta| = 1), \qquad X(z) = \begin{pmatrix} z^m & 0 \\ 0 & z^{-m} \end{pmatrix} (I + O(z^{-1})) \qquad (z \to \infty).$$

The model problem (12) is obtained by putting the diagonal scaling at $z \to \infty$ into the jump matrix.

with

$$e_k(z) = 1 + z + \frac{z^2}{2!} + \cdots + \frac{z^{k-1}}{(k-1)!} = e^z \frac{\Gamma(k,z)}{\Gamma(k)}, \tag{13}$$

where $\Gamma(z)$ and $\Gamma(k,z)$ denote the Gamma function and the incomplete Gamma function. In particular, we observe that $Y_{12}(0) = -1 \neq 0$.

The nontrivial 12-component v of a Riemann–Hilbert problem with lower triangular jump matrices, such as (11) or (12), can be expressed independently of the other components, it satisfies a homogeneous scalar Riemann–Hilbert problem of its own. Namely, denoting the 11-component of G by g, we get

$$v_+(\zeta) = g(\zeta) v_-(\zeta) \quad (\zeta \in \Gamma), \qquad v(z) = O(z^{-1}) \quad (z \to \infty). \tag{14}$$

If the contour is a cycle as in (11), or as in the model problem above, the general theory [17, Sect. 127] of Riemann–Hilbert problems with Hölder continuous boundary regularity states that the Noether index[5] κ of (14) is given by the winding number

$$\kappa = \operatorname{ind}_\Gamma g.$$

More precisely, the nullity is the sum of the positive partial indices and the deficiency is the sum of the magnitudes of the negative partial indices, see [17, Eq. (127.30)]. Since there is just one partial index in the scalar case, the nullity of (14) is κ if $\kappa > 0$, and the deficiency is $-\kappa$ if $\kappa < 0$.

Thus, in the case of the RHP (11), the nullity of the scalar sub-RHP for the 12-component is

$$\operatorname{ind}_\Gamma g = \operatorname{ind}_{\Gamma_1} 1 + \operatorname{ind}_{\Gamma_2} \zeta^{(n+m)/2} = \frac{n+m}{2},$$

in the case of the model RHP (12) the corresponding nullity is m. In both cases, the unique non-zero solution of (14) that is induced by the solution of the defining 2×2 RHP is precisely selected by the compatibility conditions set up by the remaining linear relations of that RHP: the homogeneous part of these relations must then have Noether index $-\kappa$.

Impact on Numerical Methods

This particular substructure of a Riemann–Hilbert problem with lower triangular jump matrices G is a major challenge for numerical methods. If a discretization of the 2×2 RHP induces a discretization of the scalar subproblem (14) that results in

[5]Here, we identify a RHP with an equivalent linear operator equation $Tu = \cdots$, see, e.g., (15) in the next section. We recall that $\lambda = \dim \ker T$ is called the *nullity*, $\mu = \dim \operatorname{coker} T$ the *deficiency* and $\kappa = \lambda - \mu$ the *Noether index* of a linear operator T with closed range.

a homogeneous linear system with a *square* matrix S_N (that is, the same number of equations and unknowns), there are just two (non exclusive) options:

- S_N is non-singular, which results in a 12-component $v_N = 0$ that does *not* converge;
- the full system is singular and therefore numerically of not much use (ill-conditioning and convergence issues will abound).

Such methods compute fake lower triangular solutions, are ill-conditioned, or both.

To understand this claim, let us denote the 12-component of the 2×2 discrete solution matrix by v_N and the vector of the three other components by w_N. By inheriting the subproblem structure such as (14) for the 12-component, the discretization results then in a linear system of the block matrix form

$$\underbrace{\begin{pmatrix} S_N & 0 \\ \bullet & T_N \end{pmatrix}}_{=A_N} \begin{pmatrix} v_N \\ w_N \end{pmatrix} = \begin{pmatrix} 0 \\ \bullet \end{pmatrix}$$

Because of $\det(A_N) = \det(S_N)\det(T_N)$ a non-singular discretization matrix A_N implies a non-singular S_N and, thus, a non-convergent trivial component $v_N = 0$. Such a non-convergent zero 12-component is what one gets, for example, if one applies the spectral collocation method of [18] (with square contours replacing the circles) to the Riemann–Hilbert problems (11) or to the model problem (14). As a hint of failure, the resulting discrete system is ill-conditioned; details which can be found in the thesis of the fourth author G.W. [24, Sect. 5.4].

The deeper structural reason for this problem can be seen in the fact that the Noether index of finite-dimensional square matrices is always zero, whereas the index of the infinite-dimensional subproblem (14) is strictly positive.

We suggest two approaches to deal with this problem: first, an infinite-dimensional discretization using sequence spaces, that is, without truncation, and using infinite-dimensional numerical linear algebra, and second, using underdetermined discretizations with rectangular linear systems that are complemented by a set of explicit compatibility conditions.

5 RHPs as Integral Equations with Singular Kernels

In this section, we recall a way to express the RHP (11), with standard normalization at infinity, as a particular system of singular integral equations, cf. [11, 16, 18]. We introduce the Cauchy transform

$$Cf(z) = \frac{1}{2\pi i} \int_\Gamma \frac{f(\zeta)}{\zeta - z}\, d\zeta \qquad (z \notin \Gamma)$$

and their directional limits $C_\pm$ when approaching the left or right of the oriented contour Γ, defined by

$$C_\pm f(\eta) = \lim_{z \to \eta_\pm} \frac{1}{2\pi i} \int_\Gamma \frac{f(\zeta)}{\zeta - z}\, d\zeta \qquad (\eta \in \Gamma).$$

Note that $C_\pm$ can be extended as bounded linear operators mapping $L^2(\Gamma)$ (or spaces of Hölder continuous functions) into itself, and C (suitably extended) maps such functions into functions that are holomorphic on $\mathbb{C} \setminus \Gamma$, see [12, p. 100]. By using the decomposition $C_+ - C_- = \mathrm{id}$, the ansatz (by letting C act componentwise on the matrix-valued function u)

$$X(z) = I + Cu(z), \qquad u \in L^2(\Gamma, \mathbb{C}^{2\times 2}), \tag{15a}$$

establishes the equivalence of a RHP of the form (11) and the system of singular integral equations

$$(\mathrm{id} - (G - I)C_-)u = G - I \tag{15b}$$

As the following theorem shows, singular integral operators of the form

$$T_G = \mathrm{id} - (G - I)C_- : L^2(\Gamma, \mathbb{C}^{2\times 2}) \to L^2(\Gamma, \mathbb{C}^{2\times 2})$$

can be preconditioned by operators of exactly the same form.

Theorem 1 *Let Γ be a smooth, bounded, and non-self intersecting*[6] *contour system and $G : \Gamma \to \mathrm{GL}(2)$ a system of jump matrices which continues analytically to a vicinity of Γ. Then, $T_{G^{-1}}$ is a Fredholm regulator of T_G, that is, $T_{G^{-1}} T_G = \mathrm{id} + K$ with a compact operator $K : L^2(\Gamma, \mathbb{C}^{2\times 2}) \to L^2(\Gamma, \mathbb{C}^{2\times 2})$ that can be represented as a regular integral operator.*

Proof The Sokhotski–Plemelj formula [17, Eq. (17.2)] gives that $2C_- = -\mathrm{id} + H$, where H denotes a variant of the Hilbert transform (normalized as in [17]),

$$Hf(\zeta) = \frac{1}{\pi i} \int_\Gamma \frac{f(\eta)}{\eta - \zeta}\, d\eta \qquad (\zeta \in \Gamma),$$

with the integral understood in the sense of principle values. This way, we have

[6] Points of self intersection are allowed if certain cyclic conditions are satisfied [13]: at such a point the product of the corresponding parts of the jump matrix should be the identity matrix. These conditions guarantee smoothness in the sense of [26], where the analog of Theorem 1 is proved for the general smooth Riemann–Hilbert data.

$$T_G = A_1\,\mathrm{id} + B_1 H, \qquad A_1 = \frac{1}{2}(I+G), \quad B_1 = \frac{1}{2}(I-G),$$
$$T_{G^{-1}} = A_2\,\mathrm{id} + B_2 H, \qquad A_2 = \frac{1}{2}(I+G^{-1}), \quad B_2 = \frac{1}{2}(I-G^{-1}).$$

By a product formula of Muskhelishvili [17, Eq. (130.15)], which directly follows from the Poincaré–Betrand formula [17, Eq. (23.8)], one has

$$T_{G^{-1}} T_G = A\,\mathrm{id} + B\,H + K,$$

where K represents a *regular* integral operator and the coefficient matrices A and B are given by the expressions

$$A = A_2 A_1 + B_2 B_1, \qquad B = A_2 B_1 + B_2 A_1.$$

Here, we thus obtain $A = I$ and $B = 0$, which finally proves the assertion. □

This theorem implies that the operator T_G is *Fredholm*, that is, its nullity and deficiency are *finite*. In fact, since in our examples $\det G \equiv 1$, we have that the Noether index of T_G is zero. The possibility to use the Fredholm theory is extremely important in studying RHPs: it allows one to use, when proving the solvability of Riemann-Hilbert problems, the "vanishing lemma" [26], see also [12, Chap. 5]. For the use of Fredholm regulators in iterative methods applied to solving singular integral equations, see [23].

6 A Well-Conditioned Spectral Method for Closed Contours

We follow the ideas of Olver and Townsend [20] on spectral methods for differential equations, recently extended by Olver and Slevinsky [19] to singular integral equations. First, the solution u and the data $G - I$ of the singular integral equation (15b) are expanded[7] in the Laurent bases of the circles that built up the cycle Γ. Next, the resulting linear system is solved using the framework of *infinite-dimensional* linear algebra [14, 21], built out of the adaptive QR factorization introduced in [20].

To be specific, we describe the details for the model RHP (12), where the cycle Γ is just the unit circle. Here, we have the expansions

$$u(\zeta) = \sum_{k=-\infty}^{\infty} U_k \zeta^k, \qquad G(\zeta) - I = \sum_{k=-\infty}^{\infty} A_k \zeta^k \qquad (\zeta \in \Gamma),$$

[7] It is actually implemented this way in `SingularIntegralEquations.jl`, a JULIA software package described in [19].

both rapidly decaying with 2×2 coefficient matrices U_k and A_k. In the Laurent basis, the operator C_- acts diagonally in the simple form

$$C_- \zeta^k = \begin{cases} 0 & k \geqslant 0, \\ -\zeta^k & k < 0. \end{cases}$$

which gives

$$C_- u(\zeta) = -\sum_{k=1}^{\infty} U_{-k} \zeta^{-k} \qquad (\zeta \in \Gamma).$$

Note that $-C_-$ acts as a projection to the subspace spanned by the basis elements with negative index. This way, the system (15b) of singular integral equations is transformed to[8]

$$U_k + \sum_{j=-\infty}^{\infty} [k - j < 0]\, A_j U_{k-j} = A_k \qquad (k \in \mathbb{Z}). \tag{16}$$

Up to a given accuracy, we may assume that the data is given as a finite sum,

$$G(\zeta) - I \approx \sum_{k=-n_1}^{n_1} A_k \zeta^k,$$

likewise for $G^{-1}(\zeta) - I$ with a truncation at n_2. Thus, writing the discrete system (16) in matrix-vector form, the corresponding double-infinite matrix has a bandwidth of order $O(n_1)$. Preconditioning this system, following Theorem 1, by the multiplication with the double-infinite matrix belonging to G^{-1} instead of G, results in a double-infinite matrix that has a bandwidth of order $O(n_1 + n_2)$. Since the right hand side of (16) is truncated at indices of magnitude $O(n_1)$, application of the adaptive QR factorization [20], after re-ordering the double-infinite coefficients as $U_0, U_{-1}, U_1, \ldots$ in order to be singly infinite, will result in an algorithm that has a complexity of order $O((n_1 + n_2)^2 n_3)$, where n_3 is the number of coefficients needed to resolve u, dictated by a specified tolerance.

Remark 1 The extension to systems Γ of closed contours built from several circles is straightforward. The jump data and the solution, restricted to a circle centered at a are expanded in the Laurent basis $(z-a)^k$, $k \in \mathbb{Z}$. When instead evaluated at a circle centered at b, a change of basis is straightforwardly computed using

$$(z-a)^j = \sum_{k=0}^{\infty} \binom{j}{k} (b-a)^{j-k} (z-b)^k \qquad (j \in \mathbb{Z}),$$

[8] We use the Iverson bracket of a condition: $[\mathscr{P}] = 1$ if the predicate $\mathscr{P}$ is true, $[\mathscr{P}] = 0$ otherwise.

valid for $|z-b| < |b-a|$. Because of a geometric decay, one can truncate those series at $k = O(1)$ as long as $|z-b| < \theta|b-a|$ with $0 < \theta < 1$ small enough. The adaptive QR factorization can then be applied by interlacing the Laurent coefficients on each circle to obtain a singly infinite unknown vector of coefficients.

Numerical Example 1: Model problem

Because of the entries ζ^m and ζ^{-m} in the jump matrix of the model problem (12), we have that $n_1, n_2, n_3 = O(m)$ in order to resolve the data and the solution; hence the computational complexity of the method scales as $O(m^3)$. Using the JULIA software package `SingularIntegralEquations.jl`[9] (v0.0.1) the problem is numerically solved by the following short code showing that the user has to do little more than just providing the data and entering the singular integral equation (15b) as a mathematical expression:

```
using ApproxFun, SingularIntegralEquations

m = 100
Γ = Circle(0.0,1.0)
G = Fun(z -> [z^m 0; exp(z) 1/z^m],Γ)
C = Cauchy(-1)
@time u = (I-(G-I)*C)\(G-I)
 Y = z ->I+cauchy(u,z)
err = norm(Y(0)-[0 -1; 1 (-1)^m*exp(-lfact(m))],2)
```

The run time[10] is 2.8 seconds, the error of $Y(0)$ is $4.22 \cdot 10^{-15}$ (spectral norm), which corresponds to a loss of one digit in absolute error.

Numerical Example 2: Riemann–Hilbert Problem for the Discrete $Z^{2/3}$

Now, we apply the method to the Riemann–Hilbert problem (11) encoding the discrete Z^a map. Here, because of the exponents $-m$, $-n$ and $\pm(n+m)/2$ in (10), we have $n_1, n_2, n_3 = O(n+m)$ in order to resolve the data and the solution, see Fig. 8; hence the computational complexity scales as $O((n+m)^3)$. Note that this is far from optimal, using the stabilized recursion of Sect. 2 to compute a table including $Z^a_{n,m}$ would give a complexity of order $O((n+m)^2)$. Once more, however, the code requires little more than typing the mathematical equations of the RHP.

```
using ApproxFun, SingularIntegralEquations

a = 2/3
n = 6; m = 8; # n+m must be even
pow = z -> exp(1im*a*pi/4)*exp(-a/2*log(z/1im))
Γ = Circle(-1.0,0.3) ∪ Circle(+1.0,0.3) ∪ Circle(0.0,3.0)
```

[9] `https://github.com/ApproxFun/SingularIntegralEquations.jl`, cf. [19].
[10] Using a MacBook Pro with a 3.0 GHz Intel Core i7-4578U processor and 16 GB of RAM.

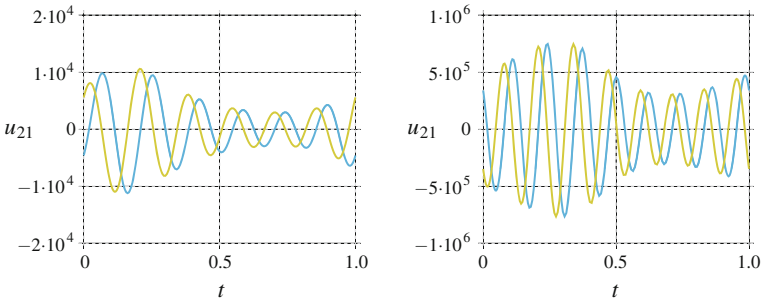

Fig. 8 *Left* $u_{21}(\zeta)$ on the circle $\zeta = -1 + 0.3e^{2\pi it}$; *right* $u_{21}(\zeta)$ on $\zeta = +1 + 0.3e^{2\pi it}$. The real parts are shown in *blue*, the imaginary part in *yellow*. Note that there are $m = 6$ oscillations on the *left* and $n = 8$ oscillations on the *right*; the maximum amplitude is about $1.1 \cdot 10^4$ on the *left* and $7.5 \cdot 10^5$ on the *right*

```
G = Fun(z -> in(z,Γ[3])?[z^((m+n)/2) 0; 0 1/z^((n+m)/2)]:[1 0;
    pow(z)/(z-1)^m/(z+1)^n 1],Γ)
C = Cauchy(-1)
@time u = (I-(G-I)*C)\(G-I)
X = z -> I+cauchy(u,z);
X0 = X(0)
Za0 = (-1)^(m+1)*X0[2,1]/X0[1,1]
Za1 = 3.610326860525178 + 2.568086087959661im # exact solution
    from the recursion as in Section 1.2 using bigfloats
 err = abs(Za0 - Za1)
```

The run time is 2.7 s, the absolute error of $Z_{6,8}^{2/3}$ is $3.38 \cdot 10^{-8}$, which corresponds to a loss of about 7 digits. This loss of accuracy can be explained by comparing the magnitude of the 21-component of u as shown in Fig. 8, along the two black circles of Fig. 6, with that of the corresponding component of the solution matrix at $z = 0$, namely,

$$X(0) \approx \begin{pmatrix} -3.38121 & -12.2073 + 8.68324i \\ 12.2073 + 8.68324i & 66.0758 \end{pmatrix}.$$

We observe that during the evaluation of the Cauchy transform (15a), which maps $u \mapsto X(0)$ by means of an integral, at least 5 digits must have been lost by cancellation—a loss, which structurally cannot be avoided for oscillatory integrands with *large* amplitudes. (Note that this is not an issue of frequency: just one oscillation with a large amplitude suffices to get such a severe cancellation.)

Since the amplitudes of u_{21} grow exponentially with n and m, the algorithm for computing $Z_{n,m}^a$ based on the numerical evaluation of (15) applied to the RHP (11) is *numerically unstable*. Even though the initial step, the spectral method in coefficient space applied to (15b) is perfectly stable, stability is destructed by the bad conditioning of the post-processing step, that is, the evaluation of the integral in

(15a). We refer to [7] for an analysis that algorithms with a badly conditioned post processing of intermediate solutions are generally prone to numerical instability.

7 RHPs as Integral Equations with Nonsingular Kernels

By reversing the orientation of the two small circles in the RHP (11), and by simultaneously replacing the jump matrix G_1 by $\tilde{G}_1 = G_1^{-1}$, the RHP is transformed to an equivalent one with a contour system Σ that satisfies the following properties, see Fig. 9: it is a union of non-self intersecting smooth curves, that bound a domain Ω_+ to its left. By Ω_- we will denote the (generally not connected) region which is the complement of $\Omega_+ \cup \Gamma$. Note that the model problem (12) falls into that class of contours without any further transformation.

We drop the tilde from the jump matrices and consider RHPs of the form

$$\Phi_+(\zeta) = G(\zeta)\Phi_-(\zeta) \quad (\zeta \in \Sigma), \qquad \Phi(z) = I + O(z^{-1}) \quad (z \to \infty), \tag{17}$$

on such contours systems Σ. It will either represent the aforementioned transformation of (11) or the model problem (12). In particular, G is lower triangular and can be analytically continued to a vicinity of Σ.

The classical theory developed by Plemelj (see [17, Sect. 126]) for such problems teaches the following: the directed boundary values Φ_- of the unique analytic solution $\Phi : \mathbb{C} \setminus \Sigma \to \mathrm{GL}(2)$ of the RHP (17) satisfy a Fredholm integral equation [17, Eq. (126.5)] of the second kind on Σ, namely

$$\Phi_-(\zeta) - \frac{1}{2\pi i} \int_\Sigma \frac{G^{-1}(\zeta)G(\eta) - I}{\eta - \zeta} \Phi_-(\eta)\, d\eta = I \qquad (\zeta \in \Sigma), \tag{18}$$

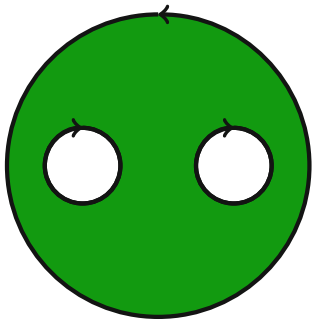

Fig. 9 A modified, but equivalent, contour system Σ for the for the RHP (11) obtained by reversing the orientation and by simultaneously replacing the jump matrix G_1 by G_1^{-1}. Now, there is a bounded domain Ω_+ (marked in *green*) to the *left* of Σ, cf. the original system shown in Fig. 6

understood here as an integral equation in $L^2(\Sigma, \mathbb{C}^{2\times 2})$. The matrix kernel of this equation, that is,

$$K(\zeta,\eta) = \frac{G^{-1}(\zeta)G(\eta) - I}{\eta - \zeta} = G^{-1}(\zeta)\frac{G(\eta) - G(\zeta)}{\eta - \zeta},$$

is smooth on $\Sigma \times \Sigma$, since it extends as an analytic function and since the singularity at $\zeta = \eta$ is removable. Integral equations of the form (18) with a smooth kernel are, in principle, amenable to fast quadrature based methods, see the next section.

We note that, given the boundary values $\Phi_-(\zeta)$ for $\zeta \in \Sigma$, the solution of the RHP (17) can be reconstructed by

$$\Phi(z) = \begin{cases} I - \dfrac{1}{2\pi i}\displaystyle\int_\Sigma \frac{\Phi_-(\zeta)}{\zeta - z}\,d\zeta & z \in \Omega_-, \\[2ex] \dfrac{1}{2\pi i}\displaystyle\int_\Sigma \frac{G(\zeta)\Phi_-(\zeta)}{\zeta - z}\,d\zeta & z \in \Omega_+. \end{cases} \tag{19}$$

In general, however, the Fredholm equation (18) is not equivalent to the RHP, see [17, p. 387]: the Fredholm equation has but a kernel of the same dimension as the kernel of the *associated* homogeneous RHP, defined as

$$\Psi_+(\zeta) = G^{-1}(\zeta)\Psi_-(\zeta) \quad (\zeta \in \Sigma), \qquad \Psi(z) = O(z^{-1}) \quad (z \to \infty). \tag{20}$$

As we will show now, the kernel of the associated RHP is *nontrivial* in the examples studied in this work.

First, we observe, by the lower triangular form of G, that the 11- and the 12-components of Ψ both satisfy a scalar RHP of the form (14) with a jump function g that has a winding number which is

$$\operatorname{ind}_\Sigma g = -\frac{n+m}{2}$$

for the discrete map Z^a, and which is $\operatorname{ind}_\Sigma g = -m$ for the model problem (12). Note that this winding number has the sign opposite to the results of Sect. 4 since the underlying 2×2 RHP is based on G^{-1} instead of G. Hence, the nullity of the scalar RHPs for the 11- and the 12-components of Ψ is zero and the deficiency is $(n+m)/2$ (m in case of the model problem). As a consequence, the 11- and the 12-components of Ψ must both be identically zero.

Next, since we now know that Ψ has a zero first row, also the 21- and 22-components of Ψ satisfy a scalar RHP of the form (14) each, but with a jump function g that has the positive winding number

$$\operatorname{ind}_\Sigma g = \frac{n+m}{2}$$

for the discrete map Z^a, and $\mathrm{ind}_\Sigma\, g = m$ for the model problem (12), just as discussed in Sect. 4. Hence, the deficiency of the scalar RHPs for the 21- and the 22-components of Ψ is zero and the nullity is $(n+m)/2$ (m in case of the model problem). Since both components are linearly independent from of each other, we have thus proven the following lemma.

Lemma 1 *The nullity of the associated homogeneous RHP* (20)*, and hence, that of the Fredholm integral equation* (18) *is* $n+m$ *in the case of the discrete map* Z^a *and* $2m$ *in the case of the model problem* (12)*.*

Example 1 For the model RHP (12) the smooth kernel of the Fredholm integral equation (18) can be constructed explicitly. Here we have

$$K(\zeta,\eta) = \frac{G^{-1}(\zeta)G(\eta) - I}{\eta - \zeta} = \begin{pmatrix} \frac{(\eta/\zeta)^m - 1}{\eta-\zeta} & 0 \\ \frac{e^\eta \zeta^m - e^\zeta \eta^m}{\eta-\zeta} & \frac{(\zeta/\eta)^m - 1}{\eta-\zeta} \end{pmatrix}.$$

A column of a matrix belonging to the kernel of (18) satisfies the equation

$$\begin{pmatrix} u_-(\zeta) \\ w_-(\zeta) \end{pmatrix} = \frac{1}{2\pi i} \int_\Sigma K(\zeta,\eta) \begin{pmatrix} u_-(\eta) \\ w_-(\eta) \end{pmatrix} d\eta \qquad (\zeta \in \Sigma), \tag{21}$$

where Σ is the positively oriented unit circle. We will construct solutions that extend analytically as $u_-(z)$ and $w_-(z)$ for $z \neq 0$, such that

$$\begin{pmatrix} u_-(z) \\ w_-(z) \end{pmatrix} = \mathrm{res}_{\eta=0}\, K(z,\eta) \begin{pmatrix} u_-(\eta) \\ w_-(\eta) \end{pmatrix} \qquad (z \neq 0).$$

By recalling the notation introduced in (13) we observe, for $k = 0, \ldots, m-1$, that

$$\begin{aligned} \mathrm{res}_{\eta=0}\, K_{11}(z,\eta)\eta^{k-m} &= z^{k-m}, \\ \mathrm{res}_{\eta=0}\, K_{21}(z,\eta)\eta^{k-m} &= -z^k e_{m-k}(z), \\ \mathrm{res}_{\eta=0}\, K_{22}(z,\eta)\eta^{k} &= -z^k. \end{aligned}$$

Using the coefficients $a_{jk}^{(m)}$ that induce a change of polynomial basis by

$$z^k = \sum_{k=0}^{m-1} a_{kj}^{(m)} z^j e_{m-j}(z) \qquad (k = 0, \ldots, m-1),$$

we define the polynomials

$$p_k^{(m)}(z) = \sum_{j=0}^{m-1} a_{kj}^{(m)} z^j \qquad (k = 0, \ldots, m-1),$$

each of which has degree at most $m-1$. Then, the m linear independent vectors

$$\begin{pmatrix} u_-(\zeta) \\ w_-(\zeta) \end{pmatrix} = \begin{pmatrix} -2\zeta^{-m} p_k^{(m)}(\zeta) \\ \zeta^k \end{pmatrix} \qquad (k = 0, \ldots, m-1) \tag{22}$$

are solutions of (21) each. Thus, since its dimension is $2m$ by Lemma 1, the kernel of the integral equation (18) is spanned by the 2×2 matrices whose columns are linear combinations of these vectors. □

The unique solution Φ_- of the RHP (17) can be picked among the solutions of (18) by imposing additional linear conditions, namely $n+m$ independent such conditions in the case of the discrete map Z^a and $2m$ in the case of the model problem. Specifically, for the model problem (12), we obtain such conditions as follows. First, since $\Phi_-(z)$ continues analytically to $|z| > 1$ and since $\Phi_-(z) = I + O(z^{-1})$ as $z \to \infty$, we get by Cauchy's formula for the Laurent coefficients at $z = \infty$ that

$$\frac{1}{2\pi i} \int_\Sigma \Phi_-(\zeta) \frac{d\zeta}{\zeta^k} = [k = 1] \cdot I \qquad (k = 1, 2, \ldots).$$

Second, by restricting this relation to the *second row* of the matrix Φ_- for $k = 1, \ldots, m$, we get the conditions

$$\frac{1}{2\pi i} \int_\Sigma \begin{pmatrix} 0 & 1 \end{pmatrix} \cdot \Phi_-(\zeta) \frac{d\zeta}{\zeta^k} = \begin{pmatrix} 0 & [k = 1] \end{pmatrix} \qquad (k = 1, \ldots, m). \tag{23}$$

In fact, these conditions force all the components of the columns (22) that would span an offset from the kernel of (18) to be zero.

For the Z^a-RHP, similar arguments prove that the kernel of (17) is spanned by matrices whose second row extends to polynomials of degree smaller than $(n+m)/2$ to the outside of the outer circle in Fig. 9. Thus, the same form of conditions as in (23) can be applied for picking the proper solution $\Phi_-(\zeta)$, except that one would have to replace Σ by that outer circle and the upper index m by $(n+m)/2$.

8 A Modified Nyström Method

Fredholm integral equations of the second kind with smooth kernels defined on a system of circular contours are best discretized by the classical Nyström method [15, Sect. 12.2]. Here, one uses the composite trapezoidal rule as the underlying quadrature formula, that is,

$$\frac{1}{2\pi i} \int_{\partial B_r(z_0)} f(z)\, dz \approx \frac{r}{N} \sum_{j=0}^{N-1} f\left(z_0 + r e^{2\pi i j/N}\right) e^{2\pi i j/N}.$$

For integrands that extend analytically to a vicinity of the contour, this quadrature formula is spectrally accurate, see, e.g., [9, §2] or [22, §2].

Since the Fredholm integral equation (18) has a positive nullity, applying the Nyström method to it will yield, for N large enough, a numerically singular linear system. However, the theory of the last section suggests a simple modification of the Nyström method: we use the conditions (23) (after approximating them by the same quadrature formula as for the Nyström method) as additional equations and solve the resulting *overdetermined* linear system by the least squares method.

Numerical Example 1: Model problem

We apply the modified Nyström method to the Fredholm integral equation representing the model problem (12). By the sampling condition, see, e.g., [9, §2], the number N of quadrature points will scale as $N = O(m)$, hence the computational complexity scales as $O(m^3)$. To check the accuracy we compare with

$$Y(0) = \frac{1}{2\pi i}\int_\Gamma G(\zeta)\Phi_-(\zeta)\frac{d\zeta}{\zeta}, \qquad I = \frac{1}{2\pi i}\int_\Gamma \Phi_-(\zeta)\frac{d\zeta}{\zeta},$$

evaluated by the same quadrature formula as for the Nyström method. For the particular parameters $m = 100$ and $N = 140$ we get, within a run-time of 0.49 s for a straightforward Matlab implementation, a maximum error of these two quantities, measured in 2-norm, of $1.33 \cdot 10^{-14}$. The condition number of the least squares matrix grows just moderately with m: it is about 23 for $m = 1$ and about 650 for $m = 1000$.

Numerical Example 2: Discrete $Z^{2/3}$

Now, we apply the modified Nyström method to the Fredholm integral equation representing the RHP (11) subject to a transformation to the form (17). Here, the sampling condition requires $N = O(n + m)$, hence the computational complexity scales as $O((n + m)^3)$. For $Z^{2/3}_{6,8}$, the modified Nyström method yields the convergence plot shown in Fig. 10: it exhibits exponential (i.e., spectral) convergence until a noise level of about 10^{-9} is reached, which corresponds to a loss of about 6 digits. The reason for this loss is that this method for approximating the discrete Z^a suffers the same issue with a bad conditioning of the post-processing step, that is, of

$$\Phi_-(\cdot) \mapsto X(0) = \frac{1}{2\pi i}\int_\Gamma G(\zeta)\Phi_-(\zeta)\frac{d\zeta}{\zeta},$$

as the spectral method for the singular integral equation discussed in Sect. 6. Here, the amplitude of the real and imaginary part of $\Phi_-(\zeta)$ along the two inner circles is of the order 10^4 which causes a cancellation of at least 4 significant digits.

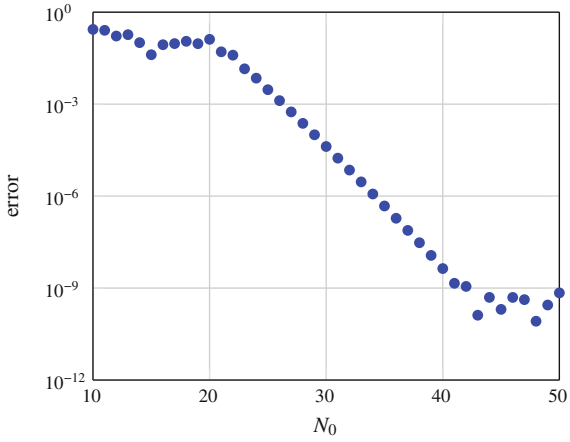

Fig. 10 Absolute error of the approximation of $Z^{2/3}_{6,8}$ by the modified Nyström method vs. the number of quadrature points N_0 on each of the three circles in Fig. 9 (the radii are $1/2$ for the inner circles, 3 for the outer one); the total number of quadrature points is then $N = 3 \times N_0$. One observes, after a threshold caused by a sampling condition, exponential (i.e., spectral) convergence that saturates at a level of numerical noise at an error of about 10^{-9}. Run time of a Mathematica implementation with $N_0 = 42$ is about 0.15 s

9 Conclusion

To summarize, there are two fundamental options for the stable numerical evaluation of the discrete map $Z^a_{n,m}$.

- Computing all the values of the array $1 \leqslant n, m \leqslant N$ at once by, first, computing the diagonal using a boundary value solve for the discrete Painlevé II equation (5) and, then, by recursing from the diagonal to the boundary using the discrete differential equation (2). This approach has optimal complexity $O(N^2)$.
- Computing just a single value for a given index pair (n, m) by using the RHP (11) and one of the methods discussed in Sect. 6 or 8. Since both methods suffer from an instability caused by a post-processing quadrature for larger values of n and m, one would rather mix this approach with the asymptotics (4). For instance, using the numerical schemes for $n, m \leqslant 10$, and the asymptotics otherwise, gives a uniform precision of about 5 digits for $a = 2/3$. Higher accuracy would require the calculation of the next order terms of the asymptotics as in Sect. 2. This mixed numerical-asymptotic method has optimal complexity $O(1)$.

Acknowledgments The research of F.B., A.I., and G.W. was supported by the DFG-Collaborative Research Center, TRR 109, "Discretization in Geometry and Dynamics."

References

1. Agafonov, S.I., Bobenko, A.: Discrete Z^γ and Painlevé equations. Int. Math. Res. Notices **2000**(4), 165–193 (2000)
2. Baik, J., Deift, P., Johansson, K.: On the distribution of the length of the longest increasing subsequence of random permutations. J. Am. Math. Soc. **12**(4), 1119–1178 (1999)
3. Bobenko, A.: Discrete conformal maps and surfaces. Symmetries and Integrability of Difference Equations (Canterbury. 1996), London Mathematical Society Lecture Note Series, vol. 255, pp. 97–108. Cambridge University Press, Cambridge (1999)
4. Bobenko, A., Its, A.: The asymptotic behaviour of the discrete holomorphic map Z^a via the Riemann–Hilbert method (2014). arXiv:1409.2667
5. Bobenko, A., Pinkall, U.: Discrete isothermic surfaces. J. Reine Angew. Math. **475**, 187–208 (1996)
6. Bobenko, A., Pinkall, U.: Discretization of surfaces and integrable systems. Discrete Integrable Geometry and Physics (Vienna, 1996). Oxford Lecture Series in Mathematics and Its Applications, vol. 16, pp. 3–58. Oxford University Press, New York (1999)
7. Bornemann, F.: A model for understanding numerical stability. IMA J. Numer. Anal. **27**(2), 219–231 (2007)
8. Bornemann, F.: On the numerical evaluation of distributions in random matrix theory: a review. Markov Process. Rel. Fields **16**(4), 803–866 (2010)
9. Bornemann, F.: Accuracy and stability of computing high-order derivatives of analytic functions by Cauchy integrals. Found. Comput. Math. **11**(1), 1–63 (2011)
10. Bornemann, F., Wechslberger, G.: Optimal contours for high-order derivatives. IMA J. Numer. Anal. **33**(2), 403–412 (2013)
11. Deift, P., Zhou, X.: A priori L^p-estimates for solutions of Riemann-Hilbert problems. Int. Math. Res. Not. **40**, 2121–2154 (2002)
12. Fokas, A.S., Its, A.R., Kapaev, A.A., Novokshenov, V.Y.: Painlevé Transcendents-The Riemann-Hilbert Approach. American Mathematical Society, Providence (2006)
13. Fokas, A.S., Zhou, X.: On the solvability of Painlevé II and IV. Comm. Math. Phys. **144**(3), 601–622 (1992)
14. Hansen, A.C.: Infinite-dimensional numerical linear algebra: theory and applications. Proc. R. Soc. Lond. Ser. A Math. Phys. Eng. Sci. **466**(2124), 3539–3559 (2010)
15. Kress, R.: Linear Integral Equations, vol. 82, 3rd edn. Springer, New York (2014)
16. Litvinchuk, G.S., Spitkovskii, I.M.: Factorization of Measurable Matrix Functions. Birkhäuser Verlag, Basel (1987)
17. Muskhelishvili, N.I.: Singular Integral Equations. Wolters-Noordhoff Publ, Groningen (1972)
18. Olver, S.: A general framework for solving Riemann-Hilbert problems numerically. Numer. Math. **122**(2), 305–340 (2012)
19. Olver, S., Slevinsky, R.M.: A fast and well-conditioned spectral method for singular integral equations (2015). arXiv:1507.00596
20. Olver, S., Townsend, A.: A fast and well-conditioned spectral method. SIAM Rev. **55**(3), 462–489 (2013)

21. Olver, S., Townsend, A.: A practical framework for infinite-dimensional linear algebra. In: Proceedings of the First Workshop for High Performance Technical Computing in Dynamic Languages, pp. 57–62 (2014)
22. Trefethen, L.N., Weideman, J.A.C.: The exponentially convergent trapezoidal rule. SIAM Rev. **56**(3), 385–458 (2014)
23. Trogdon, T.: On the application of GMRES to oscillatory singular integral equations. BIT **55**(2), 591–620 (2015)
24. Wechslberger, G.: Automatic Contour Deformation of Riemann–Hilbert Problems. Ph.D. thesis, Technische Universität München (2015)
25. Wechslberger, G., Bornemann, F.: Automatic deformation of Riemann-Hilbert problems with applications to the Painlevé II transcendents. Constr. Approx. **39**(1), 151–171 (2014)
26. Zhou, X.: The Riemann-Hilbert problem and inverse scattering. SIAM J. Math. Anal. **20**(4), 966–986 (1989)

A Variational Principle for Cyclic Polygons with Prescribed Edge Lengths

Hana Kouřimská, Lara Skuppin and Boris Springborn

Abstract We provide a new proof of the elementary geometric theorem on the existence and uniqueness of cyclic polygons with prescribed side lengths. The proof is based on a variational principle involving the central angles of the polygon as variables. The uniqueness follows from the concavity of the target function. The existence proof relies on a fundamental inequality of information theory. We also provide proofs for the corresponding theorems of spherical and hyperbolic geometry (and, as a byproduct, in $1+1$ spacetime). The spherical theorem is reduced to the Euclidean one. The proof of the hyperbolic theorem treats three cases separately: Only the case of polygons inscribed in compact circles can be reduced to the Euclidean theorem. For the other two cases, polygons inscribed in horocycles and hypercycles, we provide separate arguments. The hypercycle case also proves the theorem for "cyclic" polygons in $1+1$ spacetime.

1 Introduction

This article is concerned with cyclic polygons, i.e., convex polygons inscribed in a circle. We will provide a new proof of the following elementary theorem in Sect. 2.

Theorem 1.1 *There exists a Euclidean cyclic polygon with $n \geq 3$ sides of lengths $\ell_1, \dots, \ell_n \in \mathbb{R}_{>0}$ if and only if they satisfy the polygon inequalities*

H. Kouřimská · L. Skuppin · B. Springborn (✉)
Inst. für Mathematik, Technische Universität Berlin,
Straße des 17. Juni 136, 10623 Berlin, Germany
e-mail: boris.springborn@tu-berlin.de

H. Kouřimská
e-mail: kourim@math.tu-berlin.de

L. Skuppin
e-mail: skuppin@math.tu-berlin.de

A.I. Bobenko (ed.), *Advances in Discrete Differential Geometry*,
DOI 10.1007/978-3-662-50447-5_5

$$\ell_k < \sum_{\substack{i=1 \\ i \neq k}}^{n} \ell_i, \tag{1}$$

and this cyclic polygon is unique.

Our proof involves a variational principle with the central angles as variables. The variational principle has a geometric interpretation in terms of volume in 3-dimensional hyperbolic space (see Remark 2.6). Another striking feature of our proof is the use of a fundamental inequality of information theory:

Theorem (Information Inequality) *Let* $p = (p_1, \ldots, p_m)$ *and* $q = (q_1, \ldots, q_m)$ *be discrete probability distributions, then*

$$\sum_{k=1}^{m} p_k \log \frac{p_k}{q_k} \geq 0, \tag{2}$$

and equality holds if and only if $p = q$.

The left hand side of inequality (2) is called the *Kullback–Leibler divergence* or *information gain* of q from p, also the *relative entropy* of p with respect to q. The inequality follows from the strict concavity of the logarithm function (see, e.g., Cover and Thomas [3]).

In Sects. 3 and 4 we provide proofs for non-Euclidean versions of Theorem 1.1. The spherical version requires an extra inequality:

Theorem 1.2 *There exists a spherical cyclic polygon with* $n \geq 3$ *sides of lengths* $\ell_1, \ldots, \ell_n \in \mathbb{R}_{>0}$ *if and only if they satisfy the polygon inequalities* (1) *and*

$$\sum_{i=1}^{n} \ell_i < 2\pi, \tag{3}$$

and this cyclic spherical polygon is unique.

Inequality (3) is necessary because the perimeter of a circle in the unit sphere cannot be greater than 2π, and the perimeter of the inscribed polygon is a lower bound. We require strict inequality to exclude polygons that degenerate to great circles (with all interior angles equal to π).

In Sect. 3, we prove Theorem 1.2 by a straightforward reduction to Theorem 1.1: connecting the vertices of a spherical cyclic polygon by straight line segments in the ambient Euclidean $\mathbb{R}^3$, one obtains a Euclidean cyclic polygon.

In the case of hyperbolic geometry, the notion of "cyclic polygon" requires additional explanation. We call a convex hyperbolic polygon *cyclic* if its vertices lie on a curve of constant non-zero curvature. Such a curve is either

- a hyperbolic circle if the curvature is greater than 1,
- a horocycle if the curvature is equal to 1,
- a hypercycle, i.e., a curve at constant distance from a geodesic if the curvature is strictly between 0 and 1.

Theorem 1.3 *There exists a hyperbolic cyclic polygon with $n \geq 3$ sides of lengths $\ell_1, \ldots, \ell_n \in \mathbb{R}$ if and only if they satisfy the polygon inequalities* (1)*, and this cyclic hyperbolic polygon is unique.*

We prove this theorem in Sect. 4. The case of hyperbolic polygons inscribed in circles can be reduced to Theorem 1.1 by considering the hyperboloid model of the hyperbolic plane: Connecting the vertices of a hyperbolic polygon inscribed in a circle by straight line segments in the ambient $\mathbb{R}^{2,1}$, one obtains a Euclidean cyclic polygon.

The cases of polygons inscribed in horocycles and hypercycles cannot be reduced to the Euclidean case because the intrinsic geometry of the affine plane of the polygon is not Euclidean: In the horocycle case, the scalar product is degenerate with a 1-dimensional kernel. Hence, this case reduces to the case of degenerate polygons inscribed in a straight line. It is easy to deal with. In the hypercycle case, the scalar product is indefinite. This case reduces to polygons inscribed in hyperbolas in flat $1 + 1$ spacetime. The variational principle of Sect. 2 can be adapted for this case (see Sect. 5), but the corresponding target function fails to be concave or convex. It may be possible to base a proof of existence and uniqueness on this variational principle, perhaps using a min-max-argument, but we do not pursue this route in this article. Instead, we deal with polygons inscribed in hypercycles using a straightforward analytic argument.

Some history, from ancient to recent. Theorems 1.1–1.3 belong to the circle of results connected with the classical isoperimetric problem. As the subject is ancient and the body of literature is vast, we can only attempt to provide a rough historical perspective and ask for leniency regarding any essential work that we fail to mention.

The early history of the relevant results about polygons is briefly discussed by Steinitz [13, Sect. 16]. Steinitz goes on to discuss analogous results for polyhedra, a topic into which we will not go. A more recent and comprehensive survey of proofs of the isoperimetric property of the circle was given by Blåsjö [2].

It was known to Pappus that the regular n-gon had the largest area among n-gons with the same perimeter, and that the area grew with the number of sides. This was used to argue for the isoperimetric property of the circle:

Theorem 1.4 (Isoperimetric Theorem) *Among all closed planar curves with given length, only the circle encloses the largest area.*

It is not clear who first stated the following theorem about polygons:

Theorem 1.5 (Secant Polygon) *Among all n-gons with given side lengths, only the one inscribed in a circle has the largest area.*

This was proved by Moula [8], by L'Huilier [5] (who cites Moula), and by Steiner [12] (who cites L'Huilier). L'Huilier also proved the following theorem:

Theorem 1.6 (Tangent Polygon) *Among all convex n-gons with given angles, only the one circumscribed to a circle has the largest area when the perimeter is fixed and and smallest perimeter when the area is fixed.*

Steiner also proves versions of Theorems 1.5 and 1.6 for spherical polygons. None of these authors deemed it necessary to prove the existence of a maximizer, an issue that became generally recognized only after Weierstrass [14]. For polygons, the existence of a maximizer follows by a standard compactness argument.

Blaschke [1, Sect. 12], notes that the quadrilateral case ($n = 4$) of Theorem 1.5 can easily be deduced from the Isoperimetric Theorem 1.4 using Steiner's four-hinge method. Conversely, one can similarly deduce Theorem 1.4 and the general Theorem 1.5 from the quadrilateral case of Theorem 1.5. He remarks that the quadrilateral case of Theorem 1.5 can be proved directly by deriving the following equation for the area A of a quadrilateral with sides ℓ_k:

$$A^2 = (s - \ell_1)(s - \ell_2)(s - \ell_3)(s - \ell_4) - \ell_1\ell_2\ell_3\ell_4 \cos^2\theta, \tag{4}$$

where $s = (\ell_1 + \ell_2 + \ell_3 + \ell_4)/2$ is half the perimeter, and θ is the arithmetic mean of two opposite angles.

Neither Blaschke, nor Steiner, L'Huilier, or Moula provide an argument for the uniqueness of the maximizer in Theorem 1.5 or 1.6. It seems that even after Weierstrass, the fact that the sides determine a cyclic polygon uniquely was considered too obvious to deserve a proof.

Penner [9, Theorem 6.2] gives a complete proof of Theorem 1.1. He proceeds by showing that there is one and only one circumcircle radius that allows the construction of a Euclidean cyclic polygon with given sides (provided they satisfy the polygon inequalities).

Schlenker [11] proves Theorems 1.2 and 1.3, and also the isoperimetric property of non-Euclidean cyclic polygons, i.e., the spherical and hyperbolic versions of Theorem 1.5. His proofs of the isoperimetric property are based on the remarkable equation

$$\sum \dot{\alpha}_i v_i = 0 \tag{5}$$

characterizing the change of angles α_i of a spherical or hyperbolic polygon under infinitesimal deformations with fixed side lengths. Here, $v_i \in \mathbb{R}^3$ are the position vectors of the polygon's vertices in the sphere or in the hyperboloid, respectively. To prove the uniqueness of spherical and hyperbolic cyclic polygons with given sides he uses separate arguments similar to Penner's.

2 Euclidean Polygons. Proof of Theorem 1.1

To construct an inscribed polygon with given side lengths $\ell = (\ell_1, \ldots, \ell_n) \in \mathbb{R}^n_{>0}$ (see Fig. 1) is equivalent to finding a point $(\alpha_1, \ldots \alpha_n)$ in the set

$$D_n = \left\{ \alpha \in \mathbb{R}^n_{>0} \;\middle|\; \sum_{k=1}^{n} \alpha_k = 2\pi \right\} \subset \mathbb{R}^n \tag{6}$$

satisfying, for some $R \in \mathbb{R}$ and for all $k \in \{1, \ldots, n\}$,

$$\frac{\ell_k}{2} = R \sin \frac{\alpha_k}{2}. \tag{7}$$

This problem admits the following variational formulation. Define the function $f_\ell : \mathbb{R}^n \to \mathbb{R}$ by

$$f_\ell(\alpha) = \sum_{k=1}^{n} \left(\mathrm{Cl}_2(\alpha_k) + \log(\ell_k)\, \alpha_k \right) \tag{8}$$

where Cl_2 denotes Clausen's integral [4]:

$$\mathrm{Cl}_2(x) = -\int_0^x \log \left| 2 \sin \frac{t}{2} \right| dt. \tag{9}$$

Clausen's integral is closely related to Milnor's Lobachevsky function [6]:

$$\Pi(x) = \frac{1}{2}\, \mathrm{Cl}_2(2x).$$

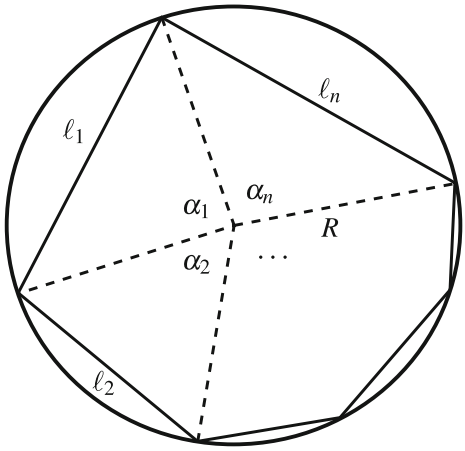

Fig. 1 Euclidean polygon inscribed in a circle

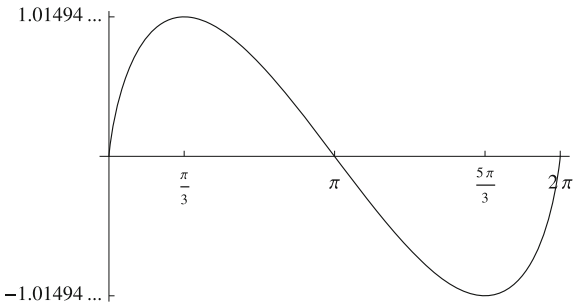

Fig. 2 Graph of Clausen's integral $\mathrm{Cl}_2(x)$

The function $\mathrm{Cl}_2 : \mathbb{R} \to \mathbb{R}$ is continuous, 2π-periodic, and odd. It is differentiable except at integer multiples of 2π where the graph has vertical tangents (see Fig. 2).

Proposition 2.1 (Variational Principle) *A point $\alpha \in D_n$ is a critical point of f_ℓ restricted to D_n if and only if there exists an $R \in \mathbb{R}$ satisfying equations* (7).

Proof A point $\alpha \in D_n$ is a critical point of f_ℓ restricted to D_n if and only if there exists a Lagrange multiplier $\log R$ such that $\nabla f_\ell(\alpha) = (\log R)\nabla g(\alpha)$ for the constraint function $g(\alpha) = \sum \alpha_k$, i.e.,

$$\begin{pmatrix} -\log\left|2\sin\frac{\alpha_1}{2}\right| + \log \ell_1 \\ \vdots \\ -\log\left|2\sin\frac{\alpha_n}{2}\right| + \log \ell_n \end{pmatrix} = \log R \begin{bmatrix} 1 \\ \vdots \\ 1 \end{bmatrix}.$$

Since $0 < \alpha_k < 2\pi$ we may omit the absolute value signs, obtaining equations (7). □

Thus, to prove Theorem 1.1, we need to show that f_ℓ has a critical point in D_n if and only if the polygon inequalities (1) are satisfied, and that this critical point is then unique. The following proposition and corollary deal with the uniqueness claim.

Proposition 2.2 *The function f_ℓ is strictly concave on D_n.*

Corollary 2.3 *If f_ℓ has a critical point in D_n, it is the unique maximizer of f_ℓ in the closure $\bar{D}_n = \{\alpha \in \mathbb{R}^n_{\geq 0} \mid \sum \alpha_k = 2\pi\}$.*

This proves the uniqueness claim of Theorem 1.1.

Proof (of Proposition 2.2) We will show that

$$V_n(\alpha) = \sum_{k=1}^{n} \mathrm{Cl}_2(\alpha_k) \tag{10}$$

is strictly concave on D_n. Since V_n differs from f_ℓ by a linear function, this is equivalent to the claim.

Rivin [10, Theorem 2.1] showed that V_3 is strictly concave on D_3. For $n > 3$ we proceed by induction on n by "cutting off a triangle": first, note the obvious identity

$$V_n(\alpha_1, \dots, \alpha_n) = V_{n-1}(\alpha_1, \dots, \alpha_{n-1} + \alpha_n) - \mathrm{Cl}_2(\alpha_{n-1} + \alpha_n) + \mathrm{Cl}_2(\alpha_{n-1}) + \mathrm{Cl}_2(\alpha_n).$$

Since Clausen's integral is 2π-periodic and odd,

$$-\mathrm{Cl}_2(\alpha_{n-1} + \alpha_n) = \mathrm{Cl}_2(2\pi - \alpha_{n-1} - \alpha_n) = \mathrm{Cl}_2\left(\sum_{k=1}^{n-2} \alpha_k\right),$$

so

$$V_n(\alpha_1, \dots, \alpha_n) = V_{n-1}(\alpha_1, \dots, \alpha_{n-1} + \alpha_n) + V_3\left(\sum_{k=1}^{n-2} \alpha_k, \alpha_{n-1}, \alpha_n\right).$$

Hence, if V_{n-1} and V_3 are strictly concave on D_{n-1} and D_3, respectively, the claim for V_n follows. □

Since f_ℓ attains its maximum on the compact set $\bar{D}_n$, it remains to show that the maximum is attained in D_n if and only if the polygon inequalities (1) are satisfied. This is achieved by the following Propositions 2.4 and 2.5.

Note that $\bar{D}_n$ is an $(n-1)$-dimensional simplex in $\mathbb{R}^n$. Its vertices are the points $2\pi e_1, \dots, 2\pi e_n$, where e_k are the canonical basis vectors of $\mathbb{R}^n$. The relative boundary of the simplex $\bar{D}_n$ is

$$\partial \bar{D}_n = \{\alpha \in \bar{D}_n \mid \alpha_k = 0 \text{ for at least one } k\}. \tag{11}$$

Proposition 2.4 *If the function f_ℓ attains its maximum on the simplex $\bar{D}_n$ at a boundary point $\alpha \in \partial \bar{D}_n$, then α is a vertex.*

Proof Suppose $\alpha \in \partial \bar{D}_n$ is not a vertex. We need to show that f_ℓ does not attain its maximum at α. This follows from the fact that the derivative of f_ℓ in a direction pointing towards D_n is $+\infty$.

Indeed, suppose $v \in \mathbb{R}^n_{\geq 0}$, $\sum_k v_k = 0$ and $v_k > 0$ if $\alpha_k = 0$. Then $\alpha + tv \in D_n$ for small enough $t > 0$, and because $\lim_{x \to 0} \mathrm{Cl}_2'(x) = +\infty$,

$$\lim_{t \to 0} \frac{d}{dt} f_\ell(\alpha + tv) = +\infty. \tag{12}$$

Hence $f_\ell(\alpha + tv) > f_\ell(\alpha)$ for small enough $t > 0$. □

Proposition 2.5 *The function f_ℓ attains its maximum on $\bar{D}_n$ at a vertex $2\pi e_k$ if and only if*

$$\ell_k \geq \sum_{\substack{i=1 \\ i \neq k}}^{n} \ell_i. \tag{13}$$

Proof By symmetry, it is enough to consider the case $k = n$, i.e., to show that the function f_ℓ attains its maximum on $\bar{D}_n$ at the vertex $(0, \ldots, 0, 2\pi)$ if and only if $\ell_n \geq \sum_{k=1}^{n-1} \ell_k$. To this end, we will calculate the directional derivative of f_ℓ in directions $v \in \mathbb{R}^n$ pointing inside D_n, i.e., satisfying

$$v_k \geq 0 \quad \text{for} \quad k \in \{1, \ldots, n-1\}, \quad v_n = -\sum_{k=1}^{n-1} v_k < 0.$$

Since we are only interested in the sign, we may assume v to be scaled so that

$$\sum_{k=1}^{n-1} v_k = 1, \qquad v_n = -1.$$

Clausen's integral has the asymptotic behavior

$$\mathrm{Cl}_2(x) = -x \log |x| + x + o(x) \quad \text{as} \quad x \to 0. \tag{14}$$

This can be seen by considering

$$\mathrm{Cl}_2(x) = -\int_0^x \log \left| (2 \sin \tfrac{t}{2})/t \right| \, dt - \int_0^x \log |t| \, dt.$$

Using (14) and the 2π-periodicity of Clausen's integral, one obtains

$$\begin{aligned} f_\ell(2\pi e_n + tv) - f_\ell(2\pi e_n) &= \sum_{k=1}^{n} \big(- t v_k \log |v_k| + t v_k \log \ell_k \big) + o(t) \\ &= -\sum_{k=1}^{n-1} t v_k \log \frac{v_k}{\ell_n} - t \log \ell_n + o(t), \end{aligned}$$

and hence

$$\frac{d}{dt}\Big|_{t=0} f(2\pi e_n + tv) = -\sum_{k=1}^{n-1} v_k \log \frac{v_k}{\ell_k} - \log \ell_n.$$

Now we invoke the information inequality (2) for the discrete probability distributions $(v_1, \ldots, v_{n-1})$ and $(\ell_1, \ldots, \ell_{n-1}) / \sum_{k=1}^{n-1} \ell_k$. Thus,

$$\frac{d}{dt}\Big|_{t=0} f(2\pi e_n + tv) = \underbrace{-\sum_{k=1}^{n-1} v_k \log\left(\frac{v_k}{\ell_n / \sum_{m=1}^{n-1} \ell_m}\right)}_{\leq 0} + \log\left(\frac{\sum_{k=1}^{n-1} \ell_k}{\ell_n}\right).$$

If $\ell_n \geq \sum_{k=1}^{n-1} \ell_k$, then

$$\frac{d}{dt}\Big|_{t=0} f(2\pi e_n + tv) \leq 0.$$

With the concavity of f_ℓ (Proposition 2.2), this implies that f_ℓ attains its maximum on $\bar{D}_n$ at $(0, \ldots, 0, 2\pi)$.

If, on the other hand, $\ell_n < \sum_{k=1}^{n-1} \ell_k$, then we obtain, for $v_k = \ell_k / \sum_{m=1}^{n-1} \ell_m$,

$$\frac{d}{dt}\Big|_{t=0} f(2\pi e_n + tv) > 0.$$

This implies that f_ℓ does not attain its maximum at $(0, \ldots, 0, 2\pi)$. □

This completes the proof of Theorem 1.1.

Remark 2.6 The function V_n has the following interpretation in terms of hyperbolic volume [6]. Consider a Euclidean cyclic n-gon with central angles $\alpha_1, \ldots, \alpha_n$. Imagine the Euclidean plane of the polygon to be the ideal boundary of hyperbolic 3-space in the Poincaré upper half-space model. Then the vertical planes through the edges of the polygon and the hemisphere above its circumcircle bound a hyperbolic pyramid with vertices at infinity. Its volume is $\frac{1}{2} V_n(\alpha_1, \ldots, \alpha_n)$. Together with Schläfli's differential volume equation (rather, Milnor's generalization that allows for ideal vertices [7]), this provides another way to prove Proposition 2.1.

3 Spherical Polygons. Proof of Theorem 1.2

The polygon inequalities (1) are clearly necessary for the existence of a spherical cyclic polygon because every side is a shortest geodesic. That inequality (3) is also necessary was already noted in the introduction. It remains to show that these inequalities are also sufficient, and that the polygon is unique.

We reduce the spherical case to the Euclidean one as shown in Fig. 3. Connecting the vertices of a spherical cyclic polygon with line segments in the ambient Euclidean space, one obtains a Euclidean cyclic polygon whose circumradius is smaller than 1. Conversely, every Euclidean polygon inscribed in a circle of radius less than 1 corresponds to a unique spherical cyclic polygon. The spherical side lengths ℓ are related to the Euclidean lengths $\bar{\ell}$ by

$$\bar{\ell} = 2 \sin \frac{\ell}{2}. \tag{15}$$

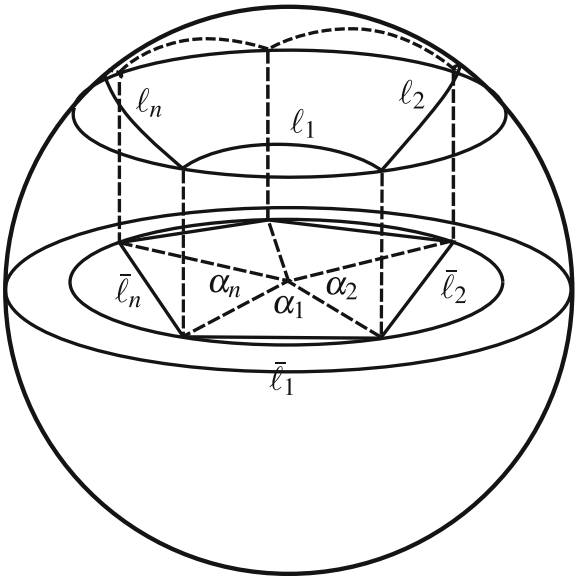

Fig. 3 Spherical and Euclidean polygons

It remains to show the following two propositions:

Proposition 3.1 *If the spherical lengths $\ell \in \mathbb{R}^n_{>0}$ satisfy the inequalities* (1) *and* (3)*, then the Euclidean lengths $\bar{\ell}$ defined by* (15) *satisfy the inequalities* (1) *as well. By Theorem 1.1 there is then a unique Euclidean cyclic polygon $P_{\bar{\ell}}$ with side lengths $\bar{\ell}$.*

Proposition 3.2 *The circumradius $\bar{R}$ of the polygon $P_{\bar{\ell}}$ of Proposition 3.1 is strictly less than* 1.

We will use the following estimate in the proof of Proposition 3.1:

Lemma 3.3 (Sum of Sines Estimate) If $\beta_1, \ldots, \beta_n \in \mathbb{R}_{\geq 0}$ satisfy $\sum_{k=1}^n \beta_k \leq \pi$, then

$$\sin\left(\sum_{k=1}^{n} \beta_k\right) \leq \sum_{k=1}^{n} \sin \beta_k. \tag{16}$$

Proof (of Lemma 3.3) By induction on n, the base case $n = 1$ being trivial. For the inductive step, use the addition theorem,

$$\sin\left(\sum_{k=1}^{n+1} \beta_k\right) = \sin\left(\sum_{k=1}^{n} \beta_k\right) \cos \beta_{n+1} + \cos\left(\sum_{k=1}^{n} \beta_k\right) \sin \beta_{n+1},$$

and note that the cosines are ≤ 1. □

Remark 3.4 The statement of Lemma 3.3 can be strengthened. Equality holds in (16) if and only if at most one β_k is greater than zero. This is easy to see, but we do not need this stronger statement in the following proof.

Proof (of Proposition 3.1) Suppose $\ell_1, \ldots, \ell_n \in \mathbb{R}_{>0}$ satisfy the polygon inequalities (1) and (3). We need to show that $\bar{\ell}_1, \ldots, \bar{\ell}_n$ defined by (15) satisfy

$$\bar{\ell}_k < \sum_{i \neq k} \bar{\ell}_i. \tag{17}$$

To this end, we will show that

$$\sin \frac{\ell_k}{2} < \sin \left(\sum_{i \neq k} \frac{\ell_i}{2} \right), \tag{18}$$

from which inequality (17) follows by Lemma 3.3. To prove inequality (18), we consider two cases separately.

- $\sum_{i \neq k} \ell_i \leq \pi$. Inequality (18) simply follows from the polygon inequality $\ell_k < \sum_{i \neq k} \ell_i$ and the monotonicity of the sine function on the closed interval $[0, \frac{\pi}{2}]$.
- $\sum_{i \neq k} \ell_i \geq \pi$. Note that $2\pi > \sum_i \ell_i$ implies $2\pi - \ell_k > \sum_{i \neq k} \ell_i$, and hence

$$2\pi > 2\pi - \ell_k > \sum_{i \neq k} \ell_i \geq \pi. \tag{19}$$

  Inequality (18) follows from $\sin \frac{\ell_k}{2} = \sin(\pi - \frac{\ell_k}{2})$ and the monotonicity of the sine function on the closed interval $[\frac{\pi}{2}, \pi]$.

This completes the proof of (18) and hence the proof of Proposition 3.1. □

Proof (of Proposition 3.2) Let α_k be the central angles of the Euclidean cyclic polygon $P_{\bar{\ell}}$. Then

$$\sin \frac{\ell_k}{2} = \frac{\bar{\ell}_k}{2} = \bar{R} \sin \frac{\alpha_k}{2}, \tag{20}$$

by (7) and (15). Note that α_k are the central angles of both the Euclidean and the spherical polygon (provided it exists). We consider two cases separately.

First, suppose that $\alpha_k \leq \pi$ for all k. Since $\sum_k \ell_k < 2\pi = \sum_k \alpha_k$, there is some k such that $\ell_k < \alpha_k$. Then $\sin \frac{\ell_k}{2} < \sin \frac{\alpha_k}{2}$, and equation (20) implies that $\bar{R} < 1$.

Otherwise, since $\sum_k \alpha_k = 2\pi$, there is exactly one i such that $\alpha_i > \pi$, and $\alpha_k < \pi$ for all $k \neq i$. By symmetry, it is enough to consider the case

$$\alpha_1 > \pi, \quad \alpha_k < \pi \quad \text{for} \quad k \in \{2, \ldots, n\}.$$

For future reference, we note that $\alpha_1 > \pi$ implies that $\bar{\ell}_1$ is the longest side of $P_{\bar{\ell}}$. (Use (20) and the monotonicity of the sine function.)

We will show $\bar{R} < 1$ by induction on n. First, assume $n = 3$. Then (18) says

$$\sin \frac{\ell_1}{2} < \sin \frac{\ell_2 + \ell_3}{2}.$$

By (20) and using $2\pi - \alpha_1 = \alpha_2 + \alpha_3$, we have

$$\sin\frac{\ell_1}{2} = \bar{R}\sin\frac{\alpha_2}{2}\cos\frac{\alpha_3}{2} + \bar{R}\cos\frac{\alpha_2}{2}\sin\frac{\alpha_3}{2}, \tag{21}$$

and

$$\begin{aligned}\sin\frac{\ell_2+\ell_3}{2} &= \sin\frac{\ell_2}{2}\cos\frac{\ell_3}{2} + \cos\frac{\ell_2}{2}\sin\frac{\ell_3}{2} \\ &= \bar{R}\sin\frac{\alpha_2}{2}\cos\frac{\ell_3}{2} + \bar{R}\cos\frac{\ell_2}{2}\sin\frac{\alpha_3}{2}\,.\end{aligned} \tag{22}$$

For at least one $k \in \{2, 3\}$, $\cos\frac{\alpha_k}{2} < \cos\frac{\ell_k}{2}$ and hence $\sin\frac{\alpha_k}{2} > \sin\frac{\ell_k}{2}$. Equation (20) implies $\bar{R} < 1$.

Now assume that $\bar{R} < 1$ has already been shown if $P_{\bar{\ell}}$ has at most n sides. Suppose $P_{\bar{\ell}}$ has $n+1$ sides. The idea of the following argument is to cut off a triangle with sides $\bar{\ell}_n$, $\bar{\ell}_{n+1}$, and $\bar{\lambda} = 2\bar{R}\sin\frac{\alpha_n+\alpha_{n+1}}{2}$. Since $\bar{\lambda} \le \bar{\ell}_1$ (the longest side), and $\bar{\ell}_1 \le 2$ by (15), we may define $\lambda = 2\arcsin\frac{\bar{\lambda}}{2}$. Now assume $\bar{R} \ge 1$. Then, by the inductive hypothesis, the polygon inequalities (1) or (3) are violated for the cut-off triangle and the remaining n-gon. Inequality (3) cannot be violated because it was assumed to hold for $\ell_1, \dots, \ell_{n+1}$. Hence,

$$\ell_1 \ge \ell_2 + \cdots + \ell_{n-1} + \lambda \quad \text{and} \quad \lambda \ge \ell_n + \ell_{n+1}.$$

This implies $\ell_1 \ge \ell_2 + \cdots + \ell_{n+1}$. Conversely, if (1) and (3) hold, then $\bar{R} < 1$. This completes the proof of Proposition 3.2. □

4 Hyperbolic Polygons. Proof of Theorem 1.3

The polygon inequalities (1) are clearly necessary for the existence of a hyperbolic cyclic polygon, because every side is a shortest geodesic. It remains to show that they are also sufficient, and that the polygon is unique, i.e., Proposition 4.2. First, we review some basic facts from hyperbolic geometry.

As in the spherical case (Sect. 3), we will connect vertices by straight line segments in the ambient vector space. But instead of the sphere, we consider the hyperbolic plane in the hyperboloid model,

$$\mathbb{H}^2 = \{x \in \mathbb{R}^{2,1} \mid \langle x, x\rangle = -1,\ x_3 > 0\},$$

where $\mathbb{R}^{2,1}$ denotes the vector space $\mathbb{R}^3$ equipped with the scalar product

$$\langle x, y\rangle = x_1y_1 + x_2y_2 - x_3y_3,$$

and lengths and angles in $\mathbb{H}^2$ are measured using the Riemannian metric induced by this scalar product.

Straight lines (i.e., geodesics) in $\mathbb{H}^2$ are the intersections of $\mathbb{H}^2$ with 2-dimensional subspaces of $\mathbb{R}^3$. The length ℓ of the geodesic segment connecting points $p, q \in \mathbb{H}^2$ is determined by

$$\cosh \ell = -\langle p, q \rangle.$$

The length of the straight line segment connecting points $p, q \in \mathbb{H}^2$ in the ambient $\mathbb{R}^{2,1}$ is

$$\bar{\ell} = \sqrt{\langle p - q, p - q \rangle}.$$

This chordal length $\bar{\ell}$ and the hyperbolic distance ℓ are related by

$$\frac{\bar{\ell}}{2} = \sinh \frac{\ell}{2}. \tag{23}$$

An affine plane in $\mathbb{R}^{2,1}$ is called spacelike, lightlike, or timelike, if the restriction of the scalar product $\langle \cdot, \cdot \rangle$ to (the tangent space of) the affine plane is positive definite, positive semidefinite, or indefinite, respectively. In terms of the standard Euclidean metric on $\mathbb{R}^3$, a plane is spacelike, lightlike, or timelike if its slope is less than, equal to, or greater than 45°.

A curve of intersection of $\mathbb{H}^2$ with an affine plane in $\mathbb{R}^{2,1}$ that does not contain 0 is a hyperbolic circle, a horocycle, or a hypercycle, depending on whether the plane is spacelike, lightlike, or timelike.

Thus, connecting the vertices of a hyperbolic cyclic polygon by straight line segments in the ambient $\mathbb{R}^{2,1}$, one obtains a planar polygon in $\mathbb{R}^{2,1}$, but the intrinsic geometry of the plane will only be Euclidean if the hyperbolic polygon is inscribed in a circle (see Fig. 4). If the polygon is inscribed in a horocycle or hypercycle, then the geometry of the plane will be degenerate with signature $(+, 0)$ or a $1 + 1$-spacetime with signature $(+, -)$, respectively.

Proposition 4.1 *Let P_ℓ be a hyperbolic cyclic polygon with side lengths $\ell_1, \ldots, \ell_n \in \mathbb{R}_{>0}$, and let $\bar{\ell}_k$ be the chordal lengths* (23)*. If P_ℓ is inscribed in*

(i) a circle then

$$\bar{\ell}_k < \sum_{\substack{i=1 \\ i \neq k}}^{n} \bar{\ell}_i \quad \text{for all } k. \tag{24}$$

(ii) a horocycle then

$$\bar{\ell}_k = \sum_{\substack{i=1 \\ i \neq k}}^{n} \bar{\ell}_i \quad \text{for one } k. \tag{25}$$

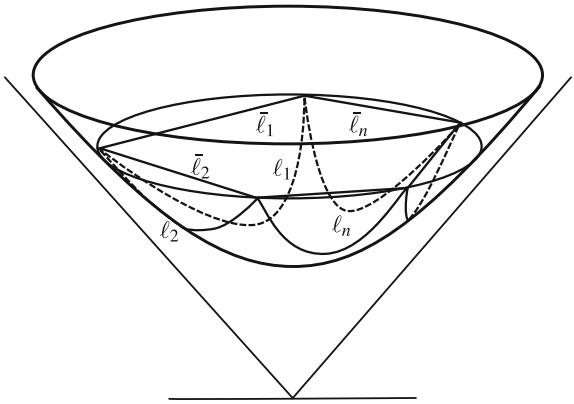

Fig. 4 Hyperbolic polygon inscribed in a circle, shown in the hyperboloid model

(iii) a hypercycle then

$$\bar{\ell}_k > \sum_{\substack{i=1 \\ i \neq k}}^{n} \bar{\ell}_i \quad \textit{for one } k. \tag{26}$$

Proof (i) If P_ℓ is inscribed in a circle, then the chordal polygon obtained by connecting the vertices of P_ℓ by straight line segments in $\mathbb{R}^{2,1}$ is a Euclidean polygon. Hence, its side lengths $\bar{\ell}$ satisfy (24).

(ii) If P_ℓ is inscribed in a horocycle, then the chordal length $\bar{\ell}_k$ of a side is equal to the length of the arc of the horocycle between its vertices (see Fig. 5). Since one horocycle arc comprises all others, this implies (25).

(iii) If P_ℓ is inscribed in a hypercycle at distance R from a geodesic g, then the chordal lengths $\bar{\ell}_k$, the hypercycle "radius" R, and the distances a_k between the foot points of the perpendiculars from the vertices to g (see Fig. 6) are related by

$$\frac{\bar{\ell}_k}{2} = \cosh(R) \sinh \frac{a_k}{2}. \tag{27}$$

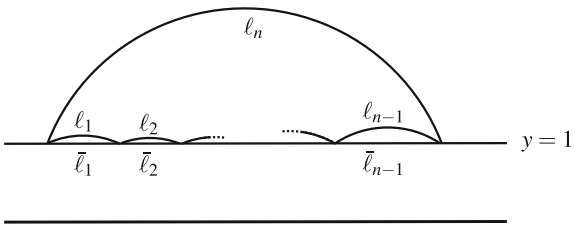

Fig. 5 Polygon inscribed in a horocycle, shown in the Poincaré half-plane model. Here, $\bar{\ell}_n = \sum_{i \neq n} \bar{\ell}_i$ is the largest chordal length. Since all horocycles are congruent, we may without loss of generality assume that the polygon is inscribed in the horocycle $y = 1$

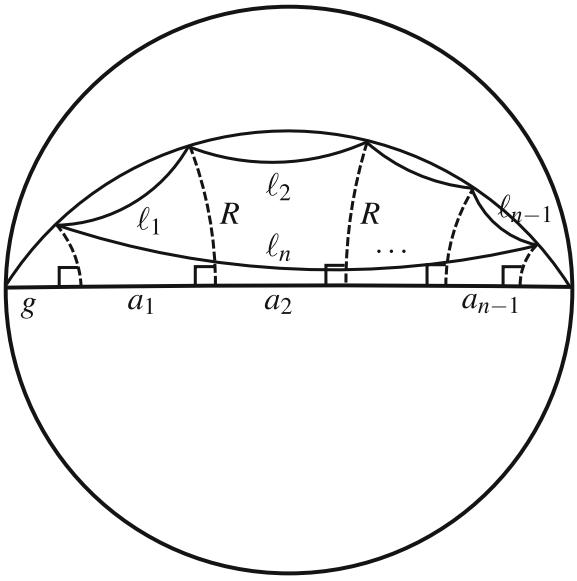

Fig. 6 Polygon inscribed in a hypercycle, shown in the Poincaré disk model. Here, ℓ_n and $\bar{\ell}_n$ are the largest side length and chordal length, respectively

Since one of the segments of g comprises all others,

$$a_k = \sum_{i \neq k} a_i \quad \text{for one } k.$$

With (27) this implies (26):

$$\frac{\bar{\ell}_k}{2} = \cosh(R) \sinh\Big(\sum_{i \neq k} \frac{a_i}{2}\Big) > \sum_{i \neq k} \cosh(R) \sinh \frac{a_i}{2} = \sum_{i \neq k} \frac{\bar{\ell}_i}{2},$$

where we have used the inequality $\sinh(x + y) > \sinh(x) + \sinh(y)$, which holds for positive x, y. This follows immediately from the addition theorem for the hyperbolic sine function.

This completes the proof of Proposition 4.1. □

Proposition 4.2 *If $\ell \in \mathbb{R}^n_{>0}$ satisfies the polygon inequalities* (1)*, then there exists a unique hyperbolic cyclic polygon with these side lengths.*

Proof Suppose $\ell \in \mathbb{R}^n_{>0}$ satisfies the polygon inequalities (1). Let $\bar{\ell}$ be the corresponding chordal lengths (23). We will treat each case of Proposition 4.1 separately. In each case, we will tacitly use Proposition 4.1 and its proof. Our treatment of case (iii) is analogous to Penner's proof [9] of Theorem 1.1 (his Theorem 6.2).

(i) If the chordal lengths $\bar{\ell}$ satisfy condition (24), then the existence and uniqueness of a hyperbolic cyclic polygon with side lengths ℓ follows from the existence and uniqueness of a Euclidean cyclic polygon with side lengths $\bar{\ell}$, i.e., from Theorem 1.1 (see Fig. 4).

(ii) If the chordal lengths $\bar{\ell}$ satisfy condition (25), then the corresponding hyperbolic cyclic polygon can be constructed by marking off the lengths $\bar{\ell}_i$ for $i \neq k$ along a horocycle (see Fig. 5). To see the uniqueness claim, note that all horocycles are congruent.

(iii) It remains to consider the case that the chordal lengths $\bar{\ell}$ satisfy condition (26). For simplicity, we will assume that ℓ_n is the largest side length. Then $\bar{\ell}_n$ is the largest chordal length and condition (26) says

$$\bar{\ell}_n > \sum_{k=1}^{n-1} \bar{\ell}_k. \tag{28}$$

Now suppose P_ℓ is a hyperbolic polygon with side lengths ℓ that is inscribed in a hypercycle at distance R from its geodesic g, and let

$$\bar{R} = \cosh R. \tag{29}$$

Then the distances a_k between the foot points (see Fig. 6) satisfy

$$a_n = \sum_{k=1}^{n-1} a_k,$$

Using (27), one obtains

$$\operatorname{arsinh}\Big(\frac{\bar{\ell}_n}{2\bar{R}}\Big) = \sum_{k=1}^{n-1} \operatorname{arsinh}\Big(\frac{\bar{\ell}_k}{2\bar{R}}\Big). \tag{30}$$

Conversely, if, for given ℓ, a number $\bar{R} > 1$ satisfies (30) then R defined by (29) is the correct hypercycle distance. More precisely, one can then construct a hyperbolic cyclic polygon with side lengths ℓ by marking off the distances $a_1, \ldots, a_{n-1}$ determined by (27) along a geodesic and intersect the perpendiculars in the marked points with a hypercycle at distance R (see Fig. 6).

It remains to show that there is exactly one $\bar{R} > 1$ satisfying (30). To this end, consider the function

$$\Phi(x) = \operatorname{arsinh}\Big(\frac{\bar{\ell}_n}{2x}\Big) - \sum_{k=1}^{n-1} \operatorname{arsinh}\Big(\frac{\bar{\ell}_k}{2x}\Big). \tag{31}$$

We need to show that Φ has exactly one zero in the interval $(1, \infty)$. Using (23), we see

$$\Phi(1) = \frac{1}{2}\Big(\ell_n - \sum_{k=1}^{n-1} \ell_k\Big) < 0. \tag{32}$$

For $x \to \infty$,

$$\Phi(x) = \frac{1}{2x}\Big(\bar{\ell}_n - \sum_{k=1}^{n-1} \bar{\ell}_k\Big) + o\Big(\frac{1}{x}\Big), \tag{33}$$

so

$$\Phi(x) > 0 \quad \text{for large } x.$$

By continuity, Φ has at least one zero in the interval $(1, \infty)$.

Finally, we will show that the derivative

$$\Phi'(x) = \frac{1}{x}\Bigg(- \frac{\frac{\bar{\ell}_n}{2x}}{\sqrt{1 + \big(\frac{\bar{\ell}_n}{2x}\big)^2}} + \sum_{k=1}^{n-1} \frac{\frac{\bar{\ell}_k}{2x}}{\sqrt{1 + \big(\frac{\bar{\ell}_k}{2x}\big)^2}}\Bigg), \tag{34}$$

is positive at the positive zeroes of Φ. This implies that Φ has at most one zero in $\mathbb{R}_{>0}$. Let us define

$$a_k(x) = \operatorname{arsinh}\Big(\frac{\bar{\ell}_k}{2x}\Big),$$

so

$$\Phi(x) = a_n(x) - \sum_{k=1}^{n-1} a_k(x),$$

and

$$\Phi'(x) = \frac{1}{x}\Big(- \tanh a_n(x) + \sum_{k=1}^{n-1} \tanh a_k(x)\Big).$$

The claim follows from the inequality

$$\tanh \sum_{j=1}^{m} a_j < \sum_{j=1}^{m} \tanh a_j,$$

which holds for $m \geq 2$ and positive numbers a_j. (Use induction on m and the addition theorem for tanh for the base case $m = 2$.)

This concludes the proof of Proposition 4.2. □

5 Concluding Remarks on 1 + 1 Spacetime

The scalar product of $\mathbb{R}^{1,1}$ is

$$\langle x, y\rangle_{1,1} = x_1 y_1 - x_2 y_2,$$

and the length of a spacelike vector x is $\ell = \sqrt{\langle x, x\rangle_{1,1}}$. The proof of Theorem 1.3 for polygons inscribed in hypercycles (Sect. 4) also proves the following theorem about "cyclic" polygons in $1+1$ spacetime.

Theorem 5.1 *There exists a polygon in $\mathbb{R}^{1,1}$ with $n \geq 3$ spacelike sides with lengths $\ell_1, \ldots, \ell_n > 0$ that is inscribed in one branch of a hyperbola $\langle x, x\rangle_{1,1} = -R^2$ if and only if*

$$\ell_k > \sum_{\substack{i=1 \\ i \neq k}}^{n} \ell_i \quad \text{for one } k, \tag{35}$$

and this polygon is unique.

Without loss of generality, we will assume that the nth side is the longest, i.e., $k = n$ in (35). Like in the Euclidean case (Sect. 2), the construction of such an inscribed polygon in $\mathbb{R}^{1,1}$ is equivalent to the following analytic problem: Find a point $a \in \mathbb{R}^n_{>0}$ satisfying

$$a_n = \sum_{i=1}^{n-1} a_i \tag{36}$$

and

$$\frac{\ell_k}{2} = R \sinh \frac{a_k}{2} \tag{37}$$

for some $R \in \mathbb{R}$ and all $k \in \{1, \ldots, n\}$.

This problem admits the following variational formulation. Define the function $\varphi_\ell : \mathbb{R}^n \to \mathbb{R}$ by

$$\varphi_\ell(a) = \sum_{k=1}^{n-1} \big(\mathrm{Clh}_2(a_k) + \log(\ell_k)\, a_k\big) - \big(\mathrm{Clh}_2(a_n) + \log(\ell_n)\, a_n\big),$$

where Clh_2 denotes the "hyperbolic version" of Clausen's integral,

$$\mathrm{Clh}_2(x) = -\int_0^x \log \left|2 \sinh \frac{t}{2}\right| dt.$$

(This notation is not standard.) The function $\mathrm{Clh}_2(x)$ can be expressed in terms of the real part of the dilogarithm function:

$$\mathrm{Clh}_2(x) = \mathrm{Re}\, \mathrm{Li}_2(e^x) + \frac{x^2}{4} - \frac{\pi^2}{6}.$$

Like in the Euclidean case, one sees that $a \in \mathbb{R}^n_{>0}$ is a critical point of φ_ℓ under the constraint (36) if and only if there is an R satisfying equations (37). However, the function φ_ℓ is neither concave nor convex on the subspace (36), so any proof

of Theorem 5.1 (or the hypercycle case of Theorem 1.3) based on this variational principle would have to be more involved.

Acknowledgments This research was supported by DFG SFB/TRR 109 "Discretization in Geometry and Dynamics".

References

1. Blaschke, W.: Kreis und Kugel. Veit u. Co., Leipzig (1916)
2. Blåsjö, V.: The isoperimetric problem. Am. Math. Monthly **112**(6), 526–566 (2005)
3. Cover, T.M., Thomas, J.A.: Elements of Information Theory. Wiley, New York (1991)
4. Lewin, L.: Polylogarithms and Associated Functions. North-Holland Publishing Co., New York-Amsterdam (1981)
5. L'Huilier, S.: De relatione mutua capacitatis et terminorum figurarum, geometrice considerata: seu de maximis et minimis. Michael Gröll, Warsaw (1782). http://dx.doi.org/10.3931/e-rara-4049
6. Milnor, J.: Hyperbolic geometry: the first 150 years. Bull. Am. Math. Soc. (N.S.) **6**(1), 9–24 (1982)
7. Milnor, J.: The Schläfli differential equality. In: Collected Papers, vol. 1, pp. 281–295. Publish or Perish Inc., Houston (1994)
8. Moula, F.: De maximis in figuris rectilineis. In: Commentarii Academiae Scientiarum Imperialis Petropolitanae, vol. 9, pp. 138–159. Typis Academiae, Petropolis (1737). http://www.archive.org/details/commentariiacade09impe
9. Penner, R.C.: The decorated Teichmüller space of punctured surfaces. Comm. Math. Phys. **113**(2), 299–339 (1987)
10. Rivin, I.: Euclidean structures on simplicial surfaces and hyperbolic volume. Ann. Math. (2) **139**(3), 553–580 (1994)
11. Schlenker, J.M.: Small deformations of polygons and polyhedra. Trans. Am. Math. Soc. **359**(5), 2155–2189 (2007)
12. Steiner, J.: Sur le maximum et le minimum des figures dans le plan, sur la sphère, et dans l'espace en général. J. Reine Angew. Math. **24**, 93–152, 190–250 (1842). http://dx.doi.org/10.1515/crll.1842.24.93
13. Steinitz, E.: Polyeder und Raumeinteilungen. In: Enzyklopädie der mathematischen Wissenschaften mit Einschluss ihrer Anwendungen, vol. 3-1-2, chap. IIIAB12. B. G. Teubner, Leipzig (1914–1931)
14. Weierstrass, K.: Mathematische Werke. VII. Vorlesungen über Variationsrechnung. Georg Olms Verlagsbuchhandlung, Hildesheim; Johnson Reprint Corp., New York (1967)

Complex Line Bundles Over Simplicial Complexes and Their Applications

Felix Knöppel and Ulrich Pinkall

Abstract Discrete vector bundles are important in Physics and recently found remarkable applications in Computer Graphics. This article approaches discrete bundles from the viewpoint of Discrete Differential Geometry, including a complete classification of discrete vector bundles over finite simplicial complexes. In particular, we obtain a discrete analogue of a theorem of André Weil on the classification of hermitian line bundles. Moreover, we associate to each discrete hermitian line bundle with curvature a unique piecewise-smooth hermitian line bundle of piecewise-constant curvature. This is then used to define a discrete Dirichlet energy which generalizes the well-known cotangent Laplace operator to discrete hermitian line bundles over Euclidean simplicial manifolds of arbitrary dimension.

1 Introduction

Vector bundles are fundamental objects in Differential Geometry and play an important role in Physics [2]. The Physics literature is also the main place where discrete versions of vector bundles were studied: First, there is a whole field called Lattice Gauge Theory where numerical experiments concerning connections in bundles over discrete spaces (lattices or simplicial complexes) are the main focus. Some of the work that has been done in this context is quite close to the kind of problems we are going to investigate here [3, 4, 6].

Vector bundles make their most fundamental appearance in Physics in the form of the complex line bundle whose sections are the wave functions of a charged particle in a magnetic field. Here the bundle comes with a connection whose curvature is given by the magnetic field [2]. There are situations where the problem itself suggests a natural discretization: The charged particle (electron) may be bound to a

F. Knöppel (✉) · U. Pinkall
Inst. für Mathematik, Technische Universität Berlin,
Straße des 17. Juni 136, 10623 Berlin, Germany
e-mail: knoeppel@math.tu-berlin.de

U. Pinkall
e-mail: pinkall@math.tu-berlin.de

A.I. Bobenko (ed.), *Advances in Discrete Differential Geometry*,
DOI 10.1007/978-3-662-50447-5_6

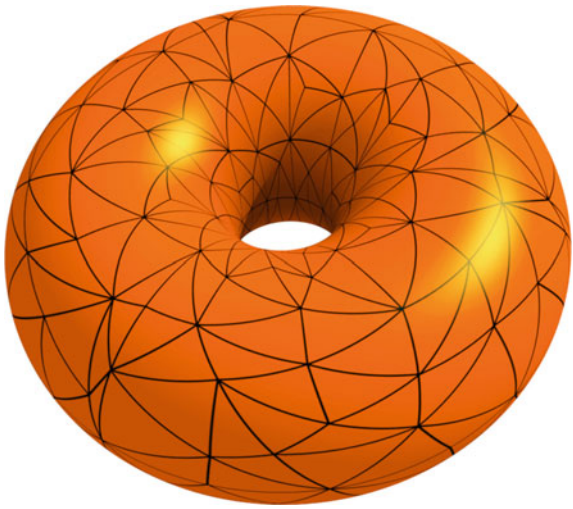

Fig. 1 A smooth triangulation of a manifold

certain arrangement of atoms. Modelling this situation in such a way that the electron can only occupy a discrete set of locations then leads to the "tight binding approximation" [1, 12, 15].

Recently vector bundles over discrete spaces also have found striking applications in Geometry Processing and Computer Graphics. We will describe these in detail in Sect. 2.

In order to motivate the basic definitions concerning vector bundles over simplicial complexes let us consider a smooth manifold $\tilde{\mathrm{M}}$ that comes with smooth triangulation (Fig. 1).

Let $\tilde{\mathrm{E}}$ be a smooth vector bundle over $\tilde{\mathrm{M}}$ of rank $\mathfrak{K}$. Then we can define a discrete version E of $\tilde{\mathrm{E}}$ by restricting $\tilde{\mathrm{E}}$ to the vertex set $\mathcal{V}$ of the triangulation. Thus E assigns to each vertex $i \in \mathcal{V}$ the $\mathfrak{K}$-dimensional real vector space $\mathrm{E}_i := \tilde{\mathrm{E}}_i$. This is the way vector bundles over simplicial complexes are defined in general: Such a bundle E assigns to each vertex i a $\mathfrak{K}$-dimensional real vector space E_i in such a way that $\mathrm{E}_i \cap \mathrm{E}_j = \emptyset$ for $i \neq j$.

So far the notion of a discrete vector bundle is completely uninteresting mathematically: The obvious definition of an isomorphism between two such bundles E and $\hat{\mathrm{E}}$ just would require a vector space isomorphism $f_i : \mathrm{E}_i \to \hat{\mathrm{E}}_i$ for each vertex i. Thus, unless we put more structure on our bundles, any two vector bundles of the same rank over a simplicial complex are isomorphic.

Suppose now that $\tilde{\mathrm{E}}$ comes with a connection ∇. Then we can use the parallel transport along edges ij of the triangulation to define vector space isomorphisms

$$\eta_{ij} : \tilde{\mathrm{E}}_i \to \tilde{\mathrm{E}}_j$$

This leads to the standard definition of a connection on a vector bundle over a simplicial complex: Such a connection is given by a collection of isomorphisms $\eta_{ij} : \mathrm{E}_i \to \mathrm{E}_j$ defined for each edge ij such that

$$\eta_{ji} = \eta_{ij}^{-1}.$$

Now the classification problem becomes non-trivial because for an isomorphism f between two bundles E and $\hat{\mathrm{E}}$ with connection we have to require compatibility with the transport maps η_{ij}:

$$f_j \circ \eta_{ij} = \hat{\eta}_{ij} \circ f_i.$$

Given a connection η and a closed edge path $\gamma = e_\ell \cdots e_1$ (compare Sect. 4) of the simplicial complex we can define the monodromy $P_\gamma \in \mathrm{Aut}(\mathrm{E}_i)$ around γ as

$$P_\gamma = \eta_{e_\ell} \circ \ldots \circ \eta_{e_1}.$$

In particular the monodromies around triangular faces of the simplicial complex provide an analog for the smooth curvature in the discrete setting. In Sect. 4 we will classify vector bundles with connection in terms of their monodromies.

Let us look at the special case of a rank 2 bundle E that is oriented and comes with a Euclidean scalar product. Then the 90°-rotation in each fiber makes it into 1-dimensional complex vector space, so we effectively are dealing with a hermitian complex line bundle. If ijk is an oriented face of our simplicial complex, the monodromy $P_{\partial ijk} : \mathrm{E}_i \to \mathrm{E}_i$ around the triangle ijk is multiplication by a complex number h_{ijk} of norm one. Writing $h_{ijk} = e^{\imath \alpha_{ijk}}$ with $-\pi < \alpha_{ijk} \leq \pi$ we see that this monodromy can also be interpreted as a real curvature $\alpha_{ijk} \in (-\pi, \pi]$. It thus becomes apparent that the information provided by the connection η cannot encode any curvature that integrated over a single face is larger than $\pm\pi$. This can be a serious restriction for applications: We effectively see a cutoff for the curvature that can be contained in a single face.

Remember however our starting point: We asked for structure that can be naturally transferred from the smooth setting to the discrete one. If we think again about a triangulated smooth manifold it is clear that we can associate to each two-dimensional face ijk the integral Ω_{ijk} of the curvature 2-form over this face. This is just a discrete 2-form in the sense of discrete exterior calculus [5]. Including this discrete curvature 2-form with the parallel transport η brings discrete complex line bundles much closer to their smooth counterparts:

Definition *A hermitian line bundle with curvature over a simplicial complex $\mathcal{X}$ is a triple* $(\mathrm{E}, \eta, \Omega)$. *Here* E *is complex hermitian line bundle over $\mathcal{X}$, for each edge ij the maps $\eta_{ij} : \mathrm{E}_i \to \mathrm{E}_j$ are unitary and the closed real-valued* 2*-form Ω on each face ijk satisfies*

$$\eta_{ki} \circ \eta_{jk} \circ \eta_{ij} = e^{\imath \Omega_{ijk}} \, \mathrm{id}_{\mathrm{E}_i}.$$

In Sect. 7 we will prove for hermitian line bundles with curvature the discrete analog of a well-known theorem by André Weil on the classification of hermitian line bundles.

In Sect. 8 we will define for hermitian line bundles with curvature a degree (which can be an arbitrary integer) and we will prove a discrete version of the Poincaré-Hopf index theorem concerning the number of zeros of a section (counted with sign and multiplicity).

Finally we will construct in Sect. 10 for each hermitian line bundle with curvature a piecewise-smooth bundle with a curvature 2-form that is constant on each face. Sections of the discrete bundle can be canonically extended to sections of the piecewise-smooth bundle. This construction will provide us with finite elements for bundle sections and thus will allow us to compute the Dirichlet energy on the space of sections.

2 Applications of Vector Bundles in Geometry Processing

Several important tasks in Geometry Processing (see the examples below) lead to the problem of coming up with an optimal normalized section ϕ of some Euclidean vector bundle E over a compact manifold with boundary M. Here "normalized section" means that ϕ is defined away from a certain singular set and where defined it satisfies $|\phi| = 1$.

In all the mentioned situations E comes with a natural metric connection ∇ and it turns out that the following method for finding ϕ yields surprisingly good results:

Among all sections ψ of E *find one which minimizes* $\int_M |\nabla\psi|^2$ *under the constraint* $\int_M |\psi|^2 = 1$. *Then away from the zero set of ψ use* $\phi = \psi/|\psi|$.

The term "optimal" suggests that there is a variational functional which is minimized by ϕ and this is in fact the case. Moreover, in each of the applications there are heuristic arguments indicating that ϕ is indeed a good choice for the problem at hand. For the details we refer to the original papers. Here we are only concerned with the Discrete Differential Geometry involved in the discretization of the above variational problem.

2.1 Direction Fields on Surfaces

Here M is a surface with a Riemannian metric, $E = TM$ is the tangent bundle and ∇ is the Levi-Civita connection. Figure 2 shows the resulting unit vector field ϕ. If we consider TM as a complex line bundle, normalized sections of the tensor square $L = TM \otimes TM$ describe unoriented direction fields on M. Similarly, "higher order direction fields" like cross fields are related to higher tensor powers of TM. Higher order direction fields also have important applications in Computer Graphics.

Fig. 2 An optimal direction field on a surface

2.2 Stripe Patterns on Surfaces

A *stripe pattern* on a surface M is a map which away from a certain singular set assigns to each point $p \in \mathrm{M}$ an element $\phi(p) \in \mathbb{S} = \{z \in \mathbb{C} | |z| = 1\}$. Such a map ϕ can be used to color M in a periodic fashion according to a color map that assigns a color to each point on the unit circle $\mathbb{S}$. Suppose we are given a 1-form ω on M that specifies a desired direction and spacing of the stripes, which means that ideally we would wish for something like $\phi = e^{i\alpha}$ with $d\alpha = \omega$. Then the algorithm in [9] says that we should use a ϕ that comes from taking E as the trivial bundle $\mathrm{E} = \mathrm{M} \times \mathbb{C}$ and $\nabla\psi = d\psi - i\omega\psi$. Sometimes the original data come from an unoriented direction field and (in order to obtain the 1-form ω) we first have to move from M to a double branched cover $\tilde{\mathrm{M}}$ of M. This is for example the case in Fig. 3.

2.3 Decomposing Velocity Fields into Fields Generated by Vortex Filaments

The velocity fields that arise in fluid simulations quite often can be understood as a superposition of interacting vortex rings. It is therefore desirable to have an algorithm that reconstructs the underlying vortex filaments from a given velocity field. Let the velocity field $\mathbf{v}$ on a domain $\mathrm{M} \subset \mathbb{R}^3$ be given as a 1-form $\omega = \langle \mathbf{v}, \cdot \rangle$. Then the algorithm proposed in [19] uses the function $\phi : \mathrm{M} \to \mathbb{C}$ that results from taking the trivial bundle $\mathrm{E} = \mathrm{M} \times \mathbb{C}$ endowed with the connection $\nabla\psi = d\psi - i\omega\psi$. Note that so far this is just a three-dimensional version of the situation in Sect. 2.2. This time however we even forget ϕ in the end and only retain the zero set of ψ as the filament configuration we are looking for (Fig. 4).

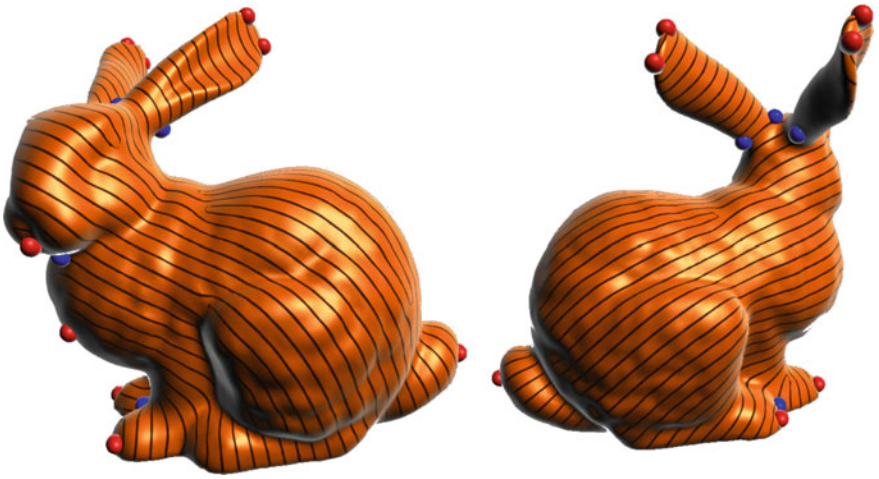

Fig. 3 An optimal stripe pattern aligned to an unoriented direction field

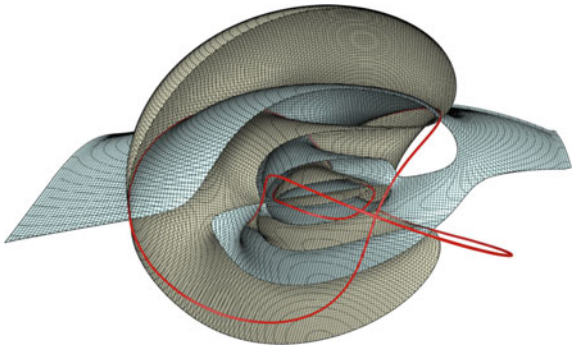

Fig. 4 A knotted vortex filament defined as the zero set of a complex valued function ψ. It is shown as the intersection of the zero set of $\mathrm{Re}\,\psi$ with the zero set of $\Im\,\psi$

2.4 Close-To-Conformal Deformations of Volumes

Here the data are a domain $\mathrm{M} \subset \mathbb{R}^3$ and a function $u : \mathrm{M} \to \mathbb{R}$. The task is to find a map $f : \mathrm{M} \to \mathbb{R}^3$ which is approximately conformal with conformal factor e^u, i.e. for all tangent vectors $X \in \mathrm{TM}$ we want

$$|df(X)| \approx e^u |X|.$$

The only exact solutions of this equations are the Möbius transformations. For these we find

$$df(X) = e^u \overline{\psi} X \psi$$

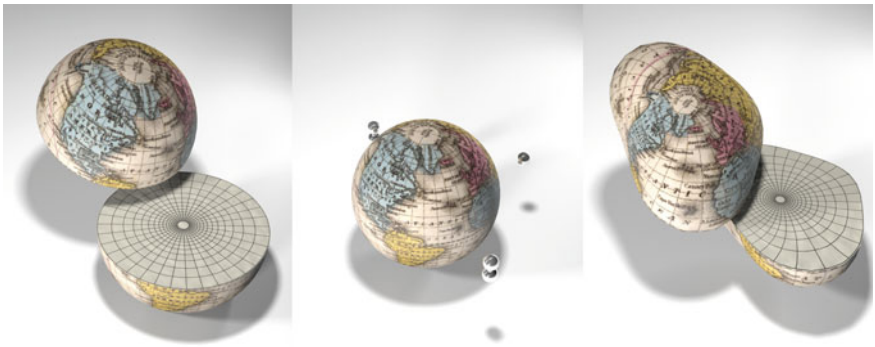

Fig. 5 Close-to-conformal deformation of a sphere based on a desired conformal factor specified as the potential of a collection of point charges

for some map $\psi : \mathrm{M} \to \mathbb{H}$ with $|\psi| = 1$ which in addition satisfies

$$d\psi(X) = -\tfrac{1}{2}(\operatorname{grad} u \times X)\,\psi.$$

Note that here we have identified $\mathbb{R}^3$ with the space of purely imaginary quaternions. Let us define a connection ∇ on the trivial rank 4 vector bundle $\mathrm{M} \times \mathbb{H}$ by

$$\nabla_X \psi := d\psi(X) + \tfrac{1}{2}(\operatorname{grad} u \times X)\psi.$$

Then we can apply the usual method and find a section $\phi : \mathrm{M} \to \mathbb{H}$ with $|\phi| = 1$. In general there will not be any $f : \mathrm{M} \to \mathbb{R}^3$ that satisfies

$$df(X) = e^u \overline{\phi} X \phi \tag{1}$$

exactly but we can always look for an f that satisfies (1) in the least squares sense. See Fig. 5 for an example.

3 Discrete Vector Bundles with Connection

An *(abstract) simplicial complex* is a collection $\mathcal{X}$ of finite non-empty sets such that if σ is an element of $\mathcal{X}$ so is every non-empty subset of σ [14].

An element of a simplicial complex $\mathcal{X}$ is called a *simplex* and each non-empty subset of a simplex σ is called a *face of* σ. The elements of a simplex are called *vertices* and the union of all vertices $\mathcal{V} = \cup_{\sigma \in \mathcal{X}} \sigma$ is called the *vertex set of* $\mathcal{X}$. The *dimension of a simplex* is defined to be one less than the number of its vertices:

$\dim \sigma := |\sigma| - 1$. A simplex of dimension k is also called a *k-simplex*. The *dimension of a simplicial complex* is defined as the maximal dimension of its simplices.

To avoid technical difficulties, we will restrict our attention to *finite* simplicial complexes only. The main concepts are already present in the finite case. Though, the definitions carry over verbatim to infinite simplicial complexes.

Definition 3.1 Let $\mathbb{F}$ be a field and let $\mathcal{X}$ be a simplicial complex with vertex set $\mathcal{V}$. A *discrete $\mathbb{F}$-vector bundle* of rank $\mathfrak{K} \in \mathbb{N}$ over $\mathcal{X}$ is a map $\pi : \mathrm{E} \to \mathcal{V}$ such that for each vertex $i \in \mathcal{V}$ the *fiber over i*

$$\mathrm{E}_i := \pi^{-1}(\{i\})$$

has the structure of a $\mathfrak{K}$-dimensional $\mathbb{F}$-vector space.

Most of the time, we slightly abuse notation and denote a discrete vector bundle over a simplicial complex schematically by $\mathrm{E} \to \mathcal{X}$.

The usual vector space constructions carry fiberwise over to discrete vector bundles. So we can speak of tensor products or dual bundles. Moreover, the fibers can be equipped with additional structures. In particular, a real vector bundle whose fibers are Euclidean vector spaces is called a *discrete Euclidean vector bundle*. Similarly, a complex vector bundle whose fibers are hermitian vector spaces is called a *discrete hermitian vector bundle*.

So far discrete vector bundles are completely uninteresting from the mathematical viewpoint—the obvious definition of an isomorphism f between two discrete vector bundles E and $\tilde{\mathrm{E}}$ just requires isomorphisms between the fibers $f_i : \mathrm{E}_i \to \tilde{\mathrm{E}}_i$. Thus any two bundles of rank $\mathfrak{K}$ are isomorphic. This changes if we connect the fibers along the edges by isomorphisms.

Let $\sigma = \{i_0, \ldots, i_k\}$ be a k-simplex. We define two orderings of its vertices to be equivalent if they differ by an even permutation. Such an equivalence class is then called an *orientation* of σ and a simplex together with an orientation is called an *oriented simplex*. We will denote the oriented k-simplex just by the word $i_0 \cdots i_k$. Further, an oriented 1-simplex is called an *edge*.

Definition 3.2 Let $\mathrm{E} \to \mathcal{X}$ be a discrete vector bundle over a simplicial complex. A *discrete connection on* E is a map η which assigns to each edge ij an isomorphism $\eta_{ij} : \mathrm{E}_i \to \mathrm{E}_j$ of vector spaces such that

$$\eta_{ji} = \eta_{ij}^{-1}.$$

Remark 3.3 Here and in the following a morphism of vector spaces is a linear map that also preserves all additional structures—if any present. E.g., if we are dealing with hermitian vector spaces, then a morphism is a complex-linear map that preserves the hermitian metric, i.e. it is a complex linear isometric immersion.

Definition 3.4 A *morphism of discrete vector bundles with connection* is a map $f : \mathrm{E} \to \mathrm{F}$ between discrete vector bundles $\mathrm{E} \to \mathcal{X}$ and $\mathrm{F} \to \mathcal{X}$ with connections η and θ (resp.) such that

(i) for each vertex i we have that $f(\mathrm{E}_i) \subset \mathrm{F}_i$ and the map $f_i = f|_{\mathrm{E}_i} : \mathrm{E}_i \to \mathrm{F}_i$ is a morphism of vector spaces,
(ii) for each edge ij the following diagram commutes:

$$\begin{array}{ccc} \mathrm{F}_i & \xrightarrow{\theta_{ij}} & \mathrm{F}_j \\ {\scriptstyle f_i}\uparrow & = & \uparrow{\scriptstyle f_j} \\ \mathrm{E}_i & \xrightarrow[\eta_{ij}]{} & \mathrm{E}_j \end{array},$$

i.e. $\theta_{ij} \circ f_i = f_j \circ \eta_{ij}$.

An *isomorphism* is a morphism which has an inverse map, which is also a morphism. Two discrete vector bundles with connection are called *isomorphic*, if there exists an isomorphism between them.

Again let $\mathcal{V}$ denote the vertex set of $\mathcal{X}$. A discrete vector bundle $\mathrm{E} \to \mathcal{X}$ with connection η is called *trivial*, if it is isomorphic to the *product bundle*

$$\underline{\mathbb{F}^{\mathfrak{K}}} := \mathcal{V} \times \mathbb{F}^{\mathfrak{K}}$$

over $\mathcal{X}$ equipped with the connection which assigns to each edge the identity $\mathrm{id}_{\mathbb{F}^{\mathfrak{K}}}$.

It is a natural question to ask how many non-isomorphic discrete vector bundles with connection exist on a given simplicial complex $\mathcal{X}$.

Remark 3.5 For $k \in \mathbb{N}$, the k-skeleton $\mathcal{X}^k$ of a simplicial complex $\mathcal{X}$ is the subcomplex that consists of all simplices $\sigma \in \mathcal{X}$ of dimension $\leq k$,

$$\mathcal{X}^k := \big\{\sigma \in \mathcal{X} \mid \dim \sigma \leq k\big\}.$$

The classification of vector bundles over $\mathcal{X}$ only involves its 1-skeleton $\mathcal{X}^1$ and could be equally done just for discrete vector bundles over 1-dimensional simplicial complexes, i.e. graphs. Later on, when we consider discrete hermitian line bundles with curvature in Sect. 7, the 2- and 3-skeleton come into play and finally, in Sect. 11, we will use the whole simplicial complex.

4 Monodromy—A Discrete Analogue of Kobayashi's Theorem

Let $\mathcal{X}$ be a simplicial complex. Each edge ij of $\mathcal{X}$ has a start vertex $s(ij) := i$ and a target vertex $t(ij) := j$. A *edge path* γ is a sequence of successive edges $(e_1, \ldots, e_\ell)$, i.e. $s(e_{k+1}) = t(e_k)$ for all $k = 1, \ldots, \ell - 1$, and will be denoted by the word:

$$\gamma = e_\ell \cdots e_1.$$

If $i = s(e_1)$, we say that γ starts at i, and if $j = t(e_\ell)$ that γ ends at j. The complex $\mathcal{X}$ is called *connected*, if any two of its vertices can be joined by an edge path. From now on we will only consider connected simplicial complexes.

Now, let $\mathrm{E} \to \mathcal{X}$ be a discrete vector bundle with connection η. To each edge path $\gamma = e_\ell \cdots e_1$ from i to j, we define the *parallel transport* $P_\gamma : \mathrm{E}_i \to \mathrm{E}_j$ *along* γ by

$$P_\gamma := \eta_{e_\ell} \circ \cdots \circ \eta_{e_1}.$$

To each edge path $\gamma = e_\ell \cdots e_1$ we can assign an *inverse path* γ^{-1}. If $\tilde{\gamma} = e_m \cdots e_{\ell+1}$ starts where γ ends, we can build the *concatenation* $\tilde{\gamma}\gamma$: With the notation $ij^{-1} := ji$, we have

$$\gamma^{-1} := e_1^{-1} \cdots e_\ell^{-1}, \quad \tilde{\gamma}\gamma := e_m \cdots e_{\ell+1} e_\ell \cdots e_1.$$

Whenever $\tilde{\gamma}\gamma$ is defined,

$$P_{\tilde{\gamma}\gamma} = P_{\tilde{\gamma}} \circ P_\gamma, \quad P_{\gamma^{-1}} = P_\gamma^{-1}. \tag{2}$$

The elements of the fundamental group are identified with equivalence classes of *edge loops*, i.e. edge paths starting and ending a given *base vertex* i of $\mathcal{X}$, where two such loops are identified if they differ by a sequence of *elementary moves* [16]:

$$e_\ell \cdots e_{k+1} e^{-1} e\, e_k \cdots e_1 \longleftrightarrow e_\ell \cdots e_{k+1} e_k \cdots e_1.$$

Now, by Eq. (2), we see that the parallel transport descends to a representation of the fundamental group $\pi_1(\mathcal{X}^1, i)$. We encapsulate this in the following

Proposition 4.1 *Let* $\mathrm{E} \to \mathcal{X}$ *be a discrete vector bundle with connection over a connected simplicial complex. The parallel transport descends to a representation of the fundamental group* $\pi_1(\mathcal{X}^1, i)$*:*

$$\mathfrak{M} : \pi_1(\mathcal{X}^1, i) \to \mathrm{Aut}(\mathrm{E}_i), \quad [\gamma] \mapsto P_\gamma.$$

The representation $\mathfrak{M}$ *will be called the monodromy of the discrete vector bundle* E.

If we change the base vertex this leads to an isomorphic representation—an isomorphism is just given by the parallel transport P_γ along an edge path joining the two base vertices. Moreover, if $f : \mathrm{E} \to \tilde{\mathrm{E}}$ is an isomorphism of discrete vector bundles with connection over the simplicial complex $\mathcal{X}$, for any edge path $\gamma = e_\ell \cdots e_1$ from a vertex i to a vertex j the following equality holds:

$$\tilde{P}_\gamma = f_j \circ P_\gamma \circ f_i^{-1}.$$

Here P and $\tilde{P}$ denote the parallel transports of E and $\tilde{\mathrm{E}}$. Thus we obtain:

Proposition 4.2 *Isomorphic discrete vector bundles with connection have isomorphic monodromies.*

In fact, the monodromy completely determines a discrete vector bundle with connection up to isomorphism, which provides a complete classification of discrete vector bundles with connection: Let $\mathcal{X}$ be a connected simplicial complex. Let $\mathrm{E} \to \mathcal{X}$ be a discrete $\mathbb{F}$-vector bundle of rank $\mathfrak{K}$ with connection and let $\mathfrak{M} : \pi_1(\mathcal{X}^1, i) \to \mathrm{Aut}(\mathrm{E}_i)$ denote its monodromy. Any choice of a basis of the fiber E_i determines a group homomorphism $\rho \in \mathrm{Hom}\big(\pi_1(\mathcal{X}^1, i), \mathrm{GL}(\mathfrak{K}, \mathbb{F})\big)$. Any other choice of basis determines a group homomorphism $\tilde{\rho}$ which is related to ρ by conjugation, i.e. there is $S \in \mathrm{GL}(\mathfrak{K}, \mathbb{F})$ such that

$$\tilde{\rho}([\gamma]) = S \cdot \rho([\gamma]) \cdot S^{-1} \textit{ for all } [\gamma] \in \pi_1(\mathcal{X}^1, i).$$

Hence the monodromy $\mathfrak{M}$ determines a well-defined conjugacy class of group homomorphisms from $\pi_1(\mathcal{X}^1, i)$ to $\mathrm{GL}(\mathfrak{K}, \mathbb{F})$, which we will denote by $[\mathfrak{M}]$. The group $\mathrm{GL}(\mathfrak{K}, \mathbb{F})$ will be referred to as the *structure group of* E.

Let $\mathfrak{V}_{\mathbb{F}}^{\mathfrak{K}}(\mathcal{X})$ denote the *set of isomorphism classes of* $\mathbb{F}$*-vector bundles of rank* $\mathfrak{K}$ *with connection over* $\mathcal{X}$ and let $\mathrm{Hom}\big(\pi_1(\mathcal{X}^1, i), \mathrm{GL}(\mathfrak{K}, \mathbb{F})\big)/_{\sim}$ denote the *set of conjugacy classes of group homomorphisms from the fundamental group* $\pi_1(\mathcal{X}^1, i)$ *into the structure group* $\mathrm{GL}(\mathfrak{K}, \mathbb{F})$.

Theorem 4.3 $F : \mathfrak{V}_{\mathbb{F}}^{\mathfrak{K}}(\mathcal{X}) \to \mathrm{Hom}\big(\pi_1(\mathcal{X}^1, i), GL(\mathfrak{K}, \mathbb{F})\big)/_{\sim}$, $[\mathrm{E}] \mapsto [\mathfrak{M}]$ *is bijective.*

Proof By Proposition 4.2, F is well-defined. First we show injectivity. Consider two discrete vector bundles E, $\tilde{\mathrm{E}}$ over $\mathcal{X}$ with connections η, $\tilde{\eta}$ and let $\mathfrak{M}$, $\tilde{\mathfrak{M}}$ denote their monodromies. Suppose that $[\mathfrak{M}] = [\tilde{\mathfrak{M}}]$. If we choose bases $\{X_i^1, \ldots, X_i^{\mathfrak{K}}\}$ of E_i and $\{\tilde{X}_i^1, \ldots, \tilde{X}_i^{\mathfrak{K}}\}$ of $\tilde{\mathrm{E}}_i$, then $\mathfrak{M}$ and $\tilde{\mathfrak{M}}$ are represented by group homomorphisms $\rho, \tilde{\rho} \in \mathrm{Hom}\big(\pi_1(\mathcal{X}^1, i), \mathrm{GL}(\mathfrak{K}, \mathbb{F})\big)$ which are related by conjugation. Without loss of generality, we can assume that $\rho = \tilde{\rho}$. Now, let $\mathcal{T}$ be a spanning tree of $\mathcal{X}$ with root i. Then for each vertex j of $\mathcal{X}$ there is an edge path $\gamma_{i,j}$ from the root i to the vertex j entirely contained in $\mathcal{T}$. Since $\mathcal{T}$ contains no loops, the path $\gamma_{i,j}$ is essentially unique, i.e. any two such paths differ by a sequence of elementary moves. Thus we can use the parallel transport to obtain bases $\{X_j^1, \ldots, X_j^{\mathfrak{K}}\} \subset \mathrm{E}_j$ and $\{\tilde{X}_j^1, \ldots, \tilde{X}_j^{\mathfrak{K}}\} \subset \tilde{\mathrm{E}}_j$ at every vertex j of $\mathcal{X}$. With respect to these bases the connections η and $\tilde{\eta}$ are represented by elements of $\mathrm{GL}(\mathfrak{K}, \mathbb{F})$. By construction, for each edge e in $\mathcal{T}$ the connection is represented by the identity matrix. Moreover, to each edge $e = jk$ not contained in $\mathcal{T}$ there corresponds a unique $[\gamma_e] \in \pi_1(\mathcal{X}^1, i)$. With the notation above, it is given by $\gamma_e = \gamma_{i,k}^{-1} e \, \gamma_{i,j}$. In particular, on the edge e both connections are represented by the same matrix $\rho([\gamma_e]) = \tilde{\rho}([\gamma_e])$. Thus, if we define $f : \mathrm{E} \to \tilde{\mathrm{E}}$ by $f(X_j^m) := \tilde{X}_j^m$ for $m = 1, \ldots, \mathfrak{K}$, we obtain an isomorphism, i.e. $\mathrm{E} \cong \tilde{\mathrm{E}}$. Hence F is injective.

To see that F is surjective we use $\mathcal{T}$ to equip the product bundle $\mathrm{E} := \mathcal{V} \times \mathbb{F}^{\mathfrak{K}}$ with a particular connection η. Let $\rho \in \mathrm{Hom}\big(\pi_1(\mathcal{X}^1, i), \mathrm{GL}(\mathfrak{K}, \mathbb{F})\big)$. If e lies in $\mathcal{T}$ we set $\eta_e = \mathrm{id}$ else we set $\eta_e := \rho([\gamma_e])$. By construction, $F([\mathrm{E}]) = [\rho]$. Thus F is surjective. □

Remark 4.4 Note that Theorem 4.3 can be regarded as a discrete analogue of a theorem of S. Kobayashi [10, 13], which states that the equivalence classes of connections on principal G-bundles over a manifold M are in one-to-one correspondence with the conjugacy classes of continuous homomorphisms from the *path group* $\Phi(\mathrm{M})$ to the structure group G. In fact, the fundamental group of the 1-skeleton is a discrete analogue of $\Phi(\mathrm{M})$.

5 Discrete Line Bundles—The Abelian Case

In this section we want to focus on *discrete line bundles*, i.e. discrete vector bundle of rank 1. Here the monodromy descends to a group homomorphism from the closed 1-chains to the multiplicative group $\mathbb{F}_* := \mathbb{F} \setminus \{0\}$ of the underlying field. This leads to a description by discrete differential forms (Sect. 6).

Let $\mathrm{L} \to \mathcal{X}$ be discrete $\mathbb{F}$-line bundle over a connected simplicial complex. In this case the structure group is just $\mathbb{F}_*$, which is abelian. Thus we obtain

$$\mathrm{Hom}\big(\pi_1(\mathcal{X}^1, i), \mathbb{F}_*)\big)/_\sim = \mathrm{Hom}\big(\pi_1(\mathcal{X}^1, i), \mathbb{F}_*\big).$$

$\mathrm{Hom}\big(\pi_1(\mathcal{X}^1, i), \mathbb{F}_*\big)$ carries a natural group structure. Moreover, the isomorphism classes of discrete line bundles over $\mathcal{X}$ form an abelian group. The group structure is given by the tensor product: For $[\mathrm{L}], [\tilde{\mathrm{L}}] \in \mathfrak{V}^1_{\mathbb{F}}(\mathcal{X})$, we have

$$[\mathrm{L}][\tilde{\mathrm{L}}] = [\mathrm{L} \otimes \tilde{\mathrm{L}}], \quad [\mathrm{L}]^{-1} = [\mathrm{L}^*].$$

The identity element is given by the trivial bundle. In the following we will denote the *group of isomorphism classes of* $\mathbb{F}$*-line bundles over* $\mathcal{X}$ by $\mathcal{L}^{\mathbb{F}}_{\mathcal{X}}$.

The map $F : \mathcal{L}^{\mathbb{F}}_{\mathcal{X}} \to \mathrm{Hom}\big(\pi_1(\mathcal{X}^1, i), \mathbb{F}_*\big)$, $[\mathrm{L}] \mapsto [\mathfrak{M}]$ is a group homomorphism. By Theorem 4.3, F is then an isomorphism.

Now, since $\mathbb{F}_*$ is abelian, each homomorphism $\rho \in \mathrm{Hom}\big(\pi_1(\mathcal{X}^1, i), \mathbb{F}_*\big)$ factors through the *abelianization*

$$\pi_1(\mathcal{X}^1, i)_{ab} = \pi_1(\mathcal{X}^1, i)/[\pi_1(\mathcal{X}^1, i), \pi_1(\mathcal{X}^1, i)],$$

i.e. for each $\rho \in \mathrm{Hom}\big(\pi_1(\mathcal{X}^1, i), \mathbb{F}_*\big)$ there is a unique $\rho_{ab} \in \mathrm{Hom}\big(\pi_1(\mathcal{X}^1, i)_{ab}, \mathbb{F}_*\big)$ such that

$$\rho = \rho_{ab} \circ \pi_{ab}.$$

Here $\pi_{ab} : \pi_1(\mathcal{X}^1, i) \to \pi_1(\mathcal{X}^1, i)_{ab}$ denotes the canonical projection. This yields an isomorphism between $\mathrm{Hom}\big(\pi_1(\mathcal{X}^1, i), \mathbb{F}_*\big)$ and $\mathrm{Hom}\big(\pi_1(\mathcal{X}^1, i)_{ab}, \mathbb{F}_*\big)$. In particular,

$$\mathcal{L}_{\mathcal{X}}^{\mathbb{F}} \cong \mathrm{Hom}\big(\pi_1(\mathcal{X}^1, i)_{ab}, \mathbb{F}_*\big).$$

As we will see below, the abelianization $\pi_1(\mathcal{X}^1, i)_{ab}$ is naturally isomorphic to the group of closed 1-chains.

The *group of k-chains* $\mathrm{C}_k(\mathcal{X}, \mathbb{Z})$ is defined as the free abelian group which is generated by the k-simplices of $\mathcal{X}$. More precisely, let $\mathcal{X}_k^{or}$ denote the *set of oriented k-simplices of* $\mathcal{X}$. Clearly, for $k > 0$, each k-simplex has two orientations. Interchanging these orientations yields a fixed-point-free involution $\rho_k : \mathcal{X}_k^{or} \to \mathcal{X}_k^{or}$. The group of k-chains is then explicitly given as follows:

$$\mathrm{C}_k(\mathcal{X}, \mathbb{Z}) := \big\{c : \mathcal{X}_k^{or} \to \mathbb{Z} \mid c \circ \rho_k = -c\big\}.$$

Since simplices of dimension zero have only one orientation, $\mathcal{X}_0^{or} = \mathcal{X}_0$. Thus,

$$\mathrm{C}_0(\mathcal{X}, \mathbb{Z}) := \big\{c : \mathcal{X}_k^{or} \to \mathbb{Z}\big\}.$$

It is common to identify an oriented k-simplex σ with its *elementary k-chain*, i.e. the chain which is 1 for σ, -1 for the oppositely oriented simplex and zero else. With this identification a k-chain c can be written as a formal sum of oriented k-simplices with integer coefficients:

$$c = \sum_{i=1}^{m} n_i \sigma_i, \quad n_i \in \mathbb{Z},\ \sigma_i \in \mathcal{X}_k^{or}.$$

The *boundary operator* $\partial_k : \mathrm{C}_k(\mathcal{X}, \mathbb{Z}) \to \mathrm{C}_{k-1}(\mathcal{X}, \mathbb{Z})$ is then the homomorphism which is uniquely determined by

$$\partial_k\, i_0 \cdots i_k = \sum_{j=0}^{k} (-1)^j\, i_0 \cdots \widehat{i_j} \cdots i_k.$$

It well-known that $\partial_k \circ \partial_{k+1} \equiv 0$. Thus we get a chain complex

$$0 \xleftarrow{\partial_0} \mathrm{C}_0(\mathcal{X}, \mathbb{Z}) \xleftarrow{\partial_1} \mathrm{C}_1(\mathcal{X}, \mathbb{Z}) \xleftarrow{\partial_2} \cdots \xleftarrow{\partial_k} \mathrm{C}_k(\mathcal{X}, \mathbb{Z}) \xleftarrow{\partial_{k+1}} \cdots .$$

The *simplicial Homology groups* $\mathrm{H}_k(\mathcal{X}, \mathbb{Z})$ may be regarded as a measure for the deviation of exactness:

$$\mathrm{H}_k(\mathcal{X}, \mathbb{Z}) := \ker \partial_k / \mathrm{im}\, \partial_{k+1}.$$

The elements of $\ker \partial_k$ are called *k-cycles*, those of $\mathrm{im}\, \partial_{k+1}$ are called *k-boundaries*.

It is a well-known fact that the abelianization of the first fundamental group is the first homology group (see e.g. [7]). Now, since the first homology of the 1-skeleton consists exactly of all closed chains of $\mathcal{X}$, we obtain

$$\pi_1(\mathcal{X}^1, i)_{ab} \cong \ker \partial_1.$$

The isomorphism is induced by the map $\pi_1(\mathcal{X}^1, i) \to \ker \partial_1$ given by $[\gamma] \mapsto \sum_j e_j$, where $\gamma = e_\ell \cdots e_1$. We summarize the above discussion in the following theorem.

Theorem 5.1 *The group of isomorphism classes of line bundles $\mathcal{L}_{\mathcal{X}}^{\mathbb{F}}$ is naturally isomorphic to the group* $\mathrm{Hom}(\ker \partial_1, \mathbb{F}_*)$*:*

$$\mathcal{L}_{\mathcal{X}}^{\mathbb{F}} \cong \mathrm{Hom}(\ker \partial_1, \mathbb{F}_*).$$

The isomorphism of Theorem 5.1 can be made explicit using discrete $\mathbb{F}_*$-valued 1-forms associated to the connection of a discrete line bundle.

6 Discrete Connection Forms

Throughout this section $\mathcal{X}$ denotes a connected simplicial complex.

Definition 6.1 Let $\mathfrak{G}$ be an abelian group. The *group of $\mathfrak{G}$-valued discrete k-forms* is defined as follows:

$$\Omega^k(\mathcal{X}, \mathfrak{G}) := \big\{\omega : \mathrm{C}_k(\mathcal{X}) \to \mathfrak{G} \mid \omega \text{ group homomorphism}\big\}.$$

The *discrete exterior derivative* d_k is then defined to be the adjoint of ∂_{k+1}, i.e.

$$d_k : \Omega^k(\mathcal{X}, \mathfrak{G}) \to \Omega^{k+1}(\mathcal{X}, \mathfrak{G}), \quad d_k\omega := \omega \circ \partial_{k+1}.$$

By construction, we immediately get that $d_{k+1} \circ d_k \equiv 0$. The corresponding cochain complex is called the *discrete de Rahm complex with coefficients in* $\mathfrak{G}$:

$$0 \to \Omega^0(\mathcal{X}, \mathfrak{G}) \xrightarrow{d_0} \Omega^1(\mathcal{X}, \mathfrak{G}) \xrightarrow{d_1} \cdots \xrightarrow{d_{k-1}} \Omega^k(\mathcal{X}, \mathfrak{G}) \xrightarrow{d_k} \cdots.$$

In analogy to the construction of the homology groups, the *k-th de Rahm Cohomology group* $\mathrm{H}^k(\mathcal{X}, \mathfrak{G})$ *with coefficients in* $\mathfrak{G}$ is defined as the quotient group

$$\mathrm{H}^k(\mathcal{X}, \mathfrak{G}) := \ker d_k / \mathrm{im}\, d_{k-1}.$$

The discrete k-forms in $\ker d_k$ are called *closed*, those in $\mathrm{im}\, d_{k-1}$ are called *exact*.

Now, let $\mathfrak{C}_{\mathrm{L}}$ denote the *space of connections* on the discrete $\mathbb{F}$-line bundle $\mathrm{L} \to \mathcal{X}$:

$$\mathfrak{C}_{\mathrm{L}} := \big\{\eta \mid \eta \textit{ connection on } \mathrm{L}\big\}.$$

Any two connections $\eta, \theta \in \mathfrak{C}_{\mathrm{L}}$ differ by a unique discrete 1-form $\omega \in \Omega^1(\mathcal{X}, \mathbb{F}_*)$:

$$\theta = \omega\eta.$$

Hence the group $\Omega^1(\mathcal{X}, \mathbb{F}_*)$ acts simply transitively on the space of connections $\mathfrak{C}_{\mathrm{L}}$. In particular, each choice of a *base connection* $\beta \in \mathfrak{C}_{\mathrm{L}}$ establishes an identification

$$\mathfrak{C}_{\mathrm{L}} \ni \eta = \omega\beta \longleftrightarrow \omega \in \Omega^1(\mathcal{X}, \mathbb{F}_*).$$

Remark 6.2 Note that each discrete vector bundle admits a trivial connection. To see this choose for each vertex a basis of the corresponding fiber. The corresponding coordinates establish an identification with the product bundle. Then there is a unique connection that makes the diagrams over all edges commute.

Definition 6.3 Let $\eta \in \mathfrak{C}_{\mathrm{L}}$. A *connection form representing the connection* η is a 1-form $\omega \in \Omega^1(\mathcal{X}, \mathbb{F}_*)$ such that $\eta = \omega\beta$ for some trivial base connection β.

Clearly, there are many connection forms representing a connection. We want to see how two such forms are related.

More generally, two connections η and θ in $\mathfrak{C}_{\mathrm{L}}$ lead to isomorphic discrete line bundles if and only if for each fiber there is a vector space isomorphism $f_i : \mathrm{L}_i \to \mathrm{L}_i$, such that for each edge ij:

$$\theta_{ij} \circ f_i = f_j \circ \eta_{ij}.$$

Since η_e and θ_e are linear, this boils down to discrete $\mathbb{F}_*$-valued functions and the relation characterizing an isomorphism becomes

$$\theta_{ij} = \big(g_j g_i^{-1}\big)\eta_{ij} = (dg)_{ij}\eta_{ij},$$

i.e. η and θ differ by an exact discrete $\mathbb{F}_*$-valued 1-form. In particular, the difference of two connection forms representing the same connection η is exact.

Thus we obtain a well-defined map sending a discrete line bundle L with connection to the corresponding equivalence class of connection forms

$$[\omega] \in \Omega^1(\mathcal{X}, \mathbb{F}_*)/d\Omega^0(\mathcal{X}, \mathbb{F}_*).$$

Theorem 6.4 *The map* $F : \mathcal{L}^{\mathbb{F}}_{\mathcal{X}} \to \Omega^1(\mathcal{X}, \mathbb{F}_*)/d\Omega^0(\mathcal{X}, \mathbb{F}_*)$, $[\mathrm{L}] \mapsto [\omega]$, *where* ω *is a connection form of* L, *is an isomorphism of groups.*

Proof Clearly, F is well-defined. Let L and $\tilde{\mathrm{L}}$ be two discrete complex line bundle with connections η and θ, respectively. If $\beta \in \mathfrak{C}_{\mathrm{L}}$ and $\tilde{\beta} \in \mathfrak{C}_{\tilde{\mathrm{L}}}$ are trivial, so is $\beta \otimes \tilde{\beta} \in \mathfrak{C}_{\mathrm{L}\otimes\tilde{\mathrm{L}}}$. Hence, with $\eta = \omega\beta$ and $\tilde{\eta} = \tilde{\omega}\tilde{\beta}$, we get

$$F([\mathrm{L} \otimes \tilde{\mathrm{L}}]) = [\omega\tilde{\omega}] = [\omega][\tilde{\omega}] = F([\mathrm{L}])F([\tilde{\mathrm{L}}]).$$

By the preceding discussion, F is injective. Surjectivity is also easily checked. □

Next we want to prove that the map given by

$$\Omega^1(\mathcal{X}, \mathbb{F}_*)/d\Omega^0(\mathcal{X}, \mathbb{F}_*) \ni [\omega] \mapsto \omega|_{\ker \partial_1} \in \mathrm{Hom}(\ker \partial_1, \mathbb{F}_*)$$

is a group isomorphism. Clearly, it is a well-defined group homomorphism. We show its bijectivity in two steps. First, the surjectivity is provided by the following

Lemma 6.5 *Let $\mathcal{X}$ be a simplicial complex and $\mathfrak{G}$ be an abelian group. Then the restriction map $\Phi : \Omega^k(\mathcal{X}, \mathfrak{G}) \to \mathrm{Hom}(\ker \partial_k, \mathfrak{G})$, $\omega \mapsto \omega|_{\ker \partial_k}$ is surjective.*

Proof If we choose an orientation for each simplex in $\mathcal{X}$, then ∂_k is given by an integer matrix. Now, there is a unimodular matrix U such that $\partial_k U = (0|H)$ has Hermite normal form. Write $U = (A|B)$, where $\partial_k A = 0$ and $\partial_k B = H$ and let a_i denote the columns of A, i.e. $A = (a_1, \ldots, a_\ell)$. Clearly, $a_i \in \ker \partial_k$. Moreover, if $c \in \ker \partial_k$, then $0 = \partial_k c = (0|H)U^{-1}c$. Hence $U^{-1}c = (q, 0)^\top$, $q \in \mathbb{Z}^\ell$, and thus $c = Aq$. Therefore $\{a_i \mid i = 1, \ldots, \ell\}$ is a basis of $\ker \partial_k$. Now, let $\mu \in \mathrm{Hom}(\ker \partial_k, \mathbb{Z})$. A homomorphism is completely determined by its values on a basis. We define $\omega = (\mu(a_1), \ldots, \mu(a_\ell), 0 \ldots, 0)U^{-1}$. Then $\omega \in \Omega^k(\mathcal{X}, \mathbb{Z})$ and $\omega A = (\mu(a_1), \ldots, \mu(a_\ell))$. Hence $\Phi(\omega) = \mu$ and Φ is surjective for forms with coefficients in $\mathbb{Z}$. Now, let $\mathfrak{G}$ be an arbitrary abelian group. And $\mu \in \mathrm{Hom}(\ker \partial_k, \mathfrak{G})$. Now, if $a_1, .., a_\ell$ is an arbitrary basis of $\ker \partial_k$, then there are forms $\omega_1, \ldots, \omega_\ell \in \Omega^k(\mathcal{X}, \mathbb{Z})$ such that $\omega_i(a_j) = \delta_{ij}$. Since $\mathbb{Z}$ acts on $\mathfrak{G}$, we can multiply ω_i with elements $g \in \mathfrak{G}$ to obtain forms with coefficients in $\mathfrak{G}$. Now, set $\omega = \sum_{i=1}^{\ell} \omega_i \cdot \mu(a_i)$. Then $\omega \in \Omega^k(\mathcal{X}, \mathfrak{G})$ and $\omega(a_i) = \mu(a_i)$ for $i = 1, \ldots, \ell$. Thus $\Phi(\omega) = \mu$. Hence Φ is surjective for forms with coefficients in arbitrary abelian groups. □

The injectivity is actually easy to see: If $\omega|_{\ker \partial_1} = 0$, we define an $\mathbb{F}_*$-valued function f by *integration along paths*: Fix some vertex i. Then

$$f(j) := \int_\gamma \omega := \sum_{e \in \gamma} \omega(e),$$

where γ is some path joining i to j. Since $\omega|_{\ker \partial_1} = 0$, the value $f(j)$ does not depend on the choice of the path γ. Moreover, $df = \omega$. Together with Lemma 6.5, this yields the following theorem.

Theorem 6.6 *The map $F : \Omega^1(\mathcal{X}, \mathbb{F}_*)/d\Omega^0(\mathcal{X}, \mathbb{F}_*) \to \mathrm{Hom}(\ker \partial_1, \mathbb{F}_*)$ given by $[\omega] \mapsto \omega|_{\ker \partial_1}$ is an isomorphism of groups.*

Now, let us relate this to Theorem 5.1. Let $\mathrm{L} \to \mathcal{X}$ be a line bundle with connection η and ω be a connection form representing η, i.e. $\eta = \omega\beta$ for some trivial base connection β. Let $[\gamma] \in \pi_1(\mathcal{X}^1, i)$, where $\gamma = e_\ell \cdots e_1$. By linearity and since trivial connections have vanishing monodromy, we obtain

$$\mathfrak{M}([\gamma]) = \eta_{e_\ell} \circ \cdots \circ \eta_{e_1} = \omega_{e_\ell} \cdots \omega_{e_1} \cdot \beta_{e_\ell} \circ \cdots \circ \beta_{e_1} = \omega(\pi_{ab}([\gamma])) \cdot \mathrm{id}|_{\mathrm{L}_i} .$$

Hence, by the uniqueness of $[\mathfrak{M}]_{ab}$, we obtain the following theorem that brings everything nicely together.

Theorem 6.7 *Let $\mathrm{L} \to \mathcal{X}$ be a line bundle with connection η. Let $\mathfrak{M}$ denote its monodromy and let ω be some connection form representing η. Then, with the identifications above,*

$$[\mathfrak{M}]_{ab} = [\omega].$$

7 Curvature—A Discrete Analogue of Weil's Theorem

In this section we describe complex and hermitian line bundles by their curvature. For the first time we use more than the 1-skeleton.

Let $\mathcal{X}$ be a connected simplicial complex and $\mathfrak{G}$ an abelian group. Since $d^2 = 0$, the exterior derivative descends to a well-defined map on $\Omega^k(\mathcal{X}, \mathfrak{G})/d\Omega^{k-1}(\mathcal{X}, \mathfrak{G})$, which again will be denoted by d. Explicitly,

$$d : \Omega^k(\mathcal{X}, \mathfrak{G})/d\Omega^{k-1}(\mathcal{X}, \mathfrak{G}) \to \Omega^{k+1}(\mathcal{X}, \mathfrak{G}), \quad [\omega] \mapsto d\omega.$$

Definition 7.1 The $\mathbb{F}_*$-*curvature* of a discrete $\mathbb{F}$-line bundle $\mathrm{L} \to \mathcal{X}$ is the discrete 2-form $\Omega \in \Omega^2(\mathcal{X}, \mathbb{F}_*)$ given by

$$\Omega = d[\omega],$$

where $[\omega] \in \Omega^1(\mathcal{X}, \mathbb{F}_*)/d\Omega^0(\mathcal{X}, \mathbb{F}_*)$ represents the isomorphism class [L].

Remark 7.2 Note that Ω just encodes the parallel transport along the boundary of the oriented 2-simplices of $\mathcal{X}$—the "local monodromy".

From the definition it is obvious that the $\mathbb{F}_*$-curvature is invariant under isomorphisms. Thus, given a prescribed 2-form $\Omega \in \Omega^2(\mathcal{X}, \mathbb{F}_*)$, it is a natural question to ask how many non-isomorphic line bundles have curvature Ω.

Actually, this question is answered easily: If $d[\omega] = \Omega = d[\tilde{\omega}]$, then the difference of ω and $\tilde{\omega}$ is closed. Factoring out the exact 1-forms we see that the space of non-isomorphic line bundles with curvature Ω can be parameterized by the first

cohomology group $\mathrm{H}^1(\mathcal{X}, \mathbb{F}_*)$. Furthermore, the existence of a line bundle with curvature $\Omega \in \Omega^2(\mathcal{X}, \mathbb{F}_*)$ is equivalent to the exactness of Ω.

But when is a k-form Ω exact? Certainly it must be closed. Even more, it must vanish on every closed k-chain: If $\Omega = \operatorname{im} d$ and S is a closed k-chain, then

$$\Omega(S) = d\omega(S) = \omega(\partial S) = 0.$$

For $k = 1$, as we have seen, this criterion is sufficient for exactness. For $k > 1$ this is not true with coefficients in arbitrary groups.

Example 7.3 Consider a triangulation $\mathcal{X}$ of the real projective plane $\mathbb{R}\mathrm{P}^2$. The zero-chain is the only closed 2-chain and hence each $\mathbb{Z}_2$-valued 2-form vanishes on every closed 2-chain. But $\mathrm{H}^2(\mathcal{X}, \mathbb{Z}_2) = \mathbb{Z}_2$ and hence there exists a non-exact 2-form.

In the following we will see that this cannot happen for fields of characteristic zero or, more generally, for groups that arise as the image of such fields.

Clearly, there is a natural pairing of $\mathbb{Z}$-modules between $\Omega^k(\mathcal{X}, \mathfrak{G})$ and $\mathrm{C}_k(\mathcal{X}, \mathbb{Z})$:

$$\langle ., . \rangle : \Omega^k(\mathcal{X}, \mathfrak{G}) \times \mathrm{C}_k(\mathcal{X}, \mathbb{Z}) \to \mathfrak{G}, \quad (\omega, c) \mapsto \omega(c).$$

This pairing is degenerate if and only if all elements of $\mathfrak{G}$ have bounded order. In particular, if $\mathfrak{G}$ is a field $\mathbb{F}$ of characteristic zero, $\langle ., . \rangle$ yields a group homomorphism

$$F_k : \mathrm{C}_k(\mathcal{X}, \mathbb{Z}) \to \mathrm{Hom}_{\mathbb{F}}(\Omega^k(\mathcal{X}, \mathbb{F}), \mathbb{F}) = (\Omega^k(\mathcal{X}, \mathbb{F}))^*.$$

A basis of $\mathrm{C}_k(\mathcal{X}, \mathbb{Z})$ is mapped under F_k to a basis of $(\Omega^k(\mathcal{X}, \mathbb{F}))^*$ and hence $\mathrm{C}_k(\mathcal{X}, \mathbb{Z})$ appears as an n_k-dimensional lattice in $(\Omega^k(\mathcal{X}, \mathbb{F}))^*$.

Let d_k^* denote the adjoint of the discrete exterior derivative d_k with respect to the natural pairing between $\Omega^k(\mathcal{X}, \mathbb{F})$ and $(\Omega^k(\mathcal{X}, \mathbb{F}))^*$. Clearly,

$$d_k^* \circ F_k = F_k \circ \partial_{k+1}.$$

Now, since the simplicial complex is finite, we can choose bases of $\mathrm{C}_k(\mathcal{X}, \mathbb{Z})$ for all k. This in turn yields bases of $(\Omega^k(\mathcal{X}, \mathbb{F}))^*$ and hence, by duality, bases of $\Omega^k(\mathcal{X}, \mathbb{F})$. With respect to these bases we have

$$\mathrm{C}_k(\mathcal{X}, \mathbb{Z}) = \mathbb{Z}^{n_k} \subset \mathbb{F}^{n_k} = (\Omega^k(\mathcal{X}, \mathbb{F}))^* = \Omega^k(\mathcal{X}, \mathbb{F}), \tag{3}$$

where n_k denotes the number of k-simplices. Moreover, the pairing is represented by the standard product. The operator $d_{k-1}^* = \partial_k$ is then just an integer matrix and

$$\partial_k = d_{k-1}^\top.$$

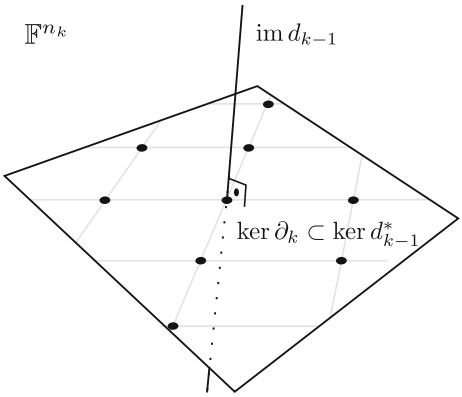

Fig. 6 With the identifications (3), the space of k-forms becomes a direct sum of the image of d_{k-1} and the kernel of its adjoint d_{k-1}^*, the latter of which contains the closed k-chains as a lattice

We have $\operatorname{im} d_{k-1} \perp \ker d_{k-1}^*$. Moreover, by the rank-nullity theorem,

$$n_k = \dim \operatorname{im} d_{k-1}^* + \dim \ker d_{k-1}^* = \dim \operatorname{im} d_{k-1} + \dim \ker d_{k-1}^*.$$

Hence, under the identifications above, we have that $\mathbb{F}^{n_k} = \operatorname{im} d_{k-1} \oplus_\perp \ker d_{k-1}^*$ (see Fig. 6). Moreover, $\ker \partial_k$ contains a basis of $\ker d_{k-1}^*$. From this we conclude immediately the following lemma.

Lemma 7.4 *Let $\omega \in \Omega^k(\mathcal{X}, \mathbb{F})$, where $\mathbb{F}$ is a field of characteristic zero. Then*

$$\omega \in \operatorname{im} d_{k-1} \iff \langle \omega, c \rangle = 0 \text{ for all } c \in \ker \partial_k.$$

Remark 7.5 Note, that for boundary cycles the condition is nothing but the closedness of the form ω. Thus Lemma 7.4 states that a closed form $\omega \in \Omega^k(\mathcal{X}, \mathbb{F})$ is exact if and only if the integral over all homology classes $[c] \in \mathrm{H}_k(\mathcal{X}, \mathbb{Z})$ vanishes.

Let $\mathfrak{G}$ be an abelian group. The sequence below will be referred to as the *k-th fundamental sequence of forms with coefficients in $\mathfrak{G}$*:

$$\Omega^{k-1}(\mathcal{X}, \mathfrak{G}) \xrightarrow{d_{k-1}} \Omega^k(\mathcal{X}, \mathfrak{G}) \xrightarrow{\Phi_k} \operatorname{Hom}(\ker \partial_k, \mathfrak{G}) \to 0,$$

where Φ_k denotes the restriction to the kernel of ∂_k, i.e. $\Phi_k(\omega) := \omega|_{\ker \partial_k}$.

Combining Lemmas 6.5 and 7.4 we obtain that the fundamental sequence with coefficients in a field $\mathbb{F}$ of characteristic zero is exact for all $k > 1$. This serves as an anchor point. The exactness propagates under surjective group homomorphisms.

Lemma 7.6 *Let $\mathfrak{A} \xrightarrow{f} \mathfrak{B} \to 0$ be a an exact sequence of abelian groups. Then, if the k-th fundamental sequence of forms is exact with coefficients in $\mathfrak{A}$, so it is with coefficients in $\mathfrak{B}$.*

Proof By Lemma 6.5 the restriction map Φ_k is surjective for every abelian group. It is left to check that $\ker \Phi_k = \operatorname{im} d_{k-1}$ with coefficients in $\mathfrak{B}$. Let $\Omega \in \Omega^k(\mathcal{X}, \mathfrak{B})$ such that $\Phi_k(\Omega) = 0$. Since $f : \mathfrak{A} \to \mathfrak{B}$ is surjective, there is a form $\Xi \in \Omega^k(\mathcal{X}, \mathfrak{A})$ such that $\Omega = f \circ \Xi$. Since $0 = \Phi_k(\Omega) = f \circ \Phi_k(\Xi)$, we obtain that $\Phi_k(\Xi)$ takes its values in $\ker f$. Since Φ_k is surjective for arbitrary groups, there is $\Theta \in \Omega^k(\mathcal{X}, \ker f)$ such that $\Phi_k(\Xi) = \Phi_k(\Theta)$. Hence $\Phi_k(\Xi - \Theta) = 0$. Thus there is a form $\xi \in \Omega^{k-1}(\mathcal{X}, \mathfrak{A})$ such that $d_{k-1}\xi = \Xi - \Theta$. Now, let $\omega := f \circ \xi \in \Omega^{k-1}(\mathcal{X}, \mathfrak{B})$. Then

$$d_{k-1}\omega = d_{k-1} f \circ \xi = f \circ d_{k-1}\xi = f \circ (\Xi - \Theta) = f \circ \Xi = \Omega.$$

Hence $\ker \Phi_k = \operatorname{im} d_{k-1}$ and the sequence (with coefficients in $\mathfrak{B}$) is exact. □

Remark 7.7 The map $f : \mathbb{C} \to \mathbb{C}$, $z \mapsto \exp(2\pi\imath\, z)$ provides a surjective group homomorphism from $\mathbb{C}$ onto $\mathbb{C}_*$, and similarly from $\mathbb{R}$ onto $\mathbb{S}$. Hence the k-th fundamental sequence of forms is exact for coefficients in $\mathbb{C}_*$ and in the unit circle $\mathbb{S}$.

Remark 7.8 The k-th fundamental sequence with coefficients in an abelian group $\mathfrak{G}$ is exact if and only if $\Omega^k(\mathcal{X}, \mathfrak{G})/d\Omega^{k-1}(\mathcal{X}, \mathfrak{G}) \cong \operatorname{Hom}(\ker \partial_k, \mathfrak{G})$. The isomorphism is induced by the restriction map Φ_k.

The following corollary is a consequence of Remark 7.7. It nicely displays the fibration of the complex line bundles by their $\mathbb{C}_*$-curvature.

Corollary 7.9 *For $\mathfrak{G} = \mathbb{S}$, $\mathbb{C}_*$ the following sequence is exact:*

$$1 \to \mathrm{H}^1(\mathcal{X}, \mathfrak{G}) \hookrightarrow \Omega^1(\mathcal{X}, \mathfrak{G})/d\Omega^0(\mathcal{X}, \mathfrak{G}) \xrightarrow{d} \Omega^2(\mathcal{X}, \mathfrak{G}) \to \operatorname{Hom}(\ker \partial_2, \mathfrak{G}) \to 1.$$

Definition 7.10 Let $\Omega^* \in \Omega^k(\mathcal{X}, \mathbb{S})$. A real-valued form $\Omega \in \Omega^2(\mathcal{X}, \mathbb{R})$ is called *compatible with Ω^** if $\Omega^* = \exp(\imath\, \Omega)$. A *discrete hermitian line bundle with curvature* is a discrete hermitian line bundle L with connection equipped with a closed 2-form compatible with the $\mathbb{S}$-curvature of L.

For real-valued forms it is common to denote the natural pairing with the k-chains by an integral sign, i.e. for $\omega \in \Omega^k(\mathcal{X}, \mathbb{R})$ and $c \in \mathrm{C}_k(\mathcal{X}, \mathbb{Z})$ we write

$$\int_c \omega := \langle \omega, c \rangle = \omega(c).$$

Theorem 7.11 *Let* L *be a discrete hermitian line bundle with curvature Ω. Then Ω is integral, i.e.*

$$\int_c \Omega \in 2\pi\,\mathbb{Z}, \quad \textit{for all } c \in \ker \partial_2.$$

Proof By definition the curvature form Ω satisfies $\exp(\imath\Omega) = d\omega$ for some connection form $\omega \in \Omega^1(\mathcal{X}, \mathbb{S})$. Thus, if $c \in \ker \partial_2$,

$$\exp\Big(\imath \int_c \Omega\Big) = \langle \exp(\imath\Omega), c\rangle = \langle d\omega, c\rangle = \langle \omega, \partial c\rangle = 1.$$

This proves the claim. □

Conversely, Corollary 7.9 yields a discrete version of a theorem of André Weil [11, 18], which states that any closed smooth integral 2-form on a manifold M can be realized as the curvature of a hermitian line bundle. This plays a prominent role in the process of prequantization [17].

Theorem 7.12 *If $\Omega \in \Omega^2(\mathcal{X}, \mathbb{R})$ is integral, then there exists a hermitian line bundle with curvature Ω.*

Proof Consider $\Omega^* := \exp(i\Omega)$. Since Ω is integral, $\langle \Omega^*, c\rangle = 1$ for all $c \in \ker \partial_2$. By Corollary 7.9, there exists $r \in \Omega^1(\mathcal{X}, \mathbb{S})$ such that $dr = \Omega^*$. This in turn defines a hermitian line bundle with curvature Ω. □

Remark 7.13 Moreover, Corollary 7.9 shows that the connections of two such bundles differ by an element of $\mathrm{H}^1(\mathcal{X}, \mathbb{S})$. Thus the space of discrete hermitian line bundles with fixed curvature Ω can be parameterized by $\mathrm{H}^1(\mathcal{X}, \mathbb{S})$.

8 The Index Formula for Hermitian Line Bundles

Before we define the degree of a discrete hermitian line bundle with curvature or the index form of a section, let us first recall the situation in the smooth setting. Therefore, let $\mathrm{L} \to \mathrm{M}$ be a smooth hermitian line bundle with connection. Since the curvature tensor R^∇ of ∇ is a 2-form taking values in the skew-symmetric endomorphisms of L, it is completely described by a closed real-valued 2-form $\Omega \in \Omega^2(\mathrm{M}, \mathbb{R})$,

$$R^\nabla = -\imath\Omega.$$

The following theorem shows an interesting relation between the index sum of a section $\psi \in \Gamma(\mathrm{L})$, the curvature 2-form Ω, and the *rotation form* ξ^ψ *of* ψ. This form is defined as follows:

$$\xi^\psi := \frac{\langle \nabla\psi, \imath\psi\rangle}{\langle \psi, \psi\rangle}.$$

Theorem 8.1 *Let* $\mathrm{L} \to \mathrm{M}$ *be a smooth hermitian line bundle with connection and* Ω *its curvature* 2*-form. Let* $\psi \in \Gamma(\mathrm{L})$ *be a section with a discrete zero set* Z*. Then, if* C *is a finite smooth* 2*-chain such that* $\partial C \cap Z = \emptyset$*,*

$$2\pi \sum_{p \in C \cap Z} \mathrm{ind}_p^\psi = \int_{\partial C} \xi^\psi + \int_C \Omega.$$

Proof We can assume that C is a single smooth triangle. Then we can express ψ on C in terms of a complex-valued function z and a pointwise-normalized local section ϕ, i.e. $\psi = z\,\phi$. Since $\mathrm{Im}(\frac{dz}{z}) = d\arg(z)$, we obtain

$$\xi^\psi = \frac{1}{|z|^2}\langle dz\,\phi + z\,\nabla\phi, \imath z\,\phi\rangle = \langle \frac{dz}{z}\,\phi, \imath\phi\rangle + \langle \nabla\phi, \imath\phi\rangle = d\arg(z) + \langle \nabla\phi, \imath\phi\rangle.$$

Moreover, away from zeros, we have

$$d\langle \nabla\phi, \imath\phi\rangle = \langle R^\nabla\phi, \imath\phi\rangle + \langle \nabla\phi \wedge \imath\nabla\phi\rangle = \langle R^\nabla\phi, \imath\phi\rangle = -\Omega.$$

Hence we obtain

$$\int_{\partial C} \xi^\psi = \int_{\partial C} d\arg(z) + \int_{\partial C} \langle \nabla\phi, \imath\phi\rangle = 2\pi \sum_{p \in C \cap Z} \mathrm{index}_p(\psi) - \int_C \Omega.$$

This proves the claim. □

In the case that L is a hermitian line bundle with connection over a closed oriented surface M, Theorem 8.1 tells us that $\int_\mathrm{M} \Omega \in 2\pi\mathbb{Z}$. This yields a well-known topological invariant—the *degree of* L:

$$\deg(\mathrm{L}) := \frac{1}{2\pi}\int_\mathrm{M} \Omega.$$

From Theorem 8.1 we immediately obtain the famous Poincaré-Hopf index theorem.

Theorem 8.2 *Let* $\mathrm{L} \to \mathrm{M}$ *be a smooth hermitian line bundle over a closed oriented surface. Then, if* $\psi \in \Gamma(\mathrm{L})$ *is a section with isolated zeros,*

$$\deg(\mathrm{L}) = \sum_{p \in \mathrm{M}} \mathrm{ind}_p^\psi.$$

Now, let us consider the discrete case. In general, a *section* of a discrete vector bundle $\mathrm{E} \to \mathcal{X}$ with vertex set $\mathcal{V}$ is a map $\psi : \mathcal{V} \to \mathrm{E}$ such that the following diagram commutes

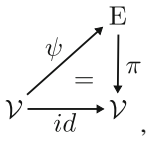

i.e. $\pi \circ \psi = id$. As in the smooth case, the space of sections of E is denoted by $\Gamma(\mathrm{E})$.

Now, let $\mathrm{L} \to \mathcal{X}$ be a discrete hermitian line bundle with curvature Ω and let $\psi \in \Gamma(\mathrm{L})$ be a nowhere-vanishing section such that

$$\eta_{ij}(\psi_i) \neq -\psi_j \tag{4}$$

for each edge ij of $\mathcal{X}$. Here η denotes the connection of L as usual. The *rotation form* ξ^ψ of ψ is then defined as follows:

$$\xi^\psi_{ij} := \arg\Big(\frac{\psi_j}{\eta_{ij}(\psi_i)}\Big) \in (-\pi, \pi).$$

Remark 8.3 Equation (4) can be interpreted as the condition that no zero lies in the 1-skeleton of $\mathcal{X}$ (compare Sect. 11). Actually, given a consistent choice of the argument on each oriented edge, we could drop this condition. Figuratively speaking, if a section has a zero in the 1-skeleton, then we decide whether we push it to the left or the right face of the edge.

Now we can define the *index form* of a discrete section:

Definition 8.4 Let $\mathrm{L} \to \mathcal{X}$ be a discrete hermitian line bundle with curvature Ω. For $\psi \in \Gamma(\mathrm{L})$, we define the *index form of* ψ by

$$\mathrm{ind}^\psi := \frac{1}{2\pi}\big(d\xi^\psi + \Omega\big).$$

Theorem 8.5 *The index form of a nowhere-vanishing discrete section is $\mathbb{Z}$-valued.*

Proof Let L be a discrete hermitian line bundle with curvature and let η be its connection. Let $\psi \in \Gamma(\mathrm{L})$ be a nowhere-vanishing section. Now, choose a connection form ω, i.e. $\eta = \omega\beta$, where β is a trivial connection on L. Then we can write ψ with respect to a non-vanishing parallel section ϕ of β, i.e. there is a $\mathbb{C}$-valued function z such that $\psi = z\phi$. Then $\xi^\psi_{ij} = \arg\big(\frac{z_j}{\omega_{ij} z_i}\big)$ and thus

$$\exp\big(2\pi\imath\, d\xi^\psi_{ijk}\big) = \exp\big(\imath\, \arg\big(\frac{z_i}{\omega_{ki} z_k}\big) + \imath\, \arg\big(\frac{z_j}{\omega_{ij} z_i}\big) + \imath\, \arg\big(\frac{z_k}{\omega_{jk} z_j}\big)\big) = \frac{1}{d\omega_{ijk}}.$$

Thus

$$\exp\bigl(2\pi\imath\,\mathrm{ind}_{ijk}^{\psi}\bigr) = \frac{\exp\bigl(\imath\,\Omega_{ijk}\bigr)}{d\omega_{ijk}} = 1.$$

This proves the claim. □

If L is a discrete hermitian line bundle with curvature Ω over a closed oriented surface $\mathcal{X}$, then we define the *degree of* L just as in the smooth case:

$$\deg\bigl(\mathrm{L}\bigr) := \frac{1}{2\pi}\int_{\mathcal{X}} \Omega.$$

Here we have identified $\mathcal{X}$ by the corresponding closed 2-chain. From Theorem 7.11 we obtain the following corollary.

Corollary 8.6 *The degree of a discrete hermitian line bundle with curvature is an integer:*

$$\deg\bigl(\mathrm{L}\bigr) \in \mathbb{Z}.$$

The discrete Poincaré-Hopf index theorem follows easily from the definitions:

Theorem 8.7 *Let* $\mathrm{L} \to \mathcal{X}$ *be a discrete hermitian line bundle with curvature* Ω *over an oriented simplicial surface. If* $\psi \in \Gamma(\mathrm{L})$ *is a non-vanishing discrete section, then*

$$\deg\bigl(\mathrm{L}\bigr) = \sum_{ijk\in\mathcal{X}} \mathrm{ind}_{ijk}^{\psi}.$$

Proof Since the integral of an exact form over a closed oriented surface vanishes,

$$2\pi\deg\bigl(\mathrm{L}\bigr) = \int_{\mathcal{X}} \Omega = \int_{\mathcal{X}} d\xi^{\psi} + \Omega = 2\pi \sum_{ijk\in\mathcal{X}} \mathrm{ind}_{ijk}^{\psi},$$

as was claimed. □

9 Piecewise-Smooth Vector Bundles over Simplicial Complexes

It is well-known that each abstract simplicial complex $\mathcal{X}$ has a geometric realization which is unique up to simplicial isomorphism. In particular, each abstract simplex is realized as an affine simplex. Moreover, each face σ' of a simplex $\sigma \in \mathcal{X}$ comes with an affine embedding

$$\iota_{\sigma'\sigma} : \sigma' \hookrightarrow \sigma.$$

In the following, we will not distinguish between the abstract simplicial complex and its geometric realization.

Definition 9.1 A piecewise-smooth vector bundle E over a simplicial complex $\mathcal{X}$ is a topological vector bundle $\pi : \mathrm{E} \to \mathcal{X}$ such that

(a) for each $\sigma \in \mathcal{X}$ the restriction $\mathrm{E}_\sigma := \mathrm{E}|_\sigma$ is a smooth vector bundle over σ,
(b) for each face σ' of $\sigma \in \mathcal{X}$, the inclusion $\mathrm{E}_{\sigma'} \hookrightarrow \mathrm{E}_\sigma$ is a smooth embedding.

As a simplicial complex, $\mathcal{X}$ has no tangent bundle. Nonetheless, differential forms survive as collections of smooth differential forms defined on the simplices which are compatible in the sense that they agree on common faces:

Definition 9.2 Let E be a piecewise-smooth vector bundle over $\mathcal{X}$. An E-valued differential k-form is a collection $\omega = \{\omega_\sigma \in \Omega^k(\sigma, \mathrm{E}_\sigma)\}_{\sigma\in\mathcal{X}}$ such that for each face σ' of a simplex $\sigma \in \mathcal{X}$ the following relation holds:

$$\iota^*_{\sigma'\sigma}\omega_\sigma = \omega_{\sigma'},$$

where $\iota_{\sigma'\sigma} : \sigma' \hookrightarrow \sigma$ denotes the inclusion. The space of E-valued differential k-forms is denoted by $\Omega^k_{ps}(\mathcal{X}, \mathrm{E})$.

Remark 9.3 Note that a 0-form defines a continuous map on the simplicial complex. Hence the definition includes functions and, more generally, sections: A piecewise-smooth section of E is a continuous section $\psi : \mathcal{X} \to \mathrm{E}$ such that for each simplex $\sigma \in \mathcal{X}$ the restriction $\psi_\sigma := \psi|_\sigma : \sigma \to \mathrm{E}_\sigma$ is smooth, i.e.

$$\Gamma_{ps}(\mathrm{E}) := \big\{\psi : \mathcal{X} \to \mathrm{E} \mid \psi_\sigma \in \Gamma(\mathrm{E}_\sigma) \textit{ for all } \sigma \in \mathcal{X}\big\}.$$

Since the pullback commutes with the wedge-product $\wedge$ and the exterior derivative d of real-valued forms, we can define the wedge product and the exterior derivative of piecewise-smooth differential forms by applying it componentwise.

Definition 9.4 For $\omega = \{\omega_\sigma\}_{\sigma\in\mathcal{X}} \in \Omega^k_{ps}(\mathcal{X}, \mathbb{R})$, $\eta = \{\eta_\sigma\}_{\sigma\in\mathcal{X}} \in \Omega^\ell_{ps}(\mathcal{X}, \mathbb{R})$,

$$\omega \wedge \eta := \{\omega_\sigma \wedge \eta_\sigma\}_{\sigma\in\mathcal{X}}, \quad d\omega := \{d\omega_\sigma\}_{\sigma\in\mathcal{X}}.$$

All the standard properties of $\wedge$ and d also hold in the piecewise-smooth case.

Definition 9.5 A *connection* on a piecewise-smooth vector bundle E over $\mathcal{X}$ is a linear map $\nabla : \Gamma_{ps}(\mathrm{E}) \to \Omega^1_{ps}(\mathcal{X}, \mathrm{E})$ such that

$$\nabla(f\psi) = df\,\psi + f\,\nabla\psi, \quad \textit{for all } f \in \Omega^0_{ps}(\mathcal{X}, \mathbb{R}),\ \psi \in \Gamma_{ps}(\mathrm{E}).$$

Once we have a connection on a smooth vector bundle we obtain a corresponding exterior derivative d^∇ on E-valued forms.

Theorem 9.6 *Let* E *be a piecewise-smooth vector bundle over* $\mathcal{X}$*. Then there is a unique linear map* $d^\nabla : \Omega^k_{ps}(\mathcal{X}, \mathrm{E}) \to \Omega^{k+1}_{ps}(\mathcal{X}, \mathrm{E})$ *such that* $d^\nabla \psi = \nabla\psi$ *for all* $\psi \in \Gamma_{ps}(\mathrm{E})$ *and*

$$d^\nabla(\omega \wedge \eta) = d\omega \wedge \eta + (-1)^k \omega \wedge d^\nabla \eta$$

for all $\omega \in \Omega^k_{ps}(\mathcal{X}, \mathbb{R})$ *and* $\eta \in \Omega^\ell_{ps}(\mathcal{X}, \mathrm{E})$.

The curvature tensor survives as a piecewise-smooth End(E)-valued 2-form:

Definition 9.7 Let $\mathrm{E} \to \mathcal{X}$ be a piecewise-smooth vector bundle. The endomorphism-valued curvature 2-form of a connection ∇ on E is defined as follows:

$$d^\nabla \circ d^\nabla \in \Omega^2_{ps}(\mathcal{X}, \mathrm{End}(\mathrm{E})).$$

10 The Associated Piecewise-Smooth Hermitian Line Bundle

Let $\tilde{\mathrm{L}} \to \mathcal{X}$ be a piecewise-smooth hermitian line bundle with connection ∇ over a simplicial complex. Just as in the smooth case the endomorphism-valued curvature 2-form takes values in the skew-adjoint endomorphisms and hence is given by a piecewise-smooth real-valued 2-form $\tilde{\Omega}$:

$$d^\nabla \circ d^\nabla = -\imath\,\tilde{\Omega}.$$

Since each simplex of $\mathcal{X}$ has an affine structure, we can speak of piecewise-constant forms.

The goal of this section will be to construct for each discrete hermitian line bundle with curvature a piecewise-smooth hermitian line bundle with piecewise-constant curvature which in a certain sense naturally contains the discrete bundle. We first prove two lemmata.

Lemma 10.1 *To each closed discrete real-valued* k*-form* ω *there corresponds a unique piecewise-constant piecewise-smooth* k*-form* $\tilde{\omega}$ *such that*

$$\omega(c) = \int_c \tilde{\omega}, \quad \text{for all } c \in \mathrm{C}_k(\mathcal{X}, \mathbb{Z}).$$

The form $\tilde{\omega}$ *will be called the piecewise-smooth form associated to* ω.

Proof It is enough to consider just a single n-simplex σ. We denote the space of piecewise-constant piecewise-smooth k-forms on σ by Ω^k_c and the space of discrete

k-forms on σ by Ω_d^k. Consider the linear map $F : \Omega_c^k \to \Omega_d^k$ that assigns to $\tilde{\omega} \in \Omega_c^k$ the discrete k-form given by

$$F(\tilde{\omega})_{\sigma'} := \int_{\sigma'} \tilde{\omega}.$$

Clearly, F is injective. Moreover, since each piecewise-constant piecewise-smooth form is closed, we have im $F \subset \ker d_k$, where d_k denotes the discrete exterior derivative. Hence it is enough to show that the space of closed discrete k-forms on σ is of dimension $\binom{n}{k}$. This we do by induction. Clearly, $\dim \ker d_0 = 1 = \binom{n}{0}$. Now suppose that $\dim \ker d_{k-1} = \binom{n}{k-1}$. By Lemma 7.4, we have $\ker d_k = \operatorname{im} d_{k-1}$. Hence

$$\dim \ker d_k = \dim \operatorname{im} d_{k-1} = \dim \Omega_d^k - \dim \ker d_{k-1} = \binom{n+1}{k} - \binom{n}{k-1} = \binom{n}{k}.$$

Therefore, for each closed discrete k-form we obtain a unique piecewise-constant piecewise-smooth k-form which has the desired integrals on the k-simplices. □

It is a classical result that on star-shaped domains $U \subset \mathbb{R}^N$ each closed form is exact: If $\Omega \in \Omega^k(U, \mathbb{R})$ is closed, then there exists a form $\omega \in \Omega^{k-1}(U, \mathbb{R})$ such that $\Omega = d\omega$. Moreover, the potential can be constructed explicitly by the map $K : \Omega^k(U, \mathbb{R}) \to \Omega^{k-1}(U, \mathbb{R})$ given by

$$K(\Omega) = \sum_{i_1 < \cdots < i_k} \sum_{\alpha=1}^{k} (-1)^{\alpha-1} \Big(\int_0^1 t^{k-1} \Omega_{i_1 \cdots i_k}(tx) dt \Big) x_{i_\alpha} \, dx_{i_1} \wedge \ldots \wedge \widehat{dx_{i_\alpha}} \wedge \ldots \wedge dx_{i_k},$$

where $\Omega = \sum_{i_1 < \cdots < i_k} \Omega_{i_1 \cdots i_k} \, dx_{i_1} \wedge \ldots \wedge dx_{i_k}$. One directly can check that

$$K(d\Omega) + d\, K(\Omega) = \Omega.$$

Hence, if $d\Omega = 0$, we get $\Omega = d\, K(\Omega)$. The same construction works for piecewise-smooth forms defined on the star of a simplex. This yields the following piecewise-smooth version of the Poincaré-Lemma.

Lemma 10.2 *On the star of a simplex each closed piecewise-smooth form is exact.*

Now we are ready to prove the main result of this section.

Theorem 10.3 *Let* $\mathrm{L} \to \mathcal{X}$ *be a discrete hermitian line bundle with curvature* Ω *over a simplicial complex and let* $\tilde{\Omega}$ *be the piecewise-smooth* 2*-form associated to* Ω*. Then there is a piecewise-smooth hermitian line bundle* $\tilde{\mathrm{L}} \to \mathcal{X}$ *with connection* $\tilde{\nabla}$ *of curvature* $\tilde{\Omega}$ *such that* $\tilde{\mathrm{L}}_i = \mathrm{L}_i$ *for each vertex* i *and the parallel transports coincide along each edge path. The bundle* $\tilde{\mathrm{L}}$ *is unique up to isomorphism.*

Proof First we construct the piecewise-smooth hermitian line bundle. Let $\mathrm{L} \to \mathcal{X}$ be a discrete hermitian line bundle with curvature Ω and let η denote its connection. Let $\mathcal{V}$ be the vertex set of $\mathcal{X}$ and let S_i denote the open vertex star of the vertex i.

Further, since Ω is closed, by Lemma 10.1, there is a piecewise-constant piecewise-smooth form $\tilde{\Omega}$ associated to Ω. Now, consider the set

$$\hat{\mathrm{L}} := \bigsqcup_{i \in \mathcal{V}} S_i \times \mathrm{L}_i .$$

Note, that $S_i \cap S_j \neq \emptyset$ if and only if ij is an edge of $\mathcal{X}$ or $i = j$. Thus, if we set $\eta_{ii} := \mathrm{id}|_{\mathrm{L}_i}$, we can define an equivalence relation on $\hat{\mathrm{L}}$ as follows:

$$(i, p, u) \sim (j, q, v) :\Longleftrightarrow p = q \text{ and } v = \exp\big(-\imath \int_{\Delta_{ij}^p} \tilde{\Omega}\big)\eta_{ij}(u),$$

where Δ_{ij}^p denotes the oriented triangle spanned by the point i, j and p. Note here that Δ_{ij}^p is completely contained in some simplex of $\mathcal{X}$. Let us check shortly that this really defines an equivalence relation. Here the only non-trivial property is transitivity. Therefore, let $(i, p, u) \sim (j, q, v)$ and $(j, q, v) \sim (k, r, w)$. Thus we have $p = q = r$ and p lies in a simplex which contains the oriented triangle ijk. Clearly, the 2-chain $\Delta_{ij}^p + \Delta_{jk}^p + \Delta_{ki}^p$ is homologous to ijk and since piecewise-constant forms are closed we get

$$\int_{\Delta_{ij}^p + \Delta_{jk}^p} \tilde{\Omega} = -\int_{\Delta_{ki}^p} \tilde{\Omega} + \int_{ijk} \tilde{\Omega} = \int_{\Delta_{ik}^p} \tilde{\Omega} + \Omega_{ijk}.$$

Hence we obtain

$$\begin{aligned} w &= \exp\big(-\imath \int_{\Delta_{jk}^p} \tilde{\Omega}\big)\eta_{jk}\Big(\exp\big(-\imath \int_{\Delta_{ij}^p} \tilde{\Omega}\big)\eta_{ij}(u)\Big) \\ &= \exp\big(-\imath \int_{\Delta_{ij}^p + \Delta_{jk}^p} \tilde{\Omega}\big)\eta_{jk} \circ \eta_{ij}(u) \\ &= \exp\big(-\imath \int_{\Delta_{ik}^p} \tilde{\Omega} - \imath\,\Omega_{ijk}\big)\eta_{jk} \circ \eta_{ij}(u) \\ &= \exp\big(-\imath \int_{\Delta_{ik}^p} \tilde{\Omega}\big)\eta_{ik}(u), \end{aligned}$$

and thus $(i, p, u) \sim (k, r, w)$. Hence $\sim$ defines an equivalence relation. One can check now that the quotient $\tilde{\mathrm{L}} := \hat{\mathrm{L}}/_{\sim}$ is a piecewise-smooth line bundle over $\mathcal{X}$. The local trivializations are then basically given by the inclusions $S_i \times \mathrm{L}_i \hookrightarrow \tilde{\mathrm{L}}$ sending a point to the corresponding equivalence class. Moreover, all transition maps are unitary so that the hermitian metric of L extends to $\tilde{\mathrm{L}}$ and turns $\tilde{\mathrm{L}}$ into a hermitian line bundle. Clearly, $\tilde{\mathrm{L}}\Big|_{\mathcal{V}} = \mathrm{L}$.

Next, we need to construct the connection. Therefore we will use an explicit system of local sections: Choose for each vertex $i \in \mathcal{V}$ a unit vector $X_i \in \mathrm{L}_i$ and define $\phi_i(p) := [i, p, X_i]$. This yields for each vertex i a piecewise-smooth section

ϕ_i define on the star S_i. For each non-empty intersection $S_i \cap S_j \neq \emptyset$ we then obtain a function $g_{ij} : S_i \cap S_j \to \mathbb{S}$. By the above construction, we find that, if $\eta_{ij}(X_i) = r_{ij} X_j$,

$$g_{ij}(p) = r_{ij} \exp\big(-\imath \int_{\Delta_{ij}^p} \tilde{\Omega}\big). \tag{5}$$

Since $\tilde{\Omega}$ is closed, Lemma 10.2 tells us that $\tilde{\Omega}|_{S_i}$ is exact. Hence there is a piecewise-smooth 1-form ω_i defined on S_i such that $d\omega_i = \tilde{\Omega}|_{S_i}$. In general, the form ω_i is only unique up to addition of an exact 1-form, but among those there is a unique form ω_i which is zero along the radial directions originating from i. To see this, just choose some potential $\tilde{\omega}_i$ of $\Omega|_{S_i}$ and define a function $f : S_i \to \mathbb{R}$ as follows:

For $p \in S_i$, let $f(p) := \int_{\gamma_i^p} \tilde{\omega}_i$, where γ_i^p denote the linear path from the vertex i to the point p. Then $\omega_i := \tilde{\omega}_i - df$ is a piecewise-smooth potential of $\Omega|_{S_i}$ and vanishes on radial directions. For the uniqueness, let $\hat{\omega}_i$ be another such potential. Then, the difference $\omega_i - \hat{\omega}_i$ is closed and hence exact on S_i, i.e. there is $f : S_i \to \mathbb{R}$ such that $df = \omega_i - \hat{\omega}_i$. Since df vanishes on radial directions f is constant on radial lines starting at i and hence constant on S_i. Thus $\omega_i = \hat{\omega}_i$.

Suppose that for each edge ij the forms ω_i and ω_j are *compatible*, i.e., wherever both are defined,

$$\imath\omega_j = \imath\omega_i + d \log g_{ij}.$$

Then we can define a connection ∇ as follows: Let $\psi \in \Gamma\big(\tilde{\mathrm{L}}\big)$ and let $X \in \mathrm{T}_p\sigma$ for some simplex σ of $\mathcal{X}$, then there is some $S_i \ni p$. On S_i we can express ψ with respect to ϕ_i, i.e. $\psi = z\,\phi_i$ for some piecewise-smooth function $z : S_i \to \mathbb{C}$. Then we define

$$\nabla_X \psi := \big(dz(X) - \imath\omega_i(X) z\big)\phi_i. \tag{6}$$

In general there are several stars that contain the point p. From compatibility easily follows that the definition does not depend on the choice of the vertex. Hence we have constructed a piecewise smooth connection ∇. One easily checks that ∇ is unitary and since $d\omega_i = \tilde{\Omega}|_{S_i}$ we get $d^\nabla \circ d^\nabla = -\imath\tilde{\Omega}$ as desired.

So it is left to check the compatibility of the forms ω_{ij} constructed above. Let ij be some edge and let p_0 be a point in its interior. Since $\omega_i - \omega_j$ is closed, we can define $\varphi : S_i \cap S_j \to \mathbb{R}$ by $\varphi(p) := \int_{\gamma_p} \omega_i - \omega_j$, where γ_p is some path in $S_i \cap S_j$ from the point p_0 to the point p. Then, for $p \in S_i \cap S_j$,

$$\int_{\Delta_p} \Omega = \int_{\partial\Delta_p} \omega_j = \int_{ij+\gamma_j^p-\gamma_i^p} \omega_j = -\int_{\gamma_i^p} \omega_j = \int_{\gamma_i^p} \omega_i - \omega_j = \varphi(p),$$

where as above γ_i^p denotes the linear path from i to p and, similarly, γ_j^p denotes the linear path from j to the point p. From this we obtain

$$\omega_i - \omega_j = d\varphi = d \int_{\Delta_p} \Omega$$

and in particular $\imath\omega_j = \imath\omega_i + d \log g_{ij}$. This shows the existence.

Now suppose there are two such piecewise-smooth bundles $\tilde{\mathrm{L}}$ and $\hat{\mathrm{L}}$ with connection $\tilde{\nabla}$ and $\hat{\nabla}$, respectively. We want to construct an isomorphism between $\tilde{\mathrm{L}}$ and $\hat{\mathrm{L}}$. Therefore we again use local systems. Explicitly, we choose a discrete direction field $X \in \mathrm{L}$. This yields for each vertex i a vector $X_i \in \tilde{\mathrm{L}}_i = \hat{\mathrm{L}}_i$ which extends by parallel transport along rays starting at i to a local sections $\tilde{\phi}_i$ of $\tilde{\mathrm{L}}$ and, similarly, to a local section $\hat{\phi}_i$ of $\hat{\mathrm{L}}$ defined on S_i.

Now we define $F : \tilde{\mathrm{L}} \to \hat{\mathrm{L}}$ to be unique map which is linear on the fibers and satisfies $F(\tilde{\phi}_i) = \hat{\phi}_i$ on S_i. To see that F is well-defined, we need to check that it is compatible with the transition maps. But by construction both systems have equal transition maps, namely the the functions g_{ij} from Eq. (5) with r_{ij} given by $\eta_{ij}(X_i) = r_{ij} X_j$. Now, if $z_i\, \tilde{\phi}_i = z_j\, \tilde{\phi}_j$, then $z_i = z_j\, g_{ij}$ and hence

$$F(z_i \tilde{\phi}_i) = z_i\, \hat{\phi}_i = z_i\, g_{ij} \hat{\phi}_j = z_j\, \hat{\phi}_j = F(z_j\, \tilde{\phi}_j).$$

Using Eq. (6) one similarly shows that $F \circ \tilde{\nabla} = \hat{\nabla} \circ F$. Thus $\tilde{\mathrm{L}} \cong \hat{\mathrm{L}}$. □

11 Finite Elements for Hermitian Line Bundles with Curvature

In this section we want to present a specific finite element space on the associated piecewise-smooth hermitian line bundle of a discrete hermitian line with curvature. They are constructed from the local systems that played such a prominent role in the proof of Theorem 10.3 and the usual piecewise-linear hat function.

Let $\tilde{\mathrm{L}}$ be the associated piecewise-smooth bundle of a discrete hermitian line bundle $\mathrm{L} \to \mathcal{X}$ and let $x_i : \mathcal{X} \to \mathbb{R}$ denote the barycentric coordinate of the vertex $i \in \mathcal{V}$, i.e. the unique piecewise-linear function such that $x_i(j) = \delta_{ij}$, where δ is the Kronecker delta. Clearly,

$$\Gamma(\mathrm{L}) = \bigoplus_{i \in \mathcal{V}} \mathrm{L}_i.$$

To each $X \in \mathrm{L}_i$ we now construct a piecewise-smooth section $\tilde{\psi}$ as follows: First, we extend X to the vertex star S_i of the vertex i using the parallel transport along rays starting at i. To get a global section $\tilde{\psi} \in \Gamma_{ps}(\mathrm{L})$ we use x_i to scale $\tilde{\phi}$ down to zero on ∂S_i and extend it by zero to $\mathcal{X}$, i.e.

$$\tilde{\psi}_p := \begin{cases} x_i(p) \tilde{\phi}_p & \text{for } p \in S_i, \\ 0 & \text{else.} \end{cases}$$

The above construction yields a linear map $\iota : \Gamma(\mathrm{L}) \to \Gamma_{ps}(\tilde{\mathrm{L}})$. Clearly, ι is injective—a left-inverse is just given by the restriction map

$$\Gamma_{ps}(\tilde{\mathrm{L}}) \ni \tilde{\psi} \mapsto \tilde{\psi}\big|_{\mathcal{V}} \in \Gamma(\mathrm{L}).$$

Definition 11.1 The *space of piecewise-linear sections* is given by $\Gamma_{pl}(\tilde{\mathrm{L}}) := \operatorname{im} \iota$.

Thus we identified each section of a discrete hermitian line bundle with curvature with a piecewise-linear section of the associated piecewise-smooth bundle. This allows to define a discrete hermitian inner product and a discrete Dirichlet energy on $\Gamma(\mathrm{L})$, which is a generalization of the well-known cotangent Laplace operator for discrete functions on triangulated surfaces. Before we come to the Dirichlet energy, we define Euclidean simplicial complexes.

Similarly to piecewise-smooth forms we can define piecewise-smooth (contravariant) k-tensors as collections of compatible k-tensors: A *piecewise-smooth k-tensor* is a collection $T = \{T_\sigma\}_{\sigma \in \mathcal{X}}$ of smooth contravariant k-tensors T_σ on σ such that

$$\iota^*_{\sigma'\sigma} T_\sigma = T_{\sigma'},$$

whenever σ' is a face of σ. A *Riemannian simplicial complex* is then a simplicial complex $\mathcal{X}$ equipped with a *piecewise-smooth Riemannian metric*, i.e. a piecewise-smooth positive-definite symmetric 2-tensor g on $\mathcal{X}$.

The following lemma tells us that the space of constant piecewise-smooth symmetric tensors is isomorphic to functions on 1-simplices.

Lemma 11.2 *Let $\mathcal{X}$ be a simplicial complex and let $\mathcal{E}$ denote the set of its 1-simplices. For each function $f : \mathcal{E} \to \mathbb{R}$ there exists a unique constant piecewise-smooth symmetric 2-tensor S such that for each 1-simplex $e = \{i, j\}$*

$$S_e(j - i, j - i) = f(e).$$

Proof It is enough to consider a single affine n-simplex $\sigma = \{i_0, \ldots, i_n\}$ with vector space V. Consider the map F that sends a symmetric 2-tensor S on V to the function given by

$$F(S)(e) := S(i_k - i_j, i_k - i_j), \quad e = \{i_j, i_k\} \subset \sigma.$$

Clearly, F is linear. Moreover, if Q denotes the quadratic form corresponding to S, i.e. $Q(X) := S(X, X)$, then

$$S(X, Y) = \tfrac{1}{2}\big(Q(X) + Q(Y) - Q(X - Y)\big).$$

Hence, from $F(S) = 0$ follows $S = 0$. Thus F is injective. Clearly, the space of symmetric bilinear forms is of dimension $n(n + 1)/2$, which equals the number of 1-simplices. Thus F is an isomorphism. This proves the claim. □

It is also easy to write down the corresponding symmetric tensor in coordinates: Let $\sigma = \{i_0, \dots, i_n\}$ be a simplex. The vectors $e_j := i_j - i_0$, $j = 1, \dots, n$, then yield a basis of the corresponding vector space. Let f be a function defined on the unoriented edges of σ and let x_{i_j} denote the barycentric coordinates of its vertices i_j, then the corresponding symmetric bilinear form S^f_σ is given by

$$S^f_\sigma = \sum_{1 \le j \le n} f_{i_0 i_j}\, dx_{i_j} \otimes dx_{i_j} + \sum_{1 \le j,k \le n,\ j \ne k} \tfrac{1}{2}\big(f_{i_0 i_j} + f_{i_0 i_k} - f_{i_j i_k}\big)\, dx_{i_j} \otimes dx_{i_k}. \quad (7)$$

Thus starting with a positive function f, by Sylvester's criterion, it has to satisfy on each n-simplex $n-1$ inequalities to determine a positive-definite form. If the corresponding piecewise-smooth form is positive-definite, we call f a discrete metric.

Definition 11.3 A *Euclidean simplicial complex* is a simplicial complex $\mathcal{X}$ equipped with a *discrete metric*, i.e. a map ℓ that assigns to each 1-simplex e a length $\ell_e > 0$ such that for each simplex σ the symmetric tensor S^ℓ_σ is positive-definite.

Now, let $\mathcal{X}$ be a Euclidean simplicial manifold of dimension n and denote by $\mathcal{X}_n$ the set of its top-dimensional simplices. Since each simplex of $\mathcal{X}$ is equipped with a scalar product it comes with a corresponding density and hence we know how to integrate functions over the simplices of $\mathcal{X}$. Now, we define the *integral over* $\mathcal{X}$ as follows:

$$\int_{\mathcal{X}} f := \sum_{\sigma \in \mathcal{X}_n} \int_\sigma f_\sigma, \quad f \in \Omega^0_{ps}(\mathcal{X}, \mathbb{R}).$$

Moreover, given a piecewise-smooth hermitian line bundle $\tilde{\mathrm{L}} \to \mathcal{X}$ with curvature, then there is a canonical hermitian product $\langle\!\langle ., . \rangle\!\rangle$ on $\Gamma_{ps}(\tilde{\mathrm{L}})$: If $\tilde\psi, \tilde\phi \in \Gamma_{ps}(\tilde{\mathrm{L}})$, then

$$\langle\!\langle \tilde\psi, \tilde\phi \rangle\!\rangle = \int_{\mathcal{X}} \langle \tilde\psi, \tilde\phi \rangle.$$

In particular, if $\tilde{\mathrm{L}}$ is the associated piecewise-smooth bundle of a discrete hermitian line bundle L with curvature Ω, then we can use ι to pull $\langle\!\langle ., . \rangle\!\rangle$ back to $\Gamma(\mathrm{L})$. Since ι is injective this yields a hermitian product on $\Gamma(\mathrm{L})$.

Now we want to compute this metric explicitly in terms of given discrete data.

Definition 11.4 A piecewise-linear section $\tilde\psi \in \Gamma_{pl}(\tilde{\mathrm{L}})$ is called *concentrated at a vertex* i, if it is of the form $\tilde\psi = \iota(\psi_i)$ for some vector $\psi_i \in \mathrm{L}_i$.

It is basically enough to compute the product of two such concentrated sections. Therefore, let $\psi_i \in \mathrm{L}_i$ and $\psi_j \in \mathrm{L}_j$ and let $\tilde\psi^i$ and $\tilde\psi^j$ denote the corresponding piecewise-linear concentrated sections.

Now consider their product $\langle \tilde{\psi}^i, \tilde{\psi}^j \rangle$. Clearly, this product has support $S_i \cap S_j$. For simplicity, we extend the discrete connection η to arbitrary pairs ij in such way that $\eta_{ii} = \mathrm{id}$ and $\eta_{ij} : \mathrm{L}_i \to \mathrm{L}_j$ is zero whenever $\{i, j\} \notin \mathcal{X}$. With this convention, Eq. (5) yields

$$\langle \tilde{\psi}^j, \tilde{\psi}^i \rangle = \langle \psi_j, \eta_{ij}(\psi_i) \rangle \, x_i x_j \, \exp\bigl(-\imath \int_{\Delta^p_{ij}} \tilde{\Omega}\bigr), \tag{8}$$

where $\tilde{\Omega}$ denotes the constant piecewise-smooth curvature form associated to Ω.

Now, let us express the integral over Δ^p_{ij} on a given n-simplex. Therefore consider an n-simplex $\sigma = \{i_0, \ldots, i_n\}$. The hat functions $x_{i_1}, \ldots, x_{i_n}$ yield affine coordinates on σ and we can express any 2-form with respect to the basis forms $dx_{i_j} \wedge dx_{i_k}$. One can show that

$$\int_{\sigma'} dx_{i_j} \wedge dx_{i_k} = \begin{cases} \pm\frac{1}{2} & \text{for } \sigma' = \pm i_j i_k i_\ell, \\ 0 & \text{else.} \end{cases}$$

Thus we obtain

$$\tilde{\Omega} = \sum_{1 \le j < k \le n} 2\, \Omega_{i_0 i_j i_k}\, dx_{i_j} \wedge dx_{i_k}.$$

Now we want to compute the integral over the triangle $\Delta^p_{i_0 i_1} \subset \sigma$. By Stokes theorem,

$$\int_{\Delta^p_{i_0 i_1}} dx_{i_j} \wedge dx_{i_k} = \int_{i_0}^{i_1} x_{i_j}\, dx_{i_k} + \int_{i_1}^{p} x_{i_j}\, dx_{i_k} + \int_{p}^{i_0} x_{i_j}\, dx_{i_k},$$

where the integrals are computed along straight lines. A small computation shows

$$\int_{\Delta^p_{i_0 i_1}} dx_{i_j} \wedge dx_{i_k} = \frac{1}{2}\bigl(\delta_{1j}\, x_{i_k}(p) - \delta_{1k}\, x_{i_j}(p)\bigr),$$

Thus, for $j < k$, we get $\int_{\Delta^p_{i_0 i_1}} dx_{i_j} \wedge dx_{i_k} = \frac{1}{2}\delta_{1j}\, x_{i_k}(p)$ and hence

$$\int_{\Delta^p_{i_0 i_1}} \tilde{\Omega} = \sum_{1 \le j < k \le n} 2\, \Omega_{i_0 i_j i_k} \int_{\Delta^p_{i_0 i_1}} dx_{i_j} \wedge dx_{i_k} = \sum_j \Omega_{i_0 i_1 i_j} x_{i_j}(p),$$

where we have used the convention that Ω vanishes on all triples not representing an oriented 2-simplex of $\mathcal{X}$. With this convention Eq. (8) becomes

$$\langle \tilde{\psi}^j, \tilde{\psi}^i \rangle = \langle \psi_j, \eta_{ij}(\psi_i) \rangle \, x_i x_j \, \exp\bigl(-\imath \sum_k \Omega_{ijk} x_k\bigr). \tag{9}$$

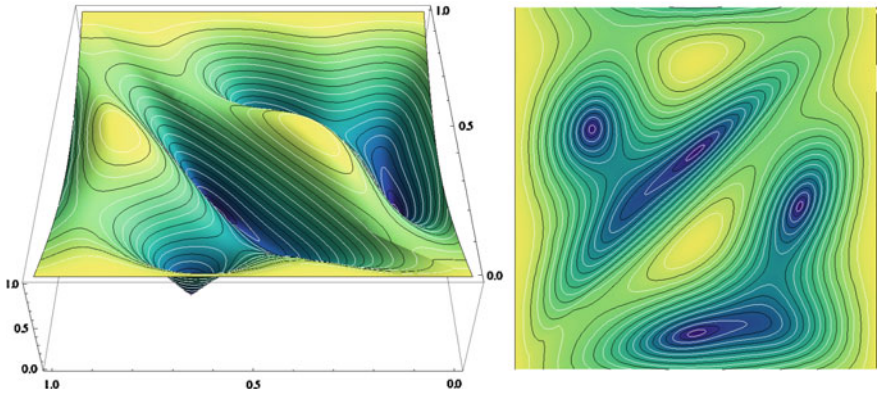

Fig. 7 The graph of the norm of a piecewise-linear section of a bundle over a torus consisting of two triangles. Its two smooth parts fit continuously together along the diagonal. In this example the curvature of the bundle over each triangles is equal to 4π. Note that the section has 4 zeros—just as predicted

In particular, using Eq. (9), we can compute the norm of a piecewise-linear section $\tilde{\psi}$ on a given triangle ijk. Therefore we distinguish one of its vertices, say i, and write $\tilde{\psi}$ with respect to a section which is radially parallel with respect to i. Now, one checks that

$$|\tilde{\psi}| = |c_i + x_j(c_j e^{i\Omega_{ijk}x_k} - c_i) + x_k(c_k e^{-i\Omega_{ijk}x_j} - c_i)|,$$

where $c_i, c_j, c_k \in \mathbb{C}$ are constants depending on the explicit form of $\tilde{\psi}$. An example of the norm of a piecewise-linear section is shown in Fig. 7.

As the next proposition shows, the identification of discrete and piecewise-linear sections perfectly fits together with the definitions in Sect. 8.

Proposition 11.5 *Let $\psi \in \Gamma(\mathrm{L})$ be a discrete section and let $\tilde{\psi} \in \Gamma_{pl}(\tilde{\mathrm{L}})$ be the corresponding piecewise-linear section, i.e. $\tilde{\psi} = \iota(\psi)$. Then, if $\tilde{\psi}$ has no zeros on edges, the discrete rotation form ξ^{ψ} and the piecewise-smooth rotation form $\xi^{\tilde{\psi}}$ are related as follows: For each oriented edge ij,*

$$\xi^{\psi}_{ij} = \int_{ij} \xi^{\tilde{\psi}}.$$

Proof The claim follows easily by expressing $\tilde{\psi}$ with respect to some non-vanishing parallel section along the edge ij. □

In particular, by Theorem 8.1, the index form of a non-vanishing section of a discrete hermitian line bundle with curvature counts the number of (signed) zeros of the corresponding piecewise-linear section of the associated piecewise-smooth bundle.

Let us continue with the computation of the metric on $\Gamma(\mathrm{L})$. To write down the formula we give the following definition.

Definition 11.6 Let $\mathcal{X}$ be an n-dimensional simplicial manifold and let $\Omega \in \Omega^2(\mathcal{X}, \mathbb{R})$. To an n-simplex σ and vertices i, j, k, l of $\mathcal{X}$ we assign the value

$$\Theta^{\Omega}_{\sigma,i,j}(k,l) := \frac{1}{\mathrm{vol}\,(\sigma)} \int_{\sigma} x_k x_l \, \exp\Big(-\imath \sum_m \Omega_{ijm} x_m\Big),$$

where we have chosen for integration an arbitrary discrete metric on $\mathcal{X}$.

Remark 11.7 Note that the functions $\Theta^{\Omega}_{\sigma,i,j}$ are indeed well-defined. On a simplex, any two such measures induced by a discrete metric differ just by a constant.

With Definition 11.6 and Eq. (9) we obtain the following form of the metric:

Theorem 11.8 (Product of Discrete Sections) *Let* L *be a discrete hermitian line bundle with curvature Ω over an n-dimensional Euclidean simplicial manifold $\mathcal{X}$, then the product on $\Gamma(\mathrm{L})$ induced by the associated piecewise-smooth hermitian line bundle is given as follows: Given two discrete sections $\psi = \sum_i \psi_i$, $\phi = \sum_i \phi_i$,*

$$\langle\!\langle \psi, \phi \rangle\!\rangle = \sum_{i,j} \mu^{ij}_{\Omega} \, \langle \psi_j, \eta_{ij}(\phi_i) \rangle, \quad \textit{where} \quad \mu^{ij}_{\Omega} = \sum_{\{i,j\} \supset \sigma \in \mathcal{X}_n} \Theta^{\Omega}_{\sigma,i,j}(i,j)\,\mathrm{vol}\,(\sigma).$$

Note that $\Theta^{\Omega}_{\sigma,i,j}(k,l)$, and hence μ^{ij}_{Ω}, can be computed explicitly using Fubini's theorem and the following small lemma, which can be shown by induction.

Lemma 11.9 *Let $c \in \mathbb{C}_*$, $n \in \mathbb{N}$ and $[a,b] \subset \mathbb{R}$ be an interval. Then*

$$\int_a^b x^n \exp(cx) dx = \frac{n!}{c^{n+1}} \Big(\sum_{k=0}^{n} (-1)^k \frac{(cx)^{n-k}}{(n-k)!} \Big) \exp(cx) \Big|_a^b.$$

Next, we would like to compute the *Dirichlet energy* of a section $\tilde{\psi} \in \Gamma_{pl}(\tilde{\mathrm{L}})$, i.e.

$$\mathrm{E}_D(\tilde{\psi}) = \int_{\mathcal{X}} |\nabla \tilde{\psi}|^2.$$

Note, that the Dirichlet energy comes with a corresponding positive-semidefinite hermitian form $\langle\!\langle ., . \rangle\!\rangle_D$—called the *Dirichlet product*. Clearly, like the metric, the Dirichlet product is completely determined by the values it takes on concentrated sections.

In general, if $\tilde{\psi} \neq 0$ is piecewise-linear section concentrated at i, it is given on the vertex star S_i as a product $\tilde{\psi} = x_i \, \tilde{\phi}$, where x_i denotes the barycentric coordinate of the vertex i and $\tilde{\phi}$ is a local section radially parallel with respect to i. Clearly,

$$\nabla \tilde{\psi} = dx_i \, \tilde{\phi} + \imath \, x_i \, \omega_i \, \tilde{\phi},$$

where ω_i denotes the rotation form of $\tilde{\phi}$, i.e. $\nabla\tilde{\phi} = \imath\omega_i\,\tilde{\phi}$. Note here that ω_i does not depend on the actual value of $\tilde{\psi}$ at i, but is the same for all non-vanishing piecewise-linear sections concentrated at i.

To compute the rotation form ω_i at a given point $p_0 \in S_i$, we use a local section ζ which is radially parallel with respect to p_0 such that $\zeta_{p_0} = \tilde{\phi}_{p_0}$. Then we can express $\tilde{\phi}$ in terms of ζ, i.e.

$$\tilde{\phi} = z\,\zeta,$$

for some piecewise-smooth $\mathbb{C}_*$-valued function z defined locally at p_0. Clearly, $|z|$ is constant, and hence

$$\imath\omega_i|_{p_0}\;\tilde{\phi}_{p_0} = \nabla\tilde{\phi}\Big|_{p_0} = dz|_{p_0}\;\zeta_{p_0} + z(p_0)\;\nabla\zeta|_{p_0} = d\log z|_{p_0}\,\tilde{\phi}_{p_0} = \imath\, d\arg z|_{p_0}\;\tilde{\phi}_{p_0}.$$

The clue is that we can now use the relation of parallel transport and curvature to obtain an explicit formula for z. If p is sufficiently close to p_0, then the three points p, i and p_0 determine an oriented triangle Δ^p which is contained in a simplex of $\mathcal{X}$. Its boundary curve γ_p consists of three line segments $\gamma_1, \gamma_2, \gamma_3$ connecting p to i, i to p_0 and p_0 back to p. Hence on each of these segments either $\tilde{\phi}$ of ζ is parallel and

$$\zeta_p = P_{\gamma_p}(\tilde{\phi}_p) = \exp\big(\imath\int_{\Delta^p}\tilde{\Omega}\big)\tilde{\phi}_p.$$

Thus we obtain that $z(p) = \exp\big(-\imath\int_{\Delta^p}\tilde{\Omega}\big)$ and hence

$$\omega_i\Big|_{p_0} = -d\Big(\int_{\Delta^p}\tilde{\Omega}\Big)\Big|_{p_0}.$$

Now, if Δ^p is contained in a simplex $\sigma = \{i_0, \ldots, i_n\}$, one verifies that

$$\int_{\Delta^p} dx_{i_j}\wedge dx_{i_k} = \frac{1}{2}\big(x_{i_j}(p_0)x_{i_k}(p) - x_{i_k}(p_0)x_{i_j}(p)\big).$$

Thus,

$$\begin{aligned} d\Big(\int_{\Delta^p}\tilde{\Omega}\Big)\Big|_{p_0} &= \sum_{1\le j<k\le n} 2\,\Omega_{i_0 i_j i_k}\, d\Big(\int_{\Delta^p} dx_{i_j}\wedge dx_{i_k}\Big)\Big|_{p_0} \\ &= \sum_{1\le j<k\le n} \Omega_{i_0 i_j i_k}\left(x_{i_j}dx_{i_k} - x_{i_k}dx_{i_j}\right)\Big|_{p_0}, \\ &= \sum_{1\le j\le n}\Big(\sum_{k\ne j}\Omega_{i_0 i_j i_k}x_{i_k}\Big)dx_{i_j}\Big|_{p_0} \end{aligned}$$

and, using the convention on Ω from above, we find the following simple formula:

$$\omega_i = \sum_j \Big(\sum_k \Omega_{ijk}\, x_k\Big)\, dx_j\Big|_{S_i}, \tag{10}$$

where we sum over the whole vertex set of $\mathcal{X}$.

Now, given this local form expressions, we can finally return to the computation of the products which we are actually interested in. Therefore we consider two piecewise-linear sections concentrated at the vertices i and j:

$$\tilde{\psi}^i := \iota(\psi_i), \quad \tilde{\psi}^j := \iota(\psi_j),$$

for some $\psi_i \in \mathrm{L}_i$ and $\psi_j \in \mathrm{L}_j$. On their common support $S_i \cap S_j$ both section can be expressed, just as above, as products of a real-valued piecewise-linear hat functions x_i and x_j and radially parallel local sections $\tilde{\phi}^i$ and $\tilde{\phi}^j$:

$$\tilde{\psi}^i = x_i\, \tilde{\phi}^i, \quad \tilde{\psi}^j = x_j\, \tilde{\phi}^j.$$

Clearly,

$$\begin{aligned}\langle\!\langle \tilde{\psi}^j, \tilde{\psi}^i \rangle\!\rangle_D &= \int_{S_i \cap S_j} \langle dx_j \tilde{\phi}^j + \imath x_j \omega_j\, \tilde{\phi}^j, dx_i \tilde{\phi}^i + \imath x_i \omega_i\, \tilde{\phi}^i \rangle \\ &= \int_{S_i \cap S_j} \langle dx_j + \imath x_j \omega_j, dx_i + \imath x_i \omega_i \rangle\, \langle \tilde{\phi}^j, \tilde{\phi}^i \rangle.\end{aligned}$$

With Eq. (9) we see that

$$\langle \tilde{\phi}^j, \tilde{\phi}^i \rangle = \langle \psi_j, \eta_{ij}(\psi_i) \rangle\, \exp\big(-\imath \sum_m \Omega_{ijm} x_m\big).$$

Moreover, by Eq. (10),

$$\begin{aligned}\langle dx_j + \imath x_j \omega_j, dx_i + \imath x_i \omega_i \rangle =& \Big[\langle dx_j, dx_i \rangle + \sum_{k',k'',l',l''} \Omega_{ik'l'} \Omega_{jk''l''} x_j x_i x_{l'} x_{l''} \langle dx_{k'}, dx_{k''} \rangle\Big] \\ &+ \imath \Big[\sum_{k',l'} (\Omega_{ik'l'} x_i x_{l'} \langle dx_j, dx_{k'} \rangle - \Omega_{jk'l'} x_j x_{l'} \langle dx_{k'}, dx_i \rangle)\Big].\end{aligned}$$

The constants $\langle dx_{k'}, dx_{l'} \rangle$ are basically provided by the following lemma.

Lemma 11.10 *Let $\sigma = \{v_0, \ldots, v_n\}$ be a Euclidean simplex of dimension $n > 0$ and let x_i denote its barycentric coordinate functions. Then*

$$grad x_i = -\frac{1}{h_i} N_i,$$

where h_i denotes the distance between v_i and $\sigma_i = \sigma \setminus \{v_i\}$ and N_i denotes the outward-pointing unit normal of σ_i.

Proof This immediately follows from two basic facts: First, $dx_i(v_j - v_0) = \delta_{ij}$ for $i, j > 0$. Second, $h_i = \langle v_0 - v_i, N_i \rangle$. □

Lemma 11.10 yields almost immediately a higher dimensional analogue of the well-known cotangent formula for surfaces.

Theorem 11.11 (Cotangent Formula) *Let σ be a simplex of a Euclidean simplicial complex $\mathcal{X}$ and let* $\dim \sigma > 1$. *If $i \neq j$,*

$$c_\sigma^{ij} := \int_\sigma \langle dx_i, dx_j \rangle = \begin{cases} -\frac{1}{n(n-1)} \cot \alpha_\sigma^{ij} \operatorname{vol}\big(\sigma \setminus \{i, j\}\big), & \text{if } \{i, j\} \subset \sigma, \\ 0 & \text{else.} \end{cases}$$

Here α_σ^{ij} denotes the angle between the faces $\sigma \setminus \{i\}$ and $\sigma \setminus \{j\}$. Moreover,

$$c_\sigma^{ii} := \int_\sigma |dx_i|^2 = \begin{cases} \frac{1}{n\, h_i} \operatorname{vol}\big(\sigma \setminus \{i\}\big), & \text{if } i \in \sigma, \\ 0 & \text{else,} \end{cases}$$

where h_i denotes the distance between the vertex i and the face $\sigma \setminus \{i\}$.

Proof Clearly, if $\{i, j\} \not\subset \sigma$, then $\int_\sigma \langle dx_i, dx_j \rangle = 0$. Now, let $\{i, j\} \subset \sigma, i \neq j$. With the notation of Lemma 11.10, we have

$$\int_\sigma \langle dx_i, dx_j \rangle = \langle \operatorname{grad} x_i, \operatorname{grad} x_j \rangle \operatorname{vol} \sigma = \frac{\langle N_i, N_j \rangle}{h_i h_j} \operatorname{vol} \sigma.$$

Furthermore, $\cos \alpha_\sigma^{ij} = -\langle N_i, N_j \rangle$ and $n! \operatorname{vol} \sigma = (n-2)!\, h_i h_j \sin \alpha_\sigma^{ij} \operatorname{vol}\big(\sigma \setminus \{i, j\}\big)$. This yields the first part of the theorem. Similarly, $n \operatorname{vol} \sigma = h_i \operatorname{vol}\big(\sigma \setminus \{i\}\big)$. Setting then $i = j$ yields the second part. □

Definition 11.12 Let $\mathcal{X}$ be an n-dimensional simplicial manifold and let $\Omega \in \Omega^2(\mathcal{X}, \mathbb{R})$. Let σ be an n-simplex and i, j, k, l be vertices of $\mathcal{X}$. Then, let

$$\Lambda_{\sigma,i,j}^{\Omega} := \frac{1}{\operatorname{vol}(\sigma)} \int_\sigma \exp\Big(-\imath \sum_m \Omega_{ijm} x_m\Big),$$

$$\Xi_{\sigma,i,j}^{\Omega}(k, l) := \frac{1}{\operatorname{vol}(\sigma)} \int_\sigma x_i x_j x_k x_l \, \exp\Big(-\imath \sum_m \Omega_{ijm} x_m\Big),$$

where we choose for the integration an arbitrary discrete metric on $\mathcal{X}$.

Remark 11.13 Just like the functions $\Theta_{\sigma,i,j}^{\Omega}$, the values $\Lambda_{\sigma,i,j}^{\Omega}$ and the functions $\Xi_{\sigma,i,j}^{\Omega}$ and are well-defined (compare Remark 11.7).

Now, with these definitions, we can summarize the above discussion by the following theorem.

Theorem 11.14 *(*Discrete Dirichlet Energy*) Let* L *be a discrete hermitian line bundle with curvature Ω over an n-dimensional Euclidean simplicial manifold $\mathcal{X}$, then the Dirichlet product on $\Gamma(\mathrm{L})$ induced by the associated piecewise-smooth hermitian line bundle is given as follows: If $\phi = \sum_i \phi_i$ and $\psi = \sum_i \psi_i$ are two discrete sections,*

$$\langle\!\langle \phi, \psi \rangle\!\rangle_D = \sum_{i,j} w^{ij}_{\Omega} \, \langle \phi_j, \eta_{ij}(\psi_i) \rangle, \quad w^{ij}_{\Omega} = \sum_{\{i,j\} \supset \sigma \in \mathcal{X}_n} W^{\Omega}_{\sigma,i,j},$$

where

$$\begin{aligned} W^{\Omega}_{\sigma,i,j} = & \Big[c^{ij}_{\sigma} \, \Lambda^{\Omega}_{\sigma,i,j} + \sum_{k',k',l',l''} \Omega_{ik'l'} \Omega_{jk'l''} \, c^{k'k'}_{\sigma} \, \Xi^{\Omega}_{\sigma,i,j}(l',l'') \Big] \\ & + \imath \Big[\sum_{k',l'} \big(\Omega_{ik'l'} \, c^{jk'}_{\sigma} \, \Theta^{\Omega}_{\sigma,i,j}(i,l') - \Omega_{jk'l'} \, c^{ik'}_{\sigma} \, \Theta^{\Omega}_{\sigma,i,j}(j,l') \big) \Big]. \end{aligned} \tag{11}$$

12 Discrete Energies on Surfaces—An Example

While the computation of the Dirichlet product $\langle\!\langle ., . \rangle\!\rangle_D$ and the metric $\langle\!\langle ., . \rangle\!\rangle$ of discrete sections is quite complicated and tedious for higher dimensional simplicial manifolds, it is manageable for the 2-dimensional case. We are going to compute it explicitly.

Throughout this section let L denote a discrete hermitian line bundle with curvature Ω over a Euclidean simplicial surface $\mathcal{X}$ and let $\sigma = \{i, j, k\}$ be one of its triangles.

The metric $\langle\!\langle ., . \rangle\!\rangle$ is easily obtained. We basically just need to compute the values $\Theta^{\Omega}_{\sigma,i,i}(i,i)$ and $\Theta^{\Omega}_{\sigma,i,j}(i,j)$, which can be done over the standard triangle. We get

$$\Theta^{\Omega}_{\sigma,i,i}(i,i) = \frac{1}{6}, \quad \Theta^{\Omega}_{\sigma,i,j}(i,j) = 2 \frac{\exp(-\imath \, \Omega_{ijk}) - 1 + \imath \, \Omega_{ijk} + \frac{1}{2} \Omega^2_{ijk} - \imath \, \frac{1}{6} \Omega^3_{ijk}}{\Omega^4_{ijk}}. \tag{12}$$

Now, we compute the Dirichlet product $\langle\!\langle ., . \rangle\!\rangle_D$ on $\mathcal{X}$. For $n = 2$, the expressions $W^{\Omega}_{\sigma,i,i}$ and $W^{\Omega}_{\sigma,i,j}$ simplify drastically. First, we look at the diagonal terms. We have

$$\begin{aligned} & \sum_{k',k',l',l''} c^{k'k'}_{\sigma} \, \Omega_{ik'l'} \Omega_{ik'l''} \, \Xi^{\Omega}_{\sigma,i,i}(l',l'') \\ & \qquad = \Big(c^{jj}_{\sigma} \, \Xi^{\Omega}_{\sigma,i,i}(k,k) - 2 c^{jk}_{\sigma} \, \Xi^{\Omega}_{\sigma,i,i}(j,k) + c^{kk}_{\sigma} \, \Xi^{\Omega}_{\sigma,i,i}(j,j) \Big) \Omega^2_{ijk}, \end{aligned}$$

and with

$$\Lambda_{\sigma,i,i} = 1, \quad \Xi_{\sigma,i,i}(j,j) = \frac{1}{90} = \Xi_{\sigma,i,i}(k,k), \quad \Xi_{\sigma,i,i}(j,k) = \frac{1}{180}$$

we get the following formula:

$$W^{\Omega}_{\sigma,i,i} = c^{ii}_{\sigma} + \frac{c^{jj}_{\sigma} - c^{jk}_{\sigma} + c^{kk}_{\sigma}}{90}\Omega^2_{ijk}.$$

Now we would like to obtain a similar formula for the off-diagonal terms. Since $dx_i + dx_j = -dx_k$, we have $c^{jk}_{\sigma} + c^{ki}_{\sigma} = -c^{kk}_{\sigma}$. Hence,

$$\sum_{k',k',l',l'} c^{k'k'}_{\sigma}\,\Omega_{ik'l'}\Omega_{jk'l'}\,\Xi^{\Omega}_{\sigma,i,j}(l',l'') = -\Big(c^{ij}_{\sigma}\,\Xi^{\Omega}_{\sigma,i,j}(k,k) + c^{kk}_{\sigma}\big(\Xi^{\Omega}_{\sigma,i,j}(i,j) + \Xi^{\Omega}_{\sigma,i,j}(j,k)\big)\Big)\Omega^2_{ijk}.$$

This time the expressions become more complicated. We get

$$\Xi^{\Omega}_{\sigma,i,j}(k,k) = \frac{2}{\Omega^6_{ijk}}\Big(20 - 12\imath\,\Omega_{ijk} - 3\Omega^2_{ijk} + \tfrac{1}{3}\imath\,\Omega^3_{ijk} + \big(-20 - 8\imath\,\Omega_{ijk} + \Omega^2_{ijk}\big)\exp\big(-\imath\,\Omega_{ijk}\big)\Big),$$

$$\Xi^{\Omega}_{\sigma,i,j}(i,j) + \Xi^{\Omega}_{\sigma,i,j}(j,k) = \frac{2}{\Omega^6_{ijk}}\Big(-6 + 4\imath\,\Omega_{ijk} + \Omega^2_{ijk} + \tfrac{1}{12}\Omega^4_{ijk} - \tfrac{1}{30}\imath\,\Omega^5_{ijk} + \big(6 + 2\imath\,\Omega_{ijk}\big)\exp\big(-\imath\,\Omega_{ijk}\big)\Big).$$

Thus,

$$\sum_{k',k',l',l''} c^{k'k'}_{\sigma}\,\Omega_{ik'l'}\Omega_{jk'l'}\,\Xi^{\Omega}_{\sigma,i,j}(l',l'') = \frac{2}{\Omega^4_{ijk}}\Big(\big[6c^{kk}_{\sigma} - 20c^{ij}_{\sigma}\big] + \big[12c^{ij}_{\sigma} - 4c^{kk}_{\sigma}\big]\imath\,\Omega_{ijk} + \big[3c^{ij}_{\sigma} - c^{kk}_{\sigma}\big]\Omega^2_{ijk} - \tfrac{c^{ij}_{\sigma}}{3}\imath\,\Omega^3_{ijk} - \tfrac{c^{kk}_{\sigma}}{12}\Omega^4_{ijk} + \tfrac{c^{kk}_{\sigma}}{30}\imath\,\Omega^5_{ijk} + \big(\big[20c^{ij}_{\sigma} - 6c^{kk}_{\sigma}\big] + \big[8c^{ij}_{\sigma} - 2c^{kk}_{\sigma}\big]\imath\,\Omega_{ijk} - c^{ij}_{\sigma}\Omega^2_{ijk}\big)\exp\big(-\imath\,\Omega_{ijk}\big).\Big)$$

Now, let us look at the second sum in Eq. (11). We have

$$\imath\sum_{k',l'}\big(\Omega_{ik'l'}c^{jk'}_{\sigma}\Theta^{\Omega}_{\sigma,i,j}(i,l') - \Omega_{jk'l'}c^{ik'}_{\sigma}\Theta^{\Omega}_{\sigma,i,j}(j,l')\big) = \Big(c^{ii}_{\sigma}\Theta^{\Omega}_{\sigma,i,j}(j,k) + c^{jj}_{\sigma}\Theta^{\Omega}_{\sigma,i,j}(k,i) + c^{kk}_{\sigma}\Theta^{\Omega}_{\sigma,i,j}(i,j)\Big)\imath\,\Omega_{ijk}.$$

The formula for $\Theta^{\Omega}_{\sigma,i,j}(i,j)$ is already given in Eq. (12). Further, we have

$$\Theta^{\Omega}_{\sigma,i,j}(j,k) = \frac{2}{\Omega^4_{ijk}}\Big(3 - 2\imath\,\Omega_{ijk} - \tfrac{1}{2}\Omega^2_{ijk} + \big(-3 + \imath\,\Omega_{ijk}\big)\exp\big(-\imath\,\Omega_{ijk}\big)\Big) = \Theta^{\Omega}_{\sigma,i,j}(k,i).$$

Thus we get

$$\imath \sum_{k',l'} \big(\Omega_{ik'l'} c_\sigma^{jk'} \Theta^{\Omega}_{\sigma,i,j}(i,l') - \Omega_{jk'l'} c_\sigma^{ik'} \Theta^{\Omega}_{\sigma,i,j}(j,l')\big) =$$
$$\frac{2}{\Omega^4_{ijk}} \Big(\big[3(c_\sigma^{ii} + c_\sigma^{jj}) - c_\sigma^{kk}\big] \imath \Omega_{ijk} + \big[2(c_\sigma^{ii} + c_\sigma^{jj}) - c_\sigma^{kk}\big] \Omega^2_{ijk} + \tfrac{1}{2}\big[c_\sigma^{kk} - c_\sigma^{ii} - c_\sigma^{jj}\big] \imath \Omega^3_{ijk}$$
$$+ \tfrac{c_\sigma^{kk}}{6} \Omega^4_{ijk} + \big(\big[c_\sigma^{kk} - 3(c_\sigma^{ii} + c_\sigma^{jj})\big] \imath \Omega_{ijk} + \big[c_\sigma^{ii} + c_\sigma^{jj}\big] \Omega^2_{ijk} \big) \exp(-\imath \Omega_{ijk}) \Big).$$

Hence, with

$$\Lambda^{\Omega}_{\sigma,i,j} = \frac{2}{\Omega^4_{ijk}} \Big(\Omega^2_{ijk} - \imath \Omega^3_{ijk} - \Omega^2_{ijk} \exp(-\imath \Omega_{ijk}) \Big),$$

Equation (11) becomes

$$W^{\Omega}_{\sigma,i,j} = \frac{2}{\Omega^4_{ijk}} \Big(\big[6\sigma^{kk} - 20 c_\sigma^{ij}\big] + \big[12 c_\sigma^{ij} + 3(c_\sigma^{ii} + c_\sigma^{jj}) - 5 c_\sigma^{kk}\big] \imath \Omega_{ijk} + \big[4 c_\sigma^{ij} + 2(c_\sigma^{ii} + c_\sigma^{jj} - c_\sigma^{kk})\big] \Omega^2_{ijk}$$
$$+ \tfrac{1}{6}\big[3(c_\sigma^{kk} - c_\sigma^{ii} - c_\sigma^{jj}) - 8 c_\sigma^{ij}\big] \imath \Omega^3_{ijk} + \tfrac{1}{12} c_\sigma^{kk} \Omega^4_{ijk} + \tfrac{1}{30} c_\sigma^{kk} \Omega^4_{ijk}$$
$$+ \big(\big[20 c_\sigma^{ij} - 6 c_\sigma^{kk}\big] + \big[8 c_\sigma^{ij} - 3(c_\sigma^{ii} + c_\sigma^{jj}) - c_\sigma^{kk}\big] \imath \Omega_{ijk} + \big[c_\sigma^{ii} - 2 c_\sigma^{ij} + c_\sigma^{jj}\big] \Omega^2_{ijk} \big) \exp(-\imath \Omega_{ijk}) \Big).$$

Since $n = 2$, the weights c_σ^{ij} are just given as follows:

$$c_\sigma^{ij} = -\frac{\cot \alpha_\sigma^{ij}}{2}, \quad c_\sigma^{kk} = \frac{\ell_{ij}}{2h_k},$$

where ℓ_{ij} denotes the edge length. We would like to express them explicitly in terms of the Euclidean metric g of σ. In fact, we can distinguish the vertex k as origin and use the hat functions x_i and x_j as coordinates on σ. With respect to these coordinates, the metric is given by a matrix:

$$g = \begin{pmatrix} g_{11} & g_{12} \\ g_{21} & g_{22} \end{pmatrix}.$$

In terms of g the cotangent weights are given as follows:

$$c_\sigma^{ij} = -\frac{g_{12}}{2\sqrt{\det g}}, \qquad c_\sigma^{jk} = -\frac{g_{11} - g_{12}}{2\sqrt{\det g}}, \qquad c_\sigma^{ki} = -\frac{g_{22} - g_{12}}{2\sqrt{\det g}},$$
$$c_\sigma^{kk} = \frac{g_{11} - 2g_{12} + g_{22}}{2\sqrt{\det g}}, \qquad c_\sigma^{ii} = \frac{g_{22}}{2\sqrt{\det g}}, \qquad c_\sigma^{jj} = \frac{g_{11}}{2\sqrt{\det g}},$$

and we have rederived the formulas in [8]:

$$W^{\Omega}_{\sigma,i,j} = \frac{1}{\mathrm{vol}\,(\sigma)\Omega^4_{ijk}}\Big(\big[3g_{11}+4g_{12}+3g_{22}\big] - \big[g_{11}+g_{12}+g_{22}\big]\imath\,\Omega_{ijk} + \tfrac{g_{12}}{6}\imath\,\Omega^3_{ijk} + \tfrac{g_{11}-2g_{12}+g_{22}}{24}\Omega^4_{ijk} + \tfrac{g_{11}-2g_{12}+g_{22}}{60}\Omega^4_{ijk} - \big(\big[3g_{11}+4g_{12}+3g_{22}\big] + \big[2g_{11}+3g_{12}+2g_{22}\big]\imath\,\Omega_{ijk} - \tfrac{1}{2}\big[g_{11}+2g_{12}+g_{22}\big]\Omega^2_{ijk}\big)\exp\big(-\imath\,\Omega_{ijk}\big)\Big).$$

Acknowledgments This research was supported by the DFG Collaborative Research Center TRR 109, "Discretization in Geometry and Dynamics".

References

1. Avron, J., Osadchy, D., Seiler, R.: A topological look at the quantum Hall effect. Phys. Today **56**, 38–42 (2003)
2. Bott, R.: On some recent interactions between mathematics and physics. Canad. Math. Bull. **28**, 129–164 (1985)
3. Christiansen, S., Halvorsen, T.: A gauge invariant discretization on simplicial grids of the Schrödinger eigenvalue problem in an electromagnetic field. SIAM J. Numer. Anal. **49**, 331–345 (2011)
4. Christiansen, S., Halvorsen, T.: A simplicial gauge theory. J. Math. Phys. **53** (2012)
5. Desbrun, M., Kanso, E., Tong, Y.: Discrete differential forms for computational modeling. In: Discrete Differential Geometry, pp. 287–324. Birkhäuser Basel (2008)
6. Halvorsen, T., Sørensen, T.: Simplicial gauge theory and quantum gauge theory simulation. Nucl. Phys. B **854**, 166–183 (2012)
7. Hatcher, A.: Algebraic Topology. Cambridge University Press (2002)
8. Knöppel, F., Crane, K., Pinkall, U., Schröder, P.: Globally optimal direction fields. ACM Trans. Graph. **32** (2013)
9. Knöppel, F., Crane, K., Pinkall, U., Schröder, P.: Stripe patterns on surfaces. ACM Trans. Graph. **34** (2015)
10. Kobayashi, S.: La connexion des variétés fibrés I and II. Comptes Rendus de l'Académie Sciences, Paris **54**(318–319), 443–444 (1954)
11. Kostant, B.: Quantization and unitary representations. In: Lectures in Modern Analysis and Applications III, vol. 170, pp. 87–208. Springer (1970)
12. Kreft, C., Seiler, R.: Models of the Hofstadter type. J. Math. Phys. **37**, 5207–5243 (1996)

13. Morrison, K.: Yang-Mills connections on surfaces and representations of the path group. Proc. Am. Math. Soc. **112**, 1101–1106 (1991)
14. Munkres, J.R.: Elements of algebraic topology. In: Advanced Book Classics. Perseus Books (1984)
15. Sasaki, K., Kawazoe, Y., Saito, R.: Aharonov-Bohm effect in higher genus materials. Physica A **321**, 369–375 (2004)
16. Seifert, H., Threlfall, W.: Lehrbuch der Topologie: mit 132 Figuren. Chelsea Scientific Books, Chelsea (1934)
17. Simms, D.J., Woodhouse, N.M.J.: Lectures on geometric quantization. In: Lecture Notes in Physics. Springer, Berlin (1976)
18. Weil, A.: Introduction a l'etude des varietes Kähleriennes. Actualités Scientifiques et Industrielles. Hermann (1958)
19. Weißmann, S., Pinkall, U., Schröder, P.: Smoke rings from smoke. ACM Trans. Graph. **33** (2014)

Holomorphic Vector Fields and Quadratic Differentials on Planar Triangular Meshes

Wai Yeung Lam and Ulrich Pinkall

Abstract Given a triangulated region in the complex plane, a discrete vector field Y assigns a vector $Y_i \in \mathbb{C}$ to every vertex. We call such a vector field holomorphic if it defines an infinitesimal deformation of the triangulation that preserves length cross ratios. We show that each holomorphic vector field can be constructed based on a discrete harmonic function in the sense of the cotan Laplacian. Moreover, to each holomorphic vector field we associate in a Möbius invariant fashion a certain holomorphic quadratic differential. Here a quadratic differential is defined as an object that assigns a purely imaginary number to each interior edge. Then we derive a Weierstrass representation formula, which shows how a holomorphic quadratic differential can be used to construct a discrete minimal surface with prescribed Gauß map and prescribed Hopf differential.

1 Introduction

Consider an open subset U in the complex plane $\mathbb{C} \cong \mathbb{R}^2$ with coordinates $z = x + iy$ together with a holomorphic vector field

$$Y = f \frac{\partial}{\partial x}.$$

Here Y is a real vector field. It assigns to each $p \in \mathbb{R}^2$ the vector $f(p) \in \mathbb{C} \cong \mathbb{R}^2$. We do not consider objects like $\frac{\partial}{\partial z}$ which are sections of the complexified tangent bundle $(\mathrm{T}\,\mathbb{R}^2)^{\mathbb{C}}$.

W.Y. Lam (✉) · U. Pinkall
Technische Universität Berlin, Inst. Für Mathematik,
Straße des 17. Juni 136, 10623 Berlin, Germany
e-mail: lam@math.tu-berlin.de

U. Pinkall
e-mail: pinkall@math.tu-berlin.de

A.I. Bobenko (ed.), *Advances in Discrete Differential Geometry*,
DOI 10.1007/978-3-662-50447-5_7

Note $f : U \to \mathbb{C}$ is a holomorphic function, i.e.

$$0 = f_{\bar{z}} = \frac{1}{2}\left(\frac{\partial f}{\partial x} + i\frac{\partial f}{\partial y}\right).$$

Let $t \mapsto g_t$ denote the local flow of Y (defined for small t on open subsets of U with compact closure in U). Then the euclidean metric pulled back under g_t is conformally equivalently to the original metric:

$$g_t^*\langle\,,\rangle = e^{2u}\langle\,,\rangle$$

for some real-valued function u. The infinitesimal change in scale $\dot{u}$ is given by

$$\dot{u} = \frac{1}{2}\operatorname{div} Y = \operatorname{Re}(f_z).$$

Note that $\dot{u}$ is a harmonic function:

$$\dot{u}_{z\bar{z}} = 0.$$

On the other hand, differentiating $\dot{u}$ twice with respect to z yields one half the third derivative of f:

$$\dot{u}_{zz} = \frac{1}{2} f_{zzz}.$$

It is well-known that the vector field Y corresponds to an infinitesimal Möbius transformation of the extended complex plane $\overline{\mathbb{C}}$ if and only if f is a quadratic polynomial. In this sense f_{zzz} measures the infinitesimal "change in Möbius structure" under Y (Möbius structures are sometimes also called "complex projective structures" [6]). Moreover, the holomorphic quadratic differential

$$q := f_{zzz}\, dz^2$$

is invariant under Möbius transformations Φ. This is equivalent to saying that q is unchanged under a change of variable $\Phi(z) = w = \xi + i\eta$ whenever Φ is a Möbius transformation. This is easy to see if $\Phi(z) = az + b$ is an affine transformation. In this case

$$dw = a\, dz$$
$$\frac{d}{dw} = \frac{1}{a}\frac{d}{dz}$$

and therefore

$$Y = \tilde{f}\frac{\partial}{\partial \xi}$$

with

$$\tilde{f} = a\, f.$$

Thus we indeed have

$$\tilde{f}_{www}\, dw^2 = f_{zzz}\, dz^2.$$

A similar argument applies to $\Phi(z) = \frac{1}{z}$ and therefore to all Möbius transformations.

For realizations from an open subset U of the Riemann sphere $\mathbb{C}\mathrm{P}^1$ the vanishing of the Schwarzian derivative characterizes Möbius transformations. The quadratic differential q plays a similar role for vector fields. We call q the *Möbius derivative* of Y.

An important geometric context where holomorphic quadratic differentials arise comes from the theory of minimal surfaces: Given a simply connected Riemann surface M together with a holomorphic immersion $g : M \to S^2 \subset \mathbb{R}^3$ and a holomorphic quadratic differential q on M, there is a minimal surface $F : M \to \mathbb{R}^3$ (unique up to translations) whose Gauß map is g and whose second fundamental form is $\mathrm{Re}\, q$.

In this paper we will provide a discrete version for all details of the above story. Instead of smooth surfaces we will work with triangulated surfaces of arbitrary combinatorics. The notion of conformality will be that of conformal equivalence as explained in [3]. Holomorphic vector fields will be defined as infinitesimal conformal deformations.

There is also a completely parallel discrete story where conformal equivalence of planar triangulations is replaced by preserving intersection angles of circumcircles. To some extent we also tell this parallel story that belongs to the world of circle patterns.

The results on planar triangular meshes in this paper are closely related to isothermic triangulated surfaces in Euclidean space [8].

2 Discrete Conformality

In this section, we review two notions of discrete conformality for planar triangular meshes. We first start with some notations of triangular meshes.

Definition 2.1 A triangular mesh M is a simplicial complex whose underlying topological space is a connected 2-manifold (with boundary). The set of vertices (0-cells), edges (1-cells) and triangles (2-cells) are denoted as V, E and F.

We denote E_{int} the set of interior edges and V_{int} the set of interior vertices. Without further notice we will assume that all triangular meshes under consideration are oriented.

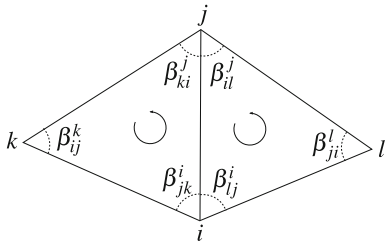

Fig. 1 Two neighboring and oriented triangles

Definition 2.2 A *realization* $z : V \to \mathbb{C}$ of a triangular mesh M in the extended complex plane assigns to each vertex $i \in V$ a point $z_i \in \overline{\mathbb{C}}$ in such a way that for each triangle $\{ijk\} \in F$ the points corresponding to its three vertices are not collinear.

Given two complex numbers $z_1, z_2 \in \mathbb{C}$ we write

$$\langle z_1, z_2 \rangle := \mathrm{Re}(\bar{z}_1 z_2).$$

We are looking for suitable definitions of conformal structure of a realization z. In particular, we want z to be conformally equivalent to $g \circ z$ whenever $g : \overline{\mathbb{C}} \to \overline{\mathbb{C}}$ is a Möbius transformations. This requirement will certainly be met if we base our definitions on complex cross ratios: Given a triangular mesh $z : V \to \mathbb{C}$, we associate a complex number to each interior edge $\{ij\} \in E_{int}$, namely the *cross ratio* of the corresponding four vertices (See Fig. 1)

$$\mathrm{cr}_{z,ij} = \frac{(z_j - z_k)(z_i - z_l)}{(z_k - z_i)(z_l - z_j)}.$$

Notice that $\mathrm{cr}_{z,ij} = \mathrm{cr}_{z,ji}$ and hence $\mathrm{cr}_z : E_{int} \to \mathbb{C}$ is well defined. It is easy to see that two realizations differ only by a Möbius transformation if and only if their corresponding cross ratios are the same. In order to arrive at a more flexible notion of conformality we need to relax the condition that demands the equality of all cross ratios. Two natural ways to do this is to only require equality of either the norm or alternatively the argument of the cross ratios. This leads to two different notions of discrete conformality: *conformal equivalence theory* [9, 13] and *circle pattern theory* [11].

Note that for the sake of simplicity of exposition we are ignoring here realizations in $\overline{\mathbb{C}}$ where one of the vertices is mapped to infinity.

2.1 Conformal Equivalence

The edge lengths of a triangular mesh realized in the complex plane provide a discrete counterpart for the induced Euclidean metric in the smooth theory. A notion

of conformal equivalence based on edge lengths was proposed by Luo [9]. Later Bobenko et al. [3] stated this notion in the following form:

Definition 2.3 Two realizations of a triangular mesh $z, w : V \to \mathbb{C}$ are *conformally equivalent* if the norm of the corresponding cross ratios are equal:

$$|\,\mathrm{cr}_z\,| \equiv |\,\mathrm{cr}_w\,|,$$

i.e. for each interior edge $\{ij\}$

$$\frac{|(z_j - z_k)||(z_i - z_l)|}{|(z_k - z_i)||(z_l - z_j)|} = \frac{|(w_j - w_k)||(w_i - w_l)|}{|(w_k - w_i)||(w_l - w_j)|}.$$

This definition can be restated in an equivalent form that closely mirrors the notion of conformal equivalence of Riemannian metrics:

Theorem 2.4 *Two realizations of a triangular mesh $z, w : V \to \mathbb{C}$ are conformally equivalent if and only if there exists $u : V \to \mathbb{R}$ such that*

$$|w_j - w_i| = e^{\frac{u_i + u_j}{2}} |z_j - z_i|.$$

Proof It is easy to see that the existence of u implies conformal equivalence. Conversely, for two conformally equivalent realizations z, w, we define a function $\sigma : E \to \mathbb{R}$ by

$$|w_j - w_i| = e^{\sigma_{ij}} |z_j - z_i|.$$

Since z, w are conformally equivalent σ satisfies for each interior edge $\{ij\}$

$$\sigma_{jk} - \sigma_{ki} + \sigma_{il} - \sigma_{lj} = 0.$$

For any vertex i and any triangle $\{ijk\}$ containing it we then define

$$e^{u_i} := e^{\sigma_{ki} + \sigma_{ij} - \sigma_{jk}}.$$

Note the vertex star of i is a triangulated disk if i is interior, or is a fan if i is a boundary vertex. Hence the value u_i defined in this way is independent of the chosen triangle. □

2.2 Circle Patterns

Given a triangular mesh realized in the complex plane we consider the circumscribed circles of its triangles. These circles inherit an orientation from their triangles. The intersection angles of these circles from neighboring triangles (Fig. 2)

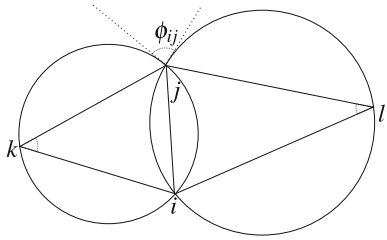

Fig. 2 The intersection angle of two neighboring circumscribed circles

define a function $\phi : E_{int} \to [0, 2\pi)$ which is related to the argument of the corresponding cross ratio via

$$\phi_{ij} = \mathrm{Arg}(\mathrm{cr}_{z,ij}). \tag{1}$$

Based on these angles we obtain another notion of discrete conformality which reflects the angle-preserving property that we have in the smooth theory.

Definition 2.5 Two realizations of a triangular mesh $z, w : V \to \mathbb{C}$ have the same *pattern structure* if the corresponding intersection angles of neighboring circumscribed circles are equal:

$$\mathrm{Arg}(\mathrm{cr}_{z,ij}) = \mathrm{Arg}(\mathrm{cr}_{w,ij}),$$

i.e. for each interior edge $\{ij\}$

$$\mathrm{Arg}\,\frac{(z_j - z_k)(z_i - z_l)}{(z_k - z_i)(z_l - z_j)} = \mathrm{Arg}\,\frac{(w_j - w_k)(w_i - w_l)}{(w_k - w_i)(w_l - w_j)}.$$

Just as conformal equivalence was related to scale factors u at vertices, having the same pattern structure is related to the existence of certain angular velocities α located at vertices:

Theorem 2.6 *Two realizations of a triangular mesh $z, w : V \to \mathbb{C}$ have the same pattern structure if and only if there exists $\alpha : V \to [0, 2\pi)$ such that*

$$\frac{w_j - w_i}{|w_j - w_i|} = e^{i\frac{\alpha_i + \alpha_j}{2}} \frac{z_j - z_i}{|z_j - z_i|}.$$

Proof The argument is very similar to the one for Theorem 2.4. In particular, the existence of the function α easily implies equality of the pattern structures. Conversely, assuming identical pattern structures we take any $\omega : E \to \mathbb{R}$ that satisfies

$$\frac{w_j - w_i}{|w_j - w_i|} = e^{i\omega_{ij}} \frac{z_j - z_i}{|z_j - z_i|}.$$

For any vertex i and any triangle $\{ijk\}$ containing it we define $\alpha_i \in [0, 2\pi)$ such that

$$e^{i\alpha_i} = e^{i(\omega_{ki}+\omega_{ij}-\omega_{jk})}.$$

Note the vertex star of i is a triangulated disk if i is interior, or is a fan if i is a boundary vertex. Hence having the same pattern structure implies that the value α_i is independent of the chosen triangle. □

3 Infinitesimal Deformations and Linear Conformal Theory

We will linearize both of the above notions of discrete conformality by considering infinitesimal deformations. This will allow us to relate them to linear discrete complex analysis, based on a discrete analogue of the Cauchy Riemann equations [4, 5, 10] (See the survey [12]).

Definition 3.1 An *infinitesimal conformal deformation* of a realization $z : V \to \mathbb{C}$ of a triangular mesh is a map $\dot{z} : V \to \mathbb{C}$ such that there exists $u : V \to \mathbb{R}$ satisfying

$$\mathrm{Re}\frac{\dot{z}_j - \dot{z}_i}{z_j - z_i} = \frac{\langle \dot{z}_j - \dot{z}_i, z_j - z_i \rangle}{|z_j - z_i|^2} = \frac{u_i + u_j}{2}.$$

We call u the *scale change* at vertices.

Definition 3.2 An *infinitesimal pattern deformation* of a realization $z : V \to \mathbb{C}$ of a triangular mesh is a map $\dot{z} : V \to \mathbb{C}$ such that there exists $\alpha : V \to \mathbb{R}$ satisfying

$$\mathrm{Im}\frac{\dot{z}_j - \dot{z}_i}{z_j - z_i} = \frac{\langle \dot{z}_j - \dot{z}_i, i(z_j - z_i) \rangle}{|z_j - z_i|^2} = \frac{\alpha_i + \alpha_j}{2}.$$

We call α the *angular velocities* at vertices.

Example 3.3 The infinitesimal deformations $\dot{z} := az^2 + bz + c$, where $a, b, c \in \mathbb{C}$ are constants, are both conformal and pattern deformations since

$$\frac{\dot{z}_j - \dot{z}_i}{z_j - z_i} = (az_i + b/2) + (az_j + b/2).$$

Infinitesimal conformal deformations and infinitesimal pattern deformations are closely related:

Theorem 3.4 *Suppose $z : V \to \mathbb{C}$ is a realization of a triangular mesh. Then an infinitesimal deformation $\dot{z} : V \to \mathbb{C}$ is conformal if and only if $i\dot{z}$ is a pattern deformation.*

Proof Notice

$$\frac{\langle \dot{z}_j - \dot{z}_i, z_j - z_i \rangle}{|z_j - z_i|^2} = \frac{\langle i\dot{z}_j - i\dot{z}_i, i(z_j - z_i) \rangle}{|z_j - z_i|^2}.$$

and the claim follows from Definition 3.1 and 3.2. □

3.1 Infinitesimal Deformations of a Triangle

Let $z : V \to \mathbb{C}$ be a realization of a triangulated mesh and $\dot{z}$ an infinitesimal deformation. Up to an infinitesimal translation $\dot{z}$ is completely determined by the infinitesimal scalings and rotations that it induces on each edge. These infinitesimal scalings and rotations of edges satisfy certain compatibility conditions on each triangle. These conditions involve the cotangent coefficients well known from the theory of discrete Laplacians. As we will see in Sect. 3.2, for conformal deformations (as well as for pattern deformations) the infinitesimal scalings and rotations of edges are indeed discrete harmonic functions.

Consider three pairwise distinct points $z_1, z_2, z_3 \in \mathbb{C}$ that do not lie on a line. In the following i, j, k denotes any cyclic permutation of the indexes 1, 2, 3. The triangle angle at the vertex i is denoted by β_i. We adopt the convention that all $\beta_1, \beta_2, \beta_3$ have positive sign if the triangle z_1, z_2, z_3 is positively oriented and a negative sign otherwise. Suppose we have an infinitesimal deformation of this triangle. Then there exists $\sigma_{ij}, \omega_{ij} \in \mathbb{R}$ such that

$$\dot{z}_j - \dot{z}_i = (\sigma_{ij} + i\omega_{ij})(z_j - z_i). \tag{2}$$

The scalars σ_{ij} and ω_{ij} describe the infinitesimal scalings and rotations of the edges. They satisfy the following compatibility conditions:

Lemma 3.5 *Given $\sigma_{ij}, \omega_{ij} \in \mathbb{R}$ the following statements are equivalent:*
(a) There exist $\dot{z}_i$ such that (2) holds.
(b) We have

$$0 = (\sigma_{12} + i\omega_{12})(z_2 - z_1) + (\sigma_{23} + i\omega_{23})(z_3 - z_2) + (\sigma_{31} + i\omega_{31})(z_1 - z_3). \tag{3}$$

(c) There exists $\omega \in \mathbb{R}$ such that

$$\begin{aligned} i\omega &= i\omega_{23} + i\cot\beta_1(\sigma_{31} - \sigma_{12}) \\ &= i\omega_{31} + i\cot\beta_2(\sigma_{12} - \sigma_{23}) \\ &= i\omega_{12} + i\cot\beta_3(\sigma_{23} - \sigma_{31}). \end{aligned}$$

(d) There exist $\sigma \in \mathbb{R}$ such that

$$\begin{aligned}\sigma &= \sigma_{23} + i\cot\beta_1(i\omega_{31} - i\omega_{12})\\ &= \sigma_{31} + i\cot\beta_2(i\omega_{12} - i\omega_{23})\\ &= \sigma_{12} + i\cot\beta_3(i\omega_{23} - i\omega_{31}).\end{aligned}$$

Proof The relation between (a) and (b) is obvious. We show the equivalence between (b) and (c). With A denoting the signed triangle area we have the following identities:

$$\begin{aligned}0 &= \langle i(z_j - z_i), z_j - z_i\rangle,\\ 2A &= \langle i(z_j - z_i), z_k - z_j\rangle,\\ \langle i(z_j - z_i), i(z_j - z_i)\rangle &= \langle z_j - z_i, z_j - z_i\rangle.\end{aligned}$$

Using these identities and $z_3 - z_2 \in \mathrm{span}_{\mathbb{R}}\{i(z_1 - z_3), i(z_2 - z_1)\}$ we obtain

$$z_3 - z_2 = \cot(\beta_3)i(z_2 - z_1) - \cot(\beta_2)i(z_1 - z_3). \tag{4}$$

Cyclic permutation yields

$$\begin{aligned}z_1 - z_3 &= \cot(\beta_1)i(z_3 - z_2) - \cot(\beta_3)i(z_2 - z_1),\\ z_2 - z_1 &= \cot(\beta_2)i(z_1 - z_3) - \cot(\beta_1)i(z_3 - z_2).\end{aligned}$$

Substituting these identities into Equation (3) we obtain

$$\begin{aligned}0 = \quad & \sigma_1\big(\cot(\beta_3)i(z_2 - z_1) - \cot(\beta_2)i(z_1 - z_3)\big) + \omega_{23}i(z_3 - z_2)\\ & + \sigma_2\big(\cot(\beta_1)i(z_3 - z_2) - \cot(\beta_3)i(z_2 - z_1)\big) + \omega_{31}i(z_1 - z_3)\\ & + \sigma_3\big(\cot(\beta_2)i(z_1 - z_3) - \cot(\beta_1)i(z_3 - z_2)\big) + \omega_{12}i(z_2 - z_1)\\ = \quad & \big(\omega_1 + \cot\beta_1(\sigma_2 - \sigma_3)\big)i(z_3 - z_2)\\ & + \big(\omega_2 + \cot\beta_2(\sigma_3 - \sigma_1)\big)i(z_1 - z_3)\\ & + \big(\omega_3 + \cot\beta_3(\sigma_1 - \sigma_2)\big)i(z_2 - z_1).\end{aligned}$$

Now we use that $\lambda_1, \lambda_2, \lambda_3 \in \mathbb{C}$ satisfy

$$\lambda_1 i(z_3 - z_2) + \lambda_2 i(z_1 - z_3) + \lambda_3 i(z_2 - z_1) = 0,$$

if and only if $\lambda_1 = \lambda_2 = \lambda_3$. This establishes the equivalence of (b) and (c). The equivalence of (b) and (d) is seen in a similar fashion by eliminating $i(z_j - z_i)$ in (3) instead of $(z_j - z_i)$. □

The quantity ω above describes the average rotation speed of the triangle. Similarly, it can be verified that the above σ satisfies

$$\sigma = \frac{\dot{R}}{R}$$

where R denotes the circumradius of the triangle. Thus σ signifies an average scaling of the triangle.

3.2 Harmonic Functions with Respect to the Cotangent Laplacian

In smooth complex analysis conformal maps are closely related to harmonic functions. If a conformal map preserves orientation it is holomorphic and satisfies the Cauchy Riemann equations. In particular, its real part and the imaginary part are conjugate harmonic functions. Conversely, given a harmonic function on a simply connected surface then it is the real part of some conformal map.

A similar relationship manifests between discrete harmonic functions (in the sense of the cotangent Laplacian) and infinitesimal deformations of triangular meshes. Discrete harmonic functions can be regarded as the real part of holomorphic functions which satisfies a discrete analogue of the Cauchy Riemann equations. In particular, a relation between discrete harmonic functions and infinitesimal pattern deformations was found by Bobenko, Mercat and Suris [2]. Integrable systems were involved in this context. We extend their result to include the case of infinitesimal conformal deformations.

Theorem 3.6 *Let $z : V \to \mathbb{C}$ be a simply connected triangular mesh realized in the complex plane and $h : V \to \mathbb{R}$ be a function. Then the following are equivalent:*

(a) h is a harmonic function with respect to the cotangent Laplacian, i.e. using the notation of Fig. 1, for all interior vertices $i \in V_{int}$ we have

$$\sum_j (\cot \beta_{ij}^k + \cot \beta_{ji}^l)(h_j - h_i) = 0. \tag{5}$$

(b) There exists an infinitesimal conformal deformation $\dot{z} : V \to \mathbb{C}$ with scale factors given by h. It is unique up to infinitesimal rotations and translations.

(c) There exists an infinitesimal pattern deformation $i\dot{z} : V \to \mathbb{C}$ with h as angular velocities. It is unique up to infinitesimal scalings and translations.

Proof We show the equivalence of the first two statements. The equivalence of the first and the third follows similarly.

Suppose h is a harmonic function. Since the triangular mesh is simply connected, equation (5) implies the existence of a function $\tilde{\omega} : F \to \mathbb{R}$ such that for all interior edges $\{ij\}$ we have

$$i\tilde{\omega}_{ijk} - i\tilde{\omega}_{jil} = i(\cot \beta_{ij}^k + \cot \beta_{ji}^l)(h_j - h_i).$$

Here $\tilde{\omega}$ is unique up to an additive constant and called the *conjugate harmonic function* of h. Using $\tilde{\omega}$ we define a function $\omega : E \to \mathbb{R}$ via

$$i\omega_{ij} = i\tilde{\omega}_{ijk} - i \cot \beta_{ij}^k (h_j - h_i).$$

Lemma 3.5 now implies that there exists $\dot{z} : V \to \mathbb{C}$ such that

$$(\dot{z}_j - \dot{z}_i) = \left(\frac{h_i + h_j}{2} + i\omega_{ij} \right) (z_j - z_i).$$

This gives us the desired infinitesimal conformal deformation of z with h as scale factors.

To show uniqueness, suppose $\dot{z}, \dot{z}'$ are infinitesimal conformal deformations with the same scale factors. Then $\dot{z} - \dot{z}'$ preserves all the edge lengths of the triangular mesh and hence is induced from an Euclidean transformation.

Conversely, given an infinitesimal conformal deformation $\dot{z}$ with scale factors h. We write

$$\dot{z}_j - \dot{z}_i = \left(\frac{h_i + h_j}{2} + i\omega_{ij} \right) (z_j - z_i)$$

for some $\omega : E \to \mathbb{R}$. Lemma 3.5 implies that there is a function $\tilde{\omega} : F \to \mathbb{R}$ such that

$$i\tilde{\omega}_{ijk} = i\omega_{ij} + i \cot \beta_{ij}^k (h_j - h_i).$$

We have

$$i\tilde{\omega}_{ijk} - i\tilde{\omega}_{jil} = i(\cot \beta_{ij}^k + \cot \beta_{ji}^l)(h_j - h_i)$$

and

$$\sum_j (\cot \beta_{ij}^k + \cot \beta_{ji}^l)(h_j - h_i) = 0.$$

Therefore h is harmonic. □

4 Holomorphic Quadratic Differentials

In this section, we introduce a discrete analogue of holomorphic quadratic differentials. We illustrate their correspondence to discrete harmonic functions. It reflects the property in the smooth theory that holomorphic quadratic differentials parametrize Möbius structures on Riemann surfaces ([6, Chap. 9]).

To simplify the notation, we make use of discrete differential forms. We denote $\vec{E}$ the set of oriented edges and $\vec{E}_{int}$ the set of oriented interior edges. Given an oriented triangular mesh M, a complex-valued function $\eta : \vec{E} \to \mathbb{C}$ is called a *discrete 1-form* if

$$\eta(e_{ij}) = -\eta(e_{ji}) \quad \forall e_{ij} \in \vec{E}.$$

It is *closed* if for every face $\{ijk\}$

$$\eta(e_{ij}) + \eta(e_{jk}) + \eta(e_{ki}) = 0.$$

It is *exact* if there exists a function $f : V \to \mathbb{C}$ such that

$$\eta(e_{ij}) = df(e_{ij}) := f_j - f_i.$$

Similarly, we can consider discrete 1-forms on the dual graph M^* of M and these are called *dual 1-forms*. Given an oriented edge e, we denote e^* its dual edge oriented from the right face of e to its left face. The set of oriented dual edges is denoted by $\vec{E}^*$.

Definition 4.1 Given a triangular mesh $z : V \to \mathbb{C}$ realized on the complex plane, a function $q : E_{int} \to i\mathbb{R}$ defined on interior edges is a *discrete holomorphic quadratic differential* if it satisfies for every interior vertex $i \in V_{int}$

$$\sum_j q_{ij} = 0,$$
$$\sum_j q_{ij}/dz(e_{ij}) = 0.$$

Theorem 4.2 *Let $q : E_{int} \to i\mathbb{R}$ be a holomorphic quadratic differential on a realization $z : V \to \mathbb{C}$ of a triangular mesh. Suppose $\Phi : \overline{\mathbb{C}} \to \overline{\mathbb{C}}$ is a Möbius transformation which does not map any vertex to infinity. Then q is again a holomorphic quadratic differential on $w := \Phi \circ z$.*

Proof Since Möbius transformations are generated by Euclidean transformations and inversions, it suffices to consider the inversion in the unit circle at the origin

$$w := \Phi(z) = 1/z.$$

We have

$$\sum_j q_{ij}/dw(e_{ij}) = \sum_j -z_i z_j q_{ij}/dz(e_{ij}) = -z_i \sum_j q_{ij} - z_i^2 \sum_j q_{ij}/dz(e_{ij}) = 0.$$

Hence the claims follow. □

We are going to show that on a simply connected triangular mesh, there is a correspondence between discrete holomorphic quadratic differentials and discrete harmonic functions.

We first show how to construct a discrete holomorphic quadratic differential from a harmonic function. Given a function $u : V \to \mathbb{R}$ on a realization of $z : V \to \mathbb{C}$ of a triangular mesh M. If we interpolate it piecewise-linearly over each triangular face, its gradient is constant on each face and we have $\mathrm{grad}_z u : F \to \mathbb{C}$ given by

$$\mathrm{grad}_z u_{ijk} = i \frac{u_i dz(e_{jk}) + u_j dz(e_{ki}) + u_k dz(e_{ij})}{2A_{ijk}}.$$

Note that we ignore here the non-generic case (which leads to the vanishing of the area) where the triangle degenerates in the sense that its circumcircle passes through the point at infinity. Also note that for a non-degenerate triangle that is mapped by z in $\mathbb{C}$ in an orientation reversing fashion the area A_{ijk} is considered to have a negative sign. Granted this, one can verify that the gradient of u satisfies

$$\langle \mathrm{grad}_z u_{ijk}, dz(e_{ij}) \rangle = u_j - u_i \quad \forall \{ij\} \subset \{ijk\} \in F.$$

We define $u_z : F \to \mathbb{C}$ by

$$u_z := \frac{1}{2} \overline{\mathrm{grad}_z u}.$$

and the dual 1-form $du_z : \vec{E}^*_{int} \to \mathbb{C}$ on M by

$$du_z(e^*_{ij}) := (u_z)_{ijk} - (u_z)_{jil}$$

where $\{ijk\}$ is the left face and $\{jil\}$ is the right face of the oriented edge e_{ij}.

Lemma 4.3 *Given a function $u : V \to \mathbb{R}$ on a realization of a triangular mesh $z : V \to \mathbb{C}$, we have*

$$\begin{aligned} &du_z(e^*_{ij}) dz(e_{ij}) \\ =&\frac{-i}{2}\big(\cot \beta^i_{jk}(u_k - u_j) + \cot \beta^j_{ki}(u_k - u_i) + \cot \beta^j_{il}(u_l - u_i) + \cot \beta^i_{lj}(u_l - u_j)\big) \end{aligned}$$

which is purely imaginary (Fig. 1).

Proof Since

$$\langle \operatorname{grad}_z u_{ijk}, dz(e_{ij})\rangle = u_j - u_i = \langle \operatorname{grad}_z u_{jkl}, dz(e_{ij})\rangle,$$

we have

$$\operatorname{Re}(du_z(e_{ij}^*)dz(e_{ij})) = 0.$$

On the other hand, using equation (4) we get

$$\begin{aligned}
&\operatorname{Re}(du_z(e_{ij}^*)i\,dz(e_{ij}))\\
=&\operatorname{Re}(((u_z)_{ijk} - (u_z)_{jil})i\,dz(e_{ij}))\\
=&(\langle \operatorname{grad}_z u_{ijk}, \cot\beta_{jk}^i dz(e_{jk}) - \cot\beta_{ki}^j dz(e_{ki})\rangle\\
&+\langle \operatorname{grad}_z u_{jil}, \cot\beta_{il}^j dz(e_{il}) - \cot\beta_{lj}^i dz(e_{lj})\rangle)/2\\
=&\frac{1}{2}\big(\cot\beta_{jk}^i(u_k-u_j) + \cot\beta_{ki}^j(u_k-u_i) + \cot\beta_{il}^j(u_l-u_i) + \cot\beta_{lj}^i(u_l-u_j)\big).
\end{aligned}$$

Hence the claim follows. □

Lemma 4.4 *Given a realization $z : V \to \mathbb{C}$ of a triangular mesh. A function $u : V \to \mathbb{R}$ is harmonic if and only if the function $q : E_{int} \to i\mathbb{R}$ defined by*

$$q_{ij} := du_z(e_{ij}^*)dz(e_{ij})$$

is a holomorphic quadratic differential.

Proof Note q is well defined since

$$q_{ij} = du_z(e_{ij}^*)dz(e_{ij}) = du_z(e_{ji}^*)dz(e_{ji}) = q_{ji}.$$

It holds for general functions $u : V \to \mathbb{R}$ that

$$\begin{aligned}
&\operatorname{Re}(q) \equiv 0\\
&\sum_j q_{ij}/dz(e_{ij}) = \sum_j du_z(e_{ij}^*) = 0 \quad \forall i \in V_{int}.
\end{aligned}$$

We know from Lemma 4.3 that for every interior vertex $i \in V_{int}$

$$\sum_j q_{ij} = \sum_j du_z(e_{ij}^*)dz(e_{ij}) = \frac{i}{2}\sum_j(\cot\beta_{ij}^k + \cot\beta_{ji}^l)(u_j - u_i).$$

Hence, u is harmonic if and only if q is a holomorphic quadratic differential. □

Lemma 4.5 *Let $z : V \to \mathbb{C}$ be a realization of a simply connected triangular mesh. Given a function $q : E_{int} \to i\mathbb{R}$ such that for every interior vertex $i \in V_{int}$*

$$\sum_j q_{ij}/dz(e_{ij}) = 0,$$

there exists a function $u : V \to \mathbb{R}$ such that for every interior edge $\{ij\}$

$$q_{ij} = du_z(e_{ij}^*)dz(e_{ij}).$$

Proof We consider a dual 1-form τ on M defined by

$$\tau(e_{ij}^*) = q_{ij}/dz(e_{ij}).$$

Since M is simply connected and

$$\sum_j \tau(e_{ij}^*) = \sum_j q_{ij}/dz(e_{ij}) = 0,$$

there exists a function $h : F \to \mathbb{C}$ such that

$$dh(e_{ij}^*) := h_{ijk} - h_{jil} = \tau(e_{ij}^*).$$

It implies we have $\mathrm{Re}(dh(e^*)dz(e)) = \mathrm{Re}(q) \equiv 0$ and

$$\omega(e_{ij}) := \langle 2\bar{h}_{ijk}, dz(e_{ij})\rangle = \langle 2\bar{h}_{jil}, dz(e_{ij})\rangle$$

is a well-defined $\mathbb{R}$-valued 1-form. Since the triangular mesh is simply connected and for every face $\{ijk\}$

$$\omega(e_{ij}) + \omega(e_{jk}) + \omega(e_{ki}) = 0,$$

there exists a function $u : V \to \mathbb{R}$ such that for every oriented edge e_{ij}

$$du(e_{ij}) = u_j - u_i = \omega(e_{ij}).$$

It can be verified that

$$h = \frac{1}{2}\overline{\mathrm{grad}_z\, u} = u_z.$$

Hence we obtain

$$q_{ij} = \tau(e_{ij}^*)dz(e_{ij}) = dh(e_{ij}^*)dz(e_{ij}) = du_z(e_{ij}^*)dz(e_{ij})$$

for every interior edge $\{ij\}$. □

Theorem 4.6 *Suppose $z : V \to \mathbb{C}$ is a realization of a simply connected triangular mesh. Then any holomorphic quadratic differential $q : E_{int} \to i\mathbb{R}$ is of the form*

$$q_{ij} = du_z(e_{ij}^*)dz(e_{ij}) \quad \forall e_{ij} \in \vec{E}_{int}$$

for some harmonic function $u : V \to \mathbb{R}$.

Furthermore, the space of holomorphic quadratic differentials is a vector space isomorphic to the space of discrete harmonic functions module linear functions.

Proof The first part of the statement follows from Lemmas 4.4 and 4.5. In order to show the second part, it suffices to observe that

$$du_z \equiv 0 \iff \operatorname{grad} u \equiv a \iff du = \langle a, dz \rangle \iff u = \langle a, z \rangle + b$$

for some $a, b \in \mathbb{C}$. □

In previous sections, we showed that every harmonic function corresponds to an infinitesimal conformal deformation. The following shows that discrete holomorphic quadratic differentials are the change in the intersection angles of circumscribed circles.

Theorem 4.7 *Let $z : V \to \mathbb{C}$ be a realization of a simply connected triangular mesh. Suppose $u : V \to \mathbb{R}$ is a discrete harmonic function and $\dot{z}$ is an infinitesimal conformal deformation with u as scale factors. Then we have*

$$du_z dz = -\frac{1}{2}\frac{\dot{\mathrm{cr}}_z}{\mathrm{cr}_z} = -\frac{i}{2}\dot{\phi}$$

where $\dot{\phi} : E_{int} \to \mathbb{R}$ denotes the change in the intersection angles of neighboring circumscribed circles.

Proof We write $(\dot{z}_j - \dot{z}_i) = (\frac{h_i + h_j}{2} + i\omega_{ij})(z_j - z_i)$. Applying Lemma 4.3 we have

$$\begin{aligned}
\dot{\mathrm{cr}}_{z,ij} / \mathrm{cr}_{z,ij} &= i\omega_{jk} - i\omega_{ki} + i\omega_{il} - i\omega_{lj} \\
&= i\big(\cot \beta_{jk}^i (u_k - u_j) + \cot \beta_{ki}^j (u_k - u_i) + \cot \beta_{il}^j (u_l - u_i) + \cot \beta_{lj}^i (u_l - u_j)\big) \\
&= -2du_z(e_{ij}^*)dz(e_{ij}).
\end{aligned}$$

The equality

$$\frac{\dot{\mathrm{cr}}_z}{\mathrm{cr}_z} = i\dot{\phi}$$

follows from Equation (1). □

5 Conformal Deformations in Terms of End($\mathbb{C}^2$)

In this section we show how an infinitesimal conformal deformation gives rise to a discrete analogue of a holomorphic null curve in $\mathbb{C}^3$. Later we will see that the real parts of such a "holomorphic null curve" can be regarded as the Weierstrass representation of a discrete minimal surface.

Up to now we have mostly treated the Riemann sphere $\mathbb{C}\mathrm{P}^1$ as the extended complex plane $\overline{\mathbb{C}} = \mathbb{C} \cup \{\infty\}$. In this section we will take a more explicitly Möbius geometric approach: We will represent fractional linear transformations of $\overline{\mathbb{C}}$ by linear transformations of $\mathbb{C}^2$ with determinant one. Actually, the group of Möbius transformations is

$$\mathrm{M\ddot{o}b}(\overline{\mathbb{C}}) \cong \mathrm{PSL}\,(2,\mathbb{C}) \cong \mathrm{SL}\,(2,\mathbb{C})/(\pm I). \tag{6}$$

However, since we are mainly interested in infinitesimal deformations and any map into $\mathrm{PSL}(2,\mathbb{C})$ whose values stay close to the identity admits a canonical lift to $\mathrm{SL}(2,\mathbb{C})$, we can safely ignore the difference between $\mathrm{PSL}(2,\mathbb{C})$ and $\mathrm{SL}(2,\mathbb{C})$.

Given a realization $z : V \to \mathbb{C}$ of a triangular mesh we consider its lift $\psi : V \to \mathbb{C}^2$

$$\psi := \begin{pmatrix} z \\ 1 \end{pmatrix}$$

and regard the realization as a map $\Psi : V \to \mathbb{C}\mathrm{P}^1$ where

$$\Psi := \mathbb{C}\begin{pmatrix} z \\ 1 \end{pmatrix} = [\psi].$$

The action of a Möbius transformation on the Riemann sphere is given by a matrix $A \in \mathrm{SL}(2,\mathbb{C})$, which is unique up to sign:

$$[\varphi] \mapsto [A\varphi].$$

Before we investigate infinitesimal deformations we first consider finite deformations of a triangular mesh $\Psi : V \to \mathbb{C}\mathrm{P}^1$. Given such a finite deformation, the change in the positions of the three vertices of a triangle $\{ijk\}$ can be described by a Möbius transformation, which is represented by $G_{ijk} \in \mathrm{SL}(2,\mathbb{C})$. They satisfy a compatibility condition on each interior edge $\{ij\}$ (see Fig. 1):

$$[G_{ijk}\psi_i] = [G_{jil}\psi_i],$$
$$[G_{ijk}\psi_j] = [G_{jil}\psi_j].$$

Suppose now that the mesh is simply connected. Then up to a global Möbius transformation the map $G : F \to \mathrm{SL}(2, \mathbb{C})$ can be uniquely reconstructed from the *multiplicative dual 1-form* defined as

$$G(e^*_{ij}) := G_{jil}^{-1} G_{ijk}.$$

$G(e^*_{ij})$ is defined whenever $\{ij\}$ is an interior edge and we have

$$G(e^*_{ij}) = G(e^*_{ji})^{-1}.$$

Moreover, for every interior vertex i we have

$$\prod_j G(e^*_{ij}) = I.$$

The compatibility conditions imply that for interior each edge $\{ij\}$ there exist $\lambda_{ij,i}, \lambda_{ij,j} \in \mathbb{C}\backslash\{0\}$ such that

$$G(e^*_{ij})\psi_i = \lambda_{ij,i}\psi_i$$
$$G(e^*_{ij})\psi_j = \lambda_{ij,j}\psi_j.$$

Since $\lambda_{ij,i}\,\lambda_{ij,j} = \det(G(e^*_{ij})) = 1$, we have

$$\lambda_{ij} := \lambda_{ij,i} = 1/\lambda_{ij,j}.$$

Because of $G(e^*_{ij}) = G(e^*_{ij})^{-1}$ we know

$$\lambda_{ij} = \lambda_{ij,i} = 1/\lambda_{ji,i} = \lambda_{ji}.$$

Hence λ defines a complex-valued function on the set E_{int} of interior edges.

We now show that for each interior edge λ_{ij} determines the change in the cross ratio of the four points of the two adjacent triangles. Note that the cross ratio of four points in $\mathbb{C}\mathrm{P}^1$ can expressed as

$$\mathrm{cr}([\psi_j], [\psi_k], [\psi_i], [\psi_l]) = \frac{\det(\psi_k, \psi_j)\det(\psi_l, \psi_i)}{\det(\psi_i, \psi_k)\det(\psi_j, \psi_l)}.$$

Lemma 5.1 *Suppose we are given four points* $[\psi_i], [\psi_j], [\psi_k], [\psi_l] \in \mathbb{C}\mathrm{P}^1$ *and* $G \in \mathrm{SL}(2, \mathbb{C})$ *with*

$$G\psi_i = \lambda^{-1}\psi_i$$
$$G\psi_j = \lambda\psi_j$$

for some $\lambda \in \mathbb{C}\backslash\{0\}$. *Then the cross ratio of the four transformed points*

$$[\tilde{\psi}_i] = [G\psi_i], \quad [\tilde{\psi}_j] = [G\psi_j], \quad [\tilde{\psi}_k] = [G\psi_k], \quad [\tilde{\psi}_l] = [\psi_l]$$

is given by

$$\mathrm{cr}([\tilde{\psi}_j], [\tilde{\psi}_k], [\tilde{\psi}_i], [\tilde{\psi}_l]) = \mathrm{cr}([\psi_j], [\psi_k], [\psi_i], [\psi_l])/\lambda^2.$$

Proof

$$\begin{aligned}\mathrm{cr}([\tilde{\psi}_j], [\tilde{\psi}_k], [\tilde{\psi}_i], [\tilde{\psi}_l]) &= \frac{\det(G\psi_k, G\psi_j)\det(\psi_l, G\psi_i)}{\det(G\psi_i, G\psi_k)\det(G\psi_j, \psi_l)} \\ &= \mathrm{cr}([\psi_j], [\psi_k], [\psi_i], [\psi_l])/\lambda^2.\end{aligned}$$

□

We now can summarize the information about finite deformations of a realization as follows:

Theorem 5.2 *Let* $\Psi : V \to \mathbb{C}\mathrm{P}^1$ *be a realization of a simply connected triangular mesh. Then there is a bijection between finite deformations of* Ψ *in* $\mathbb{C}\mathrm{P}^1$ *modulo global Möbius transformations and multiplicative dual 1 forms* $G : \vec{E}^*_{int} \to \mathrm{SL}(2, \mathbb{C})$ *satisfying for every interior vertex i*

$$\prod_j G(e^*_{ij}) = I$$

and for every interior edge

$$\begin{aligned}G(e^*_{ij}) &= G(e^*_{ji})^{-1} \\ G(e^*_{ij})\psi_i &= \lambda_{ij}^{-1}\psi_i \\ G(e^*_{ij})\psi_j &= \lambda_{ij}\psi_j.\end{aligned}$$

Here $\lambda : E_{int} \to \mathbb{C}\backslash\{0\}$. *We denote* $\mathrm{cr} : E_{int} \to \mathbb{C}$ *the cross ratios of* Ψ *and* $\widetilde{\mathrm{cr}} : E_{int} \to \mathbb{C}$ *the cross ratios of a new realization described by G. Then*

$$\widetilde{\mathrm{cr}} = \mathrm{cr}\,/\lambda^2.$$

In particular,

$$\begin{aligned}|\lambda| \equiv 1 &\implies \textit{the deformation is conformal.} \\ \mathrm{Arg}(\lambda) \equiv 0 &\implies \textit{the deformation is a pattern deformation.}\end{aligned}$$

Suppose we have a family of deformations described by dual 1-forms $G_t : \vec{E}_{int} \to \mathrm{SL}(2,\mathbb{C})$ with $G_0 \equiv I$. By considering $\eta := \frac{d}{dt}|_{t=0} G_t$ we obtain the following description of infinitesimal deformations:

Corollary 5.3 *Let $\Psi : V \to \mathbb{C}\mathrm{P}^1$ be a realization of a simply connected triangular mesh. Then there is a bijection between infinitesimal deformations of Ψ in $\mathbb{C}\mathrm{P}^1$ modulo infinitesimal Möbius transformations and dual 1 forms $\eta : \vec{E}_{int} \to \mathrm{sl}(2,\mathbb{C})$ satisfying for every interior vertex i*

$$\sum_j \eta(e_{ij}^*) = 0 \tag{7}$$

and for every interior edge

$$\begin{aligned} \eta(e_{ij}^*) &= -\eta(e_{ji}^*) \\ \eta(e_{ij}^*)\psi_i &= -\mu_{ij}\,\psi_i \\ \eta(e_{ij}^*)\psi_j &= \mu_{ij}\,\psi_j. \end{aligned}$$

Here $\mu : E_{int} \to \mathbb{C}$. We denote $\mathrm{cr} : E_{int} \to \mathbb{C}$ the cross ratios of Ψ and $\dot{\mathrm{cr}} : E_{int} \to \mathbb{C}$ the rate of change in cross ratios induced by the infinitesimal deformation described by η. Then

$$\mu = -\frac{1}{2}\frac{\dot{\mathrm{cr}}}{\mathrm{cr}}.$$

In particular,

$$\begin{aligned} Re(\mu) \equiv 0 &\implies \textit{the infinitesimal deformation is conformal}, \\ Im(\mu) \equiv 0 &\implies \textit{the infinitesimal deformation is a pattern deformation.} \end{aligned}$$

Note that given a mesh, the 1-form η is uniquely determined by the eigenfunction μ. We now investigate the constraints on μ implied by the closedness condition (7) of η.

Consider the symmetric bilinear form $(\,,\,) : \mathbb{C}^2 \times \mathbb{C}^2 \to \mathrm{sl}(2,\mathbb{C})$

$$(\phi,\varphi)v := \det(\phi, v)\varphi + \det(\varphi, v)\phi.$$

For $\psi_i \neq \psi_j \in \mathbb{C}^2$ we define

$$m_{ij} := \frac{1}{\det(\psi_i, \psi_j)}(\psi_j, \psi_i) \in \mathrm{sl}(2,\mathbb{C}).$$

The matrix m_{ij} is independent of the representatives of $[\psi_i], [\psi_j] \in \mathbb{C}\mathrm{P}^1$ and we have

$$\begin{aligned} m_{ij} &= -m_{ji} \\ m_{ij}\psi_i &= -\psi_i \\ m_{ij}\psi_j &= \psi_j. \end{aligned}$$

Using the representatives $\psi_i = \begin{pmatrix} z_i \\ 1 \end{pmatrix}$ we obtain

$$\begin{aligned} \eta(e_{ij}^*) =& \frac{\mu_{ij}}{\det(\psi_j, \psi_i)}(\psi_i, \psi_j) \\ =& \frac{\mu_{ij}}{z_j - z_i} \begin{pmatrix} z_i + z_j & -2z_i z_j \\ 2 & -z_i - z_j \end{pmatrix}. \end{aligned}$$

Hence

$$\sum_j \eta(e_{ij}^*) = 0 \quad \Longleftrightarrow \quad \sum_j \mu_{ij} = 0 \quad \text{and} \quad \sum_j \mu_{ij}/(z_j - z_i) = 0. \tag{8}$$

We consider the Pauli matrices

$$\sigma_1 = \begin{pmatrix} 0 & 1 \\ 1 & 0 \end{pmatrix}, \quad \sigma_2 = \begin{pmatrix} 0 & i \\ -i & 0 \end{pmatrix}, \quad \sigma_3 = \begin{pmatrix} 1 & 0 \\ 0 & -1 \end{pmatrix}$$

which form a basis of $\mathrm{sl}(2, \mathbb{C})$. Then

$$\eta(e_{ij}^*) = \frac{\mu_{ij}}{z_j - z_i}((1 - z_i z_j)\sigma_1 + i(1 + z_i z_j)\sigma_2 + (z_i + z_j)\sigma_3).$$

If we now identify $\mathrm{sl}(2, \mathbb{C})$ with $\mathbb{C}^3$ via

$$\sigma_i \mapsto \begin{pmatrix} 1 \\ 0 \\ 0 \end{pmatrix}, \sigma_2 \mapsto \begin{pmatrix} 0 \\ 1 \\ 0 \end{pmatrix}, \sigma_3 \mapsto \begin{pmatrix} 0 \\ 0 \\ 1 \end{pmatrix},$$

we obtain

$$\eta(e_{ij}^*) = \frac{\mu_{ij}}{z_j - z_i} \begin{pmatrix} 1 - z_i z_j \\ i(1 + z_i z_j) \\ z_i + z_j \end{pmatrix}. \tag{9}$$

Thus to every infinitesimal deformation of a realized triangular mesh we can associate a closed $\mathrm{sl}(2, \mathbb{C})$-valued dual 1-form. In the special case of an infinitesimal conformal deformation (i.e. μ is real-valued) we will see that this yields a discrete analogue of the Weierstrass representation for minimal surfaces.

6 Weierstrass Representation of Discrete Minimal Surfaces

The Weierstrass representation for minimal surfaces in $\mathbb{R}^3$ is the most classical example for applications of complex analysis:

Theorem 6.1 *Given two meromorphic functions $g, h : U \subset \mathbb{C} \to \mathbb{C}$ such that $g^2 h$ is holomorphic. Then $f : U \to \mathbb{R}^3$ defined by*

$$df = Re\left(\begin{pmatrix} 1-g^2 \\ i(1+g^2) \\ 2g \end{pmatrix} h(z)dz\right) = Re\left(\begin{pmatrix} 1-g^2 \\ i(1+g^2) \\ 2g \end{pmatrix} \frac{q}{dg}\right)$$

is a minimal surface. Its Gauß map n is the stereographic projection of g

$$n = \frac{1}{|g|^2+1}\begin{pmatrix} 2Reg \\ 2Img \\ |g|^2-1 \end{pmatrix}.$$

The holomorphic quadratic differential $q := hg_z dz^2$ is called the Hopf differential of f and encodes its second fundamental form: The direction defined by a nonzero tangent vector W is

$$\begin{aligned} \textit{an asymptotic direction} &\iff q(W) \in i\mathbb{R}. \\ \textit{a principal curvature direction} &\iff q(W) \in \mathbb{R}. \end{aligned}$$

Locally, every minimal surface can be written in this form.

We now develop a discrete version of this theorem for arbitrary triangular meshes realized in the complex plane. A similar formula for quadrilateral meshes with factorized real cross ratios was established by Bobenko and Pinkall [1]. Here we will use the definition of a discrete minimal surface f with Gauß map n given in [8]:

Definition 6.2 Let $n : V \to \mathbb{S}^2$ be a realization of a triangular mesh on the unit sphere in $\mathbb{R}^3$. Then a map $f : F \to \mathbb{R}^3$ defined on the set F of faces is called a discrete minimal surface with Gauß map n if for all oriented interior edges e_{ij} we have

$$(n_j - n_i) \times (f_{ijk} - f_{jil}) = 0.$$

Here $\{ijk\}$ and $\{jil\}$ denote the left and the right faces of e_{ij}.

This definition mirrors the fact from the smooth theory that minimal surfaces are Christoffel duals of their Gauß maps (Fig. 3). The correspondence between discrete harmonic functions and discrete minimal surfaces was observed in [8]. Here is a Weierstrass representation for discrete minimal surfaces in terms of their Gauß map and their Hopf differential:

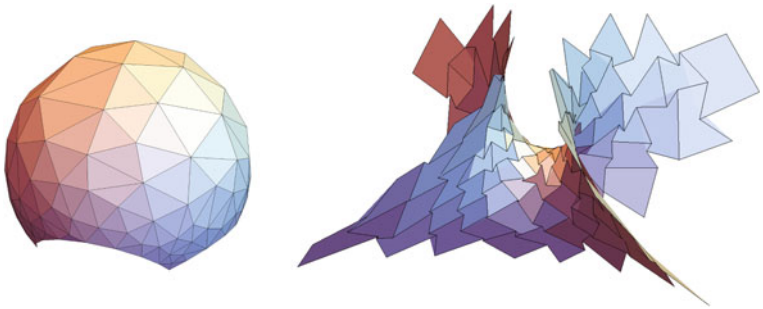

Fig. 3 *Left* A triangulated surface $n : V \to \mathbb{S}^2$ with vertices on the unit sphere. *Right* A discrete minimal surface $f : F \to \mathbb{R}^3$ satisfying Definition 6.2

Theorem 6.3 *Let $z : V \to \mathbb{C}$ be a realization of a simply connected triangular mesh and $q : E_{int} \to i\mathbb{R}$ a holomorphic quadratic differential. Then there exists $f : F \to \mathbb{R}^3$ such that for every interior edge $\{ij\}$*

$$df(e_{ij}^*) = Re\left(\frac{q_{ij}}{i(z_j - z_i)}\begin{pmatrix} 1 - z_i z_j \\ i(1 + z_i z_j) \\ z_i + z_j \end{pmatrix}\right). \tag{10}$$

Moreover f is a discrete minimal surface with Gauß map

$$n = \frac{1}{|z|^2 + 1}\begin{pmatrix} 2Rez \\ 2Imz \\ |z|^2 - 1 \end{pmatrix}.$$

Locally, every discrete minimal surface can be written in this form.

Proof Suppose $q : E_{int} \to i\mathbb{R}$ is a holomorphic quadratic differential. Then by (8) and (9) the dual 1-form η defined as

$$\eta(e_{ij}^*) := \frac{q_{ij}}{i(z_j - z_i)}\begin{pmatrix} 1 - z_i z_j \\ i(1 + z_i z_j) \\ z_i + z_j \end{pmatrix}$$

satisfies

$$\sum_j \eta(e_{ij}^*) = 0$$

for all interior vertices i. Therefore, since the triangular mesh is simply connected, there exists $\mathfrak{F} : F \to \mathbb{C}^3$ such that for any interior edge e we have

$$d\mathfrak{F}(e^*) = \eta(e^*).$$

Thus the map $f : F \to \mathbb{R}^3$ defined by $f := \mathrm{Re}\mathfrak{F}$ satisfies Eq. (10). To show that f is a discrete minimal surface we define a function $k : E_{int} \to \mathbb{R}$ by

$$k_{ij} := -i\, q_{ij}/|z_j - z_i|^2.$$

Then by direct computation we obtain

$$df(e^*_{ij}) = \frac{k_{ij}(1+|z_i|^2)(1+|z_j|^2)}{2}(n_j - n_i). \tag{11}$$

This shows that f is a discrete minimal surface with Gauß map n. The converse is straightforward: Given a discrete minimal surface f with Gauß map n we define $k : E_{int} \to \mathbb{R}$ via (11). Then it can be shown that the function

$$q_{ij} := i\, k_{ij}|z_j - z_i|^2$$

is a holomorphic quadratic differential. □

Remark 6.4 The discrete minimal surfaces given by (10) are trivalent meshes with planar vertex stars for purely imaginary q. It is closely related to discrete asymptotic nets. The factor i in front of $z_j - z_i$ appears since the integration is taken over a dual mesh while in the smooth theory $*dz = idz$.

Note that we could also consider the periodic one-parameter family of maps $f^\alpha : F \to \mathbb{R}^3$ defined for $\alpha \in \mathbb{R}$ by

$$f^\alpha := \mathrm{Re}(e^{i\alpha}\mathfrak{F}).$$

This family of discrete surfaces can be regarded as an associate family of minimal surfaces and is investigated in [7].

Acknowledgments This research was supported by DFG SFB/TRR 109 "Discretization in Geometry and Dynamics"

References

1. Bobenko, A., Pinkall, U.: Discrete isothermic surfaces. J. Reine Angew. Math. **475**, 187–208 (1996)
2. Bobenko, A.I., Mercat, C., Suris, Y.B.: Linear and nonlinear theories of discrete analytic functions. Integrable structure and isomonodromic Green's function. J. Reine Angew. Math. **583**, 117–161 (2005)
3. Bobenko, A.I., Pinkall, U., Springborn, B.A.: Discrete conformal maps and ideal hyperbolic polyhedra. Geom. Topol. **19**(4), 2155–2215 (2015)
4. Duffin, R.J.: Basic properties of discrete analytic functions. Duke Math. J. **23**, 335–363 (1956)
5. Ferrand, J.: Fonctions préharmoniques et fonctions préholomorphes. Bull. Sci. Math. **2**(68), 152–180 (1944)
6. Gunning, R.C.: Lectures on Riemann surfaces. Princeton Mathematical Notes. Princeton University Press, Princeton (1966)
7. Lam, W.Y.: Discrete minimal surfaces: critical points of the area functional from integrable systems (2015). arXiv:1510.08788
8. Lam, W.Y., Pinkall, U.: Isothermic triangulated surfaces (2015). arXiv:1501.02587
9. Luo, F.: Combinatorial Yamabe flow on surfaces. Commun. Contemp. Math. **6**(5), 765–780 (2004)
10. Mercat, C.: Discrete Riemann surfaces and the Ising model. Comm. Math. Phys. **218**(1), 177–216 (2001)
11. Schramm, O.: Circle patterns with the combinatorics of the square grid. Duke Math. J. **86**(2), 347–389 (1997)
12. Smirnov, S.: Discrete complex analysis and probability. Proceedings of the International Congress of Mathematicians. Volume I, pp. 595–621. Hindustan Book Agency, New Delhi (2010)
13. Springborn, B., Schröder, P., Pinkall, U.: Conformal equivalence of triangle meshes. ACM Trans. Graph. **27**(3), 77:1–77:11 (2008)

Vertex Normals and Face Curvatures of Triangle Meshes

Xiang Sun, Caigui Jiang, Johannes Wallner and Helmut Pottmann

Abstract This study contributes to the discrete differential geometry of triangle meshes, in combination with discrete line congruences associated with such meshes. In particular we discuss when a congruence defined by linear interpolation of vertex normals deserves to be called a 'normal' congruence. Our main results are a discussion of various definitions of normality, a detailed study of the geometry of such congruences, and a concept of curvatures and shape operators associated with the faces of a triangle mesh. These curvatures are compatible with both normal congruences and the Steiner formula.

1 Introduction

The system of lines orthogonal to a surface (called the *normal congruence* of that surface) has close relations to the surface's curvatures and is a well studied object of classical differential geometry, see e.g. [14]. It is quite surprising that this natural correspondence has not been extensively exploited in discrete differential geometry: most notions of discrete curvature are constructed in a way not involving normals, or involving normals only implicitly. There are however applications such as support structures and shading/lighting systems in architectural geometry where line congruences, and in particular normal congruences, come into play [21]. We continue

X. Sun · C. Jiang
King Abdullah Univ. of Science and Technology, Thuwal 23955, Saudi Arabia
e-mail: xiang.sun@kaust.edu.sa

C. Jiang
e-mail: caigui.jiang@kaust.edu.sa

J. Wallner (✉)
Graz University of Technology, 8010 Graz, Austria
e-mail: j.wallner@tugraz.at

H. Pottmann
Vienna University of Technology, 1040 Wien, Austria
e-mail: pottmann@geometrie.tuwien.ac.at

A.I. Bobenko (ed.), *Advances in Discrete Differential Geometry*,
DOI 10.1007/978-3-662-50447-5_8

this study, elaborate on discrete normal congruences in more depth and present a novel discrete curvature theory for triangle meshes which is based on discrete line congruences.

Contributions and overview. We organize our presentation as as follows. Section 2 summarizes properties of smooth congruences and elaborates on an important example arising in the context of linear interpolation of surface normals.

Section 3 first recalls discrete congruences following the work of Wang et al. [21] and then focuses on the interesting geometry of a new version of discrete normal congruences (defined over triangle meshes). We shed new light onto the behavior of linearly interpolated surface normals and discuss the problem of choosing vertex normals.

In Sect. 4, discrete normal congruences lead to a curvature theory for triangle meshes which has many analogies to the classical smooth setting. Unlike most other concepts of discrete curvature, it assigns values of the curvatures (principal, mean, Gaussian) to the faces of a triangle mesh. We discuss internal consistency of this theory and show by examples (Sect. 5), that it is well suited for curvature estimation and other applications.

Previous work. Smooth line congruences represent a classical subject. An introduction may be found in the monograph by Pottmann and Wallner [16]. Discrete congruences have appeared both in discrete differential geometry and geometry processing. Let us first mention contributions which study congruences based on triangle meshes: A computational framework for normal congruences and for estimating focal surfaces of meshes with known or estimated normals has been presented by Yu et al. [22]. The paper by Wang et al. [21] is described in more detail below.

Congruences associated with quad meshes are discrete versions of parametrized congruences associated with parametrized surfaces. In particular, the so-called torsal parametrizations are discussed from the integrable systems perspective by Bobenko and Suris [3]. An earlier contribution in this direction is due to Doliwa et al. [6]. These special parametrizations also occur as node axes in torsion-free support structures in architectural geometry [12, 15, 17].

Curvatures of triangle meshes are a well studied subject. One may distinguish between numerical approximation schemes (such as the jet fitting approach [4] or integral invariants [18]) on the one hand, and extensive studies from the discrete differential geometry perspective on the other hand. Without going into any detail we mention that these include discrete exterior calculus [5], the geometry of offset-like sets and distance functions [13], or various ways of defining shape operators [8, 9]. Naturally, also Yu et al. [22] address this topic when studying discrete normal congruences and focal surfaces. We present here yet another definition of curvatures for triangle meshes which is based on discrete normal congruences, and which is at the same time motivated by the Steiner formula (which also plays an important role in [2, 13, 15]).

2 Smooth Line Congruences

The introduction into line congruences in this section follows the paper by Wang et al. [21]. A line congruence $\mathcal{L}$ is a smooth 2D manifold of lines described locally by lines $L(u, v)$ which connect corresponding points $\mathbf{a}(u, v)$ and $\mathbf{b}(u, v)$ of two surfaces. With $\mathbf{e}(u, v) = \mathbf{b}(u, v) - \mathbf{a}(u, v)$ indicating the direction of the line $L(u, v)$ (see Fig. 1), we employ the volumetric parametrization

$$\mathbf{x}(u, v, \lambda) = \mathbf{a}(u, v) + \lambda \mathbf{e}(u, v) = (1 - \lambda)\mathbf{a}(u, v) + \lambda \mathbf{b}(u, v).$$

Any 1-parameter family $\mathcal{R}(t) = L(u(t), v(t))$ of lines results in a ruled surface $\mathbf{r}(t, \lambda) = \mathbf{x}(u(t), v(t), \lambda)$ contained in the congruence. We are particularly interested in *developable* ruled surfaces: The developability condition reads

$$\begin{aligned} &u_t^2[\mathbf{e}_u, \mathbf{a}_u, \mathbf{e}] + u_t v_t([\mathbf{e}_u, \mathbf{a}_v, \mathbf{e}] + [\mathbf{e}_v, \mathbf{a}_u, \mathbf{e}]) + v_t^2[\mathbf{e}_v, \mathbf{a}_v, \mathbf{e}] \\ &= (u_t, v_t) \begin{pmatrix} [\mathbf{e}_u, \mathbf{a}_u, \mathbf{e}] & [\mathbf{e}_u, \mathbf{a}_v, \mathbf{e}] + [\mathbf{e}_v, \mathbf{a}_u, \mathbf{e}] \\ \text{symm.} & [\mathbf{e}_v, \mathbf{a}_v, \mathbf{e}] \end{pmatrix} \begin{pmatrix} v_t \\ u_t \end{pmatrix} = 0, \end{aligned} \tag{1}$$

if we use subscripts to indicate differentiation and square brackets for the determinant. Equation (1) tells us that for any (u, v) there are up to two so-called *torsal* directions $u_t : v_t$ which belong to developable surfaces. This behaviour is quite analogous to the fact that for any point in a smooth surface there are two *principal* tangent directions which belong to principal curvature lines. By integrating the torsal directions one creates ruled surfaces which are developable, which is analogous to finding principal curvature lines by integrating principal directions.

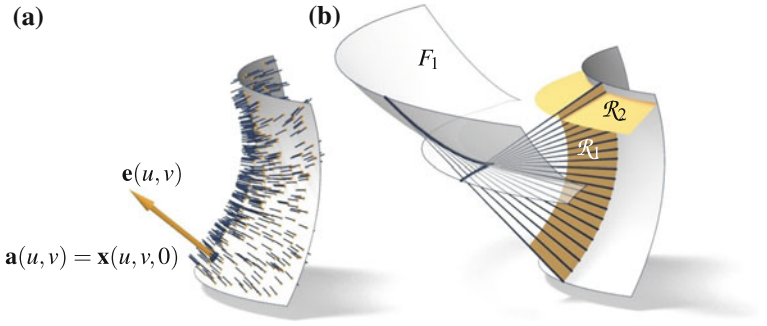

Fig. 1 **(a)** A line congruence $\mathcal{L}$ is described by a surface $\mathbf{a}(u, v)$, and direction vectors $\mathbf{e}(u, v)$. **(b)** Developables $\mathcal{R}_1$, $\mathcal{R}_2$ contained in $\mathcal{L}$. The set of all regression curves c_i of these developables makes up the focal sheets F_1, F_2 of the congruence (here only F_1 is shown). The tangent planes of $\mathcal{R}_1$, $\mathcal{R}_2$ along the common line are the torsal planes or focal planes of that line. These images are taken from [21]

Normal Congruences.

The normals of a surface constitute the normal congruence of that surface. For such congruences the analogy between torsal directions and principal directions mentioned above is actually an equality: The surface normals along a curve form a developable surface if and only if that curve is a principal curvature line [14].

The reference surface $\mathbf{a}(u, v)$ might be the base surface the lines of $\mathcal{L}$ are orthogonal to, but this does not have to be the case. The congruence does not change if the reference surface is changed to $\mathbf{a}^*(u, v) = \mathbf{a}(u, v) + \lambda(u, v)\mathbf{e}(u, v)$, so deciding whether or not $\mathcal{L}$ is a normal congruence depends on existence of an alternative reference surface $\mathbf{a}^*$ orthogonal to the lines of $\mathcal{L}$, i.e., $\langle \mathbf{e}, \mathbf{a}^*_u \rangle = \langle \mathbf{e}, \mathbf{a}^*_v \rangle = 0$. Assuming without loss of generality that $\|\mathbf{e}(u, v)\| = 1$ and using $\langle \mathbf{e}, \mathbf{e}_u \rangle = \langle \mathbf{e}, \mathbf{e}_v \rangle = 0$ the orthogonality condition reduces to $\lambda_u = -\langle \mathbf{a}_u, \mathbf{e} \rangle$, $\lambda_v = -\langle \mathbf{a}_v, \mathbf{e} \rangle$. This PDE for the function λ has a solution if and only if the integrability condition $\lambda_{uv} = \lambda_{vu}$ holds. It is easy to see that this is equivalent to

$$\langle \mathbf{a}_u, \mathbf{e}_v \rangle = \langle \mathbf{a}_v, \mathbf{e}_u \rangle. \tag{2}$$

It is not difficult to see that (2) is equivalent to the condition that developables contained in $\mathcal{L}$ intersect at right angles.

Focal surfaces and focal planes.

Loosely speaking, an intersection point of a line in $\mathcal{L}$ with an infinitesimally neighbouring line produces a *focal point* of the congruence $\mathcal{L}$. The rigorous definition of focal point is a point $\mathbf{x}(u, v, \lambda)$ where the derivatives of $\mathbf{x}$ are not linearly independent: One gets the condition

$$[\mathbf{x}_u, \mathbf{x}_v, \mathbf{x}_\lambda] = [\mathbf{e}_u, \mathbf{e}_v, \mathbf{e}]\lambda^2 + \big([\mathbf{a}_u, \mathbf{e}_v, \mathbf{e}] + [\mathbf{e}_u, \mathbf{a}_v, \mathbf{e}]\big)\lambda + [\mathbf{a}_u, \mathbf{a}_v, \mathbf{e}] = 0, \tag{3}$$

i.e., up to two focal points per line. It is not difficult to see that such singularities are exactly the singularities of developables contained in $\mathcal{L}$, see Fig. 1b. For this reason, the tangent planes of developables contained in $\mathcal{L}$ are called *focal planes* as well as *torsal planes*. Such a focal plane/torsal plane is spanned by a line $L(u, v)$ together with a torsal direction.

For normal congruences, the focal points are precisely the principal centers of curvature; they exist always unless one of the principal curvatures is zero. In each point of the surface, the focal plane (i.e., torsal plane) is spanned by the surface normal and a principal tangent.

Example: Congruences defined by linear interpolation.

Congruences of the special form

$$\begin{aligned} \mathbf{x}(u, v, \lambda) &= (1 - \lambda)\big(\mathbf{a}_0 + \mathbf{a}_{10}u + \mathbf{a}_{20}v\big) + \lambda\big(\mathbf{b}_0 + \mathbf{b}_{10}u + \mathbf{b}_{20}v\big) \\ &= \big(\mathbf{a}_0 + \mathbf{a}_{10}u + \mathbf{a}_{20}v\big) + \lambda\big(\mathbf{e}_0 + \mathbf{e}_{10}u + \mathbf{e}_{20}v\big) \end{aligned} \tag{4}$$

play an important role, both for us and in other places: for example, the set of lines described by such a congruence is the one generated by Phong shading, when one linearly interpolates vertex normals in a triangle.

We consider the planes "P_α" which are defined as the set of all points $\mathbf{x}(u, v, \alpha)$, and we study the affine mappings

$$\phi_{\alpha\beta} : P_\alpha \to P_\beta, \quad \mathbf{x}(u, v, \alpha) \mapsto \mathbf{x}(u, v, \beta).$$

The lines $L(u, v)$ of the congruence are precisely the lines which connect points $\mathbf{x}(u, v, \alpha) \in P_\alpha$ and $\mathbf{x}(u, v, \beta) \in P_\beta$. These congruences are studied e.g. in [16, Ex. 7.1.2]. Let us summarize some of their properties, which are illustrated by Fig. 2.

(i) Each intersection line $L = P_\alpha \cap P_\beta$ of two planes in the family P_λ is contained in the congruence $\mathcal{L}$. This follows from the fact that L is spanned by the points $X = \phi_{\alpha\beta}^{-1}(L) \cap L$ and $\phi_{\alpha\beta}(X) = L \cap \phi_{\alpha\beta}(L)$.

(ii) The lines $P_\alpha \cap P_\beta$ with α fixed, constitute a developable surface $\mathcal{R}_\alpha \subset \mathcal{L}$ which is planar and contained in P_α (in general, it is the tangent surface of a parabola r_α).

(iii) For properties of the focal surface, see Fig. 2.

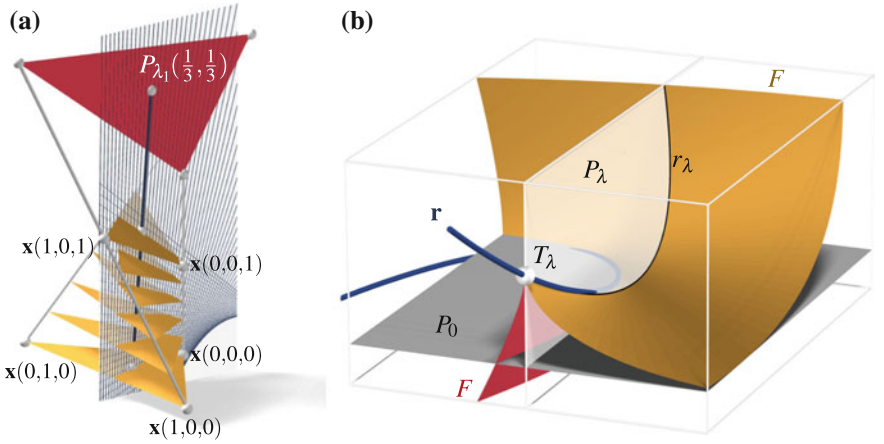

Fig. 2 Congruences defined by a "linear" volumetric parametrization $\mathbf{x}(u, v, \lambda)$ turn out to be useful for linear interpolation of triangle meshes, but they have counter-intuitive properties. **(a)** Planes P_λ defined by $\lambda = \text{const}$ are visualized as triangles. Interestingly, all of these triangles contain a planar developable $\mathcal{R}_\lambda \subset \mathcal{L}$ with a parabola r_λ as curve of regression. In particular the *red triangle* P_{λ_1} represents a torsal plane for the *blue line* $L(\frac{1}{3}, \frac{1}{3})$ which connects the barycenters of triangles P_λ. The image further shows many lines $P_{\lambda_1} \cap P_\beta$, of the planar developable $\mathcal{R}_{\lambda_1}$. **(b)** The focal surface F of $\mathcal{L}$ agrees with the envelope of the family of planes P_λ. It is in general the tangent surface of a cubic polynomial curve $\mathbf{r}$. We show in *red* and *yellow* the two sheets of this tangent surface F which are separated by the regression curve $\mathbf{r}$. We also indicate the point of tangency T_λ where P_λ touches $\mathbf{r}$. The hyperbolic congruence lines (those which are contained in two focal planes) are bitangents of the focal surface, i.e., they touch F in two points. The regression parabolas r_λ are contained in F and are obtained by intersecting F with one of its tangent planes P_λ

3 Discrete Normal Congruences

Wang et al. [21] define discrete congruences by means of correspondences between combinatorially equivalent triangle meshes A, B with vertices $\{\mathbf{a}_i\}$ and $\{\mathbf{b}_i\}$. Each pair of corresponding triangles $\mathbf{a}_i\mathbf{a}_j\mathbf{a}_k$ and $\mathbf{b}_i\mathbf{b}_j\mathbf{b}_k$ defines, via linear interpolation, a piece of a smooth line congruence of the kind described by Eq. (4):

$$\begin{aligned}
&\mathbf{x}(u, v, \lambda) = \mathbf{a}(u, v) + \lambda\mathbf{e}(u, v),\\
&\mathbf{a}(u, v) = \mathbf{a}_i + u\mathbf{a}_{ji} + v\mathbf{a}_{ki}, \quad \mathbf{e}(u, v) = \mathbf{e}_i + u\mathbf{e}_{ji} + v\mathbf{e}_{ki}, \quad \text{where}\\
&\mathbf{e}_i = \mathbf{b}_i - \mathbf{a}_i, \quad \mathbf{a}_{ij} = \mathbf{a}_i - \mathbf{a}_j, \quad \mathbf{e}_{ij} = \mathbf{e}_i - \mathbf{e}_j.
\end{aligned} \tag{5}$$

If the domain is restricted to $u \geq 0$, $v \geq 0$, $u + v \leq 1$, then the correspondence $\mathbf{x}(u, v, 0) \longmapsto \mathbf{x}(u, v, 1)$ is precisely the affine mapping of triangle $\mathbf{a}_i\mathbf{a}_j\mathbf{a}_k$ to triangle $\mathbf{b}_i\mathbf{b}_j\mathbf{b}_k$. Equations (1) and (3) serve to compute torsal directions and focal points of this congruence, and also to trace the developables contained in this congruence (see Fig. 3).

Discrete normal congruences—Version 1.

It is not straightforward to define which correspondence between triangle meshes defines a *normal* congruence. Firstly this is because congruences of the form (4) are never normal except for degenerate cases. Secondly such a normal congruence would automatically lead to a good definition of constant-distance offset mesh of a triangle mesh which is lacking so far.

We discuss two suitable definitions of "normal congruence" and start with a version already published. Wang et al. [21] require normality to hold only in the barycenters of faces (i.e., they require that Eq. (2) holds for barycenters of faces), see Fig. 4. Figure 5 shows an example demonstrating the efficiency of this definition. Proposition 3.1 below gives an equivalent analytic condition.

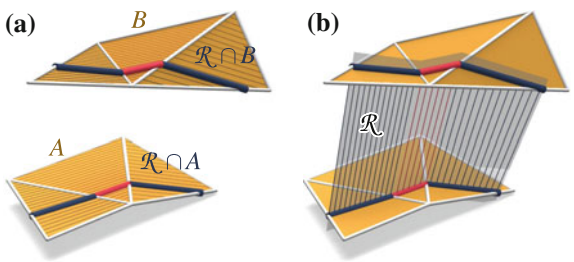

Fig. 3 A piecewise-linear correspondence between meshes A and B defines a piecewise-smooth congruence $\mathcal{L}$. **(a)** Integrating torsal directions yields corresponding polylines in meshes A and B. **(b)** Connecting corresponding points of those two polylines yields a piecewise-flat developable $\mathcal{R} \subset \mathcal{L}$. These images are taken from [21]

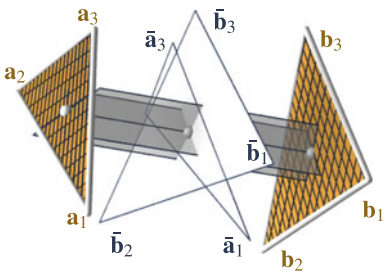

Fig. 4 Congruences defined by the piecewise-affine correspondence of meshes A, B can be called *discrete-normal*, if the normality condition is fulfilled for barycenters of faces. This figure also illustrates the auxiliary projection used by Eq. (7). This normality condition is called 'version 1 normality' here (image taken from [21])

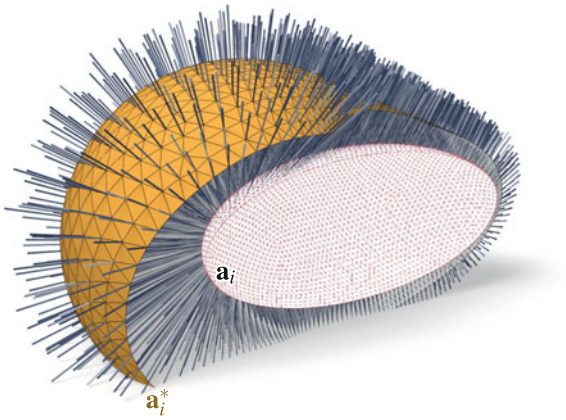

Fig. 5 We demonstrate that Eq. (7) is a working definition of normality: Given a triangle mesh $\{\mathbf{a}_i\}$ (*white*), we find unit vectors $\mathbf{e}_i$ by optimizing for shading effects according to Wang et al. [21] under the normality constraint (7). Subsequently we check if a triangle mesh $\{\mathbf{a}_i^*\}$ orthogonal to the congruence can be found. We let $\mathbf{a}_i^* = \mathbf{a}_i + \lambda_i \mathbf{e}_i$ and solve for λ_i such that the faces of the new mesh are orthogonal to the congruence in their barycenters. The result of this computation yields a mesh $\{\mathbf{a}_i^*\}$ (*yellow*) where face normals and congruence lines (in face barycenters) differ by an angle β, which assumes a maximum of 4.1°, a mean of 0.9°, and a median of 0.8°. Instead of the mesh computed here, any constant-distance offset would have been a solution as well. We chose one which lies at a small distance from the original mesh

Proposition 3.1 *Consider two combinatorially equivalent triangle meshes and the line congruence $\mathcal{L}$ defined by the piecewise-linear correspondence of faces. For each pair $\mathbf{a}_1\mathbf{a}_2\mathbf{a}_3$, $\mathbf{b}_1\mathbf{b}_2\mathbf{b}_3$ of corresponding faces perform orthogonal projection in direction of the line which connects their respective barycenters, yielding triangles $\bar{\mathbf{a}}_1\bar{\mathbf{a}}_2\bar{\mathbf{a}}_3$, $\bar{\mathbf{b}}_1\bar{\mathbf{b}}_2\bar{\mathbf{b}}_3$. Then $\mathcal{L}$ is normal in the barycenters of the two faces if and only if the following analogue of* (2) *holds:*

$$\langle \bar{\mathbf{a}}_j - \bar{\mathbf{a}}_i, \bar{\mathbf{b}}_k - \bar{\mathbf{b}}_i \rangle = \langle \bar{\mathbf{a}}_k - \bar{\mathbf{a}}_i, \bar{\mathbf{b}}_j - \bar{\mathbf{b}}_i \rangle, \quad \textit{or equivalently}, \tag{6}$$

$$\langle \bar{\mathbf{a}}_j - \bar{\mathbf{a}}_i, \bar{\mathbf{e}}_k - \bar{\mathbf{e}}_i \rangle = \langle \bar{\mathbf{a}}_k - \bar{\mathbf{a}}_i, \bar{\mathbf{e}}_j - \bar{\mathbf{e}}_i \rangle, \quad \textit{where} \quad \mathbf{e}_i = \mathbf{b}_i - \mathbf{a}_i. \tag{7}$$

It is sufficient that these conditions hold for at least one choice of indices $i, j, k \in \{1, 2, 3\}$, $i \neq j \neq k$.

Discrete normal congruences—Version 2.

There is an obvious analogy between conditions (2) and (7): they express normality in the smooth and discrete cases respectively. However Eq. (7) is not entirely satisfying as a definition since it involves a projection operator. It is therefore natural to define discrete-normality by the following two equations which replace Eqs. (6), (7):

$$\langle \mathbf{a}_j - \mathbf{a}_i, \mathbf{b}_k - \mathbf{b}_i \rangle = \langle \mathbf{a}_k - \mathbf{a}_i, \mathbf{b}_j - \mathbf{b}_i \rangle \quad \text{or, equivalently,} \tag{6*}$$

$$\langle \mathbf{a}_j - \mathbf{a}_i, \mathbf{e}_k - \mathbf{e}_i \rangle = \langle \mathbf{a}_k - \mathbf{a}_i, \mathbf{e}_j - \mathbf{e}_i \rangle. \tag{7*}$$

We will show that theses conditions are suitable to define normality of discrete congruences defined by a correspondence of triangle meshes. Besides numerical experiments (see later), we show geometric properties of congruences which fulfill these conditions. The first property is a discrete version of the following two facts (i) A normal congruence $\mathcal{L}$ has a 1-parameter family of surfaces orthogonal to it, and (ii) for any point in such a surface there are 3 mutually orthogonal planes spanned by the normal and the two principal directions. We show that in the discrete-normal case, there are analogous *principal trihedra*:

Proposition 3.2 *Consider two combinatorially equivalent triangle meshes and the line congruence* $\mathcal{L}$ *defined by the piecewise-affine correspondence of faces, and consider in particular one such pair* $\mathbf{a}_1\mathbf{a}_2\mathbf{a}_3$, $\mathbf{b}_1\mathbf{b}_2\mathbf{b}_3$ *of corresponding faces. In the generic case, the normality condition* (6*) *implies the following property:*

For each plane P_λ *spanned by the vertices* $(1-\lambda)\mathbf{a}_i + \lambda\mathbf{b}_i$ *there is a congruence line* $N_\lambda = L(u_\lambda, v_\lambda)$ *such that the two focal planes of that line together with* P_λ *form a trihedron of mutually orthogonal planes.*

The meaning of "generic" is discussed in the proof.

Proof Generically, vectors $\mathbf{e}_i = \mathbf{b}_i - \mathbf{a}_i$ are linearly independent, so we can express a normal vector $\mathbf{n}$ of the triangle $\mathbf{a}_1\mathbf{a}_2\mathbf{a}_3$ (which spans P_0) as a linear combination $\mathbf{n} = \sum_{i=1}^{3} \alpha_i \mathbf{e}_i$. Generically, $\sum \alpha_i \neq 0$, so by multiplying $\mathbf{n}$ with a factor we can achieve $\sum \alpha_i = 1$ and by relabeling the coefficients α_i we get $\mathbf{n} = (1 - u - v)\mathbf{e}_1 + u\mathbf{e}_2 + v\mathbf{e}_3$. Then Equation (5) shows that the line $L(u, v)$ is orthogonal to P_0.

Consider the affine correspondence of triangles $\mathbf{a}_1\mathbf{a}_2\mathbf{a}_3$ and $\mathbf{b}_1\mathbf{b}_2\mathbf{b}_3$ followed by orthogonal projection onto P_0. A vertex $\mathbf{a}_i$ is mapped to $\bar{\mathbf{b}}_i = \mathbf{b}_i + \lambda_i \mathbf{n}$. There is a linear mapping α with $\alpha(\mathbf{a}_i - \mathbf{a}_j) = \bar{\mathbf{b}}_i - \bar{\mathbf{b}}_j$. It is clear from Fig. 3 that the eigenvectors of α indicate the directions of torsal planes through the line $L(u, v)$. Conditions (6*), (7*) imply

$$\begin{aligned}
&\langle \mathbf{a}_j - \mathbf{a}_i, \bar{\mathbf{b}}_k - \bar{\mathbf{b}}_i \rangle - \langle \mathbf{a}_k - \mathbf{a}_i, \bar{\mathbf{b}}_j - \bar{\mathbf{b}}_i \rangle \\
&= \langle \mathbf{a}_j - \mathbf{a}_i, \mathbf{b}_k + \lambda_k \mathbf{n} - \mathbf{b}_i - \lambda_i \mathbf{n} \rangle - \langle \mathbf{a}_k - \mathbf{a}_i, \mathbf{b}_j + \lambda_j \mathbf{n} - \mathbf{b}_i - \lambda_i \mathbf{n} \rangle \\
&= \langle \mathbf{a}_j - \mathbf{a}_i, \mathbf{b}_k - \mathbf{b}_i \rangle - \langle \mathbf{a}_k - \mathbf{a}_i, \mathbf{b}_j - \mathbf{b}_i \rangle = 0,
\end{aligned}$$

i.e., symmetry of α and orthogonality of eigenvectors of α. This shows orthogonality of torsal planes and verifies the statement for the case $\lambda = 0$. The case $\lambda = 1$ is analogous, since condition (6*) is invariant if we replace $\mathbf{a}_i$ by $\mathbf{b}_i$ and vice versa. For all other values $\lambda \neq 1$ we note that replacing vertices $\mathbf{b}_i$ by vertices $\mathbf{a}_i + \lambda \mathbf{e}_i$ inflicts the change $\mathbf{e}_i \to \lambda \mathbf{e}_i$ without changing $\mathbf{a}_i$, which does not affect the normality condition (7*).

As illustrated by Fig. 2, congruences defined by the affine correspondence of triangles have counter-intuitive properties: The planes P_λ generated by linear interpolation of the defining triangles at the same time are the focal planes of $\mathcal{L}$ (and vice versa) since any P_λ carries the developable surface generated by the lines $\{P_\lambda \cap P_\alpha\}_{\alpha \in \mathbb{R}}$. The torsal planes P_λ are tangent to the focal surface F of $\mathcal{L}$. It is known that F is the tangent surface of a cubic polynomial curve, cf. [16, Ex. 7.1.2]. Proposition 3.2 now tells us that this curve has infinitely many triples of mutually orthogonal tangent planes. Translating these planes (the principal trihedra) through the origin, they become tangent planes of the directing cone of F, which is a quadratic cone. This cone is quadratic and must likewise have infinitely many orthogonal circumscribed trihedra. It is therefore a so-called *Monge cone*, see Fig. 6.

There is a phenomenon in geometry, called *porism*, cf. [7]. It refers to situations where existence of one object of a certain kind implies existence of an entire 1-parameter family of such objects. Monge cones are an instance of a porism: If a quadratic cone has one circumscribed orthogonal trihedron, then one can move this trihedron around the cone while it remains tangential. This fact is classical knowledge in projective geometry, see e.e. [1, pp. 33–34].

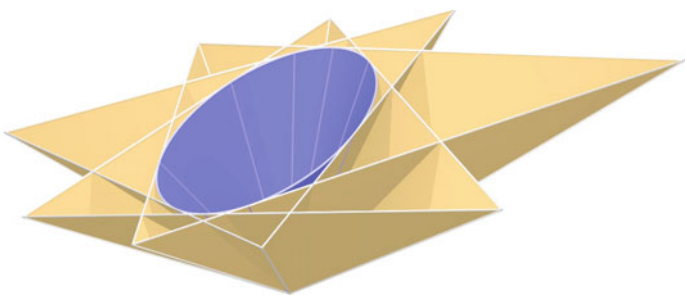

Fig. 6 The "principal" trihedra mentioned in Proposition 3.2, when moved to the origin, lie tangent to a so-called *Monge cone*. Since these planes rotate about an entire cone as the interpolation parameter λ varies, one cannot without restrictions interpret these principal trihedra as tangent planes plus principal planes of an offset family of surfaces. Such an interpretation is valid only for small λ

The same porism is hidden in the proof of Proposition 3.2: The normality condition (6*) was equivalent to existence of the principal trihedron associated with P_0, but it also implied existence of the trihedron for all P_λ.

Details on principal trihedra in discrete-normal congruences.

We wish to interpret the three mutually orthogonal planes referred to by Proposition 3.2 as the tangent plane and principal planes of a surface. In particular the normal vector $\mathbf{n}_\lambda$ of P_λ shall be the normal vector, and the line N_λ shall be the surface normal, while the torsal planes should represent the principal directions. In order to understand better the behaviour of the objects involved, we study the volumetric parametrization according to Eq. (4) in an adapted coordinate system: the plane P_0 is the xy plane, and the two torsal planes associated with it shall be the xz and zy planes. Since the affine correspondence between planes P_0, P_1 may be defined by *any* pair of corresponding triangles, we choose $\mathbf{a}_1 = \mathbf{o}, \mathbf{a}_2 = (1, 0, 0), \mathbf{a}_3 = (0, 1, 0)$. We may still change the plane P_1 without changing the congruence, so we choose $\mathbf{b}_1 = (0, 0, 1)$. The vertices $\mathbf{b}_2, \mathbf{b}_3$ must lie in the xy and xz planes because of our assumption on the torsal planes. Thus we get

$$\begin{aligned} \mathbf{x}(u, v, \lambda) &= \begin{pmatrix} u \\ v \\ 0 \end{pmatrix} + \lambda \begin{pmatrix} -\kappa_1 u \\ -\kappa_2 v \\ au + bv + 1 \end{pmatrix} \\ \implies \mathbf{n}_\lambda &= \frac{\partial \mathbf{x}}{\partial u} \times \frac{\partial \mathbf{x}}{\partial v} = \begin{pmatrix} a\lambda(\kappa_2\lambda - 1) \\ b\lambda(\kappa_1\lambda - 1) \\ (\kappa_1\lambda - 1)(\kappa_2\lambda - 1) \end{pmatrix}. \end{aligned} \tag{8}$$

We will later interpret κ_1, κ_2 as principal curvatures and vectors $(1, 0, 0)$ and $(0, 1, 0)$ as principal directions. Obviously, they are eigenvectors of the linear map α which occurs in the proof of Proposition 3.2. The plane P_λ is given as

$$\begin{aligned} n_{1,\lambda}x_1 + n_{2,\lambda}x_2 + n_{3,\lambda}x_3 - n_{0,\lambda} &= a\lambda(\kappa_2\lambda - 1)x_1 + b\lambda(\kappa_1\lambda - 1)x_2 \\ &+ (\kappa_1\lambda - 1)(\kappa_2\lambda - 1)x_3 - \lambda(\kappa_1\lambda - 1)(\kappa_2\lambda - 1) = 0. \end{aligned}$$

This is a cubic family of planes. Translating them through the origin yields the planes $n_{1,\lambda}x_1 + n_{2,\lambda}x_2 + n_{3,\lambda}x_3 = 0$, which are tangent planes of the tangent cone illustrated in Fig. 6. Since the plane coefficients satisfy the quadratic equation $(\kappa_1 - \kappa_2)n_1n_2 - an_2n_3 + bn_1n_3 = 0$, it is indeed a quadratic cone.[1]

We now look for a line $L(u_\lambda, v_\lambda)$ orthogonal to P_λ. The direction of $L(u, v)$ can be read off (8), so the condition $L(u_\lambda, v_\lambda) \parallel \mathbf{n}_\lambda$ reads

[1] The vector of coefficients (n_1, n_2, n_3) of the equation of a plane is a normal vector of that plane. This shows that the orthogonal polar cone of the Monge cone fulfills the equation $(\kappa_1 - \kappa_2)x_1x_2 - ax_2x_3 + bx_1x_3 = 0$. Since the Monge cone had many circumscribed orthogonal trihedra, its polar cone has many inscribed orthogonal frames. These frames are generated by translating the frames seen in Fig. 7b through the origin.

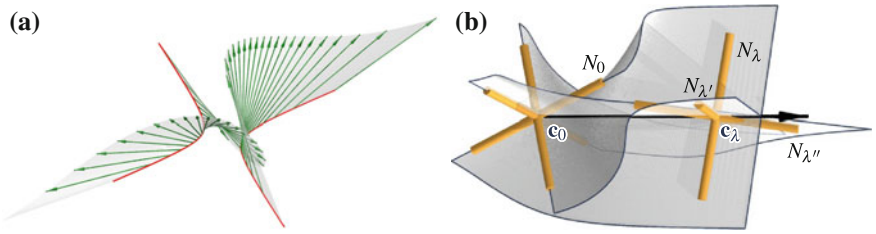

Fig. 7 Behaviour of the principal trihedron and the normal N_λ of planes P_λ in a congruence defined by the affine correspondence between two triangles. **(a)** The normals N_λ (*green*) intersect the plane P_0 in the points $\mathbf{c}(u_\lambda, v_\lambda, 0)$ of a conic (*red*). **(b)** As λ changes, the apex $\mathbf{c}_\lambda = \mathbf{x}(u_\lambda, v_\lambda, \lambda)$ of the principal trihedron (*yellow*) moves along a straight straight line (*blue*). The ruled surfaces traced out by the edges of the trihedron are shown; their union forms one algebraic ruled surface of degree four

$$\frac{\kappa_1 u_\lambda}{\kappa_2 v_\lambda} = \frac{a(\kappa_2\lambda - 1)}{b(\kappa_1\lambda - 1)}, \quad \frac{\kappa_1 u_\lambda}{a u_\lambda + b v_\lambda + 1} = \frac{a\lambda}{1 - \kappa_1\lambda}$$
$$\Longrightarrow \; u_\lambda = \frac{a\lambda\kappa_2(1 - \kappa_2\lambda)}{\nu_\lambda}, \quad v_\lambda = \frac{b\lambda\kappa_1(1 - \kappa_1\lambda)}{\nu_\lambda},$$
$$\text{where} \quad \nu_\lambda = \kappa_1\kappa_2(\kappa_1\lambda - 1)(\kappa_2\lambda - 1) + a^2\kappa_2\lambda(\kappa_2\lambda - 1) + b^2\kappa_1\lambda(\kappa_1\lambda - 1). \quad (9)$$

In particular we see that the curve $\mathbf{x}(u_\lambda, v_\lambda, 0)$, consisting of all points $N_\lambda \cap P_0$, is a conic. In fact, for every α, the curve $\{N_\lambda \cap P_\alpha\}_{\lambda\in\mathbb{R}}$ is a conic it corresponds to the curve $N_\lambda \cap P_0$ under the affine mapping $\phi_{0\alpha} : \mathbf{x}(u, v, 0) \mapsto (u, v, \alpha)$, see Fig. 7a. The surface of all N_λ's is then algebraic of 4°.

Let us now compute the "apex" $\mathbf{c}_\lambda = N_\lambda \cap P_\lambda = \mathbf{x}(u_\lambda, v_\lambda, \lambda)$ of the principal trihedron: From

$$\mathbf{c}_\lambda = \frac{\lambda(1 - \kappa_1\lambda)(1 - \kappa_2\lambda)}{\nu_\lambda} \begin{pmatrix} \kappa_2 a \\ \kappa_1 b \\ \kappa_1\kappa_2 \end{pmatrix} \quad (10)$$

we see that $\mathbf{c}_\lambda$ moves on a straight line, but the parametrization of this line is cubic. Since the planes P_λ and the torsal planes stem from the same 1-parameter family of planes, any torsal plane will play the role of $P_{\lambda'}$ for another value λ'; in total each orthogonal trihedron will occur three times, and each of the three edges of the trihedron will play the role of N_λ three times (see Fig. 7b). We summarize:

Proposition 3.3 *If a congruence is defined by the affine correspondence between two triangles* $\mathbf{a}_1\mathbf{a}_2\mathbf{a}_3$ *and* $\mathbf{b}_1\mathbf{b}_2\mathbf{b}_3$ *and satisfies the normality condition* (6*)*, then its focal surface has a 1-parameter family of circumscribed 'principal' orthogonal trihedra whose apex moves on a straight line and whose edges form an algebraic surface of degree 4 which contains that line as a triple line.*

The complicated geometry of these congruences reflects the difficulties in defining offset pairs of triangle meshes.

Discrete normal congruences — Version 3.

An elementary computation shows that either of the two conditions (6*), (7*) is implied by the stronger condition

$$\langle \mathbf{a}_j - \mathbf{a}_i, \mathbf{e}_j + \mathbf{e}_i \rangle = 0, \tag{11}$$

when imposed on all three edges of a triangle. This third version of normality is a more direct expression of the orthogonality between triangle mesh and congruence: the edges $\mathbf{a}_i\mathbf{a}_j$ of the mesh are required to be orthogonal to the arithmetic mean of normal vectors $\mathbf{e}_i, \mathbf{e}_j$ at either endpoint of the edge.

Comparison of definitions.

The various definitions of discrete normal congruences have different advantages. When one wants to design a normal congruence (as in Wang et al. [21]), version 1 may be better because it ensures orthogonality of focal planes in the part of the line congruence which is actually realized. Using version 2, orthogonal focal planes may occur outside the realized part. On the other hand, when using the normal congruence of a given surface, version 2 has the advantage that one plane of a principal frame contains the base mesh triangle; moreover discrete principal directions are orthogonal and lie in the plane of the triangle. Version 3 normality is not used here except for Fig. 8 where we show that imposing version 3 normality leads to results comparable to version 2. Since the weaker condition of version 2 is sufficient to achieve the same results, it is not necessary to impose version 3 normality.

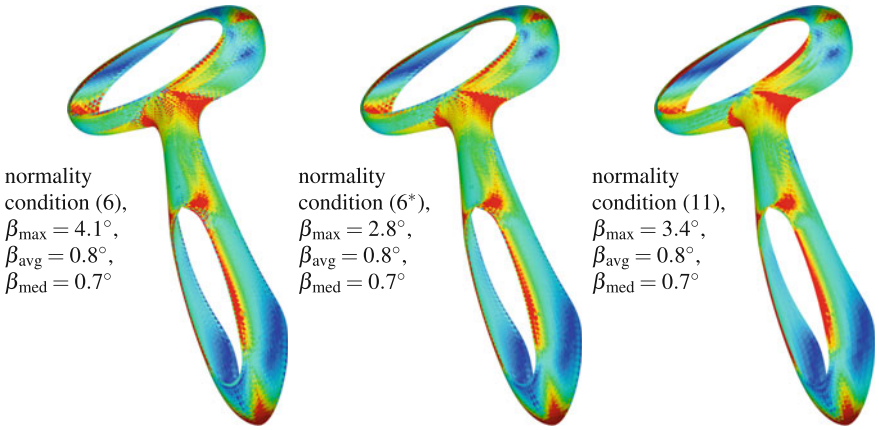

Fig. 8 Optimization of normal congruences. For a given mesh with vertices $\mathbf{a}_i$, a discrete-normal congruence, defined by unit vectors $\mathbf{e}_i$, has been found by global optimization such that one of the normality conditions considered here is fulfilled. Each of these conditions is linear, so optimization was done by least squares. It turns out that there is no substantial difference between Eqs. (6*) and (11). Faces are *colored* according to the angle β enclosed between the congruence line at the barycenter and the face's normal there. We also give statistics on β for each figure

4 Curvatures of Faces of Triangle Meshes

Recall that a smooth normal congruence $\mathcal{L}$ possesses a surface A orthogonal to the lines of $\mathcal{L}$. Then automatically all offsets A^t also lie orthogonal to $\mathcal{L}$. We assume labeling of offsets such that surfaces A^t, A^s are at constant distance $|t-s|$ from each other. Then corresponding infinitesimal surface area elements "$dA^t(u,v)$" obey Steiner's formula

$$\frac{dA^t(u,v)}{dA^0(u,v)} = 1 - 2tH(u,v) + t^2K(u,v), \tag{12}$$

where H and K denote mean and Gaussian curvature of the surface A^0, respectively. The sign of H depends on the unit normal vector field; in our case the unit normal vector field points from A^0 to the surfaces A^t with $t > 0$.

We now return to a discrete congruence $\mathcal{L}$ defined by the piecewise-linear correspondence between triangle meshes A, B. Assuming A, B approximate an offset pair of surfaces at distance 1, we consider corresponding faces $\mathbf{a}_1\mathbf{a}_2\mathbf{a}_3$ and $\mathbf{b}_1\mathbf{b}_2\mathbf{b}_3$. We write $\mathbf{b}_i = \mathbf{a}_i + \mathbf{e}_i$, where the vectors $\mathbf{e}_i$ approximate unit normal vectors of the mesh A. An offset mesh at distance approximately t then has vertices and faces

$$\mathbf{a}_i^t = \mathbf{a}_i + t\mathbf{e}_i \quad \Delta^t = \mathbf{a}_1^t\mathbf{a}_2^t\mathbf{a}_3^t.$$

We further assume that the congruence $\mathcal{L}$ is a normal congruence (which we have defined in two different ways).

- If $\mathcal{L}$ is normal in the sense of Eqs. (6) and (7), then we apply the projection mentioned in Proposition 3.1, resulting in vertices $\bar{\mathbf{a}}_1\bar{\mathbf{a}}_2\bar{\mathbf{a}}_3$, $\bar{\mathbf{b}}_1\bar{\mathbf{b}}_2\bar{\mathbf{b}}_3$. The projection is in the direction of a certain unit vector $\mathbf{n}$.
- As an alternative, the congruence may be normal in the sense of Eqs. (6*), (7*). Here we consider orthogonal projection onto the plane P_0 which contains $\mathbf{a}_1\mathbf{a}_2\mathbf{a}_3$. This projection results in vertices $\bar{\mathbf{a}}_i = \mathbf{a}_i$ and $\bar{\mathbf{b}}_i$. The projection is in direction of the unit normal vector $\mathbf{n} = \mathbf{n}_0$ of the plane P_0.

We now study the behaviour of the area of the face Δ^t as t changes. We do not measure the actual area, but apply the projection just mentioned. The area of projected triangles is measured via a determinant in the plane:

$$\text{p-area}(\mathbf{x}_1\mathbf{x}_2\mathbf{x}_3) = \frac{1}{2}[\bar{\mathbf{x}}_2 - \bar{\mathbf{x}}_1, \bar{\mathbf{x}}_3 - \bar{\mathbf{x}}_1] = \frac{1}{2}[\mathbf{n}, \bar{\mathbf{x}}_2 - \bar{\mathbf{x}}_1, \bar{\mathbf{x}}_3 - \bar{\mathbf{x}}_1] = \frac{1}{2}[\mathbf{n}, \mathbf{x}_2 - \mathbf{x}_1, \mathbf{x}_3 - \mathbf{x}_1]$$

With the notation $\bar{\mathbf{a}}_{ij} = \bar{\mathbf{a}}_i - \bar{\mathbf{a}}_j$, $\bar{\mathbf{b}}_{ij} = \bar{\mathbf{b}}_i - \bar{\mathbf{b}}_j$, $\bar{\mathbf{e}}_{ij} = \bar{\mathbf{b}}_{ij} - \bar{\mathbf{a}}_{ij}$ we get

$$\frac{\text{p-area}(\triangle^t)}{\text{p-area}(\triangle^0)} = \frac{\frac{1}{2}[\bar{\mathbf{a}}_{12} + t\bar{\mathbf{e}}_{12}, \bar{\mathbf{a}}_{13} + t\bar{\mathbf{e}}_{13}]}{\frac{1}{2}[\bar{\mathbf{a}}_{12}, \bar{\mathbf{a}}_{13}]} = 1 + t\frac{[\bar{\mathbf{a}}_{12}, \bar{\mathbf{e}}_{13}] + [\bar{\mathbf{e}}_{12}, \bar{\mathbf{a}}_{13}]}{[\bar{\mathbf{a}}_{12}, \bar{\mathbf{a}}_{13}]} + t^2\frac{[\bar{\mathbf{e}}_{12}, \bar{\mathbf{e}}_{13}]}{[\bar{\mathbf{a}}_{12}, \bar{\mathbf{a}}_{13}]}.$$

Discrete curvatures and shape operator.

The obvious similarity of this relation with (12) immediately leads to a definition of the mean curvature H and the Gauss curvature K of the face $\mathbf{a}_1\mathbf{a}_2\mathbf{a}_3$ under consideration:

$$K = \frac{[\mathbf{n}, \mathbf{e}_{12}, \mathbf{e}_{13}]}{[\mathbf{n}, \mathbf{a}_{12}, \mathbf{a}_{13}]}, \qquad 2H = -\frac{[\mathbf{n}, \mathbf{a}_{12}, \mathbf{e}_{13}] + [\mathbf{e}_{12}, \mathbf{a}_{13}]}{[\mathbf{n}, \mathbf{a}_{12}, \mathbf{a}_{13}]}. \tag{13}$$

Principal curvatures κ_1, κ_2 are defined by the relations

$$\kappa_1 + \kappa_2 = 2H, \quad \kappa_1\kappa_2 = K.$$

Completing the analogy with the smooth case, we define a shape operator Λ as the linear mapping which maps

$$\bar{\mathbf{a}}_i - \bar{\mathbf{a}}_j \overset{\Lambda}{\longmapsto} -(\bar{\mathbf{e}}_i - \bar{\mathbf{e}}_j), \quad \text{for all } i, j \in \{1, 2, 3\}.$$

Recall that the bar indicates projection (which in turn depends on which version of "normality" we employ). In analogy to the smooth case, principal directions are given by the focal planes of the congruence $\mathcal{L}$. All these notions fit together:

Proposition 4.1 *The eigenvalues of the shape operator Λ are the principal curvatures κ_1, κ_2, and its trace and determinant are given by $2H$ and K, respectively. Eigenvectors of Λ indicate the principal directions.*

Proof We first show the statement for 'version 2' normality. Recall the linear mapping α in the proof of Proposition 3.2 which maps $\bar{\mathbf{a}}_i - \bar{\mathbf{a}}_j \overset{\alpha}{\longmapsto} (\bar{\mathbf{a}}_i + \bar{\mathbf{e}}_i) - (\bar{\mathbf{a}}_j + \bar{\mathbf{e}}_j)$. Since by construction, $\Lambda = \mathrm{id} - \alpha$, Λ has the same eigenvectors as α, i.e., the torsal directions. The statement about $\mathrm{tr}\,\Lambda$ and $\det\Lambda$ follows from the relations $\det\Lambda = \frac{\det(\Lambda(\mathbf{x}),\Lambda(\mathbf{y}))}{\det(\mathbf{x},\mathbf{y})}$ and $\mathrm{tr}\,\Lambda = \frac{\det(\Lambda(\mathbf{x}),\mathbf{y})+\det(\mathbf{x},\Lambda(\mathbf{y}))}{\det(\mathbf{x},\mathbf{y})}$ which generally hold for linear mappings of $\mathbb{R}^2$. The statement about eigenvalues follows immediately.

For version 1 normality the proof is the same, only the bars have a different meaning. The mapping α is also referred to in the proof of Proposition 3.1 in [21].

Since we have defined principal curvatures κ_1, κ_2 implicitly via mean curvature H and Gauss curvature K, their relation to focal geometry is still unclear. In the smooth case, points at distance $1/\kappa_i$ from the surface are focal points of the normal congruence. This property holds in the discrete case too, if we use version 2 normality:

Proposition 4.2 *Consider a congruence with parametric representation $\mathbf{x}(u, v, \lambda)$ which is defined by the correspondence of two triangles $\mathbf{a}_1\mathbf{a}_2\mathbf{a}_3$ and $\mathbf{b}_1\mathbf{b}_2\mathbf{b}_3$. Assume that it is normal in the sense of Eq. (6*), and consider (in the notation of Proposition 3.2) the plane P_0 which contains $\mathbf{a}_1\mathbf{a}_2\mathbf{a}_3$ and the corresponding normal $L(u_0, v_0)$. Then the focal points of that line lie at distance $1/\kappa_1$, $1/\kappa_2$ from the plane P_0, with κ_i as the principal curvatures, i.e., the focal points are precisely the points $\mathbf{x}(u_0, v_0, 1/\kappa_i)$.*

Proof We consider the parametrization (8) which is with respect to an adapted coordinate system, so that $u_0 = 0$ and $v_0 = 0$. It is easy to see that the values κ_1, κ_2 occurring there are indeed the principal curvatures. A simple computation shows that for the special case $u = v = 0$, the determinant of partial derivatives of $\mathbf{x}(u, v, \lambda)$ specializes to $[\mathbf{x}_u, \mathbf{x}_v, \mathbf{x}_\lambda] = (1 - \lambda\kappa_1)(1 - \lambda\kappa_2)$. Thus we have a singularity if $\lambda = 1/\kappa_i$.

Special cases.

An *umbilic* point is characterized by equality of principal curvatures, i.e., $\kappa_1 = \kappa_2 = \kappa$. In this case some of the geometric objects discussed above simplify. E.g. the above-mentioned cubic family of planes becomes the set of tangent planes of a quadratic cone with vertex $(0, 0, 1/\kappa)$. Such an umbilic occurs every time two corresponding triangles $\mathbf{a}_1\mathbf{a}_2\mathbf{a}_3$ and $\mathbf{b}_1\mathbf{b}_2\mathbf{b}_3$ are in homothetic position, but the converse is not true.

A *parabolic* point is characterized by one principal curvature, say κ_1, being zero. In this case, Eq. (8) immediately shows that the congruence vectors $\mathbf{e}_1, \mathbf{e}_2, \mathbf{e}_3$ associated with vertices $\mathbf{a}_1, \mathbf{a}_2, \mathbf{a}_3$ are not linearly independent, so Proposition 3.2 does not apply. Along the x axis, the lines of the congruence are parallel to each other, which is in accordance with the fact that the focal point $(0, 0, 1/\kappa_1)$ has moved to infinity. The above-mentioned cubic family of planes is quadratic (in fact, it is the family of tangent planes of a parabolic cylinder).

Remark 4.3 We should mention that the approach to curvatures presented here carries over to *relative* differential geometry where the image of the Gauss map is not a sphere but a general convex body [19]. Another straightforward extension is to curvatures at vertices, which however does not lead to a shape operator in such a natural manner.

5 Results and Discussion

Numerical examples. Vertex normals of a mesh can be estimated (e.g. as area-weighted averages of face normals). Any such collection of sensible normals is not far away from being a "normal" congruence in our sense. By applying optimization, we can make it as normal as possible, meaning that (6) is fulfilled in the least-squares sense. Numerical experiments show that this improves the quality of the normal field (even if there are not enough d.o.f. to satisfy (6) fully if the vertices of the mesh are kept fixed). Since curvatures and the distribution of normals are inseparable, it makes sense to study curvatures not only as quantities derived from a mesh, but as quantities which arise naturally from the the result of the optimization procedure just mentioned. In this way the natural sensitivity of curvatures with respect to noise is moderated.

The basic task is, of course, the computation of a normal congruence for a given mesh. This is done via a standard optimization procedure, which is initialized from estimated vertex normals. We express the validity of the normality condition in terms

of least squares, and minimize subject to the constraints that (in the terminology of previous sections), vectors $\mathbf{e}_i$ are of unit length. Figure 8 shows an example. In particular one can see that normality according to Eq. (6) ("version 1") behaves differently from normality according to Eq. (6*) ("version 2"), while there is hardly any difference between conditions (6*) and (11).

Degrees of freedom and topology. When optimizing a normal congruence of a mesh with v vertices, e edges and f faces, we count $3v$ variables for the normals and $f + v$ constraints. If a number b of boundary vertices is present, we fix the normals at the boundary, resulting in $3(v - b)$ variables and $f + (v - b)$ constraints, i.e., $2v - f - 2b$ d.o.f. Elementary manipulations show that

$$\text{d.o.f.} = 2\chi - b,$$

with $\chi = f + v - e$ as the Euler characteristic. We see for meshes of sphere topology we can expect a unique solution, but topological features diminish the available degrees of freedom. If boundary normals are kept fixed, long boundaries diminish this freedom even more. By allowing vertices to move during optimization, we can achieve zero residual again, but of course a compromise has to be found between the quality of the normal congruence and the deviation of the mesh from its previous shape. Table 1 shows some numerical experiments.

Computing Curvatures. Once a normal congruence is available, we can compute curvatures (see Fig. 9) and we can integrate the field of principal curvature directions as well as the field of asymptotic directions (see Fig. 10 for an example). It must be said, however, that we do not want to compete with the many other methods for computing curvatures, and we do not regard the ability to compute curvatures a main result of this study.

Robustness by using normals. Fig. 11 demonstrates that considering a mesh and its normal congruence *together* allows us to handle optimization/smoothing in a stable way. After a mesh and its normals have been perturbed (Fig. 11b), an optimization procedure attempts to restore both. We use a target functional composed of a sum of least squares expressing condition (6*) and also the property of vectors $\mathbf{e}_i$ having

Table 1 Comparison of residuals regarding normalcy of the congruence ("*c*") and unit vectors being normalized ("*n*") when optimizing congruences

	Sphere		Torus				Disk w/holes, see Fig. 10			
	Fixed vertices		Fixed vertices		Moving vertices		Fixed vertices		Moving vertices	
	c	*n*	*c*	*n*	*c*	*n*	*c*	*n*	*c*	*n*
v. 1	7.8×10^{-3}	0	7.7×10^{0}	0	–	–	1.5×10^{0}	0	–	–
v. 2	9.7×10^{-5}	0	9.6×10^{-1}	0	6.9×10^{-5}	8.1×10^{-7}	1.9×10^{-2}	0	4.0×10^{-5}	2.2×10^{-9}
v. 3	9.0×10^{-2}	0	1.3×10^{-1}	0	6.9×10^{-4}	6.3×10^{-4}	2.4×10^{-1}	0	9.6×10^{-5}	9.5×10^{-10}

All meshes are normalized for unit average edge length, and a zero means a zero up to machine precision. The rows in this table correspond to versions 1, 2, 3 of the normalcy condition for congruences. One can see that zero residual happens only for sphere topology

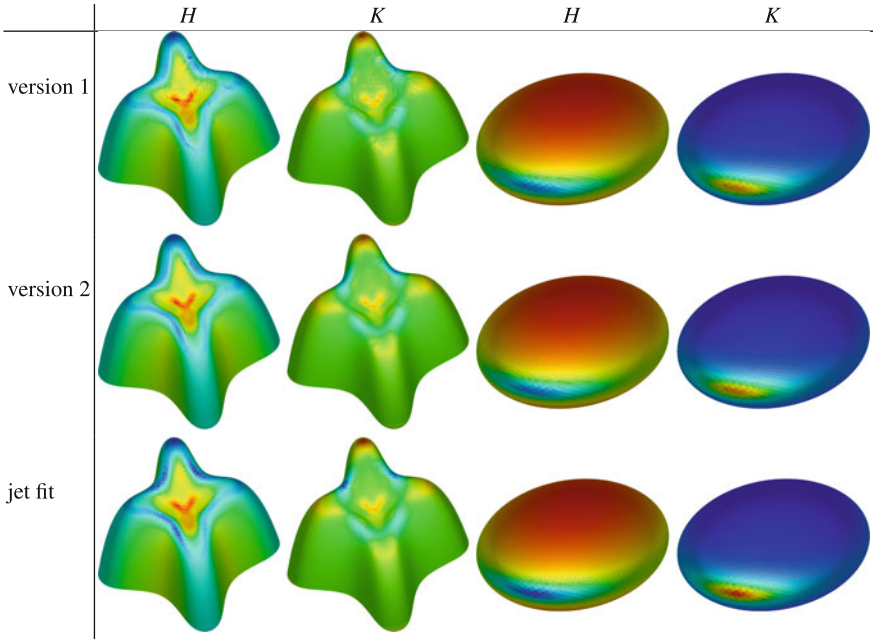

Fig. 9 Computing mean curvature H and Gaussian curvature K by means of normal congruences: "version 1" and "version 2" refer to normality defined by Eqs. (6) and (6*), respectively. Estimated normals are optimized so as to become a normal congruence which allows us to compute curvatures in faces. For comparison, curvatures computed by a 3rd order jet fit have been used, cf. [4]. The color scale is the same for each kind of curvature and each model, throughout the 3 methods of computation. One can hardly see any difference. For each mesh, normal congruences have been computed in the way employed for Fig. 8

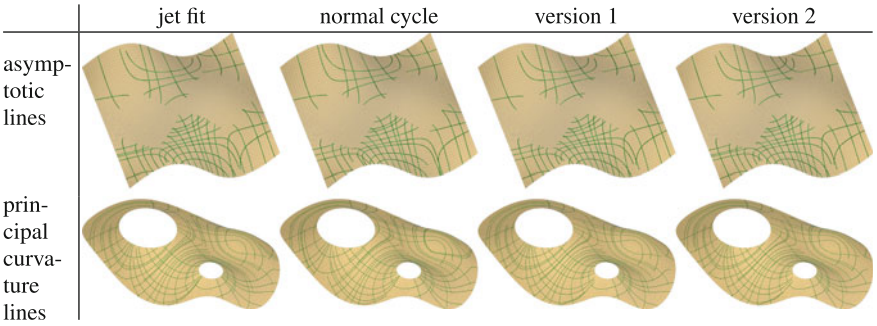

Fig. 10 We compute asymptotic lines and principal curvature lines of meshs by various means. For the figures of the first column, we have used the 3rd order jet fit method of [4]. For the second column, we used the method of normal cycles (see e.g. [20]). The 3rd and 4th column are computed using our the shape operators, where version 1 and version 2 refer to normality w.r.t. Eqs. (6), (6*), respectively. In both cases the normal congruence needed for defining the shape operator was obtained in the same way as for Fig. 8

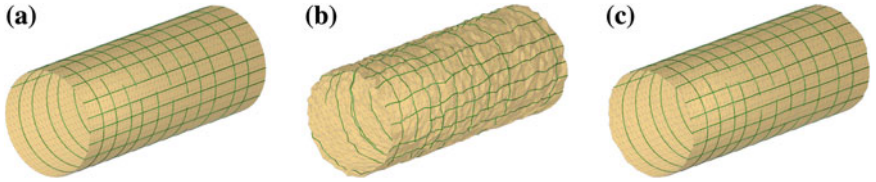

Fig. 11 Computing normals and principal curvature lines for noisy data. Subfigure **a** shows a triangulated cylinder and some of its principal curvature lines. In **b** the jet fit method has been used to obtain principal curves for data where noise has been added to both vertex coordinates and normals. Subfigure **c** shows the result of optimization applied to (**b**), which results in a smooth mesh equipped with a normal congruence. For **c** we again show the principal curvature lines computed by our method

length 1 (weight 1), proximity to the input data (weight 1/4), Laplacian fairing for the mesh (weight 10^{-6}), Laplacian fairing for the normal vectors (weight 10^{-4}) and compatibility between normal and mesh by penalizing deviation from orthogonality between congruence lines in mesh barycenters and face (weight 10^{-4}). Figure 11c shows the repaired mesh.

Relevance for discrete differential geometry.

The idea of employing the Steiner formula for defining curvatures has proved very helpful in bringing together various different notions of curvature, and indeed, various different notions of discrete surfaces (like discrete minimal surfaces and discrete cmc surfaces) which were defined in a way not involving curvature directly but by other means like Christoffel duality. We refer to [2, 3] for more details. The theory presented in [2] is restricted to offset-like pairs of polyhedral surfaces where corresponding edges and faces are parallel. There are ongoing efforts to extend this theory to more general situations (we point to recent work on quad meshes [10] and on isothermic triangle meshes of constant mean curvature [11]). It is therefore remarkable that at least for the situation described here, triangle meshes allow an approach to curvatures and even a shape operator which is likewise guided by the Steiner formula, but without the rather restrictive property of parallelity (which for triangle meshes would be even more restrictive).

Future Research.

As to discrete differential geometry, it is still unclear how known constructions of special discrete surfaces relate to the curvatures defined here: For instance, it seems difficult to gain nice geometric properties from the condition vanishing mean curvature. Nevertheless one of the known constructions of discrete minimal surfaces might be equipped with a canonical normal congruence such that, when our theory is applied, mean curvature vanishes.

Further applications of line congruences have been discussed by Wang et al. [21], but there might be other examples of geometry processing tasks where the notion of line congruence, or even normal congruence, becomes relevant.

Acknowledgments The authors are grateful to Alexander Bobenko for fruitful discussions and to the anonymous reviewers for their suggestions. This research was supported by the DFG Collaborative Research Center, TRR 109, "Discretization in Geometry and Dynamics" through grants I705 and I706 of the Austrian Science Fund (FWF).

References

1. Baker, H.F.: Principles of Geometry, vol. II, 2nd edn. Cambridge University Press (1930)
2. Bobenko, A., Pottmann, H., Wallner, J.: A curvature theory for discrete surfaces based on mesh parallelity. Math. Annalen **348**, 1–24 (2010)
3. Bobenko, A., Suris, Yu.: Discrete Differential Geometry: Integrable Structure. American Mathematical Society (2009)
4. Cazals, F., Pouget, M.: Estimating differential quantities using polynomial fitting of osculating jets. In: Kobbelt, L., Schröder, P., Hoppe, H. (eds.) Proceedings of Symposium on Geometry Processing, pp. 177–187. Eurographics Association (2003)
5. Desbrun, M., Meyer, M., Schröder, P., Barr, A.: Discrete differential-geometry operators for triangulated 2-manifolds. In: Visualization & Mathematics, vol. 3, pp. 35–57. Springer (2003)
6. Doliwa, A., Santini, P., Mañas, M.: Transformations of quadrilateral lattices. J. Math. Phys. **41**, 944–990 (2000)
7. Dragović, V., Radnović, M.: Poncelet porisms and beyond. Birkhäuser, Basel (2011)
8. Grinspun, E., Gingold, Y., Reisman, J., Zorin, D.: Computing discrete shape operators on general meshes. Comput. Graph. Forum **25**(3), 547–556 (2006). Proc. Eurographics
9. Hildebrandt, K., Polthier, K.: Generalized shape operators on polyhedral surfaces. Comput. Aided Geom. Des. **28**, 321–343 (2011)
10. Hoffmann, T., Sageman-Furnas, A., Wardetzky, M.: A discrete parametrized surface theory in $\mathbb{R}^3$. Int. Math. Res. Not. (2016), to appear
11. Lam, W.Y., Pinkall, U.: Isothermic triangulated surfaces. Math. Annalen (2016), to appear
12. Liu, Y., Pottmann, H., Wallner, J., Yang, Y.L., Wang, W.: Geometric modeling with conical meshes and developable surfaces. ACM Trans. Graphics **25**(3), 681–689 (2006). Proc. SIGGRAPH
13. Morvan, J.M.: Generalized Curvatures. Springer (2008)
14. Porteous, I.R.: Geometric Differentiation for the Intelligence of Curves and Surfaces. Cambridge University Press (1994)
15. Pottmann, H., Liu, Y., Wallner, J., Bobenko, A., Wang, W.: Geometry of multi-layer freeform structures for architecture. ACM Trans. Graphics **26**(3), # 65,1–11 (2007). Proc. SIGGRAPH
16. Pottmann, H., Wallner, J.: Computational Line Geometry. Springer (2001)
17. Pottmann, H., Wallner, J.: The focal geometry of circular and conical meshes. Adv. Comp. Math **29**, 249–268 (2008)
18. Pottmann, H., Wallner, J., Huang, Q., Yang, Y.L.: Integral invariants for robust geometry processing. Comput. Aided Geom. Des. **26**, 37–60 (2009)

19. Simon, U., Schwenck-Schellschmidt, A., Viesel, H.: Introduction to the affine differential geometry of hypersurfaces. TU Berlin & Science Univ, Tokyo (1992)
20. Sun, X., Morvan, J.M.: Curvature measures, normal cycles and asymptotic cones. Actes des recontres du C.I.R.M. **3**(1), 3–10 (2013). Proc. "Courbure discrète: théorie et applications"
21. Wang, J., Jiang, C., Bompas, P., Wallner, J., Pottmann, H.: Discrete line congruences for shading and lighting. Comput. Graph. Forum **32**(5), 53–62. Proc. Symp, Geometry Processing (2013)
22. Yu, J., Yin, X., Gu, X., McMillan, L., Gortler, S.: Focal surfaces of discrete geometry. In: Belyaev, A., Garland, M. (eds.) Proceedings of Symposium on Geometry Processing, pp. 23–32. Eurographics Association (2007)

S-Conical CMC Surfaces. Towards a Unified Theory of Discrete Surfaces with Constant Mean Curvature

Alexander I. Bobenko and Tim Hoffmann

Abstract We introduce a novel class of s-conical nets and, in particular, study s-conical nets with constant mean curvature. Moreover we give a unified description of nets of various types: circular, conical and s-isothermic. The later turn out to be interpolating between the circular net discretization and the s-conical one.

1 Introduction

A variety of approaches have been pursued to obtain a notion of discrete constant mean curvature (cmc) surfaces. Two different starting points arise from the interpretation of cmc surfaces as critical points of an area functional [9, 16], and on the other hand from an integrable systems point of view [4, 10]. One principal difference of the two approaches is that, in the first approach, the underlying combinatorial structure is naturally that of a simplicial surface, whereas the integrable systems approach demands a quadrilateral structure of the discrete surface, and one reads about discrete parametrized surfaces. Recently these two approaches were partially merged as soon as a curvature theory for general polyhedral surfaces based on the notions of parallel surfaces and mixed area was developed [5].

Restricting to quadrilateral meshes, and, in particular, to planar quadrilaterals (discrete conjugate nets), may at first sight appear to be a severe restriction. However, it turns out that every surface can be approximated by discrete nets with these

A.I. Bobenko (✉)
Inst. für Mathematik, Technische Universität Berlin,
Straße des 17. Juni 136, 10623 Berlin, Germany
e-mail: bobenko@math.tu-berlin.de

T. Hoffmann
Zentrum Mathematik – M10, Technische Universität München,
Boltzmannstr. 3, 85747 Garching bei München, Germany
e-mail: tim.hoffmann@ma.tum.de

A.I. Bobenko (ed.), *Advances in Discrete Differential Geometry*,
DOI 10.1007/978-3-662-50447-5_9

properties [3, 6], reflecting the existence of the corresponding parametrizations in the smooth case. In fact these integrable discretizations are structure preserving, i.e. they preserve the key aspects of the geometry. A characteristic feature of surfaces described by integrable systems is the existence of special transformations of Bäcklung and Darboux type that preserve the class of surfaces. In the discrete setup these transformations lead to consistent multi-dimensional nets. The last property has established itself as the integrable structure in discrete differential geometry [6].

There exists a rather developed theory of discrete cmc surfaces from an integrable point of view, reflected in numerous publications. They include Q-nets (nets with planar quadrilaterals) [5], circular nets (nets with circular quadrilaterals) [4, 6, 8, 10, 11, 14, 18, 19], semi-discrete nets [15], s-isothermic nets [12]. The latter can be characterized geometrically [6] by having a sphere at every vertex of the net such that the intersection angles of the spheres along opposite edges in every quadrilateral are the same and the four spheres either have a common orthogonal circle, share a pair of points, or (as a limiting case) all meet in exactly one point.

The key observation of the present paper is that the last subclass of s-isothermic nets is in fact conical. Although the class of conical nets introduced in [13] is very important for applications and belongs to integrable discrete differential geometry [6, 17], investigation of discrete conical surfaces with constant curvature has just started [2]. In this paper we introduce a novel class of s-conical nets and, in particular, study s-conical nets that are cmc. The identification of s-conical surfaces with special s-isothermic surfaces mentioned above leads not only to a description of conical cmc nets but also to a unified description of discrete cmc nets. One can think of s-isothermic nets as "interpolating" between the circular net discretization and the s-conical one.

2 Conical Nets

Here we consider Q-nets, which are discrete surfaces with planar quadrilateral faces. Since we are mostly developing a local theory, for simplicity we consider surfaces with the combinatorics of the square grid $f : \mathbb{Z}^2 \to \mathbb{R}^3$. Some parts of the theory can be generalized to a more general combinatorics $f : G \to \mathbb{R}^3$, where G is a quad-graph. The latter is a strongly regular cell decomposition of a two-dimensional manifold with all faces being quadrilaterals. Moreover in the developed theory of discrete CMC surfaces the quad-graph should be edge-bipartite, i.e. there is a black and white edge coloring such that for each quadrilateral opposite edges are of the same color.

Through this paper we will use a notation that indicates shifts in the various directions by subscript. For a net $f : \mathbb{Z}^2 \to \mathbb{R}^3$ we will denote a generic point $f(k, l)$ simply by f. Then it is understood that $f_1 = f(k + 1, l)$, $f_2 = f(k, l + 1)$, $f_{12} = f(k + 1, l + 1)$, $f_{\bar{1}} = f(k - 1, l)$ and so forth. This is of particular use in case of $\mathbb{Z}^n$ lattices but also as long as only one or two neighboring quadrilaterals of a quad-graph are concerned it is a useful shorthand. The following definition first appeared in [13].

Definition 2.1 A Q-net $f : \mathbb{Z}^2 \to \mathbb{R}^3$ is said to be *conical* if for each vertex all incident faces touch a common sphere σ.

The touching spheres in the Definition 2.1 of conical nets are not unique. In general there is a 1-parameter family of spheres touching all incident faces for each vertex. These spheres are inscribed in a cone, and their centers lie on the cone axis. This furnishes a canonical *normal direction* (or line) in each vertex of f.

The normal lines of neighboring vertices are coplanar. Due to this fact conical nets have parallel nets in normal direction. The following theorem as well as all properties of conical nets mentioned in this section are due to [13] (see also [5, 6]).

Theorem 2.2 *Let $f : \mathbb{Z}^2 \to \mathbb{R}^3$ be a conical net. There is a 1-parameter family of conical nets $f^t : \mathbb{Z}^2 \to \mathbb{R}^3$ such that $(f^t - f)$ lies in normal direction to f, f and f^t have parallel edges, and the distance between corresponding faces is constant.*

Proof Given a conical net $f : \mathbb{Z}^2 \to \mathbb{R}^3$ one chooses f^t at a vertex f such that $f^t - f$ is in normal direction. Then there is a touching sphere σ with center at f^t. Let r be its radius. Now one can find touching spheres σ of radius r at all other vertices. Set f^t to be their centers. Then (ff^t) is in normal direction everywhere. Consider a quadrilateral (f, f_1, f_{12}, f_2). Since the edge (ff_1) lies in the intersection of two common tangent planes of σ_1 and σ it is parallel to the difference of their centers $f_1^t - f^t$ as well (the spheres are of equal radius). Thus the corresponding edges (and hence also the faces) of the quadrilaterals (f, f_1, f_{12}, f_2) and $(f^t, f_1^t, f_{12}^t, f_2^t)$ are parallel. Moreover since all the spheres have the same radius r, the distance between the planes of these quadrilaterals is r. Since the faces of f and f^t are parallel f^t is conical as well.

Definition 2.3 Let $f : \mathbb{Z}^2 \to \mathbb{R}^3$ be a conical net. $n : \mathbb{Z}^2 \to \mathbb{R}^3$ is called a Gauss map of f if n points in normal direction and the parallel net $f^1 = f + n$ has constant face offset 1, i.e. the distance between the planes of the corresponding faces of f and f^1 is equal to 1.

Proposition 2.4 *Let $f : \mathbb{Z}^2 \to \mathbb{R}^3$ be a conical net and $n : \mathbb{Z}^2 \to \mathbb{R}^3$ its Gauss map. Then the edges of n are parallel to the edges of f and the faces of n touch the unit sphere S^2.*

Proof Since $f + n$ is parallel to f, n is parallel to f as well. Moreover since the distance between the faces of $f + n$ and f is equal to 1, the projection of n to the face normals N of f (and n) is 1. Thus the faces of n touch the unit sphere.

The parallel nets in Theorem 2.2 are then given by

$$f^t = f + tn. \tag{1}$$

We will refer to these nets as *(parallel) nets in constant distance*.

We can use the notion of parallel nets to give yet another characterization for conical nets:

Proposition 2.5 *A Q-net $f : \mathbb{Z}^2 \to \mathbb{R}^3$ is a conical net if and only if f has parallel nets with constant face offset. If f is generic the constant face offset nets lie in normal direction.*

Proof Theorem 2.2 shows that conical nets have parallel nets with constant face offset. Now if f is a net with parallel net $\tilde{f}$ in constant face distance d, then $\hat{f} = \tilde{f} - f$ is parallel to f as well, and the faces of $\hat{f}$ touch a sphere of radius d. Thus $\hat{f}$ is conical. This also ensures conicality of all its parallel nets, in particular of f and $\tilde{f}$. Finally, $\hat{f} = \tilde{f} - f$ is the cone axes for $\hat{f}$ and therefore $(f\,\tilde{f})$ is the normal direction for $\tilde{f}$ and f as well.

The following angle characterization of conical nets was proven in [20].

Proposition 2.6 *A Q-net $f : \mathbb{Z}^2 \to \mathbb{R}^3$ is a conical net if and only if at each vertex the sums of the opposite angles (of quadrilaterals) are equal.*

Example 2.7 Take any planar polygon $\gamma(k) = (\gamma^1(k), \gamma^2(k))$ with non vanishing edges and an angle $0 < \phi < \pi$. Then the discrete rotational net

$$f(k, l) = (\gamma^1(k), \cos(l\phi)\gamma^2(k), \sin(l\phi)\gamma^2(k))$$

is a conical net.

3 Curvatures of Conical Nets via Steiner's Formula

The classical Steiner formula couples the areas of a surface f and a parallel offset surface f^t with the mean and Gauss curvature of f. If f is an infinitesimal surface patch and f^t the parallel one in distance t in normal direction, then Steiner's formula gives:

$$A(f^t) = A(f)(1 - 2Ht + Kt^2), \tag{2}$$

where A is the area, and H and K are the mean and the Gauss curvatures of f.

A discrete analogue of this formula was used in [5] to define curvatures for Q-nets with a given Gauss map (see also [18] where this formula first appeared for Q-nets with circular quadrilaterals). Let $Q = (q, q_1, q_{12}, q_2)$ be a planar quadrilateral and N a unit normal of the plane of Q. Denoting its diagonals with $d_1 = q_{12} - q$ and $d_2 = q_2 - q_1$ the area $A(Q)$ can be computed as

$$A(Q) = \frac{1}{2}\det(d_1, d_2, N).$$

If P is another quadrilateral with edges parallel to the edges of Q and with diagonals c_1 and c_2 the area of $P + tQ$ is equal to

$$A(P + tQ) = A(P) + 2t\frac{1}{4}(\det(d_1, c_2, N) + \det(c_1, d_2, N)) + t^2 A(Q). \tag{3}$$

The space of all planar quadrilaterals with edges parallel to a given one Q is a four dimensional vector space. Moding out the translations leaves a two dimensional one. On this space the area is a quadratic form $A(P)$ and the mixed area is the corresponding symmetric form $A(P_1, P_2)$.

Since a conical mesh f and its Gauss map n have parallel edges, the area of the quadrilaterals of the offset net $f^t = f + tn$ is quadratic in the distance t. A discrete version of Steiner's formula suggested in [5] (see also [6]) reads as follows.

Definition 3.1 Let $f : \mathbb{Z}^2 \to \mathbb{R}^3$ be a conical net with the Gauss map $n : G \to \mathbb{R}^3$. Then the *discrete Steiner formula*

$$A(f + tn) = A(f)(1 - 2Ht + Kt^2) \tag{4}$$

defines a *discrete mean curvature* H and a *discrete Gauss curvature* K on the faces of the net f:

$$H = -\frac{A(f, n)}{A(f)}, \quad K = \frac{A(n)}{A(f)}. \tag{5}$$

Here $A(f)$ and $A(n)$ are the areas of the quadrilaterals (f, f_1, f_{12}, f_2) and (n, n_1, n_{12}, n_2) respectively, and $A(f, n)$ is their mixed area.

4 Dual Quadrilaterals and Koenigs Nets

As we mentioned already, the mixed area $A(P, Q)$ is a symmetric bilinear form on a two-dimensional vector space of quadrilaterals with parallel edges. Quadrilaterals P and Q with $A(P, Q) = 0$ are "orthogonal" with respect to this form. For any non-vanishing planar quadrilateral Q there is a P with $A(P, Q) = 0$ and P is unique up to scaling.

Definition 4.1 Two planar quadrilaterals P and Q with parallel edges are called *dual* to each other if their mixed area vanishes:

$$A(P, Q) = 0.$$

Whenever scaling is unimportant we will simply talk about *the* dual quadrilateral P^*, satisfying $A(P, P^*) = 0$.

Let $P = (p, p_1, p_{12}, p_2)$ and $Q = (q, q_1, q_{12}, q_2)$ be two planar quadrilaterals with parallel edges and let N be their common normal then (3) implies the following formula for their *mixed area*

$$A(P, Q) = \frac{1}{4}\left(\det(p_{12} - p, q_2 - q_1, N) + \det(q_{12} - q, p_1 - p_2, N)\right). \tag{6}$$

The duality can be described in terms of the diagonals [5, 6].

Proposition 4.2 *The mixed area $A(P, Q)$ of two planar quadrilaterals with parallel edges $P = (p, p_1, p_{12}, p_2)$ and $Q(q, q_1, q_{12}, q_2)$ vanishes if and only if their non-corresponding diagonals are parallel, i.e. $p_{12} - p \parallel q_2 - q_1$ and $q_{12} - q \parallel p_2 - p_1$.*

Let us present also useful explicit formulas for the dual quadrilateral. Let o be the intersection point of the diagonals of a planar quadrilateral $P = (p, p_1, p_{12}, p_2)$, $e_1 = \frac{p_{12}-p}{\|p_{12}-p\|}$, $e_2 = \frac{p_2-p_1}{\|p_2-p_1\|}$ be the unit vectors of diagonals and define $\alpha, \beta, \gamma, \delta$ as the oriented lengths of the connection intervals of the intersection point o to the vertices: $p - o = \alpha e_1$, $p_{12} - o = \gamma e_1$, $p_1 - o = \beta e_2$, $p_2 - o = \delta e_2$. Then the quadrilateral $P^* = (p^*, p_1^*, p_{12}^*, p_2^*)$ determined by

$$p^* - o^* = -\frac{1}{\alpha} e_2, \; p_{12}^* - o^* = -\frac{1}{\gamma} e_2, \; p_1^* - o^* = \frac{1}{\beta} e_1, \; p_2^* - o^* = \frac{1}{\delta} e_1 \qquad (7)$$

with some o^* is dual to P.

Every planar quadrilateral has a dual one. However generic Q-nets are not dualizable as a whole. Dualizable Q-nets were introduced in [7] (see also [6]).

Definition 4.3 A Q-net $f : \mathbb{Z}^2 \to \mathbb{R}^3$ is called a *Koenigs net* if there is a Q-net $f^* : \mathbb{Z}^2 \to \mathbb{R}^3$ such that the corresponding quadrilaterals of f and f^* are dual to each other; f^* is called *(Christoffel) dual* of f.

Koenigs nets can be characterized [6, 7] in terms of the intersection points of the diagonals.

Proposition 4.4 *A Q-net $f : \mathbb{Z}^2 \to \mathbb{R}^3$ in general position (each vertex and its neighbours are not co-planar) is a Koenigs net if and only if the intersection points of the diagonals of four quadrilaterals around each vertex are coplanar.*

Since the planes of a planar quadrilateral and its dual are parallel, the conicality conditions for f^* and f are satisfied simultaneously.

Proposition 4.5 *If $f : \mathbb{Z}^2 \to \mathbb{R}^3$ is conical and Koenigs, its Christoffel dual $f^* : \mathbb{Z}^2 \to \mathbb{R}^3$ is conical as well.*

5 Conical Nets with Constant Mean Curvature and S-Conical Nets

Definition 5.1 A conical net $f : \mathbb{Z}^2 \to \mathbb{R}^3$ is called a net with *constant mean curvature* (cmc net) if its mean curvature H defined by (5) is constant. Conical nets with vanishing mean curvature are called *minimal*.

Theorem 5.2 *A conical net $f : \mathbb{Z}^2 \to \mathbb{R}^3$ is a cmc net with mean curvature $H \neq 0$ if and only if it is a Koenigs net with its Christoffel dual in constant distance $\frac{1}{H}$:*

$$H = \text{const} \Leftrightarrow f^* = f - \frac{1}{H}n. \tag{8}$$

The dual net f^* is a conical cmc net with mean curvature H as well.

Indeed, we have

$$HA(f, f) = -A(f, n) \Leftrightarrow 0 = A(f, f - \frac{1}{H}n).$$

Thus f^* exists and is given by (8).

There is a tight connection (see [6, 17]) of conical nets and circular nets, i.e. Q-nets with circular faces. Given a conical net one can choose a point on one of the face's planes arbitrarily. Mirroring this point at the planes spanned by the face's edges and their incident normals gives a circular net. Each vertex of this circular net corresponds to a face of the conical net and vice versa. This way each conical net gives rise to a 2-parameter family of circular nets. The circle centers of the circular net lie on the cone axes of the conical one.

On the other hand, given a circular net, we can choose an initial unit vertex normal arbitrarily. Mirroring that normal at the edge-bisecting planes gives rise to a consistent set of vertex normals such that neighboring normals intersect. Their orthogonal planes passing through the vertices of the circular net give rise to a conical net. This way each circular Q-net gives rise to a 2-parameter family of conical nets. We will call these conical and circular nets *corresponding* to each other.

We complete this section with an introduction of particular conical nets.

Definition 5.3 A discrete conical net $f : \mathbb{Z}^2 \to \mathbb{R}^3$ is called *s-conical* if for every vertex the intersection points of the diagonals of the quadrilaterals sharing the vertex lie on a circle, and the axis of this circle is the vertex normal (the cone axis at the vertex).

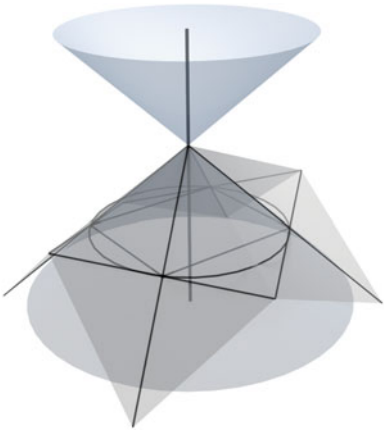

Fig. 1 To definition of s-conical nets. The cone touches all four neighboring quadrilaterals. The intersection points of the diagonals are circular, and the axis of the circle coincides with the axis of the cone

It is easy to see that an s-conical net and its circular net formed by the intersection points of the diagonals are corresponding (see Fig. 1). Indeed two triangles on two neighboring faces sharing an edge built by this edge and the intersection points of the diagonals are congruent. Therefore they are symmetric with respect to the reflection in the symmetry plane of the planes of the neighboring faces.

Theorem 5.4 *(i) S-conical nets are Koenigs nets.*
(ii) The dual net of an s-conical net is also s-conical.

Proof (i) follows from Proposition 4.4 since the intersection points of the diagonals are circular.

(ii) Consider two (congruent) triangles Δ_1, Δ_2 on two neighboring faces of f with a common edge built by this edge and the intersection points of the diagonals. As it was explained above they are symmetric with respect to the reflection in the symmetry plane P of the planes of the faces. The dualization formula (7) implies that the corresponding triangles Δ_1^*, Δ_2^* of the dual net f^* are also symmetric with respect to P. This implies that f^* is s-conical.

In Sect. 7 we give an alternative definition of this class and investigate it.

6 S-Isothermic Nets

For an s-conical net the intersection points o of the diagonals are circular with the circle centers lying on the corresponding cone axes. Let f be a vertex of an s-conical net and $o_{\bar{1}\bar{2}}, o_{\bar{2}}, o, o_{\bar{1}}$ the diagonal intersection points of the quadrilaterals incident to f. The points $o_{\bar{1}\bar{2}}, o_{\bar{2}}, o, o_{\bar{1}}$ lie on a sphere s with center f. This furnishes a map $s : \mathbb{Z}^2 \to \{\text{spheres in } \mathbb{R}^3\}$ such that each sphere s is centered at the vertex f and in each diagonals intersection point o four spheres s, s_1, s_{12}, s_2 meet. Furthermore, opposite spheres s and s_{12} as well as s_1 and s_2 touch at o.

In order to proceed further we recall some basic facts about s-isothermic nets and their Möbius geometric description (see [6] for details).

Let $\mathbb{R}^{4,1}$ be the five dimensional Minkowski space with the standard Lorenz inner product

$$\langle x, y\rangle = -x_0 y_0 + \sum_{k=1}^{4} x_k y_k.$$

There is a bijection between oriented spheres and planes s in $\mathbb{R}^3$ and unit vectors $\hat{s} \in \mathbb{R}^{4,1}$ (here we consider planes as degenerate spheres), as well as points p in $\mathbb{R}^3 \cup \infty$ and isotropic vectors $\hat{p} \in \mathbb{L}^4 \subset \mathbb{R}^{4,1}$. For points p one sets

$$\hat{p} = \left(\frac{1 + \|p\|^2}{2}, p, \frac{1 - \|p\|^2}{2}\right) \tag{9}$$

with $\langle \hat{p}, \hat{p} \rangle = 0$. The point at infinity ∞ is then given by $(1, 0, 0, 0, -1)$. An oriented sphere s with center c and radius r in $\mathbb{R}^3$is represented as

$$\hat{s} = \frac{1}{r}\left(\frac{1 + (\|c\|^2 - r^2)}{2}, c, \frac{1 - (\|c\|^2 - r^2)}{2}\right). \tag{10}$$

A plane with the normal form $\langle v, n \rangle|_{\mathbb{R}^3} = d$, $\|n\| = 1$ is is given by

$$\hat{s} = (d, n, -d).$$

In both cases $\langle \hat{s}, \hat{s} \rangle = 1$. Changing the orientation of the sphere or plane corresponds to the transformation $\hat{s} \mapsto -\hat{s}$. A point p lies on a sphere s if and only if

$$p \in s \Leftrightarrow \langle \hat{p}, \hat{s} \rangle = 0. \tag{11}$$

The intersection angle α between two spheres s_1 and s_2 can be calculated as

$$\cos \alpha = \langle \hat{s}_1, \hat{s}_2 \rangle. \tag{12}$$

In particular touching spheres satisfy

$$\langle \hat{s}_1, \hat{s}_2 \rangle = -1.$$

From here on we will use the same notation p, s for points and spheres in $\mathbb{R}^3$ and their representatives (10) in $\mathbb{R}^{4,1}$. The meaning will be clear from the context.

Definition 6.1 A net $s : \mathbb{Z}^2 \to \mathbb{R}^{4,1}$ of space-like unit vectors solving the discrete Moutard equation

$$s + s_{12} = \lambda(s_1 + s_2), \lambda \neq 0, \tag{13}$$

is called *s-isothermic*.

Proposition 6.2 *Let $s : \mathbb{Z}^2 \to \mathbb{R}^{4,1}$ be an s-isothermic net. Then*

$$\langle s_{12}, s_1 \rangle = \langle s_2, s \rangle \quad \textit{and} \quad \langle s_{12}, s_2 \rangle = \langle s_1, s \rangle. \tag{14}$$

Proof The unit length condition implies

$$1 = \langle s_{12}, s_{12} \rangle = \lambda^2 \langle s_1 + s_2, s_1 + s_2 \rangle - 2\lambda \langle s_1 + s_2, s \rangle + 1,$$

and finally

$$\lambda \langle s_1 + s_2, s_1 + s_2 \rangle - 2\langle s_1 + s_2, s \rangle = 0. \tag{15}$$

If $\langle s_1 + s_2, s_1 + s_2\rangle = 0$ (this is the touching spheres case $\langle s_1, s_2\rangle = -1$) we get from (15) $\langle s_1, s\rangle = -\langle s_2, s\rangle$. This implies $\langle s_{12}, s_1\rangle = \langle \lambda(s_1 + s_2) - s, s_1\rangle = -\langle s, s_1\rangle = \langle s, s_2\rangle$. In the non-touching case $\langle s_1 + s_2, s_1 + s_2\rangle \neq 0$ substituting λ given by (15) into (13) we obtain (14).

S-isothermic nets have the following geometric properties formulated in terms of the centers c and the radii r of the corresponding spheres (10) (see [6, 7] for the proof).

Theorem 6.3 *(i) The centers $c \in \mathbb{R}^3$ of an s-isothermic net build Koenigs nets.*
(ii) Let s be an s-isothermic net of spheres with the centers $c : \mathbb{Z}^2 \to \mathbb{R}^3$ and (signed) radii $r : \mathbb{Z}^2 \to \mathbb{R}$. The spheres s^* with the centers $c^* : \mathbb{Z}^2 \to \mathbb{R}^3$ and the radii $r^* : \mathbb{Z}^2 \to \mathbb{R}$ given by

$$c_1^* - c^* = \frac{c_1 - c}{r_1 r}, \quad c_2^* - c^* = -\frac{c_2 - c}{r_2 r}, \quad r^* = \frac{1}{r}, \tag{16}$$

build an s-isothermic net (called Christoffel dual *net).*

S-isothermic nets belong to integrable structures of discrete differential geometry [6], i.e. they can be extended consistently to the $\mathbb{Z}^N$ lattice so that all two-dimensional coordinate subnets are s-isothermic. This property can be interpreted as a transformation of two-dimensional s-isothermic nets called Darboux transformation [12].

Definition 6.4 Consider two s-isothermic nets $s : \mathbb{Z}^2 \to \mathbb{R}^{4,1}$ and $\hat{s} : \mathbb{Z}^2 \to \mathbb{R}^{4,1}$, and their spheres with the same indexes as corresponding. Thus, for example, the spheres $s, s_1, s_{12}, s_2, \hat{s}, \hat{s}_1, \hat{s}_{12}, \hat{s}_2$ build a combinatorial cube shown in Fig. 2, and we treat the faces of s and $\hat{s}$ as bottom and top faces of the cube. The s-isothermic nets s and $\hat{s}$ are said to be *Darboux transforms* of each other if the spheres corresponding to the side faces of the cube also satisfy the discrete Moutard equations (with different signs corresponding to two different pairs of opposite faces):

$$\hat{s}_1 + s = a(\hat{s} + s_1), \quad \hat{s}_{12} + s_2 = a_2(\hat{s}_2 + s_{12}),$$
$$\hat{s}_2 - s = b(\hat{s} - s_2), \quad \hat{s}_{12} - s_1 = b_1(\hat{s}_1 - s_{12}).$$

Fig. 2 A Darboux cube

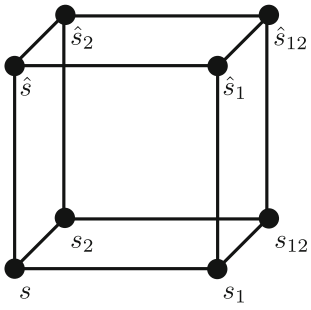

Remark 6.5 Given s its Darboux transform $\hat{s}$ is uniquely determined by one vertex of $\hat{s}$ which can be chosen arbitrary.

Remark 6.6 Note that the sides of a Darboux cube that correspond to the solutions of the Moutard equation with plus sign have embedded quadrilaterals while the ones with minus sign give rise to non-embedded quadrilaterals.

Remark 6.7 To pass to a multidimensional consistent picture mentioned above one should change the orientations of the spheres for every second line $s_{ij} \to (-1)^i s_{ij}$.

7 S-Conical Nets as S-Isothermic Nets

The Moutard equation implies that the four spheres of each quadrilateral are linearly dependent vectors in $\mathbb{R}^{4,1}$. Thus an s-isothermic net s is in particular a Q-net. We obtain three types of s-isothermic surfaces characterized by the fact that the four spheres s, s_1, s_2, s_{12}:

share a common orthogonal circle (Type 1),
intersect in a pair of points (Type 2),
intersect in exactly one point (Type 3).

These three cases are distinguished by the signature of the Lorentz metric restricted to the subspace of the corresponding spheres s, s_1, s_{12}, s_2 which span a 3-dimensional subspace $U \subset \mathbb{R}^{4,1}$. Denote its orthogonal complement by $U^\perp$. If the inner product on $U^\perp$ is positive definite the unit vectors therein form a 1-parameter family of spheres orthogonal to s, s_1, s_{12}, and s_2. This family shares a circle (given by the isotropic vectors of U) which thus is perpendicular to s, s_1, s_{12}, and s_2.

If the inner product on $U^\perp$ is indefinite and non degenerate then it contains two isotropic directions $\hat{p}_1$ and $\hat{p}_2$ which give rise to two points p_1 and p_2 that are contained in all four spheres.

Finally if the inner product is degenerate on $U^\perp$ the subspace touches the light-cone of $\mathbb{R}^{4,1}$ and that direction gives rise to one common point of s, s_1, s_{12}, and s_2.

The first type has a particularly nice special case when all the inner products are 1. In this case the four spheres for each quadrilateral touch cyclically [1, 6]. The orthogonal circle then must pass through the four touching points.

S-isothermic surfaces of type 3 are of particular interest for us. It is the case where the orthogonal circle (or the pair of common points) collapses into a point (Fig. 3).

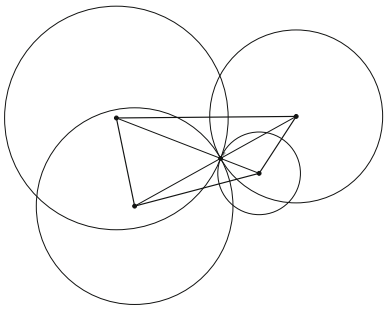

Fig. 3 An s-conical quadrilateral as an s-isothermic net of type 3

Theorem 7.1 *For a map* $s : \mathbb{Z}^2 \to \mathbb{R}^{4,1}$ *with* $\langle s, s\rangle = 1$ *the following statements are equivalent:*

(i) *s is s-isothermic of type 3.*
(ii) *s is a solution to the Moutard equation (13) and the intersection angles of the spheres are complimentary:* $\langle s, s_1\rangle = -\langle s, s_2\rangle$ *and* $|\langle s, s_1\rangle| \leq 1$.
(iii) $s + s_{12}$ *and* $s_1 + s_2$ *are parallel isotropic vectors.*
(iv) *The centers c of s form an s-conical net and the intersection points o of the diagonals lie on the corresponding spheres* s, s_1, s_{12}, s_2.

Proof $(i) \Rightarrow (ii)$. The centers of the spheres s, s_1, s_{12}, s_2 are coplanar and the opposite spheres touch in a common point. Thus this must be the intersection point of the diagonals. The intersection angle of the diagonals α and its complimentary angle $\pi - \alpha$ are exactly the intersection angles of the corresponding neighboring spheres. Then the claim follows from (12).

$(ii) \Rightarrow (iii)$. For $\langle s, s_1\rangle = -\langle s, s_2\rangle$ Eq. (15) implies that $s_1 + s_2$ is isotropic (note that $\lambda \neq 0$). Due to (13) $s_{12} + s$ is parallel and therefore isotropic as well.

$(iii) \Rightarrow (iv)$. The isotropy $\langle s_1 + s_2, s_1 + s_2\rangle = 0$ implies the touching condition $\langle s_1, s_2\rangle = -1$. Moreover $s_1 + s_2$ and $s + s_{12}$ are equivalent projective representations of the common touching point o. The centers c of the spheres form a planar quadrilateral for which the diagonals (c_1, c_2) and (c, c_{12}) intersect at the touching points o. Since $o_{\bar{1}\bar{2}}, o_{\bar{2}}, o, o_{\bar{1}}$ are the points in which the spheres $s_{\bar{1}}, s_{\bar{2}}, s_1, s_2$ touch cyclically, $o_{\bar{1}\bar{2}}, o_{\bar{2}}, o, o_{\bar{1}}$ lie on a circle,[1] which we denote by C. This implies that the net c is a Koenigs net with a circular net of points o. It remains to show that it is conical as well.

Since the quadrilateral formed by say c, o, c_2, and $o_{\bar{1}}$ is a folded kite (two pairs of non-opposing edges are equal in length), the planes spanned by c, o, c_2 and $c, c_2, o_{\bar{1}}$ are symmetric with respect to the plane spanned by c, c_2, and the axis of the circle C. The same holds for the other edges and thus c is a conical net corresponding to the circular net o.

$(iv) \Rightarrow (i)$. Let s have a central net c that is s-conical. The intersection points $o, o_{\bar{1}}, o_{\bar{1}\bar{2}}, o_{\bar{2}}$ lie on the sphere s. Since the connection line through the centers

[1] This is a simple fact from Möbius geometry that four spheres touching cyclically always have a circle through their touching points.

c, c_{12} passes through the common point o of the spheres s, s_{12}, these must touch at o. The isotropic vector of o is projectively equivalently represented by $s_{12} + s$ or $s_1 + s_2$. This implies that these vectors are parallel, thus s solves the Moutard equation. Since the four spheres share a single point the solution is of the third type.

We have shown that s-conical nets and s-isothermic nets of type 3 can be canonically identified: the centers of the spheres of an s-isothermic net of type 3 are the vertices of the corresponding s-conical net, and their intersection (touching) points o are the intersection points of the diagonals of the s-conical net.

Christoffel dualizations defined for both these classes also coincide. The following theorem follows from the dualization formulas (7) and (16).

Proposition 7.2 *The Christoffel dual net of an s-isothermic net of type 3 is an s-isothermic net of type 3. Moreover the centers c and c^* of the corresponding spheres build Christoffel dual s-conical nets in the sense of Theorem 5.4.*

Finally a Darboux transform of s-isothermic surfaces preserves nets of type 3 and therefore is well defined for s-conical surfaces.

Theorem 7.3 *Let $c : \mathbb{Z}^2 \to \mathbb{R}^3$ be s-conical with the corresponding s-isothermic net $s : \mathbb{Z}^2 \to \mathbb{R}^{4,1}$ and let $\hat{s} : \mathbb{Z}^2 \to \mathbb{R}^{4,1}$ be a Darboux transform of s with central net $\hat{c} : \mathbb{Z}^2 \to \mathbb{R}^3$. Then $\hat{c}$ is s-conical as well.*

Moreover every Darboux cube possesses a (Ribaucour) sphere $R \in \mathbb{R}^{4,1}$ which is orthogonal to all spheres $s, s_1, \ldots, \hat{s}_{12}$ of the Darboux cube,

$$\langle R, s\rangle = \langle R, s_1\rangle = \ldots = \langle R, \hat{s}_{12}\rangle = 0,$$

and passes through the intersection points $o, \hat{o}$ of diagonals of c and $\hat{c}$.

Proof Let us use the characterization (ii) of s-isothermic nets of type 3 from Theorem 7.1 that is $\langle s, s_1\rangle = -\langle s, s_2\rangle$. Due to the Moutard equation the scalar products of the spheres at the opposite edges of any face of the Darboux cube are equal (see Proposition 6.2), for example, $\langle s, s_1\rangle = \langle s^*, s_1^*\rangle$. This implies $\langle s^*, s_1^*\rangle = -\langle s^*, s_2^*\rangle$.

To prove the second claim, consider the one-parameter family of the spheres touching the quadrilateral (c, c_1, c_{12}, c_2) at the point o. They all are orthogonal to s, s_1, s_{12}, s_2. Take the sphere R from this family that is orthogonal to $\hat{s}$. Due to Moutard equations it is orthogonal to $\hat{s}_1, \hat{s}_2, \hat{s}_{12}$ as well. Thus it touches the quadrilateral $(\hat{c}, \hat{c}_1, \hat{c}_2, \hat{c}_{12})$ at $\hat{o}$.

8 S-Conical Nets with Constant Mean Curvature

In this section we consider s-conical nets with constant mean curvature $H \neq 0$. S-conical minimal surfaces, $H = 0$, build an interesting subclass of s-conical surfaces with a rich theory (associated family, Weierstrass representation, variational principle). This is a subject of a separate publication [2].

Lemma 8.1 *Let $f, f^* : \mathbb{Z}^2 \to \mathbb{R}^3$ be two s-conical nets. Then any two of the following conditions imply the third:*

(i) *f^* is a Christoffel dual of f.*
(ii) *f^* is a Darboux transform of f.*
(iii) *f^* and f are in constant face offset, and it is equal to the distance $\|o^* - o\|$ between the intersection points of diagonals of the corresponding faces of f and f^*.*

Proof 1. and 2. $\Rightarrow$ 3.:
Let s and s^* be the s-isothermic nets corresponding to f and f^* respectively. Consider the Darboux cube formed by the spheres s, s_1, s_2, s_{12} and their dual $s^*, s_1^*, s_2^*, s_{12}^*$. In the following f, f_1 etc. will denote the sphere's centers, which were previously denoted by c, c_1 etc. Since the quadrilaterals (f, f_1, f_{12}, f_2) and $(f^*, f_1^*, f_{12}^*, f_2^*)$ are dual they are parallel. Due to Theorem 7.3 they touch the Ribaucour sphere R at o and o^* respectively. This implies that the line trough o and o^* intersects these two quadrilaterals orthogonally (Fig. 4).

Next, consider two neighboring quadrilaterals (f, f_1, f_{12}, f_2) and $(f_1, f_{11}, f_{112}, f_{12})$ with their duals. The common edge $f_{12}f_1$ of the quadrilaterals is the axis of the circle $C = s_1 \cap s_{12}$. Obviously $o, o_1 \in C$. Moreover because of the orthogonality the lines (oo^*) and $(o_1o_1^*)$ are tangents to C. The same argument implies that they are also tangent to the circle $C^* = s_1^* \cap s_{12}^*$.

The circles C and C^* are co-planar and two co-planar circles have two sets of common tangents distinguished by whether they intersect the edge between the circle centers or not. Since the Darboux cubes are "flipped over" this happens for one of the lattice directions and not for the other (see Remark 6.6). Therefore $\|o^* - o\| = \|o_1 - o_1^*\|$. Since those lines are orthogonal to the quads, the face distance for the nets is constant as well.

2. and 3. $\Rightarrow$ 1.:
Again consider the Darboux cube. All sides are planar quadrilaterals and since f and f^* are in constant face distance, they have parallel edges. Moreover all the diagonal intersection points for a Darboux cube are collinear. Let us assume that the quadrilateral (f, f_1, f_1^*, f^*) is the one of the embedded sides of the Darboux cube (see Remark 6.6). Its diagonal intersection point o' and the points o, o^* are collinear. The triangles (f, f_1, o') and (f_1^*, f^*, o') are obviously similar. The triangles (f, f_1, o) and (f_1^*, f^*, o^*) are their orthogonal projections and are similar as well. Thus $f - o$ and $f_1^* - o^*$ are parallel, i.e. the diagonals for f and f^* satisfy the duality criteria of Proposition 4.2.

3. and 1. $\Rightarrow$ 2.:
Again, the planes of corresponding quadrilaterals for f and f^* are parallel since f^* is dual to f. Since (f, f_2, o) and (f_2^*, f^*, o^*) are similar triangles, the arguments of the previous item in the proof imply that the intersection points of the diagonals of all side-quadrilaterals lie on the line connecting o and o^*. In particular this is the case with the intersection point $\tilde{o}$ of the diagonals of the quadrilateral (f, f_2, f_2^*, f^*). We will prove the claim in case that this quadrilateral is non-embedded, for embedded quadrilaterals the proof differs just by a minor change of signs $\pm$.

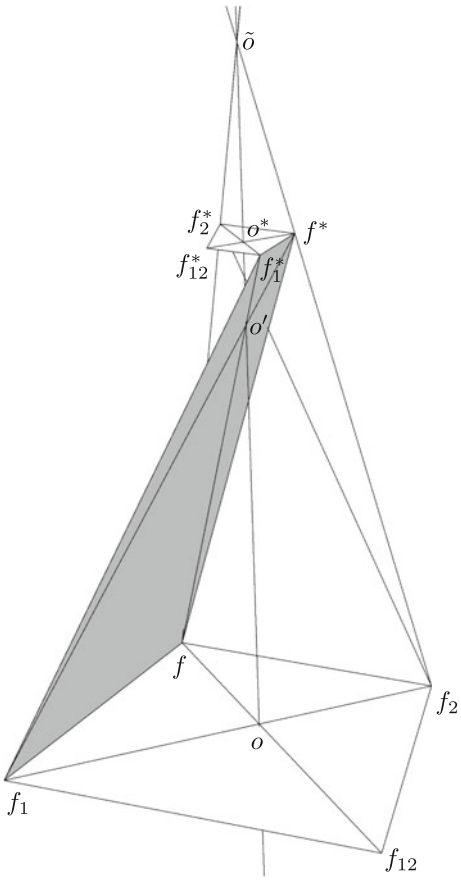

Fig. 4 A geometric cube in Lemma 8.1. The quadrilaterals $(ff_1f_{12}f_2)$, $(f^*f_1^*f_{12}^*f_2^*)$, $(ff_1f_1^*f^*)$ are embedded, the quadrilateral $(ff_2f_2^*f^*)$ is not. The diagonal intersection points $o, o^*, o', \tilde{o}$ lie on a common line orthogonal to the planes of the quadrilaterals $(ff_1f_{12}f_2)$ and $(f^*f_1^*f_{12}^*f_2^*)$

We can assume that $\tilde{o}$ lies at the origin. The triangles $(\tilde{o}, f^*, o^*)$ and $(\tilde{o}, f_2, o)$ are similar and $\|of_2\| = r_2$, $\|o^*f^*\| = r^* = \frac{1}{r}$. This implies for f^* and similarly for f_2^*:

$$f^* = \frac{1}{rr_2} f_2, \quad f_2^* = \frac{1}{rr_2} f.$$

Then the middle three coordinates (10) of the spheres s, s_2, s_2^* and s^* are equal $\frac{f}{r}, \frac{f_2}{r_2}, \frac{f_2^*}{r_2^*} = \frac{f}{r}$, and $\frac{f^*}{r^*} = \frac{f_2}{r_2}$ respectively. To prove the Moutard identity

$$s - s_2^* = \mu(s^* - s_2), \quad \mu = -\frac{r_2}{r}$$

it remains to verify it for the terms of the form $\frac{1}{r}$ and $\frac{\|f\|^2 - r^2}{r}$ in (10). The identity

$$\frac{1}{r} - \frac{1}{r_2^*} = \mu\left(\frac{1}{r^*} - \frac{1}{r_2}\right)$$

is obvious. For the terms of the form $\frac{\|f\|^2 - r^2}{r}$ the computation is slightly more involved. The claim finally follows from

$$\|f\|^2 - r^2 = \|f_2\|^2 - r_2^2 = \|\tilde{o} - o\|^2.$$

Thus the cube is Darboux.

Remark 8.2 Considering degenerated examples it is not difficult to convince yourself that the extra condition that the face distance equals the distance between the points o and o^* (or equivalently that the line (oo^*) is perpendicular to the quadrilaterals) in Lemma 8.1 cannot be dropped.

Let us recall that a parallel net in constant distance in the sense of (1) to a conical net lies in a constant distance face offset. We formulate the obtained properties of s-conical cmc nets in the following

Theorem 8.3 *(i) An s-conical net f is cmc if and only if it has a Christoffel dual f^* in constant distance. The lines (oo^*) connecting the points of intersection of diagonals of the corresponding quadrilaterals of f and f^* intersect the planes of these quadrilaterals at constant angle θ. The distance $\|oo^*\|$ is constant for the whole net.*

(ii) An s-conical net f has a Darboux transform f^D in constant distance if and only if f is cmc with $\theta = \pi/2$. Then the Darboux transform is Chistoffel dual $f^D = f^*$.

Proof The first claim in (i) is Theorem 5.2. To prove the claim about the angles, note that the the points o and o^* corresponding to four quadrilaterals with a common vertex f lie on two circles with the common axis (ff^*). Moreover the corresponding intervals oo^* are symmetric with respect to the reflections in the symmetry planes that identify the planes of the faces. This implies that the distance $\|oo^*\|$ is constant for the whole net, and the lines (oo^*) intersect the planes of the corresponding quadrilaterals at constant angle.

A Darboux transform f^D in constant distance (thus in constant distance face offset) implies that the line through the touching points of the Ribaucour sphere (oo_D) is orthogonal to the faces of the quadrilaterals, and the distance $\|oo_D\|$ is constant. Here we have denoted by o^D the diagonal intersection points of f^D. Then the Darboux transform is Chistoffel dual due to Lemma 8.1, which implies that f is cmc. The reverse statement also follows from this Lemma. Indeed, if f is cmc and f^* its dual with orthogonal (oo^*) then f^* is a Darboux transform of f.

Remark 8.4 Geometric characterizations of s-conical cmc surfaces turn out to be quite similar to the ones of circular cmc surfaces, that also can be characterized as possessing a Christoffel dual, which is simultaneously a Darboux transform, at constant distance [10].

9 Delaunay Nets

In this section we will construct s-conical Delaunay nets that are s-conical analogues of rotationally symmetric cmc surfaces.

A planar polygon $c : \mathbb{Z} \to \mathbb{R}^2$ with non-vanishing edges, gives rise to a discrete surface of revolution. Denoting the components of a vertex c_k by $c_k = (x_k, y_k)$ and choosing an angle ϕ one can form

$$f(k,l) = (x_k, \cos(l\phi)y_k, \sin(l\phi)y_k).$$

Since all the polygons $f(\cdot, l_0)$ are planar we will not distinguish between the generating polygon c and its resulting rotational symmetric net f in what follows. This abuses the notation to some extend but it is understood that shifts in the first direction are along the polygon and whenever a shift in the second direction occurs it refers to the rotational direction of the net.

By symmetry c is s-isothermic. In order for it to be of type 1 with touching spheres ($\langle s_1, s\rangle = \langle s_2, s\rangle = 1$) the polygon must satisfy in addition

$$\|c_1 - c\| = \sin\frac{\phi}{2}\,(y_1 + y).$$

Instead of the polygon c one can look at the midpoint connectors in axial direction. They form a planar polygon as well (see Fig. 5). Calling this polygon $p = (x, v)$ one finds that above condition translates to

$$\|p_1 - p\|^2 = 4\tan^2\frac{\phi}{2}\,v_1 v.$$

Thus in order to allow for the net to be s-isothermic with touching spheres one needs

$$\frac{\|p_1 - p\|^2}{v v_1} = const. \tag{17}$$

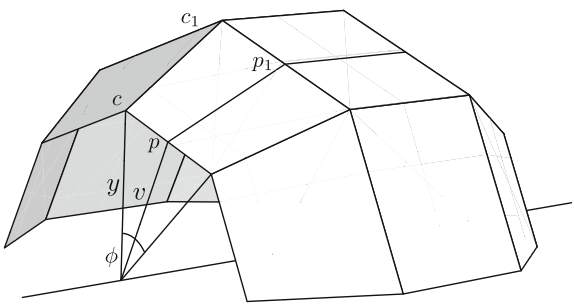

Fig. 5 Rotationally symmetric nets

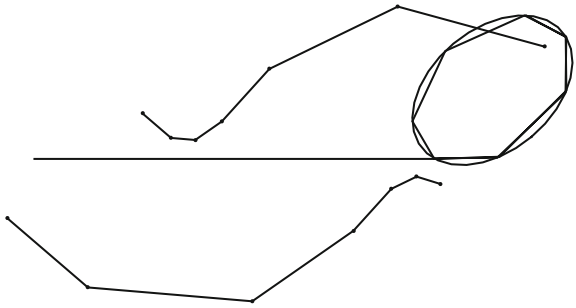

Fig. 6 Unrolling the billiard in an ellipse: consecutively place the edges of the billiard on the axis and mark the position of one of the foci. The second polygon is generated by the other focus and mirroring on the axis

This holds true in particular for a polygon p that arises when unrolling the billiard in an ellipse.

The construction is as follows [11] (see also [5]): Starting with a polygon given by a billiard in an ellipse, unroll it by placing each edge on the axis consecutively and marking the location of one of its foci in this process. This gives rise to a new polygon p (see Fig. 6). The same can be done with the other focus and after mirroring that second polygon along the axis the two polygons p and p^* are known to give rise to a pair of discrete cmc nets in the discrete isothermic sense. In particular pairs of edges p_1p and $p_1^*p^*$ form trapezoids (see Fig. 7) with constant distances and diagonals $\|p^* - p\| = d = \|p_1^* - p_1\|$ and $\|p^* - p_1\| = l = \|p_1^* - p\|$. Corresponding quadrilaterals from the two nets are dual to each other.

To see that this polygon satisfies Eq. (17) one needs to know that $\tan\alpha \tan\beta$, with the angles α, β in Fig. 7, is an integral of motion for the billiard in an ellipse, i.e.

$$\tan\frac{\alpha}{2}\tan\frac{\beta}{2} = \tan\frac{\alpha_1}{2}\tan\frac{\beta_1}{2}. \tag{18}$$

We have

$$\begin{aligned} \gamma &= \pi - \alpha - \beta, \\ \|p_1 - p\| &= 2\|p - o\| \sin\tfrac{\gamma}{2}, \\ v &= \|p - o\| \sin\alpha, \\ v_1 &= \|p - o\| \sin\beta. \end{aligned}$$

This implies

$$\frac{\|p_1 - p\|^2}{v_1 v} = \cot\frac{\alpha}{2}\cot\frac{\beta}{2} + \tan\frac{\alpha}{2}\tan\frac{\beta}{2} - 2 = \text{const}.$$

Summarizing, the billiard in an ellipse gives rise to a pair of polygons p and p^* that generate a discrete isothermic cmc surface of revolution and its dual. The same polygons $p = (x, v)$, $p^* = (x^*, v^*)$ can be read as midpoint connectors in two rotational symmetric s-isothermic nets that are generated by polygons c, c^* where

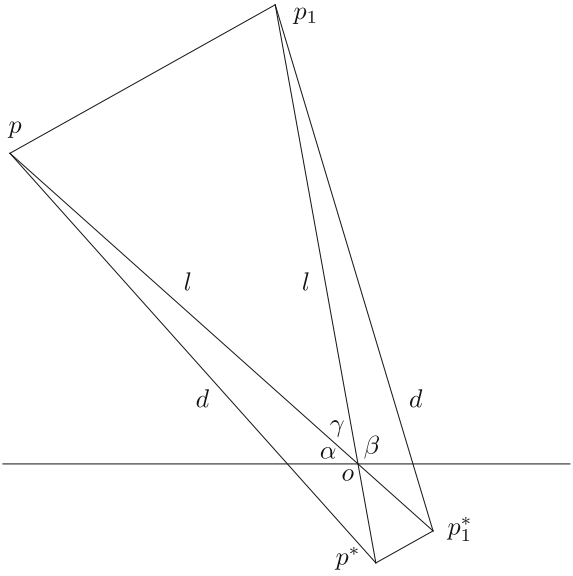

Fig. 7 The polygons from unrolling an ellipse

$$c = (x, y) = (x, \frac{v}{\cos\frac{\phi}{2}}), \quad c^* = (x^*, y^*) = (x^*, \frac{v*}{\cos\frac{\phi}{2}}).$$

Note that the corresponding scaling $(x, y) \mapsto (x, y/\cos\frac{\phi}{2})$ is an affine mapping and thus preserves parallelity. Due to Proposition 4.2 the Christoffel duality can be formulated in terms of parallel edges and diagonals, therefore dual quadrilaterals stay dual after such scaling. So, the two resulting s-isothermic nets c and c^* are dual to each other as well.

Recall that the s-isothermic nets of type 1 have an orthogonal circle for each quadrilateral of spheres and in the case of touching spheres the circle passes through the touching points. For the s-isothermic nets c and c^* one can think of the edges $p_1 p$ as diameters in the inscribed circles and we will denote the touching points along the edges $c_1 c$ with $\tilde{p}$ (see Fig. 8).

Since p, p_1, p_1^*, and p^* form a symmetric trapezoid, the circles for the quadrilaterals (c, c_1, c_{12}, c_2) and its dual $(c^*, c_1^*, c_{12}^*, c_2^*)$ are co-axial. Moreover, since the lines $(c_1 c)$ and $(c_1^* c^*)$ are parallel and tangent (in $\tilde{p}$ and $\tilde{p}^*$) to co-axial circles, their distance is $\|\tilde{p} - \tilde{p}^*\| = l$. Likewise $(c_2 c)$ and $(c_2^* c^*)$ are parallel and touch the circles in p and p^* thus their distance is $\|p^* - p\| = d$. Together we see that the two dual s-isothermic nets are in constant edge distance (but with two different distances for the two lattice directions). This is a way to define s-isothermic cmc nets (see [12]).

Now define a third pair of polygons

$$q = (x, u) = (x, \frac{y}{\cos\frac{\phi}{2}}) = (x, \frac{v}{\cos^2\frac{\phi}{2}}), \quad q^* = (x, u^*) = (x, \frac{y^*}{\cos\frac{\phi}{2}}) = (x, \frac{v^*}{\cos^2\frac{\phi}{2}}).$$

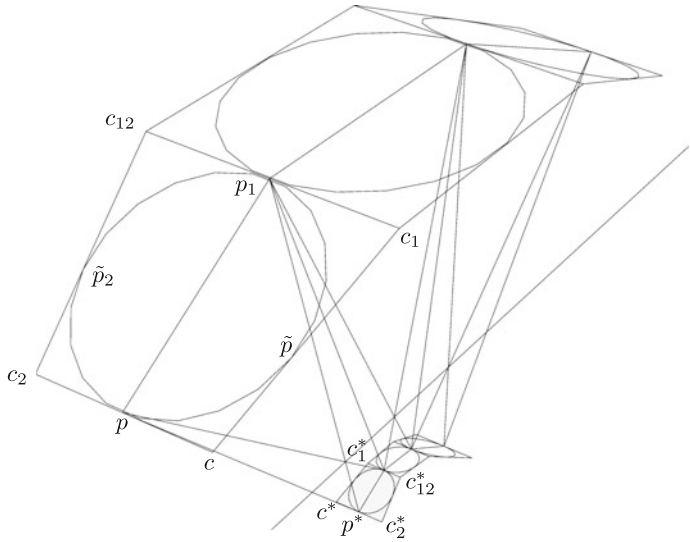

Fig. 8 The net c and its dual c^* with the inscribed circles

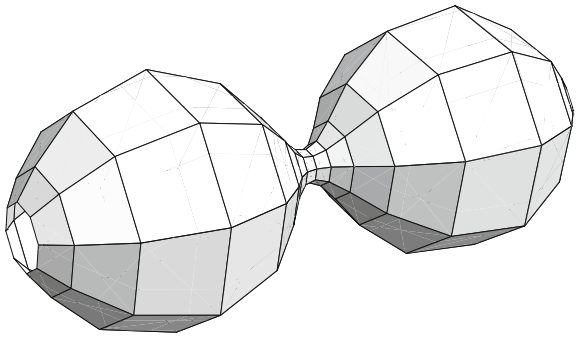

Fig. 9 An s-conical Delaunay net

Rotating these polygons one gets nets for which one can think of c and c^* as the polygons of midpoint connectors. The resulting faces for q and q^* thus will have constant face offset. Moreover they will be dual by the same argument as above.

The sphere s centered at c contains $\tilde{p}$. Since (cq) and $(c\tilde{p})$ are orthogonal a sphere t centered at q that meets $\tilde{p}$ also contains $\tilde{p}_{\bar{1}}$. By symmetry the quadrilaterals formed by the $\tilde{p}$ are circular. Finally one finds that the points $\tilde{p}$ are the diagonal intersection points of the quadrilaterals of the net q. One can see this for example by noting that the radii for the s-isothermic spheres are $r = v \tan \frac{\phi}{2}$, so $\|\tilde{p} - c\| = r$ and half an edge in rotational direction is $g = \|c - q\| = y \tan \frac{\phi}{2}$. Thus $\frac{g}{r} = \frac{y}{v}$ which is constant by construction.

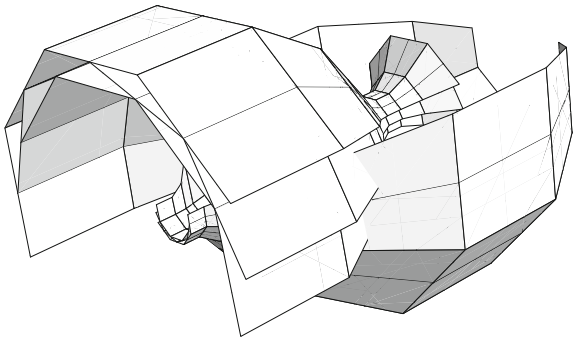

Fig. 10 Nested circular, s-isothermic, and s-conical Delaunay nets

We see that the third net formed by q is in fact an s-conical net with the dual net q^* in constant face offset equal the distance between the corresponding diagonal intersection points. Due to Theorem 8.3 this an s-conical cmc net. Figure 9 shows an example of such an s-conical Delaunay net. It is worth mentioning that the three types of discrete Delaunay nets (discrete isothermic, s-isothermic in the touching case, and s-conical) can be arranged in such a way that the second touches the first and the third touches the second as shown in Fig. 10. This is a direct consequence of the construction.

Acknowledgments This research was supported by the DFG Collaborative Research Center, TRR 109 "Discretization in Geometry and Dynamics".

References

1. Bobenko, A., Hoffmann, T., Springborn, B.: Minimal surfaces from circle patterns: geometry from combinatorics. Ann. Math. **164**(1), 231–264 (2006)
2. Bobenko, A.I., Hoffmann, T., König, B., Sechelmann, S.: S–conical minimal surfaces. Towards a unified theory of discrete minimal surfaces. (2015). Preprint
3. Bobenko, A.I., Matthes, D., Suris, Y.B.: Discrete and smooth orthogonal systems: C^∞-approximation. Int. Math. Res. Not. **2003**(45), 2415–2459 (2003)
4. Bobenko, A.I., Pinkall, U.: Discretization of surfaces and integrable systems. In: Bobenko, A.I., Seiler, R. (eds.) Discrete Integrable Geometry and Physics, pp. 3–58. Oxford University Press, New York (1999)

5. Bobenko, A.I., Pottmann, H., Wallner, J.: A curvature theory for discrete surfaces based on mesh parallelity. Math. Ann. **348**, 1–24 (2010)
6. Bobenko, A.I., Suris, Y.B.: Discrete differential geometry. Integrable structure. Graduate Studies in Mathematics, vol. 98. American Mathematical Society, Providence (2008)
7. Bobenko, A.I., Suris, Y.B.: Discrete Koenigs nets and discrete isothermic surfaces. Int. Math. Res. Not. **2009**(11), 1976–2012 (2009)
8. Burstall, F., Hertrich-Jeromin, U., Rossman, W., Santos, S.: Discrete special isothermic surfaces. Geom. Dedicata **174**, 1–11 (2015)
9. Grosse-Brauckmann, K., Polthier, K.: Numerical examples of compact surfaces of constant mean curvature. In: Elliptic and Parabolic Methods in Geometry, pp. 23–46. A K Peters, Wellesley (1996)
10. Hertrich-Jeromin, U., Hoffmann, T., Pinkall, U.: A discrete version of the Darboux transformation for isothermic surfaces. In: Bobenko, A., Seiler, R. (eds.) Discrete Integrable Geometry and Physics, pp. 59–81. Oxford University Press (1999)
11. Hoffmann, T.: Discrete rotational cmc surfaces and the elliptic billiard. In: Hege, H.C., Polthier, K. (eds.) Mathematical Visualisation, pp. 117–124. Springer (1998)
12. Hoffmann, T.: A Darboux transformation for discrete s-isothermic surfaces. J. Math-For-Industry (2010)
13. Liu, Y., Pottmann, H., Wallner, J., Wang, W., Yang, Y.: Geometric modeling with conical meshes and developable surfaces. ACM Trans. Graphics **25**(3), 681–689 (2006)
14. Müller, C.: On discrete constant mean curvature surfaces. Discrete Comput. Geom. **51**(3), 516–538 (2014)
15. Müller, C.: Semi-discrete constant mean curvature surfaces. Math. Z. **279**(1–2), 459–478 (2015)
16. Pan, H., Choi, Y.K., Liu, Y., Hu, W., Du, Q., Polthier, K., Zhang, C., Wang, W.: Robust modeling of constant mean curvature surfaces. ACM Trans. Graphics **31**(4), Article No. 85 (2012)
17. Pottmann, H., Wallner, J.: The focal geometry of circular and conical meshes. Adv. Comput. Math. **29**(3), 249–268 (2008)
18. Schief, W.K.: On the unification of classical and novel integrable surfaces. II. Difference geometry. R. Soc. Lond. Proc. Ser. A Math. Phys. Eng. Sci. **459**, 373–391 (2003)
19. Schief, W.K.: On a maximum principle for minimal surfaces and their integrable discrete counterparts. J. Geom. Phys. **56**(9), 1484–1495 (2006)
20. Wang, W., Wallner, J., Y., L.: An angle criterion for conical mesh vertices. J. Geom. Graphics **11**(2), 199–208 (2007)

Constructing Solutions to the Björling Problem for Isothermic Surfaces by Structure Preserving Discretization

Ulrike Bücking and Daniel Matthes

Abstract In this article, we study an analog of the Björling problem for isothermic surfaces (that are a generalization of minimal surfaces): given a regular curve γ in $\mathbb{R}^3$ and a unit normal vector field n along γ, find an isothermic surface that contains γ, is normal to n there, and is such that the tangent vector γ' bisects the principal directions of curvature. First, we prove that this problem is uniquely solvable locally around each point of γ, provided that γ and n are real analytic. The main result is that the solution can be obtained by constructing a family of discrete isothermic surfaces (in the sense of Bobenko and Pinkall) from data that is read off from γ, and then passing to the limit of vanishing mesh size. The proof relies on a rephrasing of the Gauss-Codazzi-system as analytic Cauchy problem and an in-depth-analysis of its discretization which is induced from the geometry of discrete isothermic surfaces. The discrete-to-continuous limit is carried out for the Christoffel and the Darboux transformations as well.

1 Introduction

Isothermic surfaces are among the most classical objects in differential geometry: these are surfaces that admit a conformal parametrization along curvature lines, see Definition 1. Like various particular geometries—special coordinate systems, minimal surfaces, surfaces of constant curvature—they have been introduced and intensively studied in the second half of the 19th century [9, 24]. Also, like the many of these classical objects, they have been "rediscovered" in the 1990s, both in connection with integrable systems and in the context of discrete differential

U. Bücking
Inst. für Mathematik, Technische Universität Berlin,
Straße des 17. Juni 136, 10623 Berlin, Germany
e-mail: buecking@math.tu-berlin.de

D. Matthes (✉)
Zentrum Mathematik – M8, Technische Universität München,
Boltzmannstr. 3, D-85747 Garching bei München, Germany
e-mail: matthes@ma.tum.de

A.I. Bobenko (ed.), *Advances in Discrete Differential Geometry*,
DOI 10.1007/978-3-662-50447-5_10

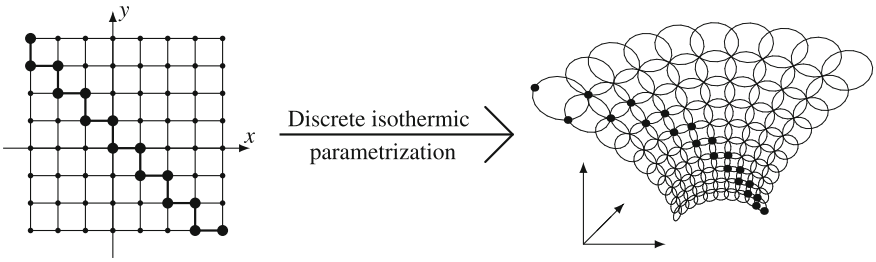

Fig. 1 Initial zig-zag on a discrete isothermic surface

geometry. The first description of isothermic surfaces as soliton surfaces is found in [11]. The first definition for discrete isothermic surfaces was made shortly after in [3]. In the most simple case, these are immersions of $\mathbb{Z}^2$ into $\mathbb{R}^3$ such that the vertices of each elementary quadrilateral are conformally equivalent to the corners of a planar square, see Definition 3.

This discrete surface class, its transformations and invariances has been studied e.g. in [7, 8, 20]. A systematic presentation of the theory of isothermic surfaces in the context of Möbius geometry can be found in [15]. Finally, we refer to [4] for a detailed overview on discrete isothermic surfaces as part of discrete differential geometry, including historical remarks.

Despite the manifold results on (classical) isothermic surfaces and the related equations, the fundamental question about their construction from suitably chosen data has apparently been left open. On the one hand, the machinery of integrable systems enables one to construct a rich variety of "solitonic" isothermic surfaces [11]. But on the other hand, nothing seems to be known about the well-posedness of an initial or boundary value problem for the Gauss-Codazzi-equations in general. The latter form a PDE system (cf. Eq. (5)) which contains both elliptic and hyperbolic equations.[1] The appearance of an elliptic equation suggests that data for the surface boundary should be prescribed, as it is done for minimal surfaces for example. The hyperbolic equations, on the other hand, suggest to provide data for two curvature lines instead, like in the case of level surfaces in triply orthogonal systems [1]. Neither of the two approaches seems promising for the coupled system.

In contrast, there is a canonical way to pose an initial value problem for a *discrete* isothermic surface. One prescribes the vertices in $\mathbb{R}^3$ for a "zig-zag"-curve in parameter space as indicated in Fig. 1. For vertices in general position, these data can be extended to a discrete isothermic surface in a unique way. In fact, all vertices on the discrete surface are easily obtained inductively from the prescribed data.

In this paper, we formulate and prove solvability of a Björling problem *for real analytic isothermic surfaces. And we prove that the solution can be obtained as the continuous limit of discrete isothermic surfaces.*

[1] The system of Gauss-Codazzi-equations can be simplified to Calapso's equation [8], which is a single scalar fourth order PDE, but unfortunately of indefinite type.

The classical Björling problem is to find a minimal surface that touches a given curve in $\mathbb{R}^3$ along prescribed tangent planes. This problem has been solved in general, see [13]. An extension of the Björling problem to surfaces of constant mean curvature has been posed (and solved) in [5]. A natural formulation of the Björling problem in the yet more general class of isothermic surfaces reads as follows.

Problem 1 *Given a regular curve γ in $\mathbb{R}^3$, and two mutually orthogonal unit vector fields v, w along γ, neither of which is tangent to γ at any point. Find an isothermic surface S containing γ such that v and w are the principal directions of curvature at each point of γ.*

We believe that this problem is solvable locally provided that γ, v and w are all real analytic. Indeed, the non-tangency of the vector fields allows to give a reformulation in terms of a non-characteristic Cauchy problem. However, we do not address the Björling problem in this full generality here, but stick to the following restricted setting, where we do not prescribe two tangent vector fields v and w individually, but only a two-dimensional tangent plane:

Problem 2 *Given a regular curve γ in $\mathbb{R}^3$, and a unit vector field n that is orthogonal to the tangent vectors γ' at each point. Find an isothermic surface S containing γ such that at each point of γ, the vector n is normal to S, and each of the two directions of principal curvature encloses an angle $\pi/4$ with γ'.*

As a corollary of the results presented here, it follows that this problem is uniquely solvable for real analytic γ and n, at least locally around each point of γ. Existence and uniqueness of a real analytic isothermic surface S for given data is the minor result of this paper, see Theorem 1. The main result is that the real analytic data can be "sampled" with a mesh width $\epsilon > 0$ in a suitable way such that the discrete isothermic surfaces S^ϵ constructed from the discrete data converge in C^1 to S. The precise formulation is given in Theorem 2.

It is remarkable that naive numerical experiments suggest that such an approximation result might *not* be true. It was already noted in [3] that discrete isothermic surfaces depend very sensitively on their initial data. The limit $\epsilon \to 0$ is delicate, and inappropriate choices of the initial zig-zag cause the sequence S^ϵ to diverge rapidly. In fact, even the possibility to construct *any* sequence of discrete isothermic surfaces that approximates a given smooth one is not obvious. Discrete isothermic surfaces are one of many examples of a discretized geometric structure for which the passage back to the original continuous structure needs a highly non-trivial approximation result, the proof of which is analysis-based and goes far beyond elementary geometric considerations. Further such non-trivial convergence results are available, for instance, for discrete surfaces of constant negative Gaussian curvature [2], for discrete triply orthogonal systems [1], and, most importantly, for circle patterns [6, 21, 22] as approximations to conformal maps.

The core of our convergence proof is a stability analysis of the *discrete Gauss-Codazzi system* that we derive for discrete isothermic surfaces. We show that the solution to the discrete Gauss-Codazzi equations with sampled data as initial condition remains close to the solution of the classical Gauss-Codazzi system for the same

(continuous) initial data. In a second step, this implies proximity of the respective discrete and continuous surfaces. We are able to quantify the approximation error in terms of the supremum-distance between analytic functions on complex domains: it is linear in the mesh size. In fact, we conjecture that this result is sub-optimal, and second-order approximation should be provable, using a more refined analysis and a more careful approximation of the data.

The techniques used in the proof are similar to those employed by one of the authors [17] to prove convergence of circle patterns to conformal maps. The geometric situation for isothermic surfaces, however, is much more complicated, and the structure of the Gauss-Codazzi system is much more complex than the Cauchy-Riemann equations. The proof of stability relies on estimates for the solution of analytic Cauchy problems in scales of Banach spaces. These estimates have been developed—in the classical, non-discretized setting—in Nagumo's famous article [18] as part of the existence proof for analytic Cauchy problems. Here, we shall rather use Nirenberg's [19] version of these estimates. For an overview over the history of analytic Cauchy problems and the related estimates, see the beautiful article of Walter [23].

Note that the convergence proof here is more direct than the one in [17]. While the latter was based on purely discrete considerations, the current proof uses semi-discrete techniques: a–somewhat artificial–extension of the discrete functions to continuous domains allows to formulate estimates more easily. The main simplification, however, is that we separate the proofs for existence of a classical solution and its approximation by discrete solutions.

The paper is organized as follows. In Sect. 2 we formulate the Gauss-Codazzi-system for smooth isothermic surfaces in the framework of analytic Cauchy problems and prove unique local solvability of the Björling problem by the Cauchy-Kowalevskaya theorem. In Sect. 3 we derive an analogous system of difference equations for discrete isothermic surfaces. For appropriate initial conditions, the convergence of the discrete solutions to the corresponding smooth ones is proven in Sect. 4. Then, in Sect. 5 we explain how to discretize the Björling initial data appropriately, and prove convergence of the discrete surfaces to the respective smooth one. Finally, in Sect. 6, the convergence result is extended to Christoffel and Darboux transformations.

2 Smooth Isothermic Surfaces

We start by summarizing basic properties of smooth isothermic surfaces and proving our first result on the local solvability of the Björling problem.

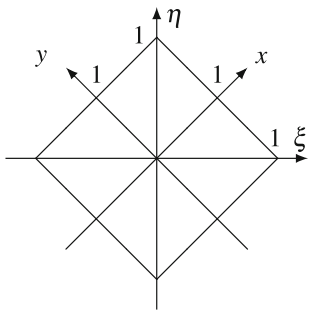

Fig. 2 Relation between the coordinates (x, y) and (ξ, η)

2.1 Coordinates and Domains

For concise statements and proofs, we need to work with two different coordinate systems (ξ, η) and (x, y) on $\mathbb{R}^2$ simultaneously. These coordinates are related to each other by

$$\xi = \frac{x - y}{2}, \quad \eta = \frac{x + y}{2} \quad \Leftrightarrow \quad x = \eta + \xi, \quad y = \eta - \xi, \tag{1}$$

see Fig. 2. Accordingly, the partial derivatives transform as follows:

$$\partial_\xi = \partial_x - \partial_y, \quad \partial_\eta = \partial_x + \partial_y.$$

Observe in particular that

$$\partial_\xi^2 + \partial_\eta^2 = 2(\partial_x^2 + \partial_y^2). \tag{2}$$

It will be convenient to consider (ξ, η) as the "basic" coordinates and (x, y) as the auxiliary ones. More precisely: in the rare cases that we need to specify explicitly the arguments of a function $g : \Omega \to \mathbb{R}$ defined on a domain $\Omega \subset \mathbb{R}^2$, then we shall write $g(\xi, \eta)$ for the value of g at the point with coordinates $x = \eta + \xi$ and $y = \eta - \xi$.

For further reference, define for $r \geq h > 0$ the domains

$$\Omega(r|h) = \big\{(\xi, \eta) \in \mathbb{R}^2 \,;\; |\xi| + |\eta| \leq r,\; -h < \eta \leq h\big\}.$$

In the (x, y)-coordinates, $\Omega(r|h)$ is a axes-parallel square of side length $2r$, centered at the origin, that is cut off at the top-right and bottom-left corners.

2.2 Definition and Equations

By abuse of notation, we use the term "(parametrized) surface" for a smooth and non-degenerate map $F : \Omega(r|h) \to \mathbb{R}^3$. Here non-degeneracy means that the vector

fields F_x and F_y are linearly independent. Every such surface comes with a smooth normal map $N : \Omega(r|h) \to \mathbb{S}^2$, given by

$$N = \frac{F_x \times F_y}{\|F_x \times F_y\|}.$$

Definition 1 $F : \Omega(r|h) \to \mathbb{R}^3$ is a (parametrized) *isothermic surface*, if

(1) F is conformal, i.e., there exists a conformal factor $u : \Omega(r|h) \to \mathbb{R}$ such that

$$\|F_x\|^2 = \|F_y\|^2 = e^{2u}, \quad \langle F_x, F_y \rangle = 0, \tag{3}$$

(2) F parametrizes along curvature lines, i.e., the normal map $N : \Omega(r|h) \to \mathbb{S}^2$ satisfies

$$\langle F_{xy}, N \rangle = 0. \tag{4}$$

The quantities $\mathfrak{k}, \mathfrak{l} : \Omega(r|h) \to \mathbb{R}$ in

$$-\langle N_x, F_x \rangle = e^u \mathfrak{k}, \quad -\langle N_y, F_y \rangle = e^u \mathfrak{l},$$

are the (scaled) principal curvatures.

Remark 1 The genuine principal curvature functions are given by $e^{-u}\mathfrak{k}$ and $e^{-u}\mathfrak{l}$. The quantities $\mathfrak{k}$ and $\mathfrak{l}$ are better suited for the calculations below.

The next result is classical.

Lemma 1 *Assume that an isothermic surface $F : \Omega(r|h) \to \mathbb{R}^3$ is given. Then the conformal factor u and the scaled curvatures $\mathfrak{k}, \mathfrak{l}$ satisfy the Gauss-Codazzi equations*

$$-(u_{xx} + u_{yy}) = \mathfrak{k}\mathfrak{l}, \quad \mathfrak{l}_x = \mathfrak{k} u_x, \quad \mathfrak{k}_y = \mathfrak{l} u_y. \tag{5}$$

Conversely, if functions $u, \mathfrak{k}, \mathfrak{l} : \Omega(r|h) \to \mathbb{R}$ satisfy the system (5), then there exists an isothermic surface $F : \Omega(r|h) \to \mathbb{R}$ that has u as its conformal factor and has scaled curvatures $\mathfrak{k}, \mathfrak{l}$. Moreover, F is uniquely determined up to Euclidean motions.

We briefly recall the proof, since we shall need some of the calculations later.

Proof (Sketch) For a given isothermic surface $F : \Omega(r|h) \to \mathbb{R}^3$, introduce the adapted frame

$$\Psi := \left(e^{-u} F_x, e^{-u} F_y, N\right) : \Omega(r|h) \to \mathrm{SO}(3)$$

and define the transition matrices $U, V : \Omega(r|h) \to \mathrm{so}(3)$ implicitly by

$$\Psi_x = \Psi U, \quad \Psi_y = \Psi V. \tag{6}$$

Using the defining properties of the isothermic parametrization, one easily obtains the following explicit expressions for U and V:

$$U = \begin{pmatrix} 0 & u_y & -\mathfrak{k} \\ -u_y & 0 & 0 \\ \mathfrak{k} & 0 & 0 \end{pmatrix}, \quad V = \begin{pmatrix} 0 & -u_x & 0 \\ u_x & 0 & -\mathfrak{l} \\ 0 & \mathfrak{l} & 0 \end{pmatrix} \tag{7}$$

The compatibility condition $U_y - V_x = UV - VU$ implies the equations in (5).

Conversely, if $u, \mathfrak{k}, \mathfrak{l}$ satisfy (5), then the matrix functions $U, V : \Omega(r|h) \to \mathrm{so}(3)$ defined by (7) satisfy compatibility condition $U_y - V_x = UV - VU$. Consequently, one can define a further matrix function $\Psi = (\Psi_1, \Psi_2, \Psi_3) : \Omega(r|h) \to \mathrm{SO}(3)$ as solution to the system (6). Clearly, the solution Ψ is uniquely determined by its value $\Psi(0) \in \mathrm{SO}(3)$ at $(x, y) = 0$. The particular form of U and V imply that

$$\partial_x(e^u \Psi_2) = \partial_y(e^u \Psi_1),$$

which further implies the existence of a map $F : \Omega(r) \to \mathbb{R}^3$ such that

$$\partial_x F = e^u \Psi_1 \quad \text{and} \quad \partial_y F = e^u \Psi_2. \tag{8}$$

The map F is non-degenerate, and it is uniquely determined by its value $F(0) \in \mathbb{R}^3$ at $(x, y) = 0$. Clearly Ψ is an adapted frame for the surface defined by F, whose normal vector field is given by Ψ_3. It follows directly from (8) that F is conformal (3). The property (4) is a further direct consequence of (6) and the special form of U and V from (7). □

A different form of the Gauss-Codazzi equations (5) is needed in the following. Remind the relation between the coordinates (x, y) and (ξ, η) by $x = \eta + \xi$ and $y = \eta - \xi$ in Sect. 2.1. Introduce auxiliary functions $v, w : \Omega(r|h) \to \mathbb{R}$ by

$$v = \frac{1}{2} u_\xi, \quad w = \frac{1}{2} u_\eta.$$

Further recall (2). Then the Gauss-Codazzi system (5) attains the form

$$v_\eta = w_\xi, \tag{9}$$

$$w_\eta = -v_\xi - \mathfrak{k}\mathfrak{l}, \tag{10}$$

$$\mathfrak{k}_y = \mathfrak{l}(w - v), \tag{11}$$

$$\mathfrak{l}_x = \mathfrak{k}(w + v). \tag{12}$$

2.3 Local Solution of the Björling Problem

The following result implies local solvability of (the restricted version of) the Björling problem for isothermic surfaces, with real analytic data. To see the equivalence to Problem 2 stated in the introduction, observe that the conformal parametrization F of an isothermic surface and our coordinates in (1) are such that the images of $\{x = \text{const}\}$ and of $\{y = \text{const}\}$ are mapped to curvature lines under F, whereas the tangent to each curve $\xi \mapsto F(\xi, \eta)$ is always at an angle of $\pi/4$ to both curvature directions.

Theorem 1 *Let an analytic and regular curve $f : (-r, r) \to \mathbb{R}^3$ and an analytic normal unit vector field $n : (-r, r) \to \mathbb{S}^2$ be given, that is $\langle f', n\rangle \equiv 0$. Then, for some $h > 0$ with $h \le r$, there exists a unique analytic isothermic surface $F : \Omega(r|h) \to \mathbb{R}^3$ such that F and its normal vector field N satisfy*

$$F(\xi, 0) = f(\xi), \quad N(\xi, 0) = n(\xi) \quad \text{for all } \xi \in (-r, r). \tag{13}$$

Remark 2 The original Björling problem consists in finding a minimal surface in $\mathbb{R}^3$ that touches a given curve along prescribed tangent planes. See [5] for an extension to constant mean curvature surfaces. Our problem is a bit different since (13) implies in addition that the tangential vector to the data curve is everywhere at angle $\pi/4$ with the directions of principal curvature, see (14). Such additional restrictions are expected to guarantee unique solvability of the Björling problem in the much larger class of isothermic surfaces.

Proof (of Theorem 1) If there exists an isothermic surface $F : \Omega(r|h) \to \mathbb{R}^3$ with the properties (13), then

$$f'(\xi) = F_\xi(\xi, 0) = F_x(\xi, 0) - F_y(\xi, 0) \tag{14}$$

at every $\xi \in (-r, r)$, and in particular

$$\|f'(\xi)\|^2 = \|F_x(\xi, 0)\|^2 + \|F_y(\xi, 0)\|^2 - \langle F_x(\xi, 0), F_y(\xi, 0)\rangle = 2e^{2u(\xi,0)}.$$

It follows that f and n determine both the conformal factor u and the adapted frame $\Psi = (e^{-u}F_x, e^{-u}F_y, N) : \Omega(r|h) \to \mathrm{SO}(3)$ uniquely on $\eta = 0$; denote the corresponding functions by $u^0 : (-r, r) \to \mathbb{R}$ and $\Psi^0 : (-r, r) \to \mathrm{SO}(3)$, respectively.

Next, introduce functions $v^0, w^0, \mathfrak{k}^0, \mathfrak{l}^0 : (-r, r) \to \mathbb{R}$ by

$$(u^0)' = 2v^0u^0, \qquad (\Psi^0)' = \Psi^0 \begin{pmatrix} 0 & 2w^0 & -\mathfrak{k}^0 \\ -2w^0 & 0 & \mathfrak{l}^0 \\ \mathfrak{k}^0 & -\mathfrak{l}^0 & 0 \end{pmatrix}. \tag{15}$$

The line $\{\eta = 0\} = \{x + y = 0\}$ is obviously non-characteristic for the system of equations (9)–(12). Hence, the Cauchy-Kowalevskaya theorem applies in this situation. For some sufficiently small $h > 0$, there exists a unique analytic solution

$v, w, \mathfrak{k}, \mathfrak{l} : \Omega(r|h) \to \mathbb{R}$ to (9)–(12) with the initial conditions $v^0, w^0, \mathfrak{k}^0, \mathfrak{l}^0$ at $\eta = 0$. Since (9) is a compatibility condition for the linear system

$$u_\xi = 2v, \quad u_\eta = 2w,$$

there exists a unique analytic solution $u : \Omega(r|h) \to \mathbb{R}$ with $u = u^0$ for $\eta = 0$. The triple $(u, \mathfrak{k}, \mathfrak{l})$ satisfies (5). Lemma 1 guarantees the existence of a unique isothermic surface $F : \Omega(r|h) \to \mathbb{R}^3$ with u as conformal factor, with scaled principle curvatures $\mathfrak{k}$ and $\mathfrak{l}$, and with the normalizations

$$F(0) = f(0), \ N(0) = n(0), \ F_x(0) - F_y(0) = f'(0). \tag{16}$$

Analyticity of F is clear from its construction in the proof. To see that F attains the initial data (13), first observe that an adapted frame Ψ necessarily satisfies $\Psi_\xi = \Psi_x - \Psi_y = \Psi(U - V)$, and so $\Psi = \Psi^0$ on $\eta = 0$, thanks to (7) and (15), (16). In particular, we have that $\Psi_3(\xi, 0) = N(\xi)$. And further, $F_\xi = \Psi_1 - \Psi_2 = \Psi_1^0 - \Psi_2^0$ implies $F = f$ on $\eta = 0$.

Concerning uniqueness: f and Ψ^0 determine the initial data $(v^0, w^0, \mathfrak{k}^0, \mathfrak{l}^0)$ for (9)–(12)—and hence also its solution $(v, w, \mathfrak{k}, \mathfrak{l})$—uniquely. Invoking again Lemma 1, it follows that F with the normalization (16) is unique as well. □

3 Discrete Isothermic Surfaces

Throughout this section, we assume that some (small) parameter $\epsilon > 0$ is given, which quantifies the average mesh width of the considered discrete isothermic surfaces. We introduce the abbreviation

$$z^* = \sqrt{1 - \epsilon^2 z^2} \tag{17}$$

for arbitrary quantities z, assuming that $|\epsilon z| < 1$.

3.1 Coordinates and Domains

Recall that we are working with the two coordinate systems from (1) simultaneously, (ξ, η) being the "basic" coordinates and (x, y) being the "auxiliary" ones. Introduce the associated shift-operators $\tau_x, \tau_y, \tau_\xi, \tau_\eta$ by

$$\tau_x(\xi, \eta) = (\xi + \frac{\epsilon}{4}, \eta + \frac{\epsilon}{4}), \qquad \tau_\xi(\xi, \eta) = (\xi + \frac{\epsilon}{2}, \eta)$$
$$\tau_y(\xi, \eta) = (\xi - \frac{\epsilon}{4}, \eta + \frac{\epsilon}{4}), \qquad \tau_\eta(\xi, \eta) = (\xi, \eta + \frac{\epsilon}{2}).$$

By slight abuse of notation, we shall use the same symbols for the associated contravariant shifts of functions $f : \Omega(r|h) \to \mathbb{R}$, i.e., $\tau_x f := f \circ \tau_x$ etc. The associated central difference quotient operators are defined by

$$\delta_x f = \frac{1}{\epsilon}(\tau_x f - \tau_x^{-1} f), \qquad \delta_\xi f = \frac{1}{\epsilon}(\tau_\xi f - \tau_\xi^{-1} f)$$
$$\delta_y f = \frac{1}{\epsilon}(\tau_y f - \tau_y^{-1} f), \qquad \delta_\eta f = \frac{1}{\epsilon}(\tau_\eta f - \tau_\eta^{-1} f).$$

It is a notorious inconvenience in discrete differential geometry that the various quantities which are derived from discrete geometric objects are associated to different natural domains of definition. To account for that, we need to single out specific subdomains inside our basic domain $\Omega(r|h)$: let

$$\Omega^{[x]_\epsilon}(r|h) = \Omega(r|h) \cap \tau_x \Omega(r|h) \cap \tau_x^{-1} \Omega(r|h),$$

be the natural domain of definition for $\delta_x f$, when f is defined on $\Omega(r|h)$. Likewise, we define $\Omega^{[y]_\epsilon}(r|h)$. The domain

$$\Omega^{[xy]_\epsilon}(r|h) = \Omega(r - \frac{\epsilon}{2}|h - \frac{\epsilon}{2})$$

is such that the mixed difference quotient $\delta_x \delta_y f$ is well-defined there; notice that $\delta_\xi f$ and $\delta_\eta f$ are well-defined on $\Omega^{[xy]_\epsilon}(r|h)$. In the same spirit, we introduce $\Omega^{[xxy]_\epsilon}(r|h)$ as domain for $\delta_x^2 \delta_y f$ etc. For each point $\zeta \in \Omega^{[xy]_\epsilon}(r|h)$, we say that the four points $\tau_\xi \zeta$, $\tau_\eta \zeta$, $\tau_\xi^{-1} \zeta$ and $\tau_\eta^{-1} \zeta$ form an *elementary ϵ-square*.

3.2 Definition of Discrete Isothermic Surfaces

In this section, we give a variant of the definition for discrete isothermic surfaces from [3], which is well-suited for the passage to the continuum limit. First, we need auxiliary notation.

Definition 2 Four points $p_1, \ldots, p_4 \in \mathbb{R}^3$ form a *(non-degenerate) conformal square* iff they lie on a circle, but no three of them are on a line, they are cyclically ordered,[2] and their mutual distances are related by

$$\|p_1 - p_2\| \cdot \|p_3 - p_4\| = \|p_1 - p_4\| \cdot \|p_2 - p_3\|. \tag{18}$$

Remark 3 The name refers to the fact that $p_1, \ldots, p_4$ form a (non-degenerate) conformal square if and only if there is a Möbius transformation of $\mathbb{R}^3$ which takes these points to the corners of the unit square, $(0, 0, 0)$, $(1, 0, 0)$, $(1, 1, 0)$ and $(0, 1, 0)$,

[2]Cyclic ordering means that walking around the circle either clockwise or anti-clockwise, one passes p_1, p_2, p_3 and p_4 in that order, see Fig. 3 *(left)*.

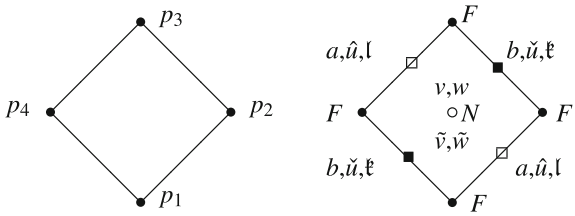

Fig. 3 Conformal squares and the association of quantities to lattice points

respectively. Notice that the non-degeneracy condition is important for the equivalence, since certain point configurations on a straight line can be Möbius transformed into the unit square as well.

Alternatively, one could define conformal squares by saying that p_1 to p_4 have cross-ratio equal to minus one, either in the sense of quaternions, see for example [15], or after identification of these points with complex numbers in their common plane. Again, non-degeneracy is important for equivalence of the definitions.

The following is an easy exercise in elementary geometry.

Lemma 2 *For any given three points $p_1, p_2, p_3 \in \mathbb{R}^3$ (with ordering) that are not collinear (and in particular pairwise distinct), there exists precisely one fourth point $p_4 \in \mathbb{R}^3$ that completes the conformal square. Moreover, the coordinates of p_4 depend analytically on those of p_1, p_2 and p_3.*

We are now going to state the main definition, namely the one for discrete isothermic surfaces. Originally [3], discrete surfaces have been introduced as particular immersed lattices in $\mathbb{R}^3$. Having the continuous limit in mind, we give a slightly different definition, which describes a continuous immersion in $\mathbb{R}^3$, corresponding to a two-parameter family of lattices.

Definition 3 A map $F^\epsilon : \Omega(r|h) \to \mathbb{R}^3$ is called (the parametrization of) a ϵ-*discrete isothermic surface*, if elementary ϵ-squares are mapped to conformal squares in $\mathbb{R}^3$.

Remark 4 Since no continuity is required for $F^\epsilon : \Omega(r|h) \to \mathbb{R}^3$, one can think of it—at this point—for instance as the piecewise constant extension of a map $\tilde{F}^\epsilon : \Lambda^\epsilon(r|h) \to \mathbb{R}^3$ that is only defined on a suitable lattice $\Lambda^\epsilon(r|h) \subset \Omega(r|h)$, e.g. on

$$\Lambda^\epsilon(r|h) = \left\{ (\xi, \eta) \in \Omega(r|h) \,;\, \frac{\xi}{\epsilon} + \frac{\eta}{\epsilon} \in \mathbb{Z} \right\}.$$

Alternatively, one can say that $F^\epsilon : \Omega(r|h) \to \mathbb{R}^3$ is a discrete isothermic surface, if and only if the four vectors

$$\tau_y \delta_x F^\epsilon,\ \tau_x \delta_y F^\epsilon,\ \tau_y^{-1} \delta_x F^\epsilon,\ \tau_x^{-1} \delta_y F^\epsilon$$

always lie in one common plane and satisfy

$$\left\|\tau_y \delta_x F^\epsilon\right\| \left\|\tau_y^{-1} \delta_x F^\epsilon\right\| = \left\|\tau_x \delta_y F^\epsilon\right\| \left\|\tau_x^{-1} \delta_y F^\epsilon\right\|. \tag{19}$$

Note that this identity is a discrete replacement for the relation $\|F_x\|^2 = \|F_y\|^2$ on smooth conformally parametrized surfaces.

3.3 The Discrete Björling Problem

We introduce the analog of the Björling problem for ϵ-discrete isothermic surfaces. In contrast to its continuous counterpart, its solution is immediate. First, we need some more notation to formulate conditions on the data.

Definition 4 A function $f^\epsilon : \Omega(r|h) \to \mathbb{R}^3$ is said to be *non-degenerate* if neither any of the point triples

$$\left(\tau_\xi^{-1} f^\epsilon, \tau_\eta^{-1} f^\epsilon, \tau_\xi f^\epsilon\right)(\xi, \eta),$$

nor any of the point triples

$$\left(\tau_\xi^{-1} f^\epsilon, \tau_\eta f^\epsilon, \tau_\xi f^\epsilon\right)(\xi', \eta')$$

are collinear, where $(\xi, \eta), (\xi', \eta') \in \Omega(r|h)$ are arbitrary points such that these respective values of f^ϵ are defined. If collinearities occur, then f^ϵ is called *degenerate*.

Definition 5 We call a function $f^\epsilon : \Omega(r|\frac{\epsilon}{2}) \to \mathbb{R}^3$ *Björling data* for the construction of an ϵ-discrete isothermic surface if it is non-degenerate.

Proposition 1 *Let $\bar{h}$ and $\epsilon > 0$ with $r > \bar{h} > \frac{\epsilon}{2}$ and Björling data f^ϵ be given. Then, there exists some maximal $h \in (\frac{\epsilon}{2}, \bar{h}]$ and a unique ϵ-discrete isothermic surface $F^\epsilon : \Omega(r|h) \to \mathbb{R}^3$ such that $F^\epsilon = f^\epsilon$ on $\Omega(r|\frac{\epsilon}{2})$. Here* maximal *has to be understood as follows: either $h = \bar{h}$, or the restriction of F^ϵ to $\Omega(r|h - \frac{\epsilon}{2})$ is degenerate.*

Proof The proof is a direct application of Lemma 2: from the data f^ϵ given on $\Omega(r|\frac{\epsilon}{2})$, one directly calculates the values of F^ϵ on $\Omega(r|\epsilon)$. These are then extended to $\Omega(r|3\frac{\epsilon}{2})$ in the next step, and so on. The procedure works as long as no degeneracies occur. □

3.4 Discrete Quantities and Basic Relations

Let some discrete isothermic surface $F^\epsilon : \Omega(r|h) \to \mathbb{R}^3$ be given. Below, we introduce quantities that play an analogous role for F^ϵ as u, $\mathfrak{k}$, $\mathfrak{l}$ etc. do for F. Figure 3 *(right)* indicates, on which lattices these respective quantities live.

Define the *discrete conformal factors* $\hat{u} : \Omega^{[x]\epsilon}(r|h) \to \mathbb{R}$ and $\check{u} : \Omega^{[y]\epsilon}(r|h) \to \mathbb{R}$, respectively, by

$$e^{\hat{u}} = \|\delta_x F^\epsilon\|, \quad e^{\check{u}} = \|\delta_y F^\epsilon\|.$$

Thanks to the property (19) of discrete isothermic surfaces, these seemingly different quantities are related to each other by the identity

$$\tau_x \check{u} + \tau_x^{-1} \check{u} = \tau_y \hat{u} + \tau_y^{-1} \hat{u}$$

that holds on $\Omega^{[xy]\epsilon}(r|h)$. We may thus unambiguously define the *discrete derivatives* $v, w : \Omega^{[xy]\epsilon}(r|h) \to \mathbb{R}$ of the conformal factor by

$$v = \frac{\tau_x \check{u} - \tau_y \hat{u}}{\epsilon} = \frac{\tau_y^{-1} \hat{u} - \tau_x^{-1} \check{u}}{\epsilon}, \quad w = \frac{\tau_x \check{u} - \tau_y^{-1} \hat{u}}{\epsilon} = \frac{\tau_y \hat{u} - \tau_x^{-1} \check{u}}{\epsilon}. \tag{20}$$

Next, define the *discrete unit tangent vectors* $a : \Omega^{[x]\epsilon}(r|h) \to \mathbb{S}^2$ and $b : \Omega^{[y]\epsilon}(r|h) \to \mathbb{S}^2$, respectively, by

$$a = e^{-\hat{u}} \delta_x F^\epsilon, \quad b = e^{-\check{u}} \delta_y F^\epsilon.$$

Since conformal squares are planar, there is a natural notion of *normal field* $N : \Omega^{[xy]\epsilon}(r|h) \to \mathbb{S}^2$, namely

$$N = \frac{\tau_y \delta_x F^\epsilon \times \tau_x \delta_y F^\epsilon}{\|\tau_y \delta_x F^\epsilon \times \tau_x \delta_y F^\epsilon\|}.$$

With the help of the discrete orthonormal frame (a, b, N), we introduce the *discrete scaled principal curvatures* $\mathfrak{k} : \Omega^{[xxy]\epsilon}(r|h) \to \mathbb{R}$ and $\mathfrak{l} : \Omega^{[xyy]\epsilon}(r|h) \to \mathbb{R}$, respectively, by

$$\epsilon\mathfrak{k} = -\langle \tau_x^{-1} N \times \tau_x N, b \rangle, \quad \epsilon\mathfrak{l} = \langle \tau_y^{-1} N \times \tau_y N, a \rangle. \tag{21}$$

Note that $\epsilon\mathfrak{k}$ and $\epsilon\mathfrak{l}$ are equal to $\sin \angle(\tau_x^{-1} N, \tau_x N)$ and to $\sin \angle(\tau_y^{-1} N, \tau_y N)$, respectively, with the signs chosen to maintain consistency with the continuous quantities.

Finally, to facilitate the calculations below, we need two more discrete functions $\tilde{v}, \tilde{w} : \Omega^{[xy]\epsilon}(r|h) \to \mathbb{R}$, given by

$$\begin{aligned}\epsilon\tilde{v} &= \frac{\langle T_y\delta_x F^\epsilon, T_x^{-1}\delta_y F^\epsilon\rangle}{\|T_y\delta_x F^\epsilon\|\|T_x^{-1}\delta_y F^\epsilon\|} = -\frac{\langle T_y^{-1}\delta_x F^\epsilon, T_x\delta_y F^\epsilon\rangle}{\|T_y^{-1}\delta_x F^\epsilon\|\|T_x\delta_y F^\epsilon\|},\\ \epsilon\tilde{w} &= \frac{\langle T_y\delta_x F^\epsilon, T_x\delta_y F^\epsilon\rangle}{\|T_y\delta_x F^\epsilon\|\|T_x\delta_y F^\epsilon\|} = -\frac{\langle T_y^{-1}\delta_x F^\epsilon, T_x^{-1}\delta_y F^\epsilon\rangle}{\|T_y^{-1}\delta_x F^\epsilon\|\|T_x^{-1}\delta_y F^\epsilon\|}.\end{aligned} \tag{22}$$

The equalities follow since opposite angles in a conformal square sum up to π. The two pairs (v, w) and $(\tilde{v}, \tilde{w})$ are just different representations of the same geometric information.

Lemma 3 *There is a one-to-one correspondence between the pairs* (v, w) *and* $(\tilde{v}, \tilde{w})$ *of functions. Specifically, recalling the* **-notation introduced in* (17)*,*

$$\sinh(\epsilon v) = \epsilon\frac{\tilde{v}\tilde{w}^*}{\tilde{v}^*} \quad \textit{and} \quad \sinh(\epsilon w) = \epsilon\frac{\tilde{w}\tilde{v}^*}{\tilde{w}^*}. \tag{23}$$

Moreover, the pair $(v, \tilde{w})$ *uniquely determines the pair* $(\tilde{v}, w)$*, and vice versa.*

Proof This is a general statement about four geometric quantities defined for conformal squares. It thus suffices to consider a single conformal square with vertices

$$p_1 = T_\eta^{-1}F^\epsilon,\ p_2 = T_\xi F^\epsilon,\ p_3 = T_\eta F^\epsilon,\ p_4 = T_\xi^{-1}F^\epsilon.$$

The respective four real numbers $v, w, \tilde{v}, \tilde{w}$ are given by

$$\begin{aligned}e^{\epsilon v} = \frac{\|p_2 - p_1\|}{\|p_1 - p_4\|} = \frac{\|p_3 - p_2\|}{\|p_4 - p_3\|},\quad e^{\epsilon w} = \frac{\|p_3 - p_2\|}{\|p_2 - p_1\|} = \frac{\|p_3 - p_4\|}{\|p_4 - p_1\|},\\ \epsilon\tilde{v} = \cos(\angle p_1p_2p_3) = -\cos(\angle p_3p_4p_1),\quad \epsilon\tilde{w} = \cos(\angle p_2p_3p_4) = -\cos(\angle p_4p_1p_2).\end{aligned}$$

Observe that

$$\begin{aligned}\|p_3 - p_2\|^2 + \|p_1 - p_2\|^2 - 2\langle p_3 - p_2, p_1 - p_2\rangle = \|p_3 - p_4\|^2\\ + \|p_1 - p_4\|^2 - 2\langle p_3 - p_4, p_1 - p_4\rangle\end{aligned}$$

since both expressions are equal to $\|p_3 - p_1\|^2$. Divide by $\|p_3 - p_2\|^2$ and use the definitions of $v, w, \tilde{v}, \tilde{w}$ to obtain, after simplification, that

$$1 + e^{-2\epsilon w} - 2\epsilon\tilde{v}e^{-\epsilon w} = e^{-2\epsilon v}(1 + e^{-2\epsilon w} + 2\epsilon\tilde{v}e^{-\epsilon w}). \tag{24}$$

The analogous considerations with $\|p_4 - p_2\|^2$ in place of $\|p_3 - p_1\|^2$ give (24) with $\tilde{w}$ in place of $\tilde{v}$, and with the roles of w and v exchanged. Clearly, these equations are uniquely solvable for $(\tilde{v}, \tilde{w})$ in terms of (v, w):

$$\epsilon\tilde{v} = \tanh(\epsilon v)\,\cosh(\epsilon w), \quad \epsilon\tilde{w} = \tanh(\epsilon w)\,\cosh(\epsilon v). \tag{25}$$

Note that in particular

$$\epsilon^2 \tilde{v}\tilde{w} = \sinh(\epsilon v)\sinh(\epsilon w). \tag{26}$$

To derive (23) from here, take the square of the equations in (25), and express $\cosh^2$ and $\tanh^2$ in terms of $\sinh^2$ only. Then use (26) to eliminate $\sinh^2(\epsilon w)$ from the first equation and $\sinh^2(\epsilon v)$ from the second one. This yields

$$\sinh^2(\epsilon v) = \left(\epsilon \frac{\tilde{v}\tilde{w}^*}{\tilde{v}^*}\right)^2, \quad \sinh^2(\epsilon w) = \left(\epsilon \frac{\tilde{w}\tilde{v}^*}{\tilde{w}^*}\right)^2.$$

Now take the square root, bearing in mind that v, $\tilde{v}$ have the same sign, and w, $\tilde{w}$ have the same sign by (25).

Finally, to calculate $\tilde{v}$ from a given $(v, \tilde{w})$ using the first relation in (23), it suffices to invert the (strictly increasing) function $\tilde{v} \mapsto \tilde{v}/\tilde{v}^*$. Then, knowing $\tilde{v}$ and $\tilde{w}$, the value of w can be obtained from the second relation in (23). □

Recall that all discrete quantities defined above depend on the parameter ϵ. To stress this fact, we will in the following use the superscript ϵ.

For later reference, we draw some first consequences of the definitions above. Specifically, we summarize the relations between the geometric quantities $(a^\epsilon, b^\epsilon, \hat{u}^\epsilon, \check{u}^\epsilon)$, and, of course, to F^ϵ itself, to the more abstract quantities $(v^\epsilon, w^\epsilon, \mathfrak{k}^\epsilon, \mathfrak{l}^\epsilon)$ that satisfy the Gauss-Codazzi system (31)–(34). These relations can be seen as a discrete analog of the frame equations (6) and (7).

Lemma 4 *On $\Omega^{[xxyy]_\epsilon}(r|h)$, one has*

$$\delta_y F^\epsilon = \exp(\hat{u}^\epsilon)a^\epsilon, \quad \delta_x F^\epsilon = \exp(\check{u}^\epsilon)b^\epsilon, \tag{27}$$

$$\delta_y \hat{u}^\epsilon = w^\epsilon - v^\epsilon, \quad \delta_x \check{u}^\epsilon = w^\epsilon + v^\epsilon, \tag{28}$$

$$\delta_y a^\epsilon = \left[\frac{(\tilde{v}^\epsilon)^*}{(\tilde{w}^\epsilon)^*}\tilde{w}^\epsilon - \tilde{v}^\epsilon\right] \tau_x^{-1} b^\epsilon + \frac{1}{\epsilon}\left[\frac{(\tilde{v}^\epsilon)^*}{(\tilde{w}^\epsilon)^*} - 1\right] \tau_y^{-1} a^\epsilon, \tag{29}$$

$$\delta_x b^\epsilon = \left[\frac{(\tilde{v}^\epsilon)^*}{(\tilde{w}^\epsilon)^*}\tilde{w}^\epsilon - \tilde{v}^\epsilon\right] \tau_y^{-1} a^\epsilon + \frac{1}{\epsilon}\left[\frac{(\tilde{v}^\epsilon)^*}{(\tilde{w}^\epsilon)^*} - 1\right] \tau_x^{-1} b^\epsilon. \tag{30}$$

Proof The two equations in (28) are obtained by rearranging the identities in (20). For the derivation of (29), one makes the ansatz

$$\tau_y a^\epsilon = \mu_a \tau_y^{-1} a^\epsilon + \mu_b \tau_x^{-1} b^\epsilon.$$

Such a representation of $\tau_y a^\epsilon$ must exist since elementary squares are mapped to (flat) quadrilaterals by F^ϵ. The coefficients μ_a and μ_b can be determined by solving the system of equations

$$1 = \|\tau_y a^\epsilon\|^2 = \mu_a^2 + \mu_b^2 - 2\epsilon\mu_a\mu_b\tilde{w}^\epsilon, \quad \epsilon\tilde{v}^\epsilon = \langle \tau_y a^\epsilon, \tau_x^{-1} b^\epsilon \rangle = -\epsilon\mu_a\tilde{w}^\epsilon + \mu_b.$$

The analogous ansatz—with the roles of a^ϵ and b^ϵ interchanged—leads to (30). □

3.5 Discrete Gauss-Codazzi System

This section is devoted to derive a discrete version of the Gauss-Codazzi equations (9)–(12). The following definition is needed to classify the difference between the continuous and the discrete system.

Definition 6 A family $(h_\epsilon)_{\epsilon>0}$ of real functions on respective domains $D_\epsilon \subset \mathbb{R}^n$ is called *asymptotically analytic on* $\mathbb{C}^n$ if the following is true. For every $M > 0$, there is an $\epsilon(M) > 0$ such that each h_ϵ with $0 < \epsilon < \epsilon(M)$ extends from D_ϵ to a complex-analytic function $\tilde{h}_\epsilon : \mathbb{D}_M^n \to \mathbb{C}$ on the n-dimensional complex multi-disc

$$\mathbb{D}_M^n = \big\{ z = (z_1, \ldots, z_n) \in \mathbb{C}^n \,\big|\, |z_j| < M \text{ for each } j = 1, \ldots, n \big\}.$$

And the extensions $\tilde{h}_\epsilon$ are bounded on $\mathbb{D}_M^n$, uniformly in $0 < \epsilon < \epsilon(M)$.

The prototypical example for a family $(h_\epsilon)_{\epsilon>0}$ that is asymptotically analytic on $\mathbb{C}$ is given by $h_\epsilon(z) = 1/z^* = (1 - \epsilon^2 z^2)^{-1/2}$. It is further easily seen that also the functions $g_\epsilon = \epsilon^{-2}(h_\epsilon - 1)$ form such a family; this is a very strong way of saying that $h_\epsilon = 1 + \mathcal{O}(\epsilon^2)$.

Proposition 2 *There are four families $(h_{1,\epsilon})_{\epsilon>0}, \ldots, (h_{4,\epsilon})_{\epsilon>0}$ of asymptotically analytic functions on $\mathbb{C}^8$ for which the following is true: let any ϵ-discrete isothermic surface $F^\epsilon : \Omega(r|h) \to \mathbb{R}^3$ be given, and define the functions $v^\epsilon, w^\epsilon, \mathfrak{k}^\epsilon, \mathfrak{l}^\epsilon$ accordingly. Then the following system of discrete equations is satisfied on $\Omega^{[xy]_\epsilon}(r|h)$:*

$$\delta_\eta v^\epsilon = \delta_\xi w^\epsilon, \tag{31}$$

$$\delta_\eta w^\epsilon = \delta_\xi v^\epsilon - (\tau_y^{-1}\mathfrak{k}^\epsilon)(\tau_x^{-1}\mathfrak{l}^\epsilon) + \epsilon h_2^\epsilon(\tau\theta^\epsilon), \tag{32}$$

$$\delta_y \mathfrak{k}^\epsilon = (\tau_x^{-1}\mathfrak{l}^\epsilon)(\tau_\eta^{-1} w^\epsilon - \tau_\xi v^\epsilon) + \epsilon^2 h_3^\epsilon(\tau\theta^\epsilon) \tag{33}$$

$$\delta_x \mathfrak{l}^\epsilon = (\tau_y^{-1}\mathfrak{k}^\epsilon)(\tau_\eta^{-1} w^\epsilon + \tau_\xi^{-1} v^\epsilon) + \epsilon h_4^\epsilon(\tau\theta^\epsilon), \tag{34}$$

where the h_j^ϵ are evaluated on

$$\tau\theta^\epsilon = \big(\tau_\xi v^\epsilon, \tau_\xi w^\epsilon, \tau_\xi^{-1} v^\epsilon, \tau_\xi^{-1} w^\epsilon, \tau_\eta^{-1} v^\epsilon, \tau_\eta^{-1} w^\epsilon, \tau_y^{-1}\mathfrak{k}^\epsilon, \tau_x^{-1}\mathfrak{l}^\epsilon\big).$$

Remark 5 Equations (31)–(34) are *explicit in η-direction* in the sense that they express the "unknown" quantities $\tau_\eta v^\epsilon$, $\tau_\eta w^\epsilon$, $\tau_y \mathfrak{k}^\epsilon$ and $\tau_x \mathfrak{l}^\epsilon$ in terms of the "given" eight quantities summarized in $\tau\theta^\epsilon$.

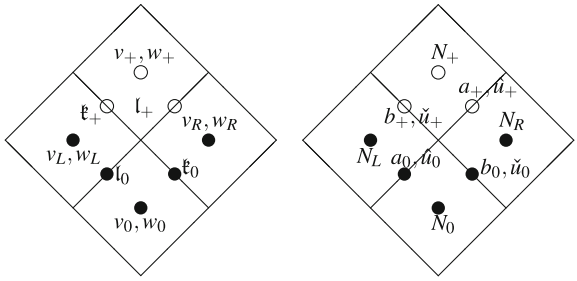

Fig. 4 Four elementary squares with discrete quantities for the Cauchy problem

The rest of this section is devoted to the proof of Proposition 2. Since $\epsilon > 0$ is fixed in the derivation of (31)–(34), we shall omit the superscript ϵ on the occurring quantities.

For the derivation of (31)–(34), one can obviously work locally: it suffices to fix some point in $\Omega^{[xxyy]^\epsilon}(r|h)$ and to consider the eight values of v, w on the midpoints of the four elementary squares incident to that vertex, and the four values of $\mathfrak{k}$, $\mathfrak{l}$ on the respective connecting edges.

The setup is visualized in Fig. 4. The "unknown" quantities v_+, w_+ and $\mathfrak{k}_+$, $\mathfrak{l}_+$ are marked by $\circ$, the "given" quantities v_0, w_0, v_L, w_L, v_R, w_R and $\mathfrak{k}_0$, $\mathfrak{l}_0$ are marked by $\bullet$. To facilitate the calculations, we also assume that values for a_0, b_0, $\hat{u}_0$, $\check{u}_0$, N_0, N_L, N_R are given; and then obtain the values of a_+, b_+, $\hat{u}_+$, $\check{u}_+$, N_+, see Fig. 4 right. Naturally, the final formulas for v_+, w_+ and $\mathfrak{k}_+$, $\mathfrak{l}_+$ will be independent of these quantities.

3.5.1 Derivation of Equation (31)

Compare the following two alternative ways to calculate $\hat{u}_+$, the logarithmic length of the edge separating the right and the top plaquettes, from $\hat{u}_0$, the logarithmic length of the edge between the plaquettes at bottom and left:

$$e^{\epsilon\hat{u}_0} e^{\epsilon v_0} e^{\epsilon w_R} = e^{\epsilon\hat{u}+} = e^{\epsilon\hat{u}_0} e^{\epsilon w_L} e^{\epsilon v_+}$$

holds by property (20) of the functions v and w. Take the logarithm to obtain (31).

3.5.2 Derivation of Equation (32)

First recall that by Lemma 3, there is a one-to-one correspondence between (v, w) and $(\tilde{v}, \tilde{w})$, so we can assume that values for $(\tilde{v}_0, \tilde{w}_0)$, $(\tilde{v}_L, \tilde{w}_L)$, $(\tilde{v}_R, \tilde{w}_R)$ are given as well. Using that N_R is the normalized cross product $a_+ \times b_0$, it is elementary to derive the following representation of a_+:

$$a_+ = \epsilon\tilde{\nu}_R b_0 + \tilde{\nu}_R^*(b_0 \times N_R). \tag{35}$$

Taking the scalar product with N_0, one obtains

$$\langle a_+, N_0\rangle = \tilde{\nu}_R^*\langle b_0, N_R \times N_0\rangle = \epsilon\tilde{\nu}_R^*\mathfrak{k}_0.$$

Hence a_+ can be expanded in the basis a_0, b_0 and N_0 as follows:

$$a_+ = \mu_a a_0 + \mu_b b_0 + \epsilon\tilde{\nu}_R^*\mathfrak{k}_0 N_0 \tag{36}$$

with some real coefficients μ_a and μ_b to be determined. Calculating the square norm on both sides gives

$$1 = \mu_a^2 + \mu_b^2 + 2\epsilon\tilde{w}_0\mu_a\mu_b + \epsilon^2(\tilde{\nu}_R^*)^2\mathfrak{k}_0^2, \tag{37}$$

and the scalar product with b_0 yields

$$\epsilon\tilde{\nu}_R = \epsilon\tilde{w}_0\mu_a + \mu_b. \tag{38}$$

Use (38) to eliminate μ_b from (37), then solve for μ_a. This gives

$$\mu_a = \frac{\tilde{\nu}_R^*\mathfrak{k}_0^*}{\tilde{w}_0^*}, \qquad \mu_b = \epsilon\tilde{\nu}_R - \epsilon\frac{\tilde{\nu}_R^*\mathfrak{k}_0^*}{\tilde{\nu}_0^*}\tilde{w}_0. \tag{39}$$

On the other hand, starting from

$$b_+ = \lambda_b b_0 + \lambda_a a_0 + \epsilon\tilde{\nu}_L^*\mathfrak{l}_0 N_0 \tag{40}$$

instead of (36), one obtains by analogous calculations that

$$\lambda_b = \frac{\tilde{\nu}_L^*\mathfrak{l}_0^*}{\tilde{w}_0^*}, \qquad \lambda_a = -\epsilon\tilde{\nu}_L - \epsilon\frac{\tilde{\nu}_L^*\mathfrak{l}_0^*}{\tilde{w}_0^*}\tilde{w}_0.$$

Since $\epsilon\tilde{w}_+ = -\langle a_+, b_+\rangle$, it eventually follows that

$$\begin{aligned}\tilde{w}_+ = {} & \frac{\tilde{\nu}_L^*\tilde{\nu}_R^*\mathfrak{k}_0^*\mathfrak{l}_0^*}{(\tilde{w}_0^*)^2}\tilde{w}_0 - \frac{\tilde{\nu}_L^*\mathfrak{l}_0^*}{\tilde{w}_0^*}\tilde{\nu}_R + \frac{\tilde{\nu}_R^*\mathfrak{k}_0^*}{\tilde{w}_0^*}\tilde{\nu}_L - \epsilon\tilde{\nu}_R^*\tilde{\nu}_L^*\mathfrak{k}_0\mathfrak{l}_0 \\ & + \epsilon^2\tilde{w}_0\left(-\tilde{\nu}_R\tilde{\nu}_L + \frac{\tilde{\nu}_R^*\tilde{\nu}_L\mathfrak{k}_0^* - \tilde{\nu}_R\tilde{\nu}_L^*\mathfrak{l}_0^*}{\tilde{w}_0^*}\tilde{w}_0 + \frac{\tilde{\nu}_R^*\tilde{\nu}_L^*\mathfrak{k}_0^*\mathfrak{l}_0^*}{(\tilde{w}_0^*)^2}\tilde{w}_0^2\right).\end{aligned} \tag{41}$$

Next, recall that one may consider (ν, w) as a function of $(\tilde{\nu}, \tilde{w})$. More precisely, by (23), one has that ν and w approximate $\tilde{\nu}$ and $\tilde{w}$, respectively, to order ϵ^2, in the sense that the family of functions

$$(\tilde{v}, \tilde{w}) \mapsto \big(\epsilon^{-2}(v-\tilde{v}), \epsilon^{-2}(w-\tilde{w})\big) = \left(\frac{1}{\epsilon^2}\left[\epsilon^{-1}\operatorname{arsinh}\left(\epsilon\frac{\tilde{v}\tilde{w}^*}{\tilde{v}^*}\right) - \tilde{v}\right], \frac{1}{\epsilon^2}\left[\epsilon^{-1}\operatorname{arsinh}\left(\epsilon\frac{\tilde{w}\tilde{v}^*}{\tilde{w}^*}\right) - \tilde{w}\right]\right)$$

is asymptotically analytic on $\mathbb{C}^2$, see Definition 6. Observe further that $\epsilon^{-2}(1-\tilde{v}^*)$ etc. are asymptotically analytic as well. With this, it is straight-forward to conclude (32) from (41).

3.5.3 Derivation of Equation (33)

In analogy to (35), one obtains by elementary considerations the following representation of a_+:

$$a_+ = -\epsilon\tilde{w}_+ b_+ + \tilde{w}_+^*(b_+ \times N_+).$$

Using the definition (21) of $\mathfrak{k}$, it then follows that

$$\langle a_+, N_L\rangle = \tilde{w}_+^*\langle b_+, N_+ \times N_L\rangle = \epsilon\tilde{w}_+^*\mathfrak{k}_+.$$

On the other hand, the computation (36)–(39) implies that

$$\begin{aligned}\langle a_+, N_L\rangle &= \mu_b\langle b_0, N_L\rangle + \epsilon\tilde{v}_R^*\mathfrak{k}_0\langle N_0, N_L\rangle \\ &= \frac{\mu_b}{\tilde{v}_L^*}\langle b_0, a_0 \times b_+\rangle + \epsilon\tilde{v}_R^*\mathfrak{l}_0^*\mathfrak{k}_0 \\ &= -\frac{\mu_b\tilde{w}_0^*}{\tilde{v}_L^*}\langle b_+, N_0\rangle + \epsilon\tilde{v}_R^*\mathfrak{l}_0^*\mathfrak{k}_0 \\ &= -\epsilon^2(\tilde{w}_0^*\tilde{v}_R - \tilde{v}_R^*\mathfrak{k}_0^*\tilde{w}_0)\mathfrak{l}_0 + \epsilon\tilde{v}_R^*\mathfrak{l}_0^*\mathfrak{k}_0.\end{aligned}$$

In combination, this yields

$$\tilde{w}_+^*\mathfrak{k}_+ = \tilde{v}_R^*\mathfrak{l}_0^*\mathfrak{k}_0 + \epsilon(\tilde{v}_R^*\mathfrak{k}_0^*\tilde{w}_0 - \tilde{w}_0^*\tilde{v}_R)\mathfrak{l}_0.$$

We can now substitute (41) to express the unknown $\tilde{w}_+$ in terms of the known quantities only. Using once again that $\epsilon^{-2}(1-\tilde{w}_+^*)$ etc. are asymptotically analytic according to Definition 6, we arrive at (33).

The derivation of Eq. (34) is analogous.

4 The Abstract Convergence Result

In this section, we analyze the convergence of solutions to the classical Gauss-Codazzi system (9)–(12) by solutions to the discrete system (31)–(34). This is the core part of the convergence proof, from which our main result will be easily deduced in the next section.

4.1 Domains

A key concept in the proof is to work with analytic extensions of the quantities v, w, $\mathfrak{k}$ and $\mathfrak{l}$ defined in Sect. 3.4. The analytic setting forces us to introduce yet another class of domains, and corresponding spaces of real analytic functions. In the following, we assume that $r > 0$ and $\bar{\rho} > 0$ are fixed parameters (which will be frequently omitted in notations), while $h \in (0, \bar{\rho})$ and $\epsilon > 0$ may vary, with the restriction that $\epsilon < h$.

For each domain $\Omega(r|h)$, introduce its *analytic fattening* $\widehat{\Omega}_{\bar{\rho}}(r|h)$ as follows:

$$\widehat{\Omega}_{\bar{\rho}}(r|h) = \left\{(\xi, \eta) \in \mathbb{C} \times \mathbb{R}\,;\ \exists(\xi', \eta) \in \Omega(r|h) \text{ s.t. } |\xi - \xi'|/\bar{\rho} + |\eta|/h < 1\right\}.$$

On these domains, we introduce the function class

$$C^{\omega}\big(\widehat{\Omega}(r|h)\big) := \left\{f : \widehat{\Omega}_{\bar{\rho}}(r|h) \to \mathbb{C}\,;\ f(\cdot, \eta) \text{ is real analytic, for each } \eta\right\}.$$

Notice that we require analyticity with respect to ξ, but not even continuity with respect to η. Next, introduce semi-norms $|\cdot|_{\eta,\rho}$ for functions $f \in C^{\omega}\big(\widehat{\Omega}(r|h)\big)$, depending on parameters $\eta \in [-h, h]$ and $\rho \in [0, \bar{\rho}]$ with $\rho/\bar{\rho} + |\eta|/h < 1$ as follows:

$$|f|_{\eta,\rho} = \sup\left\{|f(\xi, \eta)|\,;\ \xi \in \mathbb{C} \text{ s.t. } \exists(\xi', \eta) \in \Omega(r|h) \text{ with } |\xi - \xi'| < \rho\right\}.$$

These semi-norms are perfectly suited to apply Cauchy estimates; indeed, one easily proves with the Cauchy integral formula that

$$\left|\partial_{\xi} f\right|_{\eta,\rho} \leq \frac{1}{\rho' - \rho}\,|f|_{\eta,\rho'}\,, \tag{42}$$

provided that $\rho' > \rho$. The semi-norms are now combined into a genuine norm $\|\cdot\|_h$ on $C^{\omega}\big(\widehat{\Omega}(r|h)\big)$ as follows:

$$\|f\|_h = \sup\left\{\Lambda(\eta, \rho)\,|f|_{\eta,\rho}\ ;\ \frac{|\eta|}{h} + \frac{\rho}{\bar{\rho}} < 1\right\}, \tag{43}$$

where the positive weight Λ is given by

$$\Lambda(\eta, \rho) = 1 - \frac{|\eta|/h}{1 - \rho/\bar{\rho}}. \tag{44}$$

This norm makes $C^{\omega}\big(\widehat{\Omega}(r|h)\big)$ a Banach space.

There is another semi-norm $\left\{\,\cdot\,\right\}_{h,\delta}$ that will be of importance below: for each $\delta \in [0, 1]$, let

$$\left\{f\right\}_{h,\delta} = \sup\left\{|f|_{\eta,\rho}\ ;\ \frac{|\eta|}{h} + \frac{\rho}{\bar{\rho}} \leq 1 - \delta\right\}.$$

By definition (44) of the weight Λ, the following estimate is immediate:

$$\left\{f\right\}_{h,\delta} \leq \delta^{-1} \left\|f\right\|_h , \tag{45}$$

provided that $\delta > 0$.

Replacing $\Omega(r|h)$ by $\Omega^{[xy]\epsilon}(r|h)$ above yields definitions for analytically fattened domains $\widehat{\Omega}^{[xy]\epsilon}_{\bar{\rho}}(r|h)$ with respective spaces $C^\omega\left(\widehat{\Omega}^{[xy]\epsilon}(r|h)\right)$, semi-norms $|\cdot|^{[xy]\epsilon}_{\eta,\rho}$ and $\left\{\cdot\right\}^{[xy]\epsilon}_{h,\delta}$, and norms $\|\cdot\|^{[xy]\epsilon}_h$ etc.

4.2 Statement of the Approximation Result

Recall that $r > 0$ and $\bar{\rho} > 0$ are fixed parameters.

Definition 7 An *analytic solution* $\theta = (v, w, \mathfrak{k}, \mathfrak{l})$ *of the classical Gauss-Codazzi system on* $\widehat{\Omega}_{\bar{\rho}}(r|h)$ consists of four functions $v, w, \mathfrak{k}, \mathfrak{l} \in C^\omega\left(\widehat{\Omega}(r|h)\right)$ that are globally bounded on $\widehat{\Omega}_{\bar{\rho}}(r|h)$, are continuously differentiable with respect to η, and satisfy Eqs. (9)–(12) on $\widehat{\Omega}_{\bar{\rho}}(r|h)$.

An *analytic solution* $\theta^\epsilon = (v^\epsilon, w^\epsilon, \mathfrak{k}^\epsilon, \mathfrak{l}^\epsilon)$ *of the* ϵ*-discrete Gauss-Codazzi system on* $\widehat{\Omega}_{\bar{\rho}}(r|h)$ consists of four functions $v^\epsilon, w^\epsilon \in C^\omega\left(\widehat{\Omega}^{[xy]\epsilon}(r|h)\right)$, $\mathfrak{k}^\epsilon \in C^\omega\left(\widehat{\Omega}^{[xxy]\epsilon}(r|h)\right)$, $\mathfrak{l}^\epsilon \in C^\omega\left(\widehat{\Omega}^{[xyy]\epsilon}(r|h)\right)$ that satisfy Eqs. (31)–(34) on $\widehat{\Omega}^{[xxyy]\epsilon}_{\bar{\rho}}(r|h)$.

A suitable norm to measure the deviation of an ϵ-discrete solution θ^ϵ to a classical solution θ on the same domain $\widehat{\Omega}_{\bar{\rho}}(r|h)$ is given by the norms of the differences of the four components,

$$|||\theta^\epsilon - \theta|||_h = \max\left(\|v^\epsilon - v\|^{[xy]\epsilon}_h , \|w^\epsilon - w\|^{[xy]\epsilon}_h , \|\mathfrak{k}^\epsilon - \mathfrak{k}\|^{[xxy]\epsilon}_h , \|\mathfrak{l}^\epsilon - \mathfrak{l}\|^{[xyy]\epsilon}_h\right).$$

Proposition 3 *Let an analytic solution* θ *to the Gauss-Codazzi system on* $\widehat{\Omega}_{\bar{\rho}}(r|\bar{h})$ *be given, and consider a family* $(\theta^\epsilon)_{\epsilon>0}$ *of (a priori not necessarily analytic) solutions* $\theta^\epsilon = (v^\epsilon, w^\epsilon, \mathfrak{k}^\epsilon, \mathfrak{l}^\epsilon)$ *to the* ϵ*-discrete Gauss-Codazzi equations on* $\Omega(r|h^\epsilon)$*. Then there are numbers* $A, B > 0$ *and* $\bar{\epsilon} > 0$ *such that the following is true for all* $\epsilon \in (0, \bar{\epsilon})$*: if* θ^ϵ *possesses sufficient regularity to admit* ξ*-analytic complex extensions for* η *near zero such that*

$$|||\theta - \theta^\epsilon|||_\epsilon < A\epsilon, \tag{46}$$

then θ^ϵ *as a whole extends to an analytic solution* θ^ϵ *of the* ϵ*-discrete Gauss-Codazzi system on* $\widehat{\Omega}_{\bar{\rho}}(r|h)^\epsilon$*, and*

$$|||\theta - \theta^\epsilon|||_{h^\epsilon} \leq B\epsilon. \tag{47}$$

Remark 6 The formulation of the proposition suggests that the height h of the domain on which convergence takes place is small. However, this is misleading in general. As it turns out in the proof, the limitation for h is mostly determined by the value of $\bar{\rho}$. In many examples of interest, $\bar{\rho}$ is large compared to the region of interest (determined by $\bar{h}$ and r), and consequently, one has $h^\epsilon = \bar{h}$ above, i.e., convergence takes place on the entire domain of definition of θ.

The rest of this section is devoted to the proof of Proposition 3.

4.3 Consistency

We start with an evaluation of the difference between the classical and the ϵ-discrete Gauss-Codazzi equations. Here, we need yet another measure for the deviation of θ^ϵ from θ:

$$\left\{\{\theta^\epsilon - \theta\}\right\}_{h,\delta} = \max\left(\left\{v^\epsilon - v\right\}_{h,\delta}^{[xy]\epsilon}, \left\{w^\epsilon - w\right\}_{h,\delta}^{[xy]\epsilon}, \left\{\mathfrak{k}^\epsilon - \mathfrak{k}\right\}_{h,\delta}^{[xxy]\epsilon}, \left\{\mathfrak{l}^\epsilon - \mathfrak{l}\right\}_{h,\delta}^{[xyy]\epsilon}\right).$$

This semi-norm is similar to $|||\theta^\epsilon - \theta|||_h$. For further reference, we note that

$$\left\{\{\theta^\epsilon - \theta\}\right\}_{h,\delta} \leq \frac{1}{\delta}|||\theta^\epsilon - \theta|||_h, \tag{48}$$

thanks to (45), provided that $\delta > 0$. Furthermore, we denote for abbreviation the difference between corresponding discrete and continuous quantities by Δ, i.e. $\Delta v^\epsilon = v^\epsilon - v$ etc.

Lemma 5 *Let an analytic solution θ to the classical Gauss-Codazzi system and an analytic solution θ^ϵ to the ϵ-discrete Gauss-Codazzi system be given, both on $\widehat{\Omega}_{\bar{\rho}}(r|h)$. Define the residuals $\tilde{g}_1^\epsilon, \ldots, \tilde{g}_4^\epsilon \in C^\omega\left(\widehat{\Omega}^{[xxyy]\epsilon}(r|h)\right)$ by*

$$\delta_\eta \Delta v^\epsilon = \delta_\xi \Delta w^\epsilon + \epsilon \tilde{g}_1^\epsilon \tag{49}$$

$$\delta_\eta \Delta w^\epsilon = -\delta_\xi \Delta v^\epsilon + \tau_y^{-1}\mathfrak{k}^\epsilon \tau_x^{-1}\Delta \mathfrak{l}^\epsilon + \tau_y^{-1}\Delta \mathfrak{k}^\epsilon \tau_x^{-1}\mathfrak{l} + \epsilon \tilde{g}_2^\epsilon \tag{50}$$

$$\delta_y \Delta \mathfrak{k}^\epsilon = (\tau_x^{-1}\mathfrak{l}^\epsilon)\,(\tau_\eta^{-1}\Delta w^\epsilon - \tau_\xi \Delta v^\epsilon) + (\tau_x^{-1}\Delta \mathfrak{l}^\epsilon)\,(\tau_\eta^{-1} w - \tau_\xi v) + \epsilon \tilde{g}_3^\epsilon \tag{51}$$

$$\delta_x \Delta \mathfrak{l}^\epsilon = (\tau_y^{-1}\mathfrak{k}^\epsilon)\,(\tau_\eta^{-1}\Delta w^\epsilon + \tau_\xi^{-1}\Delta v^\epsilon) + (\tau_y^{-1}\Delta \mathfrak{k}^\epsilon)\,(\tau_\eta^{-1} w + \tau_\xi^{-1} v) + \epsilon \tilde{g}_4^\epsilon. \tag{52}$$

Then the $\tilde{g}_j^\epsilon$ are uniformly bounded with respect to $\epsilon < \bar{\epsilon}$ on their respective domains:

$$|\tilde{g}_j^\epsilon| \leq G \quad \text{on } \widehat{\Omega}_{\bar{\rho}}^{[xxyy]\epsilon}(r|h), \text{for each } j = 1, \ldots, 4, \tag{53}$$

with a suitable constant G that depends on θ, and θ^ϵ only via $\left\{\{\theta^\epsilon - \theta\}\right\}_{h,0}$, but is independent of ϵ.

Proof By analyticity of θ it is clear that the central difference quotients obey

$$\delta_\xi v = \partial_\xi v + \epsilon g^\epsilon_{v,\xi}, \quad \delta_\eta v = \partial_\eta v + \epsilon g^\epsilon_{v,\eta} \quad \text{etc.}$$

with functions $g^\epsilon_{v,\xi}, g^\epsilon_{v,\eta}, \ldots \in C^\omega\big(\widehat{\Omega}^{[xxyy]_\epsilon}(r|h)\big)$ that are bounded uniformly w.r.t. ϵ. The classical Gauss-Codazzi system (9)–(12) thus implies that

$$\begin{aligned}
\delta_\eta v &= \delta_\xi w + \epsilon g^\epsilon_1,\\
\delta_\eta w &= -\delta_\xi v - (\tau_y^{-1}\mathfrak{k})(\tau_x^{-1}\mathfrak{l}) + \epsilon g^\epsilon_2,\\
\delta_y \mathfrak{k} &= (\tau_x^{-1}\mathfrak{l})(\tau_\eta^{-1} w - \tau_\xi v) + \epsilon g^\epsilon_3,\\
\delta_x \mathfrak{l} &= (\tau_y^{-1}\mathfrak{k})(\tau_\eta^{-1} w + \tau_\xi^{-1} v) + \epsilon g^\epsilon_4,
\end{aligned}$$

where each of the functions g^ϵ_j is bounded on $\Omega^{[xxyy]_\epsilon}(r|h)$, with an ϵ-independent bound. Taking the difference between each equation of this system and the respective equation of the ϵ-discrete Gauss-Codazzi equation (31)–(34) yields (49)–(52), with

$$\tilde{g}^\epsilon_j = h^\epsilon_j(\tau\theta^\epsilon) - g^\epsilon_j.$$

Since the h^ϵ_j are asymptotically analytic on $\mathbb{C}^8$, it follows that the modulus of $h^\epsilon_j(\tau\theta^\epsilon)$ is uniformly controlled on $\Omega^{[xxyy]_\epsilon}(r|h)$ by the supremum of the modulus of (θ^ϵ)'s components. □

4.4 Stability

Stability is shown inductively. More precisely, we prove for each $n = 1, 2, \ldots$ with $n\frac{\epsilon}{2} \le h$ that

$$|||\theta^\epsilon - \theta|||_{n\frac{\epsilon}{2}} < B\epsilon. \tag{54}$$

In fact, there is nothing to show for $n = 1$. For $n = 2$, the claim (54) is a consequence of estimate (46) on the initial data. Now assume that (54) has been shown for some $n \ge 2$. We are going to extend the estimate to $n + 1$.

Estimate on Δv^ϵ. We begin by proving the estimate for the v-component of $\Delta\theta^\epsilon$. Since v^ϵ is defined on $\widehat{\Omega}^{[xy]_\epsilon}_{\tilde{p}}(r|h)$, the step $n \to n + 1$ requires to estimate the values of $\Delta v^\epsilon(\cdot, \eta^*)$ for $\eta^* \in ((n-1)\frac{\epsilon}{2}, n\frac{\epsilon}{2}]$. Choose such an η^*, and define accordingly ℓ such that $\eta^*_0 := \eta^* - \ell\epsilon \in (-\frac{\epsilon}{2}, \frac{\epsilon}{2}]$; in fact, $2\ell = n$ if n is even, and $n = 2\ell + 1$ if n is odd. For $0 \le k \le 2\ell$, introduce

$$\eta^*_k = \eta^* - (2\ell - k)\frac{\epsilon}{2}; \tag{55}$$

non-integer values of k are admitted. (55) is consistent with the definition of η_0^*, and moreover, $\eta^* = \eta_{2\ell}^*$. Using the evolution equation (49), we obtain

$$\begin{aligned}\Delta v^\epsilon(\cdot,\eta^*) &= \Delta v^\epsilon(\cdot,\eta_0^*) + \sum_{k=1}^{\ell} \left(\tau_\eta \Delta v^\epsilon - \tau_\eta^{-1}\Delta v^\epsilon\right)(\cdot,\eta_{2k-1}^*) \\ &= \Delta v^\epsilon(\cdot,\eta_0^*) + \epsilon \sum_{k=1}^{\ell} \delta_\xi \Delta w^\epsilon(\cdot,\eta_{2k-1}^*) + \epsilon^2 \sum_{k=1}^{\ell} \tilde{g}_1^\epsilon(\cdot,\eta_{2k-1}^*). \end{aligned} \tag{56}$$

Next, pick a $\rho^* > 0$ such that

$$\frac{\rho^*}{\bar{\rho}} + \frac{\eta^*}{h} < 1. \tag{57}$$

We estimate:

$$\begin{aligned}|\Delta v^\epsilon|_{\eta^*,\rho^*}^{[xy]\epsilon} &\le |\Delta v^\epsilon|_{\eta_0^*,\rho^*}^{[xy]\epsilon} + \epsilon \sum_{k=1}^{\ell} \left|\delta_\xi \Delta w^\epsilon\right|_{\eta_{2k-1}^*,\rho^*}^{[xy\xi]\epsilon} + \epsilon^2 \sum_{k=1}^{\ell} \left|\tilde{g}_1^\epsilon\right|_{\eta_{2k-1}^*,\rho^*}^{[xxyy]\epsilon} \\ &=: \text{(I)} + \text{(II)} + \text{(III)}. \end{aligned} \tag{58}$$

We consider the terms (I)−(III) separately. First, thanks to our hypothesis (46) on the initial conditions, we find that

$$\text{(I)} = |\Delta v^\epsilon|_{\eta_0^*,\rho^*}^{[xy]\epsilon} \le \|\Delta v^\epsilon\|_\epsilon^{[xy]\epsilon} \le A\epsilon.$$

Second, recalling the definition of $\|\cdot\|_h^{[xy]\epsilon}$, and using a Cauchy estimate (42), we obtain for given $\rho_{2k-1}^* > \rho^*$—yet to be determined—

$$\begin{aligned}\text{(II)} &= \epsilon \sum_{k=1}^{\ell} \left|\delta_\xi \Delta w^\epsilon\right|_{\eta_{2k-1}^*,\rho^*}^{[xy\xi]\epsilon} \le \epsilon \sum_{k=1}^{\ell} \left|\partial_\xi \Delta w^\epsilon\right|_{\eta_{2k-1}^*,\rho^*}^{[xy]\epsilon} \le \epsilon \sum_{k=1}^{\ell} \frac{|\Delta w^\epsilon|_{\eta_{2k-1}^*,\rho_{2k-1}^*}^{[xy]\epsilon}}{\rho_{2k-1}^* - \rho^*} \\ &\le \epsilon \left(\sum_{k=1}^{\ell} \frac{1}{(\rho_{2k-1}^* - \rho^*)\Lambda(\eta_{2k-1}^*, \rho_{2k-1}^*)} \right) \|\Delta w^\epsilon\|_{n\frac{\epsilon}{2}}^{[xy]\epsilon}. \end{aligned}$$

We make the particular choice

$$\rho_{2k-1}^* := \frac{\bar{\rho}}{2}\left(1 - \frac{\eta_{2k-1}^*}{h} + \frac{\rho^*}{\bar{\rho}}\right),$$

which yields that

$$\rho^*_{2k-1} - \rho^* = \frac{\bar\rho}{2}\left(1 - \frac{\eta^*_{2k-1}}{h} - \frac{\rho^*}{\bar\rho}\right),$$
$$\Lambda(\eta^*_{2k-1}, \rho^*_{2k-1}) = \frac{1 - \frac{\eta^*_{2k-1}}{h} - \frac{\rho^*_{2k-1}}{\bar\rho}}{1 - \frac{\rho^*_{2k-1}}{\bar\rho}} = \frac{1 - \frac{\eta^*_{2k-1}}{h} - \frac{\rho^*}{\bar\rho}}{1 + \frac{\eta^*_{2k-1}}{h} - \frac{\rho^*}{\bar\rho}}.$$

And so we obtain

$$\text{(II)} \le \frac{2}{\bar\rho}\left(1 + \frac{\eta^*}{h} - \frac{\rho^*}{\bar\rho}\right)\left(\epsilon \sum_{k=1}^{\ell}\left(1 - \frac{\eta^*_{2k-1}}{h} - \frac{\rho^*}{\bar\rho}\right)^{-2}\right) \|\Delta w^\epsilon\|^{[xy]\epsilon}_{n\frac{\epsilon}{2}}.$$

To estimate the sum above, define $\varphi : (\eta^*_0, \eta^*) \to \mathbb{R}$ by

$$\varphi(\eta) = \left(1 - \frac{\eta}{h} - \frac{\rho^*}{\bar\rho}\right)^{-2}.$$

Since φ is a convex function, Jensen's inequality implies that

$$\int_{\eta^*_{2k-2}}^{\eta^*_{2k}} \varphi(\eta)\,\mathrm{d}\eta \ge (\eta^*_{2k} - \eta^*_{2k-2})\varphi\left(\frac{1}{\eta^*_{2k} - \eta^*_{2k-2}}\int_{\eta^*_{2k-2}}^{\eta^*_{2k}} \eta\,\mathrm{d}\eta\right) = \epsilon\varphi(\eta^*_{2k-1}).$$

Hence the sum is bounded from above by the respective integral,

$$\begin{aligned}\epsilon\sum_{k=1}^{\ell}\left(1 - \frac{\eta^*_{2k-1}}{h} - \frac{\rho^*}{\bar\rho}\right)^{-2} &\le \int_{\eta^*_0}^{\eta^*_{2\ell}}\left(1 - \frac{\eta}{h} - \frac{\rho^*}{\bar\rho}\right)^{-2}\mathrm{d}\eta \\ &\le h\left(1 - \frac{\eta^*}{h} - \frac{\rho^*}{\bar\rho}\right)^{-1} = \frac{h}{\Lambda(\eta^*, \rho^*)\,(1 - \rho^*/\bar\rho)}.\end{aligned}$$

The last term (III) is estimated with the help of the bound (53). However, there is a subtlety: a priori, the constant G there is controlled in terms of $\left\{\{\theta^\epsilon - \theta\}\right\}_{n\frac{\epsilon}{2},0}$, but the induction estimate (54) is not sufficient to provide such a uniform bound, due to the weight Λ. Fortunately, a close inspection of the terms in (III) reveals in combination with (57) that we only need bounds on $|\tilde g^\epsilon_j|_{\eta,\rho}$ where $\rho/\bar\rho < 1 - \eta^*/h - \frac{\epsilon}{2}/h$. It is easily deduced from Lemma 5 that an ϵ-uniform estimate on $\left\{\{\theta^\epsilon - \theta\}\right\}_{n\frac{\epsilon}{2},\delta}$ with $\delta := \bar\rho/h\frac{\epsilon}{2} > 0$ suffices in this case, and the latter is obtained by combining (54) with (48). Enlarging G if necessary, we arrive at

$$\text{(III)} \le \epsilon^2 \sum_{k=1}^{\ell} G = (\epsilon\ell)\epsilon G \le Gh\epsilon.$$

After multiplication of (58) by $\Lambda(\eta^*, \rho^*) \leq 1$, we arrive at

$$\begin{aligned}\Lambda(\eta^*, \rho^*)\, |\Delta v^\epsilon|^{[xy]\epsilon}_{\eta^*,\rho^*} &\leq A\epsilon + \frac{2h}{\bar\rho}\frac{1+\eta^*/h-\rho^*/\bar\rho}{1-\rho^*/\bar\rho}\, \|\Delta w^\epsilon\|^{[xy]\epsilon}_{n\frac{\epsilon}{2}} + Gh\epsilon \\ &\leq \left(A + \frac{4h}{\bar\rho}B + Gh\right)\epsilon, \end{aligned} \tag{59}$$

where we have used the induction hypothesis (54) for estimation of $\|\Delta w^\epsilon\|^{[xy]\epsilon}_{n\frac{\epsilon}{2}}$, and the relation (57) for estimation of the quotient. We have just proven inequality (59) for every $\eta^* \in ((n-1)\frac{\epsilon}{2}, n\frac{\epsilon}{2}]$, and for every $\rho^* \geq 0$ that satisfies (57). Taking the supremum with respect to these quantities yields

$$\|\Delta v^\epsilon\|^{[xy]\epsilon}_{(n+1)\frac{\epsilon}{2}} \leq \left(A + \frac{4h}{\bar\rho}B + Gh\right)\epsilon. \tag{60}$$

Estimate on Δw^ϵ. For estimation of the w-component, let $\eta^* \in ((n-1)\frac{\epsilon}{2}, n\frac{\epsilon}{2}]$ be given as before, and define η^*_k as in (55). In analogy to (56), we have

$$\begin{aligned}\Delta w^\epsilon(\cdot,\eta^*) = \Delta w^\epsilon(\cdot,\eta^*_0) &+ \epsilon\sum_{k=1}^{\ell}\delta_\xi \Delta v^\epsilon(\cdot,\eta^*_{2k-1}) + \epsilon^2\sum_{k=1}^{\ell}\tilde g^\epsilon_2(\cdot,\eta^*_{2k-1}) \\ &+ \epsilon\sum_{k=1}^{\ell}\left(T_y^{-1}\mathfrak{k}^\epsilon\, T_x^{-1}\Delta\mathfrak{l}^\epsilon\right)(\cdot,\eta^*_{2k-1}) + \epsilon\sum_{k=1}^{\ell}\left(T_y^{-1}\Delta\mathfrak{k}^\epsilon\, T_x^{-1}\mathfrak{l}\right)(\cdot,\eta^*_{2k-1}).\end{aligned}$$

Taking the $|\cdot|^{[xy]\epsilon}_{\eta^*,\rho^*}$-norm on both sides, multiplying by $\Lambda(\eta^*,\rho^*) < 1$, and estimating the first couple of terms as above, we find that

$$\begin{aligned}&\Lambda(\eta^*,\rho^*)\left|\Delta w^\epsilon\right|^{[xy]\epsilon}_{\eta^*,\rho^*} \leq \left(A + \frac{4h}{\bar\rho}B + Gh\right)\epsilon \\ &+ \epsilon\sum_{k=1}^{\ell}\left(\left|\mathfrak{k}^\epsilon\right|^{[xxy]\epsilon}_{\eta^*_{2k-\frac32},\rho^*}\,\Lambda(\eta^*,\rho^*)\left|\Delta\mathfrak{l}^\epsilon\right|^{[xyy]\epsilon}_{\eta^*_{2k-\frac32},\rho^*} + \left|\mathfrak{l}\right|^{[xyy]\epsilon}_{\eta^*_{2k-\frac32},\rho^*}\,\Lambda(\eta^*,\rho^*)\left|\Delta\mathfrak{k}^\epsilon\right|^{[xxy]\epsilon}_{\eta^*_{2k-\frac32},\rho^*}\right) \\ &\leq \left(A + \frac{4h}{\bar\rho}B + Gh\right)\epsilon + \epsilon\sum_{k=1}^{\ell}\left(\left|\mathfrak{k}^\epsilon\right|^{[xxy]\epsilon}_{\eta^*_{2k-\frac32},\rho^*}\left\|\Delta\mathfrak{l}^\epsilon\right\|^{[xxy]\epsilon}_{n\frac{\epsilon}{2}} + \left|\mathfrak{l}\right|^{[xyy]\epsilon}_{\eta^*_{2k-\frac32},\rho^*}\left\|\Delta\mathfrak{k}^\epsilon\right\|^{[xxy]\epsilon}_{n\frac{\epsilon}{2}}\right).\end{aligned} \tag{61}$$

On the one hand, the analytic solution θ is bounded on $\widehat\Omega_{\bar\rho}(r|\bar h)$, and so

$$\|\mathfrak{k}\|^{[xxy]\epsilon}_{n\frac{\epsilon}{2}} \leq \Theta := \sup_{\widehat\Omega_{\bar\rho}(r|\bar h)}|\theta|. \tag{62}$$

On the other hand, since $\eta^*_{2k-\frac{3}{2}} \le \eta^* - \frac{3}{4}\epsilon$, and because of (57), we have that

$$\Lambda(\eta^*_{2k-\frac{3}{2}}, \rho^*) = \frac{1 - \eta^*_{2k-\frac{3}{2}}/h - \rho^*/\bar{\rho}}{1 - \rho^*/\bar{\rho}} \ge \frac{3}{4}\frac{\epsilon}{h},$$

and therefore, using the induction hypothesis (54),

$$|\mathfrak{k}^\epsilon|^{[xxy]\epsilon}_{\eta^*_{2k-\frac{3}{2}},\rho^*} \le |\mathfrak{k}|^{[xxy]\epsilon}_{\eta^*_{2k-\frac{3}{2}},\rho^*} + |\Delta\mathfrak{k}^\epsilon|^{[xxy]\epsilon}_{\eta^*_{2k-\frac{3}{2}},\rho^*} \le \sup_{\widehat{\Omega}_{\bar{\rho}}(r|\bar{h})} |\theta| + \frac{\|\Delta\mathfrak{k}^\epsilon\|^{[xxy]\epsilon}_{n\frac{\epsilon}{2}}}{\Lambda(\eta^*_{2k-\frac{3}{2}}, \rho^*)}$$
$$\le \Theta + \frac{B\epsilon}{(3\epsilon)/(4h)} = \Theta + \frac{4}{3}Bh. \qquad (63)$$

The remaining terms $\|\Delta\mathfrak{k}^\epsilon\|^{[xyy]\epsilon}_{n\frac{\epsilon}{2}}$ and $\|\Delta\mathfrak{l}^\epsilon\|^{[xyy]\epsilon}_{n\frac{\epsilon}{2}}$ in (61) can be estimated directly by (54). Substitution of these partial estimates into (61), and recalling that $\ell\epsilon \le h$, leads to

$$\Lambda(\eta^*, \rho^*)\,|\Delta\nu^\epsilon|^{[xy]\epsilon}_{\eta^*,\rho^*} \le \left(A + \left[\frac{4}{\bar{\rho}} + 2\Theta + \frac{4}{3}Bh\right]Bh + Gh\right)\epsilon. \qquad (64)$$

Estimate on $\Delta\mathfrak{k}^\epsilon$. Finally, let us estimate $\Delta\mathfrak{k}^\epsilon(\cdot, \eta^*)$ at some $\eta^* \in ((n - \frac{3}{2})\frac{\epsilon}{2}, (n - \frac{1}{2})\frac{\epsilon}{2}]$. For the estimates below, let in addition a $\xi^* \in \mathbb{C}$ be given such that $(\xi^*, \eta^*) \in \widehat{\Omega}^{[xxy]\epsilon}_{\bar{\rho}}(r|h)$. We need to use a slightly different normalization for the η^*_k in (55): write $\eta^* = \eta^*_{-\frac{1}{2}} + m\frac{\epsilon}{2}$ for suitable $\eta^*_{-\frac{1}{2}} \in (-\frac{\epsilon}{4}, \frac{\epsilon}{4}]$ and a (uniquely determined) $m \in \mathbb{N}$. Now define

$$\xi^*_k = \xi^* + (m - k + \frac{1}{2})\frac{\epsilon}{2}, \quad \eta^*_k = \eta^* - (m - k + \frac{1}{2})\frac{\epsilon}{2};$$

note that $\xi^* = \xi^*_{m-1/2}$ and $\eta^* = \eta^*_{m-\frac{1}{2}}$. With these notations:

$$\Delta\mathfrak{k}^\epsilon(\xi^*, \eta^*) = \Delta\mathfrak{k}^\epsilon(\xi^*_{-\frac{1}{2}}, \eta^*_{-\frac{1}{2}}) + \sum_{k=0}^{m-1}\left(\tau_y\Delta\mathfrak{k}^\epsilon - \tau_y^{-1}\Delta\mathfrak{k}^\epsilon\right)(\xi^*_k, \eta^*_k)$$
$$= \Delta\mathfrak{k}^\epsilon(\xi^*_{-\frac{1}{2}}, \eta^*_{-\frac{1}{2}}) + \epsilon\sum_{k=0}^{m-1}\mathfrak{l}^\epsilon(\xi^*_{k+\frac{1}{2}}, \eta^*_{k-\frac{1}{2}})\,\left(\Delta w^\epsilon(\xi^*_k, \eta^*_{k-1}) - \Delta v^\epsilon(\xi^*_{k+1}, \eta_k)\right)$$
$$+ \epsilon\sum_{k=0}^{m-1}\Delta\mathfrak{l}^\epsilon(\xi^*_{k+\frac{1}{2}}, \eta^*_{k-\frac{1}{2}})\,\left(w(\xi^*_k, \eta^*_{k-1}) - v(\xi^*_{k+1}, \eta^*_k)\right) + \epsilon^2\sum_{k=0}^{m-1}\tilde{g}^\epsilon_3(\xi^*_k, \eta^*_k).$$

It is straight-forward to verify that all the terms on the right-hand side are well-defined for the given arguments. For a given ρ^* that satisfies (57), we apply the semi-norm $|\cdot|^{[xxy]\epsilon}_{\eta^*,\rho^*}$ to both sides and estimate further, using the triangle inequality:

$$|\Delta \mathfrak{k}^\epsilon|^{[xxy]\epsilon}_{\eta^*,\rho^*} \leq |\Delta \mathfrak{k}^\epsilon|^{[xxy]\epsilon}_{\eta^*_{-\frac{1}{2}},\rho^*} + \epsilon \sum_{k=0}^{m-1} |\mathfrak{l}^\epsilon|^{[xxy]\epsilon}_{\eta^*_{k-\frac{1}{2}},\rho^*} \left(|\Delta w^\epsilon|^{[xy]\epsilon}_{\eta_{k-1},\rho^*} + |\Delta v^\epsilon|^{[xy]\epsilon}_{\eta_k,\rho^*} \right)$$
$$+ \epsilon \sum_{k=0}^{m-1} |\Delta \mathfrak{l}^\epsilon|^{[xxy]\epsilon}_{\eta^*_{k-\frac{1}{2}},\rho^*} \left(|w|^{[xy]\epsilon}_{\eta_{k-1},\rho^*} + |v|^{[xy]\epsilon}_{\eta^*_k,\rho^*} \right) + \epsilon^2 \sum_{k=0}^{m-1} |\tilde{g}^\epsilon_3|^{[xy]\epsilon}_{\eta^*_k,\rho^*}. \quad (65)$$

On the one hand, we have that

$$|w|^{[xy]\epsilon}_{\eta_{k-1},\rho^*} + |v|^{[xy]\epsilon}_{\eta_k,\rho^*} \leq \sup_{\widehat{\Omega}_{\bar{\rho}}(r|\bar{h})} |w| + \sup_{\widehat{\Omega}_{\bar{\rho}}(r|\bar{h})} |v| \leq 2\Theta,$$

with the bound Θ from (62). And on the other hand, arguing like in (63) on grounds of $\eta^*_{k-\frac{1}{2}} \leq \eta^* - \frac{3}{4}\epsilon$ for all $k = 0, \ldots, m-1$, we have the estimate

$$|\mathfrak{l}^\epsilon|^{[xxy]\epsilon}_{\eta^*_{k-\frac{1}{2}},\rho^*} \leq |\mathfrak{l}|^{[xxy]\epsilon}_{\eta^*_{k-\frac{1}{2}},\rho^*} + |\Delta \mathfrak{l}^\epsilon|^{[xxy]\epsilon}_{\eta^*_{k-\frac{1}{2}},\rho^*} \leq \Theta + \frac{4}{3}Bh.$$

Substitute this into (65) and multiply by $\Lambda(\eta^*, \rho^*)$ to obtain

$$\|\Delta \mathfrak{k}^\epsilon\|^{[xxy]\epsilon}_{(n+1)\frac{\epsilon}{2}} \leq \left(A + 4 \left[\Theta + \frac{1}{3}Bh \right] Bh + Gh \right) \epsilon. \quad (66)$$

Estimate on $\Delta \mathfrak{l}^\epsilon$. This is completely analogous to the estimate for $\Delta \mathfrak{k}^\epsilon$ above.

Summarizing the results in (60), (64) and (66), we obtain (54) with $n+1$ in place of n, for an arbitrary choice of $B > A$, and any corresponding $h > 0$ that is sufficiently small to make the coefficients in front of ϵ in (60), (64) and (66) smaller than B. Notice that the implied smallness condition on h is independent of ϵ.

5 The Continuous Limit of Discrete Isothermic Surfaces

We are finally in the position to formulate and prove our main approximation result.

5.1 *From Björling Data to Cauchy Data and Back*

Given analytic Björling data (f, n) in the sense of Theorem 1, first compute the associated frame Ψ^0, the conformal factor u^0, and the derived quantities v^0, w^0, $\mathfrak{k}^0$, $\mathfrak{l}^0$ as functions on $(-r, r)$ as detailed in the proof there. We claim that, for any sufficiently small $\epsilon > 0$, associated Björling data $f^\epsilon : \Omega(r|\frac{\epsilon}{2}) \to \mathbb{R}^3$ for construction of an ϵ-discrete isothermic surface can be prescribed such that the following are true:

(1) The initial surface piece and its tangent vectors are approximated to first order in ϵ,

$$\begin{aligned} f^\epsilon(\xi,\eta) &= f(\xi) + \mathscr{O}(\epsilon),\\ \delta_x f^\epsilon(\xi,\eta) &= \exp(u^0(\xi))\Psi_1^0(\xi) + \mathscr{O}(\epsilon),\\ \delta_y f^\epsilon(\xi,\eta) &= \exp(u^0(\xi))\Psi_2^0(\xi) + \mathscr{O}(\epsilon), \end{aligned} \tag{67}$$

where the $\mathscr{O}(\epsilon)$ indicate ϵ-smallness that is uniform in (ξ,η) on the domains $\Omega(r|\frac{\epsilon}{2})$ for f^ϵ, and $\Omega^{[x]\epsilon}(r|\frac{\epsilon}{2})$ for $\delta_x f^\epsilon$, and $\Omega^{[y]\epsilon}(r|\frac{\epsilon}{2})$ for $\delta_y f^\epsilon$, respectively.

(2) The derived quantities $(v^\epsilon, w^\epsilon, \mathfrak{k}^\epsilon, \mathfrak{l}^\epsilon)$ satisfy

$$v^\epsilon(\xi,\eta) = v^0(\xi), \quad \tilde{w}^\epsilon(\xi,\eta) = w^0(\xi), \quad \mathfrak{k}^\epsilon(\xi,\eta) = \mathfrak{k}^0(\xi), \quad \mathfrak{l}^\epsilon(\xi,\eta) = \mathfrak{l}^0(\xi), \tag{68}$$

at each point (ξ,η) in $\Omega^{[xy]\epsilon}(r|\epsilon)$ for $v^\epsilon, \tilde{w}^\epsilon$, in $\Omega^{[xxy]\epsilon}(r|\epsilon)$ for $\mathfrak{k}^\epsilon$, and in $\Omega^{[xyy]\epsilon}(r|\epsilon)$ for $\mathfrak{l}^\epsilon$, respectively.

Notice that the data $(v^\epsilon, w^\epsilon, \mathfrak{k}^\epsilon, \mathfrak{l}^\epsilon)$ are ξ-analytic quantities; ironically, one cannot even expect continuity of the respective data f^ϵ in general.

For later reference, we briefly sketch one possible construction of such data f^ϵ. We start by defining f^ϵ on point triples in the strip $-3\frac{\epsilon}{4} < \xi \le 3\frac{\epsilon}{4}$: let $(\xi,\eta) \in \Omega(r|\frac{\epsilon}{2})$ be a point with $-\frac{\epsilon}{4} < \xi \le \frac{\epsilon}{4}$. We distinguish two cases. If $0 < \eta \le \frac{\epsilon}{2}$, then we define $f^\epsilon(\xi, \eta - \frac{\epsilon}{2}) = f(0)$, and there is a unique way to assign data f^ϵ at the two points $(\xi - \frac{\epsilon}{2}, \eta)$ and $(\xi + \frac{\epsilon}{2}, \eta)$ such that for the vectors

$$a = \frac{1}{\epsilon}\big(f^\epsilon(\xi + \frac{\epsilon}{2}, \eta) - f^\epsilon(\xi, \eta - \frac{\epsilon}{2})\big), \quad b = \frac{1}{\epsilon}\big(f^\epsilon(\xi - \frac{\epsilon}{2}, \eta) - f^\epsilon(\xi, \eta - \frac{\epsilon}{2})\big),$$

the following is true:

(1) a is parallel to $\Psi_1^0(0)$, and b is orthogonal to $n(0)$,

(2) $\epsilon w^0(\xi) = \dfrac{\langle a, b\rangle}{\|a\|\|b\|}$,

(3) $\|a\| = \exp\big(u^0(0) + \frac{\epsilon}{2}v^0(\xi)\big)$ and $\|b\| = \exp\big(u^0(0) - \frac{\epsilon}{2}v^0(\xi)\big)$.

If instead $-\frac{\epsilon}{2} < \eta \le 0$, then we define $f^\epsilon(\xi, \eta + \frac{\epsilon}{2}) = f(0)$, and we assign data f^ϵ at $(\xi + \frac{\epsilon}{2}, \eta)$ and at $(\xi - \frac{\epsilon}{2}, \eta)$ with the respective adaptations for the conditions on the vectors.

Up to here, there has been a certain degree of freedom in the choice of the f^ϵ. From now on, there is a unique way to extend the already prescribed f^ϵ to all of $\Omega(r|\frac{\epsilon}{2})$ such that (68)—and, incidentally, also (67)—holds. We briefly indicate how to proceed in the next step; the further steps are then made inductively in the same way. Let (ξ,η) be a point with $3\frac{\epsilon}{4} < \xi \le 5\frac{\epsilon}{4}$, and with $-\frac{\epsilon}{2} < \eta \le 0$. Note that f^ϵ is already defined at the following points: $(\xi - \epsilon, \eta)$, $(\xi - \frac{\epsilon}{2}, \eta + \frac{\epsilon}{2})$ and $(\xi - 3\frac{\epsilon}{2}, \eta + \frac{\epsilon}{2})$. Let us introduce the vectors

$$a = \frac{1}{\epsilon}\big(f^\epsilon(\xi - \frac{\epsilon}{2}, \eta + \frac{\epsilon}{2}) - f^\epsilon(\xi - \epsilon, \eta)\big), \quad b = \frac{1}{\epsilon}\big(f^\epsilon(\xi - 3\frac{\epsilon}{2}, \eta + \frac{\epsilon}{2}) - f^\epsilon(\xi - \epsilon, \eta)\big).$$

Then, there is a unique choice for $f^\epsilon(\xi,\eta)$ such that the new vector

$$c = \frac{1}{\epsilon}\big(f^\epsilon(\xi - \frac{\epsilon}{2}, \eta + \frac{\epsilon}{2}) - f^\epsilon(\xi,\eta)\big)$$

satisfies the following conditions:

(1) the sin-value of the angle between the planes spanned by (a,b) and by (b,c), respectively, equals to $\epsilon \wp^0(\xi - 3\frac{\epsilon}{4})$,
(2) $\dfrac{\langle a,c\rangle}{\|a\|\|c\|} = \epsilon w^0(\xi - \dfrac{\epsilon}{2})$,
(3) $\|c\| = \|b\| \exp(\frac{\epsilon}{2} v^0(\xi - \frac{\epsilon}{2}))$.

By continuing this construction in an inductive manner, we enlarge the domain of definition with respect to ξ by $\frac{\epsilon}{2}$ in both directions in each step, until f^ϵ is defined on all of $\Omega(r|\frac{\epsilon}{2})$. It is obvious from the construction that (68) holds. The verification of (67) is a tedious but straight-forward exercise in elementary geometry that we leave to the interested reader. An important point is that the aforementioned construction only uses data that can be obtained very directly from the Björling data (f,n). Indeed, the calculation of u^0, Ψ^0 and $(v^0, w^0, \wp^0, \wp^0)$ from (f,n) only involves differentiation and inversion of matrices. In particular, all operations are local.

Definition 8 Assume that analytic Björling data (f,n) and discrete data $f^\epsilon : \Omega(r|\frac{\epsilon}{2})$ are given such that (67) and (68) are satisfied. The maximal ϵ-discrete isothermic surface $F^\epsilon : \Omega(r|h_\epsilon)$ that is obtained from f^ϵ as Björling data—see Proposition 1—is referred to as *grown from* (f,n).

5.2 Main Result

The central approximation result is the following.

Theorem 2 *Let analytic Björling data (f,n) on $(-r,r)$ be given, and let $F : \Omega(r|\bar{h}) \to \mathbb{R}^3$ be the corresponding real-analytic isothermic surface. Further, let $F^\epsilon : \Omega(r|h^\epsilon) \to \mathbb{R}^3$ be the family of ϵ-discrete isothermic surfaces that are grown from (f,n).*

Then, there are some $h > 0$ and $C > 0$, such that for all sufficiently small $\epsilon > 0$, we have that $h_\epsilon \geq h$, and

$$\|F^\epsilon(\xi,\eta) - F(\xi,\eta)\| \leq C\epsilon, \quad \|\delta_x F^\epsilon(\xi,\eta) - F_x(\xi,\eta)\| \leq C\epsilon, \quad \|\delta_y F^\epsilon(\xi,\eta) - F_y(\xi,\eta)\| \leq C\epsilon, \qquad (69)$$

for all $(\xi,\eta) \in \Omega^{[xy]\epsilon}(r|h)$.

Theorem 2 above gives an answer to the question of how to approximate the unique isothermic surface F that is determined by given Björling data by a family of ϵ-isothermic surfaces F^ϵ. Our construction of the surface F^ϵ is completely explicit,

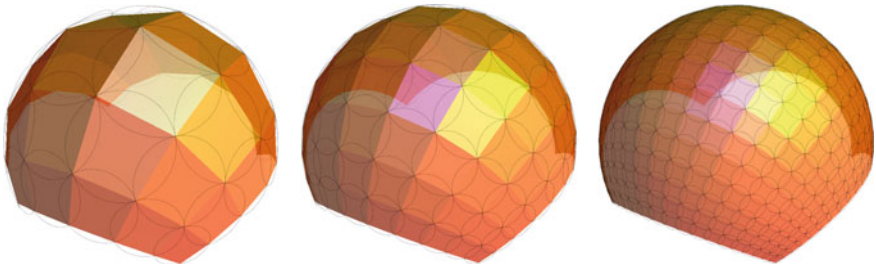

Fig. 5 A part of a sphere in different degrees of discretization

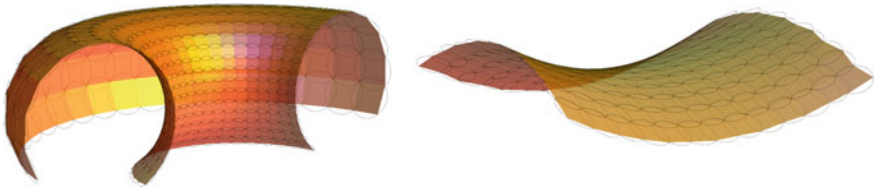

Fig. 6 Examples of discrete isothermic surfaces: torus (*left*), hyperbolic paraboloid (*right*)

and it requires no a priori knowledge about F. The plots in Figs. 5 and 6 illustrate that our construction can be used to generate pictures of the surfaces F^ϵ with just a few lines of code.

Remark 7 Note that if the discrete isothermic surfaces F^ϵ converge to a smooth isothermic surface F, then also the discrete Christoffel and Darboux transforms of F^ϵ converge to the corresponding smooth Christoffel and Darboux transforms of F. This will be proven in Sect. 6.

Proof (of Theorem 2) Since F is real-analytic on $\Omega(r|\bar{h})$, the derived quantities u, v, w and $\mathfrak{k}, \mathfrak{l}$ are real-analytic there as well, and can be extended to functions in $C^\omega\big(\widehat{\Omega}(r|\bar{h})\big)$, for a suitable choice of the "fattening parameter" $\bar{\rho} > 0$, after diminishing $\bar{h} > 0$ if necessary. The extensions satisfy the Gauss-Codazzi system (9)–(12) on the complexified domain.

Next, consider the ϵ-discrete isothermic surfaces $F^\epsilon : \Omega(r|h_\epsilon) \to \mathbb{R}$ that are grown from the Björling data (f, n). Define the associated quantities $v^\epsilon, w^\epsilon, \mathfrak{k}^\epsilon, \mathfrak{l}^\epsilon$. Thanks to (68), these are real analytic functions on $\Omega^{[xy]_\epsilon}(r|\epsilon)$, and they extend complex-analytically w.r.t. ξ to $\widehat{\Omega}^{[xy]_\epsilon}_{\bar{\rho}}(r|\epsilon)$. Since the quadruple $(v^\epsilon, w^\epsilon, \mathfrak{k}^\epsilon, \mathfrak{l}^\epsilon)$ satisfies the discrete Gauss-Codazzi equations (31)–(34), the ξ-analyticity is propagated from the initial strip to the maximal domain of existence, i.e., $v^\epsilon, w^\epsilon \in C^\omega\big(\widehat{\Omega}^{[xy]_\epsilon}(r|h_\epsilon)\big)$ etc.

Moreover, again thanks to (68), the differences Δv^ϵ, $\Delta \mathfrak{k}^\epsilon$ and $\Delta \mathfrak{l}^\epsilon$ are of order $\mathcal{O}(\epsilon)$ on the initial strip:

$$\|\Delta v^\epsilon\|_\epsilon^{[xy]_\epsilon} \leq A\epsilon, \quad \|\Delta \mathfrak{k}^\epsilon\|_\epsilon^{[xxy]_\epsilon} \leq A\epsilon, \quad \|\Delta \mathfrak{l}^\epsilon\|_\epsilon^{[xyy]_\epsilon} \leq A\epsilon,$$

with a suitable ϵ-independent constant A. For the remaining differences Δw^ϵ, it follows via Lemma 3 on the equivalence of (v^ϵ, w^ϵ) and $(\tilde{v}^\epsilon, \tilde{w}^\epsilon)$ that they satisfy the same estimate (enlarging A if necessary):

$$\|\Delta w^\epsilon\|_\epsilon^{[xy]_\epsilon} \leq A\epsilon.$$

We are thus in the situation to apply Proposition 3. From the estimate (47), it follows in particular that

$$v^\epsilon = v + \mathscr{O}(\epsilon), \quad w^\epsilon = w + \mathscr{O}(\epsilon), \quad \mathfrak{k}^\epsilon = \mathfrak{k} + \mathscr{O}(\epsilon), \quad \mathfrak{l}^\epsilon = \mathfrak{l} + \mathscr{O}(\epsilon). \tag{70}$$

Here and below, we use the slightly ambiguous notation $\mathscr{O}(\epsilon)$ to express that the discrete quantities approximate the associated continuous ones uniformly on their respective (real) domains $\Omega^{[xy]_\epsilon}(r|h_\epsilon)$ or $\Omega^{[xxy]_\epsilon}(r|h_\epsilon)$, $\Omega^{[xyy]_\epsilon}(r|h_\epsilon)$, with a maximal error of order ϵ.

Next, we conclude from (70) that also

$$a^\epsilon = a + \mathscr{O}(\epsilon), \quad b^\epsilon = b + \mathscr{O}(\epsilon), \quad \hat{u}^\epsilon = u + \mathscr{O}(\epsilon), \quad \check{u}^\epsilon = u + \mathscr{O}(\epsilon). \tag{71}$$

Indeed, it follows directly from the definition of these quantities that (71) implies

$$\delta_x F^\epsilon = \exp(\hat{u}^\epsilon) a^\epsilon = \exp\big(u + \mathscr{O}(\epsilon)\big)\big(a + \mathscr{O}(\epsilon)\big) = \exp(u)a + \mathscr{O}(\epsilon) = \partial_x F + \mathscr{O}(\epsilon),$$

and, likewise, $\delta_y F^\epsilon = \partial_y F + \mathscr{O}(\epsilon)$, which, eventually, implies further that also $F^\epsilon = F + \mathscr{O}(\epsilon)$, thanks to $F^\epsilon(\xi, \eta) = F(0)$ for $-\frac{\epsilon}{4} < \xi < \frac{\epsilon}{4}$ and $-\frac{\epsilon}{2} < \eta \leq \frac{\epsilon}{2}$ by construction. Therefore, our claim (69) is a consequence of (71).

We only sketch the proof of (71), that is little more than a repeated application of the Gronwall lemma. For further technical details, we refer the reader to [2], where the relevant estimates have been carried out in a very similar situation, see the proof of Theorem 5.4 therein.

First of all, the claim (71) holds on the strip $\Omega^{[xy]_\epsilon}(r|\epsilon)$ thanks to (67). Now compare the frame equations (6) & (7) with their discrete analogs from (28)–(30):

$$\begin{aligned}
&\partial_x u = w + v \quad \text{and} \quad \delta_x \check{u}^\epsilon = w^\epsilon + v^\epsilon,\\
&\partial_y u = w - v \quad \text{and} \quad \delta_y \hat{u}^\epsilon = w^\epsilon - v^\epsilon,\\
&\partial_x b = (w - v)(T_y^{-1} a + \mathscr{O}(\epsilon)) \quad \text{and} \quad \delta_x b^\epsilon = (w^\epsilon - v^\epsilon + \mathscr{O}(\epsilon)) T_y^{-1} a^\epsilon + \mathscr{O}(\epsilon) T_x^{-1} b^\epsilon,\\
&\partial_y a = (w - v)(T_x^{-1} b + \mathscr{O}(\epsilon)) \quad \text{and} \quad \delta_y a^\epsilon = (w^\epsilon - v^\epsilon + \mathscr{O}(\epsilon)) T_x^{-1} b^\epsilon + \mathscr{O}(\epsilon) T_y^{-1} a^\epsilon.
\end{aligned}$$

Subtract the respective equations, recall (70), and use a standard Gronwall argument to conclude that the validity of (71) extends from the "initial strip" to the entire domain $\Omega^{[xxyy]_\epsilon}(r|h)$.

A posteriori, we conclude that $h_\epsilon \uparrow h$ as $\epsilon \downarrow 0$. where $h > 0$ is the constant obtained in the proof of Proposition 3. Indeed, thanks to the uniform closeness of the discrete tangent vectors $\delta_x F^\epsilon$, $\delta_y F^\epsilon$ to their continuous counterparts $\partial_x F$, $\partial_y F$—

which are orthogonal with non-vanishing length—it easily follows that there cannot occur any degeneracies in F^ϵ at any $h^\epsilon < h$. □

6 Transformations

Isothermic surfaces have an exceptionally rich transformation theory. For the definition of discrete isothermic surfaces used in this paper this transformation theory carries over to the discrete setup.

We consider two important transformations, namely the Christoffel transformation and Darboux transformation. Their analogs for discrete isothermic surfaces may for example be found in [3, 4, 14–16]. It is a natural question whether the convergence results of Theorem 2 can be generalized to imply the convergence of the transformed surfaces.

6.1 Christoffel Transformation

We briefly remind the classical definition of the Christoffel transformation. The included existence claim was first proved by Christoffel [10].

Definition 9 Let $F : \Omega(r|h) \to \mathbb{R}^3$ be an isothermic surface. Then the $\mathbb{R}^3$-valued one-form $dF^\star$ defined by

$$F^\star_x = \frac{F_x}{\|F_x\|^2}, \qquad F^\star_y = -\frac{F_y}{\|F_y\|^2},$$

is closed. The surface $F^\star : \Omega(r|h) \to \mathbb{R}^3$, defined (up to translation) by integration of this one-form, is isothermic and is called *dual* to the surface F or *Christoffel transform* of the surface F.

Given any isothermic surface F and its dual $F^\star$, straightforward calculation leads to the following relations between corresponding quantities.

$$F^\star_x = \mathrm{e}^{-2u} F_x, \qquad F^\star_y = -\mathrm{e}^{-2u} F_y, \qquad N^\star = -N,$$
$$u^\star = -u, \qquad v^\star = -v, \qquad w^\star = -w, \qquad \mathfrak{k}^\star = -\mathfrak{k}, \qquad \mathfrak{l}^\star = \mathfrak{l}.$$

The discrete case is nearly the same, see for example [3].

Definition 10 Let $F^\epsilon : \Omega(r|h) \to \mathbb{R}^3$ be a discrete isothermic surface. Then the $\mathbb{R}^3$-valued discrete one-form $\delta(F^\star)^\epsilon$ defined by

$$\delta_x(F^\star)^\epsilon = \frac{\delta_x F^\epsilon}{\|\delta_x F^\epsilon\|^2}, \qquad \delta_y(F^\star)^\epsilon = -\frac{\delta_y F^\epsilon}{\|\delta_y F^\epsilon\|^2},$$

is closed. The surface $(F^\star)^\epsilon : \Omega(r|h) \to \mathbb{R}^3$, defined (up to translation) by integration of this discrete one-form, is a discrete isothermic surface and is called *dual* to F^ϵ or *Christoffel transform* of F^ϵ.

Corollary 1 *Under the assumptions of Theorem 2 not only the discrete isothermic surface itself converges to the corresponding smooth isothermic surface, but also the discrete Christoffel transforms converge to the corresponding Christoffel transforms of the smooth isothermic surface.*

Proof Recall the definitions of the discrete quantities in Sect. 3.4. We immediately deduce the following relations for a discrete isothermic surface F^ϵ and its dual $(F^\star)^\epsilon$. For better reading we omit the superscript ϵ.

$$a^\star = a, \quad b^\star = -b, \quad \hat{u}^\star = -\hat{u}, \quad \check{u}^\star = -\check{u}, \quad N^\star = -N,$$
$$\tilde{v}^\star = -\tilde{v}, \quad \tilde{w}^\star = -\tilde{w}, \quad v^\star = -v, \quad w^\star = -w, \quad \mathfrak{k}^\star = -\mathfrak{k}, \quad \mathfrak{l}^\star = \mathfrak{l}.$$

Now the proof follows directly from the corresponding proofs in Sects. 4 and 5. □

6.2 Darboux Transformation

The Darboux transformation for isothermic surfaces was introduced by Darboux [12]. It is a special case of a Ribaucour transformation and is closely connected to Möbius geometry as well as to the integrable system approach to isothermic surfaces, see for example [15].

Definition 11 Let $F : \Omega(r|h) \to \mathbb{R}^3$ be an isothermic surface. Then the isothermic surface $F^+ : \Omega(r|h) \to \mathbb{R}^3$ is called a *Darboux transform* of F if

$$F_x^+ = -\frac{\|F^+ - F\|^2}{C\|F_x\|^2}\left(F_x - 2\langle F_x, \frac{F^+ - F}{\|F^+ - F\|}\rangle \frac{F^+ - F}{\|F^+ - F\|}\right),$$
$$F_y^+ = \frac{\|F^+ - F\|^2}{C\|F_y\|^2}\left(F_y - 2\langle F_y, \frac{F^+ - F}{\|F^+ - F\|}\rangle \frac{F^+ - F}{\|F^+ - F\|}\right),$$

where $C \in \mathbb{R}$, $C \neq 0$, is a constant which is called *parameter of the Darboux transformation*.

In the discrete case the definition of the Darboux transformation may be interpreted as "discrete Ribaucour transformation" using intersecting instead of touching spheres.

In particular, recall the definition of the cross-ratio $q(p_1, p_2, p_3, p_4)$ of four coplanar points $p_1, \ldots, p_4$. After identification of their common plane with the complex plane $\mathbb{C}$ the cross-ratio may be calculated by the formula

$$q(p_1, p_2, p_3, p_4) := (p_1 - p_2)(p_2 - p_3)^{-1}(p_3 - p_4)(p_4 - p_1)^{-1}$$

The following definition first appeared in [16], see also [4, 15].

Definition 12 Let $F^\epsilon : \Omega(r|h) \to \mathbb{R}^3$ be a discrete isothermic surface. Then the discrete isothermic surface $(F^+)^\epsilon : \Omega(r|h) \to \mathbb{R}^3$ is called a *discrete Darboux transform* of F^ϵ if the following conditions are satisfied.

(i) The four points $\tau_x^{-1}F^\epsilon, \tau_x F^\epsilon, \tau_x^{-1}(F^+)^\epsilon, \tau_x(F^+)^\epsilon$ lie in a common plane and the same is true for $\tau_y^{-1}F^\epsilon, \tau_y F^\epsilon, \tau_y^{-1}(F^+)^\epsilon, \tau_y(F^+)^\epsilon$.

(ii) $q(\tau_x^{-1}F^\epsilon, \tau_x F^\epsilon, \tau_x(F^+)^\epsilon, \tau_x^{-1}(F^+)^\epsilon) = \dfrac{1}{\gamma}$ and

$q(\tau_y^{-1}F^\epsilon, \tau_y F^\epsilon, \tau_y(F^+)^\epsilon, \tau_y^{-1}(F^+)^\epsilon) = -\dfrac{1}{\gamma}$, where $\gamma \in \mathbb{R}, \gamma \neq 0$ is a constant which is called *parameter of the Darboux transformation*.

Note that given any discrete isothermic surface, a discrete Darboux transform may be obtained by prescribing the value of $(F^+)^\epsilon$ at one point and using the conditions of the definition to successively build a new surface which is also discrete isothermic (as long as the surface does not degenerate).

In order to obtain convergence of the discrete Darboux transform to the corresponding continuous one, we choose $\gamma = C/\epsilon^2$.

Corollary 2 *Under the assumptions of Theorem 2 not only the discrete isothermic surface itself converges to the corresponding smooth isothermic surface, but also the discrete Darboux transforms (with $\gamma = C/\epsilon^2$) converge to the corresponding Darboux transforms (with parameter C) of the smooth isothermic surface.*

Proof Assume that the discrete isothermic surface itself converges to the corresponding smooth isothermic surface with errors of order $\mathcal{O}(\epsilon)$ as in the proofs of Theorem 2. Now start with $(F^+)^\epsilon(0, 0) = F^+(0, 0)$ and build the discrete Darboux transform successively using the above definition. Denote the distance between corresponding points by $d^\epsilon = (F^+)^\epsilon - F^\epsilon$.

In order to relate corresponding discrete and smooth quantities, we first use the simple equivalence

$$\frac{(p_2 - p_1)(p_4 - p_3)}{(p_3 - p_2)(p_1 - p_4)} = \frac{1}{q} \quad \Longleftrightarrow \quad p_3 - p_2 = \frac{(p_4 - p_1) - (p_2 - p_1)}{1 - q\frac{(p_4 - p_1)}{(p_2 - p_1)}}. \tag{72}$$

Then we use the fact that in our case $(p_2 - p_1) = \mathcal{O}(\epsilon)$ and $q = C/\epsilon^2$. Thus we obtain that

$$p_3 - p_2 = \frac{(p_4 - p_1) - \epsilon\frac{(p_2-p_1)}{\epsilon}}{1 - \frac{\epsilon^2(p_4-p_1)}{C(p_2-p_1)}} = (p_4 - p_1) + \epsilon\left(\frac{(p_4 - p_1)^2}{C\frac{(p_2-p_1)}{\epsilon}} - \frac{(p_2 - p_1)}{\epsilon}\right) + \mathcal{O}(\epsilon^2).$$

Now we identify

$$(p_3 - p_2) = \tau_x d^\epsilon, \quad (p_4 - p_1) = \tau_x^{-1} d^\epsilon, \quad \frac{(p_2 - p_1)}{\epsilon} = \delta_x F^\epsilon$$

and easily deduce by straightforward identifications of complex numbers and vectors that

$$\begin{aligned}\frac{\tau_x d^\epsilon - \tau_x^{-1} d^\epsilon}{\epsilon} &= \frac{1}{C\|\delta_x F^\epsilon\|^2}(-\|\tau_x^{-1} d^\epsilon\|^2 \delta_x F^\epsilon + 2\tau_x^{-1} d^\epsilon \langle \tau_x^{-1} d^\epsilon, \delta_x F^\epsilon\rangle) - \delta_x F^\epsilon + \mathcal{O}(\epsilon) \\ &= F_x^+ - F_x + \mathcal{O}(\epsilon).\end{aligned}$$

Analogously, we obtain

$$\begin{aligned}\frac{\tau_y d^\epsilon - \tau_y^{-1} d^\epsilon}{\epsilon} &= \frac{1}{C\|\delta_y F^\epsilon\|^2}(\|\tau_y^{-1} d^\epsilon\|^2 \delta_y F^\epsilon - 2\tau_y^{-1} d^\epsilon \langle \tau_y^{-1} d^\epsilon, \delta_y F^\epsilon\rangle) - \delta_y F^\epsilon + \mathcal{O}(\epsilon) \\ &= F_y^+ - F_y + \mathcal{O}(\epsilon).\end{aligned}$$

Thus starting with $(F^+)^\epsilon(0, 0) = F^+(0, 0)$ and building the discrete Darboux transform successively using the above definition, in each step we add an error of order $\mathcal{O}(\epsilon^2)$ to the difference $d = F^+ - F$ of the Darboux pair. Therefore we obtain $(F^+)^\epsilon = F^+ + \mathcal{O}(\epsilon)$ as claimed. □

Remark 8 Using the definitions of continuous and discrete Darboux transformations, corresponding formulas for a^+, b^+, $\hat{u}^+$, $\check{u}^+$, N^+, $\tilde{v}^+$, $\tilde{w}^+$, v^+, w^+, $\mathfrak{k}^+$, $\mathfrak{l}^+$ may be deduced, which also converge under the assumptions of Theorem 2.

Acknowledgments The authors would like to thank Sepp Dorfmeister and Fran Burstall for stimulating and helpful discussions. We further thank the anonymous referee for the careful reading of the initial manuscript and various suggestions for improvement. This research was supported by the DFG Collaborative Research Center TRR 109 "Discretization in Geometry and Dynamics".

References

1. Bobenko, A.I., Matthes, D., Suris, Y.B.: Discrete and smooth orthogonal systems: C^∞-approximation. Int. Math. Res. Not. **45**, 2415–2459 (2003)
2. Bobenko, A.I., Matthes, D., Suris, Y.B.: Nonlinear hyperbolic equations in surface theory: integrable discretizations and approximation results. St. Petersburg Math. J. **17**, 39–61 (2006)
3. Bobenko, A.I., Pinkall, U.: Discrete isothermic surfaces. J. reine angew. Math. **475**, 187–208 (1996)
4. Bobenko, A.I., Suris, Y.B.: Discrete differential geometry. Integrable structure. In: Graduate Studies in Mathematics, vol. 98. AMS (2008)
5. Brander, D., Dorfmeister, J.F.: The Björling problem for non-minimal constant mean curvature surfaces. Commun. Anal. Geom. **18**(1), 171–194 (2010)
6. Bücking, U.: Approximation of conformal mapping by circle patterns. Geom. Dedicata **137**, 163–197 (2008)
7. Burstall, F.: Isothermic surfaces: conformal geometry, Clifford algebras and integrable systems. In: Terng, C.L. (ed.) Integrable Systems, Geometry and Topology, AMS/IP Studies in Advanced Math., vol. 36, pp. 1–82. American Mathematical Society (2006)
8. Burstall, F., Hertrich-Jeromin, U., Pedit, F., Pinkall, U.: Curved flats and isothermic surfaces. Math. Z. **225**(2), 199–209 (1997)
9. Cayley, A.: On the determination of the surfaces divisible into squares by means of their curves of curvature. Proc. London Math. Soc. **4**, 8–9 (1872)
10. Christoffel, E.: Ueber einige allgemeine Eigenschaften der Minimumsflächen. Crelles J. **67**, 218–228 (1867)
11. Cieśliński, J., Goldstein, P., Sym, A.: Isothermic surfaces in $\mathbf{E}^3$ as soliton surfaces. Phys. Lett. A **205**(1), 37–43 (1995)
12. Darboux, G.: Sur les surfaces isothermiques. Comptes Rendus **128**(1299–1305), 1538 (1899)
13. Dierkes, U., Hildebrandt, S., Küster, A., Wohlrab, O.: Minimal surfaces. I, Grundlehren der Mathematischen Wissenschaften [Fundamental Principles of Mathematical Sciences], vol. 295. Springer-Verlag, Berlin (1992)
14. Hertrich-Jeromin, U.: Transformations of discrete isothermic nets and discrete cmc-1 surfaces in hyperbolic space. Manuscr. Math. **102**, 465–486 (2000)
15. Hertrich-Jeromin, U.: Introduction to Möbius differential geometry. In: London Mathematical Society Lecture Note Series, vol. 300. Cambridge University Press, Cambridge (2003)
16. Hertrich-Jeromin, U., Hoffmann, T., Pinkall, U.: A discrete version of the Darboux transform for isothermic surfaces. In: Bobenko, A.I., Seiler, R. (eds.) Discrete Integrable Geometry and Physics. Oxford Lecture Ser. Math. Appl, vol. 16, pp. 59–81. Clarendon Press, Oxford (1999)
17. Matthes, D.: Convergence in discrete Cauchy problems and applications to circle patterns. Conform. Geom. Dyn. **9**, 1–23 (2005)
18. Nagumo, M.: Über das Anfangswertproblem partieller Differentialgleichungen. Jap. J. Math. **18**, 41–47 (1942)
19. Nirenberg, L.: An abstract form of the nonlinear Cauchy-Kowalewski theorem. J. Differ. Geom. **6**, 561–576 (1972)
20. Schief, W.K.: Isothermic surfaces in spaces of arbitrary dimension: integrability, discretization, and Bäcklund transformations - a discrete Calapso equation. Stud. Appl. Math. **106**(1), 85–137 (2001)
21. Schramm, O.: Circle patterns with the combinatorics of the square grid. Duke Math. J. **86**(2), 347–389 (1997)
22. Stephenson, K.: Introduction to circle packing: the theory of discrete analytic functions. Cambridge University Press, New York (2005)
23. Walter, W.: An elementary proof of the Cauchy-Kowalevsky theorem. Amer. Math. Monthly **92**(2), 115–126 (1985)
24. Weingarten, J.: Über die Differentialgleichung der Oberflächen, welche durch ihre Krümmungslinien in unendlich kleine Quadrate geteilt werden können. Sitzungsber. königl. preuß. Akad. Wiss. pp. 1163–1166 (1883)

On the Lagrangian Structure of Integrable Hierarchies

Yuri B. Suris and Mats Vermeeren

Abstract We develop the concept of pluri-Lagrangian structures for integrable hierarchies. This is a continuous counterpart of the pluri-Lagrangian (or Lagrangian multiform) theory of integrable lattice systems. We derive the multi-time Euler Lagrange equations in their full generality for hierarchies of two-dimensional systems, and construct a pluri-Lagrangian formulation of the potential Korteweg-de Vries hierarchy.

1 Introduction

In this paper, our departure point are two developments which have taken place in the field of discrete integrable systems in recent years.

- Firstly, multi-dimensional consistency of lattice systems has been proposed as a notion of integrability [8, 15]. In retrospect, this notion can be seen as a discrete counterpart of the well-known fact that integrable systems never appear alone but are organized into integrable *hierarchies*. Based on the notion of multi-dimensional consistency, a classification of two-dimensional integrable lattice systems (the so called ABS list) was given in [1]. Moreover, for all equations of the ABS list, considered as equations on $\mathbb{Z}^2$, a variational interpretation was found in [1].
- Secondly, the idea of the multi-dimensional consistency was blended with the variational formulation in [13], where it was shown that solutions of any ABS equation on any quad surface Σ in $\mathbb{Z}^N$ are critical points of a certain action functional $\int_\Sigma \mathscr{L}$ obtained by integration of a suitable discrete Lagrangian two-form $\mathscr{L}$. Moreover, it was observed in [13] that the critical value of the action remains invariant under local changes of the underlying quad-surface, or, in other words, that the 2-form $\mathscr{L}$ is closed on solutions of quad-equations, and it was suggested to consider this as a defining feature of integrability. However, later research [10] revealed that

Y.B. Suris (✉) · M. Vermeeren
Inst. für Mathematik, Technische Universität Berlin, Straße des 17. Juni 136,
10623 Berlin, Germany
e-mail: suris@math.tu-berlin.de

M. Vermeeren
e-mail: vermeer@math.tu-berlin.de

A.I. Bobenko (ed.), *Advances in Discrete Differential Geometry*,
DOI 10.1007/978-3-662-50447-5_11

$\mathscr{L}$ is closed not only on solutions of (non-variational) quad-equations, but also on general solutions of the corresponding Euler-Lagrange equations. Therefore, at least for discrete systems, the closedness condition is implicitly contained in the variational formulation.

A general theory of multi-time one-dimensional Lagrangian systems, both discrete and continuous, has been developed in [20]. A first attempt to formulate the theory for continuous two-dimensional systems was made in [21]. For such systems, a solution is a critical point of the action functional $\int_S \mathscr{L}$ on any two-dimensional surface S in $\mathbb{R}^N$, where $\mathscr{L}$ is a suitable differential two-form. The treatment in [21] was restricted to second order Lagrangians, i.e. to two-forms $\mathscr{L}$ that only depend on the second jet bundle. In the present work we will extend this to Lagrangians of any order.

As argued in [10], the unconventional idea to consider the action on arbitrary two-dimensional surfaces in the multi-dimensional space of independent variables has significant precursors. These include:

- *Theory of pluriharmonic functions* and, more generally, of pluriharmonic maps [11, 17, 19]. By definition, a pluriharmonic function of several complex variables $f : \mathbb{C}^N \to \mathbb{R}$ minimizes the Dirichlet functional $E_\Gamma = \int_\Gamma |(f \circ \Gamma)_z|^2 dz \wedge d\bar{z}$ along any holomorphic curve in its domain $\Gamma : \mathbb{C} \to \mathbb{C}^N$. Differential equations governing pluriharmonic functions,

$$\frac{\partial^2 f}{\partial z_i \partial \bar{z}_j} = 0 \qquad \text{for all} \qquad i, j = 1, \dots, N,$$

  are heavily overdetermined. Therefore it is not surprising that pluriharmonic functions (and maps) belong to the theory of integrable systems.
  This motivates the term *pluri-Lagrangian systems*, which was proposed in [9, 10].
- *Baxter's Z-invariance* of solvable models of statistical mechanics [3, 4]. This concept is based on invariance of the partition functions of solvable models under elementary local transformations of the underlying planar graphs. It is well known (see, e.g., [7]) that one can identify planar graphs underlying these models with quad-surfaces in $\mathbb{Z}^N$. On the other hand, the classical mechanical analogue of the partition function is the action functional. This suggests the relation of Z-invariance to the concept of closedness of the Lagrangian 2-form, at least at the heuristic level. This relation has been made mathematically precise for a number of models, through the quasiclassical limit [5, 6].
- The classical notion of *variational symmetry*, going back to the seminal work of E. Noether [16], has been shown to be directly related to the closedness of the Lagrangian form in the multi-time [21].

The main goal of this paper is two-fold: to derive the Euler Lagrange equations for two-dimensional pluri-Lagrangian problems of arbitrary order, and to state the (potential) KdV hierarchy as a pluri-Lagrangian system. We will also discuss the closedness of the Lagrangian two-form, which turns out to be related to the Hamiltonian theory of integrable hierarchies.

Note that the influential monograph [12], according to the foreword, is "about hierarchies of integrable equations rather than about individual equations". However, its Lagrangian part (Chaps. 19, 20) only deals with individual equations. The reason for this is apparently the absence of the concept of pluri-Lagrangian systems. We hope that this paper opens up the way for a variational approach to integrable hierarchies.

2 Pluri-Lagrangian Systems

2.1 Definition

We place our discussion in the formalism of the variational bicomplex as presented in [12, Chap. 19] (and summarized, for the reader's convenience, in Appendix A). Slightly different versions of this theory can be found in [18] and in [2].

Consider a vector bundle $X : \mathbb{R}^N \to \mathbb{R}$ and its nth jet bundle $J^n X$. Let $\mathscr{L} \in \mathscr{A}^{(0,d)}(J^n X)$ be a smooth horizontal d-form. In other words, $\mathscr{L}$ is a d-form on $\mathbb{R}^N$ whose coefficients depend on a function $u : \mathbb{R}^N \to \mathbb{R}$ and its partial derivatives up to order n. We call $\mathbb{R}^N$ the *multi-time*, u the *field*, and $\mathscr{L}$ the *Lagrangian d-form*. We will use coordinates $(t_1, \dots, t_N)$ on $\mathbb{R}^N$. Recall that in the standard calculus of variations the Lagrangian is a *volume form*, so that $d = N$.

Definition 2.1 We say that the field u solves the *pluri-Lagrangian problem* for $\mathscr{L}$ if u is a critical point of the action $\int_S \mathscr{L}$ simultaneously for all d-dimensional surfaces S in $\mathbb{R}^N$. The equations describing this condition are called the *multi-time Euler-Lagrange equations*. We say that they form a *pluri-Lagrangian system* and that $\mathscr{L}$ is a *pluri-Lagrangian structure* for these equations.

To discuss critical points of a pluri-Lagrangian problem, consider the *vertical derivative* $\delta\mathscr{L}$ of the (0,d)-form $\mathscr{L}$ in the variational bicomplex, and a *variation* $\mathscr{V}$. Note that we consider variations $\mathscr{V}$ as vertical vector fields; such a restriction is justified by our interest, in the present paper, in autonomous systems only. Besides, in the context of discrete systems only vertical vector fields seem to possess a natural analogs. The criticality condition of the action, $\delta \int_S \mathscr{L} = 0$, is described by the equation

$$\int_S \iota_{\mathrm{pr}\,\mathscr{V}}\, \delta\mathscr{L} = 0, \tag{1}$$

which has to be satisfied for any variation $\mathscr{V}$ on S that vanishes at the boundary ∂S. Recall that $\mathrm{pr}\,\mathscr{V}$ is the nth jet prolongation of the vertical vector field $\mathscr{V}$, and that ι stands for the contraction. One fundamental property of critical points can be established right from the outset.

Proposition 2.2 *The exterior derivative* $\mathrm{d}\mathscr{L}$ *of the Lagrangian is constant on critical points u.*

Proof Consider a critical point u and a small $(d+1)$-dimensional ball B. Because $S := \partial B$ has no boundary, Eq. (1) is satisfied for any variation $\mathscr{V}$. Using Stokes' theorem and the properties that $\delta \mathrm{d} + \mathrm{d}\delta = 0$ and $\iota_{\mathrm{pr}\,\mathscr{V}}\,\mathrm{d} + \mathrm{d}\,\iota_{\mathrm{pr}\,\mathscr{V}} = 0$ (Propositions A.1 and A.4 in Appendix A), we find that

$$0 = \int_{\partial B} \iota_{\mathrm{pr}\,\mathscr{V}}\,\delta\mathscr{L} = \int_B \mathrm{d}(\iota_{\mathrm{pr}\,\mathscr{V}}\,\delta\mathscr{L}) = -\int_B \iota_{\mathrm{pr}\,\mathscr{V}}\,\mathrm{d}(\delta\mathscr{L}) = \int_B \iota_{\mathrm{pr}\,\mathscr{V}}\,\delta(\mathrm{d}\mathscr{L}).$$

Since this holds for any ball B it follows that $\iota_{\mathrm{pr}\,\mathscr{V}}\,\delta(\mathrm{d}\mathscr{L}) = 0$ for any variation $\mathscr{V}$ of a critical point u. Therefore, $\delta(\mathrm{d}\mathscr{L}) = 0$, so that $\mathrm{d}\mathscr{L}$ is constant on critical points u. Note that here we silently assume that the space of critical points is connected. It would be difficult to justify this property in any generality, but it is usually clear in applications, where the critical points are solutions of certain well-posed systems of partial differential equations. □

We will take a closer look at the property $\mathrm{d}\mathscr{L} = \text{const}$ in Sect. 6, when we discuss the link with Hamiltonian theory. It will be shown that vanishing of this constant, i.e., closedness of $\mathscr{L}$ on critical points, is related to integrability of the multi-time Euler-Lagrange equations.

2.2 Approximation by Stepped Surfaces

For computations, we will use the multi-index notation for partial derivatives. For any multi-index $I = (i_1, \ldots, i_N)$ we set

$$u_I = \frac{\partial^{|I|} u}{(\partial t_1)^{i_1} \ldots (\partial t_N)^{i_N}},$$

where $|I| = i_1 + \ldots + i_N$. The notations Ik and Ik^α will represent the multi-indices $(i_1, \ldots, i_k + 1, \ldots i_N)$ and $(i_1, \ldots, i_k + \alpha, \ldots i_N)$ respectively. When convenient we will also use the notations It_k and It_k^α for these multi-indices. We will write $k \notin I$ if $i_k = 0$ and $k \in I$ if $i_k > 0$. We will denote by D_i or D_{t_i} the total derivative with respect to coordinate direction t_i,

$$\mathrm{D}_i := \mathrm{D}_{t_i} := \sum_I u_{Ii} \frac{\partial}{\partial u_I}$$

and by $\mathrm{D}_I := \mathrm{D}_{t_1}^{i_1} \ldots \mathrm{D}_{t_N}^{i_N}$ the corresponding higher order derivatives.

Our main general result is the derivation of the multi-time Euler-Lagrange equations for two-dimensional surfaces ($d = 2$). That will allow us to study the KdV hierarchy as a pluri-Lagrangian system. However, it is instructive to first derive the multi-time Euler-Lagrange equations for curves ($d = 1$).

The key technical result used to derive multi-time Euler-Lagrange equations is the observation that it suffices to consider a very specific type of surface.

Definition 2.3 A *stepped d-surface* is a d-surface that is a finite union of coordinate d-surfaces. A *coordinate d-surface* of the direction $(i_1, \ldots, i_d)$ is a d-surface lying in an affine d-plane $\{(t_1, \ldots, t_N) \mid t_j = c_j \text{ for } j \neq i_1, \ldots, i_d\}$.

Lemma 2.4 *If the action is stationary on any stepped surface, then it is stationary on any smooth surface.*

The proof of this Lemma can be found in appendix B.

2.3 Multi-time Euler-Lagrange Equations for Curves

Theorem 2.5 *Consider a Lagrangian 1-form $\mathscr{L} = \sum_{i=1}^{N} L_i \, \mathrm{d}t_i$. The multi-time Euler-Lagrange equations for curves are:*

$$\frac{\delta_i L_i}{\delta u_I} = 0 \qquad \forall I \not\ni i, \tag{2}$$

$$\frac{\delta_i L_i}{\delta u_{Ii}} = \frac{\delta_j L_j}{\delta u_{Ij}} \qquad \forall I, \tag{3}$$

where i and j are distinct, and the following notation is used for the variational derivative corresponding to the coordinate direction i:

$$\frac{\delta_i L_i}{\delta u_I} = \sum_{\alpha \geq 0} (-1)^\alpha \, \mathrm{D}_i^\alpha \frac{\partial L_i}{\partial u_{Ii^\alpha}} = \frac{\partial L_i}{\partial u_I} - \mathrm{D}_i \frac{\partial L_i}{\partial u_{Ii}} + \mathrm{D}_i^2 \frac{\partial L_i}{\partial u_{Ii^2}} - \ldots.$$

Remark 2.6 In the special case that $\mathscr{L}$ only depends on the first jet bundle, system (2)–(3) reduces to the equations found in [20]:

$$\begin{aligned}
\frac{\delta_i L_i}{\delta u} = 0 \quad &\Leftrightarrow \quad \frac{\partial L_i}{\partial u} - \mathrm{D}_i \frac{\partial L_i}{\partial u_i} = 0, \\
\frac{\delta_i L_i}{\delta u_j} = 0 \quad &\Leftrightarrow \quad \frac{\partial L_i}{\partial u_j} = 0 \quad \text{for} \quad i \neq j, \\
\frac{\delta_i L_i}{\delta u_i} = \frac{\delta_j L_j}{\delta u_j} \quad &\Leftrightarrow \quad \frac{\partial L_i}{\partial u_i} = \frac{\partial L_j}{\partial u_j} \quad \text{for} \quad i \neq j.
\end{aligned}$$

Proof (of Theorem 2.5) According to Lemma 2.4, it is sufficient to look at a general L-shaped curve $S = S_i \cup S_j$, where S_i is a line segment of the coordinate direction i and S_j is a line segment of the coordinate direction j. Denote the cusp by $p := S_i \cap S_j$. We orient the curve such that S_i induces the positive orientation on the point p and S_j the negative orientation. There are four cases, depending on how

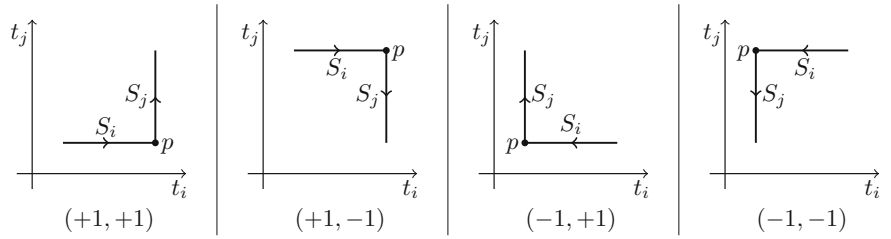

Fig. 1 The four *L-shaped curves* with their values of $(\varepsilon_i, \varepsilon_j)$

the L-shape is rotated. They are depicted in Fig. 1. To each case we associate a pair $(\varepsilon_i, \varepsilon_j) \in \{-1, +1\}^2$, where the positive value is taken if the respective piece of curve is oriented in the coordinate direction, and negative if it is oriented opposite to the coordinate direction.

The variation of the action is

$$\begin{aligned}\int_S \iota_{\mathrm{pr}\,\mathscr{V}}\,\delta\mathscr{L} &= \varepsilon_i \int_{S_i} (\iota_{\mathrm{pr}\,\mathscr{V}}\,\delta L_i)\,\mathrm{d}t_i + \varepsilon_j \int_{S_j} (\iota_{\mathrm{pr}\,\mathscr{V}}\,\delta L_j)\,\mathrm{d}t_j \\ &= \varepsilon_i \int_{S_i} \sum_I \frac{\partial L_i}{\partial u_I}\delta u_I(\mathscr{V})\,\mathrm{d}t_i + \varepsilon_j \int_{S_j} \sum_I \frac{\partial L_j}{\partial u_I}\delta u_I(\mathscr{V})\,\mathrm{d}t_j.\end{aligned}$$

Note that these sums are actually finite. Indeed, since $\mathscr{L}$ depends on the nth jet bundle all terms with $|I| := i_1 + \ldots + i_N > n$ vanish.

Now we expand the sum in the first of the integrals and perform integration by parts.

$$\begin{aligned}&\varepsilon_i \int_{S_i} (\iota_{\mathrm{pr}\,\mathscr{V}}\,\delta L_i)\,\mathrm{d}t_i \\ &= \varepsilon_i \int_{S_i} \sum_{I \not\ni i} \left(\frac{\partial L_i}{\partial u_I}\delta u_I(\mathscr{V}) + \frac{\partial L_i}{\partial u_{Ii}}\delta u_{Ii}(\mathscr{V}) + \frac{\partial L_i}{\partial u_{Ii^2}}\delta u_{Ii^2}(\mathscr{V}) + \ldots\right)\mathrm{d}t_i \\ &= \varepsilon_i \int_{S_i} \sum_{I \not\ni i} \left(\frac{\partial L_i}{\partial u_I} - \mathrm{D}_i\,\frac{\partial L_i}{\partial u_{Ii}} + \mathrm{D}_i^2\,\frac{\partial L_i}{\partial u_{Ii^2}} - \mathrm{D}_i^3\,\frac{\partial L_i}{\partial u_{Ii^3}} + \ldots\right)\delta u_I(\mathscr{V})\,\mathrm{d}t_i \\ &\quad + \sum_{I \not\ni i} \left(\frac{\partial L_i}{\partial u_{Ii}}\delta u_I(\mathscr{V}) + \frac{\partial L_i}{\partial u_{Ii^2}}\delta u_{Ii}(\mathscr{V}) - \mathrm{D}_i\,\frac{\partial L_i}{\partial u_{Ii^2}}\delta u_I(\mathscr{V})\right. \\ &\qquad\qquad \left. + \frac{\partial L_i}{\partial u_{Ii^3}}\delta u_{Ii^2}(\mathscr{V}) - \mathrm{D}_i\,\frac{\partial L_i}{\partial u_{Ii^3}}(\mathscr{V})\delta u_{Ii}(\mathscr{V}) + \mathrm{D}_i^2\,\frac{\partial L_i}{\partial u_{Ii^3}}\delta u_I(\mathscr{V}) + \ldots\right)\Big|_p.\end{aligned}$$

Using the language of variational derivatives, this reads

$$\varepsilon_i \int_{S_i} (\iota_{\mathrm{pr}\,\mathscr{V}}\,\delta L_i)\,\mathrm{d}t_i = \varepsilon_i \int_{S_i} \sum_{I \not\ni i} \frac{\delta_i L_i}{\delta u_I}\delta u_I(\mathscr{V})\,\mathrm{d}t_i$$

$$+\sum_{I\not\ni i}\left(\frac{\delta_i L_i}{\delta u_{Ii}}\delta u_I(\mathscr{V})+\frac{\delta_i L_i}{\delta u_{Ii^2}}\delta u_{Ii}(\mathscr{V})+\dots\right)\Big|_p$$
$$=\varepsilon_i\int_{S_i}\sum_{I\not\ni i}\frac{\delta_i L_i}{\delta u_I}\delta u_I(\mathscr{V})\,\mathrm{d}t_i+\sum_I\left(\frac{\delta_i L_i}{\delta u_{Ii}}\delta u_I(\mathscr{V})\right)\Big|_p.$$

The other piece, S_j, contributes

$$\varepsilon_j\int_{S_j}\iota_{\mathrm{pr}\,\mathscr{V}}\,\delta L_j\,\mathrm{d}t_j=\varepsilon_j\int_{S_j}\sum_{I\not\ni j}\frac{\delta_j L_j}{\delta u_I}\delta u_I(\mathscr{V})\,\mathrm{d}t_j-\sum_I\left(\frac{\delta_j L_j}{\delta u_{Ij}}\delta u_I(\mathscr{V})\right)\Big|_p,$$

where the minus sign comes from the fact that S_j induces negative orientation on the point p. Summing the two contributions, we find

$$\int_S\iota_{\mathrm{pr}\,\mathscr{V}}\,\delta\mathscr{L}=\varepsilon_i\int_{S_i}\sum_{I\not\ni i}\frac{\delta_i L_i}{\delta u_I}\delta u_I(\mathscr{V})\,\mathrm{d}t_i+\varepsilon_j\int_{S_j}\sum_{I\not\ni j}\frac{\delta_j L_j}{\delta u_I}\delta u_I(\mathscr{V})\,\mathrm{d}t_j$$
$$+\sum_I\left(\frac{\delta_i L_i}{\delta u_{Ii}}\delta u_I(\mathscr{V})-\frac{\delta_j L_j}{\delta u_{Ij}}\delta u_I(\mathscr{V})\right)\Big|_p. \tag{4}$$

Now require that the variation (4) of the action is zero for any variation $\mathscr{V}$. If we consider variations that vanish on S_j, then we find for every multi-index I which does not contain i that

$$\frac{\delta_i L_i}{\delta u_I}=0.$$

Given this equation, and its analogue for the index j, only the last term remains in the right hand side of Eq. (4). Considering variations around the cusp p we find for every multi-index I that

$$\frac{\delta_i L_i}{\delta u_{Ii}}=\frac{\delta_j L_j}{\delta u_{Ij}}.$$

It is clear these equations combined are also sufficient for the action to be critical. □

2.4 Multi-time Euler-Lagrange Equations for Two-Dimensional Surfaces

The two-dimensional case ($d=2$) covers many known integrable hierarchies, including the potential KdV hierarchy which we will discuss in detail later on. We consider a Lagrangian two-form $\mathscr{L}=\sum_{i<j}L_{ij}\,\mathrm{d}t_i\wedge\mathrm{d}t_j$ and we will use the notational convention $L_{ji}=-L_{ij}$.

Theorem 2.7 *The multi-time Euler-Lagrange equations for two-dimensional surfaces are*

$$\frac{\delta_{ij} L_{ij}}{\delta u_I} = 0, \qquad \forall I \not\ni i, j, \tag{5}$$

$$\frac{\delta_{ij} L_{ij}}{\delta u_{Ij}} = \frac{\delta_{ik} L_{ik}}{\delta u_{Ik}} \qquad \forall I \not\ni i, \tag{6}$$

$$\frac{\delta_{ij} L_{ij}}{\delta u_{Iij}} + \frac{\delta_{jk} L_{jk}}{\delta u_{Ijk}} + \frac{\delta_{ki} L_{ki}}{\delta u_{Iki}} = 0 \qquad \forall I, \tag{7}$$

where i, j and k are distinct, and the following notation is used for the variational derivative corresponding to the coordinate directions i, j:

$$\frac{\delta_{ij} L_{ij}}{\delta u_I} := \sum_{\alpha,\beta \geq 0} (-1)^{\alpha+\beta} \, \mathrm{D}_i^{\alpha} \, \mathrm{D}_j^{\beta} \, \frac{\partial L_{ij}}{\partial u_{Ii^{\alpha} j^{\beta}}}.$$

Remark 2.8 In the special case that $\mathscr{L}$ only depends on the second jet bundle, this system reduces to the equations stated in [21].

Before proceeding with the proof of Theorem 2.7, we introduce some terminology and prove a lemma. A two-dimensional stepped surface consisting of q flat pieces intersecting at some point p is called a *q-flower* around p, the flat pieces are called its *petals*. If the action is stationary on every q-flower, it is stationary on any stepped surface. By Lemma 2.4 the action will then be stationary on any surface. The following Lemma shows that it is sufficient to consider 3-flowers.

Lemma 2.9 *If the action is stationary on every 3-flower, then it is stationary on every q-flower for any $q > 3$.*

Proof Let F be a q-flower. Denote its petals corresponding to coordinate directions $(t_{i_1}, t_{i_2}), (t_{i_2}, t_{i_3}), \ldots, (t_{i_q}, t_{i_1})$ by $S_{12}, S_{23}, \ldots, S_{q1}$ respectively. Consider the 3-flower $F_{123} = S_{12} \cup S_{23} \cup S_{31}$, where S_{31} is a petal in the coordinate direction (t_{i_3}, t_{i_1}) such that F_{123} is a flower around the same point as F. Similarly, define $F_{134}, \ldots, F_{1\,q-1\,q}$. Then (for any integrand)

$$\int_{F_{123}} + \int_{F_{134}} + \ldots + \int_{F_{1\,q-1\,q}} = \int_{S_{12}} + \int_{S_{23}} + \int_{S_{31}} + \int_{S_{13}} + \int_{S_{34}} + \int_{S_{41}} + \ldots + \int_{S_{1\,q-1}} + \int_{S_{q-1\,q}} + \int_{S_{q1}}.$$

Here, $S_{21}, S_{32}, \ldots$ are the petals $S_{12}, S_{23}, \ldots$ but with opposite orientation (see Fig. 2). Therefore all terms where the index of S contains 1 cancel, except for the first and last, leaving

$$\int_{F_{123}} + \ldots + \int_{F_{1\,q-1\,q}} = \int_{S_{12}} + \int_{S_{23}} + \int_{S_{34}} + \ldots + \int_{S_{q-1\,q}} + \int_{S_{q1}} = \int_{F}.$$

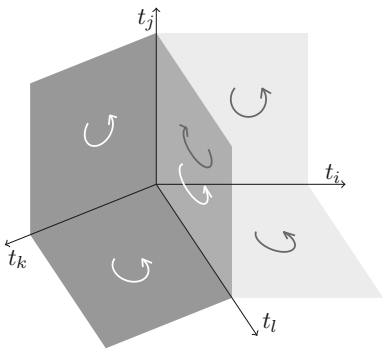

Fig. 2 Two 3-flowers composed to form a 4-flower. The common petal does not contribute to the integral because it occurs twice with opposite orientation

By assumption the action is stationary on every 3-flower, so

$$\int_F \iota_{\mathrm{pr}\,\mathscr{V}}\,\delta\mathscr{L} = \int_{F_{123}} \iota_{\mathrm{pr}\,\mathscr{V}}\,\delta\mathscr{L} + \ldots + \int_{F_{1\,q-1\,q}} \iota_{\mathrm{pr}\,\mathscr{V}}\,\delta\mathscr{L} = 0.$$

□

Proof (of Theorem 2.7) Consider a 3-flower $S = S_{ij} \cup S_{jk} \cup S_{ki}$ around the point $p = S_{ij} \cap S_{jk} \cap S_{ki}$. Denote its interior edges by

$$\partial S_i := S_{ij} \cap S_{ki}, \qquad \partial S_j := S_{jk} \cap S_{ij}, \qquad \partial S_k := S_{ki} \cap S_{jk}.$$

On ∂S_i, ∂S_j and ∂S_k we choose the orientations that induce negative orientation on p. We consider the case where these orientations correspond to the coordinate directions, as in Fig. 3. The cases where one or more of these orientations are opposite to the corresponding coordinate direction (see Fig. 4) can be treated analogously and yield the same result.

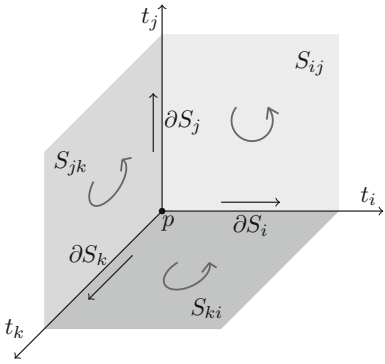

Fig. 3 A 3-flower. Different petals induce the opposite orientation on the common boundary

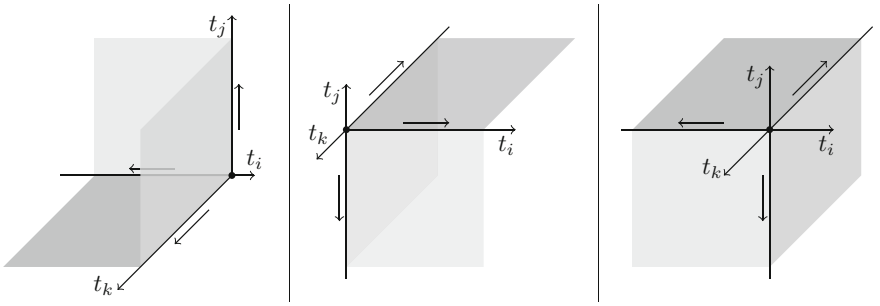

Fig. 4 Three of the other 3-flowers. The orientations of the interior edges do not all correspond to the coordinate direction

We choose the orientation on the petals in such a way that the orientations of ∂S_i, ∂S_j and ∂S_k are induced by S_{ij}, S_{jk} and S_{ki} respectively. Then the orientations of ∂S_i, ∂S_j and ∂S_k are the opposite of those induced by S_{ki}, S_{ij} and S_{jk} respectively (see Fig. 3).

We will calculate

$$\int_S \iota_{\mathrm{pr}\,\mathscr{V}}\,\delta\mathscr{L} = \int_{S_{ij}} \iota_{\mathrm{pr}\,\mathscr{V}}\,\delta\mathscr{L} + \int_{S_{jk}} \iota_{\mathrm{pr}\,\mathscr{V}}\,\delta\mathscr{L} + \int_{S_{ki}} \iota_{\mathrm{pr}\,\mathscr{V}}\,\delta\mathscr{L} \tag{8}$$

and require it to be zero for any variation $\mathscr{V}$ which vanishes on the (outer) boundary of S. This will give us the multi-time Euler-Lagrange equations.

For the first term of Eq. (8) we find

$$\begin{aligned}\int_{S_{ij}} \iota_{\mathrm{pr}\,\mathscr{V}}\,\delta\mathscr{L} &= \int_{S_{ij}} \sum_I \frac{\partial L_{ij}}{\partial u_I}\delta u_I(\mathscr{V})\,\mathrm{d}t_i\wedge\mathrm{d}t_j\\ &= \int_{S_{ij}} \sum_{I\not\ni i,j}\sum_{\lambda,\mu\geq 0}\frac{\partial L_{ij}}{\partial u_{Ii^\lambda j^\mu}}\delta u_{Ii^\lambda j^\mu}(\mathscr{V})\,\mathrm{d}t_i\wedge\mathrm{d}t_j.\end{aligned}$$

First we perform integration by parts with respect to t_i as many times as possible.

$$\begin{aligned}\int_{S_{ij}} \iota_{\mathrm{pr}\,\mathscr{V}}\,\delta\mathscr{L} = &\int_{S_{ij}} \sum_{I\not\ni i,j}\sum_{\lambda,\mu\geq 0}(-1)^\lambda\,\mathrm{D}_i^\lambda\,\frac{\partial L_{ij}}{\partial u_{Ii^\lambda j^\mu}}\delta u_{Ij^\mu}(\mathscr{V})\,\mathrm{d}t_i\wedge\mathrm{d}t_j\\ &-\int_{\partial S_j} \sum_{I\not\ni i,j}\sum_{\lambda,\mu\geq 0}\sum_{\pi=0}^{\lambda-1}(-1)^\pi\,\mathrm{D}_i^\pi\,\frac{\partial L_{ij}}{\partial u_{Ii^\lambda j^\mu}}\delta u_{Ii^{\lambda-\pi-1}j^\mu}(\mathscr{V})\,\mathrm{d}t_j.\end{aligned}$$

Next integrate by parts with respect to t_j as many times as possible.

$$\int_{S_{ij}} \iota_{\mathrm{pr}\,\mathscr{V}}\,\delta\mathscr{L} = \int_{S_{ij}} \sum_{I\not\ni i,j}\sum_{\lambda,\mu\geq 0}(-1)^{\lambda+\mu}\,\mathrm{D}_i^\lambda\,\mathrm{D}_j^\mu\,\frac{\partial L_{ij}}{\partial u_{Ii^\lambda j^\mu}}\delta u_I(\mathscr{V})\,\mathrm{d}t_i\wedge\mathrm{d}t_j \tag{9}$$

$$-\int_{\partial S_j}\sum_{I\not\ni i,j}\sum_{\lambda,\mu\geq 0}\sum_{\pi=0}^{\lambda-1}(-1)^{\pi}\,\mathrm{D}_i^{\pi}\,\frac{\partial L_{ij}}{\partial u_{Ii^{\lambda}j^{\mu}}}\delta u_{Ii^{\lambda-\pi-1}j^{\mu}}(\mathscr{V})\,\mathrm{d}t_j \tag{10}$$

$$-\int_{\partial S_i}\sum_{I\not\ni i,j}\sum_{\lambda,\mu\geq 0}\sum_{\rho=0}^{\mu-1}(-1)^{\lambda+\rho}\,\mathrm{D}_i^{\lambda}\,\mathrm{D}_j^{\rho}\,\frac{\partial L_{ij}}{\partial u_{Ii^{\lambda}j^{\mu}}}\delta u_{Ij^{\mu-\rho-1}}(\mathscr{V})\,\mathrm{d}t_i. \tag{11}$$

The signs of (10) and (11) are due to the choice of orientations (see Fig. 3). We can rewrite the integral (9) as

$$\int_{S_{ij}}\sum_{I\not\ni i,j}\frac{\delta_{ij}L_{ij}}{\delta u_I}\delta u_I(\mathscr{V})\,\mathrm{d}t_i\wedge\mathrm{d}t_j.$$

The last integral (11) takes a similar form if we replace the index μ by $\beta=\mu-\rho-1$.

$$\begin{aligned}
&-\int_{\partial S_i}\sum_{I\not\ni i,j}\sum_{\lambda,\mu\geq 0}\sum_{\rho=0}^{\mu-1}(-1)^{\lambda+\rho}\,\mathrm{D}_i^{\lambda}\,\mathrm{D}_j^{\rho}\,\frac{\partial L_{ij}}{\partial u_{Ii^{\lambda}j^{\mu}}}\delta u_{Ij^{\mu-\rho-1}}(\mathscr{V})\,\mathrm{d}t_i\\
&\quad=-\int_{\partial S_i}\sum_{I\not\ni i,j}\sum_{\beta,\lambda,\rho\geq 0}(-1)^{\lambda+\rho}\,\mathrm{D}_i^{\lambda}\,\mathrm{D}_j^{\rho}\,\frac{\partial L_{ij}}{\partial u_{Ii^{\lambda}j^{\beta+\rho+1}}}\delta u_{Ij^{\beta}}(\mathscr{V})\,\mathrm{d}t_i\\
&\quad=-\int_{\partial S_i}\sum_{I\not\ni i,j}\sum_{\beta\geq 0}\frac{\delta_{ij}L_{ij}}{\delta u_{Ij^{\beta+1}}}\delta u_{Ij^{\beta}}(\mathscr{V})\,\mathrm{d}t_i.
\end{aligned}$$

To write the other boundary integral (10) in this form we first perform integration by parts.

$$\begin{aligned}
&-\int_{\partial S_j}\sum_{I\not\ni i,j}\sum_{\lambda,\mu\geq 0}\sum_{\pi=0}^{\lambda-1}(-1)^{\pi}\,\mathrm{D}_i^{\pi}\,\frac{\partial L_{ij}}{\partial u_{Ii^{\lambda}j^{\mu}}}\delta u_{Ii^{\lambda-\pi-1}j^{\mu}}(\mathscr{V})\,\mathrm{d}t_j\\
&\quad=-\int_{\partial S_j}\sum_{I\not\ni i,j}\sum_{\lambda,\mu\geq 0}\sum_{\pi=0}^{\lambda-1}(-1)^{\pi+\mu}\,\mathrm{D}_i^{\pi}\,\mathrm{D}_j^{\mu}\,\frac{\partial L_{ij}}{\partial u_{Ii^{\lambda}j^{\mu}}}\delta u_{Ii^{\lambda-\pi-1}}(\mathscr{V})\,\mathrm{d}t_j\\
&\qquad+\sum_{I\not\ni i,j}\sum_{\lambda,\mu\geq 0}\sum_{\pi=0}^{\lambda-1}\sum_{\rho=0}^{\mu-1}(-1)^{\pi+\rho}\left(\mathrm{D}_i^{\pi}\,\mathrm{D}_j^{\rho}\,\frac{\partial L_{ij}}{\partial u_{Ii^{\lambda}j^{\mu}}}\delta u_{Ii^{\lambda-\pi-1}j^{\mu-\rho-1}}(\mathscr{V})\right)\Bigg|_p.
\end{aligned}$$

Then we replace λ by $\alpha=\lambda-\pi-1$ and in the last term μ by $\beta=\mu-\rho-1$.

$$\begin{aligned}
&-\int_{\partial S_j}\sum_{I\not\ni i,j}\sum_{\lambda,\geq 0}\sum_{\pi=0}^{\lambda-1}(-1)^{\pi}\,\mathrm{D}_i^{\pi}\,\frac{\partial L_{ij}}{\partial u_{Ii^{\lambda}j^{\mu}}}\delta u_{Ii^{\lambda-\pi-1}j^{\mu}}(\mathscr{V})\,\mathrm{d}t_j\\
&\quad=-\int_{\partial S_j}\sum_{I\not\ni i,j}\sum_{\alpha,\mu,\pi\geq 0}(-1)^{\pi+\mu}\,\mathrm{D}_i^{\pi}\,\mathrm{D}_j^{\mu}\,\frac{\partial L_{ij}}{\partial u_{Ii^{\alpha+\pi+1}j^{\mu}}}\delta u_{Ii^{\alpha}}(\mathscr{V})\,\mathrm{d}t_j
\end{aligned}$$

$$+\sum_{I\not\ni i,j}\sum_{\alpha,\beta,\pi,\rho\geq 0}\left((-1)^{\pi+\rho}\,\mathrm{D}_i^{\pi}\,\mathrm{D}_j^{\rho}\,\frac{\partial L_{ij}}{\partial u_{Ii^{\alpha+\pi+1}j^{\beta+\rho+1}}}\delta u_{Ii^{\alpha}j^{\beta}}(\mathscr{V})\right)\Big|_p$$
$$=-\int_{\partial S_j}\sum_{I\not\ni i,j}\sum_{\alpha\geq 0}\frac{\delta_{ij}L_{ij}}{\delta u_{Ii^{\alpha+1}}}\delta u_{Ii^{\alpha}}(\mathscr{V})\,\mathrm{d}t_j+\sum_{I\not\ni i,j}\sum_{\alpha,\beta\geq 0}\left(\frac{\delta_{ij}L_{ij}}{\delta u_{Ii^{\alpha+1}j^{\beta+1}}}\delta u_{Ii^{\alpha}j^{\beta}}(\mathscr{V})\right)\Big|_p.$$

Putting everything together we find

$$\int_{S_{ij}}\iota_{\mathrm{pr}\,\mathscr{V}}\,\delta\mathscr{L}=\int_{S_{ij}}\sum_{I\not\ni i,j}\frac{\delta_{ij}L_{ij}}{\delta u_I}\delta u_I(\mathscr{V})\,\mathrm{d}t_i\wedge\mathrm{d}t_j-\int_{\partial S_i}\sum_{I\not\ni i}\frac{\delta_{ij}L_{ij}}{\delta u_{Ij}}\delta u_I(\mathscr{V})\mathrm{d}t_i$$
$$-\int_{\partial S_j}\sum_{I\not\ni j}\frac{\delta_{ij}L_{ij}}{\delta u_{Ii}}\delta u_I(\mathscr{V})\,\mathrm{d}t_j+\left(\sum_I\frac{\delta_{ij}L_{ij}}{\delta u_{Iij}}\delta u_I(\mathscr{V})\right)\Big|_p.$$

Expressions for the integrals over S_{jk} and S_{ki} are found by cyclic permutation of the indices. Finally we obtain

$$\begin{aligned}\int_S\iota_{\mathrm{pr}\,\mathscr{V}}\,\delta\mathscr{L}=&\int_{S_{ij}}\sum_{I\not\ni i,j}\frac{\delta_{ij}L_{ij}}{\delta u_I}\delta u_I(\mathscr{V})\,\mathrm{d}t_i\wedge\mathrm{d}t_j\\&-\int_{\partial S_i}\left(\sum_{I\not\ni i}\frac{\delta_{ij}L_{ij}}{\delta u_{Ij}}\delta u_I(\mathscr{V})+\sum_{I\not\ni i}\frac{\delta_{ki}L_{ki}}{\delta u_{Ik}}\delta u_I(\mathscr{V})\right)\mathrm{d}t_i\\&+\sum_I\left(\frac{\delta_{ij}L_{ij}}{\delta u_{Iij}}\delta u_I(\mathscr{V})\right)\Big|_p\qquad+\text{ cyclic permutations in } i,\,j,\,k.\end{aligned}\tag{12}$$

From this we can read off the multi-time Euler-Lagrange equations. □

3 Pluri-Lagrangian Structure of the Sine-Gordon Equation

We borrow our first example of a pluri-Lagrangian system from [21].

The Sine-Gordon equation $u_{xy}=\sin u$ is the Euler-Lagrange equation for

$$L=\frac{1}{2}u_xu_y-\cos u.$$

Consider the vector field $\varphi\frac{\partial}{\partial u}$ with

$$\varphi=u_{xxx}+\frac{1}{2}u_x^3$$

and its prolongation $\mathrm{D}_\varphi := \sum_I \varphi_I \frac{\partial}{\partial u_I}$. It is known that D_φ is a variational symmetry for the sine-Gordon equation [18, p. 336]. In particular, we have that

$$\mathrm{D}_\varphi L = \mathrm{D}_x N + \mathrm{D}_y M \tag{13}$$

with

$$\begin{aligned} M &= \frac{1}{2}\varphi u_x - \frac{1}{8}u_x^4 + \frac{1}{2}u_{xx}^2, \\ N &= \frac{1}{2}\varphi u_y - \frac{1}{2}u_x^2 \cos u - u_{xx}(u_{xy} - \sin u). \end{aligned}$$

Now we introduce a new independent variable z corresponding to the "flow" of the generalized vector field D_φ, i.e. $u_z = \varphi$. Consider simultaneous solutions of the Euler-Lagrange equation $\frac{\delta L}{\delta u} = 0$ and of the flow $u_z = \varphi$ as functions of three independent variables x, y, z. Then Eq. (13) expresses the closedness of the two-form

$$\mathscr{L} = L\,dx \wedge dy - M\,dz \wedge dx - N\,dy \wedge dz.$$

The fact that $\mathrm{d}\mathscr{L} = 0$ on solutions is consistent with Proposition 2.2. Hence $\mathscr{L}$ is a reasonable candidate for a Lagrangian two-form.

Theorem 3.1 *The multi-time Euler-Lagrange equations for the Lagrangian two-form*

$$\mathscr{L} = L_{12}\,dx \wedge dy + L_{13}\,dx \wedge dz + L_{23}\,dy \wedge dz$$

with the components

$$L_{12} = \frac{1}{2}u_x u_y - \cos u, \tag{14}$$

$$L_{13} = \frac{1}{2}u_x u_z - \frac{1}{8}u_x^4 + \frac{1}{2}u_{xx}^2, \tag{15}$$

$$L_{23} = -\frac{1}{2}u_y u_z + \frac{1}{2}u_x^2 \cos u + u_{xx}(u_{xy} - \sin u), \tag{16}$$

consist of the sine-Gordon equation

$$u_{xy} = \sin u,$$

the modified KdV equation

$$u_z = u_{xxx} + \frac{1}{2}u_x^3,$$

and corollaries thereof. On solutions of either of these equations the two-form $\mathscr{L}$ is closed.

Proof Let us calculate the multi-time Euler-Lagrange Eqs. (5)–(7) one by one:

- The equation $\dfrac{\delta_{12} L_{12}}{\delta u} = 0$ yields $\ldots\ldots\ldots\ldots\ldots\ldots\ldots\ldots\ldots\ldots\ldots\ldots u_{xy} = \sin u$.

  For any $\alpha > 0$ the equation $\dfrac{\delta_{12} L_{12}}{\delta u_{z^\alpha}} = 0$ yields $0 = 0$.
- The equation $\dfrac{\delta_{13} L_{13}}{\delta u} = 0$ yields $\ldots\ldots\ldots\ldots\ldots\ldots\ldots\ldots\ldots\ldots\ldots\ldots u_{xz} = \frac{3}{2} u_x^2 u_{xx} + u_{xxxx}$.

  For any $\alpha > 0$ the equation $\dfrac{\delta_{13} L_{13}}{\delta u_{y^\alpha}} = 0$ yields $0 = 0$.
- The equation $\dfrac{\delta_{23} L_{23}}{\delta u} = 0$ yields $\ldots\ldots\ldots\ldots\ldots\ldots\ldots\ldots\ldots\ldots\ldots\ldots u_{yz} = \frac{1}{2} u_x^2 \sin u + u_{xx} \cos u$.

  The equation $\dfrac{\delta_{23} L_{23}}{\delta u_x} = 0$ yields $\ldots\ldots\ldots\ldots\ldots\ldots\ldots\ldots\ldots\ldots\ldots\ldots u_{yxx} = u_x \cos u$.

  The equation $\dfrac{\delta_{23} L_{23}}{\delta u_{xx}} = 0$ yields $\ldots\ldots\ldots\ldots\ldots\ldots\ldots\ldots\ldots\ldots\ldots\ldots u_{xy} = \sin u$.

  For any $\alpha > 2$, the equation $\dfrac{\delta_{23} L_{23}}{\delta u_{x^\alpha}} = 0$ yields $0 = 0$.
- The equation $\dfrac{\delta_{13} L_{13}}{\delta u_x} = \dfrac{\delta_{23} L_{23}}{\delta u_y}$ yields $\ldots\ldots\ldots\ldots\ldots\ldots\ldots\ldots\ldots\ldots\ldots\ldots u_z = u_{xxx} + \frac{1}{2} u_x^3$.

  The equation $\dfrac{\delta_{13} L_{13}}{\delta u_{xx}} = \dfrac{\delta_{23} L_{23}}{\delta u_{xy}}$ yields $u_{xx} = u_{xx}$.

  For any other I the equation $\dfrac{\delta_{13} L_{13}}{\delta u_{Ix}} = \dfrac{\delta_{23} L_{23}}{\delta u_{Iy}}$ yields $0 = 0$.
- The equation $\dfrac{\delta_{12} L_{12}}{\delta u_y} = \dfrac{\delta_{13} L_{13}}{\delta u_z}$ yields $\frac{1}{2} u_x = \frac{1}{2} u_x$.

  For any nonempty I, the equation $\dfrac{\delta_{12} L_{12}}{\delta u_{Iy}} = \dfrac{\delta_{13} L_{13}}{\delta u_{Iz}}$ yields $0 = 0$.
- The equation $\dfrac{\delta_{12} L_{12}}{\delta u_x} = \dfrac{\delta_{23} L_{32}}{\delta u_z}$ yields $\frac{1}{2} u_y = \frac{1}{2} u_y$.

  For any nonempty I, the equation $\dfrac{\delta_{12} L_{12}}{\delta u_{Ix}} = \dfrac{\delta_{23} L_{32}}{\delta u_{Iz}}$ yields $0 = 0$.
- For any I the equation $\dfrac{\delta_{12} L_{12}}{\delta u_{Ixy}} + \dfrac{\delta_{23} L_{23}}{\delta u_{Iyz}} + \dfrac{\delta_{13} L_{31}}{\delta u_{Izx}} = 0$ yields $0 = 0$.

It remains to notice that all nontrivial equations in this list are corollaries of the equations $u_{xy} = \sin u$ and $u_z = u_{xxx} + \frac{1}{2} u_x^3$, derived by differentiation.

The closedness of $\mathscr{L}$ can be verified by direct calculation:

$$\begin{aligned} \mathrm{D}_z L_{12} - \mathrm{D}_y L_{13} + \mathrm{D}_x L_{23} = {} & \frac{1}{2}(u_{yz} u_x + u_{xz} u_y) + u_z \sin u \\ & - \frac{1}{2} u_{yz} u_x - \frac{1}{2} u_z u_{xy} + \frac{1}{2} u_x^3 u_{xy} - u_{xx} u_{xxy} \end{aligned}$$

$$
\begin{aligned}
&- \frac{1}{2}u_{xz}u_y - \frac{1}{2}u_z u_{xy} + u_x u_{xx}\cos u - \frac{1}{2}u_x^3 \sin u \\
&+ u_{xxx}(u_{xy} - \sin u) + u_{xx}(u_{xxy} - u_x \cos u) \\
&= -\left(u_z - \frac{1}{2}u_x^3 - u_{xxx}\right)(u_{xy} - \sin u).
\end{aligned}
$$

□

Remark 3.2 The Sine-Gordon equation and the modified KdV equation are the simplest equations of their respective hierarchies. Furthermore, those hierarchies can be seen as the positive and negative parts of one single hierarchy that is infinite in both directions [14, Sect. 3c and 5k]. It seems likely that this whole hierarchy possesses a pluri-Lagrangian structure.

4 The KdV Hierarchy

Our second and the main example of a pluri-Lagrangian system will be the (potential) KdV hierarchy. This section gives an overview of the relevant known facts about KdV, mainly following Dickey [12, Sect. 3.7]. The next section will present its pluri-Lagrangian structure.

One way to introduce the *Korteweg-de Vries (KdV) hierarchy* is to consider a formal power series

$$R = \sum_{k=0}^{\infty} r_k z^{-2k-1},$$

with the coefficients $r_k = r_k[u]$ being polynomials of u and its partial derivatives with respect to x, satisfying the equation

$$R_{xxx} + 4uR_x + 2u_x R - z^2 R_x = 0. \tag{17}$$

Multiplying this equation by R and integrating with respect to x we find

$$RR_{xx} - \frac{1}{2}R_x^2 + 2\left(u - \frac{1}{4}z^2\right)R^2 = C(z), \tag{18}$$

where $C(z) = \sum_{k=0}^{\infty} c_k z^{-2k}$ is a formal power series in z^{-2}, with coefficients c_k being constants. Different choices of $C(z)$ correspond to different normalizations of the KdV hierarchy. We take $C(z) = \frac{1}{8}$, i.e. $c_0 = \frac{1}{8}$ and $c_k = 0$ for $k > 0$. The first few coefficients of the power series $R = r_0 z^{-1} + r_1 z^{-3} + r_2 z^{-5} + \dots$ are

$$r_0 = \frac{1}{2}, \quad r_1 = u, \quad r_2 = u_{xx} + 3u^2, \quad r_3 = u_{xxxx} + 10uu_{xx} + 5u_x^2 + 10u^3.$$

The Korteweg-de Vries hierarchy is defined as follows.

Definition 4.1 • The *KdV hierarchy* is the family of equations

$$u_{t_k} = (r_k[u])_x.$$

• Write $g_k[v] := r_k[v_x]$. The *potential KdV (PKdV) hierarchy* is the family of equations

$$v_{t_k} = g_k[v].$$

• The *differentiated potential KdV (DPKdV) hierarchy* is the family of equations

$$v_{xt_k} = (g_k[v])_x.$$

The right-hand sides of first few PKdV equations are

$$g_1 = v_x, \quad g_2 = v_{xxx} + 3v_x^2, \quad g_3 = v_{xxxxx} + 10v_xv_{xxx} + 5v_{xx}^2 + 10v_x^3.$$

Remark 4.2 The first KdV and PKdV equations, $u_{t_1} = u_x$, resp. $v_{t_1} = v_x$, allow us to identify x with t_1.

Proposition 4.3 *The differential polynomials $r_k[u]$ satisfy*

$$\frac{\delta r_k}{\delta u} = (4k-2)\, r_{k-1},$$

where $\frac{\delta}{\delta u}$ is shorthand notation for $\frac{\delta_1}{\delta u}$.

A proof of this statement can be found in [12, 3.7.11–3.7.14].

Corollary 4.4 *Set $h_k[v] := \frac{1}{4k+2} g_{k+1}[v]$, then the differential polynomials g_k and h_k satisfy*

$$\frac{\delta g_k}{\delta v_x} = (4k-2)\, g_{k-1} \qquad \text{and} \qquad \frac{\delta h_k}{\delta v_x} = g_k.$$

Before we proceed, let us formulate a simple Lemma.

Lemma 4.5 *For any multi-index I and for any differential polynomial $f[v]$ we have:*

$$\mathrm{D}_x\left(\frac{\delta f}{\delta v_{Ix}}\right) = \frac{\partial f}{\partial v_I} - \frac{\delta f}{\delta v_I}.$$

Proof By direct calculation:

$$\mathrm{D}_x\left(\frac{\delta f}{\delta v_{Ix}}\right) = \mathrm{D}_x\left(\frac{\partial f}{\partial v_{Ix}} - \mathrm{D}_x\frac{\partial f}{\partial v_{Ix^2}} + \mathrm{D}_x^2\frac{\partial f}{\partial v_{Ix^3}} - \dots\right)$$

$$= \mathrm{D}_x \frac{\partial f}{\partial v_{Ix}} - \mathrm{D}_x^2 \frac{\partial f}{\partial v_{Ix^2}} + \mathrm{D}_x^2 \frac{\partial f}{\partial v_{Ix^3}} - \ldots = \frac{\partial f}{\partial v_I} - \frac{\delta f}{\delta v_I}.$$

□

We can now find Lagrangians for the the DPKdV equations.

Proposition 4.6 *The DPKdV equations are Lagrangian, with the Lagrange functions*

$$L_k[v] = \frac{1}{2} v_x v_{t_k} - h_k[v].$$

Proof Since $h_k = \frac{1}{4k+2} g_{k+1}$ does not depend on v directly, it follows from Lemma 4.5 and Corollary 4.4 that

$$\frac{\delta L_k}{\delta v} = -v_{t_k x} - \frac{\delta h_k}{\delta v} = -v_{t_k x} + \mathrm{D}_x \frac{\delta h_k}{\delta v_x} = -v_{t_k x} + (g_k)_x.$$

□

5 Pluri-Lagrangian Structure of PKdV Hierarchy

Since the individual KdV and PKdV equations are evolutionary (not variational), it seems not very plausible that they could have a pluri-Lagrangian structure. However, it turns out that the PKdV hierarchy as a whole is pluri-Lagrangian. Let us stress that this structure is only visible if one considers several PKdV equations simultaneously and not individually. We consider a finite-dimensional multi-time $\mathbb{R}^N$ parametrized by $t_1, t_2, \ldots, t_N$ supporting the first N flows of the PKdV hierarchy. Recall that the first PKdV equation reads $v_{t_1} = v_x$, which allows us to identify t_1 with x.

The formulation of the main result involves certain differential polynomials introduced in the following statement.

Lemma 5.1 • *There exist differential polynomials $b_{ij}[v]$ depending on v and v_{x^α}, $\alpha > 0$, such that*

$$\mathrm{D}_x(g_i) g_j = \mathrm{D}_x(b_{ij}). \tag{19}$$

• *These polynomials satisfy*

$$b_{ij} + b_{ji} = g_i g_j. \tag{20}$$

• *The differential polynomials $a_{ij}[v]$ (depending on v_{x^α} and $v_{x^\alpha t_j}$, $\alpha \geq 0$) defined by*

$$a_{ij} := v_{t_j} \frac{\delta_1 h_i}{\delta v_x} + v_{xt_j} \frac{\delta_1 h_i}{\delta v_{xx}} + v_{xxt_j} \frac{\delta_1 h_i}{\delta v_{xxx}} + \ldots \tag{21}$$

satisfy

$$\mathrm{D}_j(h_i) + \mathrm{D}_x(g_i)v_{t_j} = \mathrm{D}_x(a_{ij}). \tag{22}$$

Proof The existence of polynomials b_{ij} is shown in [12, 3.7.9]. Since

$$\mathrm{D}_x(b_{ij} + b_{ji}) = \mathrm{D}_x(g_i)g_j + g_i\,\mathrm{D}_x(g_j) = \mathrm{D}_x(g_i g_j),$$

and since neither $b_{ij} + b_{ji}$ nor $g_i g_j$ contain constant terms, Eq. (20) follows. The last claim is a straightforward calculation using Lemma 4.5:

$$\begin{aligned}
\mathrm{D}_x(a_{ij}) &= \mathrm{D}_x\left(v_{t_j}\frac{\delta_1 h_i}{\delta v_x} + v_{xt_j}\frac{\delta_1 h_i}{\delta v_{xx}} + v_{xxt_j}\frac{\delta_1 h_i}{\delta v_{xxx}} + \dots\right)\\
&= v_{xt_j}\frac{\delta_1 h_i}{\delta v_x} + v_{xxt_j}\frac{\delta_1 h_i}{\delta v_{xx}} + v_{xxxt_j}\frac{\delta_1 h_i}{\delta v_{xxx}} + \dots\\
&\quad + v_{t_j}\,\mathrm{D}_x\left(\frac{\delta_1 h_i}{\delta v_x}\right) + v_{xt_j}\,\mathrm{D}_x\left(\frac{\delta_1 h_i}{\delta v_{xx}}\right) + v_{xxt_j}\,\mathrm{D}_x\left(\frac{\delta_1 h_i}{\delta v_{xxx}}\right) + \dots\\
&= v_{xt_j}\frac{\delta_1 h_i}{\delta v_x} + v_{xxt_j}\frac{\delta_1 h_i}{\delta v_{xx}} + v_{xxxt_j}\frac{\delta_1 h_i}{\delta v_{xxx}} + \dots\\
&\quad - v_{t_j}\frac{\delta_1 h_i}{\delta v} + v_{t_j}\frac{\partial h_i}{\partial v} - v_{xt_j}\frac{\delta_1 h_i}{\delta v_x} + v_{xt_j}\frac{\partial h_i}{\partial v_x} - v_{xxt_j}\frac{\delta_1 h_i}{\delta v_{xx}} + v_{xxt_j}\frac{\partial h_i}{\partial v_{xx}} - \dots\\
&= \mathrm{D}_j\, h_i - v_{t_j}\frac{\delta_1 h_i}{\delta v} = \mathrm{D}_j\, h_i + \mathrm{D}_x(g_i)v_{t_j}.
\end{aligned}$$

□

Now we are in a position to give a pluri-Lagrangian formulation of the PKdV hierarchy.

Theorem 5.2 *The multi-time Euler-Lagrange equations for the Lagrangian two-form* $\mathscr{L} = \sum_{i<j} L_{ij}\,\mathrm{d}t_i \wedge \mathrm{d}t_j$*, with coefficients given by*

$$L_{1i} := L_i = \frac{1}{2}v_x v_{t_i} - h_i \tag{23}$$

and

$$L_{ij} := \frac{1}{2}(v_{t_i}g_j - v_{t_j}g_i) + (a_{ij} - a_{ji}) - \frac{1}{2}(b_{ij} - b_{ji}) \quad \textit{for} \quad j > i > 1 \tag{24}$$

are the first $N-1$ *nontrivial PKdV equations*

$$v_{t_2} = g_2, \quad v_{t_3} = g_3, \quad \dots \quad v_{t_N} = g_N,$$

and equations that follow from these by differentiation.

5.1 Variational Symmetries and the Pluri-Lagrangian Form

Before proving Theorem 5.2, let us give an heuristic derivation of expression (24) for L_{ij}. The ansatz is that different flows of the PKdV hierarchy should be variational symmetries of each other. (We are grateful to V. Adler who proposed this derivation to us in a private communication.)

Fix two distinct integers $i, j \in \{2, 3, \dots, N\}$. Consider the the ith DPKdV equation, which is nothing but the conventional two-dimensional variational system generated in the (x, t_i)-plane by the Lagrange function

$$L_{1i}[v] = \frac{1}{2} v_x v_{t_i} - h_i[v].$$

Consider the evolutionary equation $v_{t_j} = g_j[v]$, i.e., the jth PKdV equation, and the corresponding generalized vector field

$$\mathrm{D}_{g_j} := \sum_{I \neq j} (\mathrm{D}_I\, g_j) \frac{\partial}{\partial v_I}.$$

We want to show that D_{g_j} is a variational symmetry of L_{1i}. For this end, we look for L_{ij} such that

$$\mathrm{D}_{g_j}(L_{1i}) - \mathrm{D}_i \left(L_{1j}^{(g_j)} \right) + \mathrm{D}_x(L_{ij}) = 0. \tag{25}$$

Here, $L_{1j}^{(g_j)}$ is the Lagrangian defined by (23) but with v_{t_j} replaced by g_j:

$$L_{1j}^{(g_j)} := \frac{1}{2} v_x g_j - h_j.$$

We have:

$$\mathrm{D}_i \left(L_{1j}^{(g_j)} \right) = \frac{1}{2} v_{t_i x} g_j + \frac{1}{2} v_x (g_j)_{t_i} - \mathrm{D}_i(h_j),$$
$$\mathrm{D}_{g_j}(L_{1i}) = \frac{1}{2} (g_j)_x v_{t_i} + \frac{1}{2} v_x (g_j)_{t_i} - \mathrm{D}_{g_j}(h_i).$$

Upon using (22) and (19), and introducing the polynomial

$$a_{ij}^{(g_j)} := g_j \frac{\delta_1 h_i}{\delta v_x} + (g_j)_x \frac{\delta_1 h_i}{\delta v_{xx}} + (g_j)_{xx} \frac{\delta_1 h_i}{\delta v_{xxx}} + \dots$$

obtained from a_{ij} through the replacement of v_{t_j} by g_j, we find:

$$\mathrm{D}_i \left(L_{1j}^{(g_j)} \right) - \mathrm{D}_{g_j}(L_{1i}) = \frac{1}{2} v_{t_i x} g_j - \frac{1}{2} (g_j)_x v_{t_i} - \mathrm{D}_i(h_j) + \mathrm{D}_{g_j}(h_i)$$

$$
\begin{aligned}
&= \frac{1}{2} v_{t_i x} g_j - \frac{1}{2} (g_j)_x v_{t_i} - (a_{ji})_x + (g_j)_x v_{t_i} + \left(a_{ij}^{(g_j)}\right)_x - (g_i)_x g_j \\
&= \frac{1}{2} v_{t_i x} g_j + \frac{1}{2} (g_j)_x v_{t_i} - \left(a_{ji} - a_{ij}^{(g_j)}\right)_x - (g_i)_x g_j \\
&= \frac{1}{2} (v_{t_i} g_j)_x + \left(a_{ij}^{(g_j)} - a_{ji}\right)_x - (b_{ij})_x .
\end{aligned}
$$

We denote the antiderivative with respect to x of this quantity by

$$
L_{ij}^{(i)} := \frac{1}{2} v_{t_i} g_j + \left(a_{ij}^{(g_j)} - a_{ji}\right) - b_{ij} .
$$

The analogous calculation with coordinates x and t_j yields

$$
\mathrm{D}_{g_i}(L_{1j}) - \mathrm{D}_j\left(L_{1i}^{(g_i)}\right) = -\frac{1}{2}(v_{t_j} g_i)_x + \left(a_{ij} - a_{ji}^{(g_i)}\right)_x + (b_{ji})_x .
$$

We denote its antiderivative by

$$
L_{ij}^{(j)} := -\frac{1}{2} v_{t_j} g_i + \left(a_{ij} - a_{ji}^{(g_i)}\right) + b_{ji} .
$$

Now we look for a differential polynomial $L_{ij}[v]$ depending on the partial derivatives of v with respect to x, t_i and t_j that reduces to $L_{ij}^{(i)}$ and to $L_{ij}^{(j)}$ after the substitutions $v_{t_j} = g_j$ and $v_{t_i} = g_i$, respectively. It turns out that there is a one-parameter family of such functions, given by

$$
L_{ij} = c v_{t_i} v_{t_j} + (a_{ij} - a_{ji}) + \left(\frac{1}{2} - c\right) v_{t_i} g_j - \left(\frac{1}{2} + c\right) v_{t_j} g_i + \frac{1}{2}(b_{ji} - b_{ij}) + c g_i g_j
$$

for $c \in \mathbb{R}$. Checking this is a straightforward calculation using Eq. (20). Our theory does not depend in any essential way on the choice of L_{ij} within this family. For aesthetic reasons we chose $c = 0$, which gives us Eq. (24).

Remark 5.3 We could also take $\mathscr{L}$ to be the c-linear part of the form we have just obtained, i.e. $\mathscr{L} = \sum_{1<i<j} (v_{t_i} - g_i)(v_{t_j} - g_j)\, \mathrm{d}t_i \wedge \mathrm{d}t_j$. One can think of this as choosing $c = \infty$. Such a two-form $\mathscr{L}$ can be considered for any family of evolutionary equations $v_{t_i} = g_i[v]$. However, due to the vanishing components L_{1i}, this form $\mathscr{L}$ has no relation to the classical variational formulation of the individual differential equations $v_{xt_i} = (g_i)_x$.

Eventually, Eq. (25) leads to the following closedness property.

Proposition 5.4 *The two-form $\mathscr{L} = \sum_{i<j} L_{ij}\, \mathrm{d}t_i \wedge \mathrm{d}t_j$, with coefficients given by (23) and (24), is closed as soon as v solves all but one of the PKdV equations $v_{t_2} = g_2, \ldots, v_{t_N} = g_N$.*

Proof We use the notation

$$\mathrm{d}\mathscr{L} = \sum_{i<j<k} M_{ijk}\,\mathrm{d}t_i \wedge \mathrm{d}t_j \wedge \mathrm{d}t_k, \quad M_{ijk} = \mathrm{D}_k L_{ij} - \mathrm{D}_j L_{ik} + \mathrm{D}_i L_{jk} \tag{26}$$

We start by showing that $M_{1jk} = \mathrm{D}_k L_{1j} - \mathrm{D}_j L_{1k} + \mathrm{D}_x L_{jk}$ vanishes as soon as either $v_{t_j} = g_j$ or $v_{t_k} = g_k$ is satisfied. Indeed, we have:

$$\begin{aligned}
M_{1jk} &= \mathrm{D}_k L_{1j} - \mathrm{D}_j L_{1k} + \mathrm{D}_x L_{jk} \\
&= \frac{1}{2} v_{t_j t_k} v_x + \frac{1}{2} v_{t_j} v_{x t_k} - \mathrm{D}_k h_j - \frac{1}{2} v_{t_j t_k} v_x - \frac{1}{2} v_{t_k} v_{x t_j} + \mathrm{D}_j h_k \\
&\quad + \frac{1}{2}\left(v_{x t_j} g_k + v_{t_j}\,\mathrm{D}_x g_k - v_{x t_k} g_j - v_{t_k}\,\mathrm{D}_x g_j\right) \\
&\quad + \mathrm{D}_k h_j + v_{t_k}\,\mathrm{D}_x g_j - \mathrm{D}_j h_k - v_{t_j}\,\mathrm{D}_x g_k - \frac{1}{2}(g_k\,\mathrm{D}_x g_j - g_j\,\mathrm{D}_x g_k) \\
&= \frac{1}{2}\Big(v_{t_j} v_{x t_k} - v_{t_k} v_{x t_j} + v_{x t_j} g_k - v_{t_j}\,\mathrm{D}_x g_k \\
&\qquad - v_{x t_k} g_j + v_{t_k}\,\mathrm{D}_x g_j - g_k\,\mathrm{D}_x g_j + g_j\,\mathrm{D}_x g_k\Big) \\
&= \frac{1}{2}\left(v_{t_j} - g_j\right)\mathrm{D}_x\left(v_{t_k} - g_k\right) - \frac{1}{2}\left(v_{t_k} - g_k\right)\mathrm{D}_x\left(v_{t_j} - g_j\right).
\end{aligned} \tag{27}$$

For the case $i, j, k > 1$, we assume without loss of generality that $v_{t_i} = g_i$ and $v_{t_j} = g_j$ are satisfied. We do not assume that $v_{t_k} = g_k$ holds, and correspondingly we do not make any identification involving $v_{t_k}, v_{x t_k}, \ldots$. Using Eq. (27), we find:

$$\begin{aligned}
\mathrm{D}_x M_{ijk} &= \mathrm{D}_x\left(\mathrm{D}_k L_{ij} - \mathrm{D}_j L_{ik} + \mathrm{D}_i L_{jk}\right) \\
&= \mathrm{D}_k\left(\mathrm{D}_i L_{1j} - \mathrm{D}_j L_{1i}\right) - \mathrm{D}_j\left(\mathrm{D}_i L_{1k} - \mathrm{D}_k L_{1i}\right) + \mathrm{D}_i\left(\mathrm{D}_j L_{1k} - \mathrm{D}_k L_{1j}\right) \\
&= 0.
\end{aligned}$$

Since these polynomials do not contain constant terms, it follows that

$$\mathrm{D}_k L_{ij} - \mathrm{D}_j L_{ik} + \mathrm{D}_i L_{jk} = 0.$$

□

Remark 5.5 Assuming that the statement of Theorem 5.2 holds true, one can easily prove a somewhat weaker claim than Proposition 5.4, namely that the two-form $\mathscr{L}$ is closed on simultaneous solutions of *all* the PKdV equations. Indeed, by Proposition 2.2, $\mathrm{d}\mathscr{L}$ is constant on solutions of the multi-time Euler-Lagrange equations $v_{t_i} = g_i$. Vanishing of this constant follows from the fact that $\mathrm{d}\mathscr{L} = 0$ on the trivial solution $v \equiv 0$.

5.2 The Multi-time Euler-Lagrange Equations

Proof (of Theorem 5.2) We check all multi-time Euler-Lagrange Eqs. (5)–(7) individually. If $N > 3$, we fix $k > j > i > 1$. If $N = 3$, we take $j = 3$, $i = 2$, and in the following ignore all equations containing k. We use the convention $L_{ji} = -L_{ij}$, etc.

Equations (7)

- The equations
$$\frac{\delta_{1i} L_{1i}}{\delta v_{I x t_i}} + \frac{\delta_{ij} L_{ij}}{\delta v_{I t_i t_j}} + \frac{\delta_{1j} L_{j1}}{\delta v_{I t_j x}} = 0$$
and
$$\frac{\delta_{ij} L_{ij}}{\delta v_{I t_i t_j}} + \frac{\delta_{jk} L_{jk}}{\delta v_{I t_j t_k}} + \frac{\delta_{ki} L_{ki}}{\delta v_{I t_k t_i}} = 0$$
are trivial because all terms vanish.

Equations (6)

- The equation
$$\frac{\delta_{1i} L_{1i}}{\delta v_x} = \frac{\delta_{ij} L_{ji}}{\delta v_{t_j}}$$
yields
$$\begin{aligned} \frac{1}{2} v_{t_i} - \frac{\delta_{1i} h_i}{\delta v_x} &= \frac{1}{2} g_i - \frac{\delta_{ij} a_{ij}}{\delta v_{t_j}} \\ &= \frac{1}{2} g_i - \frac{\delta_{ij}}{\delta v_{t_j}} \left(v_{t_j} \frac{\delta_1 h_i}{\delta v_x} + v_{t_j x} \frac{\delta_1 h_i}{\delta v_{xx}} + v_{t_j xx} \frac{\delta_1 h_i}{\delta v_{xxx}} + \dots \right) \\ &= \frac{1}{2} g_i - \frac{\delta_1 h_i}{\delta v_x}. \end{aligned}$$
This simplifies to the PKdV equation
$$v_{t_i} = g_i. \tag{28}$$

- For $\alpha > 0$, the equation
$$\frac{\delta_{1i} L_{1i}}{\delta v_{x^{\alpha+1}}} = \frac{\delta_{ij} L_{ji}}{\delta v_{t_j x^\alpha}}$$
yields
$$-\frac{\delta_{1i} h_i}{\delta v_{x^{\alpha+1}}} = -\frac{\delta_{ij}}{\delta v_{t_j x^\alpha}} \left(v_{t_j} \frac{\delta_1 h_i}{\delta v_x} + v_{t_j x} \frac{\delta_1 h_i}{\delta v_{xx}} + v_{t_j xx} \frac{\delta_1 h_i}{\delta v_{xxx}} + \dots \right)$$

$$= -\frac{\delta_1 h_i}{\delta v_{x^{\alpha+1}}},$$

which is trivial.

- Similarly, the equation

$$\frac{\delta_{1j} L_{1j}}{\delta v_x} = \frac{\delta_{ij} L_{ij}}{\delta v_{t_i}}$$

yields PKdV equation

$$v_{t_j} = g_j, \tag{29}$$

and for $\alpha > 0$, the equation

$$\frac{\delta_{1j} L_{1j}}{\delta v_{x^{\alpha+1}}} = \frac{\delta_{ij} L_{ij}}{\delta v_{t_i x^\alpha}}$$

is trivial.

- All equations of the form

$$\frac{\delta_{1i} L_{1i}}{\delta v_{xI}} = \frac{\delta_{ij} L_{ji}}{\delta v_{t_j I}} \quad (t_i \notin I) \qquad \text{and} \qquad \frac{\delta_{1j} L_{1j}}{\delta v_{xI}} = \frac{\delta_{ij} L_{ij}}{\delta v_{t_i I}} \quad (t_j \notin I)$$

where I contains any t_l $(l > 1)$ are trivial because each term is zero.

- The equations

$$\frac{\delta_{1i} L_{1i}}{\delta v_{It_i}} = \frac{\delta_{1j} L_{1j}}{\delta v_{It_j}} \qquad (x \notin I)$$

and

$$\frac{\delta_{ij} L_{ij}}{\delta v_{It_j}} = \frac{\delta_{ik} L_{ik}}{\delta v_{It_k}} \qquad (t_i \notin I)$$

are easily seen to be trivial as well.

Equations (5)

- By construction, the equations $\dfrac{\delta_{1i} L_{1i}}{\delta v} = 0$ for $i > 1$ are the equations

$$v_{xt_i} = \mathrm{D}_x\, g_i. \tag{30}$$

For I containing any $t_l, l > 1, l \neq i$, the equations $\dfrac{\delta_{1i} L_{1i}}{\delta v_{t_I}} = 0$ are trivial.

- The last family of equations we discuss as a lemma because its calculation is far from trivial.

Lemma 5.6 *The equations* $\dfrac{\delta_{ij} L_{ij}}{\delta v_{x^\alpha}} = 0$ *are corollaries of the PKdV equations.*

Proof (of Lemma 5.6) From Eq. (24) we see that the variational derivative of L_{ij} contains only three nonzero terms,

$$\frac{\delta_{ij} L_{ij}}{\delta v_{x^\alpha}} = \frac{\partial L_{ij}}{\partial v_{x^\alpha}} - \mathrm{D}_i \left(\frac{\partial L_{ij}}{\partial v_{x^\alpha t_i}} \right) - \mathrm{D}_j \left(\frac{\partial L_{ij}}{\partial v_{x^\alpha t_j}} \right). \tag{31}$$

In particular, the equation $\dfrac{\delta_{ij} L_{ij}}{\delta v} = 0$ yields $\mathrm{D}_i\, g_j - \mathrm{D}_j\, g_i = 0$, that is, the compatibility condition of the flows $v_{t_i} = g_i$ and $v_{t_j} = g_j$. To determine the first term on the right hand side of Eq. (31) for an arbitrary $\alpha > 0$, we use an indirect method. Assume that the dimension of multi-time N is at least 4 and fix $k > 1$ distinct from i and j. Let v be a solution of all PKdV equations except $v_{t_k} = g_k$. By Proposition 5.4 we have

$$\sum_I \frac{\partial L_{ij}}{\partial v_I} v_{It_k} = \mathrm{D}_k\, L_{ij} = \mathrm{D}_j\, L_{ik} - \mathrm{D}_i\, L_{jk}. \tag{32}$$

Since $\frac{\partial L_{ij}}{\partial v_I}$ does not contain any derivatives with respect to t_k, we can determine $\frac{\partial L_{ij}}{\partial v_{x^\alpha}}$ by looking at the terms in the right hand side of Eq. (32) containing $v_{x^\alpha t_k}$. These are

$$\begin{aligned} &\mathrm{D}_j \left(-\frac{1}{2} g_i v_{t_k} + v_{t_k} \frac{\delta_1 h_i}{\delta v_x} + v_{xt_k} \frac{\delta_1 h_i}{\delta v_{xx}} + \dots \right) \\ &- \mathrm{D}_i \left(-\frac{1}{2} g_j v_{t_k} + v_{t_k} \frac{\delta_1 h_j}{\delta v_x} + v_{xt_k} \frac{\delta_1 h_j}{\delta v_{xx}} + \dots \right). \end{aligned}$$

Now we expand the brackets. By again throwing out all terms that do not contain any $v_{x^\alpha t_k}$, and those that cancel modulo $v_{t_i} = g_i$ or $v_{t_j} = g_j$, we get

$$\begin{aligned} &- v_{t_k} \mathrm{D}_j \left(\frac{\delta_1 h_i}{\delta v_x} \right) + v_{xt_k} \mathrm{D}_j \left(\frac{\delta_1 h_i}{\delta v_{xx}} \right) + v_{xxt_k} \mathrm{D}_j \left(\frac{\delta_1 h_i}{\delta v_{xxx}} \right) + \dots \\ &+ v_{t_k} \mathrm{D}_i \left(\frac{\delta_1 h_j}{\delta v_x} \right) - v_{xt_k} \mathrm{D}_i \left(\frac{\delta_1 h_j}{\delta v_{xx}} \right) - v_{xxt_k} \mathrm{D}_i \left(\frac{\delta_1 h_j}{\delta v_{xxx}} \right) - \dots . \end{aligned}$$

Comparing this to Eq. (32), we find that

$$\frac{\partial L_{ij}}{\partial v_{x^\alpha}} = -\mathrm{D}_i \left(\frac{\delta_1 h_j}{\delta v_{x^{\alpha+1}}} \right) + \mathrm{D}_j \left(\frac{\delta_1 h_i}{\delta v_{x^{\alpha+1}}} \right).$$

On the other hand we have

$$-\mathrm{D}_i \left(\frac{\partial L_{ij}}{\partial v_{x^\alpha t_i}} \right) - \mathrm{D}_j \left(\frac{\partial L_{ij}}{\partial v_{x^\alpha t_j}} \right) = \mathrm{D}_i \left(\frac{\delta_1 h_j}{\delta v_{x^{\alpha+1}}} \right) - \mathrm{D}_j \left(\frac{\delta_1 h_i}{\delta v_{x^{\alpha+1}}} \right),$$

so Equation (31) implies that $\frac{\delta_{ij} L_{ij}}{\delta v_{x^\alpha}} = 0$ for any α.

Since $\frac{\delta_{23} L_{23}}{\delta v_{x^\alpha}} = 0$ does not depend on the dimension $N \geqslant 3$, the result for $N \geqslant 4$ implies the claim for $N = 3$. □

This concludes the proof of Theorem 5.2. □

6 Relation to Hamiltonian Formalism

In this last section, we briefly discuss the connection between the closedness of $\mathscr{L}$ and the involutivity of the corresponding Hamiltonians.

In Proposition 2.2 we saw that $\mathrm{d}\mathscr{L}$ is constant on solutions. For the one–dimensional case ($d = 1$) with $\mathscr{L}$ depending on the first jet bundle only, it has been shown in [20] that this is equivalent to the commutativity of the corresponding Hamiltonian flows. If the constant is zero then the Hamiltonians are in involution. Now we will prove a similar result for the two-dimensional case.

We will use a Poisson bracket on *formal integrals*, i.e. equivalence classes of functions modulo x-derivatives [12, Chap. 1–2]. In this section, the integral sign $\int$ will always denote an equivalence class, not an integration operator. The Poisson bracket due to Gardner-Zakharov-Faddeev is defined by

$$\{\textstyle\int F, \int G\} = \int \left(\mathrm{D}_x \frac{\delta_1 F}{\delta u}\right) \frac{\delta_1 G}{\delta u}.$$

Using integration by parts, we see that this bracket is anti-symmetric. Less obvious is the fact that it satisfies the Jacobi identity [18, Chap. 7]. As we did when studying the KdV hierarchy, we introduce a potential v that satisfies $v_x = u$, and we identify the space-coordinate x with the first coordinate t_1 of multi-time. We can now re-write the Poisson bracket as

$$\{\textstyle\int F, \int G\} = \int \left(\mathrm{D}_x \frac{\delta_1 F}{\delta v_x}\right) \frac{\delta_1 G}{\delta v_x} = -\int \frac{\delta_1 F}{\delta v} \frac{\delta_1 G}{\delta v_x}, \tag{33}$$

for functions F and G that depend on the x-derivatives of v but not on v itself.

Assume that the coefficients L_{1j} of the Lagrangian two-from $\mathscr{L}$ are given by

$$L_{1j} = \frac{1}{2} v_x v_{t_j} - h_j,$$

where h_j is a differential polynomial in $v_x, v_{xx}, \ldots$. This is the case for the PKdV hierarchy. The L_{1j} are Lagrangians of the equations

$$v_{xt_j} = \mathrm{D}_x\, g_j \qquad \text{or} \qquad u_{t_j} = \mathrm{D}_x\, g_j,$$

where $g_j := \frac{\delta_1 h_j}{\delta v_x}$, hence $\frac{\delta_1 h_j}{\delta v} = -\mathrm{D}_x\, g_j$. It turns out that the formal integral $\int h_j$ is the Hamilton functional for the equation $u_{t_j} = \mathrm{D}_x\, g_j$ with respect to the Poisson bracket (33). Formally:

$$\{\int h_j, u(y)\} = \{\int h_j, \int u\,\delta(\cdot - y)\} = -\int \frac{\delta_1 h_j}{\delta v}\delta(x-y) \;= \mathrm{D}_x\, g_j(y),$$

where δ denotes the Dirac delta.

Theorem 6.1 *If* $\mathrm{d}\mathscr{L} = 0$ *on solutions, then the Hamiltonians are in involution,*

$$\{\int h_i, \int h_j\} = 0.$$

Proof Recall notation (26). We have

$$\begin{aligned}
\int M_{1jk} &= \int \big(\mathrm{D}_x\, L_{jk} - \mathrm{D}_j\, L_{1k} + \mathrm{D}_k\, L_{1j}\big)\\
&= \int \big(-\mathrm{D}_j\, L_{1k} + \mathrm{D}_k\, L_{1j}\big)\\
&= \int \Big(-\frac{1}{2}v_{xt_j}v_{t_k} - \frac{1}{2}v_x v_{t_k t_j} + \mathrm{D}_j\, h_k + \frac{1}{2}v_{xt_k}v_{t_j} + \frac{1}{2}v_x v_{t_j t_k} - \mathrm{D}_k\, L_{1j}\Big)\\
&= \int \Big(\frac{1}{2}\big(v_{xt_k}v_{t_j} - v_{xt_j}v_{t_k}\big) - \mathrm{D}_k\, L_{1j} + \mathrm{D}_j\, h_k\Big)
\end{aligned}$$

Using Eq. (21) (which, as opposed to Eq. (19), is independent of the form of h_i and g_i), the evolution equations $v_{t_j} = g_j$, and integration by parts, we find that

$$\begin{aligned}
\int M_{1jk} &= \int \Big(\frac{1}{2}\big(v_{xt_k}v_{t_j} - v_{xt_j}v_{t_k}\big) - \mathrm{D}_x\, a_{jk} + v_{t_k}\,\mathrm{D}_x\, g_j + \mathrm{D}_x\, a_{kj} - v_{t_j}\,\mathrm{D}_x g_k\Big)\\
&= \int \Big(-\frac{1}{2}\big(g_j\,\mathrm{D}_x\, g_k - g_k\,\mathrm{D}_x\, g_j\big) - \mathrm{D}_x\, a_{jk} + \mathrm{D}_x\, a_{kj}\Big)\\
&= \int g_k\,\mathrm{D}_x\, g_j\\
&= -\int \frac{\delta_1 h_j}{\delta v}\frac{\delta_1 h_k}{\delta v_x}\\
&= \{\int h_j, \int h_k\}.
\end{aligned}$$

Hence if $\mathrm{d}\mathscr{L} = 0$ on solutions of the evolution equations $v_{t_j} = g_j$, then the Hamilton functionals are in involution. □

7 Conclusion

We have formulated the pluri-Lagrangian theory of integrable hierarchies, and propose it as a definition of integrability. The motivation for this definition comes from the discrete case [10, 13, 20] and the fact that we have established a relation with the Hamiltonian side of the theory. For the Hamiltonians to be in involution, we need the additional fact that the Lagrangian two-form is closed. However, we believe that the essential part of the theory is inherently contained in the pluri-Lagrangian formalism.

Since the KdV hierarchy is one of the most important examples of an integrable hierarchy, our construction of a pluri-Lagrangian structure for the PKdV hierarchy is an additional indication that the existence of a pluri-Lagrangian structure is a reasonable definition of integrability.

It is remarkable that multi-time Euler-Lagrange equations are capable of producing evolutionary equations. This is a striking difference from the discrete case, where the evolution equations (*quad equations*) imply the multi-time Euler–Lagrange equations (*corner equations*), but are themselves not variational [10].

Acknowledgments This research is supported by the Berlin Mathematical School and the DFG Collaborative Research Center TRR 109 "Discretization in Geometry and Dynamics".

A. A very short introduction to the variational bicomplex

Here we introduce the variational bicomplex and derive the basic results that we use in the text. We follow Dickey, who provides a more complete discussion in [12, Chap. 19]. Another good source on a (subtly different) variational bicomplex is Anderson's unfinished manuscript [2]. For ease of notation we restrict to real fields $u : \mathbb{R}^N \to \mathbb{R}$, rather than vector-valued fields.

The space of (p, q)-forms $\mathscr{A}^{(p,q)}$ consists of all formal sums

$$\omega^{p,q} = \sum f \, \delta u_{I_1} \wedge \ldots \wedge \delta u_{I_p} \wedge \mathrm{d}t_{j_1} \wedge \ldots \wedge \mathrm{d}t_{j_q},$$

where f is a polynomial in u and partial derivatives of u of arbitrary order with respect to any coordinates. The vertical one-forms δu_I are dual to the vector fields $\frac{\partial}{\partial u_I}$. The action of the derivative D_i on $\omega^{p,q}$ is

$$\begin{aligned}\mathrm{D}_i \, \omega^{p,q} = \sum (\mathrm{D}_i \, f) \, \delta u_{I_1} \wedge \ldots \wedge \delta u_{I_p} \wedge \mathrm{d}t_{j_1} \wedge \ldots \wedge \mathrm{d}t_{j_q} \\ + \; f \, \delta u_{I_1 i} \wedge \ldots \wedge \delta u_{I_p} \wedge \mathrm{d}t_{j_1} \wedge \ldots \wedge \mathrm{d}t_{j_q} \\ + \; \ldots + f \, \delta u_{I_1} \wedge \ldots \wedge \delta u_{I_p i} \wedge \mathrm{d}t_{j_1} \wedge \ldots \wedge \mathrm{d}t_{j_q}.\end{aligned}$$

The integral of $\omega^{p,q}$ over an q-dimensional manifold is the $(p, 0)$-form defined by

$$\int \omega^{p,q} = \sum \left(\int f \, \mathrm{d}t_{j_1} \wedge \ldots \wedge \mathrm{d}t_{j_q} \right) \delta u_{I_1} \wedge \ldots \wedge \delta u_{I_p}.$$

We call $(0,q)$-forms horizontal and $(p,0)$-forms vertical. The *horizontal exterior derivative* $\mathrm{d} : \mathscr{A}^{(p,q)} \to \mathscr{A}^{(p,q+1)}$ and the *vertical exterior derivative* $\delta : \mathscr{A}^{(p,q)} \to \mathscr{A}^{(p+1,q)}$ are defined by the anti-derivation property

(a) $$\mathrm{d}\left(\omega_1^{p_1,q_1} \wedge \omega_2^{p_2,q_2}\right) = \mathrm{d}\omega_1^{p_1,q_1} \wedge \omega_2^{p_2,q_2} + (-1)^{p_1+q_1} \omega_1^{p_1,q_1} \wedge \mathrm{d}\omega_2^{p_2,q_2},$$

$$\delta\left(\omega_1^{p_1,q_1} \wedge \omega_2^{p_2,q_2}\right) = \delta\omega_1^{p_1,q_1} \wedge \omega_2^{p_2,q_2} + (-1)^{p_1+q_1} \omega_1^{p_1,q_1} \wedge \delta\omega_2^{p_2,q_2},$$

and by the way they act on $(0,0)$-, $(1,0)$-, and $(0,1)$-forms:

(b) $$\mathrm{d}f = \sum_j \mathrm{D}_j f \, \mathrm{d}t_j = \sum_j \left(\frac{\partial f}{\partial t_j} + \sum_I \frac{\partial f}{\partial u_I} u_{Ij} \right) \mathrm{d}t_j, \quad \delta f = \sum_I \frac{\partial f}{\partial u_I} \delta u_I,$$

(c) $$\mathrm{d}(\delta u_I) = -\sum_j \delta u_{Ij} \wedge \mathrm{d}t_j, \quad \delta(\delta u_I) = 0,$$

(d) $$\mathrm{d}(\mathrm{d}t_j) = 0, \quad \delta(\mathrm{d}t_j) = 0, \quad \delta(\mathrm{d}u_I) = -\mathrm{d}(\delta u_I) = \sum_j \delta u_{Ij} \wedge \mathrm{d}t_j.$$

Properties (a)–(d) determine the action of d and δ on any form. The corresponding mapping diagram is known as the *variational bicomplex*.

$$\begin{array}{ccccccc}
\vdots & & \vdots & & \vdots & & \vdots \\
\uparrow \delta & & \uparrow \delta & & \uparrow \delta & & \uparrow \delta \\
\mathscr{A}^{(1,0)} & \xrightarrow{\mathrm{d}} & \mathscr{A}^{(1,1)} & \xrightarrow{\mathrm{d}} \ \ldots \ \xrightarrow{\mathrm{d}} & \mathscr{A}^{(1,n-1)} & \xrightarrow{\mathrm{d}} & \mathscr{A}^{(1,n)} \\
\uparrow \delta & & \uparrow \delta & & \uparrow \delta & & \uparrow \delta \\
\mathscr{A}^{(0,0)} & \xrightarrow{\mathrm{d}} & \mathscr{A}^{(0,1)} & \xrightarrow{\mathrm{d}} \ \ldots \ \xrightarrow{\mathrm{d}} & \mathscr{A}^{(0,n-1)} & \xrightarrow{\mathrm{d}} & \mathscr{A}^{(0,n)}
\end{array}$$

The following claims follow immediately from the definitions.

Proposition A.1 *We have* $\mathrm{d}^2 = \delta^2 = 0$ *and* $\mathrm{d}\delta + \delta\mathrm{d} = 0$.

Remark A.2 This implies that $\mathrm{d} + \delta : \mathscr{A}^k \to \mathscr{A}^{k+1}$, where $\mathscr{A}^k := \bigcup_{i=0}^k \mathscr{A}^{(i,k-i)}$, is an exterior derivative as well.

Proposition A.3 *We have* $\mathrm{D}_i \, \delta = \delta \, \mathrm{D}_i$.

Proposition A.4 *For a differential polynomial h, define the corresponding vertical generalized vector field by* $\partial_h := \sum_I h_I \frac{\partial}{\partial u_I}$. *We have* $\mathrm{d}\, \iota_{\partial_h} + \iota_{\partial_h} \mathrm{d} = 0$.

Proof It suffices to show this for (0,0)-forms (polynomials f in u and partial derivatives of u), for (0,1)-forms $\mathrm{d}t_j$, and for (1,0)-forms δu_I. For (0,0)-forms, both terms of the claimed identity are zero:

$$\mathrm{d}\left(\iota_{\partial_h} f \right) = 0, \quad \iota_{\partial_h}(\mathrm{d}f) = \iota_{\partial_h} \left(\sum_j \mathrm{D}_j f \, \mathrm{d}t_j \right) = 0.$$

Likewise for (0,1)-forms:

$$\mathrm{d}\Big(\iota_{\partial_h}\,\mathrm{d}t_j\Big) = 0, \quad \iota_{\partial_h}(\mathrm{d}\mathrm{d}t_j) = 0.$$

For (1,0)-forms we find:

$$\iota_{\partial_h}(\mathrm{d}\delta u_I) = \iota_{\partial_h}\left(-\sum_j \delta u_{Ij}\wedge \mathrm{d}t_j\right) = -\sum_j h_{Ij}\,\mathrm{d}t_j = -\mathrm{d}h_I = -\mathrm{d}\Big(\iota_{\partial_h}\,\delta u_I\Big).$$

□

B. Proof of Lemma 2.4

Assume that the action is stationary on all d-dimensional stepped surfaces in $\mathbb{R}^N$. Let S be a smooth d-dimensional surface in $\mathbb{R}^N$. Partition the space $\mathbb{R}^N$ into hypercubes C_i of edge length ε. We can choose this partitioning in such a way that the surface S does not contain the center of any of the hypercubes. Denote $S_i^N := S \cap C_i$.

We give each hypercube its own coordinate system $[-1,1]^N \to C_i$ and identify the hypercube with its coordinates. In each *punctured* hypercube $[-1,1]^N \setminus \{0\}$ we define a family of *balloon maps*

$$\mathscr{B}_\alpha^N : [-1,1]^N \setminus \{0\} \to [-1,1]^N \setminus \{0\} : x \mapsto \begin{cases} \dfrac{\alpha x}{\|x\|_{\max}} & \text{if } \|x\|_{\max} < \alpha \\ x & \text{if } \|x\|_{\max} \geqslant \alpha \end{cases}$$

for $\alpha \in [0,1]$. Here, $\|x\|_{\max} := \max(|x_1|, \dots |x_N|)$ denotes the maximum norm with respect to the local coordinates. The idea is that from the center of each hypercube, we inflate a square balloon which pushes the curve away from the center, until it lies on the boundary of the hypercube.

Indeed, the deformed surface $S_i^{N-1} := \mathscr{B}_1^N(S_i^N) = \mathscr{B}_1^N(S \cap C_i)$ lies on the boundary of the hypercube, i.e. within the $(N-1)$-faces of the hypercube. We want it to lie within the d-faces of the hypercube, which would imply that it is a stepped surface. To achieve this, we introduce a balloon map

$$\mathscr{B}_\alpha^{N-1,j} : [-1,1]^{N-1} \setminus \{0\} \to [-1,1]^{N-1} \setminus \{0\} : x \mapsto \begin{cases} \dfrac{\alpha x}{\|x\|_{\max}} & \text{if } \|x\|_{\max} < \alpha \\ x & \text{if } \|x\|_{\max} \geqslant \alpha \end{cases}$$

in each of the $(N-1)$-faces C_i^j of the hypercube C_i, which pushes the surface into the $(N-2)$-faces. We denote the surface we obtain this way by S_i^{N-2}. If the surface happens to contain the center of a $(N-1)$-face, we can slightly perturb the surface without affecting the argument. By iterating this procedure, using balloon maps $\mathscr{B}_\alpha^{k,j}$

in each k-face C_i^j ($N \geqslant k \geqslant d+1$), we obtain a surface S_i^d that lies in the d-faces (Figs. 5 and 6).

Consider the $(d+1)$-dimensional surface

$$M_i := \bigcup_{k=d+1}^{N} \bigcup_{\substack{j:\ C_i^j \text{ is a} \\ k\text{-face of } C_i}} \bigcup_{\alpha\in[0,1]} \mathscr{B}_\alpha^{k,j}(S_i^k \cap C_i^j)$$

that is swept out by the consecutive application of the balloon maps to $S_i^N := S \cap C_i$. Assuming that ε is small compared to the curvature of S, the $(d+1)$-dimensional volume of each of the $\bigcup_{\alpha\in[0,1]} \mathscr{B}_\alpha^{k,j}(S_i^k \cap C_i^j)$ is of the order ε^{d+1}. The number of such volumes making up M_i only depends on the dimensions N and d, not on ε, so the $(d+1)$-dimensional volume $|M_i|$ of M_i is of the order $|M_i| = \mathscr{O}(\varepsilon^{d+1})$.

Now consider a variation $\mathscr{V}$ with compact support and restrict the surface S to this support. Denote by $\widehat{S} := \bigcup_i S_i^d$ the stepped surface obtained from S by repeated application of balloon maps in all the hypercubes, and by $M := \bigcup_i M_i$ the $(d+1)$-dimensional surface swept out by these balloon maps. The bounary of M consists of S, $\widehat{S}$, and a small strip of area $\mathscr{O}(\varepsilon)$ connecting the boundaries of S and $\widehat{S}$ (the dotted line in Fig. 5). The number of hypercubes intersecting S is of order ε^{-d}, so $|M| = \mathscr{O}(\varepsilon^{-d})\mathscr{O}(\varepsilon^{d+1}) = \mathscr{O}(\varepsilon)$. It follows that

$$\begin{aligned}\left|\int_{\widehat{S}} \iota_{\mathrm{pr}}\mathscr{V}\,\delta\mathscr{L} - \int_S \iota_{\mathrm{pr}}\mathscr{V}\,\delta\mathscr{L}\right| &= \left|\int_{\partial M} \iota_{\mathrm{pr}}\mathscr{V}\,\delta\mathscr{L}\right| + \mathscr{O}(\varepsilon)\\ &= \left|\int_M \mathrm{d}(\iota_{\mathrm{pr}}\mathscr{V}\,\delta\mathscr{L})\right| + \mathscr{O}(\varepsilon) \to 0\end{aligned}$$

as $\varepsilon \to 0$. By assumption, $\int_{\widehat{S}} \iota_{\mathrm{pr}}\mathscr{V}\,\delta\mathscr{L} = 0$ for all ε, so the action on S will be stationary as well. □

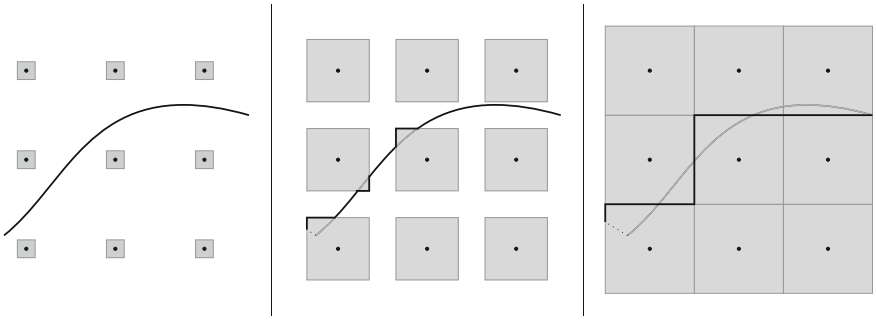

Fig. 5 Balloon maps in nine adjacent squares deforming a *curve* in $\mathbb{R}^2$. From *left* to *right*: $\alpha = 0.2$, $\alpha = 0.7$ and $\alpha = 1$

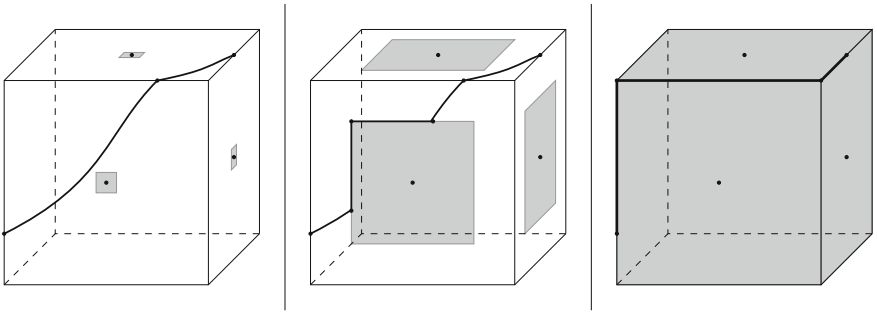

Fig. 6 The second and last iteration for a curve in $\mathbb{R}^3$. From *left* to *right*: $\alpha = 0.1$, $\alpha = 0.6$ and $\alpha = 1$

References

1. Adler, V., Bobenko, A., Suris, Y.: Classification of integrable equations on quad-graphs. the consistency approach. Commun. Math. Phys. **233**, 513–543 (2003)
2. Anderson, I.: The variational bicomplex. Preprint (1989)
3. Baxter, R.: Solvable eight-vertex model on an arbitrary planar lattice. Philos. Trans. R. Soc. Lond. **289**, 315–346 (1978)
4. Baxter, R.: Free-fermion, checkerboard and Z-invariant lattice models in statistical mechanics. Proc. R. Soc. Lond. A **404**, 1–33 (1986)
5. Bazhanov, V., Mangazeev, V., Sergeev, S.: A master solution of the quantum Yang-Baxter equation and classical discrete integrable equations. Adv. Theor. Math. Phys. **16**, 65–95 (2012)
6. Bazhanov, V., Mangazeev, V., Sergeev, S.: Faddeev-Volkov solution of the Yang-Baxter equation and discrete conformal symmetry. Nucl. Phys. B **784**, 234–258 (2007)
7. Bobenko, A., Mercat, C., Suris, Y.: Linear and nonlinear theories of discrete analytic functions. Intergable structure and isomonodromic Green's function. J. Reine Angew. Math. **583**, 117–161 (2005)
8. Bobenko, A., Suris., Y.: Integrable systems on quad-graphs. Intern. Math. Res. Not. **2002**(11), 573–611 (2002)
9. Bobenko, A., Suris, Y.: Discrete pluriharmonic functions as solutions of linear pluri-Lagrangian systems. Commun. Math. Phys. **336**, 199–215 (2015)
10. Boll, R., Petrera, M., Suris, Y.: What is integrability of discrete variational systems? Proc. R. Soc. A **470**, 20130, 550 (2014)

11. Burstall, F., Ferus, D., Pedit, F., Pinkall, U.: Harmonic tori in symmetric spaces and commuting Hamiltonian systems on loop algebras. Ann. Math. **138**, 173–212 (1993)
12. Dickey, L.: Soliton equations and Hamiltonian systems, 2nd edn. World Scientific (2003)
13. Lobb, S., Nijhoff., F.: Lagrangian multiforms and multidimensional consistency. J. Phys. A: Math. Theor. **42**, 454,013 (2009)
14. Newell, A.: Solitons in mathematics and physics. SIAM (1985)
15. Nijhoff, F.: Lax pair for the Adler (lattice Krichever-Novikov) system. Phys. Lett. A **297**, 49–58 (2002)
16. Noether, E.: Invariante Variationsprobleme. Nachrichten von der Gesellschaft der Wissenschaften zu Göttingen, Math.-Phys. Kl. 235–257 (1918)
17. Ohnita, Y., Valli, G.: Pluriharmonic maps into compact Lie groups and factorization into unitons. Proc. Lond. Math. Soc. **61**, 546–570 (1990)
18. Olver, P.: Applications of Lie groups to differential equations, 2nd edn. Springer (1993)
19. Rudin, W.: Function theory in polydiscs. Benjamin (1969)
20. Suris, Y.: Variational formulation of commuting Hamiltonian flows: multi-time Lagrangian 1-forms. J. Geom. Mech. **5**, 365–379 (2013)
21. Suris, Y.: Variational symmetries and pluri-Lagrangian systems. In: Dynamical Systems, Number Theory and Applications. A Festschrift in Honor of Armin Leutbecher's 80th Birthday, Hagen, Th., Rupp, F., Scheurle, J. (eds.) World Scientific, pp. 255–266 (2016)

On the Variational Interpretation of the Discrete KP Equation

Raphael Boll, Matteo Petrera and Yuri B. Suris

Abstract We study the variational structure of the discrete Kadomtsev-Petviashvili (dKP) equation by means of its pluri-Lagrangian formulation. We consider the dKP equation and its variational formulation on the cubic lattice $\mathbb{Z}^N$ as well as on the root lattice $Q(A_N)$. We prove that, on a lattice of dimension at least four, the corresponding Euler-Lagrange equations are equivalent to the dKP equation.

1 Introduction

We developed the theory of pluri-Lagrangian problems (integrable systems of variational origin) in recent papers [2–6, 15, 16], influenced by the fundamental insight of [11–13, 17]. In the present paper, we consider the pluri-Lagrangian formulation of the *discrete bilinear Kadomtsev-Petviashvili* (dKP) equation on three-dimensional lattices and its consistent extension to higher dimensional lattices. This equation belongs to integrable octahedron-type equations which were classified in [1]. A Lagrangian formulation of this equation was given in [13]. There, the authors consider a discrete 3-form on the lattice $\mathbb{Z}^3$ together with the corresponding Euler-Lagrange equations which are shown to be satisfied on solutions of the dKP equation. They also show that this 3-form is closed on solutions of the dKP equation, namely, the so-called 4D closure relation is satisfied. The main goal of the present paper is to provide a more precise understanding of the findings in that paper. More concretely:

- In the framework of the pluri-Lagrangian formulation, we construct the elementary building blocks of Euler-Lagrange equations, which, in the present situation, are the so-called 4D corner equations.

R. Boll · M. Petrera · Y.B. Suris (✉)
Inst. für Mathematik, Technische Universität Berlin,
Straße des 17. Juni 136, 10623 Berlin, Germany
e-mail: suris@math.tu-berlin.de

R. Boll
e-mail: boll@math.tu-berlin.de

M. Petrera
e-mail: petrera@math.tu-berlin.de

A.I. Bobenko (ed.), *Advances in Discrete Differential Geometry*,
DOI 10.1007/978-3-662-50447-5_12

- In the two-dimensional case, as noticed in [4], the corresponding 3D corner equations build a consistent system. Its solutions are more general then the solutions of the underlying hyperbolic system of quad-equations. On the contrary, in the present three-dimensional situation, the system of 4D corner equations is not consistent in the usual sense (i.e., it does not allow to determine general solutions with the maximal number of initial data). However, this system turns out to be equivalent, in a sense which we are going to explain later, to the corresponding hyperbolic system, namely the dKP equation.
- We provide a rigorous consideration of the branches of the logarithm functions involved in the Euler-Lagrange equations. This leads to the following more precise result: the system of 4D corner equations is equivalent, and thus provides a variational formulation, to two different hyperbolic equations, namely the dKP equation itself and its version obtained under inversion $x \mapsto x^{-1}$ of all fields which will be denoted by dKP^{-}.

One can consider the dKP equation on the cubic lattice $\mathbb{Z}^3$ and its higher dimensional analogues $\mathbb{Z}^N$, but, as discussed in [1, 8, 9] another natural setting the dKP equation (and related octahedron-type equations) is the three-dimensional root lattice

$$Q(A_3) := \{(n_i, n_j, n_k, n_\ell) : n_i + n_j + n_k + n_\ell = 0\}.$$

Also in this setting, the dKP equation can be extended in a consistent way to the higher dimensional lattices $Q(A_N)$ with $N > 3$.

Both lattices have their advantages and disadvantages. The cubic lattice $\mathbb{Z}^N$, on the one hand, is more manageable and easier to visualize. Its cell structure is very simple: for every dimension N, all N-dimensional elementary cells are N-dimensional cubes. On the other hand, it is less natural to consider dKP on the lattice $\mathbb{Z}^3$, because this equation depends on the variables assigned to six out of eight vertices of a (three-dimensional) cube.

The root lattice $Q(A_N)$, in contrast, has a more complicated cell structure, because the number of different N-dimensional elementary cells increases with the dimension N. For instance, for $N = 3$ there are two types of elementary cells octahedra and tetrahedra. Moreover, especially in higher dimensions, a visualization of the elementary cells is difficult, if not impossible. However, this lattice is more natural for the consideration of dKP from the combinatorial point of view, because this equation depends on variables which can be assigned to the six vertices of an octahedron, one of the elementary cells of the lattice. Furthermore, the four-dimensional elementary cells are combinatorially smaller (they contain only 10 vertices, as compared with 16 vertices of a four-dimensional cube) and possess higher symmetry than the cubic ones. Since they support the equations which serve as variational analogue of the dKP equation, this leads to a simpler situation.

We will see that a four-dimensional cube is combinatorially equivalent to the sum of four elementary cells of the root lattice $Q(A_4)$. Therefore, several results in the cubic case can be seen as direct consequences of results of the more fundamental $Q(A_N)$-case.

Let us start with some concrete definitions valid for an arbitrary N-dimensional lattice $\mathscr{X}$.

Definition 1.1 (*Discrete 3-form*) A *discrete 3-form* on $\mathscr{X}$ is a real-valued function $\mathscr{L}$ of oriented 3-cells σ depending on some field $x : \mathscr{X} \to \mathbb{R}$, such that $\mathscr{L}$ changes the sign by changing the orientation of σ.

For instance, in $Q(A_N)$, the 3-cells are tetrahedra and octahedra, and, in $\mathbb{Z}^N$, the 3-cells are 3D cubes.

Definition 1.2 (*3-dimensional pluri-Lagrangian problem*) Let $\mathscr{L}$ be a discrete 3-form on $\mathscr{X}$ depending on $x : \mathscr{X} \to \mathbb{R}$.

- To an arbitrary 3-manifold $\Sigma \subset \mathscr{X}$, i.e., a union of oriented 3-cells which forms an oriented three-dimensional topological manifold, there corresponds the *action functional*, which assigns to $x|_{V(\Sigma)}$, i.e., to the fields in the set of the vertices $V(\Sigma)$ of Σ, the number

$$S_\Sigma := \sum_{\sigma \in \Sigma} \mathscr{L}(\sigma).$$

- We say that the field $x : V(\Sigma) \to \mathbb{R}$ is a critical point of S_Σ, if at any interior point $n \in V(\Sigma)$, we have

$$\frac{\partial S_\Sigma}{\partial x(n)} = 0. \tag{1}$$

  Equation (1) are called *discrete Euler-Lagrange equations* for the action S_Σ.
- We say that the field $x : \mathscr{X} \to \mathbb{R}$ solves the *pluri-Lagrangian problem* for the Lagrangian 3-form $\mathscr{L}$ if, *for any 3-manifold* $\Sigma \subset \mathscr{X}$, the restriction $x|_{V(\Sigma)}$ is a critical point of the corresponding action S_Σ.

In the present paper, we focus on the variational formulation of the dKP equation on $Q(A_N)$ and $\mathbb{Z}^N$. Let us formulate the main results of the paper.

On the lattice $Q(A_N)$, we consider discrete 3-forms vanishing on all tetrahedra. One can show (see Corollary 2.5) that, for an arbitrary interior vertex of any 3-manifold in $Q(A_N)$, the Euler-Lagrange equations follow from certain elementary building blocks. These so-called 4D corner equations are the Euler-Lagrange equations for elementary 4-cells of $Q(A_N)$ different from 4-simplices, so-called 4-ambo-simplices. Such a 4-ambo-simplex has ten vertices. Therefore, the crucial issue is the study of the system consisting of the corresponding ten corner equations. In our case, each corner equation depends on all ten fields at the vertices of the 4-ambo-simplex. Therefore, one could call this system *consistent* if any two equations are functionally dependent. It turns out that this is *not* the case. We will prove the following statement:

Theorem 1.3 *Every solution of the system of ten corner equations for a 4-ambo-simplex in $Q(A_N)$ satisfies either the system of five dKP equations or the system of five dKP$^-$ equations on the five octahedral facets of the 4-ambo-simplex.*

Thus, one can prescribe arbitrary initial values at seven vertices of a 4-ambo-simplex. We will also prove the following theorem:

Theorem 1.4 *The discrete 3-form $\mathscr{L}$ is closed on any solution of the system of corner equations.*

In [4, 15], it was shown that in dimensions 1 and 2 the analogues of the property formulated in Theorem 1.4 are related to more traditional integrability attributes.

For the case of the cubic lattice $\mathbb{Z}^N$, the situation is similar: one can show (see Corollary 4.2) that, for an arbitrary interior vertex of any 3-manifold in $\mathbb{Z}^3$, the Euler-Lagrange equations follow from certain elementary building blocks. These so-called 4D corner equations are the Euler-Lagrange equations for elementary 4D cubes in $\mathbb{Z}^N$. A 4D cube has sixteen vertices, but in our case the action on a 4D cube turns out to be independent of the fields on two of the vertices. Therefore, the crucial issue is the study of the system consisting of the corresponding fourteen corner equations. Six of the fourteen corner equations depend each on thirteen of the fourteen fields. There do not exist pairs of such equations which are independent of one and the same field. All other equations depend each on ten of the fourteen fields. Therefore, one could call this system *consistent* if it would have the minimal possible rank 2 (assign twelve fields arbitrarily and use two of the six corner equations—depending on thirteen fields—to determine the remaining two fields, then all twelve remaining equations should be satisfied automatically). It turns out that the system of the fourteen corner equations is *not* consistent in this sense. We will prove the following analogue of Theorem 1.3:

Theorem 1.5 *Every solution of the system of fourteen corner equations for a 4D cube in $\mathbb{Z}^N$ satisfies either the system of eight dKP equations or the system of eight dKP$^-$ equations on the eight cubic facets of the 4D cube.*

Thus, one can prescribe arbitrary initial values at nine vertices of a 4D cube. Correspondingly, we will also prove the following statement:

Theorem 1.6 *The discrete 3-form $\mathscr{L}$ is closed on any solution of the system of corner equations.*

The paper is organized as follows: we start with the root lattice $Q(A_N)$, thus considering the combinatorial issues and some general properties of pluri-Lagrangian systems. Then we introduce the dKP equation and its pluri-Lagrangian structure. In the second part of the paper the present similar considerations for the cubic lattice $\mathbb{Z}^N$.

2 The Root Lattice $Q(A_N)$

We consider the root lattice

$$Q(A_N) := \{n := (n_0, n_1, \dots, n_N) \in \mathbb{Z}^{N+1} : n_0 + n_1 + \dots + n_N = 0\},$$

where $N \geq 3$. The three-dimensional sub-lattices $Q(A_3)$ are given by

$$Q(A_3) := \{(n_i, n_j, n_k, n_\ell) : n_i + n_j + n_k + n_\ell = \text{const}\}.$$

We consider fields $x : Q(A_N) \to \mathbb{R}$, and use the shorthand notations

$$x_{\bar{\imath}} = x(n - e_i), \qquad x = x(n), \qquad \text{and} \qquad x_i = x(n + e_i),$$

where e_i is the unit vector in the ith coordinate direction. Furthermore, the shift functions T_i and $T_{\bar{\imath}}$ are defined by

$$T_i x_\alpha := x_{i\alpha} \quad \text{and} \quad T_{\bar{\imath}} x_\alpha := x_{\bar{\imath}\alpha}$$

for a multiindex α. For simplicity, we sometimes abuse notations by identifying lattice points n with the corresponding fields $x(n)$.

We now give a very brief introduction to the Delaunay cell structure of the n-dimensional root lattice $Q(A_N)$ [7, 14]. Here, we restrict ourselves to a very elementary description which is appropriate to our purposes and follow the considerations in [1]. For each N there are N sorts of N-cells of $Q(A_N)$ denoted by $P(k, N)$ with $k = 1, \ldots, N$:

- Two sorts of 2-cells:

  $P(1,2)$: black triangles $\lfloor ijk \rfloor := \{x_i, x_j, x_k\}$;
  $P(2,2)$: white triangles $\lceil ijk \rceil := \{x_{ij}, x_{ik}, x_{jk}\}$;
- Three sorts of 3-cells:

  $P(1,3)$: black tetrahedra $\lfloor ijk\ell \rfloor := \{x_i, x_j, x_k, x_\ell\}$;
  $P(2,3)$: octahedra $[ijk\ell] := \{x_{ij}, x_{ik}, x_{i\ell}, x_{jk}, x_{j\ell}, x_{k\ell}\}$;
  $P(3,3)$: white tetrahedra $\lceil ijk\ell \rceil := \{x_{ijk}, x_{ij\ell}, x_{ik\ell}, x_{jk\ell}\}$;
- Four sorts of 4-cells:

  $P(1,4)$: black 4-simplices $\lfloor\!\lfloor ijk\ell m \rfloor\!\rfloor := \{x_i, x_j, x_k, x_\ell, x_m\}$;
  $P(2,4)$: black 4-ambo-simplices $\lfloor ijk\ell m \rfloor := \{x_{\alpha\beta} : \alpha, \beta \in \{i, j, k, \ell, m\}, \alpha \neq \beta\}$;
  $P(3,4)$: white 4-ambo-simplices $\lceil ijk\ell m \rceil := \{x_{\alpha\beta\gamma} : \alpha, \beta, \gamma \in \{i, j, k, \ell, m\}, \alpha \neq \beta \neq \gamma \neq \alpha\}$;
  $P(4,4)$: white 4-simplices $\lceil\!\lceil ijk\ell m \rceil\!\rceil := \{x_{ijk\ell}, x_{ijkm}, x_{ij\ell m}, x_{ik\ell m}, x_{jk\ell m}\}$.

The facets of 3-cells and 4-cells can be found in Appendix 1.

In the present paper we will consider objects on *oriented* manifolds. We say that a black triangle $\lfloor ijk \rfloor$ and white triangle $\lceil ijk \rceil$ are positively oriented if $i < j < k$ (see Fig. 1). Any permutation of two indices changes the orientation to the opposite one.

When we use the bracket notation, we always write the letters in brackets in increasing order, so, e.g., in writing $\lfloor ijk \rfloor$ we assume that $i < j < k$ and avoid the notation $\lfloor jik \rfloor$ or $\lfloor ikj \rfloor$ for the negatively oriented triangle $-\lfloor ijk \rfloor$.

There is a simple recipe to derive the orientation of facets of an N-cell: On every index in the brackets we put alternately a "+" or a "−" starting with a "+" on the

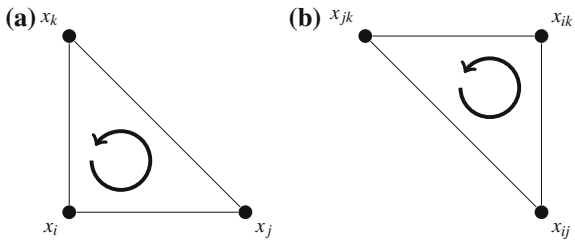

Fig. 1 Orientation of triangles: **a** the black triangle $\lfloor ijk \rfloor$; **b** the white triangle $\lceil ijk \rceil$

last index. Then we get each of its facets by deleting one index and putting the corresponding sign in front of the bracket. For instance, the black 4-ambo-simplex

$$\begin{array}{c} + - + - + \\ \lfloor\ i\ \ j\ \ k\ \ \ell\ \ m\ \rfloor \end{array}$$

has the five octahedral facets $[ijk\ell]$, $-[ijkm]$, $[ij\ell m]$, $-[ik\ell m]$, and $[jk\ell m]$.

The following two definitions are valid for arbitrary N-dimensional lattices $\mathscr{X}$.

Definition 2.1 (*Adjacent N-cell*) Given an N-cell σ, another N-cell $\bar{\sigma}$ is called *adjacent* to σ if σ and $\bar{\sigma}$ share a common $(N-1)$-cell. The orientation of this $(N-1)$-cell in σ must be opposite to its orientation in $\bar{\sigma}$.

The latter property guarantees that the orientations of the adjacent N-cells agree.

Definition 2.2 (*Flower*) A 3-manifold in $\mathscr{X}$ with exactly one interior vertex x is called a *flower* with center x. *The flower* at an interior vertex x of a given 3-manifold is the flower with center x which lies completely in the 3-manifold.

As a consequence, in $Q(A_N)$, in each flower every tetrahedron has exactly three adjacent 3-cells and every octahedron has exactly four adjacent 3-cells.

Examples for open 3-manifolds in $Q(A_N)$ are the three-dimensional sub-lattices $Q(A_3)$. Here, the flower at an interior vertex consists of eight tetrahedra (four black and four white ones) and six octahedra.

Examples of closed 3-manifolds in $Q(A_N)$ are the set of facets of a 4-ambo-simplex (consisting of five tetrahedra) and the set of facets of a 4-ambo-simplex (consisting of five tetrahedra and five octahedra).

The elementary building blocks of 3-manifolds are so-called 4D corners:

Definition 2.3 (*4D corner*) A *4D corner* with center x is a 3-manifold consisting of all facets of a 4-cell adjacent to x.

In $Q(A_N)$, there are two different types of 4D corners: a corner on a 4-simplex (consisting of a four tetrahedra) and a corner on a 4-ambo-simplex (consisting of two tetrahedra and three octahedra), see Appendix 2 for details.

The following combinatorial statement will be proven in Appendix 3:

Theorem 2.4 *The flower at any interior vertex of any 3-manifold in* $Q(A_N)$ *can be represented as a sum of 4D corners in* $Q(A_{N+2})$.

Let $\mathscr{L}$ be a discrete 3-form on $Q(A_N)$. The *exterior derivative* $d\mathscr{L}$ is a discrete 4-form whose value at any 4-cell in $Q(A_N)$ is the action functional of $\mathscr{L}$ on the 3-manifold consisting of the facets of the 4-cell. For our purposes, we consider discrete 3-forms $\mathscr{L}$ vanishing on all tetrahedra. In particular, we have

$$d\mathscr{L}(\llbracket ijk\ell m \rrbracket) \equiv 0 \quad \text{and} \quad d\mathscr{L}(\lceil ijk\ell m \rceil) \equiv 0$$

since a 4-simplices only contain tetrahedra. The exterior derivative on a black 4-ambo-simplex $\lfloor ijk\ell m \rfloor$ is given by

$$\begin{aligned} \underline{S}^{ijk\ell m} &:= d\mathscr{L}(\lfloor ijk\ell m \rfloor) \\ &= \mathscr{L}([ijk\ell]) + \mathscr{L}(-[ijkm]) + \mathscr{L}([ij\ell m]) + \mathscr{L}(-[ik\ell m]) + \mathscr{L}([jk\ell m]). \end{aligned} \tag{2}$$

The exterior derivative on a white 4-ambo-simplex $\lceil ijk\ell m \rceil$ is given by

$$\begin{aligned} \bar{S}^{ijk\ell m} &:= d\mathscr{L}(\lceil ijk\ell m \rceil) \\ &= \mathscr{L}(T_m[ijk\ell]) + \mathscr{L}(-T_\ell[ijkm]) + \mathscr{L}(T_k[ij\ell m]) + \mathscr{L}(-T_j[ik\ell m]) \\ &\quad + \mathscr{L}(T_i[jk\ell m]). \end{aligned} \tag{3}$$

Accordingly, the Euler-Lagrange equations on black 4-ambo-simplices $\lfloor ijk\ell m \rfloor$ are

$$\begin{aligned} &\frac{\partial \underline{S}^{ijk\ell m}}{\partial x_{ij}} = 0, \quad \frac{\partial \underline{S}^{ijk\ell m}}{\partial x_{ik}} = 0, \quad \frac{\partial \underline{S}^{ijk\ell m}}{\partial x_{i\ell}} = 0, \quad \frac{\partial \underline{S}^{ijk\ell m}}{\partial x_{im}} = 0, \quad \frac{\partial \underline{S}^{ijk\ell m}}{\partial x_{jk}} = 0, \\ &\frac{\partial \underline{S}^{ijk\ell m}}{\partial x_{j\ell}} = 0, \quad \frac{\partial \underline{S}^{ijk\ell m}}{\partial x_{jm}} = 0, \quad \frac{\partial \underline{S}^{ijk\ell m}}{\partial x_{k\ell}} = 0, \quad \frac{\partial \underline{S}^{ijk\ell m}}{\partial x_{km}} = 0, \quad \frac{\partial \underline{S}^{ijk\ell m}}{\partial x_{\ell m}} = 0. \end{aligned} \tag{4}$$

and the Euler-Lagrange equations on white 4-ambo-simplices $\lceil ijk\ell m \rceil$ are

$$\begin{aligned} &\frac{\partial \bar{S}^{ijk\ell m}}{\partial x_{ijk}} = 0, \quad \frac{\partial \bar{S}^{ijk\ell m}}{\partial x_{ij\ell}} = 0, \quad \frac{\partial \bar{S}^{ijk\ell m}}{\partial x_{ijm}} = 0, \quad \frac{\partial \bar{S}^{ijk\ell m}}{\partial x_{ik\ell}} = 0, \quad \frac{\partial \bar{S}^{ijk\ell m}}{\partial x_{ikm}} = 0, \\ &\frac{\partial \bar{S}^{ijk\ell m}}{\partial x_{i\ell m}} = 0, \quad \frac{\partial \bar{S}^{ijk\ell m}}{\partial x_{jk\ell}} = 0, \quad \frac{\partial \bar{S}^{ijk\ell m}}{\partial x_{jkm}} = 0, \quad \frac{\partial \bar{S}^{ijk\ell m}}{\partial x_{j\ell m}} = 0, \quad \frac{\partial \bar{S}^{ijk\ell m}}{\partial x_{k\ell m}} = 0. \end{aligned} \tag{5}$$

The last two systems are called *corner equations*.

The following statement is an immediate consequence of Theorem 2.4:

Theorem 2.5 *For discrete every 3-form on $Q(A_N)$ and every 3-manifold in $Q(A_N)$ all corresponding Euler-Lagrange equations can be written as a sum of corner equations.*

3 The dKP Equation on $Q(A_N)$

We will now introduce the dKP equation on the root lattice $Q(A_3)$. Every oriented octahedron $[ijk\ell]$ $(i < j < k < \ell)$ in $Q(A_3)$ supports the equation

$$x_{ij}x_{k\ell} - x_{ik}x_{j\ell} + x_{i\ell}x_{jk} = 0. \tag{6}$$

We can extend this system in a consistent way (see [1]) to the four-dimensional root lattice $Q(A_4)$ and higher-dimensional analogues, such that the five octahedral facets $[ijk\ell]$, $[jk\ell m]$, $-[ik\ell m]$, $[ijm\ell]$, and $-[ijkm]$ of the black 4-ambo-simplex $\lfloor ijk\ell m \rfloor$ support the equations

$$\begin{aligned}
&x_{ij}x_{k\ell} - x_{ik}x_{j\ell} + x_{i\ell}x_{jk} = 0,\\
&x_{jk}x_{\ell m} - x_{j\ell}x_{km} + x_{jm}x_{k\ell} = 0,\\
&x_{k\ell}x_{im} - x_{km}x_{i\ell} + x_{ik}x_{\ell m} = 0,\\
&x_{\ell m}x_{ij} - x_{i\ell}x_{jm} + x_{j\ell}x_{im} = 0,\\
&x_{im}x_{jk} - x_{jm}x_{ik} + x_{km}x_{ij} = 0
\end{aligned} \tag{7}$$

and the five octahedral facets $T_m[ijk\ell]$, $T_i[jk\ell m]$, $-T_j[ik\ell m]$, $T_k[ij\ell m]$, and $-T_\ell[ijkm]$ of the white 4-ambo-simplex $\lceil ijk\ell m \rceil$ support the equations

$$\begin{aligned}
&x_{ijm}x_{k\ell m} - x_{ikm}x_{j\ell m} + x_{i\ell m}x_{jkm} = 0,\\
&x_{ijk}x_{i\ell m} - x_{ij\ell}x_{ikm} + x_{ijm}x_{ik\ell} = 0,\\
&x_{jk\ell}x_{ijm} - x_{jkm}x_{ij\ell} + x_{ijk}x_{j\ell m} = 0,\\
&x_{k\ell m}x_{ijk} - x_{ik\ell}x_{jkm} + x_{jk\ell}x_{ikm} = 0,\\
&x_{i\ell m}x_{jk\ell} - x_{j\ell m}x_{ik\ell} + x_{k\ell m}x_{ij\ell} = 0.
\end{aligned} \tag{8}$$

In both systems one can derive one equation from another by cyclic permutations of indices $(ijk\ell m)$.

We propose the following discrete 3-form $\mathscr{L}$ defined on oriented octahedra $[ijk\ell]$:

$$\mathscr{L}([ijk\ell]) := \frac{1}{2}\left(\Lambda\left(\frac{x_{ij}x_{k\ell}}{x_{ik}x_{j\ell}}\right) + \Lambda\left(\frac{x_{ik}x_{j\ell}}{x_{i\ell}x_{jk}}\right) + \Lambda\left(-\frac{x_{i\ell}x_{jk}}{x_{ij}x_{k\ell}}\right)\right), \tag{9}$$

where

$$\Lambda(z) := \lambda(z) - \lambda\left(\frac{1}{z}\right) \quad \text{and} \quad \lambda(z) := -\int_0^z \frac{\log|1-x|}{x}dx. \tag{10}$$

The discrete 3-form (9) has its motivation in [13]. Indeed, in [13], the authors consider a similar discrete 3-form on the cubic lattice $\mathbb{Z}^N$. One can also consider our 3-form on the cubic lattice $\mathbb{Z}^N$. Then one would assign to each 3D cube the 3-form at its

inscribed octahedron. This 3-form differs from their one by an additive constant and a slightly different definition of the function $\lambda(z)$: they use the function

$$\mathrm{Li}_2(z) := -\int_0^z \frac{\log(1-x)}{x}dx \tag{11}$$

instead of $\lambda(z)$. Our choice of $\lambda(z)$ allows us for a more precise consideration of the branches of the occurring logarithm.

Observe that the expression (9) only changes its sign under the cyclic permutation of indices $(ijk\ell m)$. This follows from $\Lambda(z) = -\Lambda(z^{-1})$. As a consequence, the exterior derivatives $\underline{S}^{ijk\ell m}$ and $\bar{S}^{ijk\ell m}$ defined in (2) and (3), respectively, are invariant under the cyclic permutation of indices $(ijk\ell m)$. Therefore, one can obtain all corner equations in (4) and (5) by (iterated) cyclic permutation $(ijk\ell m)$ from

$$\frac{\partial \underline{S}^{ijk\ell m}}{\partial x_{ij}} = 0, \quad \frac{\partial \underline{S}^{ijk\ell m}}{\partial x_{ik}} = 0, \quad \text{and} \quad \frac{\partial \bar{S}^{ijk\ell m}}{\partial x_{ijk}} = 0, \quad \frac{\partial \bar{S}^{ijk\ell m}}{\partial x_{ij\ell}} = 0.$$

Let us study separately the corner equations on black and white 4-ambo-simplices. The corner equations which live on the black 4-ambo-simplex $\lfloor ijk\ell m \rfloor$ are given by

$$\frac{\partial \underline{S}^{ijk\ell m}}{\partial x_{ij}} = \frac{\partial \mathscr{L}([ijk\ell])}{\partial x_{ij}} + \frac{\partial \mathscr{L}(-[ijkm])}{\partial x_{ij}} + \frac{\partial \mathscr{L}([ij\ell m])}{\partial x_{ij}} = 0$$

and

$$\frac{\partial \underline{S}^{ijk\ell m}}{\partial x_{ik}} = \frac{\partial \mathscr{L}([ijk\ell])}{\partial x_{ik}} + \frac{\partial \mathscr{L}(-[ijkm])}{\partial x_{ik}} + \frac{\partial \mathscr{L}(-[ik\ell m])}{\partial x_{ik}} = 0.$$

Explicitly, they read

$$\frac{1}{x_{ij}} \log|E_{ij}| = 0 \quad \text{and} \quad \frac{1}{x_{ik}} \log|E_{ik}| = 0, \tag{12}$$

where

$$E_{ij} := \frac{x_{ij}x_{k\ell} + x_{i\ell}x_{jk}}{x_{ij}x_{k\ell} - x_{ik}x_{j\ell}} \cdot \frac{x_{ij}x_{km} - x_{ik}x_{jm}}{x_{ij}x_{km} + x_{im}x_{jk}} \cdot \frac{x_{ij}x_{\ell m} + x_{im}x_{j\ell}}{x_{ij}x_{\ell m} - x_{i\ell}x_{jm}}$$

and

$$E_{ik} := \frac{x_{ik}x_{j\ell} - x_{ij}x_{k\ell}}{x_{ik}x_{j\ell} - x_{i\ell}x_{jk}} \cdot \frac{x_{ik}x_{jm} - x_{im}x_{jk}}{x_{ik}x_{jm} - x_{ij}x_{km}} \cdot \frac{x_{ik}x_{\ell m} - x_{i\ell}x_{km}}{x_{ik}x_{\ell m} + x_{im}x_{k\ell}}.$$

For every corner equation (12) there are two classes of solutions, because any solution can either solve $E_{ij} = -1$ or $E_{ij} = 1$. Hereafter, we only consider solutions, where all fields x_{ij} are non-zero (we call such solutions non-singular).

Theorem 3.1 *Every solution of the system* (4) *solves either the system*

$$\begin{aligned} &E_{ij} = -1, \quad E_{ik} = -1, \quad E_{i\ell} = -1, \quad E_{im} = -1, \quad E_{jk} = -1, \\ &E_{j\ell} = -1, \quad E_{jm} = -1, \quad E_{k\ell} = -1, \quad E_{km} = -1, \quad E_{\ell m} = -1 \end{aligned} \tag{13}$$

or the system

$$\begin{aligned} &E_{ij} = 1, \quad E_{ik} = 1, \quad E_{i\ell} = 1, \quad E_{im} = 1, \quad E_{jk} = 1, \\ &E_{j\ell} = 1, \quad E_{jm} = 1, \quad E_{k\ell} = 1, \quad E_{km} = 1, \quad E_{\ell m} = 1. \end{aligned} \tag{14}$$

Furthermore, the system (13) *is equivalent to the system* (7) *(that is dKP on the corresponding black 4-ambo-simplex). The system* (14) *is equivalent to the system*

$$\begin{aligned} &x_{ik}x_{i\ell}x_{jk}x_{j\ell} - x_{ij}x_{i\ell}x_{jk}x_{k\ell} + x_{ij}x_{ik}x_{j\ell}x_{k\ell} = 0, \\ &x_{j\ell}x_{jm}x_{k\ell}x_{km} - x_{jk}x_{jm}x_{k\ell}x_{\ell m} + x_{jk}x_{j\ell}x_{km}x_{\ell m} = 0, \\ &x_{km}x_{ik}x_{\ell m}x_{i\ell} - x_{k\ell}x_{ik}x_{\ell m}x_{im} + x_{k\ell}x_{km}x_{i\ell}x_{im} = 0, \\ &x_{i\ell}x_{j\ell}x_{im}x_{jm} - x_{\ell m}x_{j\ell}x_{im}x_{ij} + x_{\ell m}x_{i\ell}x_{jm}x_{ij} = 0, \\ &x_{jm}x_{km}x_{ij}x_{ik} - x_{im}x_{km}x_{ij}x_{jk} + x_{im}x_{jm}x_{ik}x_{jk} = 0, \end{aligned} \tag{15}$$

which is the system (7) *after the transformation* $x \mapsto x^{-1}$ *of fields (that is dKP*$^-$ *on the corresponding black 4-ambo-simplex).*

Proof Consider a solution x of (4) that solves $E_{ij} = -1$ and $E_{jk} = -1$. We set

$$a_{ij} := x_{\ell m}x_{ij} - x_{i\ell}x_{jm} + x_{j\ell}x_{im}, \tag{16}$$

$$a_{ik} := x_{k\ell}x_{im} - x_{km}x_{i\ell} + x_{ik}x_{\ell m}, \tag{17}$$

and

$$a_{jk} := x_{jk}x_{\ell m} - x_{j\ell}x_{km} + x_{jm}x_{k\ell}, \tag{18}$$

and use these equations to substitute x_{ij}, x_{ik} and x_{jk} in $E_{ij} = -1$ and $E_{jk} = -1$. Writing down the result in polynomial form, we get

$$x_{\ell m}^2(a_{ij} + x_{i\ell}x_{jm} - x_{im}x_{j\ell})e_{ij} = 0$$

and

$$x_{\ell m}^2(a_{jk} + x_{j\ell}x_{km} - x_{jm}x_{k\ell})e_{jk} = 0,$$

where e_{ij} and e_{jk} are certain polynomials. Since for every solutions of (4) all fields are non-zero this leads us to $e_{ij} = 0$ and $e_{jk} = 0$. Computing the difference of the latter two equations we get

$$a_{ij}x_{k\ell}x_{km}(a_{ij}+x_{i\ell}x_{jm}-x_{im}x_{j\ell})-a_{jk}x_{i\ell}x_{im}(a_{jk}+x_{j\ell}x_{km}-x_{jm}x_{k\ell})=0$$

and, with the use of (16) and (18),

$$x_{\ell m}(a_{ij}x_{ij}x_{k\ell}x_{km}-a_{jk}x_{jk}x_{i\ell}x_{im})=0,$$

which depends on seven independent fields, i.e., no subset of six fields belong to one octahedron. Then comparing coefficients leads to $a_{ij}=a_{jk}=0$. Substituting

$$x_{ij}=\frac{x_{i\ell}x_{jm}-x_{im}x_{j\ell}}{x_{\ell m}} \quad \text{and} \quad x_{jk}=\frac{x_{j\ell}x_{km}-x_{jm}x_{k\ell}}{x_{\ell m}}$$

into $E_{ij}=-1$ and solving the resulting equation with respect to x_{ik}, we get

$$x_{ik}=\frac{x_{i\ell}x_{km}-x_{im}x_{k\ell}}{x_{\ell m}}.$$

Substituting x_{ij}, x_{ik} and x_{jk} in E_{ik} by using the last three equations, we get $E_{ik}=-1$.

Analogously, one can prove that, for a solution x of (4) which solves $E_{ij}=-1$ and $E_{ik}=-1$, we have $E_{jk}=-1$, and for a solution x of (4) which solves $E_{ik}=-1$ and $E_{i\ell}=-1$, we have $E_{k\ell}=-1$. Therefore, for every solution x of (4) and for every white triangle $\{x_\alpha, x_\beta, x_\gamma\}$ on the black 4-ambo-simplex $\lfloor ijk\ell m\rfloor$ we proved the following: if $E_\alpha=-1$ and $E_\beta=-1$ then $E_\gamma=-1$, too.

On the other hand, one can easily see that x solves $E_{ij}=1$ or $E_{jk}=1$ if and only if x^{-1} solves $E_{ij}=-1$ or $E_{ik}=-1$, respectively. Therefore, we also know that, if $E_\alpha=1$ and $E_\beta=1$ then $E_\gamma=1$, too.

Summarizing, we proved that every solution x of (4) solves either (13) and then also (7) or (14) and then also (15).

Consider a non-singular solution x of the system (7). Then

$$\begin{aligned}E_{ij}&=\frac{x_{ij}x_{k\ell}+x_{i\ell}x_{jk}}{x_{ij}x_{k\ell}-x_{ik}x_{j\ell}}\cdot\frac{x_{ij}x_{km}-x_{ik}x_{jm}}{x_{ij}x_{km}+x_{im}x_{jk}}\cdot\frac{x_{ij}x_{\ell m}+x_{im}x_{j\ell}}{x_{ij}x_{\ell m}-x_{i\ell}x_{jm}}\\&=\frac{x_{ik}x_{j\ell}}{-x_{i\ell}x_{jk}}\cdot\frac{-x_{im}x_{jk}}{x_{ik}x_{jm}}\cdot\frac{x_{i\ell}x_{jm}}{-x_{im}x_{j\ell}}=-1\end{aligned}$$

and

$$\begin{aligned}E_{ik}&=\frac{x_{ik}x_{j\ell}-x_{ij}x_{k\ell}}{x_{ik}x_{j\ell}-x_{i\ell}x_{jk}}\cdot\frac{x_{ik}x_{jm}-x_{im}x_{jk}}{x_{ik}x_{jm}-x_{ij}x_{km}}\cdot\frac{x_{ik}x_{\ell m}-x_{i\ell}x_{km}}{x_{ik}x_{\ell m}+x_{im}x_{k\ell}}\\&=\frac{x_{i\ell}x_{jk}}{x_{ij}x_{k\ell}}\cdot\frac{x_{ij}x_{km}}{x_{im}x_{jk}}\cdot\frac{x_{im}x_{k\ell}}{-x_{i\ell}x_{km}}=-1.\end{aligned}$$

This proves the equivalence of (13) and (7) and also the equivalence of (14) and (15) since x solves $E_{ij}=-1$ or (7) if and only if x^{-1} solves $E_{ij}=1$ or (15), respectively. □

We will present the closure relation which can be seen as a criterion of integrability:

Theorem 3.2 *(Closure relation) There holds:*

$$\underline{S}^{ijk\ell m} \pm \frac{\pi^2}{4} = 0$$

on all solutions of (13) *and* (14)*, respectively. Therefore, one can redefine the 3-form* $\mathscr{L}$ *as*

$$\tilde{\mathscr{L}}([ijk\ell]) := \mathscr{L}([ijk\ell]) \pm \frac{\pi^2}{4}$$

in order to get $\underline{S}^{ijk\ell m} = 0$ *on all solutions of* (13) *and* (14)*, respectively.*

Proof The set of solutions $\mathscr{S}^+$ of (13), as well as the set of solutions $\mathscr{S}^-$ (14), is a connected seven-dimensional algebraic manifold which can be parametrized by the set of variables $\{x_{ij}, x_{ik}, x_{i\ell}, x_{im}, x_{jk}, x_{j\ell}, x_{jm}\}$. We want to show that the directional derivatives of $\underline{S}^{ijk\ell m}$ along tangent vectors of $\mathscr{S}^{\pm}$ vanish. It is easy to see that the stronger property $\operatorname{grad}\underline{S}^{ijk\ell m} = 0$ on $\mathscr{S}^{\pm}$, where we $\underline{S}^{ijk\ell m}$ is considered as a function of ten variables x_{ij}, is a consequence of (13), respectively (14). Therefore, the function $\underline{S}^{ijk\ell m}$ is constant on $\mathscr{S}^{\pm}$.

To determine the value of $\underline{S}^{ijk\ell m}$ on solutions of (13), we consider the constant solution of (7)

$$\begin{aligned} x_{ij} = x_{jk} = x_{k\ell} = x_{\ell m} = x_{im} = a, \\ x_{ik} = x_{j\ell} = x_{km} = x_{i\ell} = x_{jm} = -1, \end{aligned} \tag{19}$$

where

$$a := \frac{1}{2} - \frac{\sqrt{5}}{2}.$$

(Indeed, for this point every equation from (7) looks like $a^2 - 1 - a = 0$.) Therefore, this point satisfies (13), because (7) and (13) are equivalent.

Consider the dilogarithm as defined in (11) and suppose that $z > 1$. According to [10], we derive:

$$\operatorname{Li}_2(z) = -\operatorname{Li}_2(z^{-1}) - \frac{1}{2}\log^2 z + \frac{\pi^2}{3} - i\pi \log z$$

and

$$\begin{aligned} \operatorname{Re}\operatorname{Li}_2(z) =& \operatorname{Re}\operatorname{Li}_2(ze^{i0}) = -\frac{1}{2}\int_0^z \frac{\log(1 - 2x\cos 0 + x^2)}{x}dx \\ =& -\frac{1}{2}\int_0^z \frac{\log(1-x)^2}{x}dx = -\int_0^z \frac{\log|1-x|}{x}dx = \lambda(z), \end{aligned}$$

where $\lambda(z)$ is the same function as in (9). Therefore, we have

$$\lambda(z) = \begin{cases} \mathrm{Li}_2(z), & z \le 1, \\ -\mathrm{Li}_2(z^{-1}) - \dfrac{1}{2}\log^2 z + \dfrac{\pi^2}{3}, & z > 1. \end{cases}$$

By using the following special values [10]

$$\begin{aligned} &\mathrm{Li}_2(a^2) = \tfrac{\pi^2}{15} - \log^2(-a), \quad \mathrm{Li}_2(-a) = \tfrac{\pi^2}{10} - \log^2(-a), \\ &\mathrm{Li}_2(a) = -\tfrac{\pi^2}{15} + \tfrac{1}{2}\log^2(-a), \ \mathrm{Li}_2(a^{-1}) = -\tfrac{\pi^2}{10} - \log^2(-a). \end{aligned}$$

a straightforward computation gives

$$\begin{aligned} \mathscr{L}([ijk\ell]) =& \mathscr{L}(-[ijkm]) = \mathscr{L}([ij\ell m]) = \mathscr{L}(-[ik\ell m]) = \mathscr{L}([jk\ell m]) \\ =& \frac{1}{2}(\Lambda(a^2) + \Lambda(-a^{-1}) + \Lambda(a^{-1})) = -\frac{\pi^2}{20} \end{aligned}$$

and

$$\begin{aligned} \underline{S}^{ijk\ell m} =& \mathscr{L}([ijk\ell]) + \mathscr{L}(-[ijkm]) + \mathscr{L}([ij\ell m]) + \mathscr{L}(-[ik\ell m]) + \mathscr{L}([jk\ell m]) \\ =& -\frac{\pi^2}{4}. \end{aligned}$$

This is, because the expression for $\mathscr{L}([ijk\ell])$ (see (9)) changes the sign under the cyclic permutation of indices $(ijk\ell)$ and the solution is invariant under cyclic permutation of indices $(ijk\ell m)$.

Let us now consider the second branch of solutions: one can easily see that

$$\begin{aligned} &x_{ij} = x_{jk} = x_{k\ell} = x_{\ell m} = x_{im} = a^{-1}, \\ &x_{ik} = x_{j\ell} = x_{km} = x_{i\ell} = x_{jm} = -1 \end{aligned} \tag{20}$$

with

$$a = \frac{1}{2} - \frac{\sqrt{5}}{2}$$

is a solution of (14) and (15), because (19) is a solution of (13) and (7). Therefore, on the solution (20) as well as on all other solutions of (14), we have

$$\underline{S}^{ijk\ell m} = \frac{\pi^2}{4},$$

where we used $\Lambda(z) = \lambda(z) - \lambda(z^{-1})$, and, therefore, $\Lambda(z^{-1}) = -\Lambda(z)$. □

Analogously, we get similar results for the white 4-ambo-simplex $\lceil ijk\ell m\rceil$. Here, the corner equations are:

$$\frac{\partial \bar{S}^{ijk\ell m}}{\partial x_{ijk}} = \frac{\partial \mathscr{L}(T_k[ij\ell m])}{\partial x_{ijk}} + \frac{\partial \mathscr{L}(-T_j[ik\ell m])}{\partial x_{ijk}} + \frac{\partial \mathscr{L}(T_i[jk\ell m])}{\partial x_{ijk}} = 0$$

and

$$\frac{\partial \bar{S}^{ijk\ell m}}{\partial x_{ij\ell}} = \frac{\partial \mathscr{L}(-T_\ell[ijkm])}{\partial x_{ij\ell}} + \frac{\partial \mathscr{L}(-T_j[ik\ell m])}{\partial x_{ij\ell}} + \frac{\partial \mathscr{L}(T_i[jk\ell m])}{\partial x_{ij\ell}} = 0.$$

Explicitly, they read

$$\frac{1}{x_{ijk}} \log|E_{ijk}| = 0 \quad \text{and} \quad \frac{1}{x_{ij\ell}} \log|E_{ij\ell}| = 0, \tag{21}$$

where

$$E_{ijk} := \frac{x_{ijk}x_{k\ell m} + x_{ikm}x_{jk\ell}}{x_{ijk}x_{k\ell m} - x_{ik\ell}x_{jkm}} \cdot \frac{x_{ijk}x_{j\ell m} - x_{ij\ell}x_{jkm}}{x_{ijk}x_{j\ell m} + x_{ijm}x_{jk\ell}} \cdot \frac{x_{ijk}x_{i\ell m} + x_{ijm}x_{ik\ell}}{x_{ijk}x_{i\ell m} - x_{ij\ell}x_{ikm}}$$

and

$$E_{ij\ell} := \frac{x_{ij\ell}x_{k\ell m} - x_{ik\ell}x_{j\ell m}}{x_{ij\ell}x_{k\ell m} + x_{i\ell m}x_{jk\ell}} \cdot \frac{x_{ij\ell}x_{jkm} - x_{ijm}x_{jk\ell}}{x_{ij\ell}x_{jkm} - x_{ijk}x_{j\ell m}} \cdot \frac{x_{ij\ell}x_{ikm} - x_{ijk}x_{i\ell m}}{x_{ij\ell}x_{ikm} - x_{ijm}x_{ik\ell}}.$$

The analogue of Theorem 3.1 reads:

Theorem 3.3 *Every solution of the system* (5) *solves either the system*

$$\begin{aligned} &E_{ijk} = -1, \quad E_{ij\ell} = -1, \quad E_{ijm} = -1, \quad E_{ik\ell} = -1, \quad E_{ikm} = -1, \\ &E_{i\ell m} = -1, \quad E_{jk\ell} = -1, \quad E_{jkm} = -1, \quad E_{j\ell m} = -1, \quad E_{k\ell m} = -1 \end{aligned} \tag{22}$$

or the system

$$\begin{aligned} &E_{ijk} = 1, \quad E_{ij\ell} = 1, \quad E_{ijm} = 1, \quad E_{ik\ell} = 1, \quad E_{ikm} = 1, \\ &E_{i\ell m} = 1, \quad E_{jk\ell} = 1, \quad E_{jkm} = 1, \quad E_{j\ell m} = 1, \quad E_{k\ell m} = 1. \end{aligned} \tag{23}$$

Furthermore the system (22) *is equivalent to the system* (8) *(that is dKP on the corresponding white 4-ambo-simplex). The system* (23) *is equivalent to the system*

$$
\begin{aligned}
&x_{ikm}x_{i\ell m}x_{jkm}x_{j\ell m} - x_{ijm}x_{i\ell m}x_{jkm}x_{k\ell m} + x_{ijm}x_{ikm}x_{j\ell m}x_{k\ell m} = 0,\\
&x_{ij\ell}x_{ijm}x_{ik\ell}x_{ikm} - x_{ijk}x_{ijm}x_{ik\ell}x_{i\ell m} + x_{ijk}x_{ij\ell}x_{ik\ell}x_{i\ell m} = 0,\\
&x_{jkm}x_{ijk}x_{j\ell m}x_{ij\ell} - x_{jk\ell}x_{ijk}x_{j\ell m}x_{ijm} + x_{jk\ell}x_{jkm}x_{j\ell m}x_{ijm} = 0,\\
&x_{ik\ell}x_{jk\ell}x_{ikm}x_{jkm} - x_{k\ell m}x_{jk\ell}x_{ikm}x_{ijk} + x_{k\ell m}x_{ik\ell}x_{ikm}x_{ijk} = 0,\\
&x_{j\ell m}x_{k\ell m}x_{ij\ell}x_{ik\ell} - x_{i\ell m}x_{k\ell m}x_{ij\ell}x_{jk\ell} + x_{i\ell m}x_{j\ell m}x_{ij\ell}x_{jk\ell} = 0,
\end{aligned}
\tag{24}
$$

which is the system (8) *after the transformation* $x \mapsto x^{-1}$ *of fields (that is dKP*$^-$ *on the corresponding white 4-ambo-simplex).*

The analogue of Theorem 3.2 reads:

Theorem 3.4 *(Closure relation) There holds:*

$$\bar{S}^{ijk\ell m} \pm \frac{\pi^2}{4} = 0$$

on all solutions of (22) *and* (23)*, respectively. Therefore, one can redefine the 3-form* $\mathscr{L}$ *as*

$$\tilde{\mathscr{L}}([ijk\ell]) := \mathscr{L}([ijk\ell]) \pm \frac{\pi^2}{4}$$

in order to get $\bar{S}^{ijk\ell m} = 0$ *on all solutions of* (22) *and* (23)*, respectively.*

4 The Cubic Lattice $\mathbb{Z}^N$

We will now consider the relation between the elementary cells of the root lattice $Q(A_N)$ and the cubic lattice $\mathbb{Z}^N$. The points of $Q(A_N)$ and of $\mathbb{Z}^N$ are in a one-to-one correspondence via

$$P_i : Q(A_N) \to \mathbb{Z}^N, \quad x(n_0, \dots, n_{i-1}, n_i, n_{i+1}, \dots, n_N) \mapsto x(n_0, \dots, n_{i-1}, n_{i+1}, \dots, n_N).$$

In the present paper, we will always apply P_i with $i < j, k, \ell, \dots$

We denote by

$$\{jk\ell\} := \{x, x_j, x_k, x_\ell, x_{jk}, x_{j\ell}, x_{k\ell}, x_{jk\ell}\}$$

the oriented 3D cubes of $\mathbb{Z}^N$. We say that the 3D cube $\{jk\ell\}$ is positively oriented if $j < k < \ell$. Any permutation of two indices changes the orientation to the opposite one. Also in this case, we always write the letters in the brackets in increasing order, so, e.g., in writing $\{jk\ell\}$ we assume that $j < k < \ell$ and avoid the notation $\{kj\ell\}$ or $\{j\ell k\}$ for the negatively oriented 3D cube $-\{jk\ell\}$.

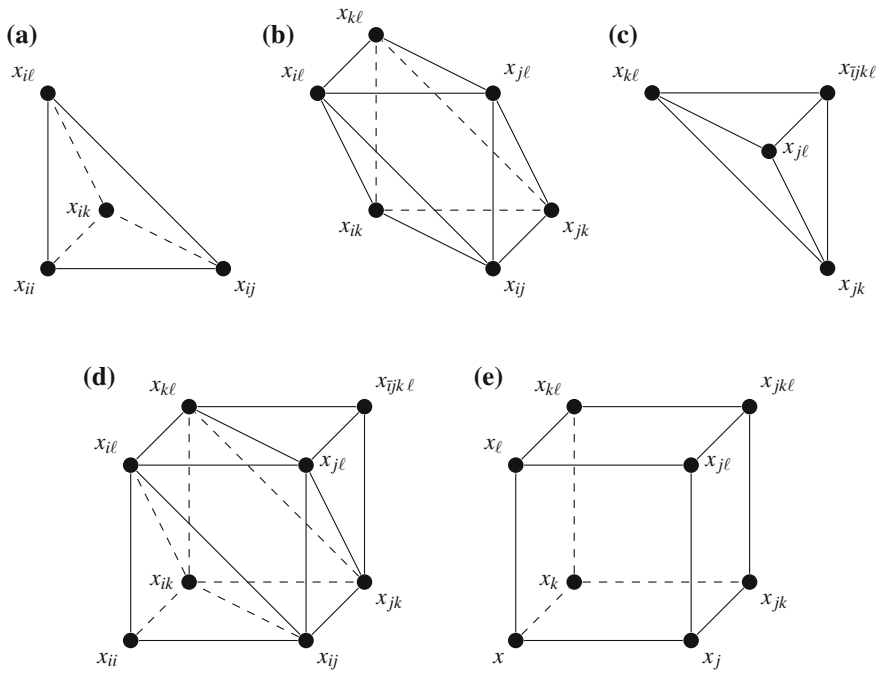

Fig. 2 Three adjacent 3-cells of the lattice $Q(A_N)$: **a** black tetrahedron $-T_i\lfloor ijk\ell\rfloor$, **b** octahedron $[ijk\ell]$, **c** white tetrahedron $-T_{\bar{\imath}}\lceil ijk\ell\rceil$. The sum **d** of these 3-cells corresponds to a 3D cube **e**

The object in $Q(A_N)$ which corresponds to the 3D cube $\{jk\ell\}$ is the sum of three adjacent 3-cells, namely

- the black tetrahedron $-T_i\lfloor ijk\ell\rfloor$ (see Fig. 2a),
- the octahedron $[ijk\ell]$ (see Fig. 2b),
- and the white tetrahedron $-T_{\bar{\imath}}\lceil ijk\ell\rceil$ (see Fig. 2c).

It contains sixteen triangles and to every quadrilateral face of $\{jkl\}$ there corresponds a pair of these triangles containing one black and one white triangle. Here, the map P_i reads as follows:

$$x_{ii} \mapsto x, \quad x_{ij} \mapsto x_j, \quad x_{jk} \mapsto x_{jk}, \quad \text{and} \quad x_{\bar{\imath}jk\ell} \mapsto x_{jk\ell}.$$

As a four-dimensional elementary cell of $\mathbb{Z}^N$, we consider an oriented 4D cube

$$\{jk\ell m\} := \{x, x_j, x_k, x_\ell, x_m, x_{jk}, x_{j\ell}, x_{jm}, x_{k\ell}, x_{km}, x_{\ell m}, x_{jk\ell}, x_{jkm}, x_{j\ell m}, x_{k\ell m}, x_{jk\ell m}\}.$$

The 4D cube $\{jk\ell m\}$ corresponds to the sum of four 4-cells in $Q(A_N)$:

- the black 4-simplex $-T_i[\![ijk\ell m]\!]$,
- the black 4-ambo-simplex $\lfloor ijk\ell m\rfloor$,

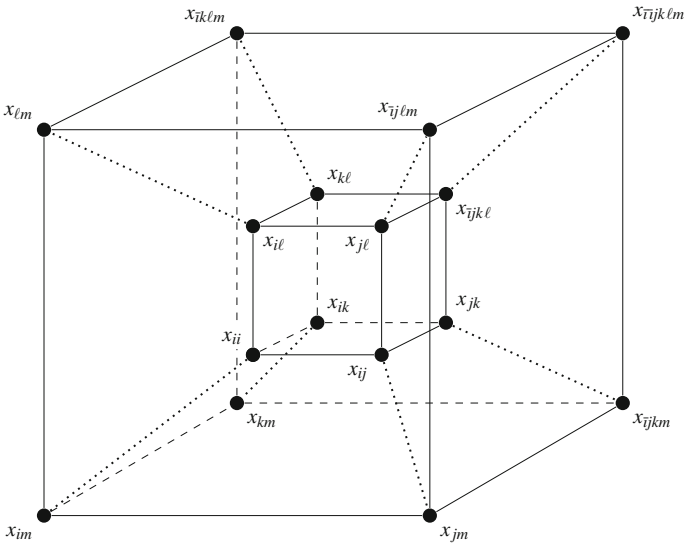

Fig. 3 The sum of the black 4-simplex $-T_i\,[\![ijk\ell m]\!]$, the adjacent black 4-ambo-simplex $\lfloor ijk\ell m\rfloor$, the adjacent white 4-ambo-simplex $-T_{\bar{\imath}}\lceil ijk\ell m\rceil$, and the adjacent white 4-simplex $T_{\bar{\imath}}T_{\bar{\imath}}\,[\![ijk\ell m]\!]$ corresponds to the 4D cube $\{jk\ell m\}$

- the white 4-ambo-simplex $-T_{\bar{\imath}}\lceil ijk\ell m\rceil$, and
- the white 4-simplex $T_{\bar{\imath}}T_{\bar{\imath}}\,[\![ijk\ell m]\!]$

(see Fig. 3). It contains sixteen tetrahedra (eight black and eight white ones) and eight octahedra. Here, the map P_i reads as follows:

$$x_{ii} \mapsto x, \quad x_{ij} \mapsto x_j, \quad x_{jk} \mapsto x_{jk}, \quad x_{\bar{\imath}jk\ell} \mapsto x_{jk\ell}, \quad \text{and} \quad x_{\bar{\imath}\bar{\imath}jk\ell m} \mapsto x_{jk\ell m}.$$

Also in the cubic case there is an easy recipe to obtain the orientation of the facets of an (oriented) 4D cube: on every index between the brackets we put alternately a "+" and a "−" starting with a "+" on the last index. Then we get each facet by deleting one index and putting the corresponding sign in front of the bracket. For instance., the 4D cube

$$\begin{array}{c} - + - + \\ \{\ j\ \ k\ \ \ell\ \ m\ \} \end{array}$$

has the eight 3D facets: $\{jk\ell\}$, $-\{jkm\}$, $\{j\ell m\}$, $-\{k\ell m\}$ and the opposite ones $-T_m\{jk\ell\}$, $T_\ell\{jkm\}$, $-T_k\{j\ell m\}$, and $T_j\{k\ell m\}$.

As a consequence of Definition 2.2, in each flower in $\mathbb{Z}^N$, every 3D cube has exactly four adjacent 3D cubes.

We will now prove the analogue of Theorem 2.5. This proof is easier than the one for $Q(A_N)$, because of the simpler combinatorial structure.

Theorem 4.1 *The flower at any interior vertex of any 3-manifold in $\mathbb{Z}^N$ can be represented as a sum of 4D corners in $\mathbb{Z}^{N+1}$.*

Proof Set $M := N + 1$ and consider the flower of an interior vertex x of an arbitrary 3-manifold in $\mathbb{Z}^N$. Over each 3D corner $\{jk\ell\}$ (petal) of the flower, we can build a 4D corner adjacent to x on the 4D cube $\{jk\ell M\}$. Then the vertical 3D cubes coming from two successive petals of the flower carry opposite orientations, so that all vertical squares cancel away from the sum of the 4D corners. □

Let $\mathfrak{L}$ be a discrete 3-form on $\mathbb{Z}^N$. The *exterior derivative* $d\mathfrak{L}$ is a discrete 4-form whose value at any 4D cube in $\mathbb{Z}^N$ is the action functional of $\mathfrak{L}$ on the 3-manifold consisting of the facets of the 4D cube:

$$\begin{aligned} S^{jk\ell m} :=& d\mathfrak{L}(\{jk\ell m\}) = \mathfrak{L}(\{jk\ell\}) + \mathfrak{L}(-\{jkm\}) + \mathfrak{L}(\{j\ell m\}) + \mathfrak{L}(-\{k\ell m\}) \\ &+ \mathfrak{L}(-T_m\{jk\ell\}) + \mathfrak{L}(T_\ell\{jkm\}) + \mathfrak{L}(-T_k\{j\ell m\}) + \mathfrak{L}(T_j\{k\ell m\}). \end{aligned}$$

Accordingly, the Euler-Lagrange equations on the 4D cube $\{jk\ell m\}$ are given by

$$\begin{aligned} &\frac{\partial S^{jk\ell m}}{\partial x} = 0, \\ &\frac{\partial S^{jk\ell m}}{\partial x_j} = 0, \frac{\partial S^{jk\ell m}}{\partial x_k} = 0, \frac{\partial S^{jk\ell m}}{\partial x_\ell} = 0, \frac{\partial S^{jk\ell m}}{\partial x_m} = 0, \\ &\frac{\partial S^{jk\ell m}}{\partial x_{jk}} = 0, \frac{\partial S^{jk\ell m}}{\partial x_{j\ell}} = 0, \frac{\partial S^{jk\ell m}}{\partial x_{jm}} = 0, \frac{\partial S^{jk\ell m}}{\partial x_{k\ell}} = 0, \frac{\partial S^{jk\ell m}}{\partial x_{km}} = 0, \frac{\partial S^{jk\ell m}}{\partial x_{\ell m}} = 0, \\ &\frac{\partial S^{jk\ell m}}{\partial x_{jk\ell}} = 0, \frac{\partial S^{jk\ell m}}{\partial x_{jkm}} = 0, \frac{\partial S^{jk\ell m}}{\partial x_{j\ell m}} = 0, \frac{\partial S^{jk\ell m}}{\partial x_{k\ell m}} = 0, \\ &\frac{\partial S^{jk\ell m}}{\partial x_{jk\ell m}} = 0. \end{aligned} \tag{25}$$

They are called *corner equations*.

The following statement is an immediate consequence of Theorem 4.1:

Theorem 4.2 *For every discrete 3-form on $\mathbb{Z}^N$ and every 3-manifold in $\mathbb{Z}^N$ all corresponding Euler-Lagrange equations can be written as a sum of corner equations.*

5 The dKP Equation on $\mathbb{Z}^N$

On the 3D cube $\{jk\ell\}$ in $\mathbb{Z}^3$ ($j < k < \ell$) we put the equation

$$x_j x_{k\ell} - x_k x_{j\ell} + x_\ell x_{jk} = 0. \tag{26}$$

We can extend this system in a consistent way (see [1]) to the four-dimensional cubic lattice $\mathbb{Z}^4$ and its higher-dimensional analogues, such that the eight facets $\{jk\ell\}$,

$-\{jkm\}$, $\{j\ell m\}$, $-\{k\ell m\}$, $-T_m\{jk\ell\}$, $T_\ell\{jkm\}$, $-T_k\{j\ell m\}$, $T_j\{k\ell m\}$ of a 4D cube $\{jk\ell m\}$ carry the equations

$$\begin{aligned}
&x_jx_{k\ell}-x_kx_{j\ell}+x_\ell x_{jk}=0, && x_{jm}x_{k\ell m}-x_{km}x_{j\ell m}+x_{\ell m}x_{jkm}=0,\\
&x_jx_{km}-x_kx_{jm}+x_mx_{jk}=0, && x_{jk}x_{k\ell m}-x_{k\ell}x_{jkm}+x_{km}x_{jk\ell}=0,\\
&x_jx_{\ell m}-x_\ell x_{jm}+x_mx_{j\ell}=0, && x_{j\ell}x_{k\ell m}-x_{k\ell}x_{j\ell m}+x_{\ell m}x_{jk\ell}=0,\\
&x_kx_{\ell m}-x_\ell x_{km}+x_mx_{k\ell}=0, && x_{jk}x_{j\ell m}-x_{j\ell}x_{jkm}+x_{jm}x_{jk\ell}=0.
\end{aligned} \tag{27}$$

Note that, in the four equations in the left column, the fields with one index always appear with increasing order of indices. The equations in the right column are shifted copies of the ones in the left column. One can derive the system (27) from the system of dKP equations (7) on the black 4-ambo-simplex $\lfloor ijk\ell m\rfloor$ and the system of dKP equations (8) on the white 4-ambo-simplex $T_{\bar{i}}\lceil ijkm\ell\rceil$, by removing the equations on the octahedra $[jk\ell m]$ and $[jkm\ell]$, respectively, from both systems and applying the transformation P_i to the fields in the remaining eight equations.

We propose the discrete 3-form $\mathfrak{L}$ defined as

$$\mathfrak{L}:=(P_i)_\star\mathscr{L},$$

where $\mathscr{L}$ is the discrete 3-form on the root lattice $Q(A_N)$ (see (9)). Therefore, $\mathfrak{L}$ evaluated at the 3D cube $\{jk\ell\}$ reads as

$$\begin{aligned}
\mathfrak{L}(\{jk\ell\}) &= ((P_i)_\star\mathscr{L})(P_i(-T_i\lfloor ijk\ell\rfloor+[ijk\ell]-T_{\bar{i}}\lceil ijk\ell\rceil))\\
&= (P_i)_\star(\underbrace{\mathscr{L}(-T_i\lfloor ijk\ell\rfloor)}_{=0}+\mathscr{L}([ijk\ell])-\underbrace{\mathscr{L}(-T_{\bar{i}}\lceil ijk\ell\rceil)}_{=0})=(P_i)_\star\mathscr{L}([ijk\ell]).
\end{aligned}$$

For this discrete 3-form, there are no corner equations on the 4D cube $\{jk\ell m\}$ centered at x and $x_{jk\ell m}$ since $S^{jk\ell m}$ does not depend on these two variables. The remaining corner equations from (25) are given by

$$\begin{aligned}
\frac{\partial S^{jk\ell m}}{\partial x_j} &= \frac{\partial\mathfrak{L}(\{jk\ell\})}{\partial x_j}+\frac{\partial\mathfrak{L}(-\{jkm\})}{\partial x_j}+\frac{\partial\mathfrak{L}(\{j\ell m\})}{\partial x_j}+\underbrace{\frac{\partial\mathfrak{L}(T_j\{k\ell m\})}{\partial x_j}}_{=0}\\
&= (P_i)_\star\left(\frac{\partial\mathscr{L}([ijk\ell])}{\partial x_{ij}}+\frac{\partial\mathscr{L}(-[ijkm])}{\partial x_{ij}}+\frac{\partial\mathscr{L}([ij\ell m])}{\partial x_{ij}}\right)=\frac{1}{x_j}\log|\mathscr{E}_j|=0,\\
\frac{\partial S^{jk\ell m}}{\partial x_{jk}} &= \frac{\partial\mathfrak{L}(\{jk\ell\})}{\partial x_{jk}}+\frac{\partial\mathfrak{L}(-\{jkm\})}{\partial x_{jk}}+\frac{\partial\mathfrak{L}(-T_k\{j\ell m\})}{\partial x_{jk}}+\frac{\partial\mathfrak{L}(T_j\{k\ell m\})}{\partial x_{jk}}\\
&= (P_i)_\star\left(\frac{\partial\mathscr{L}([ijk\ell])}{\partial x_{jk}}+\frac{\partial\mathscr{L}(-[ijkm])}{\partial x_{jk}}+\frac{\partial\mathscr{L}(-T_{\bar{i}}T_k[ij\ell m])}{\partial x_{jk}}\right.\\
&\qquad\left.+\frac{\partial\mathscr{L}(T_{\bar{i}}T_j[ik\ell m])}{\partial x_{jk}}\right)\\
&= \frac{1}{x_{jk}}\log\left|\frac{\mathscr{E}_{jk}}{\bar{\mathscr{E}}_{jk}}\right|=0,
\end{aligned}$$

$$\begin{aligned}\frac{\partial S^{jk\ell m}}{\partial x_{jk\ell}} &= \underbrace{\frac{\partial \mathfrak{L}(\{jk\ell\})}{\partial x_{jk\ell}}}_{\equiv 0} + \frac{\partial \mathfrak{L}(T_\ell\{jkm\})}{\partial x_{jk\ell}} + \frac{\partial \mathfrak{L}(-T_k\{j\ell m\})}{\partial x_{jk\ell}} + \frac{\partial \mathfrak{L}(T_j\{k\ell m\})}{\partial x_{jk\ell}} \\ &= (P_{\bar{\imath}})_\star \left(\frac{\partial \mathscr{L}(T_{\bar{\imath}} T_\ell[ijkm])}{\partial x_{\bar{\imath}jk\ell}} + \frac{\partial \mathscr{L}(-T_{\bar{\imath}} T_k[ij\ell m])}{\partial x_{\bar{\imath}jk\ell}} + \frac{\partial \mathscr{L}(T_{\bar{\imath}} T_j[ik\ell m])}{\partial x_{\bar{\imath}jk\ell}} \right) \\ &= \frac{1}{x_{jk\ell}} \log \left| \frac{1}{\mathscr{E}_{jk\ell}} \right| = 0, \end{aligned} \tag{28}$$

where

$$\mathscr{E}_j := (P_{\bar{\imath}})_\star E_{ij}, \quad \underline{\mathscr{E}}_{jk} := (P_{\bar{\imath}})_\star E_{jk}, \quad \bar{\mathscr{E}}_{jk} := (P_{\bar{\imath}})_\star E_{ijk}, \quad \text{and} \quad \mathscr{E}_{jk\ell} := (P_{\bar{\imath}})_\star E_{jk\ell}.$$

Hereafter, we only consider solutions, where all fields are non-zero (we call these solutions non-singular). As in the case of the root lattice $Q(A_N)$ every corner equation has two classes of solutions.

Theorem 5.1 *Every solution of the system* (25) *solves either the system*

$$\begin{gathered} \mathscr{E}_j = -1, \quad \mathscr{E}_k = -1, \quad \mathscr{E}_\ell = -1, \quad \mathscr{E}_m = -1, \\ \underline{\mathscr{E}}_{jk} = -1, \quad \underline{\mathscr{E}}_{j\ell} = -1, \quad \underline{\mathscr{E}}_{jm} = -1, \quad \underline{\mathscr{E}}_{k\ell} = -1, \quad \underline{\mathscr{E}}_{km} = -1, \quad \underline{\mathscr{E}}_{\ell m} = -1, \\ \bar{\mathscr{E}}_{jk} = -1, \quad \bar{\mathscr{E}}_{j\ell} = -1, \quad \bar{\mathscr{E}}_{jm} = -1, \quad \bar{\mathscr{E}}_{k\ell} = -1, \quad \bar{\mathscr{E}}_{km} = -1, \quad \bar{\mathscr{E}}_{\ell m} = -1, \\ \mathscr{E}_{jk\ell} = -1, \quad \mathscr{E}_{jkm} = -1, \quad \mathscr{E}_{j\ell m} = -1, \quad \mathscr{E}_{k\ell m} = -1 \end{gathered} \tag{29}$$

or the system

$$\begin{gathered} \mathscr{E}_j = 1, \quad \mathscr{E}_k = 1, \quad \mathscr{E}_\ell = 1, \quad \mathscr{E}_m = 1, \\ \underline{\mathscr{E}}_{jk} = 1, \quad \underline{\mathscr{E}}_{j\ell} = 1, \quad \underline{\mathscr{E}}_{jm} = 1, \quad \underline{\mathscr{E}}_{k\ell} = 1, \quad \underline{\mathscr{E}}_{km} = 1, \quad \underline{\mathscr{E}}_{\ell m} = 1, \\ \bar{\mathscr{E}}_{jk} = 1, \quad \bar{\mathscr{E}}_{j\ell} = 1, \quad \bar{\mathscr{E}}_{jm} = 1, \quad \bar{\mathscr{E}}_{k\ell} = 1, \quad \bar{\mathscr{E}}_{km} = 1, \quad \bar{\mathscr{E}}_{\ell m} = 1, \\ \mathscr{E}_{jk\ell} = 1, \quad \mathscr{E}_{jkm} = 1, \quad \mathscr{E}_{j\ell m} = 1, \quad \mathscr{E}_{k\ell m} = 1. \end{gathered} \tag{30}$$

Furthermore the system (29) *is equivalent to the system* (27) *(this is dKP on the corresponding 4D cube). The system* (30) *is equivalent to the system*

$$\begin{aligned} &x_k x_\ell x_{jk} x_{j\ell} - x_j x_\ell x_{jk} x_{k\ell} + x_j x_k x_{j\ell} x_{k\ell} = 0, \\ &x_k x_m x_{jk} x_{jm} - x_j x_m x_{jk} x_{km} + x_j x_k x_{jm} x_{km} = 0, \\ &x_\ell x_m x_{j\ell} x_{jm} - x_j x_m x_{j\ell} x_{\ell m} + x_j x_\ell x_{jm} x_{\ell m} = 0, \\ &x_\ell x_m x_{k\ell} x_{km} - x_k x_m x_{k\ell} x_{\ell m} + x_k x_\ell x_{km} x_{\ell m} = 0, \\ &x_{km} x_{\ell m} x_{jkm} x_{j\ell m} - x_{jm} x_{\ell m} x_{jkm} x_{k\ell m} + x_{jm} x_{km} x_{j\ell m} x_{k\ell m} = 0, \\ &x_{k\ell} x_{\ell m} x_{jk\ell} x_{j\ell m} - x_{j\ell} x_{\ell m} x_{jk\ell} x_{k\ell m} + x_{j\ell} x_{k\ell} x_{j\ell m} x_{k\ell m} = 0, \\ &x_{k\ell} x_{km} x_{jk\ell} x_{jkm} - x_{jk} x_{km} x_{jk\ell} x_{k\ell m} + x_{jk} x_{k\ell} x_{jkm} x_{k\ell m} = 0, \\ &x_{j\ell} x_{jm} x_{jk\ell} x_{jkm} - x_{jk} x_{jm} x_{jk\ell} x_{j\ell m} + x_{jk} x_{j\ell} x_{jkm} x_{j\ell m} = 0, \end{aligned} \tag{31}$$

which is the system (27) *after the transformation* $x \mapsto x^{-1}$ *of fields (this is dKP*$^-$ *on the corresponding 4D cube).*

Proof Let x be a solution of the system (25) such that $\mathscr{E}_j = -1$ and $\mathscr{E}_k = -1$. Then we know from the proof of Theorem 3.1 that

$$\begin{aligned} &\mathscr{E}_j = -1, \quad \mathscr{E}_k = -1, \quad \mathscr{E}_\ell = -1, \quad \mathscr{E}_m = -1, \\ &\underline{\mathscr{E}}_{jk} = -1, \quad \underline{\mathscr{E}}_{j\ell} = -1, \quad \underline{\mathscr{E}}_{jm} = -1, \quad \underline{\mathscr{E}}_{k\ell} = -1, \quad \underline{\mathscr{E}}_{km} = -1, \quad \underline{\mathscr{E}}_{\ell m} = -1 \end{aligned}$$

and that the latter system is equivalent to

$$\begin{aligned} &x_j x_{k\ell} - x_k x_{j\ell} + x_\ell x_{jk} = 0, \\ &x_j x_{km} - x_k x_{jm} + x_m x_{jk} = 0, \\ &x_j x_{\ell m} - x_\ell x_{jm} + x_m x_{j\ell} = 0, \\ &x_k x_{\ell m} - x_\ell x_{km} + x_m x_{k\ell} = 0, \\ &x_{jk} x_{\ell m} - x_{j\ell} x_{km} + x_{jm} x_{k\ell} = 0. \end{aligned}$$

On the other hand, if we consider a solution x of (25) such that $\mathscr{E}_j = 1$ and $\mathscr{E}_k = 1$, we know from the proof of Theorem 3.1 that

$$\begin{aligned} &\mathscr{E}_j = 1, \quad \mathscr{E}_k = 1, \quad \mathscr{E}_\ell = 1, \quad \mathscr{E}_m = 1, \\ &\underline{\mathscr{E}}_{jk} = 1, \quad \underline{\mathscr{E}}_{j\ell} = 1, \quad \underline{\mathscr{E}}_{jm} = 1, \quad \underline{\mathscr{E}}_{k\ell} = 1, \quad \underline{\mathscr{E}}_{km} = 1, \quad \underline{\mathscr{E}}_{\ell m} = 1 \end{aligned}$$

and that the latter system is equivalent to

$$\begin{aligned} &x_k x_\ell x_{jk} x_{j\ell} - x_j x_\ell x_{jk} x_{k\ell} + x_j x_k x_{j\ell} x_{k\ell} = 0, \\ &x_k x_m x_{jk} x_{jm} - x_j x_m x_{jk} x_{km} + x_j x_k x_{jm} x_{km} = 0, \\ &x_\ell x_m x_{j\ell} x_{jm} - x_j x_m x_{j\ell} x_{\ell m} + x_j x_\ell x_{jm} x_{\ell m} = 0, \\ &x_\ell x_m x_{k\ell} x_{km} - x_k x_m x_{k\ell} x_{\ell m} + x_k x_\ell x_{km} x_{\ell m} = 0, \\ &x_{j\ell} x_{jm} x_{k\ell} x_{km} - x_{jk} x_{jm} x_{k\ell} x_{\ell m} + x_{jk} x_{j\ell} x_{km} x_{\ell m} = 0. \end{aligned}$$

Now, let x be a solution of the system (25) such that $\mathscr{E}_{jk\ell} = -1$ and $\mathscr{E}_{jkm} = -1$. Then we know from the proof of Theorem 3.3 that

$$\begin{aligned} &\bar{\mathscr{E}}_{jk} = 1, \quad \bar{\mathscr{E}}_{j\ell} = 1, \quad \bar{\mathscr{E}}_{jm} = 1, \quad \bar{\mathscr{E}}_{k\ell} = 1, \quad \bar{\mathscr{E}}_{km} = 1, \quad \bar{\mathscr{E}}_{\ell m} = 1, \\ &\mathscr{E}_{jk\ell} = 1, \quad \mathscr{E}_{jkm} = 1, \quad \mathscr{E}_{j\ell m} = 1, \quad \mathscr{E}_{k\ell m} = 1 \end{aligned}$$

and that the latter system is equivalent to

$$
\begin{aligned}
&x_{\ell m}x_{jkm} - x_{km}x_{j\ell m} + x_{jm}x_{k\ell m} = 0,\\
&x_{km}x_{jk\ell} - x_{k\ell}x_{jkm} + x_{jk}x_{k\ell m} = 0,\\
&x_{\ell m}x_{jk\ell} - x_{k\ell}x_{j\ell m} + x_{j\ell}x_{k\ell m} = 0,\\
&x_{jm}x_{jk\ell} - x_{j\ell}x_{jkm} + x_{jk}x_{j\ell m} = 0,\\
&x_{jk}x_{\ell m} - x_{j\ell}x_{km} + x_{jm}x_{k\ell} = 0.
\end{aligned}
$$

On the other hand, if we consider a solution x of (25) such that $\mathscr{E}_j = 1$ and $\mathscr{E}_k = 1$, we know from the proof of Theorem 3.3 that

$$
\begin{aligned}
&\bar{\mathscr{E}}_{jk} = 1, \quad \bar{\mathscr{E}}_{j\ell} = 1, \quad \bar{\mathscr{E}}_{jm} = 1, \quad \bar{\mathscr{E}}_{k\ell} = 1, \quad \bar{\mathscr{E}}_{km} = 1, \quad \bar{\mathscr{E}}_{\ell m} = 1,\\
&\mathscr{E}_{jk\ell} = 1, \quad \mathscr{E}_{jkm} = 1, \quad \mathscr{E}_{j\ell m} = 1, \quad \mathscr{E}_{k\ell m} = 1
\end{aligned}
$$

and that the latter system is equivalent to

$$
\begin{aligned}
&x_{km}x_{\ell m}x_{jkm}x_{j\ell m} - x_{jm}x_{\ell m}x_{jkm}x_{k\ell m} + x_{jm}x_{km}x_{j\ell m}x_{k\ell m} = 0,\\
&x_{k\ell}x_{\ell m}x_{jk\ell}x_{j\ell m} - x_{j\ell}x_{\ell m}x_{jk\ell}x_{k\ell m} + x_{j\ell}x_{k\ell}x_{j\ell m}x_{k\ell m} = 0,\\
&x_{k\ell}x_{km}x_{jk\ell}x_{jkm} - x_{jk}x_{km}x_{jk\ell}x_{k\ell m} + x_{jk}x_{k\ell}x_{jkm}x_{k\ell m} = 0,\\
&x_{j\ell}x_{jm}x_{jk\ell}x_{jkm} - x_{jk}x_{jm}x_{jk\ell}x_{j\ell m} + x_{jk}x_{j\ell}x_{jkm}x_{j\ell m} = 0,\\
&x_{j\ell}x_{jm}x_{k\ell}x_{km} - x_{jk}x_{jm}x_{k\ell}x_{\ell m} + x_{jk}x_{j\ell}x_{km}x_{\ell m} = 0.
\end{aligned}
$$

Since a solution x of (25) cannot solve

$$x_{jk}x_{\ell m} - x_{j\ell}x_{km} + x_{jm}x_{k\ell} = 0$$

and

$$x_{j\ell}x_{jm}x_{k\ell}x_{km} - x_{jk}x_{jm}x_{k\ell}x_{\ell m} + x_{jk}x_{j\ell}x_{km}x_{\ell m} = 0$$

at the same time, this proves the theorem. □

Theorem 5.2 *(Closure relation) There holds* $S^{jk\ell m} = 0$ *on all solutions of* (25).

Proof Let x be a solution of (29) or (30). Then

$$
\begin{aligned}
S^{jk\ell m} &= d\mathfrak{L}(\{jk\ell\}) = (P_i)_\star(d\mathscr{L}(\lfloor ijk\ell m\rfloor) + d\mathscr{L}(-\lceil ijk\ell m\rceil)) = \underline{S}^{ijk\ell m} - \bar{S}^{ijk\ell m}\\
&= \pm\frac{\pi^2}{4} \mp \frac{\pi^2}{4} = 0
\end{aligned}
$$

due to Theorems 3.2 and 3.4 since every solution of (29) solves (13) and (22) after the transformation P_i of variables and every solution of (30) solves (14) and (23) after the transformation P_i of variables. □

6 Conclusion

The fact that the three-dimensional (hyperbolic) dKP equation is, in a sense, equivalent to the Euler-Lagrange equations of the corresponding action is rather surprising since for the two-dimensional (hyperbolic) quad-equations an analogous statement is not true (see [4, 6] for more details). On the other hand, in the continuous situation there is an example of a 2-form whose Euler-Lagrange equations are equivalent to the set of equations consisting of the (hyperbolic) sine-Gordon equation and the (evolutionary) modified Korteweg-de Vries equation (see [16] for more details). So, the general picture remains unclear.

In particular, the variational formulation for the other equations of octahedron type in the classification of [1] is still an open problem.

Acknowledgments This research was supported by the DFG Collaborative Research Center TRR 109 "Discretization in Geometry and Dynamics".

Appendix 1: Facets of N-Cells of the Root Lattice $Q(A_N)$

Facets of 3-cells:

Black tetrahedra $\lfloor ijk\ell \rfloor$: four black triangles $\lfloor ijk \rfloor$, $-\lfloor ij\ell \rfloor$, $\lfloor ik\ell \rfloor$, and $-\lfloor jk\ell \rfloor$;
Octahedra $[ijk\ell]$: four black triangles $T_\ell \lfloor ijk \rfloor$, $-T_k \lfloor ij\ell \rfloor$, $T_j \lfloor ik\ell \rfloor$, and $-T_i \lfloor jk\ell \rfloor$, four white triangles $\lceil ijk \rceil$, $-\lceil ij\ell \rceil$, $\lceil ik\ell \rceil$, and $-\lceil jk\ell \rceil$;
White tetrahedra $\lceil ijk\ell \rceil$: four white triangles $T_\ell \lceil ijk \rceil$, $-T_k \lceil ij\ell \rceil$, $T_j \lceil ik\ell \rceil$, and $-T_i \lceil jk\ell \rceil$;

Facets of 4-cells:

Black 4-simplices $[\![ijk\ell m]\!]$: $five black tetrahedra \lfloor ijk\ell \rfloor$, $-\lfloor ijkm \rfloor$, $\lfloor ij\ell m \rfloor$, $-\lfloor ik\ell m \rfloor$, and $\lfloor jk\ell m \rfloor$;
Black 4-ambo-simplices $\lfloor ijk\ell m \rfloor$: five black tetrahedra $T_m \lfloor ijk\ell \rfloor$, $-T_\ell \lfloor ijkm \rfloor$, $T_k \lfloor ij\ell m \rfloor$, $-T_j \lfloor ik\ell m \rfloor$, and $T_i \lfloor jk\ell m \rfloor$, and five octahedra $[ijk\ell]$, $-[ijkm]$, $[ij\ell m]$, $-[ik\ell m]$, and $[jk\ell m]$;
White 4-ambo-simplices $\lceil ijk\ell m \rceil$: five octahedra $T_m[ijk\ell]$, $-T_\ell[ijkm]$, $T_k[ij\ell m]$, $-T_j[ik\ell m]$, and $T_i[jk\ell m]$, and five white tetrahedra $\lceil ijk\ell \rceil$, $-\lceil ijkm \rceil$, $\lceil ij\ell m \rceil$, $-\lceil ik\ell m \rceil$, and $\lceil jk\ell m \rceil$;
White 4-simplices $[\![ijk\ell m]\!]$: five white tetrahedra $T_m \lceil ijk\ell \rceil$, $-T_\ell \lceil ijkm \rceil$, $T_k \lceil ij\ell m \rceil$, $-T_j \lceil ik\ell m \rceil$, and $T_i \lceil jk\ell m \rceil$.

Appendix 2: 4D Corners on 4-Cells of the Root Lattice $Q(A_N)$

Black 4-simplex $\llbracket ijk\ell m\rrbracket$:
The 4D corner with center vertex x_i contains

- the four black tetrahedra $\lfloor ijk\ell\rfloor$, $-\lfloor ijkm\rfloor$, $\lfloor ij\ell m\rfloor$, and $-\lfloor ik\ell m\rfloor$;

Black 4-ambo-simplex $\lfloor ijk\ell m\rfloor$:
The 4D corner with center vertex x_{ij} contains

- the two black tetrahedra $-T_j\lfloor ik\ell m\rfloor$, and $T_i\lfloor jk\ell m\rfloor$,
- and the three octahedra $[ijk\ell]$, $-[ijkm]$, and $[ij\ell m]$;

White 4-ambo-simplex $\lceil ijk\ell m\rceil$:
The 4D corner with center vertex x_{ijk} contains

- the three octahedra $T_k[ij\ell m]$, $-T_j[ik\ell m]$, and $T_i[jk\ell m]$,
- and the two white tetrahedra $\lceil ijk\ell\rceil$, and $-\lceil ijkm\rceil$;

White 4-simplex $\llbracket ijk\ell m\rrbracket$:
The 4D corner with center vertex $x_{ijk\ell}$ contains

- the four white tetrahedra $-T_\ell\lceil ijkm\rceil$, $T_k\lceil ij\ell m\rceil$, $-T_j\lceil ik\ell m\rceil$, and $T_i\lceil jk\ell m\rceil$.

Appendix 3: Proof of Theorem 2.4

Set $M := N+1$ and $L := N+2$. Then, for the construction of the sum Σ of 4D corners representing the flower σ centered in X, we use the following algorithm:

(i) For every black tetrahedron $\pm\lfloor ijk\ell\rfloor \in \sigma$ at the interior vertex X we add the 4D corner with center vertex X on the black 4-simplex $\pm\llbracket ijk\ell M\rrbracket$ to Σ.
(ii) For every octahedron $\pm[ijk\ell] \in \sigma$ we add the 4D corner with center vertex X on the black 4-ambo-simplex $\pm\lfloor ijk\ell M\rfloor$ to Σ.
(iii) For every white tetrahedron $\pm\lceil ijk\ell\rceil \in \sigma$ we add the 4D corner with center vertex X on the white 4-ambo-simplex $\pm\lceil ijk\ell M\rceil$ to Σ.
(iv) For every white tetrahedron $\pm\lceil ijkM\rceil \in \Sigma \setminus \sigma$ which appeared in Σ during the previous step we add the 4D corner with center vertex X on the white 4-simplex $\mp T_{\tilde{L}}\llbracket ijkML\rrbracket$ to Σ.

Therefore, we have to prove that $\Sigma = \sigma$.

Assume that $X = x_i$. Then for each black tetrahedron $\pm\lfloor ijk\ell\rfloor \in \sigma$ we added the three black tetrahedra $\mp\lfloor ijkM\rfloor$, $\pm\lfloor ij\ell M\rfloor$, and $\mp\lfloor ik\ell M\rfloor$ to Σ which do not belong to σ. Moreover, $\pm\lfloor ijk\ell\rfloor$ has three black triangular facets adjacent to x_i, namely $\pm\lfloor ijk\rfloor$, which is the common triangle with $\mp\lfloor ijkM\rfloor$ (up to orientation), $\mp\lfloor ij\ell\rfloor$, which is the common triangle with $\pm\lfloor ij\ell M\rfloor$, and $\pm\lfloor ik\ell\rfloor$, which is the common triangle with $\mp\lfloor ik\ell M\rfloor$. Therefore, each of these black tetrahedra has to

cancel away with the corresponding black tetrahedra from the 4D corner which is coming from the 3-cell adjacent to $\pm\lfloor ijk\ell\rfloor$ via the corresponding black triangle.

Assume that $X = x_{ij}$. Then for each octahedron $\pm[ijk\ell] \in \sigma$ we added the two black tetrahedra $\mp T_j\lfloor ik\ell M\rfloor$ and $\pm T_i\lfloor jk\ell M\rfloor$ as well as the two octahedra $\mp[ijkM]$ and $\pm[ij\ell M]$ to Σ which do not belong to σ. Moreover, $\pm[ijk\ell]$ has two black tetrahedral facets adjacent to x_{ij}, namely $\pm\lfloor ijk\rfloor$, which is the common triangle with $\mp T_j\lfloor ik\ell M\rfloor$, and $\mp\lfloor ij\ell\rfloor$, which is the common triangle with $\pm T_i\lfloor jk\ell M$, as well as two white tetrahedral facets adjacent to x_{ij}, namely $\pm T_j\lceil ik\ell\rceil$, which is the common triangle with $\mp[ijkM]$ and $\pm[ij\ell M]$, and $\mp\lceil jk\ell\rceil$, which is the common triangle with $\pm[ij\ell M]$. Therefore, each of the black tetrahedra $\mp T_j\lfloor ik\ell M\rfloor$ and $\pm T_i\lfloor jk\ell M$ has to cancel away with the corresponding black tetrahedron from the 4D corner which is coming from the 3-cell adjacent to$\pm[ijk\ell]$ via the corresponding black triangle, and each of the octahedra $\mp[ijkM]$ and $\pm[ij\ell M]$ has to cancel away with the corresponding octahedron coming the 4D corner which is coming from the 3-cell adjacent to $\pm[ijk\ell]$ via the corresponding white triangle.

Assume that $X = x_{ijk}$. Then for each white tetrahedron $\pm\lceil ijk\ell\rceil \in \sigma$ we added the three octahedra $\pm T_k[ij\ell M]$, $\mp T_j[ik\ell M]$, and $\pm T_i[jk\ell M]$ as well as the white tetrahedron $\mp\lceil ijkM\rceil$ to Σ which do not belong to σ. Moreover, $\pm\lceil ijk\ell\rceil$ has three white triangular facets adjacent to x_{ijk}, namely $\mp T_k\lceil ij\ell\rceil$, which is the common triangle with $\pm T_k[ij\ell M]$, $\pm T_j\lceil ik\ell\rceil$, which is the common triangle with $\mp T_j[ik\ell M]$, and $\mp T_i\lceil jk\ell\rceil$, which is the common triangle with $\pm T_i[jk\ell M]$. Therefore, each of these octahedra has to cancel away with the corresponding octahedron from the 4D corner which is coming from the 3-cell adjacent to $\pm\lceil ijk\ell\rceil$ via the corresponding white triangle.

Consider two 3-cells $\Omega, \bar{\Omega} \in \sigma$ adjacent via the black triangle $\lfloor ijk\rfloor$, say $\lfloor ijk\rfloor$ belongs to Ω and $-\lfloor ijk\rfloor$ belongs to $\bar{\Omega}$. Then the 4D corner corresponding to Ω contributes the black tetrahedron $-\lfloor ijkM\rfloor$ to Σ, whereas the 4D corner corresponding to $\bar{\Omega}$ contributes the black tetrahedron $\lfloor ijkM\rfloor$ to Σ. Therefore, the latter two black tetrahedra cancel out.

Consider two 3-cells $\Omega, \bar{\Omega} \in \sigma$ adjacent via the white triangle $\lceil ijk\rceil$, say $\lceil ijk\rceil$ belongs to Ω and $-\lceil ijk\rceil$ belongs to $\bar{\Omega}$. Then the 4D corner corresponding to Ω contributes the octahedron $-[ijkM]$ to Σ, whereas the 4D corner corresponding to $\bar{\Omega}$ contributes the octahedron $[ijkM]$ to Σ. Therefore, the latter two octahedra cancel out.

Up to now we proved that all black tetrahedra and all octahedra in $\Sigma \setminus \sigma$ cancel out. We will now consider with the white tetrahedra in $\Sigma \setminus \sigma$.

Lemma 6.1 *The white tetrahedra $\lfloor ijkM\rfloor$ arising in the third step of the algorithm build flowers which only contain white tetrahedra.*

Proof We have two prove that each of these white tetrahedra has exactly three adjacent white tetrahedra in the flowers, one via each white triangle adjacent to X. They are not adjacent to the 3-cells in σ, but each of them has three common neighbors adjacent to X with the corresponding white tetrahedron in σ. These common neighbors are octahedra which cancel out in the previous steps of the algorithm.

Consider now two white tetrahedra $T, \bar{T} \in \Sigma \setminus \sigma$ after the third step of the algorithm, where the corresponding white tetrahedra in σ are adjacent, i.e., there is a pair of octahedra with the same set of points and different orientation, one adjacent to T and the other adjacent to $\bar{T}$. Therefore, T and $\bar{T}$ share a common white triangle (up to orientation), i.e., they are adjacent.

Consider the 4D corner which we add to Σ for an octahedron. Its two octahedra which do not belong to σ share a common white triangle (up to orientation) which does no lie in σ. Furthermore, consider a sequence of adjacent octahedra in σ, where the common triangles are all white triangles. Then the octahedra in the corresponding 4D corners which are not in σ all share a common white triangle (up to orientation).

Consider now two white tetrahedra $T, \bar{T} \in \Sigma \setminus \sigma$ after the third step of the algorithm, where the corresponding tetrahedra in σ are connected by a sequence of octahedra adjacent via white triangles. Then, there is a pair of octahedra, one of them adjacent to T and the other one adjacent to $\bar{T}$, which share a common white triangle (up to orientation). This triangle does not belong to any 3-cell in σ and, therefore, is a common triangle of T and $\bar{T}$, i.e., T and $\bar{T}$ are adjacent. □

Now we continue with the proof of Theorem 2.4. We already proved that a flower containing only black tetrahedra can be written as a sum of 3D corners on black 4-simplices (see proof of step 1). Analogously, one can write every flower containing only white tetrahedra as a sum of 3D corners on white 4-simplices. So we write for each of the flowers of white tetrahedra in $\Sigma \setminus \sigma$ after the third step of the algorithm the flower of opposite orientation as a sum of 3D corners on white 4-simplices and add this sums to Σ. Then $\Sigma = \sigma$.

References

1. Adler, V.E., Bobenko, A.I., Suris, Y.B.: Classification of integrable discrete equations of octahedron type. Intern. Math. Res. Not. **2012**(8), 1822–1889 (2012)
2. Bobenko, A.I., Suris, Y.B.: Discrete pluriharmonic functions as solutions of linear pluri-Lagrangian systems. Commun. Math. Phys. **336**(1), 199–215 (2015)
3. Boll, R., Petrera, M., Suris, Y.B.: Multi-time Lagrangian 1-forms for families of Bäcklund transformations. Toda-type systems. J. Phys. A: Math. Theor. **46**(275204) (2013)
4. Boll, R., Petrera, M., Suris, Y.B.: What is integrability of discrete variational systems? Proc. R. Soc. A **470**(20130550) (2014)

5. Boll, R., Petrera, M., Suris, Y.B.: Multi-time Lagrangian 1-forms for families of Bäcklund transformations. Relativistic Toda-type systems. J. Phys. A: Math. Theor. **48**(085203) (2015)
6. Boll, R., Petrera, M., Suris, Y.B.: On integrability of discrete variational systems. Octahedron relations. Intern. Math. Research Notices **rnv140** (2015)
7. Conway, J.H., Sloane, N.J.A.: The cell structures of certain lattices. In: Hilton, P., Hirzebruch, F., Remmert, R. (eds.) Miscellanea Mathematica, pp. 71–107. Springer, Berlin (1991)
8. Doliwa, A.: Desargues maps and the Hirota-Miwa equation. Proc. R. Soc. A **466**, 1177–1200 (2010)
9. Doliwa, A.: The affine Weyl group symmetry of Desargues maps and of the non-commutative Hirota-Miwa system. Phys. Lett. A **375**, 1219–1224 (2011)
10. Lewin, L.: Polylogarithms and Associated Functions. Elsevier North Holland, New York (1981)
11. Lobb, S., Nijhoff, F.W.: Lagrangian multiforms and multidimensional consistency. J. Phys. A: Math. Theor. **42**(454013) (2009)
12. Lobb, S., Nijhoff, F.W.: Lagrangian multiform structure for the lattice Gel'fand-Dikii hierarchy. J. Phys. A: Math. Theor. **43**(072003) (2010)
13. Lobb, S., Nijhoff, F.W., Quispel, G.R.W.: Lagrangian multiform structure for the lattice KP system. J. Phys. A: Math. Theor. **42**(472002) (2009)
14. Moody, R.V., Patera, J.: Voronoi and Delaunay cells of root lattices: classification of their facets by Coxeter-Dynkin diagrams. J. Phys. A: Math. Gen. **25**(5089) (1992)
15. Suris, Y.B.: Variational formulation of commuting Hamiltonian flows: multi-Lagrangian 1-forms. J. Geom. Mech. **5**, 365–379 (2013)
16. Suris, Y.B.: Variational symmetries and pluri-Lagrangian systems. arXiv:1307.2639 [math-ph] (2013)
17. Yoo-Kong, S., Lobb, S., Nijhoff, F.W.: Discrete-time Calogero-Moser system and Lagrangian 1-form structure. J. Phys. A: Math. Theor. **44**(365203) (2011)

Six Topics on Inscribable Polytopes

Arnau Padrol and Günter M. Ziegler

Abstract We discuss six topics related to inscribable polytopes, both in dimension 3 (where the topic was started with a problem posed by Steiner in 1832) and in higher dimensions.

Jakob Steiner ended his 1832 geometry book *Systematische Entwicklung der Abhängigkeit geometrischer Gestalten von einander* [41] with a list of 85 open problems. Problem 77 reads as follows:

> 77) Wenn irgend ein convexes Polyeder gegeben ist läßt sich dann immer (oder in welchen Fällen nur) irgend ein anderes, welches mit ihm in Hinsicht der Art und der Zusammensetzung der Grenzflächen übereinstimmt (oder von gleicher Gattung ist), in oder um eine Kugelfläche, oder in oder um irgend eine andere Fläche zweiten Grades beschreiben (d.h. daß seine Ecken alle in dieser Fläche liegen oder seine Grenzflächen alle diese Fläche berühren)?

It asks whether every (3-dimensional) polytope is *inscribable*; that is, whether for every 3-polytope there is a combinatorially equivalent polytope with all the vertices on the sphere. And if not, which are the cases of 3-polytopes that do have such a realization? He also asks the same question for *circumscribable* polytopes, those that have a realization with all the facets tangent to the sphere, as well as for other surfaces of degree 2.

There was no progress on this question until 1928, when Ernst Steinitz showed that inscribability and circumscribability are polar concepts and presented the first

A. Padrol (✉)
Institut de Mathématiques de Jussieu - Paris Rive Gauche (UMR 7586),
Sorbonne Universités, UPMC Univ Paris 06, 4 place Jussieu, Case 247,
75252 Paris Cedex 05, France
e-mail: arnau.padrol@imj-prg.fr

G.M. Ziegler
Institut für Mathematik, Freie Universität Berlin,
Arnimallee 14, 14195 Berlin, Germany
e-mail: ziegler@math.fu-berlin.de

A.I. Bobenko (ed.), *Advances in Discrete Differential Geometry*,
DOI 10.1007/978-3-662-50447-5_13

examples of polytopes that cannot be inscribed/circumscribed. Since then, the interest on inscribability of polytopes has soared, partially because of tight relations with Delaunay subdivisions and hyperbolic geometry. It was in the context of the latter that, more than 50 years after Steinitz's results, Igor Rivin finally found a characterization of 3-dimensional inscribable polytopes [34]: A 3-connected planar graph describes an inscribable polytope if and only if a certain inequality system has a solution.

What about other quadric surfaces? First of all, since these are not necessarily convex, one has to decide to either consider realizations with the vertices on the surface, or realizations whose intersection with the surface are only the vertices. The weakly inscribable spherical polytopes considered in [8] belong to the first category. For the second version of the definition, Danciger et al. have very recently extended Rivin's results to arbitrary quadrics in $\mathbb{R}^3$ [9]: A 3-polytope is inscribable in the hyperboloid or the cylinder if and only if it is inscribable in the sphere and its graph is Hamiltonian.

So, is the inscribability problem completely solved? We do not think so: Many fundamental questions in this area remain still wide open. In particular, very little is known about inscribability for higher dimensional polytopes. Here we present some intriguing open questions and problems motivated by some recent (and not so recent) results on inscribable polytopes.

1 Inscribability of 3-Polytopes

Incribability and circumscribability are polar concepts: A polytope is inscribable if and only if its polar is circumscribable. Steinitz [42] (cf. [17, Thm. 13.5.2]) constructed non-circumscribable polytopes using the following simple fact. Paint some of the facets of a 3-polytope P black in such a way that there are no two neighboring black facets (just like on a soccer ball). If you can paint more than half of the facets black, then P is not circumscribable (unlike the soccer ball).

His argument was the following. Observe that each facet F has a point of contact with the sphere p_F. We associate to each edge e of F the angle with which we see e from p_F. A reflection about the plane spanned by e and the center of the sphere shows that this angle is the same for the two facets incident to e. Now, if we add all these angles for the edges incident to black facets, we get 2π for each black facet. No two of these share an edge, so if we count the contributions for the white facets we should get at least the same value. However, we get at most 2π times the number of white facets, which is smaller than the number of black facets by hypothesis. □

The same argument also works if exactly half of the facets are black as long as there is at least one edge between two white facets. This provides us with our first example of a non-circumscribable polytope: Take a simplex and truncate all its vertices. The facets arising from the truncation do not share an edge, so painting them black shows non-circumscribability.

The polar argument says that if the graph of a 3-polytope has an independent set (a subset of vertices no two of which are connected by an edge) of more than half of

the vertices (or exactly half of them but not incident to every edge), then the polytope is not inscribable. For example, the *triakis tetrahedron*, a convex polytope obtained by stacking a tetrahedron onto each facet of a tetrahedron, is not inscribable.

Steinitz's condition was later subsumed by results by Dillencourt [10] and by Dillencourt together with Smith [11]. In [10] it is shown that the graph of any inscribed polytope is *1-tough*, which means that for any k, removing k vertices splits the graph into at most k connected components.

This proves non-inscribability for polytopes with an independent set that contains more than half of the vertices, by removing the other vertices. For independent sets that collect exactly half the vertices, we need a slight improvement from [11]: the graph of an inscribable 3-polytope is either bipartite (with both sides of the same size) or 1-supertough, which means that for any $k \geqslant 2$, the removal of k vertices splits the graph into less than k components.

Toughness is a necessary combinatorial condition for inscribability that is easy to check, but it is not sufficient.

Besides the mentioned necessary conditions, Dillencourt and Smith also found some sufficient combinatorial conditions [12], which they summarize as: "*If a polyhedron has a sufficiently rich collection of Hamiltonian subgraphs, then it is of inscribable type.*" For example, this implies that 3-polytopes whose graphs are 4-connected, or where all the vertex degrees are between 4 and 6, are always inscribable.

So, how can we decide whether a given polytope is incribable? Fundamental results on hyperbolic polyhedra by Rivin [34] provided an easy way to decide inscribability/circumscribability of 3-polytopes by linear programming [19] (see also [32, 33, 35]). If one identifies the ball with the Klein model of the hyperbolic space, then an inscribed polytope is an ideal hyperbolic polyhedron. Rivin showed that the dihedral angles at the edges completely characterize these polyhedra.

Theorem 1.1 *([19, Thm. 1]) A 3-polytope P is circumscribable if and only if there exist numbers $\omega(e)$ associated to the edges e of P such that:*

- $0 < \omega(e) < \pi$,
- $\sum_{e \in F} \omega(e) = 2\pi$ *for each facet F of P, and*
- $\sum_{e \in C} \omega(e) > 2\pi$ *for each simple circuit C that does not bound a facet.*

Using this result, inscribability and circumscribability can be efficiently checked. Yet, the characterization depends on a linear programming type feasibility computation. As Dillencourt and Smith pointed out in [11], it is an outstanding open problem to find a graph-theoretical characterization of inscribable 3-polytopes. For simple polytopes, they found such a characterization [11]: A simple 3-polytope is inscribable if and only if its graph is either bipartite and has a 4-connected dual or it is 1-supertough.

Question 1.2 (Dillencourt and Smith [11]) Is there a purely combinatorial characterization of the graphs of inscribable 3-polytopes?

2 A Characterization in Higher Dimensions

It is not likely that there is a characterization as nice and simple as Rivin's for higher-dimensional inscribable polytopes. To start with, 4-dimensional polytopes already present *universality* in the sense of Mnëv: This is a very strong statement whose history took off with groundbreaking results in Nikolai Mnëv's Ph.D. thesis [25, 26], and that we discuss a little further in Sect. 5 (see also [30]). It has several implications, among them that it is already very hard to decide whether a given face lattice corresponds to a 4-polytope. And as we will see later, higher-dimensional inscribable polytopes also present universality features, so one should not expect to be able to decide inscribability in higher dimensions easily or quickly.

A more realistic goal would hence be to look for strong necessary conditions for inscribability in higher dimensions as well as for good (that is, weak) sufficient conditions. A set of necessary conditions is available, since Steinitz's proof carries over directly to higher dimensions, as Grünbaum and Jucovič have observed already in 1974 [18]. Let's see how.

Theorem 2.1 *Let P be a d-polytope with graph G. If G has an independent set that contains more than half of all the vertices, or exactly half the vertices when G is not bipartite, then P is not inscribable.*

Proof Again, we prove the polar statement. Assume that P° is circumscribed. Each facet F touches the ball in a single point p_F. To each of the facets of F, which are ridges of P°, we can intersect the cone with apex p_F spanned by the ridge with a small ball centered at p_F. The (normalized) solid angle associated to the ridge is the ratio of the volume of this intersection to the volume of the ball. Again, a reflection shows that the solid angle associated to each ridge does not depend on which of the two incident facets we take the apex from.

Now assume that the facets of P° are painted in black and white, in such a way that there are no two neighboring black facets. If we add the contributions of the angles of the ridges associated to black facets, it should be at most (or less than if the dual graph is not bipartite) the sum of the contributions for the white facets. Since the sum along each facet is 1, the number of black facets cannot exceed the number of white facets, and they also cannot be the same if there are two adjacent white facets. □

The more general necessary conditions by Dillencourt, such as 1-toughness, have however not yet been generalized to higher dimensions, as far as we know; neither have the sufficient conditions of Dillencourt and Smith. Is it true that if the graph of a d-polytope has a rich enough structure of Hamiltonian subgraphs then the corresponding polytope is inscribable? This could explain the phenomena observed in the next section.

Question 2.2 Find strong necessary and sufficient conditions for inscribability of higher-dimensional polytopes.

Firsching recently achieved a complete enumeration of the simplicial 4-polytopes with 10 vertices [13]: There are exactly 162 004 combinatorial types. Firsching also managed to decide inscribability for all but 13 of these polytopes: The remaining 161 991 are divided into 161 978 inscribable and 13 non-inscribable. So, most simplicial 4-polytopes with 10 vertices are inscribable. Moreover, the very few that are not inscribable have very few facets and edges. More precisely, every non-inscribable simplicial 4-polytope with 10 vertices has less than 27 facets and less than 37 edges, but 146 104 out of the 162 004 simplicial 4-polytopes with 10 vertices do have at least 27 facets and 37 edges. This seems indicate that there might be combinatorial sufficient conditions for inscribability based only on the f-vector.

Question 2.3 Is it true that most simplicial 4-polytopes on n vertices are inscribable, for $n \to \infty$?

In 1991 Smith [40] proved that although there are exponentially many inscribable and circumscribable 3-polytopes with n vertices (because there are many that are 4-connected), most simplicial 3-polytopes with n vertices are neither inscribable nor circumscribable. The proof consists in showing that the probability of finding a fixed non-inscribable subgraph in a random 3-connected planar triangulations tends to 1 as $n \to \infty$. The same argument can be used on random 3-connected planar graphs, see [6, Thm. 2 and Cor. 1], which shows that most combinatorial types of 3-polytopes on a given large number of edges are not inscribable/circumscribable. This contrasts with what happens with simplicial 3-polytopes with few vertices. In the same paper [40], Smith classified these according to their inscribability and circumscribility, and most turned out to be both inscribable and circumscribable. The referee for this paper suggested to use the strategy for 3-polytopes in higher dimension: To show that a large random simplicial d-polytope is likely to contain a fixed non-inscribable subcomplex.

3 Neighborly Polytopes

What is the maximal number of faces that a d-dimensional polytope with n vertices can have? The answer to this fundamental question in the combinatorial theory of polytopes was not established until 1970, by McMullen [22], although Motzkin had already guessed the answer, as we know from a 1957 abstract [27]. And the answer is that the *cyclic d-polytopes* with n *vertices* have the maximal number of k-faces among all *d-polytopes* with n vertices (for all k!). This is the polytope one obtains when taking the convex hull of n points on the moment curve given by $\gamma(t) := (t, t^2, t^3, \ldots, t^d)$.

The cyclic polytopes owe their name to Gale [14], one of several (re-) inventors (cf. [17, Sec. 7.4]), although they were essentially already known to Constantin Carathéodory in 1911 [7], who had studied the convex hull of the *trigonometric moment curve* $(\sin t, \cos t, \sin 2t, \cos 2t, \ldots, \sin kt, \cos kt)$. The representation on

the trigonometric moment curve, which is projectively equivalent to the monomial one [45, pp. 75/76], shows that in even dimensions, the cyclic polytopes are inscribable. Since then, several inscribed realizations of the cyclic polytope have been found (also in odd dimensions), see [17, p. 67], [39, p. 521] and [16, Prop. 17]. Thus the upper bound theorem is established for inscribed polytopes too.

The next natural question asks for *all* the polytopes that have this many facets. McMullen also provided the answer to this: This characterizes the simplicial *neighborly polytopes*. These are the simplicial polytopes with a complete $\lfloor \frac{d}{2} \rfloor$-skeleton. (All even-dimensional neighborly polytopes are simplicial, but not in general the odd-dimensional ones. In particular, not all odd-dimensional neighborly polytopes have the maximal number of facets, only those that are simplicial.) Even if Motzkin claimed that the cyclic polytopes are the only neighborly polytopes (in the same 1957 abstract [27] mentioned above), there are actually plenty. The number of neighborly d-polytopes with n vertices grows at least as $n^{\lfloor d/2 \rfloor n(1-o(1))}$ for fixed d [29]. Compare this to the number of d-polytopes with n vertices, which is not larger than $n^{d^2 n(1+o(1))}$ [3]. As it turns out, each one of the neighborly polytopes used to provide this lower bound is also inscribable [15] (for $d \geqslant 4$). And even more, as we discuss in the next section, they are inscribable in any strictly convex body! This surprising behavior let Gonska and Padrol [15] to ask:

Question 3.1 (Gonska and Padrol [15]) Is every (even-dimensional) neighborly polytope inscribable?

Firsching [13] undertook a quest to find a counterexample. He successfully used non-linear optimization techniques to find polytope realizations. In particular, he tried to inscribe the neighborly polytopes enumerated in [24]. The results are surprising: Every neighborly 4-polytope with $n \leqslant 11$ vertices, every simplicial neighborly 5-polytope with $n \leqslant 10$ vertices, every neighborly 6-polytope with $n \leqslant 11$ vertices, and every simplicial neighborly 7-polytope with $n \leqslant 11$ vertices is inscribable! Even more, every simplicial 2-neighborly 6-polytope with $n \leqslant 10$ vertices is also inscribable. This lead Firsching to ask whether the even stronger statement that all 2-neighborly polytopes are inscribable might be true [13, Conj. 1]. This may be a very brave conjecture, for which not much evidence is available yet. However, recall that the graph of a 2-neighborly polytope is complete, and hence has the richest possible structure of Hamiltonian subgraphs ...

Question 3.2 (Firsching [13]) Is every (simplicial) 2-neighborly polytope inscribable?

We can also ask the polar question: What about circumscribability of neighborly polytopes? The results are completely opposite. Chen and Padrol proved that, for any $d \geqslant 4$, no cyclic d-polytope on sufficiently many vertices is circumscribable [8]. (The proof will be sketched below in the last section.) They even conjecture that this holds in more generality for neighborly polytopes [8, Conj. 7.4]. Notice that, since neighborliness can be read on the f-vector, this would imply that there is an f-vector of a convex polytope that does not belong to any inscribable polytope,

namely that of the polar of a neighborly 4-polytope with sufficiently many vertices. No example of such an f-vector has been established so far. Actually, what is known points into the other direction: Every f-vector of a 3-dimensional polytope is inscribable [16]. However, f-vectors that are not k-scribable are known for $d \geqslant 4$ and $1 \leqslant k \leqslant d-2$ [8]. (A polytope is *k-scribable* if it has a realization with all its k-faces tangent to the sphere.)

Question 3.3 (Gonska and Ziegler [16]) Is there an f-vector that is not inscribable?

4 Universally Inscribable

As we just mentioned, the proof of inscribability for cyclic and many more neighborly polytopes given in [15] still works when we replace the unit ball by any other smooth strictly convex body. (This is what Oded Schramm called an *egg* in his celebrated paper "*How to cage an egg?*" [37].) Here smoothness is not very important, but strict convexity is. For example, the pigeonhole principle tells us that no simplicial d-polytope with more than $d(d+1)$ vertices can be inscribed on the boundary of a d-simplex.

Hence many neighborly polytopes (among them all cyclic polytopes) are *universally inscribable*: They can be inscribed into any egg. Other examples of such polytopes are the stacked d-polytopes arising as a join of a path with a $(d-2)$-simplex; and also Lawrence polytopes [15].

Question 4.1 (Gonska and Padrol [15]) Which polytopes are inscribable into the boundary of every (smooth) strictly convex body?

An observation of Karim Adiprasito [15] shows that being inscribable on the sphere is not sufficient for being universally inscribable. (The proof uses projectively unique polytopes [2].) We thank the anonymous reviewer for suggesting the following opposite question. (The reviewer's conjectured answer is yes.)

Question 4.2 Are there polytopes that are inscribable in every egg other than the ellipsoid?

The celebrated Koebe–Andreev–Thurston Theorem states that every 3-polytope has a realization with all its edges tangent to the sphere. This amazing result has a long history. It seems that it was first proved by Paul Koebe, but only for simple and simplicial polytopes [21]. Thurston later realized [44] that it followed from results of Andreev on hyperbolic polyhedra [4, 5]. Since then, several proofs have been found (see [46, Sect. 1.3] and references therein). Schramm went even further and proved that every 3-polytope has a realization with all its edges tangent to any given egg [37].

Theorem 4.3 *(Schramm [37]) For every 3-polytope P, and every smooth strictly convex body K, there is a realization Q of P such that each edge of Q is tangent to K.*

There is also the other side of universal inscribability, which would be to focus on the convex bodies. The mathoverflow user called Samsa asked [36]:

> Is there a convex body in $\mathbb{R}^d$ such that every combinatorial type of a d-dimensional convex polytope can be realized with vertices on its surface?

We reproduce the beautiful affirmative answer by Ivanov [20]:

> Yes, there is such a body. Actually there is one very close to the standard unit ball and containing disjoint representatives of each combinatorial type (but these representatives are very small).
>
> Indeed, every combinatorial type of a d-polytope has a realization which looks as follows: there is a "large" $(d-1)$-dimensional facet and the remaining surface is a graph over this facet. To construct such a realization, choose a $(d-1)$-facet, pick a hyperplane parallel to it and very close to it (but not intersecting the polytope), and apply a projective map which sends this hyperplane to infinity.
>
> We can further "flatten" this realization so that it is very close to its large face. Choose a very small $\varepsilon > 0$, apply a homothety such that the diameter of the polytope becomes less than ε, and place the resulting tiny polytope so that it touches the sphere by a point on its "large" face. Then consider the convex hull of the sphere and the polytope. All vertices will be on the boundary of this convex hull if the polytope is sufficiently "flattened." And the convex hull diverges from the ball only in a neighborhood of size $\sim\sqrt{\varepsilon}$.
>
> Now pick another combinatorial type of a polytope and repeat the procedure with a much smaller ε and a location on the sphere chosen so that the neighborhood affected by the second polytope does not interfere with the first one. And so on. Since there are only countably many combinatorial types, they all can be packed into the sphere, provided that ε goes to 0 sufficiently fast.

5 Universality

We move on to a slightly different topic, and a different notion of "universality." Take an inscribable polytope P, and consider the set of all inscribed realizations of P. How does this set look like? To start off, it can be parametrized by the vertex coordinates. Moreover, since any Möbius transformation that preserves the unit sphere as well as its interior sends an inscribed polytope onto an inscribed polytope, we can safely mod out the action of this group. This defines $\mathscr{R}_{\text{ins}}(P)$, the *realization space of an inscribed polytope* P (with n vertices in $\mathbb{R}^d$):

$$\mathscr{R}_{\text{ins}}(P) = \left\{A \in (\mathbb{S}^{d-1})^n \,\middle|\, \text{conv}(A) \simeq P\right\} \Big/ \text{Möb}(\mathbb{S}^{d-1}). \tag{1}$$

This concept is inspired by an analogue definition for general polytopes. In that setting, one considers $\mathscr{R}_{\text{pol}}(P)$, the set of all realizations of P, up to affine transformation. From Steinitz's proofs of Steinitz's Theorem [43] we know that these sets are relatively nice when P is of dimension at most 3: They are contractible, contain rational points, etc.; see [30, 31]. For higher-dimensional polytopes, however, the behavior of realization spaces is much wilder. This was first observed by

Mnëv, with his celebrated Universality Theorem [25, 26] for polytopes and oriented matroids. The polytopal version reads: For every primary basic [open] semi-algebraic set defined over $\mathbb{Z}$ there is a [simplicial] polytope whose realization space is stably equivalent to it. This has many consequences, among them:

- topological: $\mathscr{R}_{\text{pol}}(P)$ can have the homotopy type of any arbitrary finite simplicial complex,
- algebraic: there are polytopes that cannot be realized with rational coordinates,
- algorithmic: it is ETR-hard to decide if a lattice is the face lattice of a polytope.

Mnëv's proof provided polytopes with the desired realization spaces, but could not say anything about their dimensions. Another major step was done later by Jürgen Richter-Gebert, who proved that there is universality already for 4-dimensional polytopes [30].

The inscribed picture is similar. Up to dimension 3, inscribed realization spaces are reasonable. This follows from the results of Rivin that we have already mentioned [33], which imply that for a 3-polytope P, $\mathscr{R}_{\text{ins}}(P)$ is homeomorphic to the polyhedron of angle structures (and hence are contractible). In contrast, results of Adiprasito and Padrol with Louis Theran show that, in arbitrarily high dimensions, there is again universality [1]. We have not found yet an appropriate notion of stable equivalence for this context, while a universality theorem for general polytopes without stable equivalence is neither available nor in sight. This forces us to separate the topological, algebraic and algorithmic statements:

Theorem 5.1 *(Adiprasito et al. [1])*

- *For every primary basic semi-algebraic set there is an inscribed polytope whose realization space is homotopy equivalent to it.*
- *For every finite field extension $F/\mathbb{Q}$ of the rationals, there is an inscribed polytope that cannot be realized with coordinates in F.*
- *The problem of deciding if a poset is the face lattice of an inscribed [simplicial] polytope is polynomially equivalent to the* existential theory of the reals (ETR). *In particular, it is NP-hard.*

In the last point we can even ask the polytopes to be simplicial. This follows from a weak universality theorem for inscribed simplicial polytopes, which also appears in [1]. In this case, we can only find polytopes whose realization space retracts onto the semi-algebraic set, instead of having homotopy equivalence as in the general case.

The inscribed analogue to Richter-Gebert's result for 4-polytopes is still missing.

Question 5.2 (Adiprasito et al. [1]) Is there universality for inscribed polytopes in bounded dimension, say for 4-polytopes inscribed into $\mathbb{S}^3$?

The proof of Theorem 5.1 strongly relies on the results of Mnëv. The strategy is to start with certain polytopes with intricate realization spaces, and then to show that their inscribed realization spaces are equally involved. In particular, it does not

prove that it is hard to decide inscribability once we already know that the face lattice corresponds to a polytope. However, inscribability is itself a complex condition, and hence one can expect that it increases the complexity of the corresponding realization spaces. This could lead to a proof of universality that is intrinsic to inscribed polytopes, and hopefully to advances in the previous question. A first step in this direction could be to find a polytope P such that $\mathscr{R}_{\text{ins}}(P)$ is disconnected while $\mathscr{R}_{\text{pol}}(P)$ is not.

Question 5.3 Is there universality for the realization spaces $\mathscr{R}_{\text{ins}}(P)$ for a class of inscribable polytopes P whose general realization spaces $\mathscr{R}_{\text{pol}}(P)$ are trivial (in particular, contractible)?

6 (*i, j*)-Scribability

We have already referred to the Koebe–Andreev–Thurston Theorem. One is tempted to ask if similar behaviors might also appear in higher dimensions. The answer is no. Egon Schulte used an inductive argument over non-inscribable/non-circumscribable 3-polytopes to show that, for every $d \geqslant 4$, and every $0 \leqslant k \leqslant d-1$, there are d-polytopes that cannot be realized with all their k-faces tangent to the sphere [38]. Of course, this opens the door to ask for a characterization of k-scribable polytopes. There are almost no results in this direction, which is definitely an interesting research topic.

We will, however, consider a different problem. If we take an edge-scribed realization of a 3-polytope, it has also the following property: All the vertices are outside the ball while all the facets cut the ball. This kind of realizations are studied in [8]. Here a polytope is said to be *(i, j)-scribed* if all its i-faces "avoid" the sphere while all the j-faces "cut" it. The definitions for cutting and avoiding that seem to work better say that a face F *cuts* the ball if there is a point of the unit ball in its relative interior, and that it *avoids* the ball if there is a hyperplane H, supporting for F, which completely contains P and the ball in one of the closed halfspaces it defines. (This somehow involved definition is needed if we want a self-dual concept that reduces to classical k-scribability when $i = j = k$.)

The weakest condition occurs when $i = 0$ and $j = d-1$:

Question 6.1 Does every polytope have a realization where every vertex avoids the ball and every facet cuts the ball?

The answer is most probably no, but so far no proof has been given (although Karim Adiprasito has suggested that one should be able to obtain counterexamples from gluing some of the large projectively unique polytopes from [2]). There are some results in the opposite direction: For $d = 3$, the edge-scribed realization is also $(0, d-1)$-scribed. Every inscribable polytope has directly a $(0, d-1)$-scribed realization too. So, in particular, cyclic polytopes and many (all?) neighborly polytopes have such realizations. And obviously, circumscribable polytopes also have

such a realization. This includes stacked polytopes, which are always circumscribable [8].

What about other values of i and j? The best offenders found in [8] are even-dimensional cyclic polytopes (and their duals):

Theorem 6.2 *(Chen and Padrol [8]) If an even-dimensional cyclic polytope has sufficiently many vertices, then it is not* $(1, d-1)$*-scribable, which in particular implies that it is not circumscribable.*

Proof (Sketch) The first step is to associate to each vertex of a $(1, d-1)$-scribed cyclic polytope the spherical cap consisting of the points of $\mathbb{S}^{d-1}$ visible from it. This yields a configuration of spherical caps on $\mathbb{S}^{d-1}$. These are said to form a *k-ply* system if no point of $\mathbb{S}^{d-1}$ is contained in the interior of more than k caps.

Now the Sphere Separator Theorem of Miller et al. [23] states that the intersection graph of a k-ply system on $\mathbb{S}^{d-1}$ has a separator of size $O(k^{1/(d-1)}n^{1-1/(d-1)})$. The proof is astonishingly simple and beautiful (cf. [28, Thm. 8.5]): With a Möbius transformation, we can assume that the origin is a center-point of the centers of the caps. The next step is to compute the probability that a random linear hyperplane intersects a cap, which depends only on the area covered by the cap. Since our system is k-ply, we can estimate the sum of these volumes because we know the surface area of the sphere. This is used to show that a random linear hyperplane hits very few caps, whose removal separates the graph.

So how do we tie this in with cyclic polytopes? The key observation is that a set of points induce a k-ply system if and only if the convex hull of every k-set intersects the sphere. A *k-set* is a subset of k points that can be separated from the others with a hyperplane. Even-dimensional cyclic polytopes have a lot of nice properties, among them oriented matroid rigidity. This allows us to show that every k-set with $k \geqslant \frac{3}{2}d - 1$ contains a facet. If the realization was $(0, d-1)$-scribed, this facet would intersect the sphere, and hence the cyclic polytope induces a k-ply set. But in this case, the intersection graph consists of the edges of the polytope avoiding the sphere. If all the edges avoided the sphere, this would be a complete graph, which obviously does not have a small separator. □

Acknowledgments We are grateful to Karim Adiprasito, Hao Chen, Igor Rivin, Juanjo Rué, Francisco Santos, and the anonymous referee for very valuable discussions, suggestions, and references; and to Sergei Ivanov for letting us reproduce his mathoverflow answer.

References

1. Adiprasito, K., Padrol, A., Theran, L.: Universality theorems for inscribed polytopes and Delaunay triangulations. Discrete Comput. Geom. **54**, 412–431 (2015)
2. Adiprasito, K., Ziegler, G.M.: Many projectively unique polytopes. Inventiones Math. **199**, 581–652 (2015)
3. Alon, N.: The number of polytopes, configurations and real matroids. Mathematika **33**(1), 62–71 (1986)
4. Andreev, E.M.: On convex polyhedra in Lobačevskiĭ spaces. Math. USSR, Sb. **10**, 413–440 (1971)
5. Andreev, E.M.: On convex polyhedra of finite volume in Lobačevskiĭ space. Math. USSR, Sb. **12**, 255–259 (1971)
6. Bender, E.A., Gao, Z.C., Richmond, L.B.: Submaps of maps. I. general 0–1 laws. J. Combinat. Theory, Ser. B **55**(1), 104–117 (1992)
7. Carathéodory, C.: Über den Variabilitätsbereich der Fourier'schen Konstanten von positiven harmonischen Funktionen. Rendiconto del Circolo Matematico di Palermo **32**, 193–217 (1911)
8. Chen, H., Padrol, A.: Scribability problems for polytopes. Preprint, August 2015, 24 pp., http://arxiv.org/abs/1508.03537
9. Danciger, J., Maloni, S., Schlenker, J.M.: Polyhedra inscribed in a quadric. Preprint, October 2014, 42 pp., http://arxiv.org/abs/1410.3774
10. Dillencourt, M.B.: Toughness and Delaunay triangulations. Discrete Comput. Geom. **5**(6), 575–601 (1990)
11. Dillencourt, M.B., Smith, W.D.: A linear-time algorithm for testing the inscribability of trivalent polyhedra. Internat. J. Comput. Geom. Appl. **5**(1-2), 21–36 (1995). Eighth Annual ACM Symposium on Computational Geometry (Berlin, 1992)
12. Dillencourt, M.B., Smith, W.D.: Graph-theoretical conditions for inscribability and Delaunay realizability. Discrete Math. **161**(1–3), 63–77 (1996)
13. Firsching, M.: Realizability and inscribability for some simplicial spheres and matroid polytopes. Preprint, October 2015, 25 pp., http://arxiv.org/abs/1508.02531
14. Gale, D.: Neighborly and cyclic polytopes. In: Proceedings of Symposia in Pure Mathematics, vol. VII, pp. 225–232. American Mathematical Society, Providence (1963)
15. Gonska, B., Padrol, A.: Neighborly inscribed polytopes and Delaunay triangulations. Adv. Geom. (in press). Preprint http://arxiv.org/abs/1308.5798v2
16. Gonska, B., Ziegler, G.M.: Inscribable stacked polytopes. Adv. Geom. **13**(4), 723–740 (2013)
17. Grünbaum, B.: Convex polytopes. Graduate Texts in Mathematics, vol. 221, 2nd edn. Springer-Verlag, New York (2003)
18. Grünbaum, B., Jucovič, E.: On non-inscribable polytopes. Czechoslovak Math. J. **24**(99), 424–429 (1974)
19. Hodgson, C.D., Rivin, I., Smith, W.D.: A characterization of convex hyperbolic polyhedra and of convex polyhedra inscribed in the sphere. Bull. Amer. Math. Soc. **27**(2), 246–251 (1992)
20. Ivanov, S.: Can all convex polytopes be realized with vertices on surface of convex body? MathOverflow, http://mathoverflow.net/q/107113, September 2012
21. Koebe, P.: Kontaktprobleme der konformen Abbildung. Berichte Verh. Sächs. Akademie der Wissenschaften Leipzig, Math.-Phys. Klasse **88**, 141–164 (1936)
22. McMullen, P.: The maximum numbers of faces of a convex polytope. Mathematika **17**, 179–184 (1970)
23. Miller, G.L., Teng, S.H., Thurston, W., Vavasis, S.A.: Separators for sphere-packings and nearest neighbor graphs. J. ACM **44**(1), 1–29 (1997)
24. Miyata, H., Padrol, A.: Enumerating of neighborly polytopes and oriented matroids. Exp. Math. **24**(4), 489–505 (2015)
25. Mnëv, N.E.: The topology of configuration varieties and convex polytopes varieties. Ph.D. thesis, St. Petersburg State University, St. Petersburg, RU (1986). 116 pp., http://www.pdmi.ras.ru/~mnev/mnev_phd1.pdf

26. Mnëv, N.E.: The universality theorems on the classification problem of configuration varieties and convex polytopes varieties. In: Topology and Geometry—Rohlin Seminar. Lecture Notes in Mathematics, vol. 1346, pp. 527–544. Springer-Verlag, Berlin (1988)
27. Motzkin, T.S.: Comonotone curves and polyhedra (Abstract). Bull. Am. Math. Soc. **63**, 35 (1957)
28. Pach, J., Agarwal, P.K.: Combinatorial Geometry. Wiley-Interscience Series in Discrete Mathematics and Optimization. Wiley, New York (1995)
29. Padrol, A.: Many neighborly polytopes and oriented matroids. Discrete Comput. Geom. **50**(4), 865–902 (2013)
30. Richter-Gebert, J.: Realization spaces of polytopes. Lecture Notes in Mathematics, vol. 1643. Springer-Verlag, Berlin (1996)
31. Richter-Gebert, J., Ziegler, G.M.: Realization spaces of 4-polytopes are universal. Bull. Am. Math. Soc. **32**, 403–412 (1995)
32. Rivin, I.: On geometry of convex ideal polyhedra in hyperbolic 3-space. Topology **32**(1), 87–92 (1993)
33. Rivin, I.: Euclidean structures on simplicial surfaces and hyperbolic volume. Ann. Math. (2) **139**(3), 553–580 (1994)
34. Rivin, I.: A characterization of ideal polyhedra in hyperbolic 3-space. Ann. Math. (2) **143**(1), 51–70 (1996)
35. Rivin, I.: Combinatorial optimization in geometry. Adv. Appl. Math. **31**(1), 242–271 (2003)
36. Samsa, G.: Can all convex polytopes be realized with vertices on surface of convex body? MathOverflow. http://mathoverflow.net/q/107096, September 2012
37. Schramm, O.: How to cage an egg. Inventiones Math. **107**(3), 543–560 (1992)
38. Schulte, E.: Analogues of Steinitz's theorem about non-inscribable polytopes. In: Proceedings of "Intuitive Geometry" (Siófok, 1985). Colloq. Math. Soc. János Bolyai, vol. 48, pp. 503–516. North-Holland, Amsterdam (1987)
39. Seidel, R.: Exact upper bounds for the number of faces in d-dimensional Voronoĭ diagrams. In: Applied Geometry and Discrete Mathematics. DIMACS Ser. Discrete Math. Theoret. Comput. Sci., vol. 4, pp. 517–529. American Mathematical Society, Providence (1991)
40. Smith, W.D.: On the enumeration of inscribable graphs. Manuscript, 7 pp., NEC Research Institute, 1991; http://citeseer.ist.psu.edu/viewdoc/summary?doi=10.1.1.29.4543
41. Steiner, J.: Systematische Entwicklung der Abhängigkeit geometrischer Gestalten von einander. Fincke, Berlin (1832). Also in: Gesammelte Werke, vol. 1, Reimer, Berlin 1881, pp. 229–458
42. Steinitz, E.: Über isoperimetrische Probleme bei konvexen Polyedern. J. Reine Angew. Math. **159**, 133–143 (1928)
43. Steinitz, E., Rademacher, H.: Vorlesungen über die Theorie der Polyeder. Springer-Verlag, Berlin (1934). Reprint, Springer-Verlag (1976)
44. Thurston, W.P.: Geometry and topology of 3-manifolds. In: Lecture Notes. Princeton University, Princeton (1977–1978); http://library.msri.org/books/gt3m/
45. Ziegler, G.M.: Lectures on polytopes. Graduate Texts in Mathematics, vol. 152. Springer, New York (1995)
46. Ziegler, G.M.: Convex polytopes: extremal constructions and f-vector shapes. In: Geometric Combinatorics. IAS/Park City Math. Ser., vol. 13, pp. 617–691. American Mathematical Society, Providence (2007)

DGD Gallery: Storage, Sharing, and Publication of Digital Research Data

Michael Joswig, Milan Mehner, Stefan Sechelmann, Jan Techter and Alexander I. Bobenko

Abstract We describe a project, called the DGD Gallery, whose goal is to store geometric data and to make it publicly available. The DGD Gallery offers an online web service for the storage, sharing, and publication of digital research data.

1 Introduction

Software produces data. Mathematical software produces scientific data, and this is often worth keeping. One reason for this can be the vast amount of CPU time spent on a specific experiment. Another reason can be that the output is obtained only via a complex interaction process between the software and its user. That latter situation is typical in mathematical visualization, where producing a satisfying or even beautiful picture of a geometric object is a form of art. The purpose of this text is to describe a new project, called the "Discretization in Geometry and Dynamics Gallery", or DGD GALLERY for short, whose goal is to store geometric data and to make it publicly available. The URL of the web-site is

http://gallery.discretization.de

M. Joswig (✉) · M. Mehner · S. Sechelmann · J. Techter · A.I. Bobenko
Inst. für Mathematik, Technische Universität Berlin,
Straße des 17. Juni 136, 10623 Berlin, Germany
e-mail: joswig@math.tu-berlin.de

M. Mehner
e-mail: mmehner@math.tu-berlin.de

S. Sechelmann
e-mail: sechel@math.tu-berlin.de

J. Techter
e-mail: techter@math.tu-berlin.de

A.I. Bobenko
e-mail: bobenko@math.tu-berlin.de

A.I. Bobenko (ed.), *Advances in Discrete Differential Geometry*,
DOI 10.1007/978-3-662-50447-5_14

Today it is safe to say that finally mathematical software has reached every branch of mathematics. While computers have played a role in mathematical applications for a long time, it took considerably longer for software to be appreciated fully in parts of mathematics traditionally considered as "pure". The array of tools at our fingertips now includes solvers for linear programs and partial differential equations, but also software for dealing with real algebraic sets [1] or delicate constructions in sheaf theory [2]. To get an idea of how rich the mathematical software landscape has become, see, e.g., [3]. The success of each single software system raises the question of how the respective data produced should be stored. With an increasing number of relevant mathematical results relying on non-trivial computations in an essential way (see, e.g., the `Flyspeck` project [4]) it becomes more and more crucial to publish such results in a way such that they can be scrutinized (and used) by the mathematical community.

The mathematical data we have in mind for the DGD GALLERY are the geometric objects that occur naturally on the border between differential geometry and geometric combinatorics. This includes various classes of surfaces (embedded or immersed) in 3-space, convex polytopes and polyhedral fans of various dimensions, circle patterns, and many more. Yet, we believe that several of our design decisions and architecture ingredients will be useful for other collections of mathematical data. Key features include the following:

- structured storage of research data,
- review process for increased reliability,
- migration process for sustainability,
- licensing scheme.

To further stress the relevance of our endeavor, it is worth noting that scientific funding agencies have begun to add requirements concerning the preservation of scientific data to their regulations. For instance, in a recent announcement [5] of Deutsche Forschungsgemeinschaft (DFG) says[1]:

> The documentation of research data according to standards depending on the subject and their long-term archival are relevant for controlling the quality of scientific work. Further, these data are the basic requirements for the subsequent use of research results.

The DGD GALLERY evolved as a project within the DFG Collaborative Research Center SFB/TRR 109 "Discretization in Geometry and Dynamics". Its usage is currently restricted to the members of the center. However, it is intended that future versions allow other researchers to contribute their work, too.

The paper is organized as follows. First we compare our design to existing collections of geometric data (Sect. 2). Then, in Sect. 3, we exhibit some examples already published on the gallery. This should give a good idea of what kind of collection we have in mind. At the same time this also shows some of the technical features and capabilities. The core is Sect. 4, where we elaborate on the architecture and the design decisions. The key concept is the *model*, which is our technical realization of a geometric object. Some aspects of the implementation are covered in Sect. 5. For

[1] Translated from German.

instance, we explain how we use the XML document database BASEX [6] and meet current standards of web technology.

2 Comparison with Previous Work

To store geometric data digitally and make it accessible through a web-site is clearly not a new idea. On the contrary, since the early days of the Internet people have set up numerous web-sites with all kinds of information on geometric objects, e.g.: The Geometry Center's "Geometry Reference Archive" [7], "The Scientific Graphics Project"of MSRI [8], or David Eppstein's "Geometry Junkyard" [9], to name a few prominent examples. Clearly, all of the above still contain lots of interesting information. However, there are some shortcomings. In the case of the archive of The Geometry Center we have a static collection of data that will not see any updates or additions. Yet there is the advantage that all data is available from one source, and so it cannot degenerate over time (except for eventually outdated file formats). Not so with the "Geometry Junkyard". This is a collection of links to other interesting resources on the web. Many of the links are dead already. This is mainly due to a discontinued provider service or simply a change of position of the person who provided the data. The "Scientific Graphics Project" is mainly a collection of surfaces and differential geometry related publications. The DGD GALLERY wants to cover geometric objects from a much wider collection.

A more recent project is the "GeometrieWerkstatt" [10] maintained by a group of geometers at Tübingen University. It contains visualizations of mostly smooth constant mean curvature surfaces. Surfaces are visualized using videos, images, and interactive 3D viewers. The main difference to the DGD GALLERY is that there is no geometric data that can be accessed via the web-site. On the other hand, how to provide the data for smooth surfaces is far from obvious and cannot be separated from the mathematical methods. For the DGD GALLERY we propose to include a discretization of a smooth surface in a reasonable resolution.

"IMAGINARY—open mathematics"is a platform [11] which has a strong educational focus. It features images and mathematical software for a broad audience such as exhibitions, high school education, and museums. As an essential feature, IMAGINARY is open for the public to contribute material by cross-linking to other web-sites. In this way it works like a collection of collections.

The focus of the SymbolicData project [12] is on developing concepts and tools for profiling, testing and benchmarking Computer Algebra Software. This includes storing scientific data from various sources, but visualization does not play a role.

The project that is most similar in spirit to our DGD GALLERY is "Electronic Geometry Models" [13, 14], which is a refereed online journal for digital geometry models on the web. It features XML file formats, visualization separated from descriptions, and a reviewing process. All of these are also implemented in the DGD GALLERY.

However, our technical realization substantially differs from "Electronic Geometry Models". The DGD GALLERY employs modern web technology for the user interface and a standard data base implementation for storing. One advantage of this

is the possibility to work in teams. Each team member can contribute to a model if he/she is a registered user with the suitable permissions. Permissions can be granted by owners of content; for details see Fig. 7 below. Moreover, the entire work flow from the submission, through reviewing and revising, to the final publication has one consistent setup through a common front end. Most importantly, the overall design is highly modularized. For instance, the DGD GALLERY features a variety of media renderers with different visualization strengths to accommodate for heterogeneous hard- and software environments at the users' end. This is also relevant for being able to preserve the data over a long period.

Another difference to "Electronic Geometry Models" is that the DGD GALLERY aims at a broader outreach and therefore seeks to include more models of purely educational value. This results in a different set of criteria for accepting a model for publication. Moreover, the DGD GALLERY allows for changes to a model after publication.

3 Examples

In this section we present some selected models from the early contributions to the DGD GALLERY. They are intended as guidelines and inspiration for future models to be submitted.

3.1 Discrete S–Conical Catenoid and Helicoid

Authors: Alexander Bobenko, Tim Hoffmann, Benno König, and Stefan Sechelmann (Fig. 1)

http://gallery.discretization.de/models/sc-catenoid

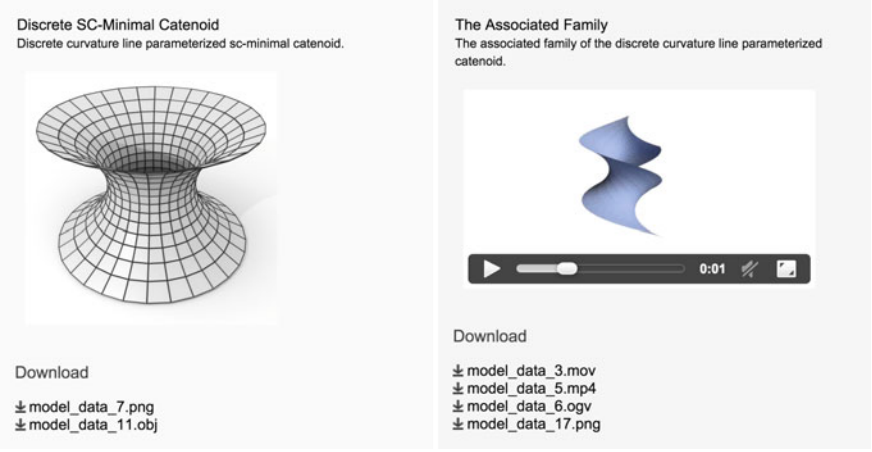

Fig. 1 Screenshot of two media objects contained in the "Discrete S-Conical Catenoid and Helicoid" model as presented by a modern web browser. *Left* Discrete s-conical catenoid. *Right* Associated family animation between s-conical catenoid and its conjugate, the discrete helicoid

This model shows discrete s-conical versions of the catenoid and the helicoid, which are classical minimal surfaces [15]. The smooth versions are among the first classical minimal surfaces ever investigated. Their s-conical counterparts are quadrilateral polyhedral surfaces with the property that at each vertex the adjacent faces are tangent to a cone of revolution. The theory of these discrete minimal surfaces is closely related to the theory of orthogonal circle patterns and Koebe polyhedra; see Sect. 3.3 below. Its features and constructions are similar to the theory of s-isothermic surfaces. A minimal surface is (Christoffel) dual to its Gauss map. This property is preserved in the discrete setup, and so discrete minimal surfaces are constructed from Koebe polyhedra. The associate family of minimal surfaces is contained in the discrete theory as well.

The model features images of the catenoid and helicoid using representations with discrete curvature line parameterizations as well as discrete asymptotic line parameterizations in the associate family. It contains a video with an animation of the associate family animating the angle parameter. Geometric data is given as OBJ files and corresponding preview images.

3.2 z^a Circle Pattern

Authors: Jan Techter and Jürgen Richter-Gebert (Fig. 2)

http://gallery.discretization.de/models/zalpha_circle_pattern

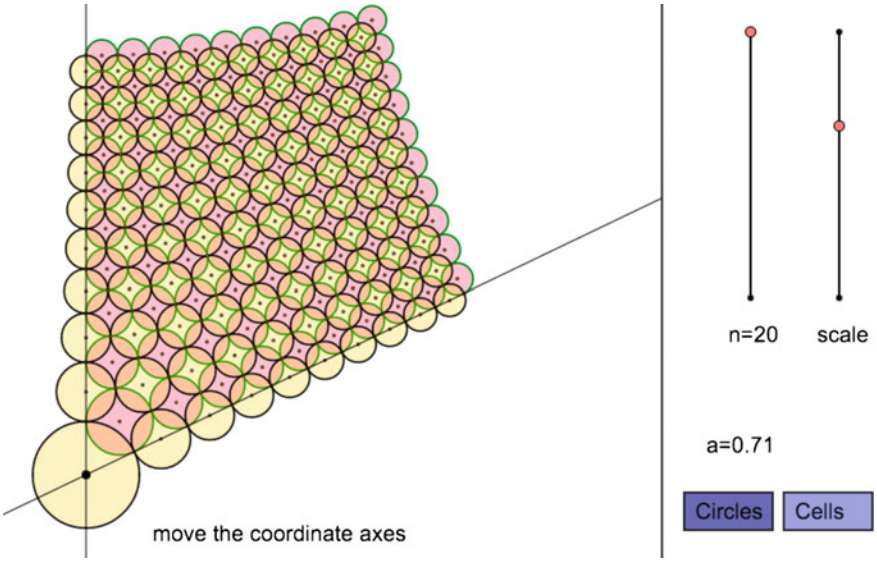

Fig. 2 Screenshot of the interactive element of the "z^a *circle pattern*" model. A user can adjust the number of *circles* in a row as well as the overall scale of the drawing. The angle α is entered by moving the axes with the mouse

The representation of discrete holomorphic functions by circle patterns with square-grid combinatorics was first studied by Schramm [16].

This model shows the Schramm type circle pattern corresponding to the holomorphic map $z \mapsto z^a$ for $0 < a < 2$ in the first quadrant of the complex plane. Taking the centers and intersections of the circles as complex fields on the first quadrant of $\mathbb{Z}^2$, the discrete map was introduced in [17] as a special isomonodromic solution of the cross-ratio equation (cross-ratio equal to -1 on each elementary quadrilateral). The numerics of these discrete maps is studied in [18].

The model features an interactive Cinderella [19] application where the user can adjust the exponent a and the number of circles, see also Sect. 5.3.

3.3 Koebe Polyhedra

Author: Stefan Sechelmann (Fig. 3)

http://gallery.discretization.de/models/koebe_polyhedra

A *Koebe polyhedron* is a 3-dimensional convex polytope whose edges are tangent to the unit sphere. Koebe polyhedra have a strong connection to the theory of circle patterns, see [20]. The theory of discrete minimal surfaces of s-isothermic and s-conical type is based on Koebe polyhedra. Each combinatorial type of 3-polytope admits a representation as Koebe polyhedron, which is unique up to Möbius transformation.

The first step for the construction of a Koebe polyhedron is to create an orthogonal circle pattern corresponding to the desired polytopal cell decomposition of the sphere. This is generally done by finding critical points of a functional expressed in the the variables $\rho_i = \log \tan \frac{r_i}{2}$ given by the spherical radii r_i. Once the radii are known

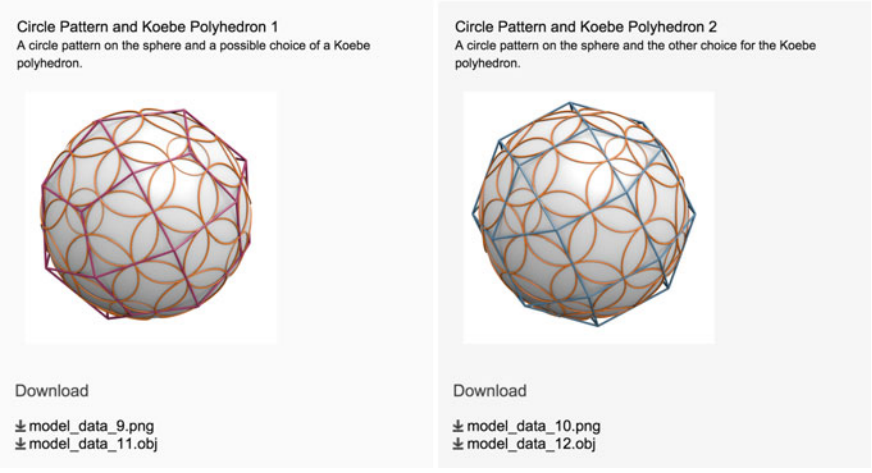

Fig. 3 Screenshot of two media objects of the "Koebe Polyhedra" model. The two images show the two corresponding Koebe polyhedra for a given *circle pattern*

the circles can be layed out. The still remaining freedom of applying a Möbius transformation can be fixed (up to a simple rotation) by requiring the center of mass to be at the sphere center. The vertices of the circumscribed Koebe polyhedron that corresponds to the circle pattern can now easily be found by inverting the euclidean centers of the circles in $\mathbb{S}^2$ (the cone tips are the points polar to the planes containing the circles). Here we have the freedom to choose one of the two orthogonal families of circles to become vertices of the Koebe polyhedron, and the other family to become faces.

The online model features a selection of Koebe polyhedra. Each one with an OBJ geometry file and a PNG image file.

3.4 Lawson's Surface Uniformization

Authors: Stefan Sechelmann, Alexander Bobenko, and Boris Springborn (Fig. 4)

http://gallery.discretization.de/models/lawsons_surface_uniformization

Fuchsian uniformizations of the Riemann surface of Lawson's genus 2 minimal surface in $\mathbb{S}^3$ [21] are presented in this model. The results were created in [22] using the discrete uniformization theory. Three different conformally equivalent representations of the surface and of the corresponding hyperbolic tilings are presented.

Lawson's minimal surface in $\mathbb{S}^3$ is conformally equivalent to the hyperelliptic curve $\mu^2 = \lambda^6 - 1$. The branch points $\lambda_1, \ldots, \lambda_6$ are the 6th roots of unity.

An embedding of Lawson's surface in $\mathbb{R}^3$, see Fig. 4, is obtained via stereographic projection from $\mathbb{S}^3$ [23]. For this surface the hyperelliptic involution of the Riemann

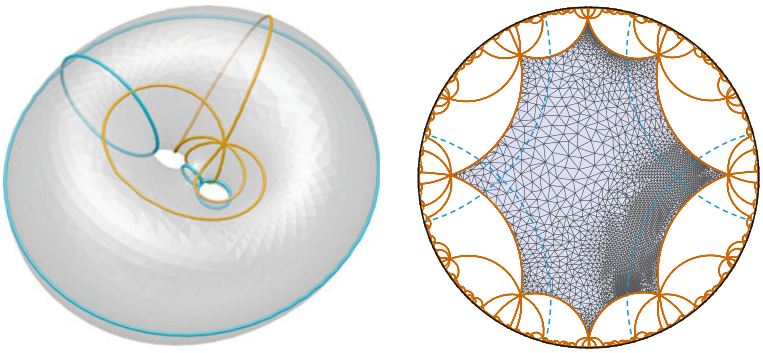

Fig. 4 *Left* The Lawson surface in $\mathbb{R}^3$, the boundary curves of the fundamental domain of the uniformizing group in the *right picture* are shown in *red*. *Blue curves* correspond to simple closed geodesics corresponding to the axes of generators of the group. *Right* The uniformization of the Lawson surface in the Poincaré model of hyperbolic space with a canonical fundamental domain (*red*) and axes of the hyperbolic generators of the uniformizing group

surface is realized as a rotation by 180°. The axis meets the surface in six points, which are the branch points of the hyperelliptic curve.

The third realization of the Riemann surface is made of squares identified along suitable edges. The fundamental domain is identified with the two others.

The model features the data of the discrete uniformizations in XML format. It contains the combinatorial data, the coordinates of the points, and the uniformizing groups data. PDF vector graphics and PNG images provide 2D renderings of objects in 3D space.

3.5 Tropical Grassmannian TropGr(2,6)

Authors: Michael Joswig and Benjamin Schröter (Fig. 5)

http://gallery.discretization.de/models/tropical_grassmannian_gr26

Tropical geometry studies piecewise linear images of classical algebraic varieties. Many interesting properties remain visible in the tropicalization. Additionally, this method reveals relations between geometry and optimization. One outcome are combinatorial algorithms for dealing with classical objects.

The *tropical Grassmannian* $\mathrm{TropGr}(d, n)$ is the tropicalization of the classical Grassmannian $\mathrm{Gr}(d, n)$, defined over some field. It parameterizes the tropical d-planes in the tropical $(n-1)$-torus; see [24, §4.3]. For $d = 2$ the tropical Grassmannian coincides with the corresponding *Dressian*, which arises as the subfan of the secondary fan of the hypersimplex $\Delta(d, n)$ corresponding to those regular decompositions whose cells are matroid polytopes [25].

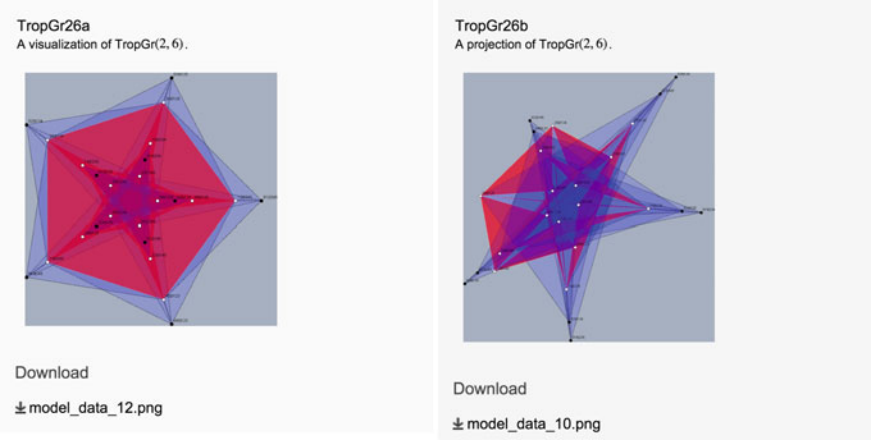

Fig. 5 Screenshots of two images contained in the "Tropical Grassmannian TropGr(2,6)" model

How to properly visualize TropGr(2, 6) is far from obvious, since (modulo its lineality space and intersected with the corresponding unit sphere) this is a 2-dimensional spherical simplicial complex naturally embedded in the 8-sphere. It has 25 vertices, 105 edges and 105 triangles. The approach here employs a fixed copy of smaller tropical Grassmannian TropGr(2, 5), obtained by deletion, as a frame of reference and uses projections. The *deletion* of a matroid as a smaller matroid which is induced on fewer elements, and this notion carries over matroid decompositions.

The media objects associated with this model are a `polymake` [26] description and pictures of various projections, in PNG format.

4 Architecture

In this section we describe the structure of a model and the organization of data within the DGD GALLERY. It is also explained how users create, edit, and interact with models using model permissions. Finally, we give details on the submission system and the review process.

4.1 What Is a Model?

The architecture of the DGD GALLERY is built around the definition of the `Model`, see Fig. 6. The `teletype` font is used to indicate that a word is the name of an abstract data type, one of its attributes, or an admissible value. From a high level perspective a *model* is a collection of files together with a description. The description contains fields for the title, authors, a description text, keywords, literature references, and the creation date. The data files associated with a model are bundled into media objects. A *media object* is a set of files together with a title and a description text. These files may be images, videos or data for specific software systems. While some file formats are more common (and more reasonable) than others, conceptually we allow for any file format to become part of a media object. In this way our design is very flexible and thus could be applied in other contexts.

The data type `Model` has a `key`, a `version` number, a `status` field, and an `edited-by` username. The model key is a unique identifier that is used, e.g., to assemble the permanent link of the model on the web. The version number is assigned automatically for keeping track of a model's history. Throughout the following the word "model" refers both to a specific version and to the entire history of a model. The standard representative of a model is given by its latest version. The `edited-by` field contains the username of the author of a particular model version. Hence, in a database a model can be uniquely identified by its key, a model version is identified by its key and version number.

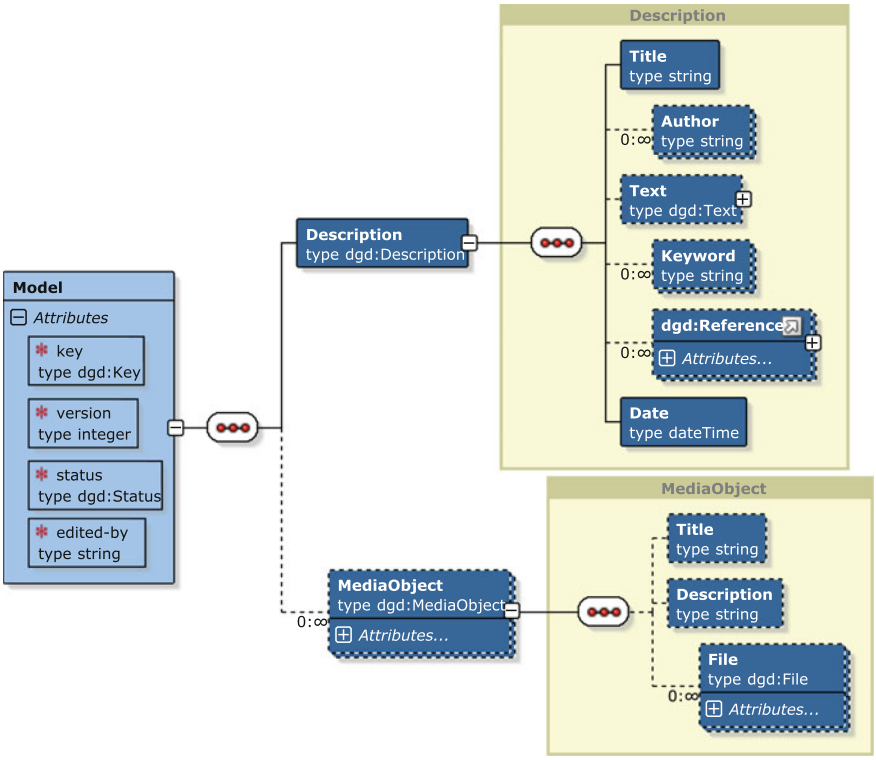

Fig. 6 The structure of a model. A model is a collection of media objects together with a description

The status of a model can take the values `edit`, `pending`, `rejected`, or `approved`. See Sect. 4.5 for a detailed description of the model status and the submission process for models in the gallery.

The model description is a collection of the following information that is provided by the editor of a model. While this somehow resembles the structure of a traditional research paper, there are some notable differences.

- The `Title` of the model.
- A sorted list of `Authors`. Since this is a frequent source of misunderstanding, it is worth explaining. The authors of the model are those who create the content that is presented online. Like for a research paper all the scientific work that leads to the model must be properly acknowledged in the references. However, clearly, the set of authors cannot comprise all the authors who contributed something to the entire history of a mathematical idea. For instance, suppose that Alice first describes a new type of surface in a traditional research paper, and Bob afterwards produces a model from Alices description (without Alice's help). Then Bob is the only author, who must cite Alice's paper.

- The description `Text`, which can contain any valid LaTeX source code that can be compiled using the MathJax library, see [27]. References to the literature or to media objects can be cited via the `\cite{.}` command. Previews of media objects can be included with the `\media{.}` command.
- A set of keywords can be assigned to the model. The keywords are used on the web-site to, e.g., improve search features.
- A set of references each of which consitsts of a reference key that is to be used in `\cite` commands and a set of key value pairs. The user interface of the gallery maps BibTeX entries to model references. Conversely a model reference is rendered and referenced using common BibTeX styles.
- The date field of the description contains the creation date of the particular version of the model.

A model contains a number of media objects for visualization and use in other software systems. This concept will be explained below.

4.2 Media Objects and Data Files

A media object is a collection of files that describe the same set of data associated with the model. For instance, several media objects might correspond to various views of the same model; e.g., see the tropical Grassmanian in Example in Sect. 3.5. A different use case for several media objects for the same model is displayed for the discrete catenoid and helicoid model in Example in Sect. 3.1. One media object shows a catenoid, whereas the other media object contains a dynamic rendering of the transformation from the catenoid to the helicoid.

The various file formats for one media object are meant to display one view of the model on several backends. For instance, the discrete catenoid media object comes with a PNG file to be displayed in a standard web browser and with an OBJ file which allows 3-dimensional interactive visualization with a suitable viewer software. The data files comprising the media objects are stored in the file system separately from the model database. The media objects of a model contain links to those data files, see Sect. 4.1.

In principle, we do not restrict the file formats for data files of any media objects. This makes the DGD Gallery very flexible, but this also creates potential trouble with file formats that are uncommon. We support the direct visualization of a few well chosen standard file formats. So far these include the following: PNG and JPG (for raster image data), SVG and PDF (for vector graphics), OBJ (for 3-dimensional geometric data), MOV, MP4, and OGV (for video content), POLY (for `polymake` data), and others. Interactive content is not excluded, see Sect. 5.3, but the danger of a particularly low stability over time should be well considered. We rely on the review process for a sound selection.

4.3 Versioning

The DGD GALLERY tracks the history of each model via the `version` attribute, see Fig. 6. Editing a model amounts to adding a new version with modified content. If a model is deleted, all versions of the model and the data files linked are deleted from the database. A data file is kept in the file system as long as there exists a link to it from some version of a model.

The version system is particularly useful for models with several authors who can collaborate through our front end.

It is worth noting that we also allow published models to be edited further and resubmitted. Upon acceptance this new version will appear as the current version of the model on the web page. The previously published versions remain visible and can be compared. This way authors can keep their models up to date; see also Sect. 5.2 below which describes our migration process.

4.4 Users

The users of the DGD GALLERY are represented by their usernames, i.e., their `login` names on the web-site. The access is password restricted, see also Sect. 5.1. In addition to the username and password we store the name and email address of the person that is associated with the user.

A user has a global user-role that can take the values `admin`, `reviewer`, or `author`. In addition to the global user-role we store model-roles for each model associated with a user. A user can be the `owner` or an `editor` of a model. The read and write access to models is restricted such that it is based on a combination of the global user-role, the model-role and the state of the model, Fig. 7. This implementation allows reviewers to act as model authors but prevents them from approving their own models.

A notable design decision is that a reviewer can modify a submitted model to correct obvious typos and other minor changes before approval. Each owner of a model can invite other users to become either owners or editors of that model.

4.5 Submission Process

The DGD GALLERY uses a submission system to publish models on the web-site. The idea is that a board of reviewers approves, sends back for revision, or rejects a submitted model. The review process should concern the quality of the content and address technical issues with the digital data. The review board has to work out and agree on some quality criteria for a model.

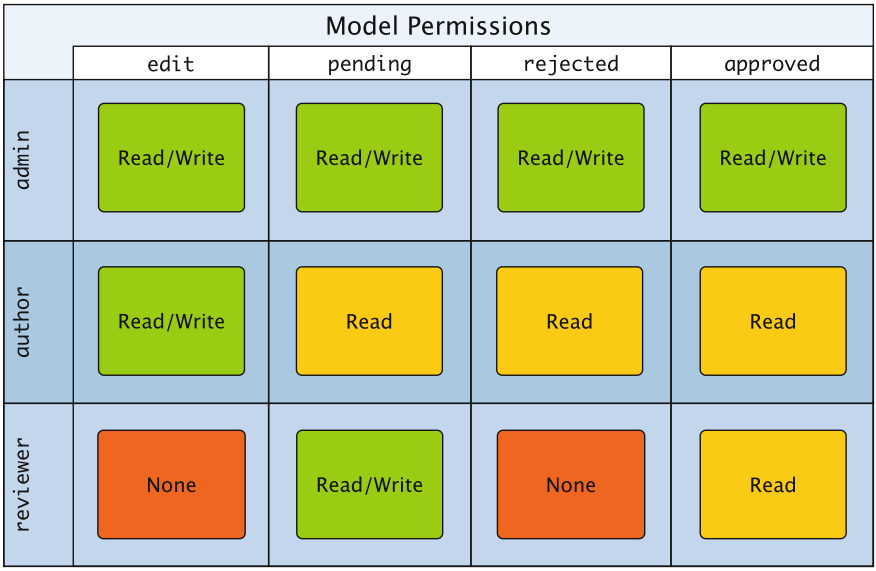

Fig. 7 Read and write permissions during the life-cycle of a model. A user with global `admin` privileges can read and write on the model at any state (*first row*). The `author` of the model can edit his model if it is in `edit` state (*second row*). A `reviewer` can edit a model if it has been submitted (`pending` state, *third row*)

During its life-cycle a model has assigned a status value. A newly created model starts its life in `edit` state. It can be previewed and edited by the `owners` of the model, typically the creator of the model, and any additional user with the `editor` model-role, see Sect. 4.4.

A model can be submitted by a user with the `owner` model-role. The status of the model changes to `pending`. A model with `pending` status is read-only for the `owner` and all `editors`.

Reviewers can preview and edit `pending` models. A reviewer edits a model to resolve small issues such as typos. If the quality of a model is sufficiently high then a reviewer can accept a model. The status of the model is changed to `approved`. If the content has flaws or technical issues that can be resolved by the creator of the model, the reviewer sends the model back to `edit` state. Any action by a reviewer is accompanied by a review text, which is presented to the authors of the model.

If a model is sent back for revision, the authors can edit the model according to the review text and resubmit. If the model is `rejected` it can neither be edited nor resubmitted. A model will be rejected if it contains major flaws or its content is not appropriate for publication in the DGD GALLERY.

Approved models become publicly available on the DGD GALLERY web-site (see Sect. 4.6). To further improve public models, e.g. by correcting errors or replacing outdated file formats, a new version of an approved model can be created, which is back in `edit` state. To publish the new version it has to be submitted und undergo the revision process again.

The model submission system dispatches messages to the users of the DGD GALLERY on every model status change. Reviewers are notified about submitted models. Model owners/editors are notified upon acceptance, rejection, or call for revision.

In principle any reviewer can accept, send back, or reject a model. We rely on a reasonable communication between the reviewers to organize the review process. Accepting a model is based on formal correctness, technical soundness, mathematical content and visualization quality.

4.6 Publication and Licensing

Content that has been approved by the board of reviewers is published on the DGD GALLERY web page. The presentation of the content on this page is equivalent to the preview during `edit` state of the model. The `key` defines the permanent absolute URL of a model:

https://gallery.discretization.de/model/

The content of the DGD GALLERY is published under the Creative Commons Attribution-ShareAlike 4.0 International license, short CC BY-SA 4.0, see [28]. This means in particular that we allow for our data to be used commercially, enabling newspapers or commercial web blogs to include content from the gallery without further complications. Appropriate credit must be given if any content is reproduced or used, and this includes a link to the DGD GALLERY.

5 Implementation

In this section we elaborate on the technical decisions that we made in order to implement the DGD GALLERY. It should give an impression of the system architecture, libraries, frameworks, and languages in use and their respective purposes.

We imposed some a priori constraints on the implementation mainly to ensure reusability and persistence of the data over time.

- **Human readable data format** (with enough structure to allow for easy validation and transformation): We chose XML for storage on the server and as the web server API data format. It fits the tree-like structure of our data and can be transformed to anything else, e.g. using XSLT. This allows for easy migrations which can range from changing the structure of the models to getting rid of XML itself (replacing it with some more sophisticated data format in the future). To ensure that all stored data, and in particular data entered by users of the system, agrees with our specifications we use the XML Schema concept [30]. This allows to validate all data on insert and during migration, see Sect. 5.2.

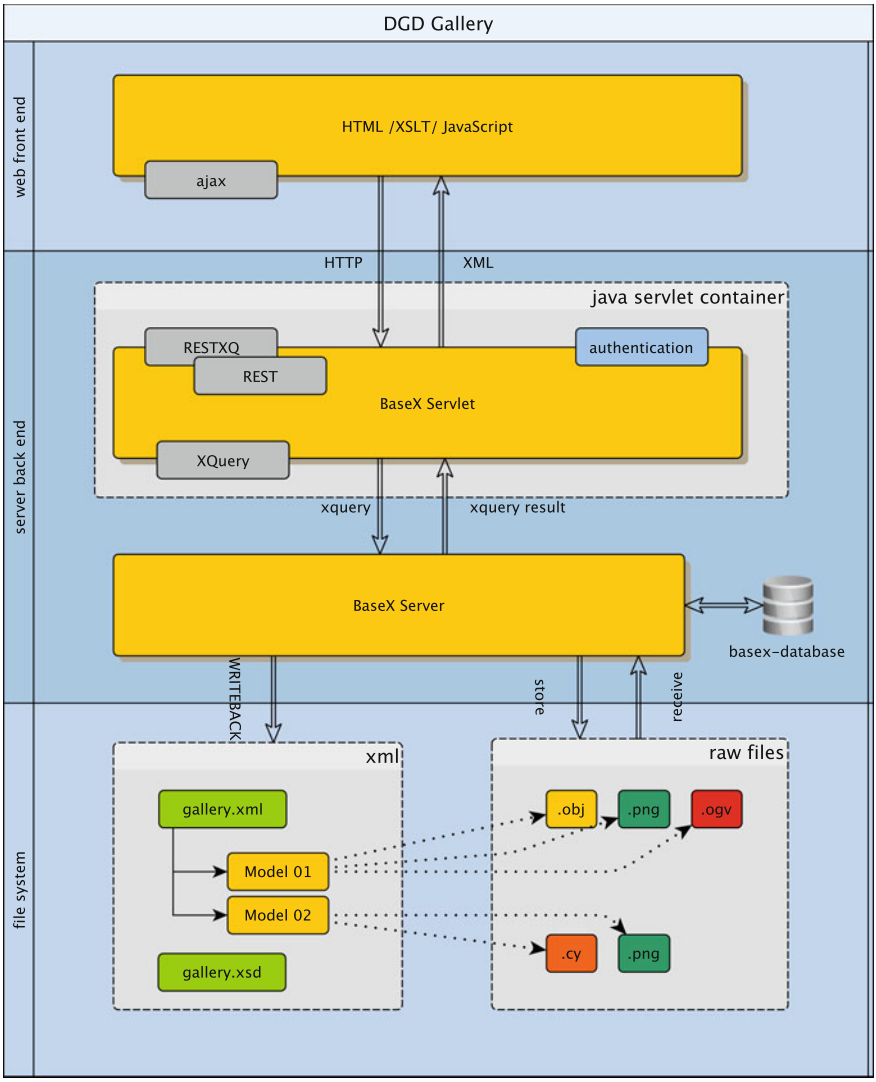

Fig. 8 System architecture of the DGD GALLERY. On the file system level we store XML model data and data files. A BASEX server manages the read/write access to the XML documents and data files. It maintains an instance of a document database to optimize access to the XML data. At the same time a BaseX servlet provides a REST API [29] to connect the HTML/Javascript web front end of the gallery. It runs inside an Apache Tomcat servlet container executed within an Apache HTTP web server. The front end uses AJAX techniques and XSLT to create an interactive application using the API provided by the application server

- **Database framework agnostic storage** (while still using a database): The XML and any binary data are stored and handled using the XML document database BASEX [6], see Sect. 5.1. This gives us low access times (for data cached in main memory) and a transparent mechanism for permanent storage on the server's file system. The binary data files of the model's media objects are stored next to the XML data and linked appropriately, see the file system section in Fig. 8.
- **Separation of data and presentation**: We separate our application into a back end (on the server for database management only) and a front end (creating a HTML representation on the client machine). The BASEX database already provides the means for a complete implementation of the back end via XQUERY. This includes the specification of a REST API [29], which is a standard way to define the communication interface between server and client in the internet. The API returns XML or binary data in response to specified HTTP requests from the front end. XML is already close to HTML, while still not carrying explicit information on the visualization. This allows for the easy generation of multiple presentations from just one XML. In Sect. 5.3 we elaborate on the front end, which is based an XSLT, JavaScript and AJAX [31].

5.1 *XML Based Backend and the XML Document Database* BASEX

We use the established XML document database BASEX for storing our data. This automatically provides us with permissions, versioning, and life-cycle management for the models. BASEX runs on any Java application server. We use Apache Tomcat 7, see [32].

BASEX allows for the implementation of (web) applications using the XML query language XQUERY, see [33]. It combines the database access and application server logic implementation into one language. Additionally BASEX can be used to implement a REST API via RESTXQ, which is a set of XQUERY annotations for handling HTTP requests and generating HTTP responses [34], see Listing 1.

```
1  (:~
2  : REST API function to create a new model.
3  :
4  : @param $title mapped to POST parameter title, the title of the
       new model
5  : @param $user optional user name if no session can be inferred by
        the server
6  : @param $pass optional password
7  :)
8  declare %rest:POST
9  %rest:path("/createmodel")
10 %rest:form-param("title", "{$title}")
11 %rest:form-param("user", "{$user}", "dummy_id")
12 %rest:form-param("pass", "{$pass}", "")
13 %output:method("text")
14 %updating function api:createModel(
15     $title as xs:string,
16     $user as xs:ID,
```

```
17      $pass as xs:string
18  ) {
19      let $user := user:checkUser($user, $pass)
20      return model:createModel($user, $title)
21  };
```

Listing 1 XQuery with RESTXQ annotations. The function api:createModel defines the web API function to create a model for a specified user and title string. The RESTXQ annotations, lines 8–13, define the REST interface of the server. User permissions are checked, line 19, and the corresponding database function to create a new model is called, line 20. User credentials (`$user`, `$pass`) are optional parameters and are transmitted using HTTPS API calls. Once logged in we use session cookies to authenticate users.

Generally, all API calls to our back end have to be authenticated. Either a username and password pair, or a session-cookie has to be provided along each request. The front end implementation uses session-cookies, which are obtained by an authenticated call to the login API function. A user's password is stored in the form of a salted bcrypt hash to provide protection against password recovery through an attacker in case of a server breach, see [35].

5.2 A Fail-Safe Release and Migration Process

While a project like the DGD GALLERY evolves the precise technical requirements for the database are likely to change. This means that old versions will have to be migrated into new ones. We implemented a release process for new versions of the web application and its data using Apache ant [36]. We use XSLT 2.0 and XML Schema to define and validate database migrations [37].

In principle this allows for more general migrations than just XML to XML conversions between different schema versions of the database. We can envision scenarios in the future where XML may turn into a legacy format and will be replaced by a more general versatile format. With XSLT we can also convert our XML data into arbitrary text based formats allowing for a final conversion into file formats entirely different from XML.

5.3 A JavaScript Web Front End

The standard way to enter a new model into the DGD GALLERY is through our web front end. This part of the application is completely separated from the back end, relying only on the REST API to BASEX for communication.

We use the AJAX scheme of web application development. The application, with its HTML, XSLT, and JavaScript components, is initially loaded from the server. The access to the database is organized as HTTP connections via JavaScript. Once XML model data has arrived from the server we process it with XSL Transformations [37]

to provide dynamic HTML and JavaScript for each client. We use the SaxonCE XSLT JavaScript framework to execute XSLT 2.0 in the browser, see [38].

Media renderers are provided for several common media formats, see Sect. 4.2. In the case of images and videos we are relying on the standards built into HTML5. We have support for the web capabilities of Cinderella to allow for interactive content [19, 39]. For the web browser in particular we use CindyJS [40], an open source JavaScript variant of Cinderella that aims to be compatible with Cinderella.

Acknowledgments This research was supported by DFG SFB/TRR 109 "Discretization in Geometry and Dynamics".

References

1. Bates, D.J., Hauenstein, J.D., Sommese, A.J., Wampler, C.W.: Numerically solving polynomial systems with Bertini, Software, Environments, and Tools, vol. 25. Society for Industrial and Applied Mathematics (SIAM), Philadelphia, PA (2013)
2. Barakat, M., Lange-Hegermann, M.: Gabriel morphisms and the computability of Serre quotients with applications to coherent sheaves (2014). Preprint arXiv:1409.2028
3. Hong, H., Yap, C. (eds.): Mathematical software–ICMS 2014. Lecture Notes in Computer Science, vol. 8592. Springer, Heidelberg (2014)
4. Hales, T., Adams, M., Bauer, G., Dang, D.T., Harrison, J., Hoang, T.L., Kaliszyk, C., Magron, V., McLaughlin, S., Nguyen, T.T., Nguyen, T.Q., Nipkow, T., Obua, S., Pleso, J., Rute, J., Solovyev, A., Ta, A.H.T., Tran, T.N., Trieu, D.T., Urban, J., Vu, K.K., Zumkeller, R.: A formal proof of the Kepler conjecture (2015). Preprint arXiv:1501.02155
5. DFG verabschiedet Leitlinien zum Umgang mit Forschungsdaten. http://www.dfg.de/foerderung/info_wissenschaft/2015/info_wissenschaft_15_66/
6. BaseX Team: BaseX. The XML database (2014). http://basex.org
7. The Geometry Center—Geometry Reference Archive (2000). http://www.geom.uiuc.edu/docs/reference/
8. Hoffman, D., Hoffman, J., Weber, M.: The Scientific Graphics Project (1998–2004). http://www.msri.org/publications/sgp/SGP/
9. Eppstein, D.: The Geometry Junkyard. https://www.ics.uci.edu/~eppstein/junkyard/
10. Bohle, C., Loose, F., Schmitt, N., Heller, S.: GeometrieWerkstatt. https://www.math.uni-tuebingen.de/ab/GeometrieWerkstatt/
11. Imaginary | open mathematics. http://imaginary.org/
12. The SymbolicData project. http://wiki.symbolicdata.org/
13. EG-Models. http://www.eg-models.de

14. Joswig, M., Polthier, K.: EG-Models—a New Journal for Digital Geometry Models. In: Borwein J., Morales M., Polthier K., Rodrigues J. (eds.) Multimedia Tools for Communicating Mathematics, pp. 165–190. Springer (2002)
15. Bobenko, A.I., Hoffmann, T., König, B., Sechelmann, S.: S-conical minimal surfaces. Towards a unifying theory of discrete minimal surfaces (2015)
16. Schramm, O.: Circle patterns with the combinatorics of the square grid. Duke Math. J. **86**, 347–389 (1997)
17. Bobenko, A.I.: Discrete conformal maps and surfaces. In: Clarkson P., Nijhof F. (eds.) Symmetries and Integrability of Difference Equations, Proceedings of the SIDE II Conference, Canterbury, July 1–5, 1996, pp. 97–108. Cambridge University Press (1999)
18. Bornemann, F., Its, A., Olver, P., Wechslberger, G.: Numerical methods for the discrete map z^a (in this volume)
19. Cinderella (2013). http://www.cinderella.de
20. Bobenko, A.I., Springborn, B.A.: Variational principles for circle patterns and Koebe's theorem. Trans. Amer. Math. Soc **356**, 659–689 (2004)
21. Lawson, H.B.J.: Complete minimal surfaces in $\mathbb{S}^3$. Annals of Mathematics **92**(3), 335–374 (1970)
22. Bobenko, A.I., Sechelmann, S., Springborn, B.: Discrete conformal maps: Boundary value problems, circle domains, Fuchsian and Schottky uniformization (In this volume)
23. Oberknapp, B., Polthier, K.: An algorithm for discrete constant mean curvature surfaces. In: Hege, H.C., Polthier, K. (eds.) Visualization and Mathematics, pp. 141–161. Springer, Berlin Heidelberg (1997)
24. Maclagan, D., Sturmfels, B.: Introduction to Tropical Geometry, Graduate Studies in Mathematics, vol. 161. American Mathematical Society, Providence, RI (2015)
25. Herrmann, S., Jensen, A., Joswig, M., Sturmfels, B.: How to draw tropical planes. Electronic J. Combin. **16**(2), R6 (2009–2010). http://www.combinatorics.org/ojs/index.php/eljc/article/view/v16i2r6
26. Gawrilow, E., Joswig, M.: `polymake`: a framework for analyzing convex polytopes. In: Polytopes—combinatorics and computation (Oberwolfach, 1997), *DMV Sem.*, vol. 29, pp. 43–73. Birkhäuser, Basel (2000)
27. The MathJax Consortium: Mathjax. https://www.mathjax.org
28. creativecommons.org: CC BY-SA 4.0. http://creativecommons.org/licenses/by-sa/4.0/
29. REST—Representational State Transfer. https://en.wikipedia.org/wiki/Representational_state_transfer
30. W3C: XML Schema (2004). http://www.w3.org/TR/xmlschema-0/
31. Ajax programming. http://wikipedia.org/wiki/Ajax_(programming)
32. Apache: Apache Tomcat (2015). https://tomcat.apache.org
33. W3C: Xquery 1.0: An xml query language (2010). http://www.w3.org/TR/xquery/
34. BaseX Team: RESTXQ documentation web page. http://docs.basex.org/wiki/RESTXQ
35. Provos, N., Mazières, D.: A future-adaptive password scheme. Proceedings of the Annual Conference on USENIX Annual Technical Conference. ATEC '99, pp. 32–32. USENIX Association, Berkeley, CA, USA (1999)
36. Apache: Apache ant (2012). http://ant.apache.org/
37. W3C: XSL Transformations (XSLT) version 2.0 (2007). http://www.w3.org/TR/xslt20/
38. Saxonica: Saxon-CE (Client Edition) (2015). http://www.saxonica.com/ce/index.xml
39. Richter-Gebert, J., Kortenkamp, U.: The Cinderella.2 Manual: Working with The Interactive Geometry Software. Springer (2012)
40. CindyJS—A JavaScript framework for interactive (mathematical) content. https://github.com/CindyJS